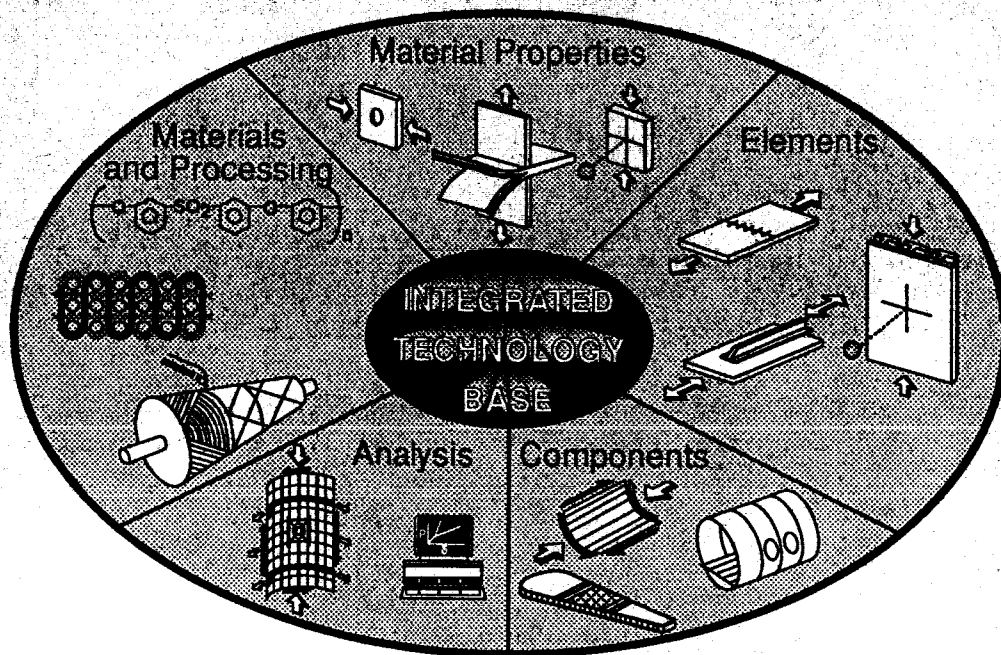


First NASA Advanced Composites Technology Conference



*Proceedings of a conference held in
Seattle, Washington
October 29–November 1, 1990*

Review for general release January 31, 1993

NASA

*NASA Conference Publication 3104
Part 1*

First NASA Advanced Composites Technology Conference

*Compiled by
John G. Davis, Jr.
NASA Langley Research Center
Hampton, Virginia*

*Herman L. Bohon
Lockheed Engineering & Sciences Company
Hampton, Virginia*

Proceedings of a conference sponsored by the
National Aeronautics and Space Administration,
Washington, D.C., and held in
Seattle, Washington
October 29–November 1, 1990



National Aeronautics and
Space Administration

Office of Management

Scientific and Technical
Information Division

1991

PREFACE

The First NASA Advanced Composites Technology Conference was sponsored by the NASA Langley Research Center to review recent advances in research and development of advanced composites technology for applications to military and commercial aircraft. The NASA Advanced Composites Technology (ACT) Program is a major new multiyear research initiative to achieve a national goal of technology readiness before the end of the decade. This initiative is carried out through a cooperative program between industry, universities, and the Government conducting research in materials processing, analysis development, innovative designs and manufacturing methodology.

The First NASA Advanced Composites Technology Conference was held in Seattle, Washington, October 29 through November 1, 1990. The conference provided a forum for the composites community to exchange information and an opportunity to observe recent progress in advanced composites technology. Fifty-two papers were organized into sessions that emphasized composite transport technology development, advances in design and manufacturing, and research in materials and structural mechanics. In addition, a session sponsored by the Department of Defense emphasized lessons learned from current applications programs. This conference publication is a compilation which contains the papers presented in these sessions.

The use of trademarks or manufacturers' names in this publication does not constitute endorsement, either expressed or implied, by the National Aeronautics and Space Administration.

John G. Davis, Jr.
Herman L. Bohon

CONFERENCE ORGANIZATION

Sponsor: Structures Technology Program Office
Structures Directorate
NASA Langley Research Center
Hampton, VA

General Chairman
John G. Davis, Jr.
NASA Langley

Technical Chairman
Herman L. Bohon
Lockheed Engineering
& Sciences Company

Administrative Assistant
Stuart E. Pendleton
Lockheed Engineering
& Sciences Company

SESSION ORGANIZERS

John G. Davis, Jr.
James H. Starnes, Jr.
Norman J. Johnston
David Beeler

NASA Langley Research Center
NASA Langley Research Center
NASA Langley Research Center
Wright Research and Development Center

SESSION OUTLINE

FIRST NASA ADVANCED COMPOSITES TECHNOLOGY CONFERENCE

Session I

Composite Transport Technology

Chairman: **Michael F. Card**, Chief, Structural Mechanics Division
NASA Langley Research Center

Session II

Advances in Design and Manufacturing

Chairman: **Darrel Tenney**, Chief, Materials Division
NASA Langley Research Center

Session III

DoD Composites Applications

Chairman: **David Beeler**, Head, Nonmetals Branch
Wright Research and Development Center

Session IV

Materials Research

Chairman: **Norman J. Johnston**, Chief Scientist, Materials Division
NASA Langley Research Center

Session V

Work in Progress - Materials and Structures

Chairman: **W. Tom Freeman**, ACT Structures Technology Program Office
NASA Langley Research Center

Session VI

Structural Mechanics Research

Chairman: **James H. Starnes Jr.**, Head, Aircraft Structures Branch
Structural Mechanics Division, NASA Langley Research Center

Consolidation of Graphite/Thermoplastic Textile Preforms for Primary Aircraft Structure	293
J. Suarez and J. Mahon	

Cost Studies for Commercial Fuselage Crown Designs	339
T. H. Walker, P. J. Smith, G. Truslove, K. S. Willden, S. L. Metschan, and C. L. Pfahl	

A Unified Approach for Composite Cost Reporting and Prediction in the ACT Program	357
W. Tom Freeman, Louis F. Vosteen, and Shahid Siddiqi	

Session III

F-15 Composite Engine Access Door	371
Ramaswamy L. Ramkumar and James C. Watson	

Fabrication of the V-22 Composite Aft Fuselage Using Automated Fiber Placement	385
Robert L. Pinckney	

Lessons Learned for Composite Structures	399
R. S. Whitehead	

Part 2*

Session IV

Preliminary Properties of a Resin From Ethynyl Terminated Materials	419
Paul M. Hergenrother and John W. Connell	

Infiltration/Cure Modeling of Resin Transfer Molded Composite Materials Using Advanced Fiber Architectures	425
Alfred C. Loos, Mark H. Weideman, Edward R. Long, Jr., David E. Kranbuehl, Philip J. Kinsley, and Sean M. Hart	

Powder Towpreg Process Development	443
Robert M. Baucom and Joseph M. Marchello	

Effects of Intra- and Inter-Laminar Resin Content on the Mechanical Properties of Toughened Composite Materials	455
Dodd H. Grande, Larry B. Ilcewicz, William B. Avery, and Willard D. Bascom	

Studies of Fiber-Matrix Adhesion on Compression Strength	477
W. D. Bascom, J. A. Nairn, and D. J. Boll	

*These papers are presented in NASA CP-3104, Part 2.

The Initiation, Propagation, and Effect of Matrix Microcracks in Cross-Ply and Related Laminates	497
John A. Nairn, Shoufeng Hu, Siulie Liu, and Jong Bark	
Comparison of Impact Results for Several Polymeric Composites Over a Wide Range of Low Impact Velocities	513
C. C. Poe, Jr., M. A. Portanova, J. E. Masters, B. V. Sankar, and Wade C. Jackson	
Delaminations in Composite Plates Under Impact Loads	549
Scott R. Finn and George S. Springer	
Micromechanics of Fatigue in Woven and Stitched Composites	579
B. N. Cox, M. S. Dadkhah, R. V. Inman, M. R. Mitchell, W. L. Morris, and S. Schroeder	
Characterization of Multiaxial Warp Knit Composites	589
H. Benson Dexter, Gregory H. Hasko, and Roberto J. Cano	
Development of Stitching Reinforcement for Transport Wing Panels	621
Raymond J. Palmer, Marvin B. Dow, and Donald L. Smith	

Session V

Development of Resins for Composites by Resin Transfer Molding	647
Edmund P. Woo, Paul M. Puckett, and Shawn J. Maynard	
Advanced Fiber/Matrix Material Systems	659
J. Timothy Hartness	
Mechanical and Analytical Screening of Braided Composites for Transport Fuselage Applications	677
Mark J. Fedro, Christian Gunther, and Frank K. Ko	
Ultrasonic Detection and Identification of Fabrication Defects in Composites	705
Edward R. Long, Jr., Susan M. Kullerd, Patrick H. Johnston, and Eric I. Madaras	
Developments in Impact Damage Modeling for Laminated Composite Structures	721
Ernest F. Dost, William B. Avery, Gary D. Swanson, and Kuen Y. Lin	
Multi-Parameter Optimization Tool for Low-Cost Commercial Fuselage Crown Designs	737
Zelda Zabinsky, Mark Tuttle, Douglas Graesser, Gun-In Kim, Darrin Hatcher, Gary Swanson, and Larry Ilcewicz	
Comparison of Hand Laid-Up Tape and Filament Wound Composite Cylinders and Panels With and Without Impact Damage	749
Dawn C. Jegley and Osvaldo F. Lopez	

Effects of Scale in Predicting Global Structural Response	761
R. B. Deo and H. P. Kan	
Design and Analysis of Grid Stiffened Concepts for Aircraft Composite Primary Structural Applications	779
Damodar R. Ambur	
Optimization of Composite Sandwich Cover Panels Subjected to Compressive Loadings	791
Juan R. Cruz	
A Comparison of Classical Mechanics Models and Finite Element Simulation of Elastically Tailored Wing Boxes	809
Lawrence W. Rehfield, Richard D. Pickings, Stephen Chang, and Michael Holl	
Advanced Fiber Placement of Composite Fuselage Structures	817
Robert L. Anderson and Carroll G. Grant	
Process and Assembly Plans for Low Cost Commercial Fuselage Structure	831
Kurtis Willden, Stephen Metschan, and Val Starkey	
<u>Session VI</u>	
Progressive Failure Methodologies for Predicting Residual Strength and Life of Laminated Composites	843
Charles E. Harris, David H. Allen, and T. Kevin O'Brien	
Multiple Methods Integration for Structural Mechanics Analysis and Design	875
J. M. Housner and M. A. Aminpour	
Probabilistic Composite Analysis	891
C. C. Chamis and P. L. N. Murthy	
A Rayleigh-Ritz Analysis Methodology for Cutouts in Composite Structures	901
Steven G. Russell	
Effects of Bolt-Hole Contact on Bearing-Bypass Damage-Onset Strength	921
John H. Crews, Jr. and Rajiv A. Naik	
Prediction of Stiffener-Skin Separation in Composite Panels	939
Han-Pin Kan, Mary A. Mahler, and Ravi B. Deo	
Experimental Behavior of Graphite-Epoxy Y-Stiffened Specimens Loaded in Compression	953
P. D. Sydow and M. J. Stuart	
Structural Response of Bead-Stiffened Thermoplastic Shear Webs	969
Marshall Rouse	

Evaluation of Some Scale Effects in the Response and Failure of Composite Beams 979
Karen E. Jackson and John Morton

An Overview of the Crash Dynamics Failure Behavior of Metal and Composite Aircraft Structures 1005
Huey D. Carden, Richard L. Boitnott, Edwin L. Fasanella, and Lisa E. Jones

Tailored Composite Wings With Elastically Produced Chordwise Camber 1037
Lawrence W. Rehfield, Stephen Chang, Peter J. Zischka, Richard D. Pickings, and Michael W. Holl

Part 1

* * *

Luncheon Address

* * *

COMPOSITES: A VIABLE OPTION

John E. McCarty

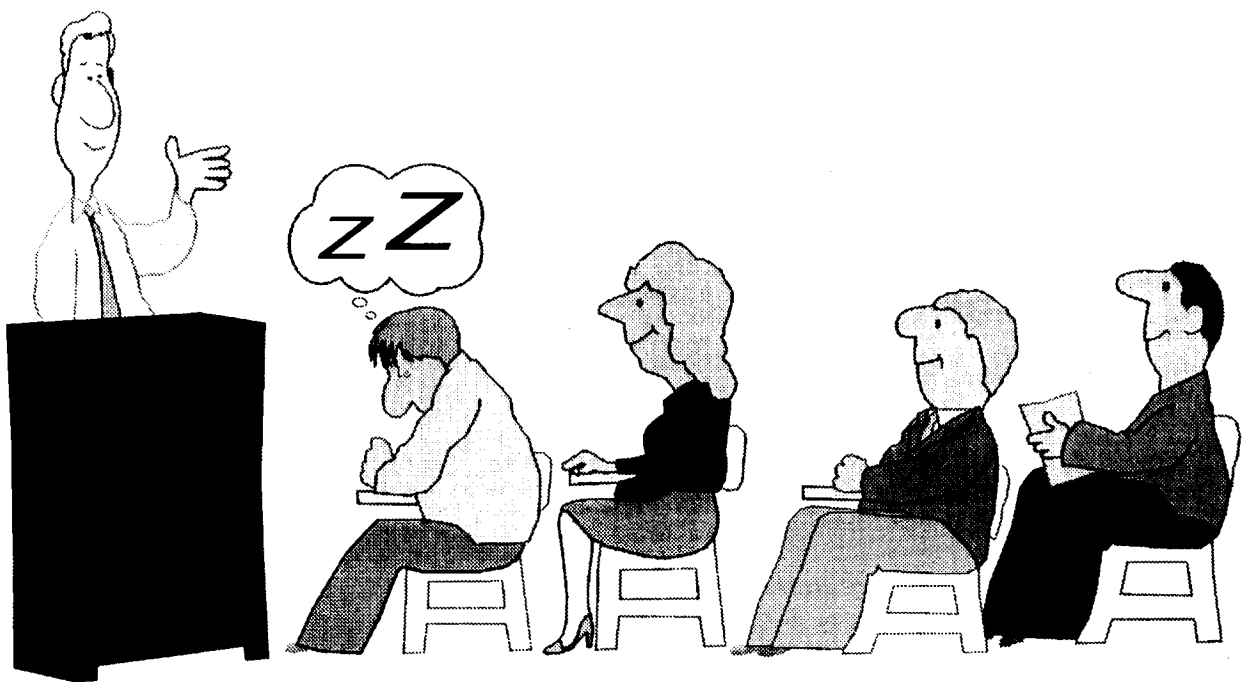
While it sounded great to be asked to talk about composites, I found it difficult to select subject areas that would be of real interest. My choice is based on saying some things about where the maturity of the composite aircraft structures is today and what that means in terms of future criteria for application. This focus was the basis for my title selection. The other issue that will be addressed was requested by NASA and focuses on composites structures cost. This fits well with the state-of-the-art interpretations I will discuss first, since the cost issue must be viewed from both the current status and future points of view. The difficulty in presenting something in these areas is not in the subjects themselves but in trying to present a real world viewpoint to an audience of composite experts. So, with recognition of the expertise of the audience, I hope you will see something in this presentation about how to view composite aircraft structure.

Introduction

- NASA - introduction and vision
- Composite aircraft - option validation
- Aircraft structure
- Composite cost considerations
- Composite potential - commercial

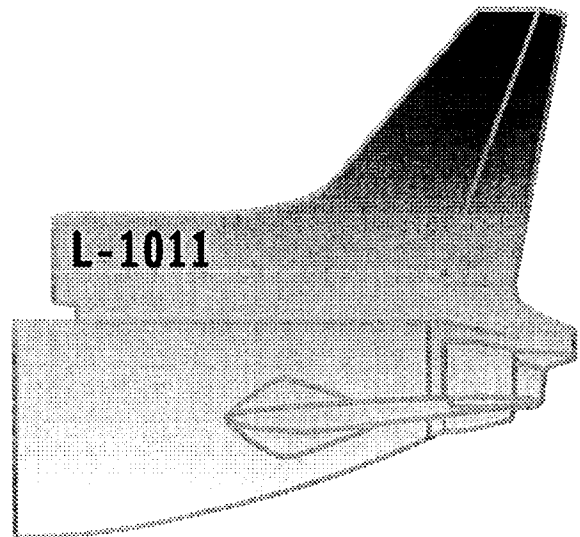
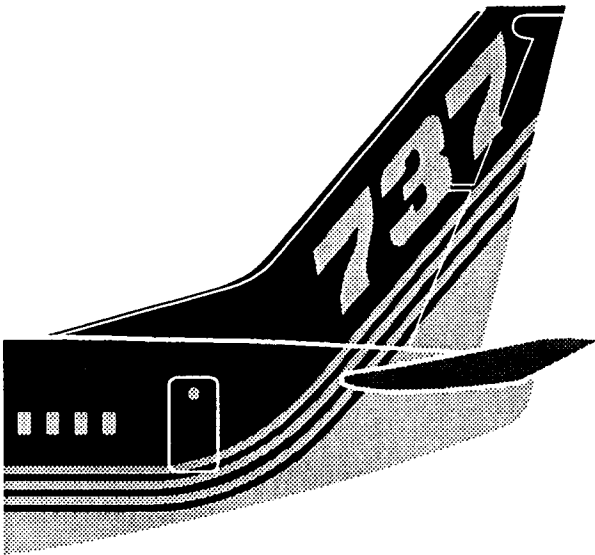
As noted, my initiation into the composite field and my association with NASA began at basically the same time. My first trip to NASA Langley was to take over contract management of Boeing's first composite contract with NASA that Reid June had won and was managing. Boeing management had decided that Reid was to help out on SST and I was to replace him on the NASA contract. My flight to NASA was one of those that I am sure all of you who have traveled a lot have experienced. I arrived at Newport News at 4:00 o'clock in the morning with the scheduled review on the contract at 8:00 o'clock. As the picture shows, about a minute after Reid introduced me as the new contract manager and the lights were dimmed for the presentation, I caught up on my missed night's sleep. There were and are those at NASA that have taken many opportunities to remind me of this, their initial impression of me.

NASA - Introduction



I feel it is only fair play that I give my friends at NASA the similar type of reminder they have often given me on my introduction to them. This chart is to remind them about the NASA/ACEE program initial bid phase that was won by Lockheed. As all company managements will, Boeing's wanted to know why they lost the contract bid. Since Reid and I were the ones preparing the bid, we of course went with our bosses to NASA to find out what we did wrong. There were several reasons expressed by NASA for Boeing's loss. A simple one was that Lockheed just had a better overall proposal. But one point that NASA focused on and that they said was one of the keys for our loss was our use of the 737 vertical tail component, since the 737 represented an aircraft with little future sales potential. My only response to NASA now is to say I hope your vision into the future is better now.

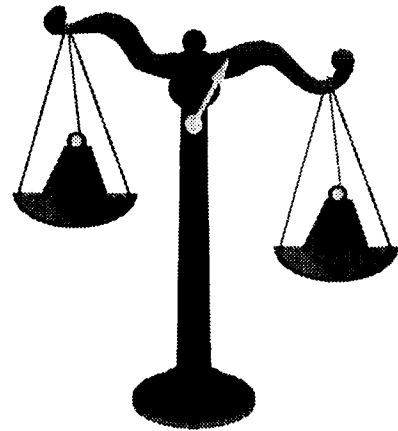
NASA: Vision



With this discussion of the past, between those I hope I can still call friends, let's take a look at the status of composites technology from the point of view of the presentation title. I selected the title because I had a boss that said, "When a material is considered during the preliminary design and product development phase of an aircraft program on an equal basis with other material options, it has become a viable option." I believe this is the status of composite materials today. What does this mean in terms of the selection and potential usage on future commercial transport aircraft. To understand this you need to understand the evolutionary changes that take place in commercial aircraft and the role the service usage plays in the design approaches taken. The selection of a viable material also means that it is not selected because it is the fad or to start the technology learning process. The scale on the chart emphasizes the equal weighing of all the structure material options on their merits. This means no bias criteria for or against a material systems selection. I am sure all the members of the audience that have been promoters of composites have experienced the imposition of special criteria on composites by those not wanting to change from metals. Finally, the things that are needed to make the change are a need to improve the product, an inhouse champion at the appropriate management level, and a need in the marketplace for a new aircraft in a competitive environment. The key here again is the acceptance of composites on an equal basis and weighed on a scale with the same acceptance parameters.

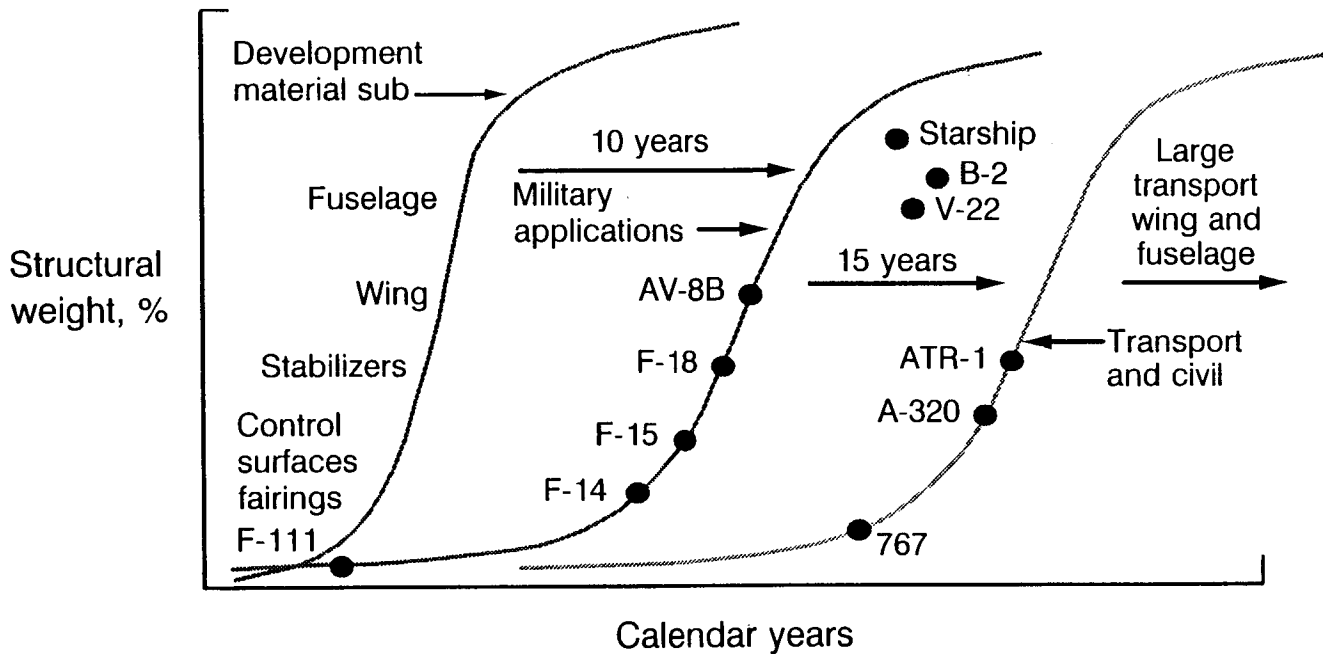
Composite Structures Selection

- Commercial aircraft design environment
 - Evolution
 - Service time
- Selection from the options
 - Criteria bias
 - Weighing of options
- Making the change
 - Need
 - Champion
 - Market



This chart simply displays that we now have a significant history of composite applications in military, civil, and commercial aircraft. This history also suggests that with this background the technology base is such that the material is truly a viable option for future designs.

Composite Structure Applications



One of the questions often asked by management when stepping up to the selection of a new material system is "Do we know how to certify it?" This list of civil and commercial aircraft components and aircraft that have been certified should emphatically answer that question in a positive manner. The certification process has been experienced by all the large commercial airframe manufacturers. The FAA now has the experience to deal with composite structural systems and to feel confident in their certification process. This certification question can no longer be a basis for not selecting composites on an equal basis with metals.

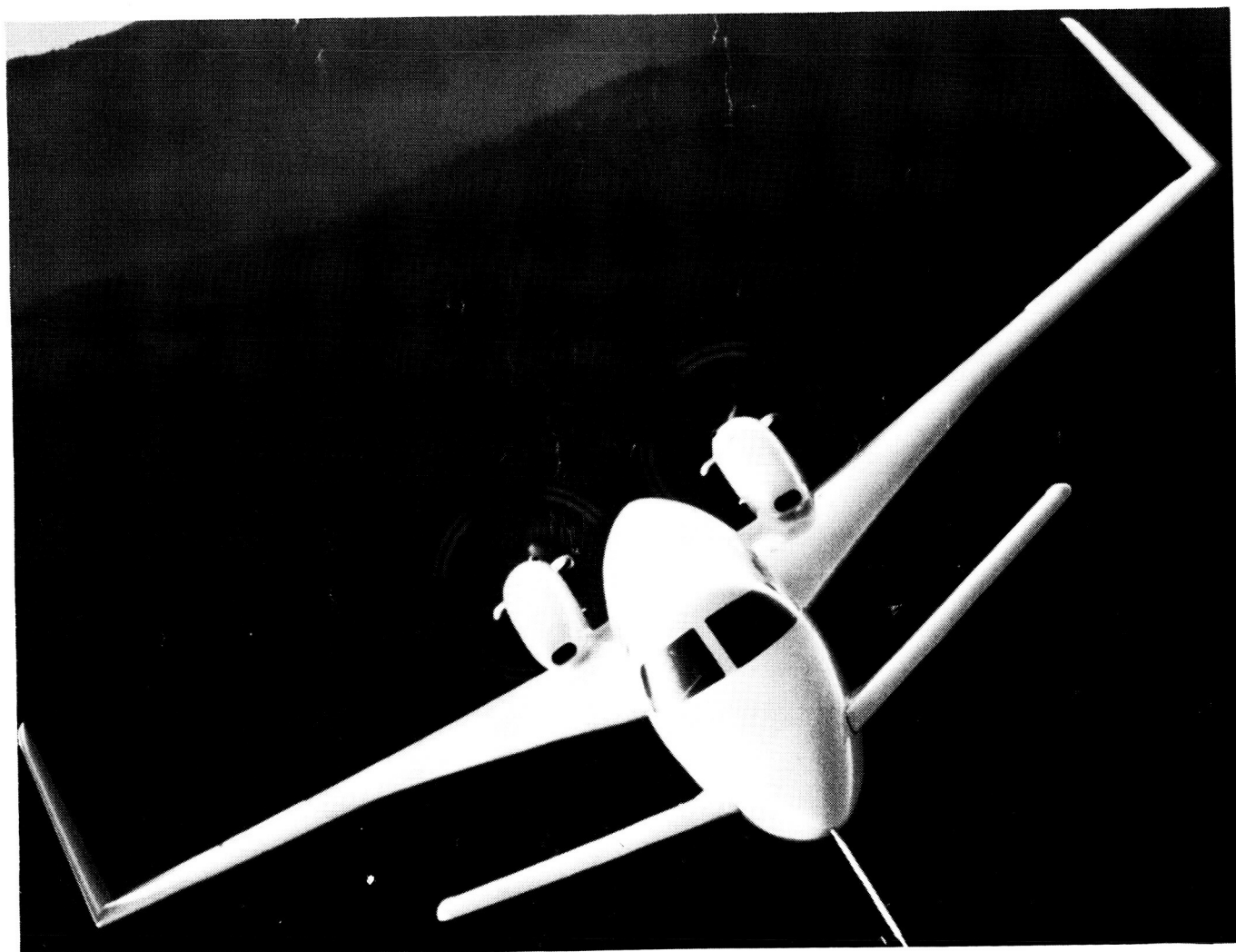
Certified - Applications

Key Primary Structure

- Transport category
 - Aerospatiale/Aeritalia outboard wing 11/15/89
 - Airbus A300-600 vertical stabilizer 3/28/88
 - Airbus A310-300 vertical stabilizer 6/10/87
 - Airbus A320 vertical and horizontal stabilizer 12/15/88
 - DC-10 vertical stabilizer 6/03/86
 - Boeing 737 horizontal stabilizer 11/14/84
- Normal (civil) category
 - Windecker Eagle entire aircraft 12/18/69
 - Beech 2000 (Starship) entire aircraft 6/14/88
 - Piaggio P-180 empennage, canard, and aft fuselage 5/07/90

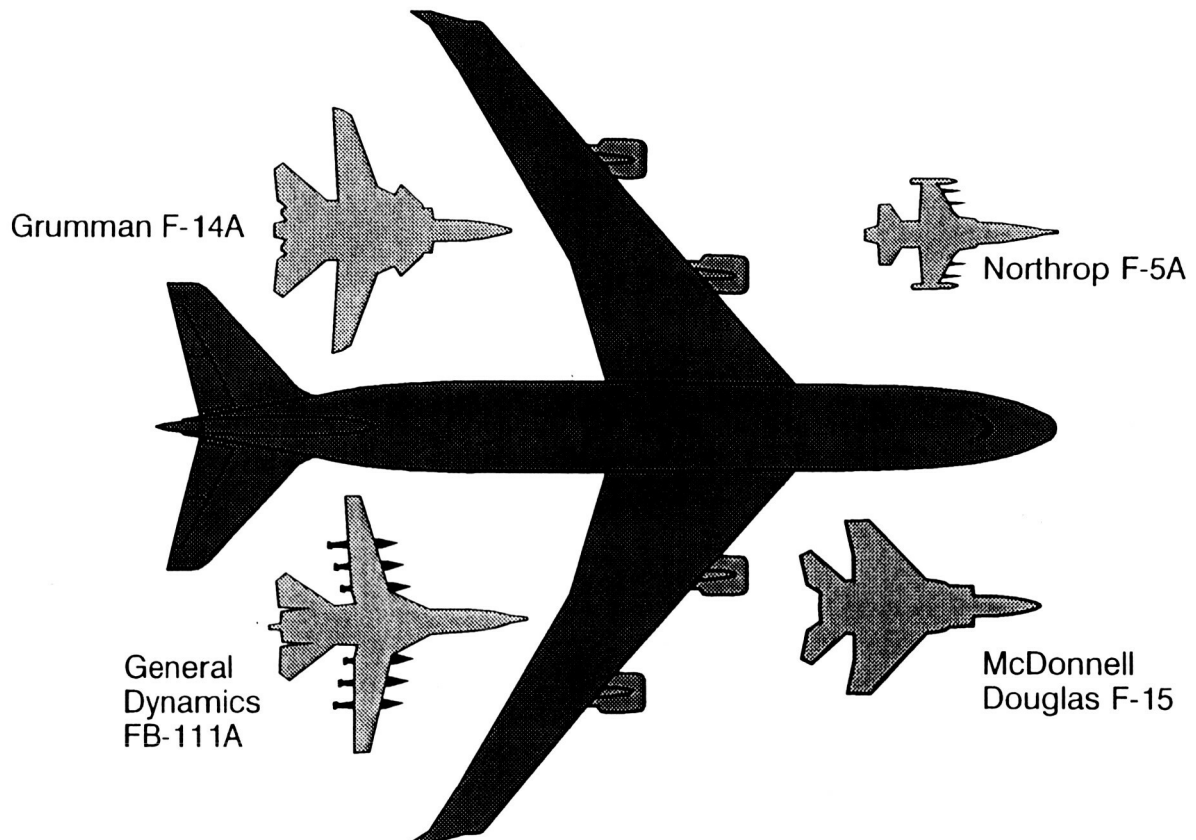
I show this picture of the Beech Starship since it is certified and in production. It represents what can certainly be called an all composite aircraft. The issues of fuel in the wing and a fuselage pressurized shell were both accounted for in its certification process. With the production underway it will be the aircraft by which all future composite civil aircraft will be measured. My salute to Beech Aircraft Company for the development and certification of the Starship.

Starship



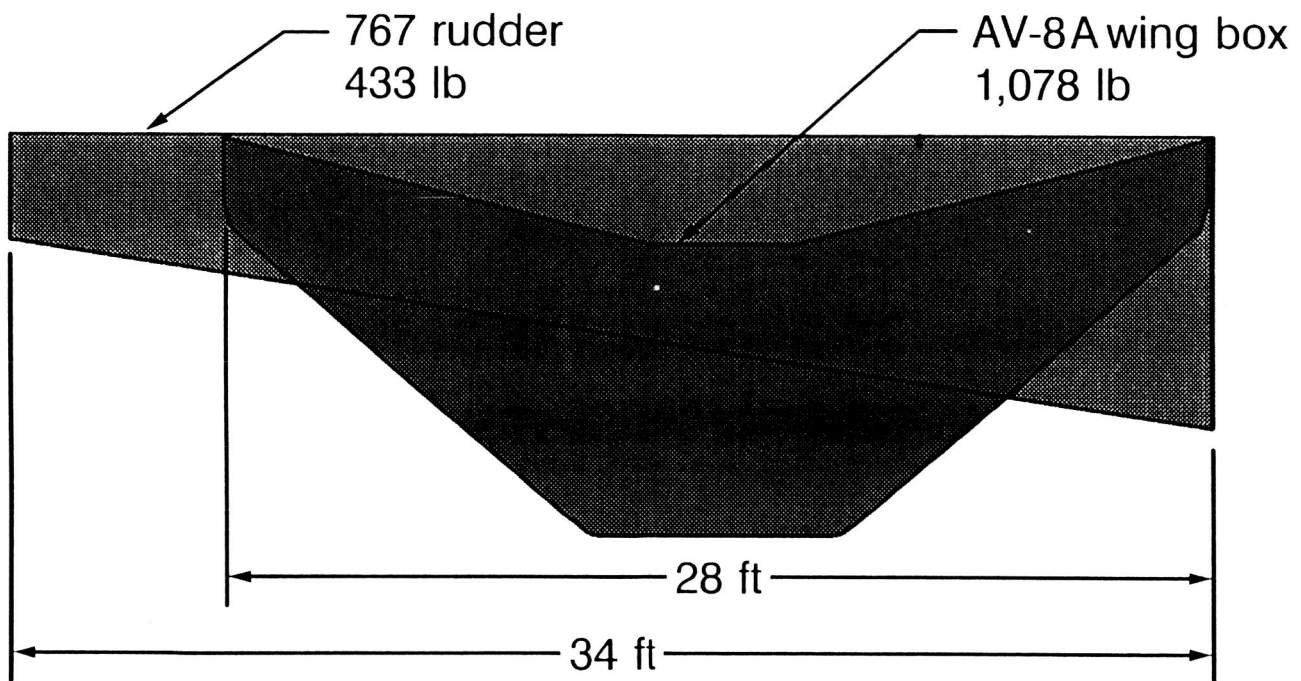
Almost all my general or overview presentations have shown this picture, since I believe it clearly dramatizes the size considerations that must be part of the stepping up to commitment of composites to commercial aircraft. The risk from a manufacturing and cost point of view is directly related to this size effect. The structural mechanics are not different between fighters and commercial transports, but the manufacturing differences are as great as the differences shown in this picture. Those who have worked on large aircraft production readily recognize this size effect.

Aircraft Size Considerations



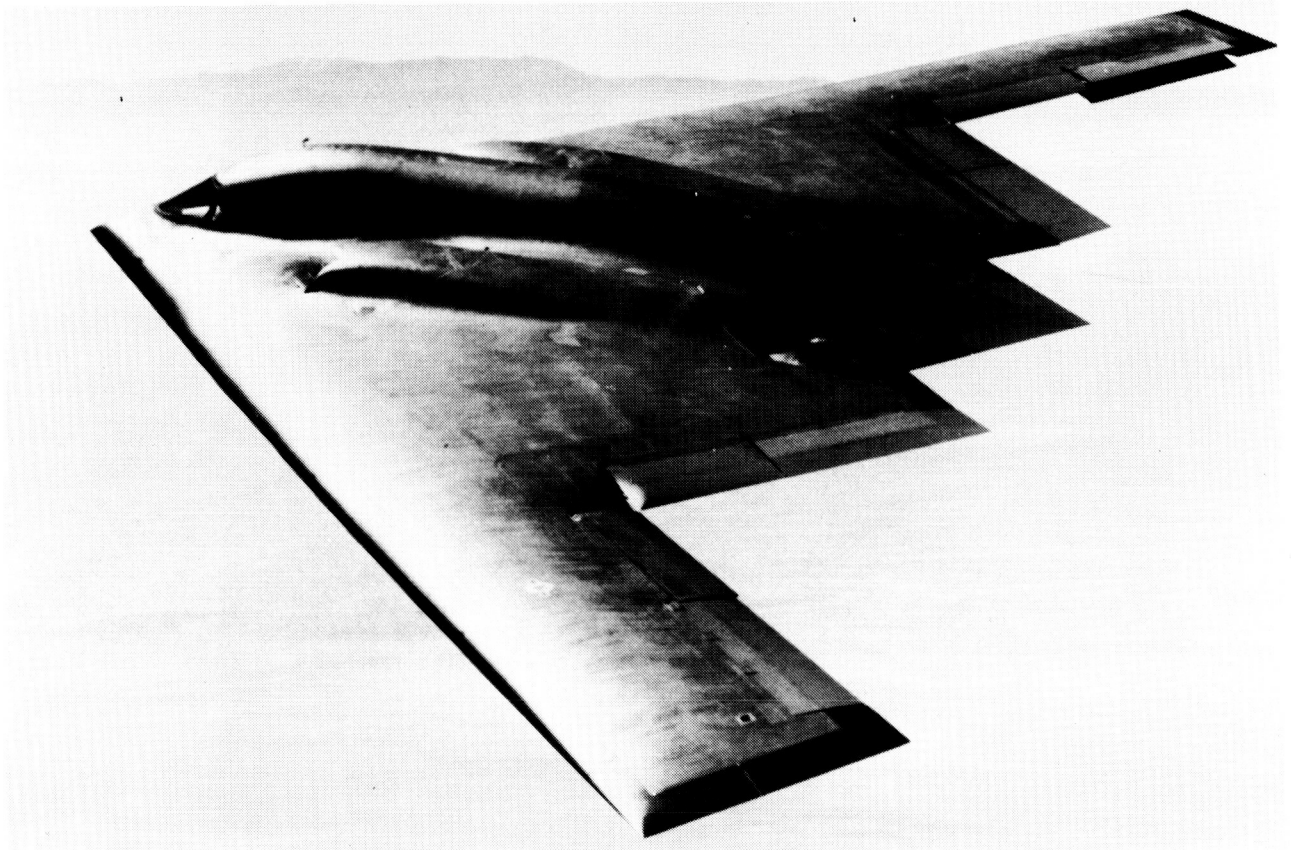
This is just another way of expressing the effect of size. It simply says that as expected there are major structural differences in the 767 rudder and the AV-8A wing. These differences are simply reflected in their weight differences, even though their dimensions are very similar. The difference in their design requirements obviously makes significant difference in their design details and the manufacturing cost of those details.

Application Considerations

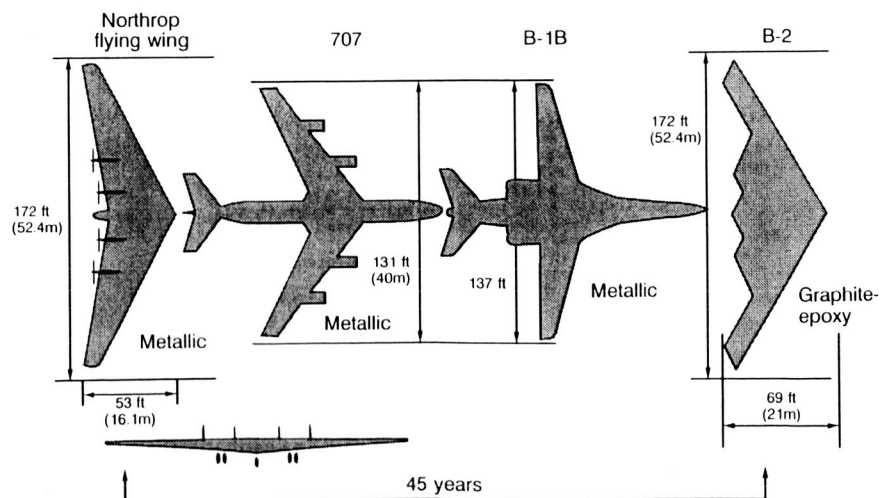


These two pictures show that the technology for design of composite components covers not only the fighter size airframes but now covers wing spans that are similar to large commercial aircraft. Therefore, to continue the argument that industry does not have the background in large airframes is no longer a valid view of composite airframe structures. This preceding discussion states simply and clearly that it is now time and the industry is ready to complete the technology steps to the large commercial aircraft of composites, a viable material option.

B-2 Bomber

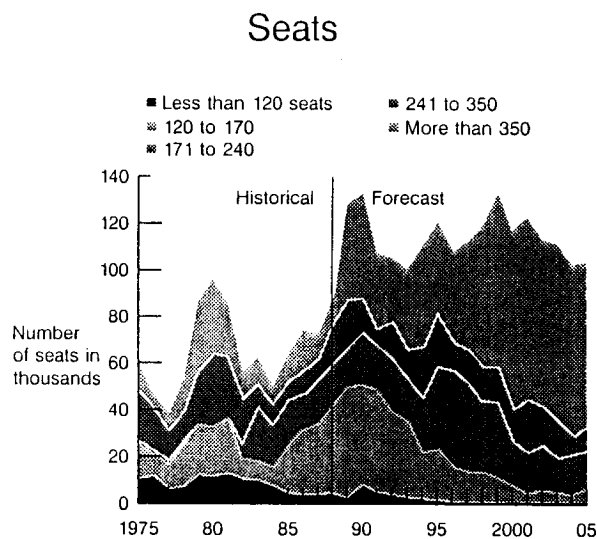
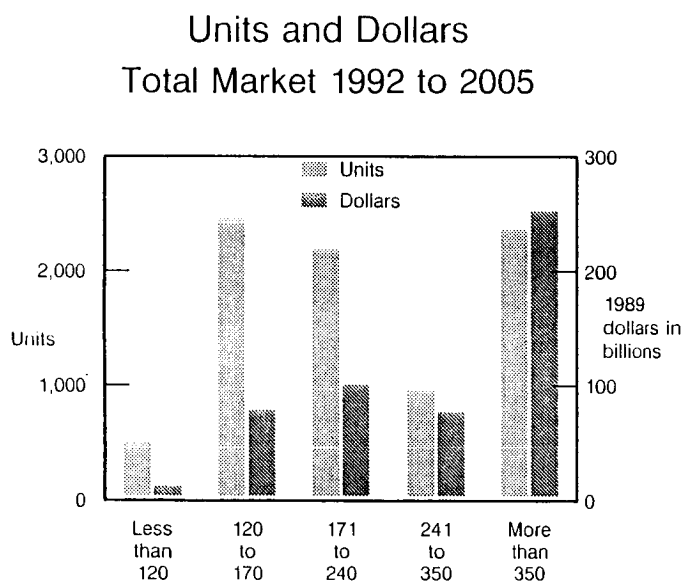


Transport Size Transition to Composites



The next step in assessing if the large commercial aircraft industry should step up to the design and development of the final major components of wing and fuselage lies with the need for new aircraft. The cycle for new commercial aircraft (those not government subsidized) continues to grow in time. The past time cycle was 7 to 10 years and has more recently expanded to 12 to 15 years. This chart simply shows that even with the new aircraft coming along now, there should be a market for another new round of aircraft in the period 2005 to 2015. Therefore, the final developments needed for cost risk reduction in producing a commercial aircraft should be addressed now. The current NASA ACT program, which this meeting is about, has the right timing to aid the US commercial airframe companies to compete with the rest of the world.

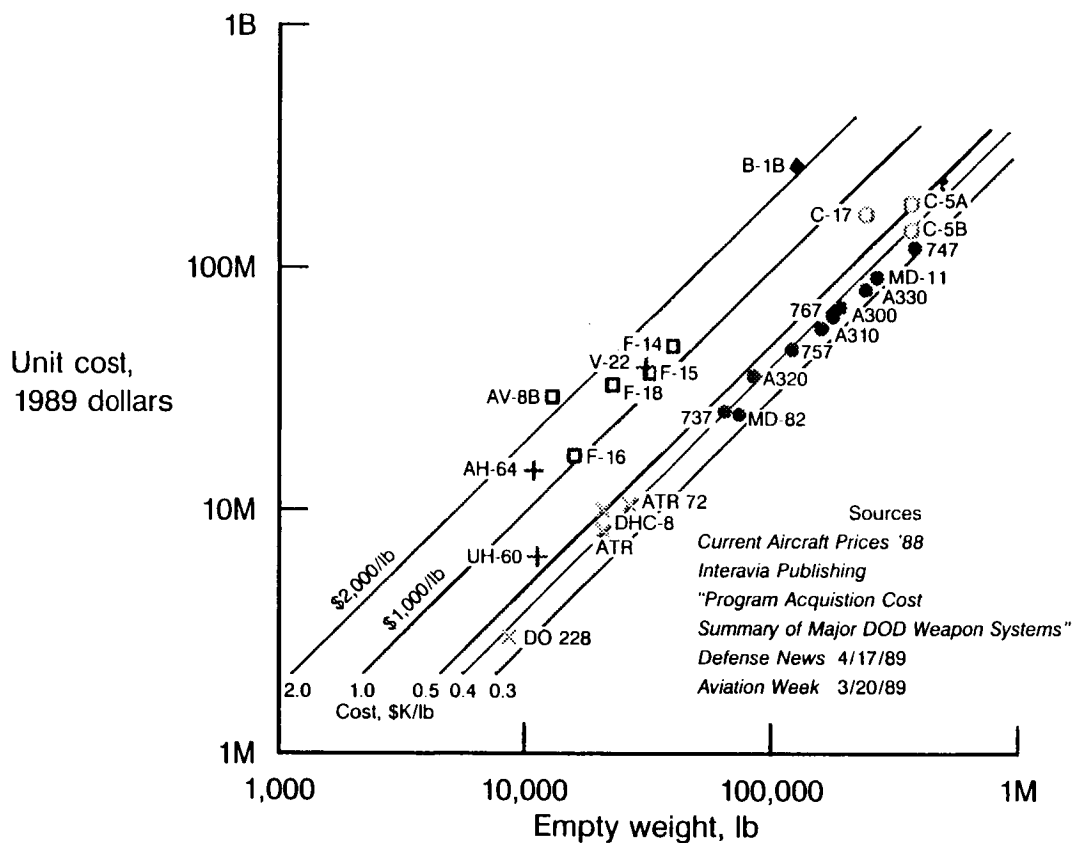
Market Forecast - Share by Airplane Size



This chart shows that the cost of aircraft has followed a fairly well defined pattern and that to compete in the future the cost of the aircraft must meet or beat this established pattern. No company will risk the initiation of a new aircraft within its own funding capabilities if it cannot be sure of its ability to not only project the cost but to control the manufacturing cost after commitment to production. This scenario leads directly to the reason that cost of composite structures is now the issue, not structural technology. The evaluation and design of the structure will require the continued development of better composite structural analysis tools. However, the technology to manufacture that structure in an economical manner is the key to the risk acceptance for the manufacturers. The measuring stick for assessing the success of development of the manufacturing processes and tools will be the comparison of the cost of large composite structures against the 50 to 60 year base for metals structures, a tough comparison for composite structures.

Aircraft Cost Trends

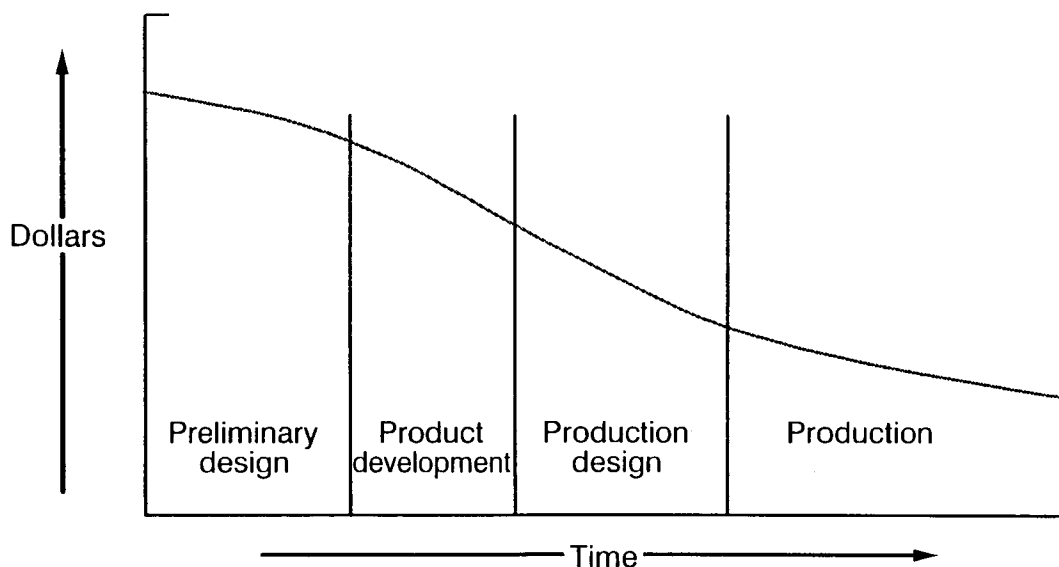
Aircraft Costs 1988 to 1989



This chart shows what we must consider in a plan to assess how to meet that tough comparison with the manufacturing experience base of metal structures and has been seen by many of you at other presentations and conferences. I show it here because I believe in what it tells us so strongly. Our ability as structural engineers and manufacturing engineers to save cost and weight decreases with program time. As the program progresses to each following phase, opportunities for cost and weight savings are lost. The first person to have the largest chance at cost and weight savings is the configuration engineer as he draws the first three view drawings and establishes the aircraft arrangement. From the aircraft arrangement comes the structural arrangement against which various material systems and structural concepts are assessed. There is complete freedom for structural considerations in this stage of design development within the constraints of the airplane mission. As can be expected, each following phase is constrained by decisions made in the preceding phase. This scenario clearly suggests that cost and weight be a significant consideration at the initial step as well as performance or mission requirements.

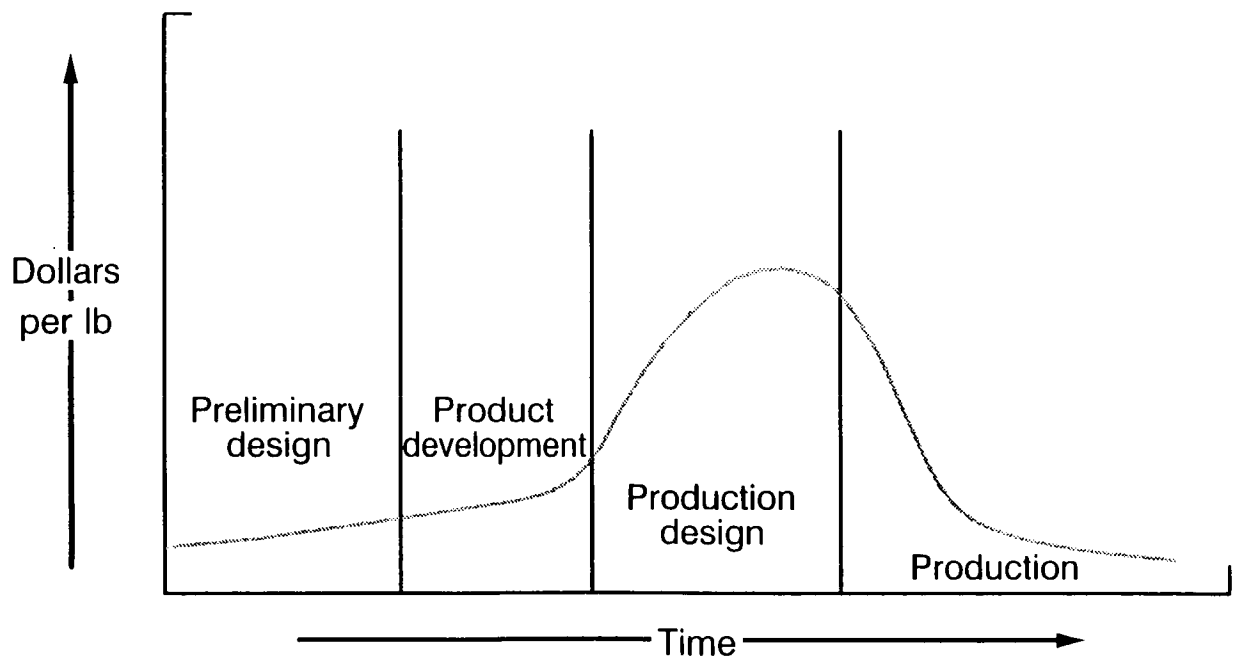
Program Schedule and Cost Savings

Decreasing Opportunities for Cost Savings



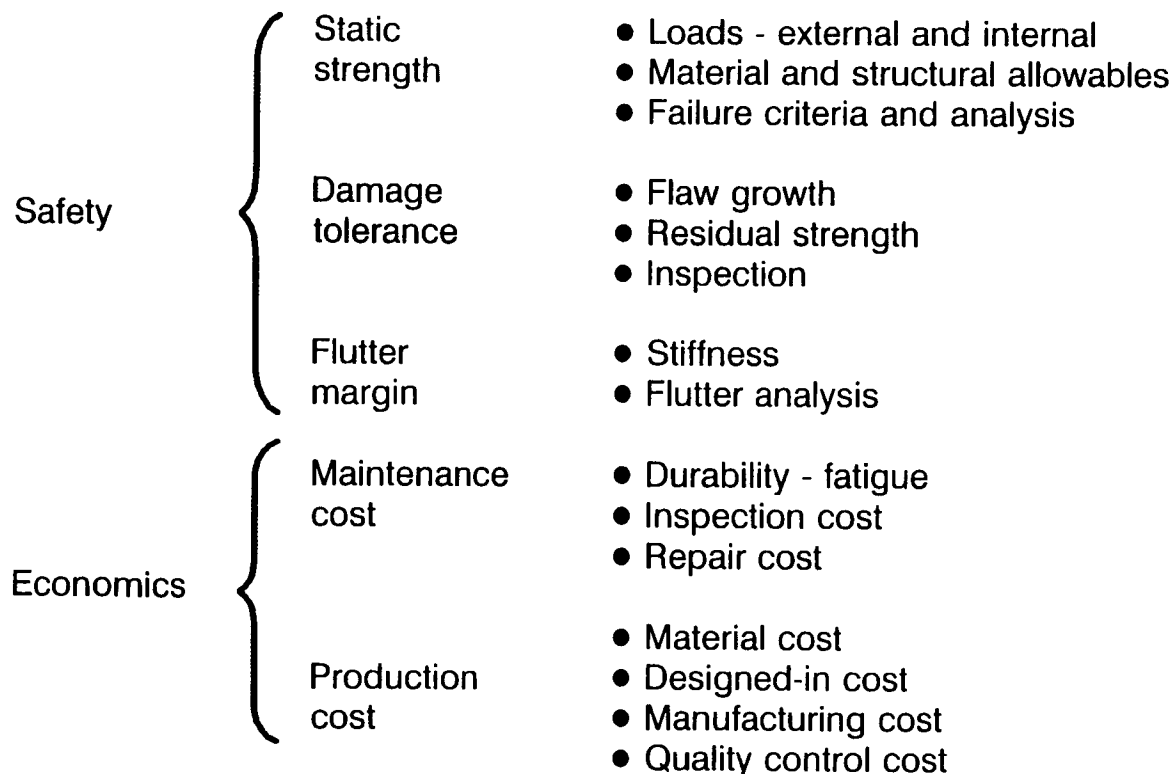
This chart shows how the idea of the value of weight savings varies with the same development cycle. During the initial phase it is not a very large number since the optimism is that the design will easily meet weight projections and performance requirements. When the cycle reaches the production drawing release, the real weight numbers begin to appear and panic sets in to meet weight targets and performance specifications. This raises the value of weight savings, and this is when all the awards for weight savings are given. These two charts together suggest that the awards in the production drawing release phase may add to the weight savings needed to solve the overweight problem when recognized. However, since the savings are evaluated on a dollars/pound basis, this is a cost issue as well as a weight issue and perhaps the award for both cost and weight saving should be issued in the preliminary design phases as well. Simply stated, we may be giving awards at the wrong time.

Program Schedule and Value of Weight Savings



This chart (upper section) is one that I have used many times to focus on the issues of static strength and damage tolerance of composites. The lower half of the chart addresses the cost, considering both the manufacturing costs and the in service maintenance cost. The bottom four items are of direct interest to this presentation. The material cost is one of the issues that is being discussed at this conference. The other is the so called "designed-in cost". Those are the costs that the designer causes to occur due to the design he selects. The influence of the design process on cost is the single greatest influence on product cost. The facilities that are available and the manufacturing techniques selected by manufacturing rate second to the designer effect on cost. The designer must be aware of and understand how his design selection is affected by the available facilities and manufacturing methods. There has been considerable written and said about the design and manufacturing interface required on composites, and there is no need to repeat that here. I will, however, add that I believe the need for this interface is much greater for composites than for metal structures. However, as the next chart illustrates, the designer is the key to real cost savings.

Structural Design Drivers



To allow the designer to make effective assessments of the cost of his design, he requires tools to do it in the same manner that he meets the other requirement displayed on this chart. This does not mean he must become a cost estimator, but he needs tools that allow him to make cost one of the tradeable items as he goes through the thought process for his design development. I believe that the post design cost evaluation by an estimator does not allow the same degree of design innovation as allowing the designer to work cost as one of his design parameters. Since the design process that selects from many options occurs at various design stages and detail levels, cost tools are needed at each stage and level. Real design cost improvement can be made if we provide the designer with real cost evaluation tools. These tools do not have to represent the dollar cost of the design, only the relative cost of one design approach to another. With such tools in the hands of the designers we will see considerable improvement in the "designed-in cost" of composite airframe structures.

Designer's Tools

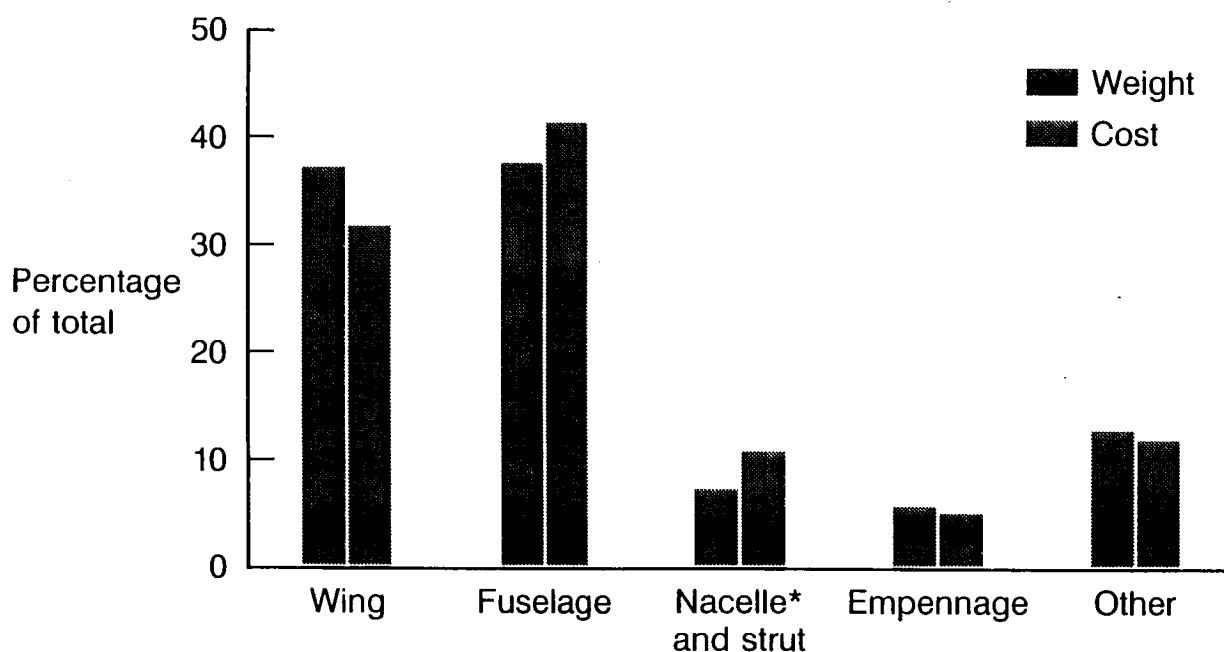
Design parameter	Designer's tools	Design incentives
Safety (strength)	$f_b = \frac{Mc}{I}$ M.S. = $\frac{f_b}{F_b} - 1.0$	Regulators (FAA)
Durability	f_{max} , DFR, N reg	Warranty Service life
Weight	Density x volume = weight	Performance
Cost	?	Sales Profit



This weight and cost chart is an old one that we put together in the early 70's and has been used repeatedly by many people at Boeing. What it displays does not present anything different from what you would expect to see. The two major components each make up about the same percentage of the total structural weight. In a similar manner, the costs that are shown are as expected because of the size of these components; they are a high percentage of the total cost. The fuselage costs more because of its higher part count. However, when used in connection with the next chart, one can begin to assess where to work the weight savings the hardest and where to make cost the key design driver. These charts can tell you how to approach design solutions such as damage tolerance as well. The approach to each area of design can be initially established with this level of information. The distribution may vary in small percentages—commercial transport to transport—but not significantly enough to not allow for this information to provide guidance of some up-front design approach decisions to be made.

Weight and Cost Distribution

Commercial Aircraft



*Powerplant weight and cost excluded

A simple and perhaps extreme example of cost as the key driver, is the intermediate ribs. These ribs do not support any external attachments or form fuel bays. They simply maintain box shape and support the skin/stringers surface panels. They usually have their web gages set by fuel slosh and must maintain a reasonable stiffness to support the surface panels. These requirements limit their potential weight savings. Therefore, the chart assumption was only a 10% weight savings, which results in a negligible weight saving to the total airframe. However, in a study we did in the same time period that we generated these weight/cost charts, we found that on a dollar per pound basis these ribs were the most costly element of the wing. Therefore, some simple review of the weight and cost history can guide you, as it would for this example, to make cost the key design driver for intermediate ribs. This can be done in those early pay-off design phases previously discussed. Similarly, very obvious is the selection of the surface panels of the wing for weight saving potential. Since it is a large contributor to total cost, the design must also reflect the best cost options while allowing the maximum weight saving to be gained. Again, many early inputs to the design process can be made from simple information and design histories regardless of the material system. To most of you good composite designers in the audience this is nothing new.

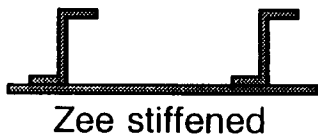
Weight-Saving Areas Selection

	Structural element, %	Wing, %	Fuselage, %	Total aircraft, %
Wing				
• Skin and stiffeners	25	15.5		5.7
• Spars	20	3.0		1.1
• SOB	15	1.2		0.4
• Special ribs	20	1.0		0.4
• Intermediate ribs	10	0.4		0.0
• Center-section beams	20	<u>0.4</u>		<u>0.0</u>
		21.5		7.6
Fuselage				
• Skin, stringers, and frames	25		10.8	4.0
• Keel and wheelwell	20		3.2	1.2
• Floors and floorbeams	20		2.4	0.9
• Doors	15		1.7	0.6
• Bulkheads	20		2.0	0.7
• Windows	15		<u>0.8</u>	<u>0.3</u>
			20.9	7.7

- Aircraft total (wing and fuselage): 15.3%

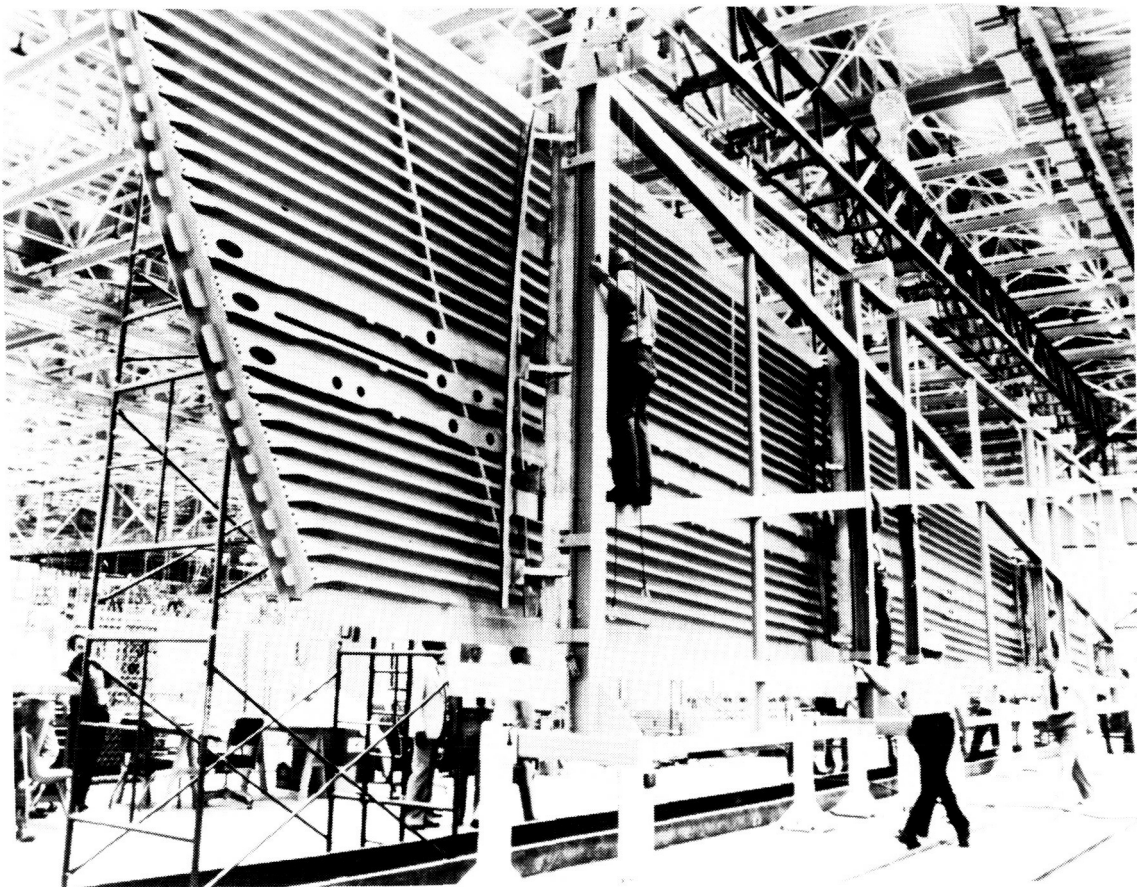
There has been and continues to be much discussion about composite designs being "black aluminum" designs. The discussions say that if the designs were not so black aluminum looking we could save more cost and weight. This chart shows we should stop looking for the non-black aluminum. The geometry of the cross section of aircraft structures looks the way it does because those are the most efficient structural shapes. How those shapes are made out of composites is a separate issue from the shapes. Ply orientations and lay-up sequences are the real design differences with composite structures. These shapes were taken from an old paper, *Optimization of Multirib and Multiweb Wing Box Structure Under Shear and Moment Loads*, by Donald H. Emero and Leonard Spunt of North American. I have not shown all the cross sections displayed in that paper on this chart. If you can review that paper and come up with some additional cross sections of significant differences, I would like to hear from you. Let's focus our development time on the real issues remaining to produce cost effective composite structures and not waste it looking for the non-black aluminum shape or geometry.

Structural Concepts



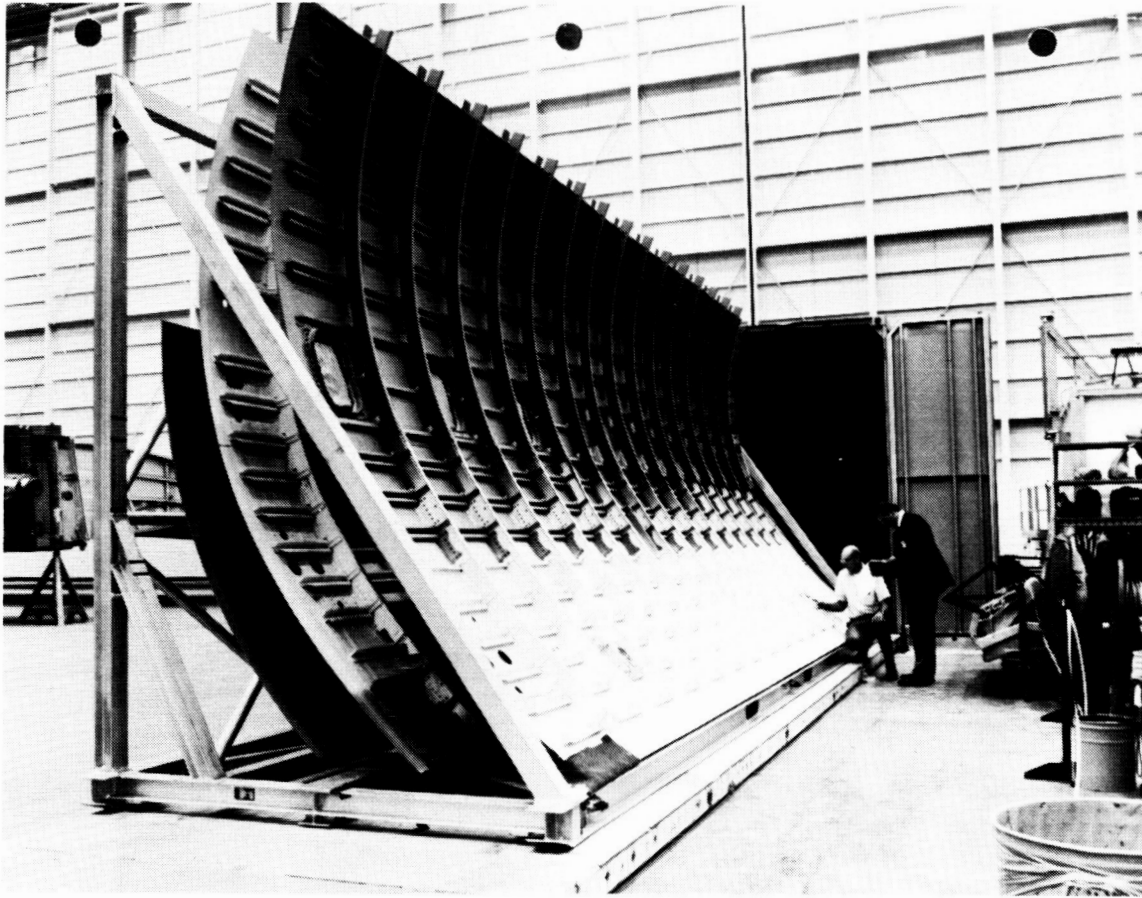
These two photo charts are shown to add to my just discussed issue of "black aluminum." The key surface panels of commercial aircraft are made of basically long skinny members and panels. I believe that again to look for something different is a total waste of development funds. The real question to be addressed with development funds is how to design these shapes for the low manufacturing cost while selecting those that will perform well structurally and save weight. The development of manufacturing methods along with the design of these shapes needs to be the focus. The manufacturing methods development must be focused not on just those methods that are simply the lowest cost (without the recognition that these methods must have the ability to produce these two shapes). Those manufacturing methods that do not, from the start, recognize the effects of commercial airframe size and these shape requirements will be a waste of development effort and funds. I want to be careful here and not to forget to say that as the manufacturing methods for these two factors are developed, there is a requirement for continuing development to improve and enhance the structural data base and analysis tools. They offer the means of opening the options door to the fullest for the design engineer.

Structural Elements



Wing Skin and Stringers

Fuselage Skin, Stringers, and Frames



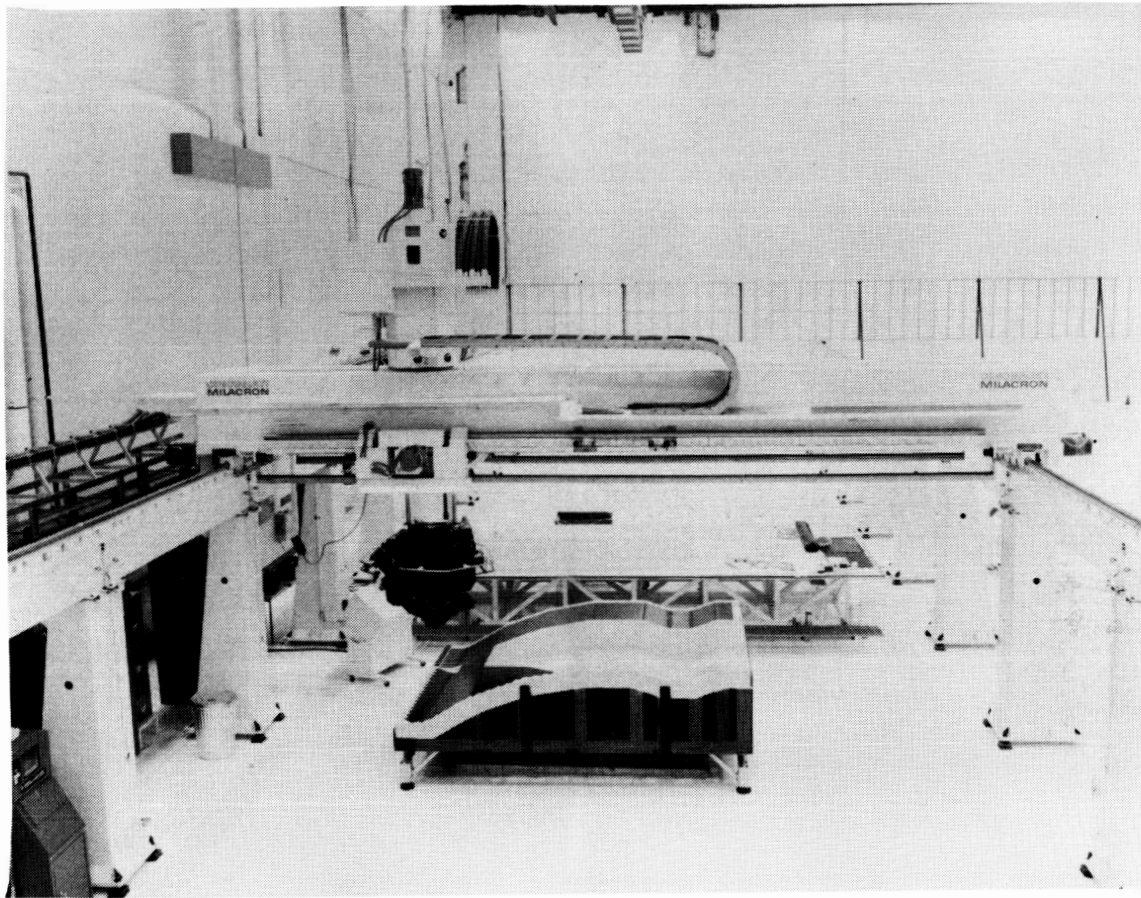
I have just made my case for not looking for the non-black aluminum designs and the recognition of the key structural elements. These charts validate that industry is effectively doing that in spite of continuing discussion of looking for non-black aluminum designs. We have developed the tape laying machine that does in effect the same job that the skin mill does. In the next chart we are developing pultrusion machines we hope will make long skinny members like we machine on spar mills. I present these pictures to show you have already recognized what I just previously said. To improve on that you should continue to look further at the processes that can produce these required shapes. I believe we have to take the correct steps while allowing the non-knowledgeable to continue to look for the wrong thing, non-black aluminum designs. We need to focus our effort on continuing to explore new manufacturing methods that can reduce the cost of making the real structural shapes required.

Metal and Composite - Skins



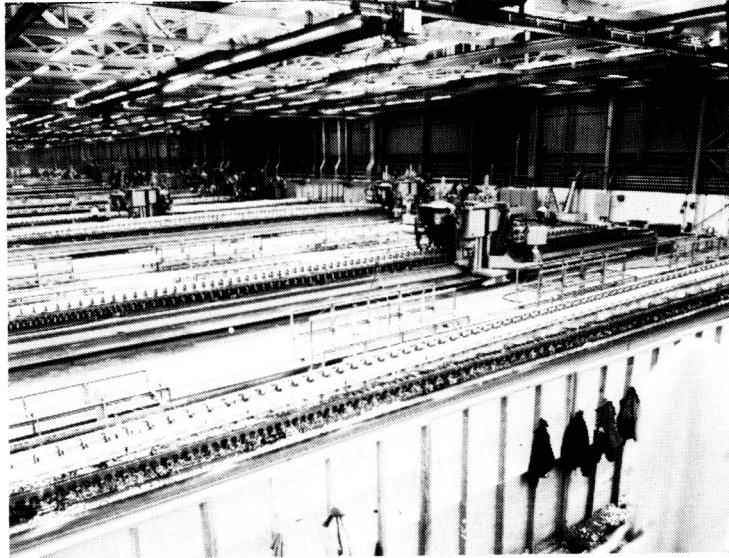
Skin Mills

Tape Layup Machine

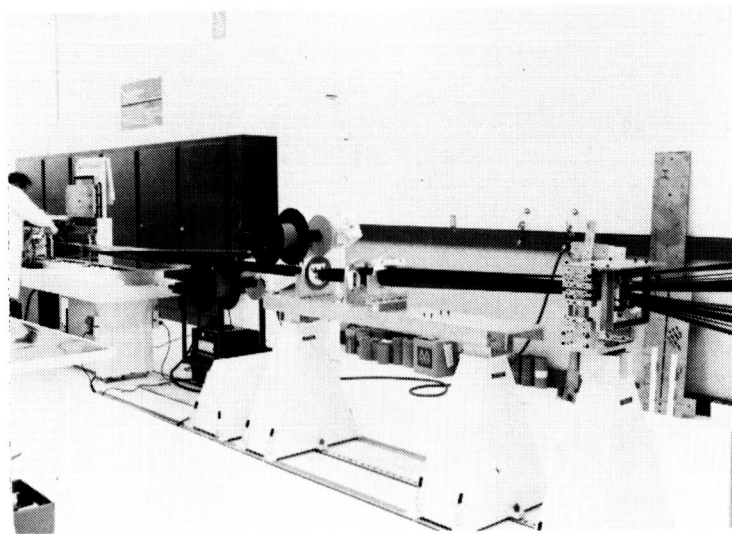


No additional discussion is needed for this chart in addition to information presented previously. Let's just keep a continued focus on the right manufacturing methods development. The following charts will show that we have at least as many options as metals, if not more.

Metal and Composite – Stringers



Spar Mills



Pultrusion Machine

In continuing to address the cost issues the question often arises as to the structural and manufacturing options available with composites. They are still viewed by some as a new structural system, but I am certain not by those of you in this audience. A reduced set of structural and manufacturing options seem to be implied. This may be limiting the usage of composite structural applications. These two charts are presented to show simply that I don't see it that way and that the options in both cases are equal. We have yet to see all that might become available for composites. We may still have some development or learning to apply to what I show here, but I believe they are all possible.

Structural Options

Options	Metal	Composite
● Joining		
● Mechanical	*	*
● Bonding	*	*
● Integral	*	* (Cocure)
● Configurations		
● Skin and frame	*	*
● Skin, frame, and major longerons	*	*
● Skin, frame, and stringer	*	*
● Honeycomb and frame	*	*
● Honeycomb shell	*	*
● Grid stiffened and frame	*	*
● Grid shell	*	*

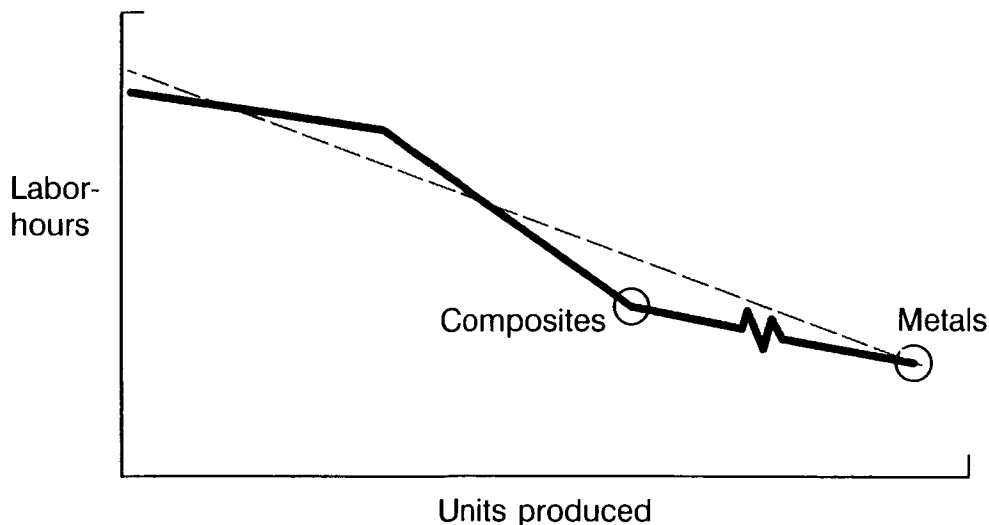
This chart makes a similar statement about the fabrications options available for composites. Neither of these charts is said to be complete in terms of all possibilities but to be reasonably representative of the current development status.

Form and Fabrication Options

Metal	Composite
● Element forms	
● Sheet and plate	Tape layup and filament winding
● Extrusion	Pultrusion
● Forging	Resin infusion
● Shaping	
● Roll forming	*
● Hydropress	Hot forming and thermoplastic
● Machining	Hot forming and thermoplastic
● Stretch forming	Aligned discontinuous fibers and thermoplastic
● Joining	
● Mechanical fastening	*
● Bonding	*
● Diffusion bonding	Cocuring
● Welding	Thermoplastic fusion

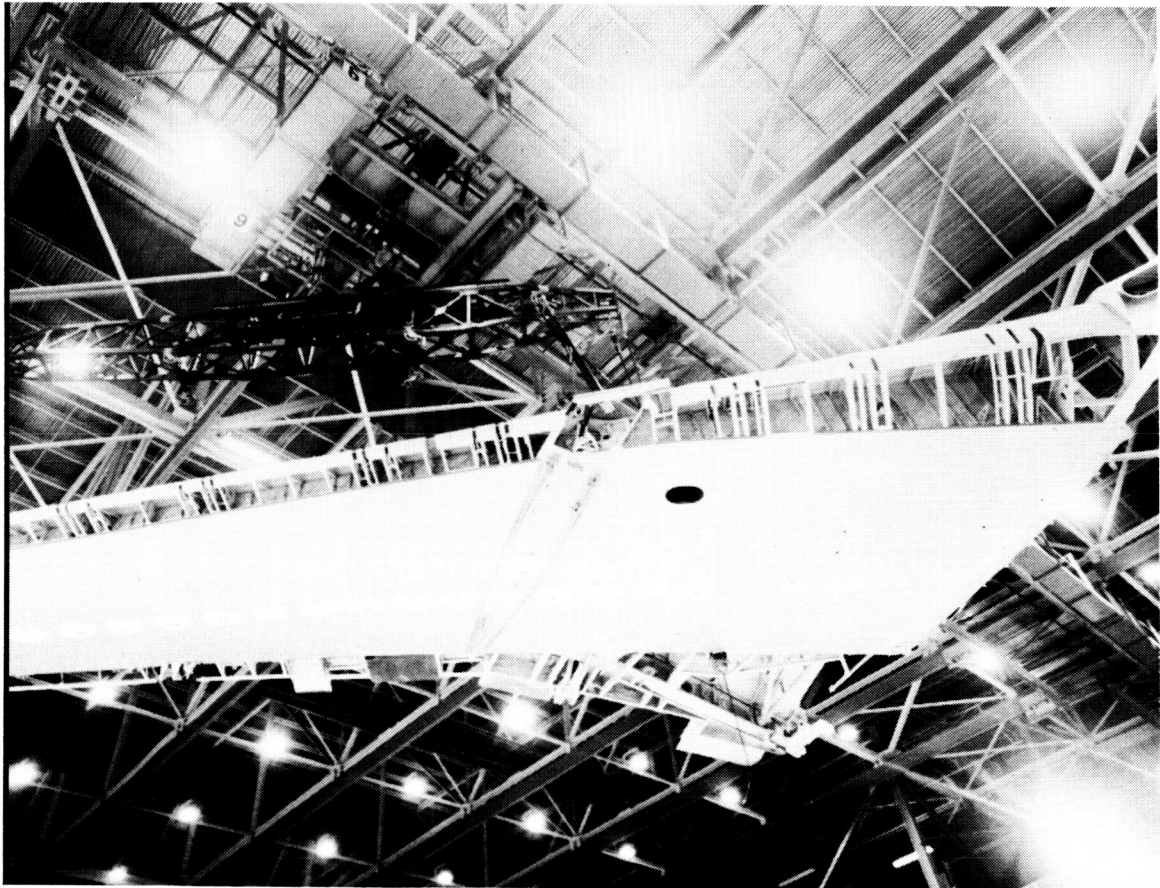
From the two previous charts I tried to show that the composite designer has the same degree of options open to him as the metal designer. The manufacturing methods offer the same level of options. I did not say that the manufacturing methods were equal in cost or efficiency. Metals manufacturing has a considerable head start in both the development and applications aspects of the methods. This chart addresses an applications aspect that may sometimes be overlooked when making cost comparisons. This chart shows that the learning curve, I believe, is not straight as often depicted by the dashed line, but is more like the solid line. The solid line shows that in the production of the first 30 to 40 aircraft there is little so-called learning going on. This is due to the high number of changes that usually occur as the aircraft goes into production and both engineering and manufacturing correct their mistakes. The steep slope indicates that changes are reduced and the real people-learning takes place. This is followed by a lower but continuing reduction in man-hours per aircraft. This slope does not represent any continued people-learning improvements but those improvements due to manufacturing methods and tooling changes that are made to reduce cost. These changes are only made when the cost savings can be shown to be effective over the remaining production run. These changes and ideas are carried forward to the next design. The point of the chart is that this carry over is not zero for composites but it does not have the years of background that metals have available. While the composites are not at zero as I show (relative to the final slope), they are so close to that for commercial transport major components that it represents the real position relative to the metals for 50 to 60 years. This number of years' difference makes it very difficult for composites to compete on cost alone.

Learning Curve



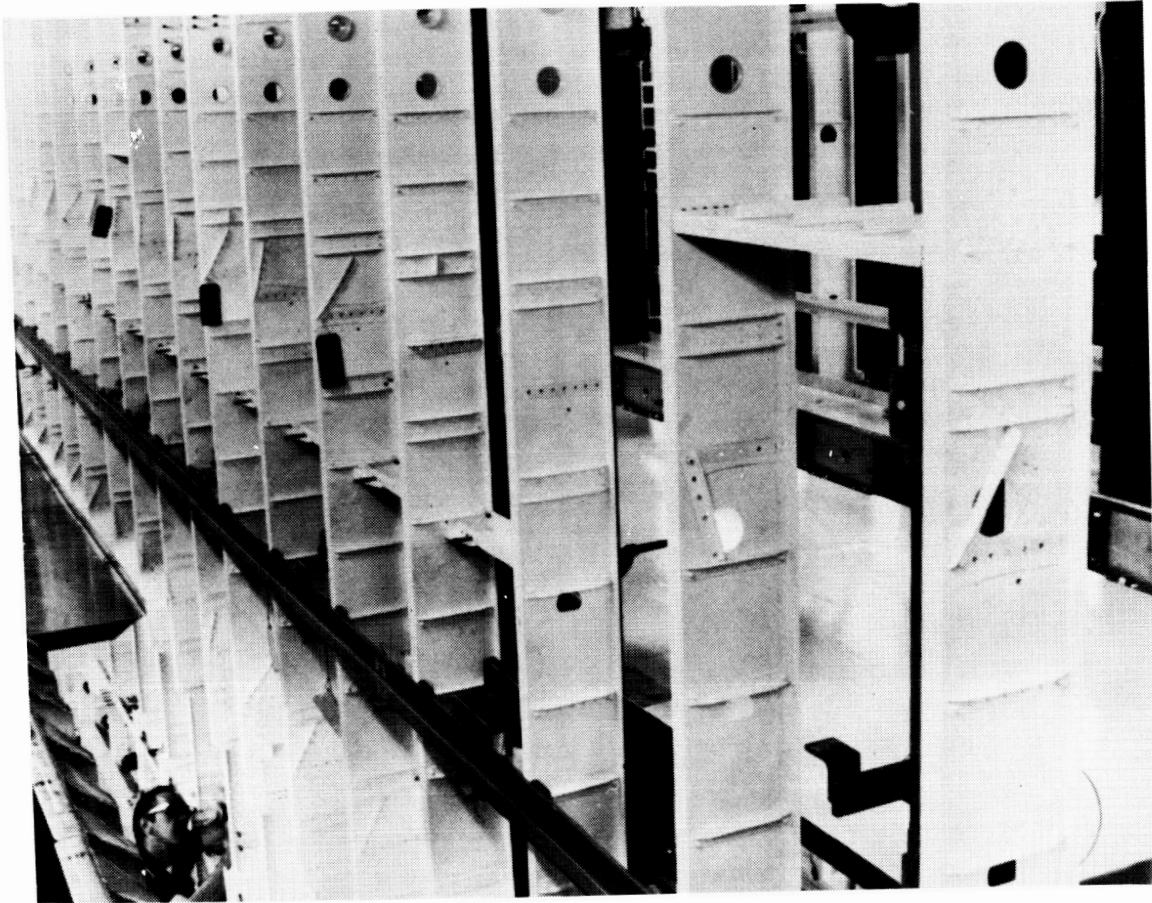
This chart suggests one of those areas that can be addressed now, and I do not believe it is being addressed in competition with metal. If I need a clip or short stiffener of composite material, it is usually manufactured for that specific location and usage. In metals I have standards books of extruded shapes and possibly a set of rolled shapes. From these I can often select what I need. If one looks at the many uses of clips or brackets and web stiffeners used in aircraft, one wonders why a supplier has not come forward for this structural element. A large number of metal extrusion dies have been developed over the years just noted. Maybe it's time to start something similar in composites. I made a very rough estimate of the number of short stiffeners or attachment clips on a commercial transport. My estimate is that more than a million feet per year would be needed based on 10, 767 size airplanes a month. If a simple angle were produced in a standard lay-up and angle, say 90 degrees, there are many locations where it could be used. It is possible that if that angle were made of thermoplastic, it could be used for angles other than 90 degrees by placing it in a heated die to change the shape angle. If there are other items to be addressed as composite structural standards, I leave that to this audience.

Stiffeners - Requirements



Spar Stiffeners

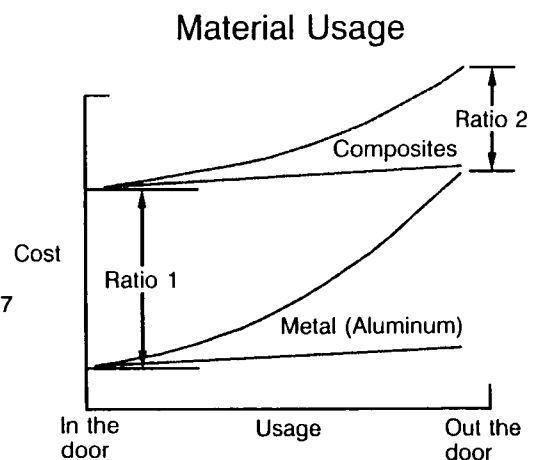
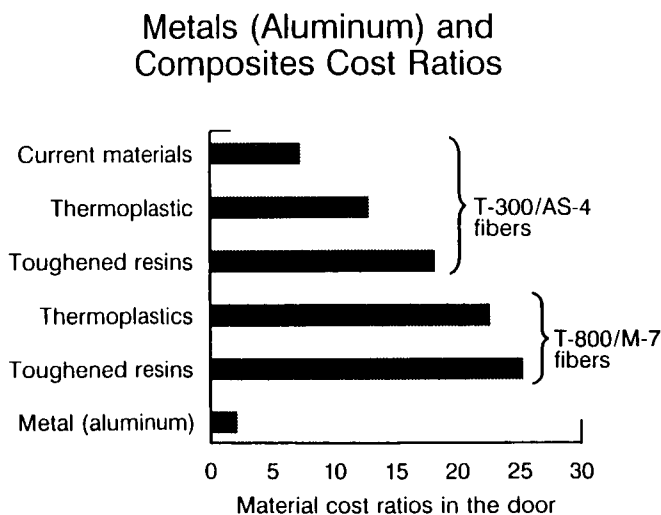
Floorbeam Stiffeners



We are hearing a lot about the cost of composite materials and that it is difficult for composites to compete with aluminum on the basis of just the basic material cost alone. This chart is based on some data from a NASA document looking at the cost of composite material relating to type of composite material. I have taken that data and ratioed it to the cost of aluminum. The displayed ratios agree that composite material costs are high. When we have ratios this high in comparison with aluminum it is difficult for composites to compete on a cost basis. However, I offer the right hand graph on this chart as another look at this cost ratio. If we consider the out-the-door cost of the materials rather than just the in-the-door cost, we get a different picture. For wing skins, we order special large roll taper skins, and we often machine away 60 to 70 percent of the material. For certain airlines that like shiny fuselage skin, we order premium sheet. Neither of these elements, that are part of the previously shown major weight contributors, are purchased at the base price of aluminum. Second, when we consider the 60 to 70 percent chips in the machined skins (even with the 50-a-pound resale on the chips) the cost ratios are significantly altered for the out-the-door cost ratios. I should note that my comparison on material cost only addresses the material cost and amount used; no labor is included. The general utilization of composite materials is in the 120% range. That is, we need 120% of the out-the-door weight in-the-door to make the parts. This comparison changes the ratio to about 20 to 30% of the in-the-door ratio between aluminum and composites. Let's be sure we recognize this aspect before we say how expensive composite materials are as compared to metals.

Material Cost Comparison

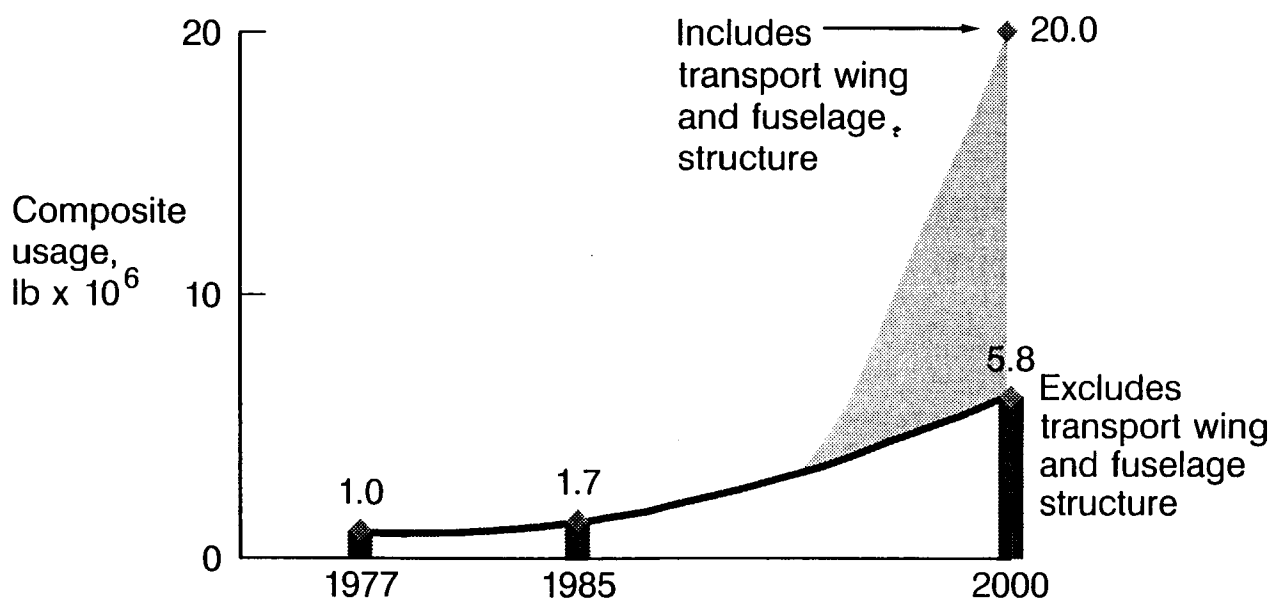
Composite Versus Metal (Aluminum)



While I have just defended the cost of composite materials, I would like to send a message to the material suppliers here by again using a chart from a NASA report. If this chart is right, and I believe the trend it shows is correct, then the suppliers need to examine their marketing approach and recognize the business potential out there for them if the price of composite materials can be reduced. The reduction in cost can make the application expand to the major structural elements of the airframe, namely the wing and fuselage. I believe continuing effort on the part of the suppliers is needed and should be part of all future research and development. The airframers need to continue to clearly define their needs and their manufacturing approaches, while the supplier needs to identify the items in the airframer's requirements that are the key cost drivers in the product. They, of course need to, on their own, continue to look for ways to reduce their cost so they can pass it on in the reduced price of composite materials. The market target potential is so large with the development of an all composite commercial transport that this cost aspect is as important as any needing attention.

Composite Material Usage

Projection of Potential Usage



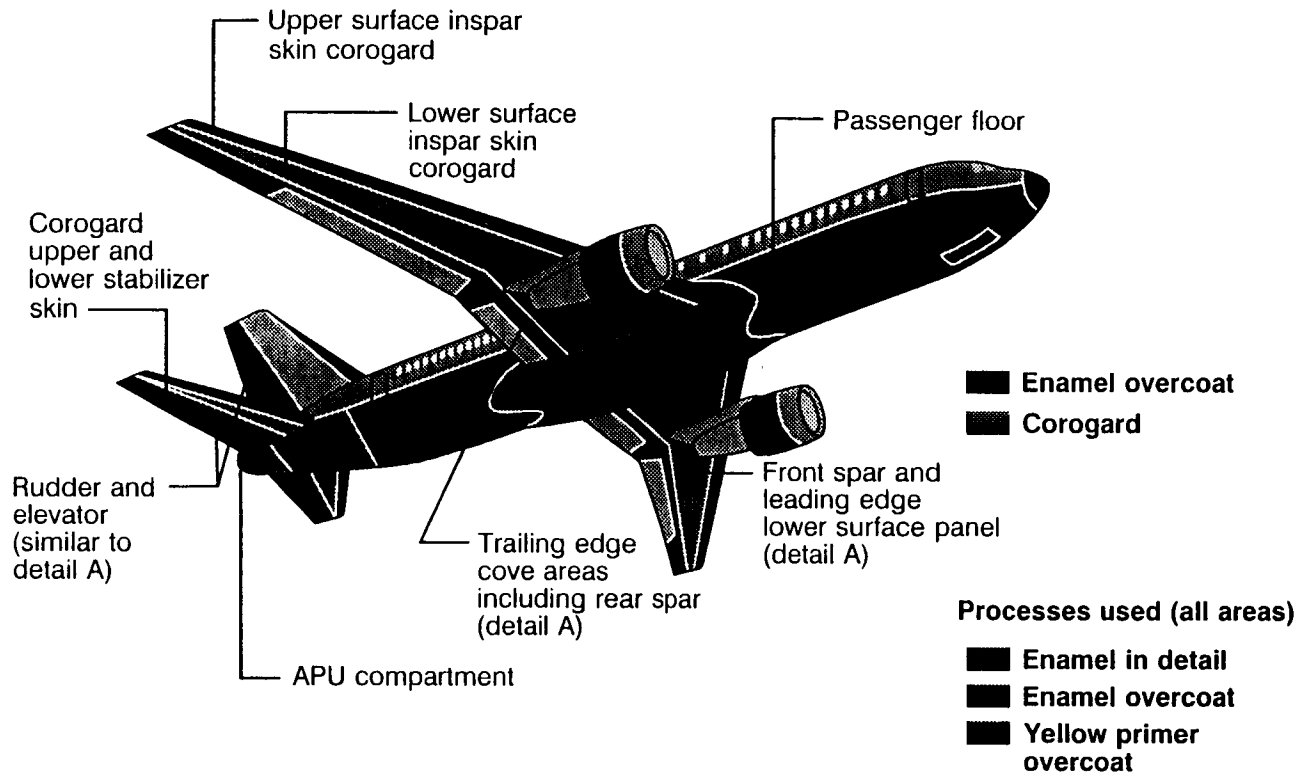
All of us here, as well as those involved in the development of composite structure, have, I am sure, tried to dream up as many reasons possible that composites produce benefits to both the airframe manufacturer and the aircraft user. The ones I have selected here I believe are real. They are either well defined today for composites or will be in the future when fully applied to the commercial transports. We have shown over and over again we can save weight, and you have heard that again at this conference. The performance resulting from that saving certainly can produce fuel saving and again, in today's world climate, that is becoming an issue for the airlines. In terms of maintenance the fatigue characteristics of composites will continue to reduce the fatigue maintenance requirements significantly. The area that composite structures has not received enough benefits credit for is the area of corrosion. Many dollars go into the airframe manufacturing process for the addition of corrosion protection of the structure. Similarly, the airlines spend many dollars maintaining this corrosion protection in their fleets. The use of composites eliminates a major portion of this requirement for corrosion protection. The chart on the right shows only a small part of the corrosion protection applications applied to Boeing aircraft. Finally, I believe as we continue our learning process in how to produce large commercial transport composite structures, we will see more and more opportunities to reduce the cost of composite structures and accrue additional benefits.

Composite Application Benefits

- Performance improvements - weight saving
 - Fuel savings
 - Improved DOCs
- Reduced maintenance
 - Large reduction in fatigue problems
 - Corrosion maintenance greatly reduced
- Potential manufacturing cost reduction
 - Better material usage
 - Reduced assembly (more monolithic parts)

As noted, this chart does not show all the corrosion protection areas for commercial transport (which is a significant cost item in the manufacture and maintenance of the aircraft).

Corrosion Protection and Maintenance



Where are the key development needs? As I see it, this list presents my best assessment of the continuing development needs as they relate to commercial transport aircraft. I am sure that not everyone will agree with this list, but I believe it encompasses some of the key needs. Many at this conference have talked about the cost of composite structures, and I have briefly addressed it today. Cost may represent the largest stumbling block to the application of composites to commercial aircraft. The large pressure shell considerations are the key concerns for the application of composite to commercial aircraft fuselages. The Aloha Airlines incident of a couple of years ago keeps before us the fatigue and pressure issue in metals and reminds us not to short change those same issues in composites. If we expand the use of composites, we will surely want to raise the strain levels used with time, and in doing so, the low strain level of usage we have employed previously will not provide the error protection of the past. Therefore, we need to continue to expand our knowledge on the issues of fatigue and flaw growth, even if we plan to design to a "no growth" approach with composites. Finally, for commercial transport aircraft certifications we need to continue to address the issue of the effect of environment on composite structure full scale validation tests. Also, the issue of proof of the "no growth" approach needs very careful review. I believe the enhanced loads approach to be totally wrong; therefore, I included this issue in the needs list of areas for continuing development support.

Composites Continuing Development

Development Needs

- Material cost reduction
- Manufacturing cost reduction
- Fuselage pressure shells - damage tolerance
- Industry accepted - failure theory
- Effects higher strain utilization
 - Fatigue
 - Flaw growth
- Certification - additional validation of -
 - Ambient full-scale testing
 - Flaw "no growth" approach

This chart is one that an oldtimer has the privilege of presenting. The whys and wherefores of these dates are many and well developed by my personal prejudices on composites, but I thought I would leave them with you as reasonable targets and challenges for the commercial airplane people in the audience.

I again want to thank NASA for inviting me to make this presentation and to say thanks to those many friends at NASA who have helped me over the years. Also my thanks goes to those of you in the audience that I have worked with on committees and contracts that have helped me and been my friends for these many years in composites. And, of course, to many associates and friends at Boeing who are here, thanks for your great support and help over the years. I hope that all the goals of the ACT program are achieved and the benefits well recognized by the non-technical community as well as by the technical community.

Application Projections

Large Commercial Transports

- **Complete composite structures**
 - **Wing - before year 2000**
 - **Fuselage - by year 2010**

Page intentionally left blank

ADVANCED COMPOSITE STRUCTURAL CONCEPTS AND MATERIAL

TECHNOLOGIES FOR PRIMARY AIRCRAFT STRUCTURES

Anthony Jackson
Lockheed Aeronautical Systems Company

SUMMARY

Structural weight savings using advanced composites have been demonstrated for many years. Most military aircraft today use these materials extensively and Europe has taken the lead in their use in commercial aircraft primary structures. A major inhibitor to the use of advanced composites in the United States is cost. Material costs are high and will remain high relative to aluminum. The key therefore lies in the significant reduction in fabrication and assembly costs. The largest cost in most structures today is assembly.

As part of the NASA Advanced Composite Technology Program, Lockheed Aeronautical Systems Company has a contract to explore and develop advanced structural and manufacturing concepts using advanced composites for transport aircraft.

Wing and fuselage concepts and related trade studies are discussed. These concepts are intended to lower cost and weight through the use of innovative material forms, processes, structural configurations and minimization of parts. The approach to the trade studies and the downselect to the primary wing and fuselage concepts is detailed. The expectations for the development of these concepts is reviewed.

INTRODUCTION

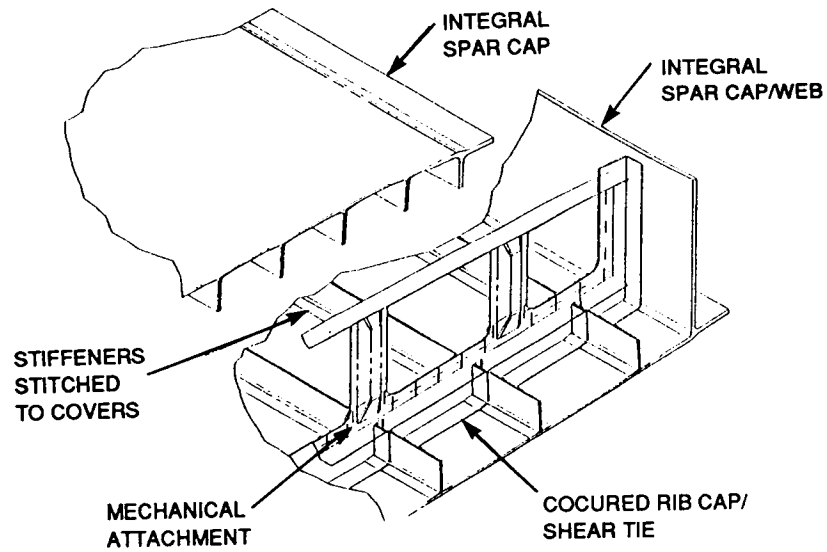
The Lockheed program consists of two phases. Phase 1 is currently underway and Phase 2 is an option scheduled to start in 1992. Phase 1 consists of five tasks: Task 1, Design/Manufacturing Concept Assessment, is the subject of this paper; Task 2, Structural Response and Failure Analysis, involves structural analysis methods development; Task 3, Advanced Materials Concepts, covers the development of new polymeric matrix systems for HSCT; Task 4, Assessment Review, is the phase final review leading to a decision on whether to exercise the option for Phase 2; and Task 5, Box Beam, the subject of another paper at this conference, involves the fabrication and assembly of the C-130 wing center box developed under a previous NASA contract.

The goals of this program are to identify emerging technologies which will lead to a 25 percent cost saving, a 40 to 50 percent weight saving, and a 50 percent reduction in parts count to validate the low cost manufacturing and to verify both the structural response and the weight savings.

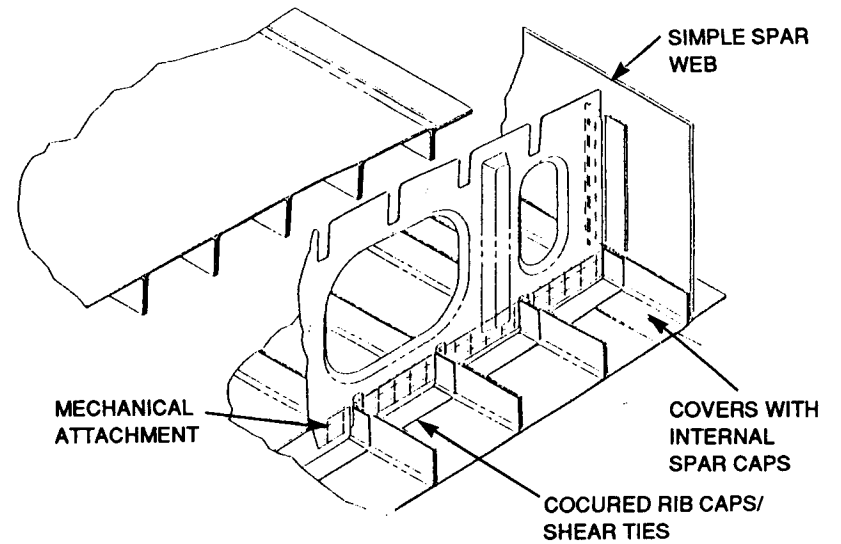
APPROACH

Four wing and three fuselage concepts were selected for this program. These concepts are shown in Figure 1. The concepts were selected based on their potential for meeting the criteria, with a moderate risk. The Lockheed L-1011 was selected as

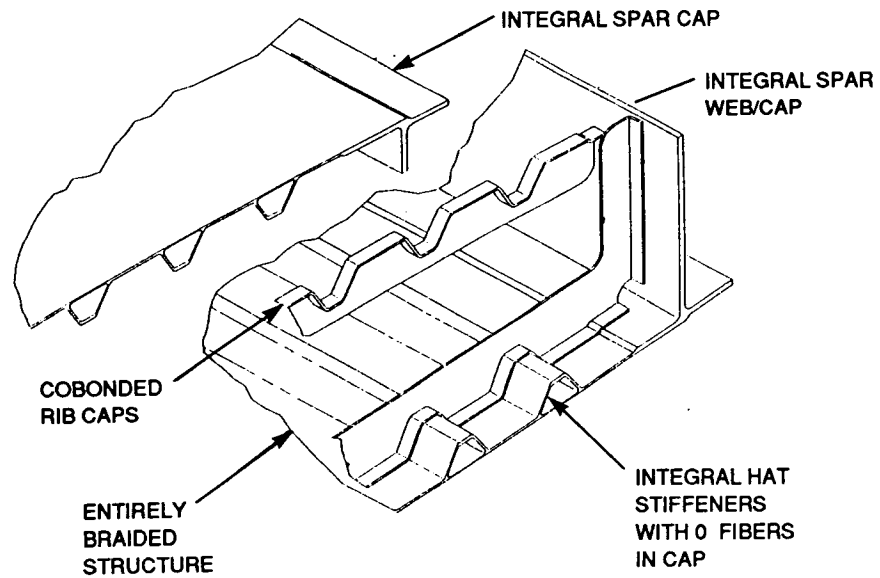
RESIN TRANSFER MOLDED WING DESIGN



AUTOMATIC TOW PLACEMENT WING DESIGN



BRAIDED WING DESIGN



MODULAR WINGBOX DESIGN

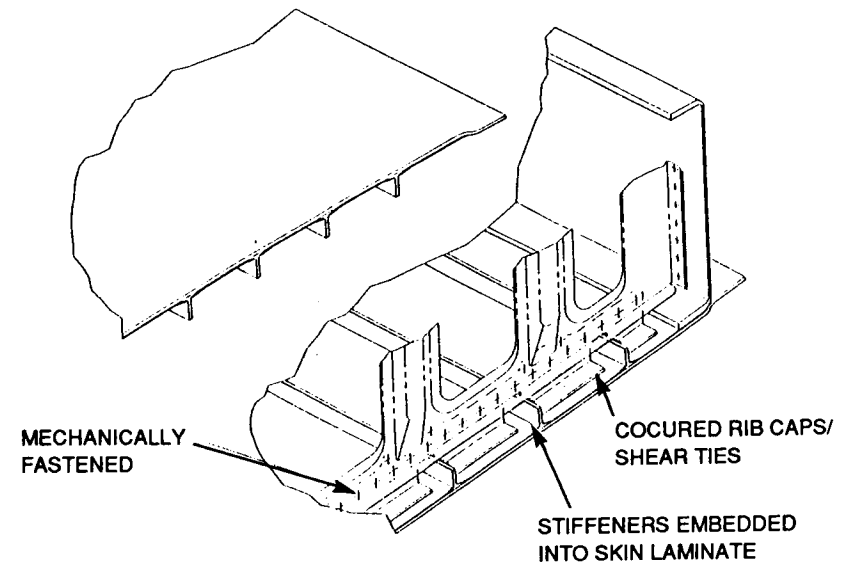
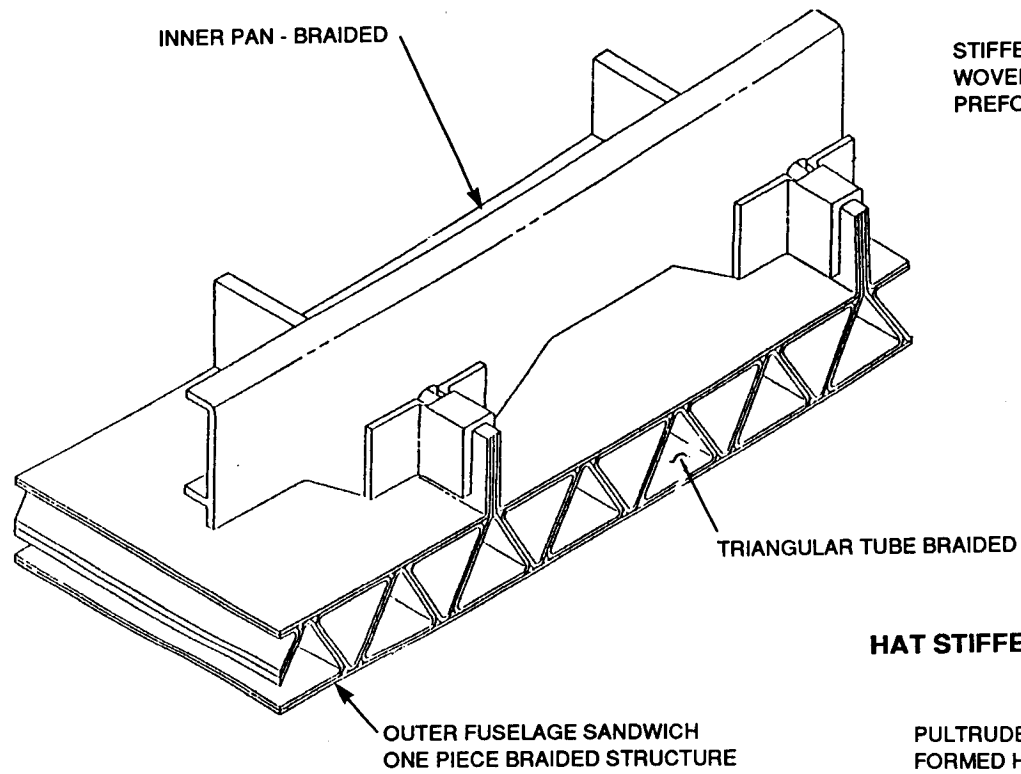


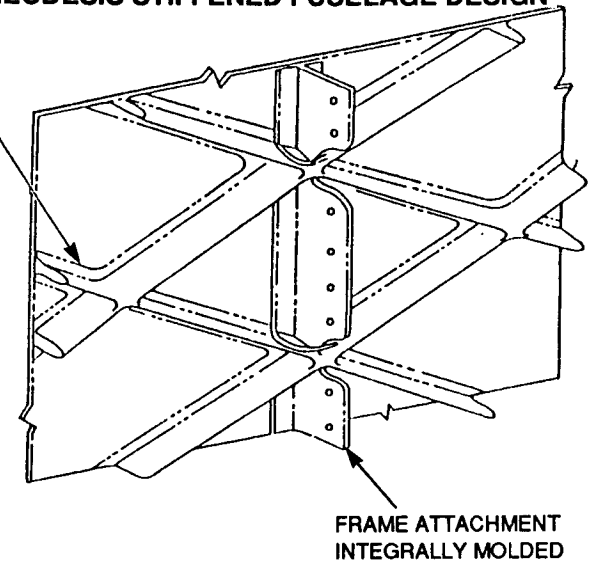
Figure 1a. Wing Concepts

SANDWICH FUSELAGE DESIGN



GEODESIC STIFFENED FUSELAGE DESIGN

STIFFENER OVERWRAP
WOVEN OR KNITTED
PREFORM



HAT STIFFENED FUSELAGE DESIGN

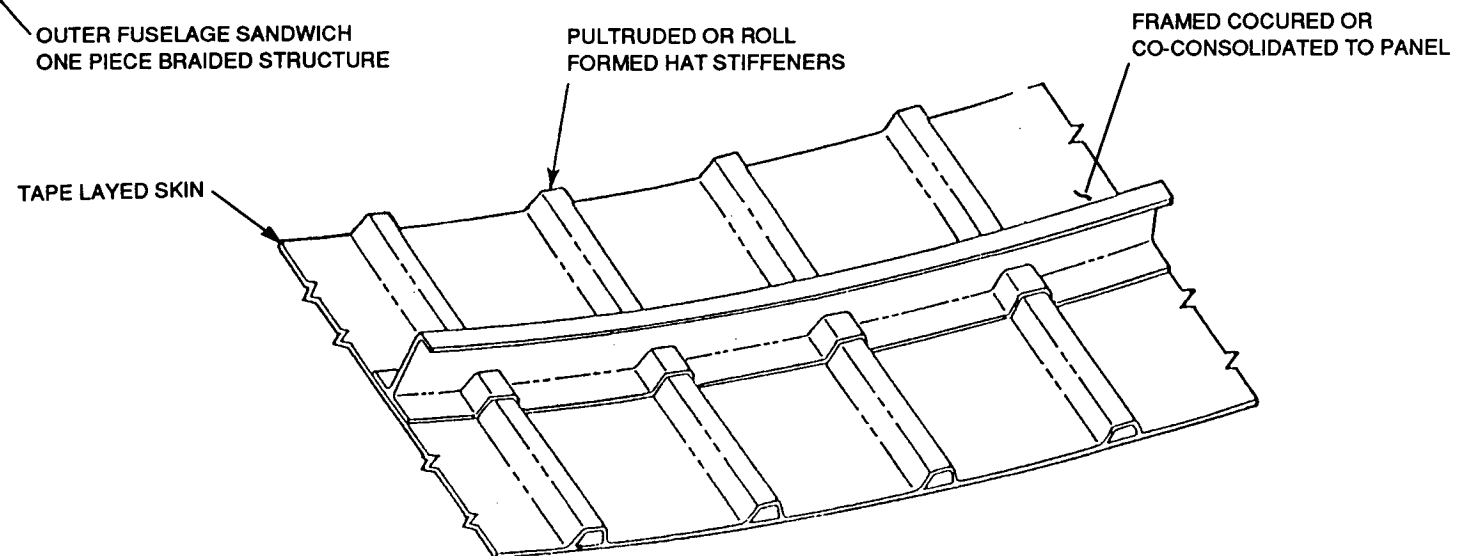


Figure 1b. Fuselage Concepts

the baseline airplane for this study. A wing location was selected which is relatively highly loaded and will yield test panels which can be tested in existing test machines and fixtures. The upper surface has to be buckling critical. The fuselage location was selected in a similar manner. Figure 2 shows the location of the wing section, and Figure 3 shows the location of the fuselage section. The design criteria for the wing are shown in Figure 4 and for the fuselage in Figure 5.

WING CONCEPTS

Four wing concepts were selected for the trade studies. Concept #1 is the Modular Wing. This concept is built up of various components each of which is fabricated using a different process. The stiffeners are pultruded, the skins are automatic tape placed, the ribs are press formed and the spars are filament wound. Concept #2 is the Resin Transfer Molded Wing. This concept is made from woven stitched preforms and is molded in two pieces. Concept #3 is the Advanced Tow Placement Wing. This concept also involves other fabrication processes, but the covers are made by automatic tow placement (ATP). Concept #4 is the Braided Wing. This concept is fabricated mainly by 2D and 3D braiding.

CONCEPT #1 - MODULAR WING

This design is shown in Figure 6. The covers, spars and ribs are fabricated separately and are assembled by conventional methods. The covers are blade stiffened. The stiffeners are fabricated from dry preforms which are resin infused and either B-staged or fully cured Tee sections. The skins are fabricated in two parts. The inner skin is discontinuous at the stiffeners. It can be laid up by automatic tape dispenser and can be cut into strips by a waterjet cutter or by a Gerber cutter. The outer skin is laid up over a tool containing the stiffeners and inner skin strips by automatic tape dispenser. The fabrication sequence is shown in Figure 7.

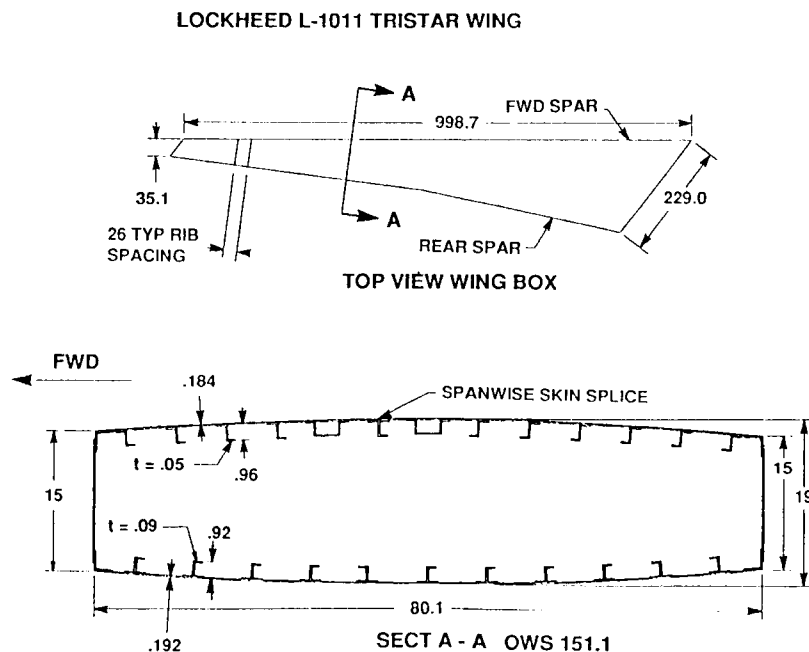


Figure 2. Baseline Wing and Study Location

LOCKHEED L-1011 TRISTAR FUSELAGE

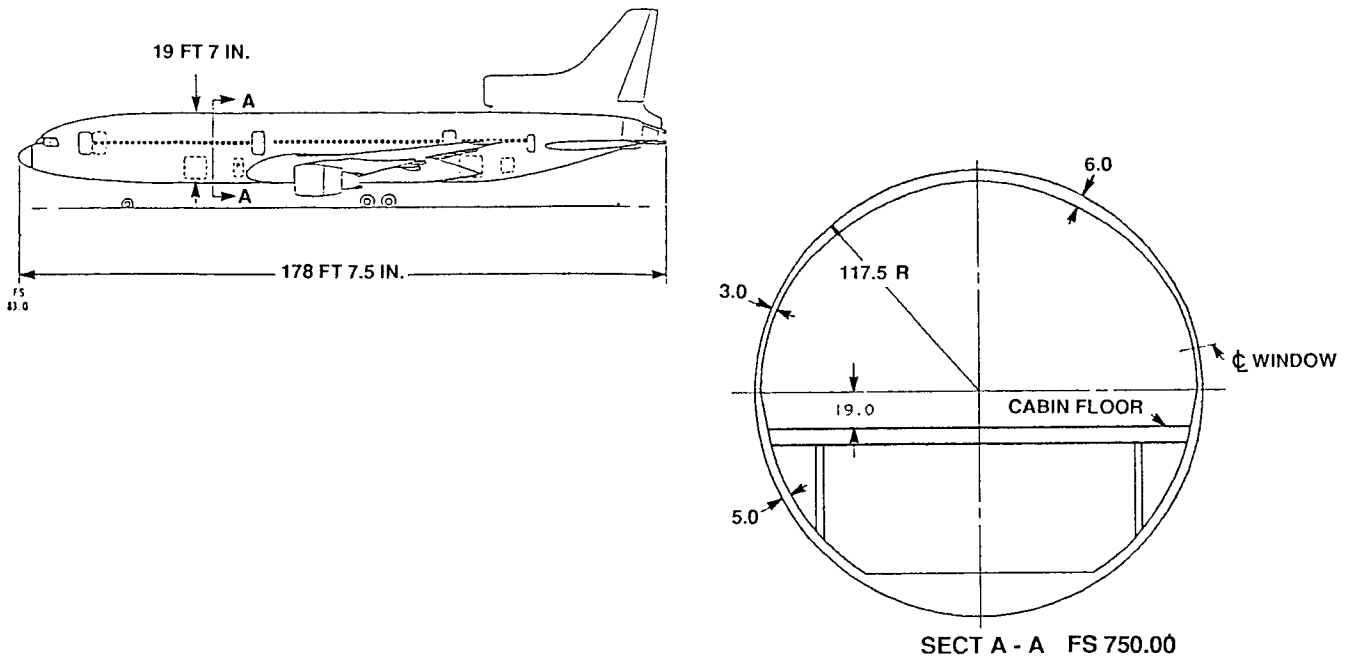


Figure 3. Baseline Fuselage and Study Location

NX	14,000 LB/IN
NXY	2,000 LB/IN
P	10.38 PSI BURST
	7.82 PSI CRUSHING
ECCENTRICITY	.1%
Gt MIN.	.70 E6 PSI

UPPER COVER LOADS O.W.S. 151.00

- COVERS BUCKLING RESISTANT
- MAX. ALLOWABLE STRAIN .006 IN/IN TENSION
.0044 IN/IN COMPRESSION

Figure 4. Wing Design Criteria

CONDITION	CROWN	SIDEWALL	KEEL
MAXIMUM TENSION (LB/IN)	1307	432	318
MAXIMUM COMPRESSION (LB/IN)	489	705	943
SHEAR (LB/IN)	150	600	300

LOADS AT F.S. 750.00

- SKINS SHEAR BUCKLING RESISTANT BELOW 1G
- MAX. ALLOWABLE STRAIN .006 IN/IN TENSION
.0044 IN/IN COMPRESSION

Figure 5. Fuselage Design Criteria

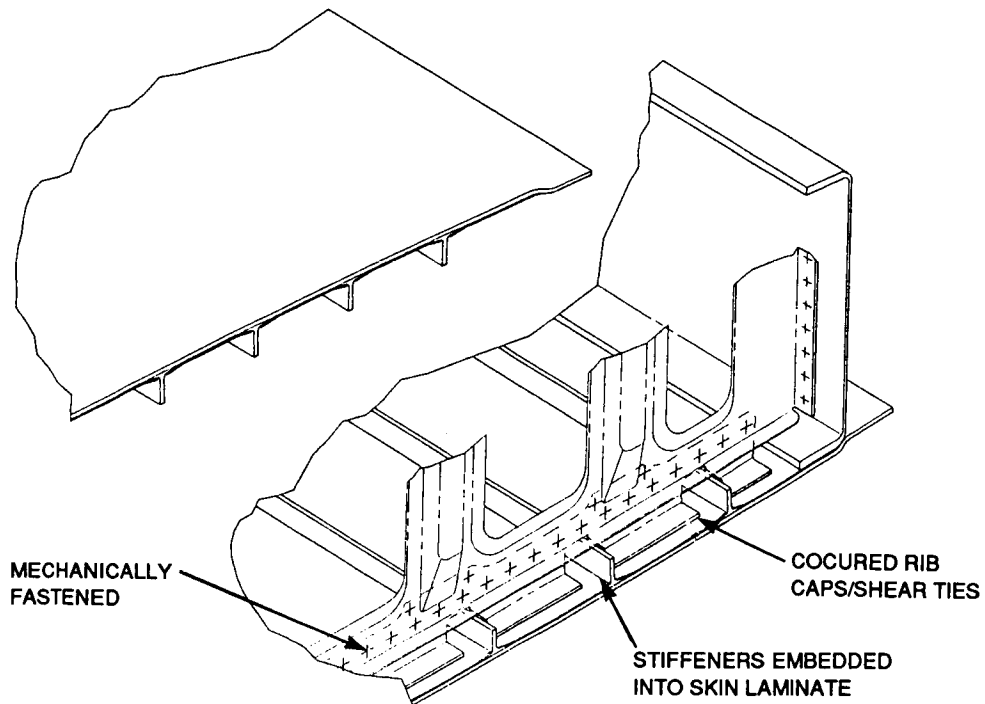


Figure 6. Modular Wing Concept

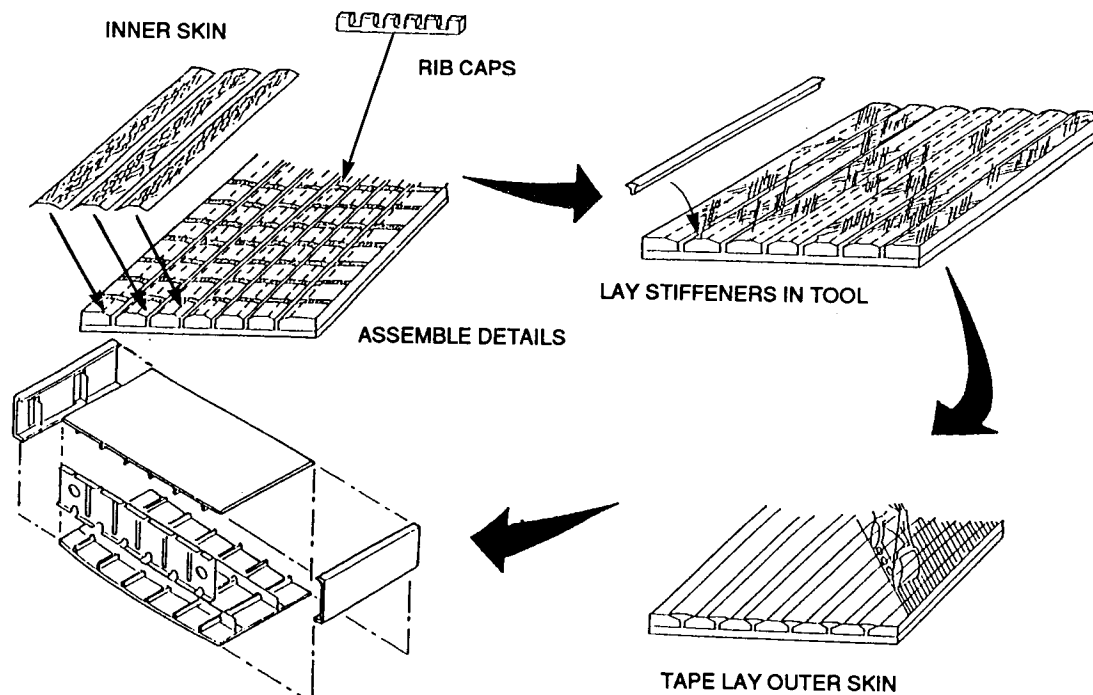


Figure 7. Modular Wing Fabrication

The front and rear spars are fabricated by automatic tow placement. Alternatives are filament winding or tape winding. The spars are designed as C-sections and can be wound as pairs in the form of a rectangular box and cut into C-sections after cure.

The ribs are fabricated as separate caps and webs. Prepreg plies are cut by Gerber cutter, stacked, formed to shape and B-staged. The rib caps are then placed in the cover fabrication tool along with the inner skin strips and the stiffeners before the outer skin is laid directly on the curing tool. A caul plate is placed over the assembly which is then bagged and cured.

The rib webs are compression molded using either thermosets or thermoplastics.

Final assembly is achieved by using mechanical fasteners.

CONCEPT #2 - RESIN TRANSFER MOLDED WING

The design concept for the resin transfer molded (RTM) wing is shown in Figure 8. The design calls for the wing box to be fabricated in two halves. Each half consists of one complete cover and part of the integral front and rear spars and with integral rib caps. Consequently, this design has no mechanical fasteners penetrating the outer surfaces.

The wing box would require large woven/stitched preforms. Close stitching would be required to debulk the preforms sufficiently to allow them to be assembled in the RTM tool. Assembly of the final molded halves would be accomplished by mechanical fasteners in the spar webs and by mechanical attachment of the separately molded rib webs. Figure 9 shows the fabrication approach.

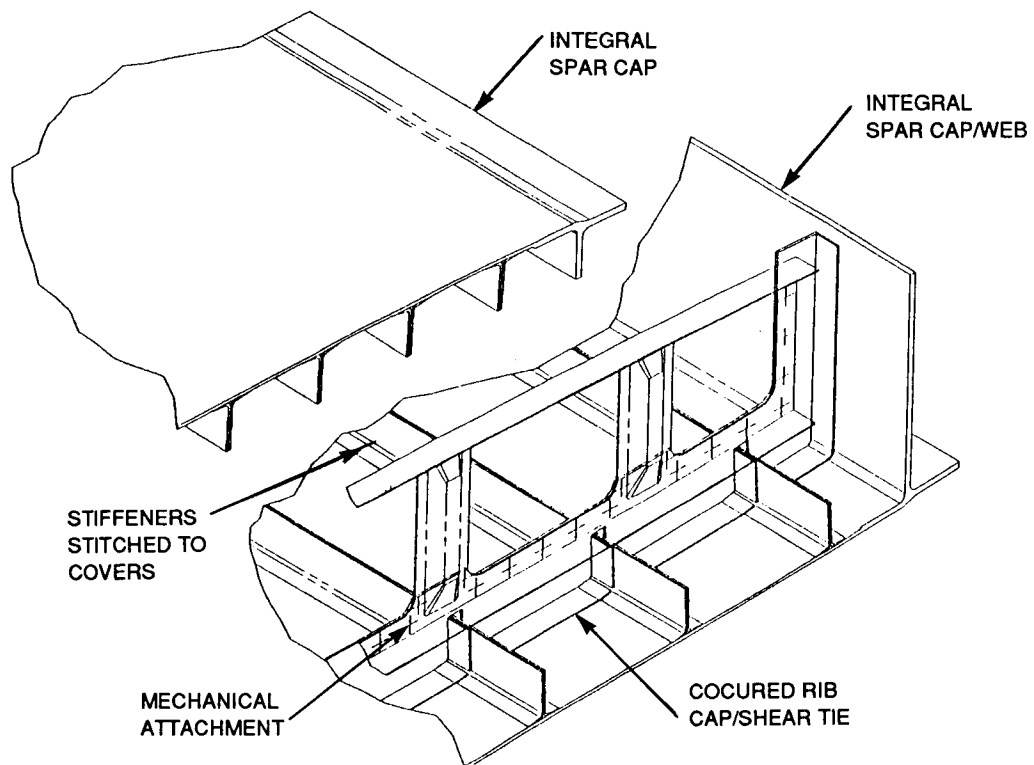


Figure 8. RTM Wing Concept

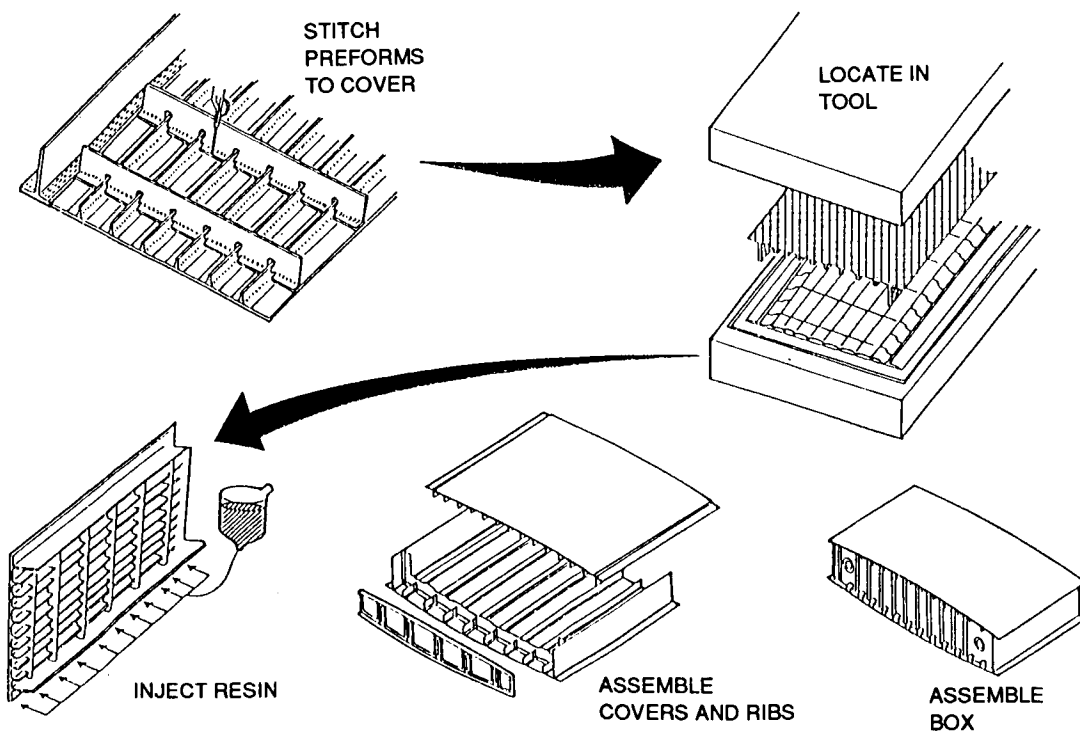


Figure 9. RTM Wing Fabrication

The wing cover assemblies will weigh approximately 2500 pounds. The largest RTM assemblies fabricated today weigh about 250 pounds. This design would thus require considerable scale-up of current technology.

A major concern with this design is the large number of tool parts which would be required. Stiffeners are usually normal to the skin, thus giving closed angles which would require segmented tools between each adjacent pair of stiffeners. At various locations along the wing span and probably chordwise, sets of vents would be required for resin to escape and to release trapped air. These vents would be closed progressively as the resin migrates outward from the injection ports. After all vents are closed some pressure would be maintained via the injection port to reduce the chance of entrapped air settling and causing voids.

CONCEPT #3 - ADVANCED TOW PLACEMENT WING

The design concept for the advanced tow placement (ATP) wing is shown in Figure 10. This design calls for the wing box to be tow placed and cured on a single mandrel. The large size of the wing box, however, made the handling of a single mandrel a major logistical problem. Consequently, the design was modified to fabricate the covers and spars separately. Rectangular tubes would be tape wound on mandrels and cut into two channel sections to form the blade stiffeners. This process allows plies to be picked up and dropped off to add localized reinforcements and 0 degree plies in the stiffener webs.

Spars can be tow placed in pairs around mandrels. An alternative approach would be to incorporate the spar caps in the covers and to tow place the webs in groups. The fabrication approach is shown in Figure 11.

The ribs would be press or diaphragm formed.

CONCEPT #4 - BRAIDED WING

The design concept for the braided wing is shown in Figure 12. This design calls for a one-piece wing box. Both 2D and 3D braiding were considered. The physical size of the wing box being considered does not fit within the confines of any current or planned braider. Today's largest 2D braider would have difficulty braiding 45-degree angles with 12k tow over a one-foot diameter mandrel. The size of carrier for this type of braider is five feet in diameter. A machine capable of braiding an L-1011 size wing box would require an enormous amount of floor and air space. More importantly, the individual carriers could not dispense a high enough quantity of fiber to make the process automatable. The carriers would require such frequent replacement that the process is not feasible in the foreseeable future.

This is also partly true for 3D braiding. The limitations of closed section tubular structures is less severe. Atlantic Research has developed an automated 3D braider which utilizes 9216 fiber carriers. A fabrication approach is shown in Figure 13.

Because of the problems in fabricating a complete wing box, this concept was dropped from further consideration. The braiding process was retained as an option for smaller assemblies as part of the modular wing box concept.

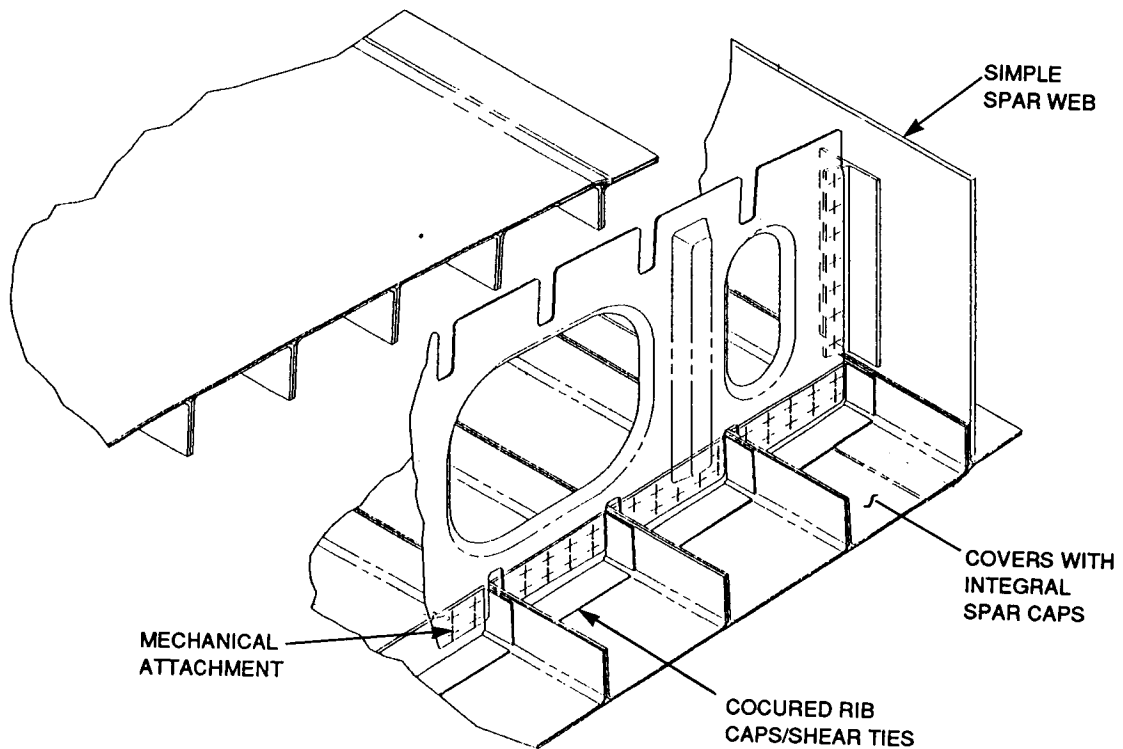


Figure 10. ATP Wing Concept

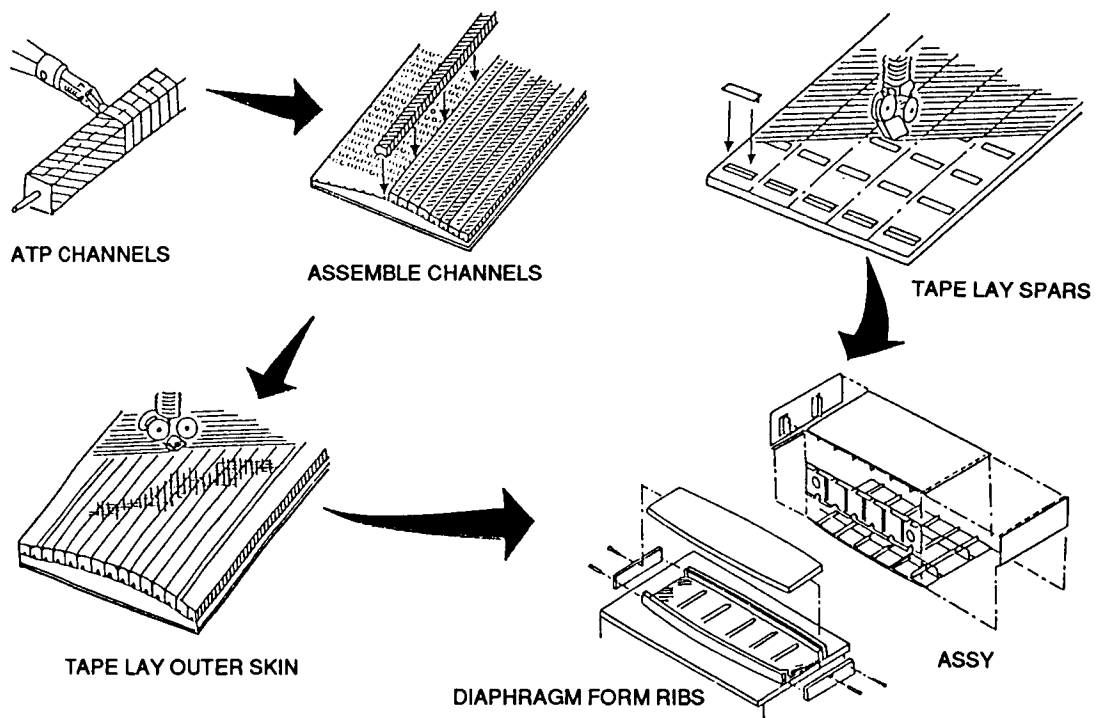


Figure 11. ATP Wing Fabrication

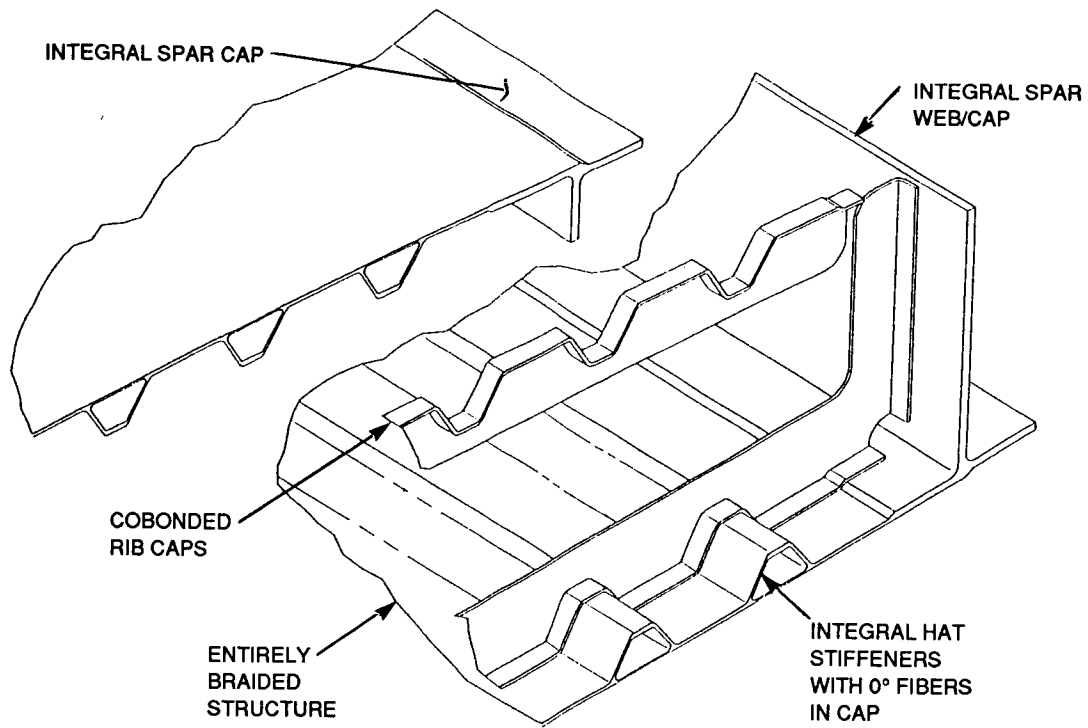


Figure 12. Braided Wing Concept

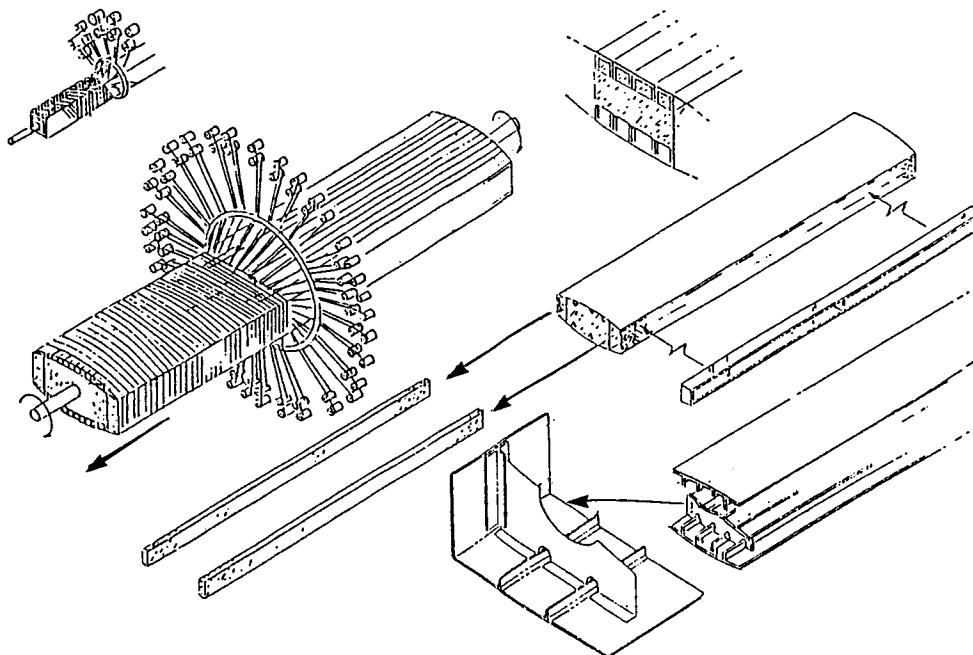


Figure 13. Braided Wing Fabrication

FUSELAGE CONCEPTS

Three fuselage concepts were selected for the trade studies. Concept #1 is a sandwich design incorporating braided triangular tubes in the sandwich. Concept #2 is a geodesic design based on an isogrid concept. Concept #3 is a hat stiffened shell design.

CONCEPT #1 - SANDWICH STIFFENED SHELL

The design concept for the sandwich shell is shown in Figure 14. This design consists of a sandwich using braided triangular tubes as the core. The tubes are oriented longitudinally. Periodically, there are flanged tubes as shown in Figure 15 which act as longerons.

The fabrication approach is to braid the tubes using dry fiber, then to pultrude through a resin bath and B stage. A fly-away foam mandrel would be required with this approach. The tubes can be fully cured and then assembled using an adhesive. This would eliminate the need for foam mandrels but would create many bond lines which would be difficult to inspect.

The inner skin is built up from C-sections which could also be pultruded. The outer skin is formed by overwrapping with tow or tape. The fabrication plan for a complete barrel section is shown in Figure 16.

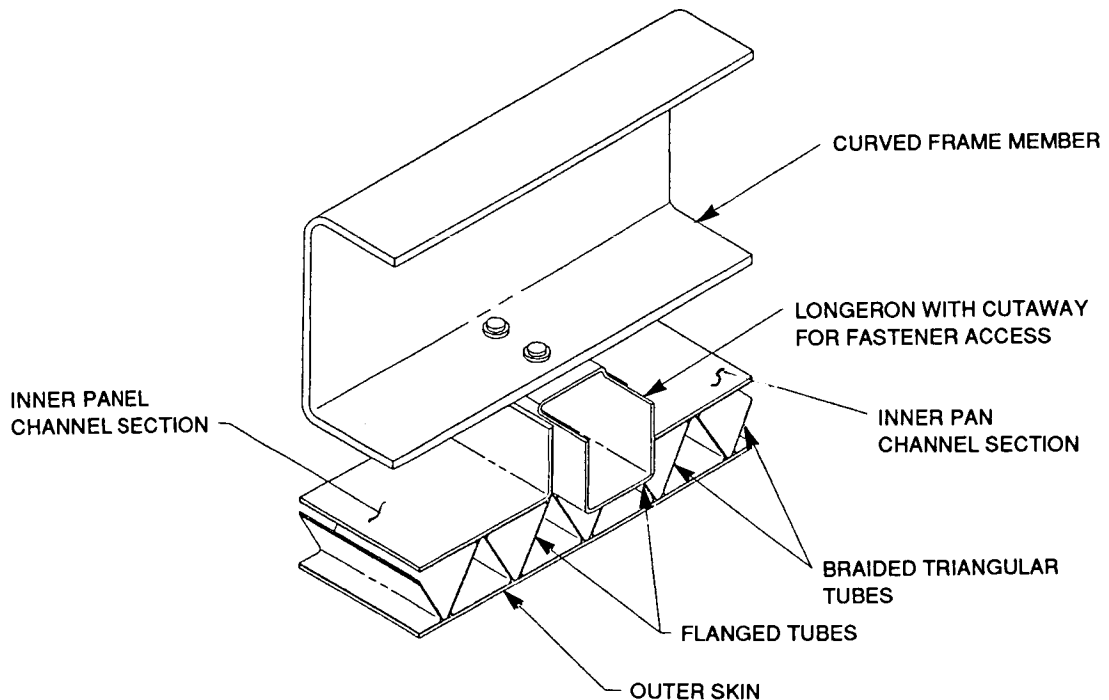


Figure 14. Sandwich Stiffened Shell Concept

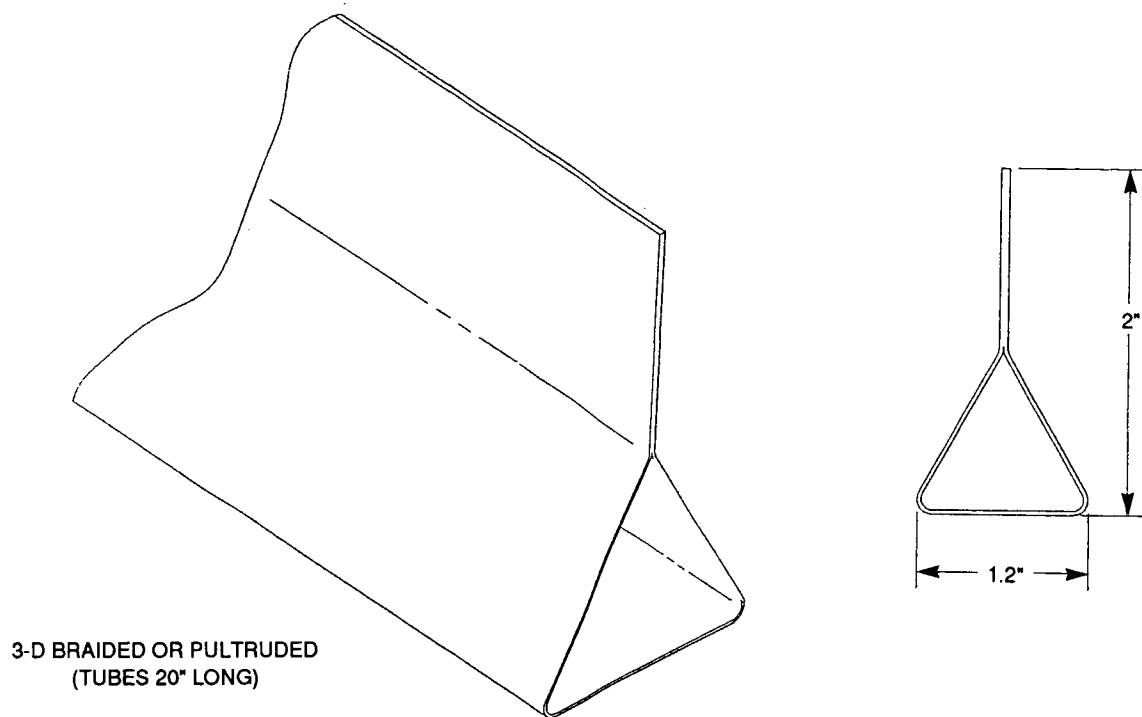


Figure 15. Flanged Triangular Tube Section

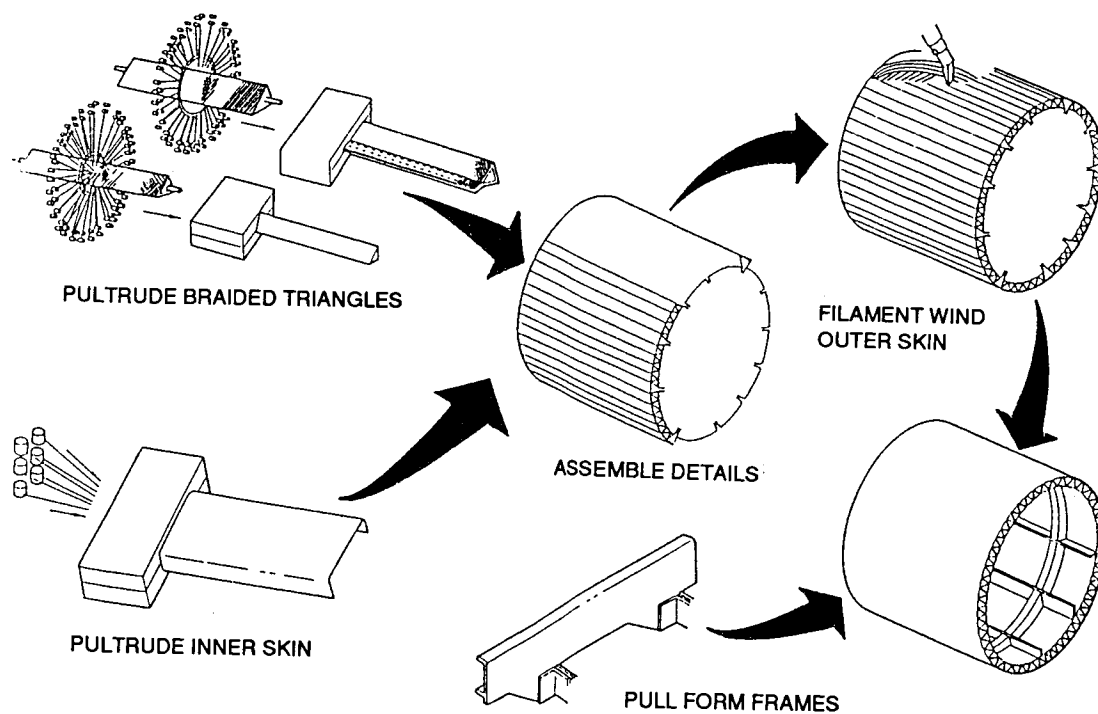


Figure 16. Sandwich Fuselage Fabrication

CONCEPT #2 - GEODESIC FUSELAGE

The design concept for the geodesic fuselage is shown in Figure 17. This design calls for an isogrid stiffened shell. The helical stiffeners are formed by winding Filcoat material alternately in each direction. Filcoat is a patented Lockheed designed material consisting of Gr/Ep tape coated with an equal thickness of epoxy filled with glass micro-balloons called syntactic. At intersections the syntactic is squeezed out. Figure 18 shows a schematic of an intersection. The fibers in each direction are continuous and the intersections are the same height as the stiffeners.

The hoop stiffeners are not continuous. They are pull-formed and cut to their individual lengths. Intersection clips and overwraps are stitched dry fiber forms containing mainly ± 45 degree and 90 degree plies to provide shear and flange bending strength. These clips and overwraps can be combined to minimize parts and are resin transfer molded and B-staged.

The skin is finally tape or tow wrapped over a mandrel. The fabrication process is shown in Figure 19.

CONCEPT #3 - HAT STIFFENED SHELL FUSELAGE

The design concept for the hat stiffened shell fuselage is shown in Figure 20. This design consists of pultruded hat stiffeners cocured to an advance tow placed skin. The frames are designed to be resin infusion molded and the complete assembly is cocured. An alternative fabrication method for the stiffeners is to braid prior to pultrusion. The fabrication process is illustrated in Figure 21.

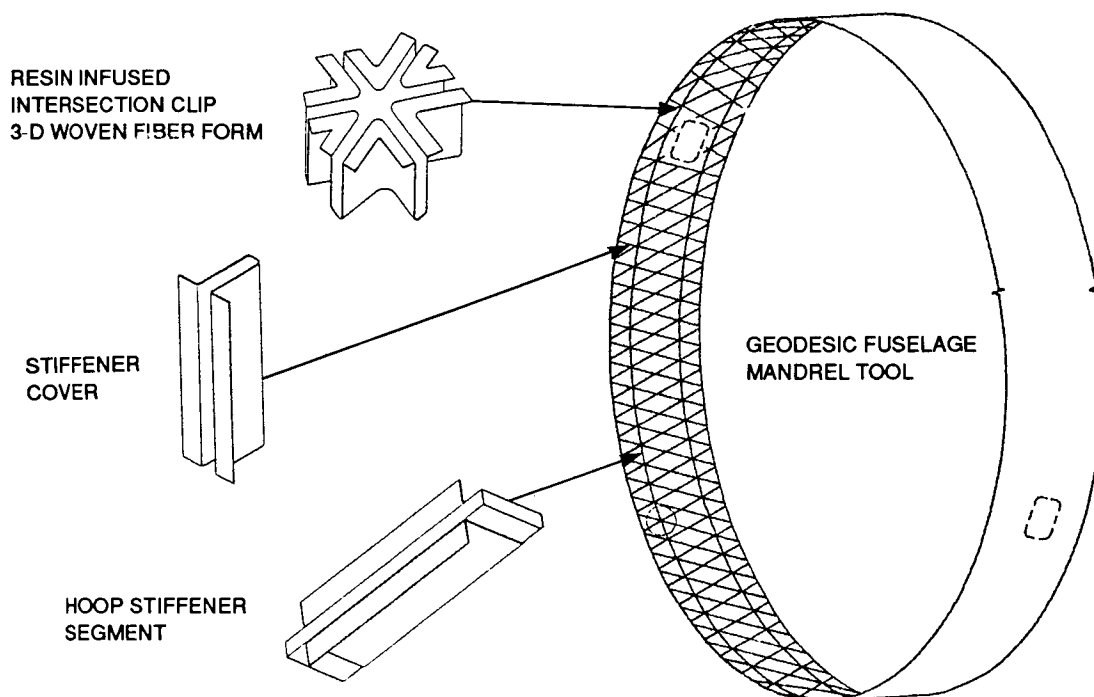


Figure 17. Geodesic Fuselage Concept

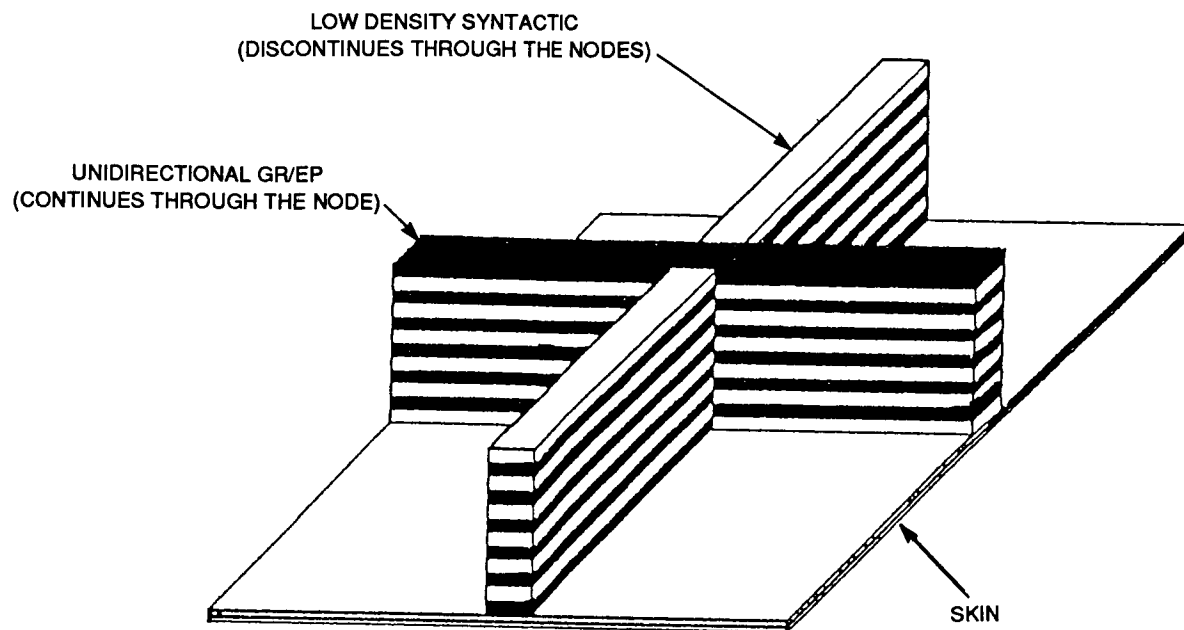


Figure 18. Geodesic Intersection

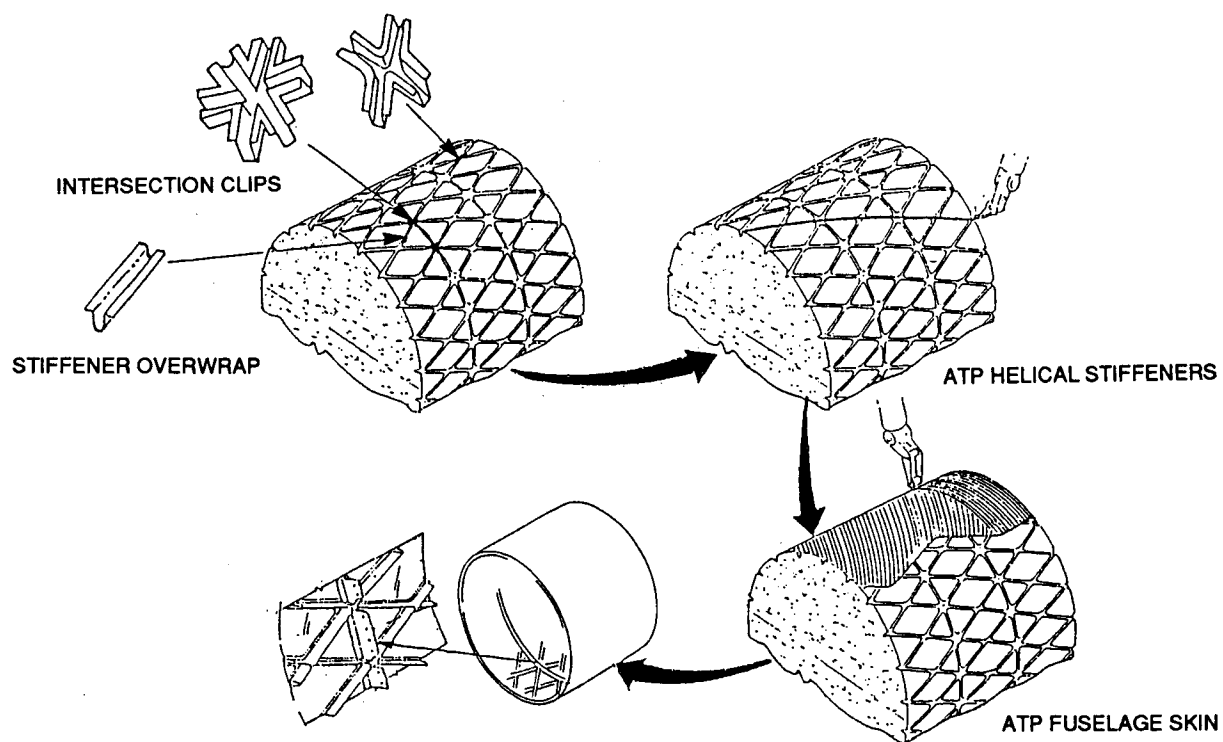
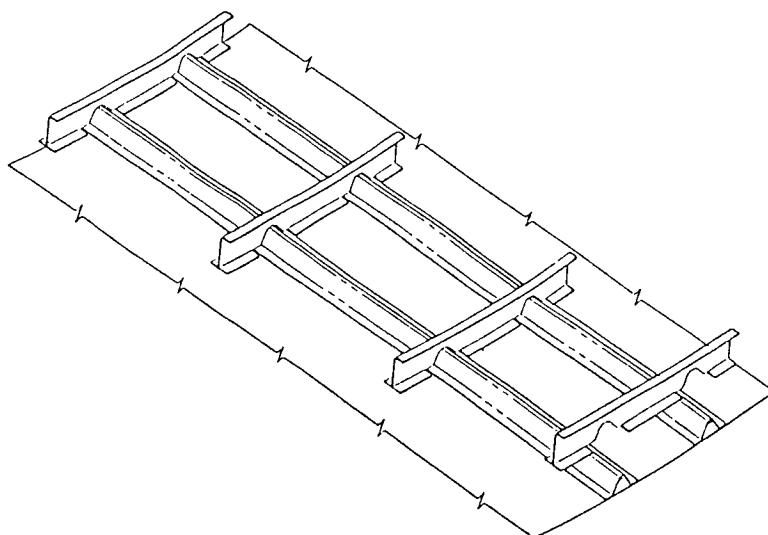


Figure 19. Geodesic Fuselage Fabrication



DESIGN FEATURES

- HAT STIFFENED TO INCREASE SPACING BETWEEN STIFFENERS
- CO-CURED ASSY
- GOOD DAMAGE TOLERANCE
- RFI FRAMES
- PULTRUDED HAT STIFFENERS

Figure 20. Stiffened Fuselage Shell Concept

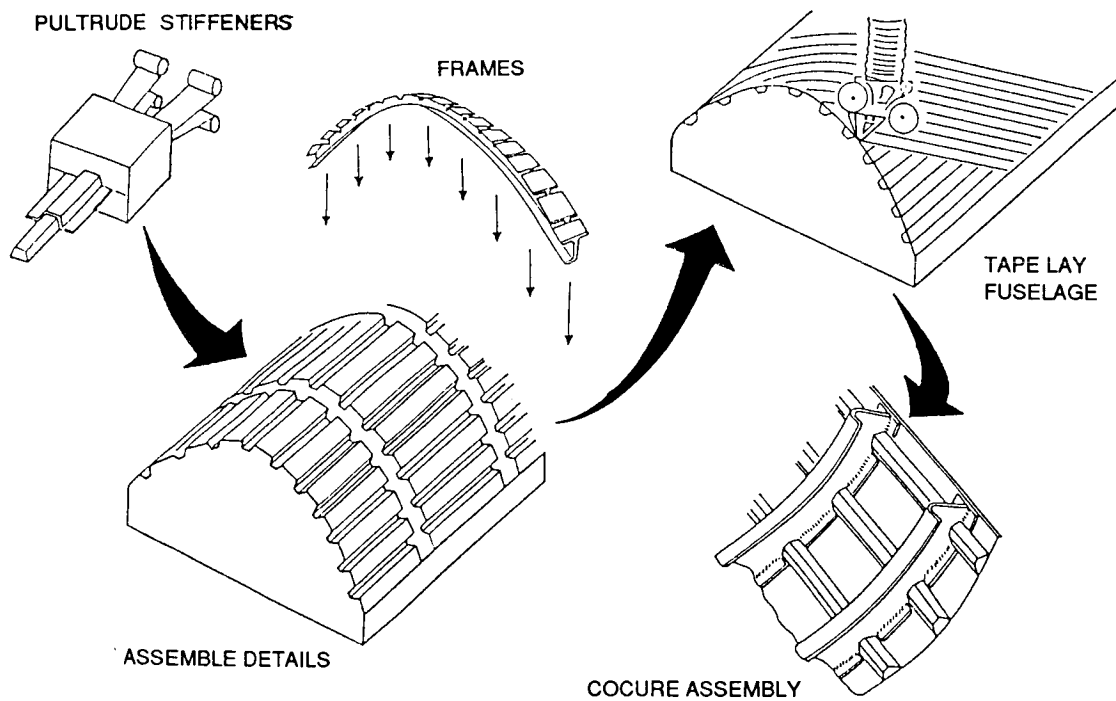


Figure 21. Stiffened Shell Fuselage Fabrication

The most effective way to fabricate these panels is as quarter panels. Essentially, upper, lower and side panels would be required. The use of closed hat stiffeners in the lower, or keel section, needs to be studied further because of problems associated with entrapment of bilge fluids. This is not considered to be a major problem as composites do not corrode. Drainage must, however, be provided to prevent accumulation of fluids and bacteria growth as well as the additional weight.

TRADE STUDIES

Figure 22 shows a summary of the options which were considered during the trade studies.

Blade, Jay and hat stiffeners were considered as options for wing skin stiffening. The Jay stiffener was eliminated because it is more difficult to fabricate than the blade and it did not show a significant enough weight saving to justify a higher cost. Hat stiffeners posed several problems in fuel tanks. They can trap fuel, they can provide leak paths and, being wide, they are difficult to terminate outboard effectively. This led to the use of blade stiffeners in all of the wing concepts. The blade configurations are, however, different. The blade configurations for the three concepts which were carried to completion are shown in Figure 23. The ATP stiffeners are built up from side by side channel sections. For the modular wing the stiffeners are pultruded with tapered flanges so that they can be buried in the skin. For the RTM wing the stiffeners are built up from woven stitched fabric.

The fuselage concepts are unique in themselves, so the stiffener configuration was not tradeable.


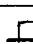

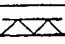
CONCEPT	CONFIGURATION				FABRICATION METHODS				MATERIALS	
					BRAID	ATP	RTM/RFI	PULT	T/S	T/P
MODULAR WING	•	•	•		•	•	•	•	•	•
RTM WING	•		•		•		•		•	•
ATP WING	•					•		•	•	•
BRAIDED WING	•		•		•				•	•
SANDWICH FUSELAGE				•	•	•	•	•	•	
GEODESIC FUSELAGE	•					•	•		•	
STIFFENED SHELL FUSELAGE			•		•	•	•	•	•	•

Figure 22. Trade Study Options

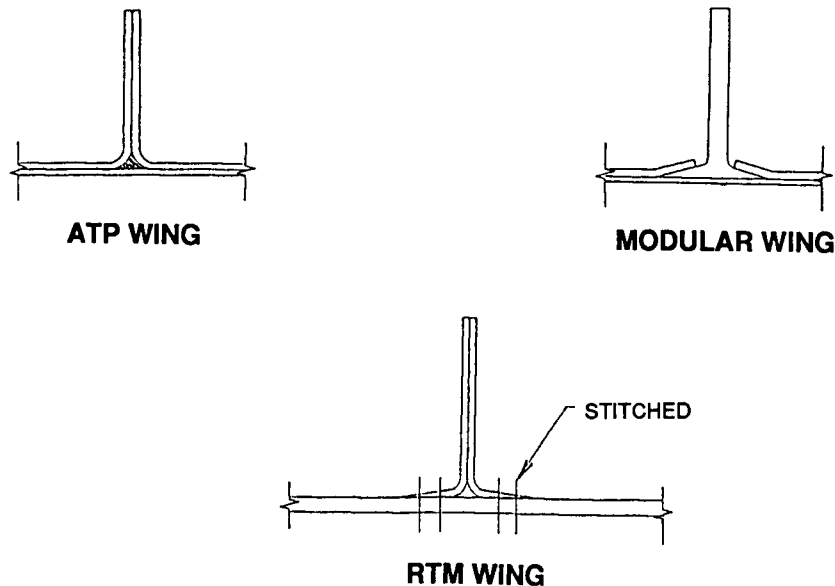


Figure 23. Stiffener Comparison

The fabrication methods looked at for each concept are summarized in Figure 22. The method selected for each component has already been discussed.

The trade study also looked at the possible use of thermoplastic materials instead of thermosets. The high cost of thermoplastic materials today makes their use in subsonic aircraft unlikely. The inherent toughness of the thermoplastic materials has some advantages, but the toughened thermosets are much more cost effective. Thermoplastics do look good for press formed ribs and even for frames. The main disadvantage of mixing materials is that mechanical fasteners would be required for assembly as thermosets and thermoplastics are very difficult to bond together. Figure 24 shows typical thermoplastic material costs today. Figure 25 shows a comparison of current and projected material costs. If projected prices do in fact become reality, then thermoplastics may be viable candidates for future commercial subsonic transports.

CONCEPT EVALUATION

Each concept was evaluated for cost, weight, design technology advancement, manufacturing technology advancement, producibility, damage tolerance, inspectability, maintainability and repair. The ability of the concept to meet the program goals was a major consideration. The scoring system used in the evaluation gave 40 points to cost, 30 points to weight and 30 points to all other factors. The cost score is the cost goal divided by the concept cost multiplied by 40. The weight score is the weight goal divided by the concept weight multiplied by 30. The other factors' score is the total of all points other than cost and weight divided by the maximum possible score multiplied by 30. This is summarized in Figure 26. The individual scores for the other factors are shown in the appendix along with the rationale.

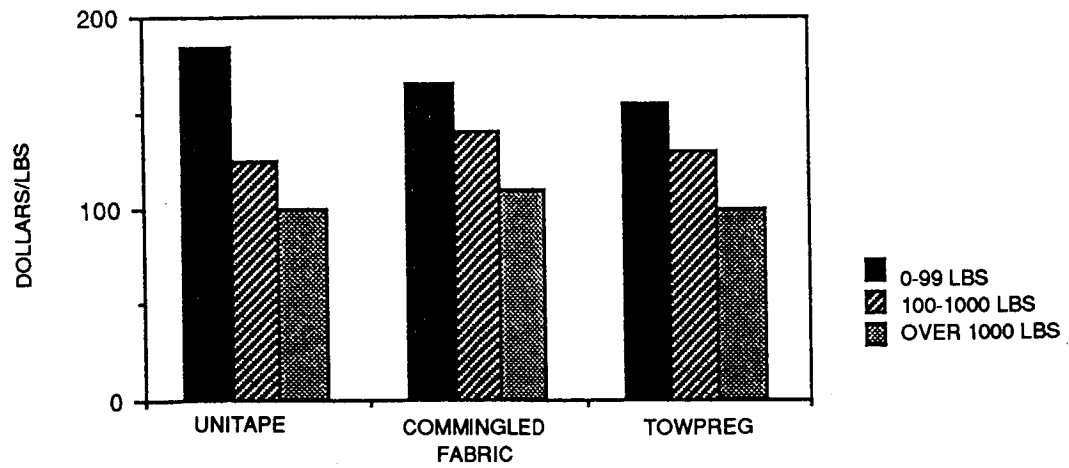


Figure 24. Thermoplastic Material Forms Cost Comparison

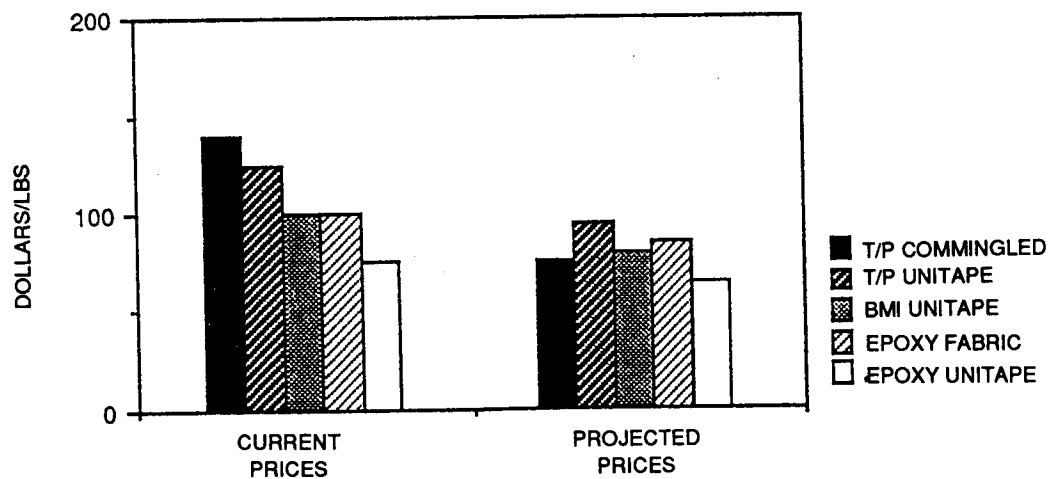


Figure 25. Cost of Various Composites

EACH CONCEPT WAS ALLOCATED A MINIMUM SCORE OF 100 POINTS BROKEN DOWN AS

- **COST (40 POINTS)**

$$\text{COST SCORE} = (\text{COST GOAL} / \text{COST OF DESIGN}) \times 40$$

- **WEIGHTS (30 POINTS)**

$$\text{WEIGHTS SCORE} = (\text{WEIGHT GOAL} / \text{WEIGHT OF DESIGN}) \times 30$$

- **OTHER FACTORS (30 POINTS)**

$$\text{OTHER FACTORS SCORE} = (\text{SUM OF POINTS OF DESIGN} / \text{MAXIMUM POSSIBLE POINTS}) \times 30$$

Figure 26. Scoring System

WEIGHT TRADES

The weights for the wing concepts were based on the total weight of the wing box structure per aircraft. Optimum sizing of the structure at outer wing station 151.1 was obtained. A spanwise variation was then used based on previous wing studies. Additional weight was added to account for landing gear attach fittings, engine mount fittings and access doors.

Weights for the fuselage concepts were based on sizing of the upper shell at station 750. The sizing assumed maximum tension and shear or maximum compression and shear. The sizing was then conservatively assumed to be constant at all circumferential locations. Total weight between Fuselage Stations 235 and 983 was taken.

A comparison of wing box weights is shown in Figure 27 and the fuselage segment weights in Figure 28. A summary of the weight trade study is shown in Figure 29.

COST TRADES

The cost trades were based on recurring costs only, although nonrecurring costs were considered in the producibility trades. Recurring costs were based on a production run of 300 ship sets at a rate of five per month. Labor rates are 1995 projected as agreed among the ACT program contractors at the Cost Workshops. Material costs were assumed to be \$40/lb. A sensitivity study on material cost will be performed. It was assumed that there would be no purchase of facilities or equipment. The fly to buy was dependent on fabrication method. The cost analysis program used was ACCEM. It includes material burden, support labor, quality control, learning curves and industrial engineering standards. A comparison of the wing concept costs is shown in Figure 30 and a comparison of the fuselage costs is shown in Figure 31. The cost trade study results are summarized in Figure 32.

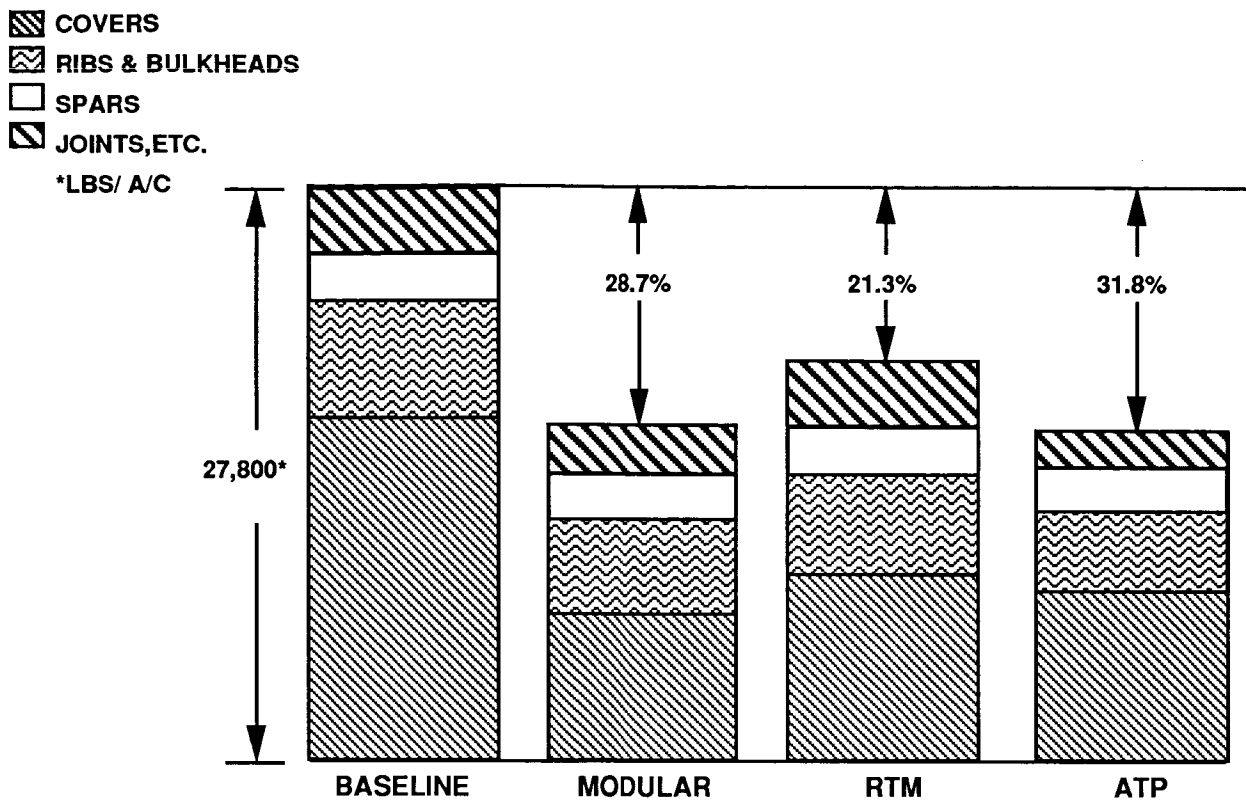


Figure 27. Wing Box Weights

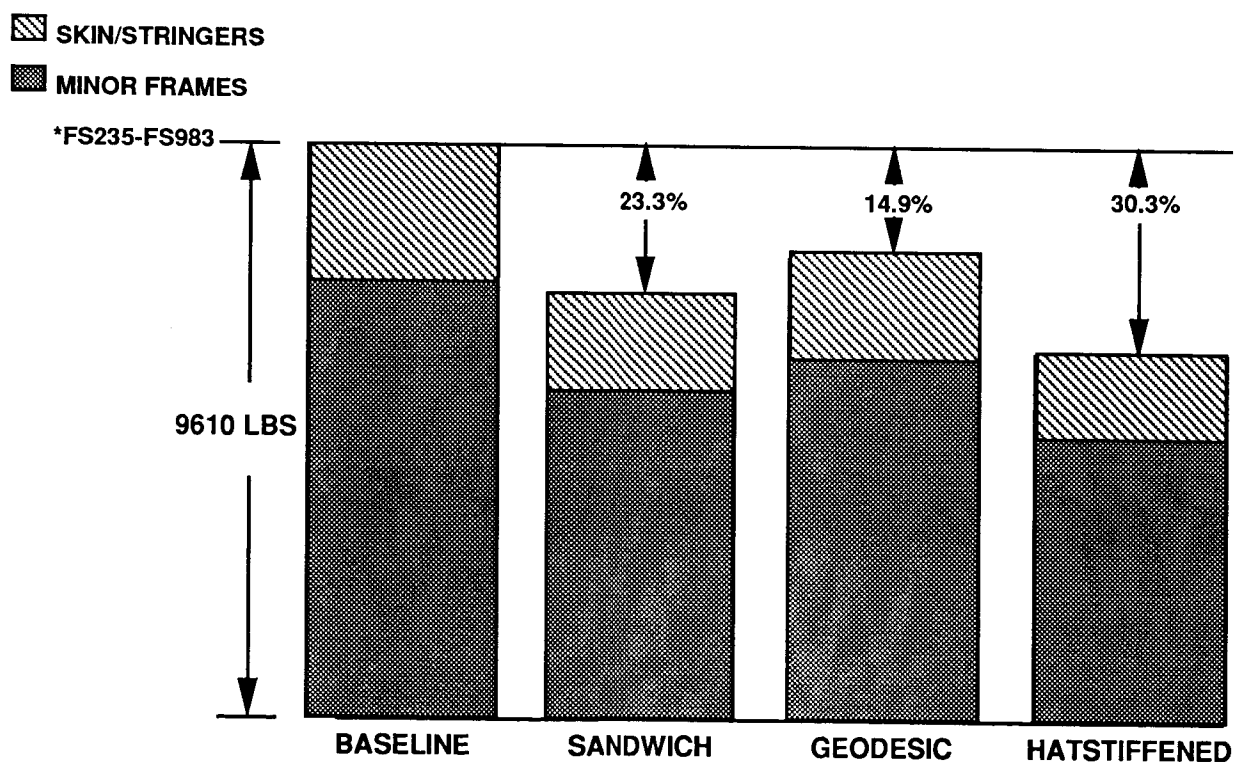


Figure 28. Fuselage Shell Weights

	CONCEPT	WEIGHT	SCORE
WING	BASELINE (GOAL)-34%	27,800 (17,792)	
	MODULAR	19,831	26.91
	RTM	21,976	24.29
	ATP	18,953	28.16
FUSELAGE	BASELINE (GOAL)-34%	9,610 (6,150)	
	SANDWICH	7,367	25.04
	GEODESIC	8,175	22.57
	HAT STIFFENED	6,700	27.54

Figure 29. Weight Trade Study Results

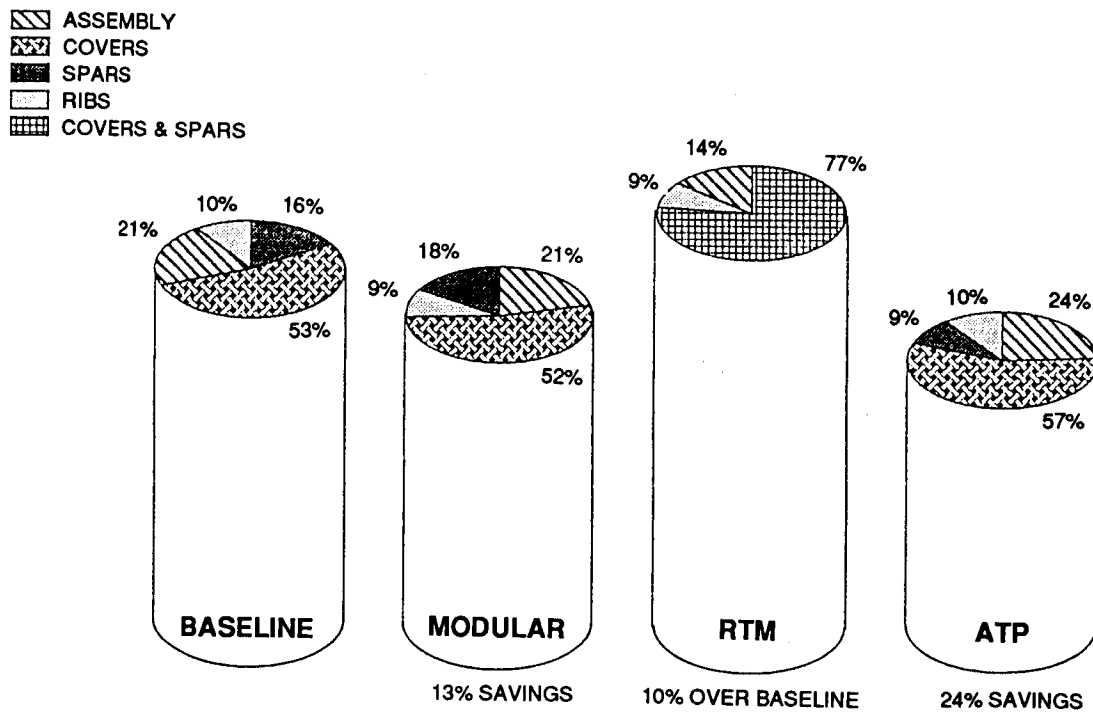


Figure 30. Wing Concept Cost Comparisons

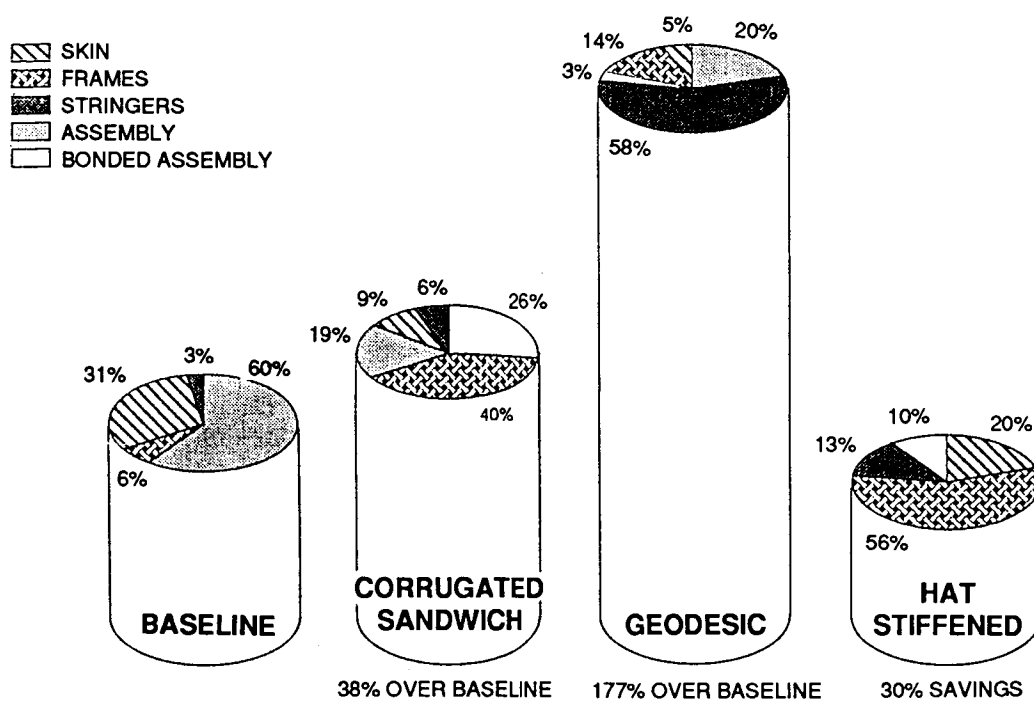


Figure 31. Fuselage Concept Cost Comparison

	CONCEPT	COST \$	SCORE
WING	BASELINE (GOAL)-25%	2,636,425 (1,977,318)	
	MODULAR	2,301,918	34.36
	RTM	2,912,135	27.16
	ATP	2,002,760	39.49
FUSELAGE	BASELINE (GOAL)-25%	161,704 (121,278)	
	SANDWICH	221,985	21.85
	GEODESIC	448,918	10.81
	HAT STIFFENED	112,962	42.95

Figure 32. Cost Trade Study Results

Cost benefits and drivers for each concept are summarized in Figure 33.

DOWNSELECT

Based on the trade studies, one wing and one fuselage concept was selected from the concepts shown in Figures 34 and 35. Figure 36 shows a summary of the rankings of the concepts. The Advanced Tow Placement Wing and the Hat Stiffened Shell Fuselage designs finished the clear winners. Both came close to the 25 percent cost saving target and the 40 percent weight saving target and exceeded the 50 percent reduction in parts count. The weight saving goal shown has been reduced to 34 percent to account for resizing. The 34 percent was an overall goal bearing in mind the fact that the wing would be expected to have a larger savings from resizing than would the fuselage which has volume constraints. The selected concepts are shown in Figures 37 and 38.

The original program plan had called for continuing with a backup design for both the wing and the fuselage through the end of Phase 1. The primary concepts, however, emerged as such clear winners that it was decided to put all the remaining effort into developing and validating the primary concepts.

EXPECTATIONS FOR DEVELOPMENT

Both the selected concepts depend on minimization of mechanical fasteners and the fabrication of large components. The development of these concepts depends on the minimization of discontinuities, the development of analytical methods, the demonstration of repeatable process and the use of in-process controls which will in

CONCEPT	COST BENEFITS	COST DRIVERS
MODULAR WING	<ul style="list-style-type: none">• MORE EFFICIENT USE OF MATERIALS	<ul style="list-style-type: none">• TOOL LOADING• MATERIAL COST• ADDITIONAL FASTENERS• INCREASED ASSEMBLY
RTM WING	<ul style="list-style-type: none">• STIFFENER SIMPLICITY• REDUCED PART COUNT• MINIMAL MECHANICAL ASSEMBLY	<ul style="list-style-type: none">• TOOL LOADING• COMPLEX TOOLING• MATERIAL COST
ATP WING	<ul style="list-style-type: none">• USE OF ATP EQUIPMENT• INTEGRAL SPAR CAPS• REDUCED ASSEMBLY	<ul style="list-style-type: none">• HANDLING• TOOL LOADING
SANDWICH FUSELAGE	<ul style="list-style-type: none">• USE OF AUTOMATED FABRICATION PROCESSES	<ul style="list-style-type: none">• HIGH PART COUNT• ASSEMBLY• MATERIAL COST
GEODESIC FUSELAGE	<ul style="list-style-type: none">• COMMONALITY OF DETAILS	<ul style="list-style-type: none">• HIGH PART COUNT• HAND PLACEMENT OF DETAILS• MATERIAL COST
STIFFENED SHELL FUSELAGE	<ul style="list-style-type: none">• REDUCED NUMBER OF PARTS• COCURED FRAMES	<ul style="list-style-type: none">• COMPLEX TOOLING

Figure 33. Cost Benefits and Cost Drivers

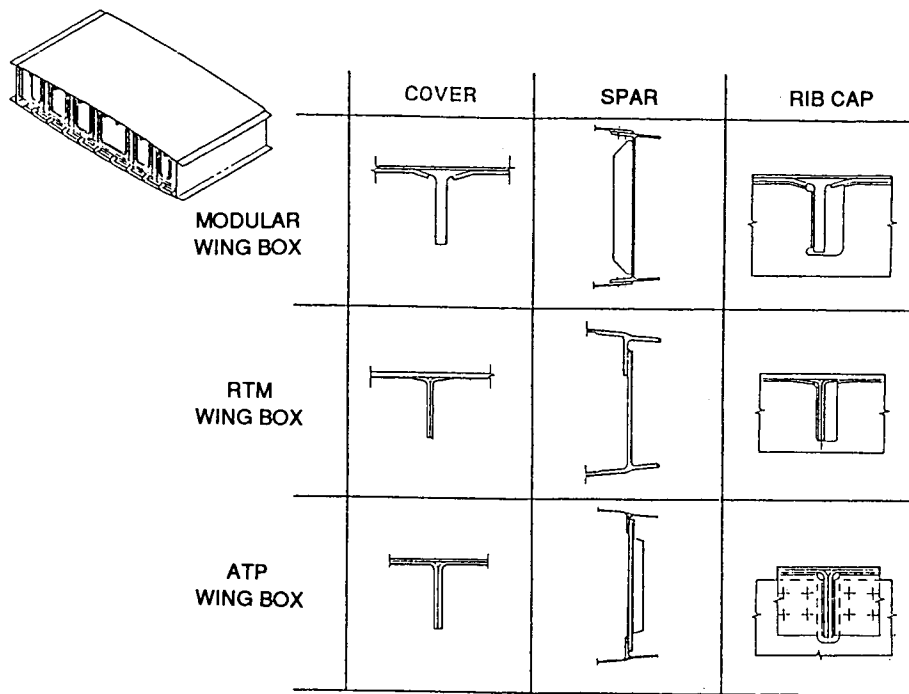


Figure 34. Wing Box Concepts

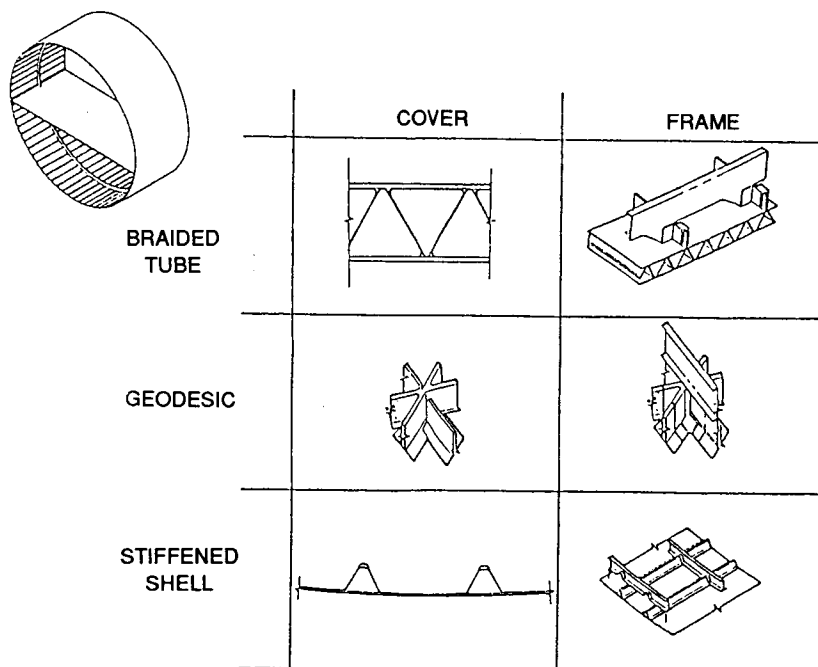
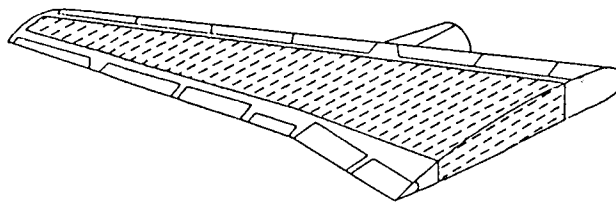


Figure 35. Fuselage Concepts

CONCEPT		WEIGHT	COST	ILITIES	TOTAL	RANK
WING	MODULAR	26.91	34.36	12.5	73.77	2
	RTM	24.29	27.16	20.5	71.95	3
	ATP	28.16	39.49	18.0	85.65	1
FUSELAGE	SANDWICH	25.05	21.85	17.0	63.90	2
	GEODESIC	22.57	10.81	15.5	48.88	3
	STIFFENED SHELL	27.54	42.95	17.5	87.99	1

Figure 36. Downselect Summary



DESIGN FEATURES:

- ONE PIECE DESIGN - NO SPANWISE/ CHORDWISE JOINTS
- INTEGRAL CONTINUOUS BLADE STIFFENERS
- UPPER/LOWER COVERS WITH INTEGRAL SPAR CAPS
- NO FASTENERS/LEAK PATHS THROUGH THE COVERS
- INTEGRAL RIB CAPS WITH SHEAR CLIPS

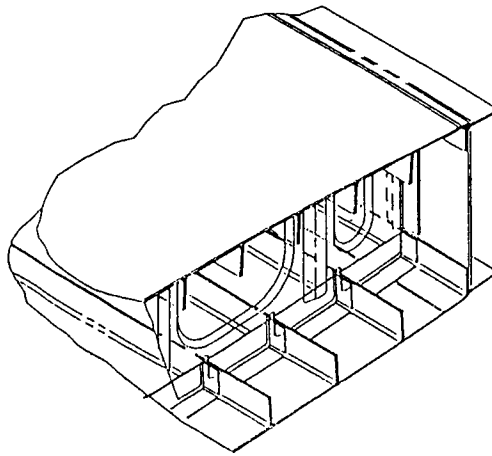
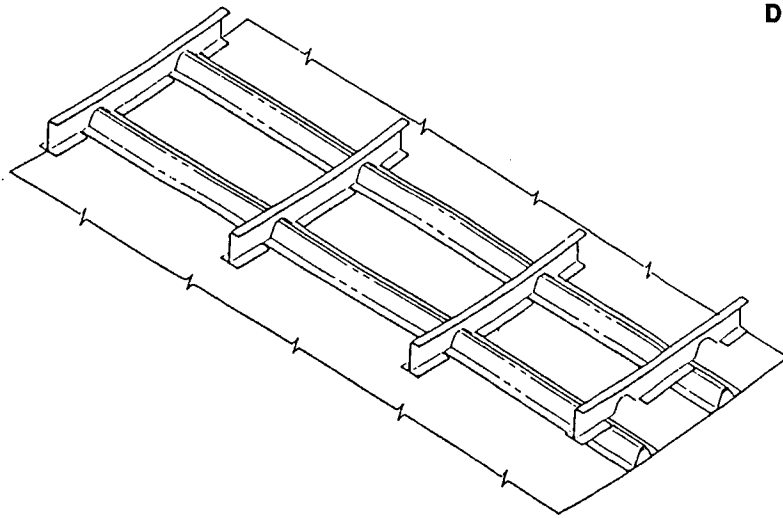


Figure 37. Selected Wing Concept



DESIGN FEATURES:

- HAT STIFFENED TO INCREASE SPACING BETWEEN STIFFENERS
- CO-CURED ASSY
- GOOD DAMAGE TOLERANCE
- RFI FRAMES
- PULTRUDED HAT STIFFENERS

Figure 38. Selected Fuselage Concept

effect build in the quality and minimize scrap and buy-off. The concepts involve a moderate risk but can be approached in an incremental manner which will improve the chances of success. Neither concept involves an all or nothing approach and alternative paths are available if needed.

SUMMARY AND CONCLUSIONS

Advanced structural and material trade studies were carried out on four wing and three fuselage concepts. The trade studies showed that the Advanced Tow Placement Wing concept and the Hat Stiffened Shell Fuselage concept both showed excellent potential for meeting the program goals. The weight savings are close enough to the goal that there is a reasonable chance of meeting or exceeding this goal with further development and refinement. The wing cost is within one percent of the goal and the cost of the fuselage concept exceeds the goal. Efforts are now underway to validate these designs by more detailed analyses and by fabrication and test.

APPENDIX

CONCEPT	DESIGN TECHNOLOGY ADVANCEMENT	RATIONALE
MODULAR WING	4	CONVENTIONAL ASSEMBLY METHODS. LARGE COCURED COVER ASSEMBLIES REPRESENT A SLIGHT TECHNOLOGY ADVANCEMENT.
RTM WING	5	CONVENTIONAL DESIGN CONFIGURATION WITH EXCEPTION OF COVER/SPAR INTEGRATION AND STITCHED PREFORM.
ATP WING	5	CONVENTIONAL DESIGN CONFIGURATION. EMPHASIS ON LARGE COCURED ASSEMBLIES. MECHANICAL FASTENERS SIGNIFICANTLY REDUCED.
SANDWICH FUSELAGE	8	UNIQUE DESIGN CONCEPT AMENABLE TO AUTOMATED FABRICATION TECHNIQUES. SIMPLIFIED FRAME TO COVER ATTACHMENT.
GEODESIC FUSELAGE	6	HIGHLY EFFICIENT, DAMAGE TOLERANT DESIGN. DESIGN SUITABLE FOR AUTOMATED MANUFACTURING METHODS.
STIFFENED SHELL FUSELAGE	4	DESIGN CONCEPT IS CURRENT STATE OF THE ART. CONFIGURATION ALLOWS FOR COCURING OF ALL STRUCTURAL ELEMENTS.

CONCEPT	TECHNOLOGY ADVANCEMENT MANUFACTURING	RATIONALE
MODULAR WING	3	DIFFICULT TO LAY UP RIB CAPS AND COCURING TO THE COVER AND STIFFENERS. LITTLE TECHNOLOGY ADVANCEMENT.
RTM WING	9	ONE-SHOT COMPLETE RTM WING HALF WOULD BE A TREMENDOUS ADVANCEMENT OF THE TECHNOLOGY. DESIGN ELIMINATES MANY COMPONENTS AND FASTENERS.
ATP WING	7	ATP OF C-CHANNEL BLOCKS AND ASSEMBLY TO FORM COVERS REPRESENTS AN ADVANCEMENT OVER CURRENT METHODS. CO-CURING OF INTEGRAL RIB CAPS IS A SIGNIFICANT ADVANCEMENT.
SANDWICH FUSELAGE	7	SIGNIFICANT ADVANCEMENT IN MANDREL TECHNOLOGY. SOME ADVANCEMENT IN COMPONENT LOCATION ARENA WITH THE MANY TUBES. A SIGNIFICANT ADVANCEMENT IF PULTRUDED.
GEODESIC FUSELAGE	7	ATP OF HELICAL STIFFENERS AND RFI OF INTERSECTION CLIPS IS A SIGNIFICANT ADVANCEMENT. PULL FORMING OF FRAMES IS AN EXTENSION OF TECHNOLOGY.
STIFFENED SHELL FUSELAGE	3	LITTLE ADVANCEMENT ASIDE FROM THE FACT THAT THE FRAMES ARE COCURED.

APPENDIX

CONCEPT	INSPECT- ABILITY	RATIONALE
MODULAR WING	6	SEPARATE COMPONENTS CAN BE INSPECTED, BUT ALSO WILL REQUIRE EXTENSIVE POST PROCESS INSPECTION DUE TO COCONSOLIDATION AND/OR BONDING
RTM WING	8	PREFORM MAY BE INSPECTED BEFORE MOLD FILLING. WIDE RANGE OF IN-PROCESSMETHODS COULD BE USED FOR MONITORING THE MOLD FILL AND CURE, INCLUDING PROCESS MODELS.
ATP WING	6	TOW QUALITY, SIZE AND PLACEMENT MUST BE MONITORED AT ALL TIMES, WILL DEPEND ON MACHINE. PLACEMENT MONITORING NEEDS TO BE DEVELOPED.
SANDWICH FUSELAGE	5	TUBES COULD BE INSPECTED IN-LINE, BUT POST PROCESS WILL BE VERY DIFFICULT BETWEEN TUBES.
GEODESIC FUSELAGE	2	VERY COMPLEX GEOMETRY. THE TRUSS INTERSECTIONS ARE UNINSPECTABLE.
STIFFENED SHELL FUSELAGE	8	HIGH SCORE BECAUSE COMPONENTS MAY BE INSPECTED BEFORE FINAL CURE. IN-PROCESS INSPECTION OF PULTRUDED HATS AND RTM FRAMES HAVE EASY GOEMTRY.

CONCEPT	MAINTAIN- ABILITY	RATIONALE
MODULAR WING	6	MODULAR CONSTRUCTION FACILITATES LESS COSTLY REPAIR TECHNOLOGY. HEAVY STRUCTURAL DAMAGE IS UNREPAIRABLE AT FIELD LEVEL.
RTM WING	6	LEAK PATHS ARE ELIMINATED. CONSTRUCTION FACILITATES LESS COSTLY REPAIR TECHNOLOGY. HEAVY STRUCTURAL DAMAGE IS UNREPAIRABLE AT FIELD LEVEL.
ATP WING	7	LEAK PATHS ARE ELIMINATED. REPAIR AT FIELD LEVEL IS LESS COSTLY. HEAVY DAMAGE WILL INDUCE REMOVE AND REPLACEMENT OF ENTIRE STRUCTURE.
SANDWICH FUSELAGE	8	COMPOSITE MATERIALS ELIMINATE MOST MAINTAINABILITY ISSUES. REPAIR CAN BE EASILY DONE AT THE FIELD LEVEL.
GEODESIC FUSELAGE	4	CREATES REPAIR PROBLEMS THAT CANNOT BE SATISFIED WITHOUT MAJOR RECONSTRUCTION OF LARGE AREAS. REQUIRES EXCESSIVE SPARE /REPAIR PARTS INVENTORY.
STIFFENED SHELL FUSELAGE	6	REPAIR PROBLEMS IN TRANSFERING LOAD ACROSS DAMAGED AREA.

APPENDIX

CONCEPT	PRODUCIBILITY	RATIONALE
MODULAR WING	3	RIB CAP CONFIGURATION DIFFICULT TO FABRICATE AND EXPENSIVE. NO PROVISION FOR TOLERANCE FLOAT. LIMITED ACCESS FOR INTERNAL FAST.
RTM WING	6	THIS CONCEPT IS HIGH RISK, BUT HAS HIGH PAY-OFF. ALSO, HAS SAME ACCESS PROBLEMS AS THE MODULAR DESIGN.
ATP WING	6	CONCEPT HAS LESS RISK THAN RTM DESIGN, AND ALSO LESS PAY-OFF. SAME ACCESS PROBLEMS AS OTHER WING CONCEPTS.
SANDWICH FUSELAGE	3	TOO MANY PIECES. THE LENGTH AND SMALL CROSS SECTION OF THE TRIANGLES MAKE MANDREL REMOVAL DIFFICULT. INSPECTION OF BONDED ASSEMBLY PRESENTS PROBLEMS.
GEODESIC FUSELAGE	3	TOO MANY PARTS. JUNCTION CLIPS VERY DIFFICULT TO FAB WITH CONTINUOUS FIBER COMPOSITES. VERY COMPLEX TOOLING, MANY PARTS.
STIFFENED SHELL FUSELAGE	8	ALL PROCESSES ARE AUTOMATED INCLUDING RTM, PULTRUSION AND FILAMENT WINDING.

CONCEPT	DURABILITY / DAMAGE TOLERANCE	RATIONALE
MODULAR WING	3	CONCERN IS THAT IMPACT DAMAGE WILL CAUSE STIFFENER TO PULL AWAY FROM SKIN DRASTICALLY REDUCING MECHANICAL PROPERTIES.
RTM WING	7	THROUGH THE THICKNESS REINFORCEMENT SHOULD PREVENT STIFFENER UNBOND AND MINIMIZE IMPACT DAMAGE. LOWER FIBER VOLUME IS STILL A CONCERN, AS IT WOULD REDUCE STRUCTURAL INTEGRITY.
ATP WING	5	THIS IS TYPICAL OF CURRENT STRUCTURES.
SANDWICH FUSELAGE	3	THINNESS OF FACINGS IS A DURABILITY CONCERN. IMPACT COULD CAUSE SEPERATION OF TRIANGULAR TUBES OVER A LARGE REGION. THIS COULD REDUCE RESIDUAL PROPERTIES.
GEODESIC FUSELAGE	9	THIS CONFIGURATION IS HIGHLY REDUNDANT AND SHOULD HAVE OUT-STANDING DURABILITY AND DAMAGE TOLERANCE. HOWEVER, THERE IS A HIGH RISK OF CRITICAL MANUFACTURING FLAWS IN THE DIAGONAL CROSS-OVERS.
STIFFENED SHELL FUSELAGE	6	CONSIDERED SLIGHTLY BETTER THAN CURRENT STRUCTURES BECAUSE OF THE ELIMINATION OF FASTENERS AND HOLES.

APPENDIX

CONCEPT	TECHNOLOGY ADVANCEMENT		PRODUCIBILITY	DAMAGE TOL/ DURABILITY	INSPECTABILITY	MAINTAINABILITY/ REPAIR	TOTAL	SCORE
	DESIGN	MFG						
MODULAR WING	4	3	3	3	6	6	25	12.5
RTM WING	5	9	6	7	8	6	41	20.5
ATP WING	5	7	6	5	6	7	36	18.0
SANDWICH FUSELAGE	8	7	3	3	5	8	34	17.0
GEODESIC FUSELAGE	6	7	3	9	2	4	31	15.5
STIFFENED SHELL FUSELAGE	4	3	8	6	8	6	35	17.5

Page intentionally left blank

COMPOSITES TECHNOLOGY FOR TRANSPORT PRIMARY STRUCTURE

VICTOR CHEN, ARTHUR HAWLEY,
MAX KLOTZSCHE, ALAN MARKUS,
RAY PALMER
DOUGLAS AIRCRAFT COMPANY

The ACT contract activity being performed by the McDonnell Douglas Corporation is divided into two separate activities: one effort by Douglas Aircraft in Long Beach, California with a focus on Transport Primary Wing and Fuselage Structure, and the other effort by McDonnell Aircraft in St. Louis, Missouri with a focus on Advanced Combat Aircraft Center Wing-Fuselage Structure. This presentation is on the Douglas Aircraft Transport Structure portion of the ACT program called ICAPS - Innovative Composite Aircraft Primary Structure. The McDonnell Aircraft portion of the ACT program will be presented by Mike Renieri in a presentation scheduled for tomorrow.

COMPOSITE APPLICATION GOALS

The Douglas Aircraft Company has a goal to have the wing technology readiness in hand in early 1993. It is anticipated that both a military and a civil application that require start of engineering development will occur during that year. Plans to initiate specific development design and tests have been identified.

The goal for a pressurized fuselage is to have the technology readiness in hand in early 1994 so that the preliminary designs can be finalized and start of engineering development can occur in early 1995. Douglas has targeted a specific vehicle, the MD-XX, to incorporate this technology.

START ENGINEERING DEVELOPMENT OF A WING BOX ON A SHORT-HAUL TRANSPORT IN 1993

START ENGINEERING DEVELOPMENT OF A PRESSURIZED FUSELAGE IN 1995

OBJECTIVE

There are several specific objectives in this program as well as the Douglas funded effort. First and foremost is cost savings. In the ACT May 1989 kickoff review meeting at NASA Langley Research Center, we had one chart on key barriers - one of which was "COST." We have attacked the major cost drivers as well as almost all of the other cost areas.

The weight savings on individual parts can be as much as 50% compared to metal, but on an overall assembly for primary structure the specific objective is to exceed 30%.

For a production program the objective is to have Development (non-recurring) and Production (recurring) costs to be equivalent to a metal system. This has been demonstrated on a few secondary composite structures already.

To achieve the weight savings we have to have a high strength after impact damage. Today to get that value we use toughened resin/high strength fibers which cost much more than the currently used material systems in secondary structures. Our objective is to use material systems that are less costly than today's, yet end up with a component that has high strength after damage as well as better tolerance to all types of impact.

**COST SAVINGS OF 40% FROM STATE-OF-THE-ART
COMPOSITES**

**WEIGHT SAVINGS OF 30% OF METAL ON ASSEMBLED
STRUCTURE**

**DEVELOPMENT AND PRODUCTION COSTS EQUIVALENT
TO METAL SYSTEM**

**DAMAGE TOLERANCE EQUIVALENT TO TOUGHENED
RESIN/HIGH-STRENGTH FIBER MATERIAL SYSTEMS**

**ABILITY TO ANALYTICALLY PREDICT STRUCTURAL
BEHAVIOR AND FAILURE**

OVERALL FOCUS OF ICAPS

Evaluation in the mid-80's indicated that to make a cost breakthrough, a deviation from the current trend of fabrication had to be made. Douglas focused on the dry preform resin transfer concept. From early testing it was evident that a considerable improvement in the damage tolerance could be obtained, equivalent to the toughened resin high strength fiber prepregs just reaching the marketplace. These new systems were also higher in cost. The preliminary stitched preform concepts were sponsored by Douglas and were further evaluated under NASA contract in the late 80's to broaden the understanding. With the advent of the ACT program it was an opportunity to develop a more comprehensive evaluation program. While Douglas funds were developing the wing section using the new toughened resins, the NASA ICAPS program focused on the dry stitched preform concept. The stitching parameter development will be explained in the later presentation by Marvin Dow of NASA. All current stitching work is being accomplished by our old (but modified) Douglas sewing machine. A more versatile machine was needed to evaluate the speed-up of the stitching concept. After numerous equipment developer visits, a general specification was developed and the solicitation, proposal evaluation, and source selection process was accomplished. Several new resins are being evaluated that are more suitable for the RTM (pressure and/or vacuum) process. Tools for each process are fabricated for the subcomponent and testing is in progress. As test results are analyzed, the design/prediction methods are further evaluated. As the larger components are made, the cost projection analysis will be re-evaluated.

SIMPLE DESIGN

- ACCOMMODATES FABRICATION, INSPECTION, AND REPAIR

UNIQUE COMPOSITE MATERIAL

- STITCHED FABRIC PREFORMS AND RESIN TRANSFER MOLDING

PROCESSES AND TOOLING

- RTM AND ATP WITH POTENTIAL FOR USE ON LARGE INTEGRATED STRUCTURES

DEVELOPMENT TESTING

- DESIGN VALIDATION AND PERFORMANCE PREDICTION DATA

STRUCTURAL MECHANICS

- ENGINEERING FOUNDATION FOR FUTURE DESIGNS, PERFORMANCE PREDICTIONS, AND CERTIFICATION

PRIOR TO ACT PROGRAM

The selected baseline transport configuration used for the advanced technology related to subsonic transports in 1984 were the D3300 configuration for the wing and the MD-100 for the fuselage. The specific features addressed on the wing and fuselage would be utilized in a next generation new transport that would utilize organic composite structures. The composite joints and cutouts program under NASA contract used loads and design criteria from these baseline aircraft. These development contracts were awarded after the ACEE program and preceded the ACT program.

BASELINE STUDIES

- **ADVANCED DESIGN HIGH-ASPECT-RATIO WING**
- **DOUGLAS DEVELOPMENT PROGRAM**

BASELINE DESIGN

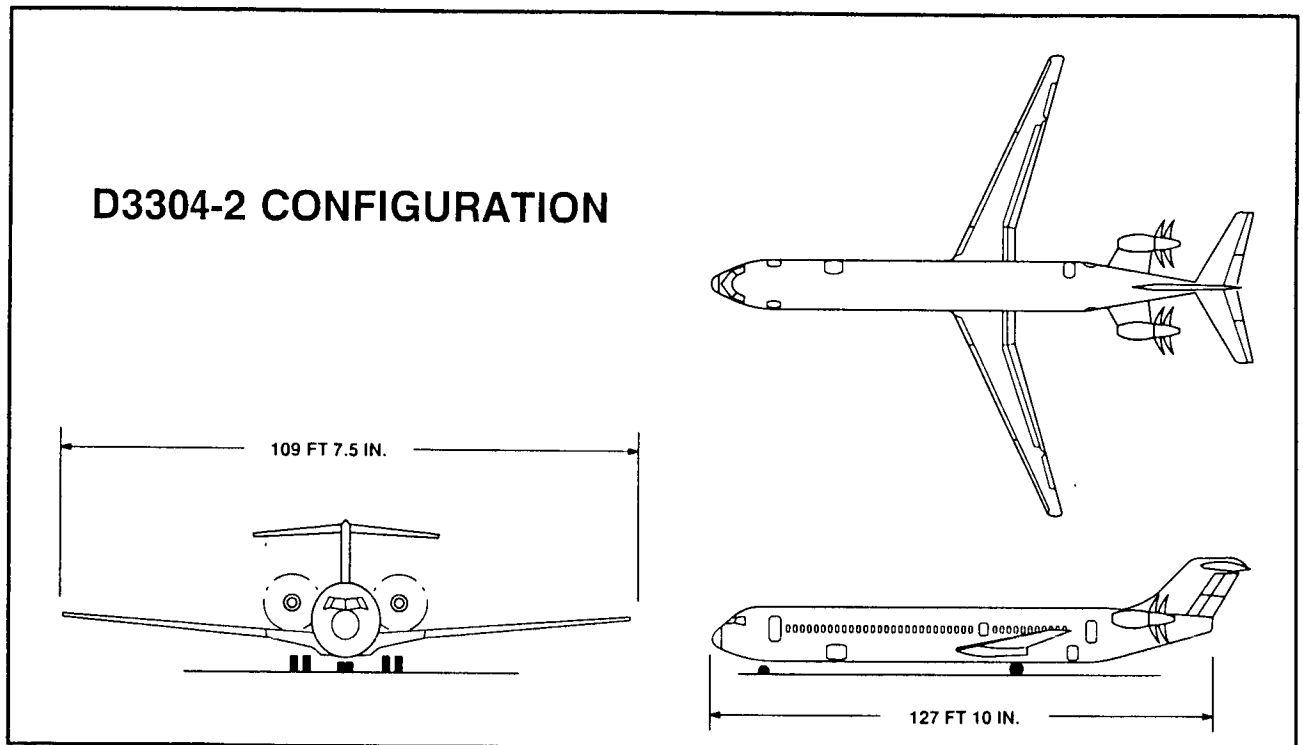
- **LOW STRAIN CONCEPT**
- **BLADE-STIFFENED WING/J-STIFFENED FUSELAGE**
- **FEATURES**
 - **SKIN, BLADE LAYUP PATTERN IDENTICAL**
 - **REPAIRABLE**
- **DOUGLAS TOUGHENED RESIN WING BOX PROGRAM**

DEVELOPMENT

- **NASA JOINT AND CUTOUT CONTRACTS**
- **NASA PANEL FABRICATION CONTRACT**
- **DOUGLAS COMPONENT DEVELOPMENT**

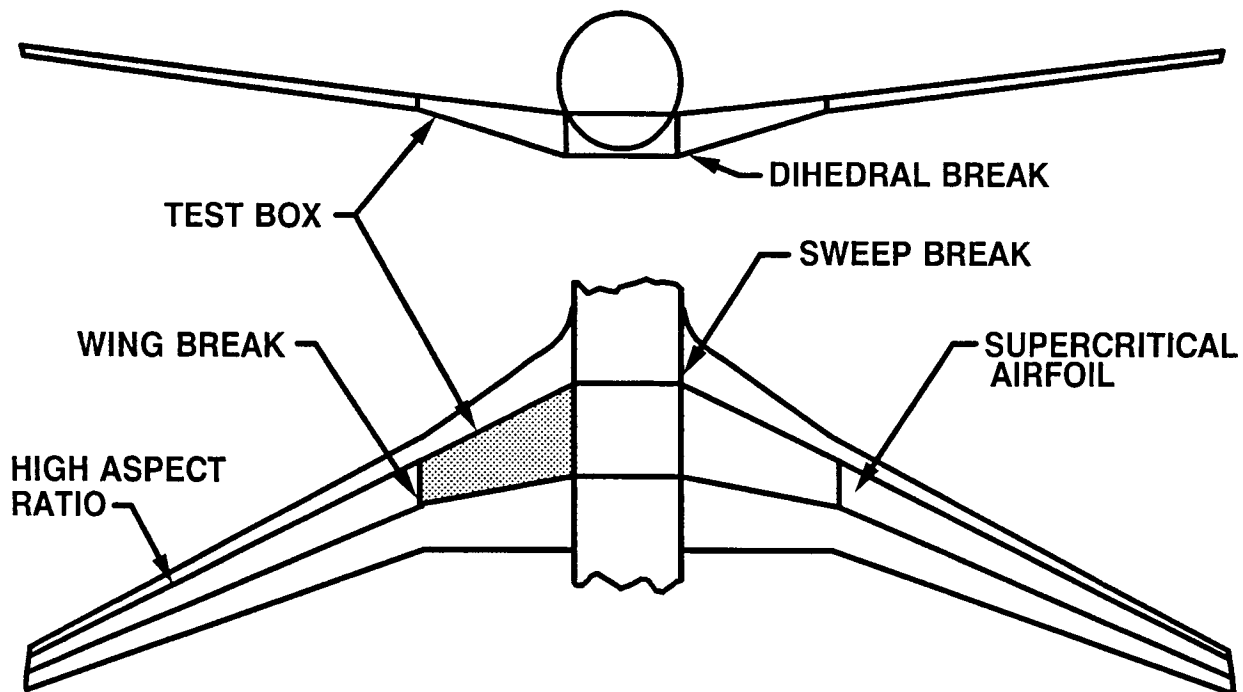
WING BASELINE AIRCRAFT

The D3300 configuration was an intermediate range 200-passenger aircraft for which detailed wing loading and configuration data was generated. Today the Douglas Operating Plan refers to this aircraft as the MD-XX and is focusing on very high bypass ducted fan engines, but an unducted counter rotating system could still be a consideration.



BASELINE WING TEST BOX RELATIONSHIP

The test units for both Douglas and ICAPS Program is identified on the baseline wing plan form. The section is at the side of the body to the wing aerobreak, which is approximately twelve feet. For the baseline wing configuration used in this program the test units are full scale.



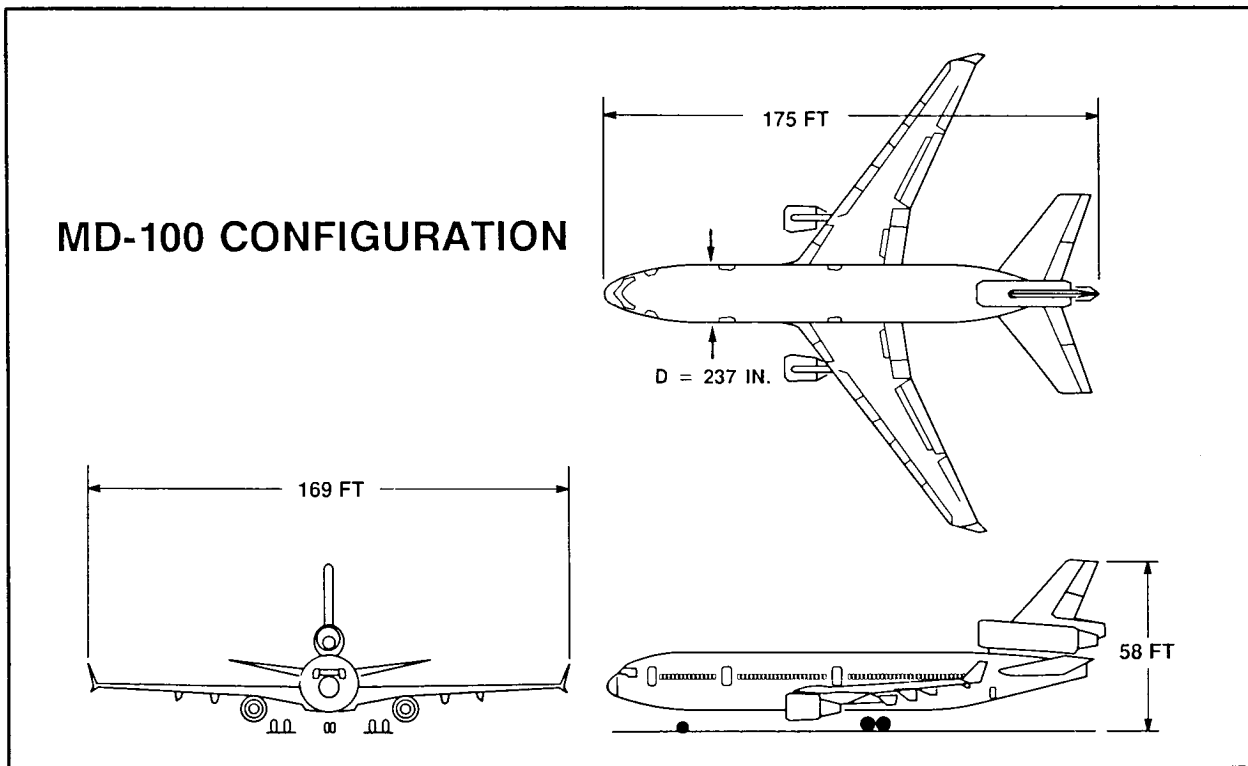
WING DESIGN CRITERIA

Wing loads and criteria are summarized. Shear and bending loadings are a maximum at the aerobreak station (outboard end of the test box) rather than at the root. This is because, even though root shear and bending moments are higher, this is offset by the much greater box dimensions at the root station. The design fuel pressures derive from the 9g crash condition. Minimum flexural and torsional stiffnesses are those required to meet dynamics and aileron effectiveness requirements.

COVER PANELS - MAXIMUM SPANWISE LOADING	N _x LB/IN. ULTIMATE [AVERAGED ACROSS BOX]	TENSION	23,200
		COMPRESSION	23,600
SPARS - MAXIMUM SHEAR FLOW	N _{xy} LB/IN. ULTIMATE [AVERAGED OVER SPAR DEPTH]		3,700
REQUIRED FLEXURAL STIFFNESS (ROOT)	(EI) 10 ⁶ LB/IN. ²		261,300
REQUIRED SHEAR STIFFNESS (ROOT)	(GK) 10 ⁶ LB/IN. ²		137,500
MAXIMUM FUEL PRESSURE	LB/IN. ² ULTIMATE	INNER WING	36.2
		OUTER WING	46.7

FUSELAGE BASELINE AIRCRAFT

The MD-100 configuration was a pre MD-11 configuration on which advanced structural configuration changes were evaluated. The NASA contract on fuselage cutouts and joints for composite structures used loads from this preliminary design. A considerable number of composite structural configurations were evaluated and the "J" stiffened panel was selected.



FUSELAGE DESIGN CRITERIA

The fuselage loadings given represent maximum forward fuselage conditions that occur at the front spar station. Hoop loading due to internal pressure differential are based on the 2.0 ultimate factor condition with no other loads present.

CONDITION		CROWN	SIDE	KEEL
MAXIMUM LONGITUDINAL TENSION LOADING	N_x LB/IN.	4,600	3,200	2,300
MAXIMUM LONGITUDINAL COMPRESSION LOADING	N_x LB/IN.	-1,700	-3,000	-2,100
MAXIMUM SHEAR FLOW	N_{xy} LB/IN.	800	1,500	1,000
MAXIMUM HOOP TENSION LOADING (PRESSURE = 9.1 PSI)	N_y LB/IN.	2,157 (AT 2p)		

ALL LOADS ARE ULTIMATE

EVOLUTION OF DESIGN STRAINS

The baseline composite wing is not based on a high strain concept since this is not an option because of stiffness and supportability constraints. A simple, easily producible and repairable design based on 4,000 strains was shown in an earlier NASA program to be weight-competitive on a damage tolerance basis with high strain concepts. Further reductions in design strain have been introduced to meet specific stiffness and repair criteria. The wing is designed to be repairable at any location by mechanically fastened patches.

HIGH STRAIN WING HAS HIGHER FABRICATION COMPLEXITY AND REPAIR LIMITATION

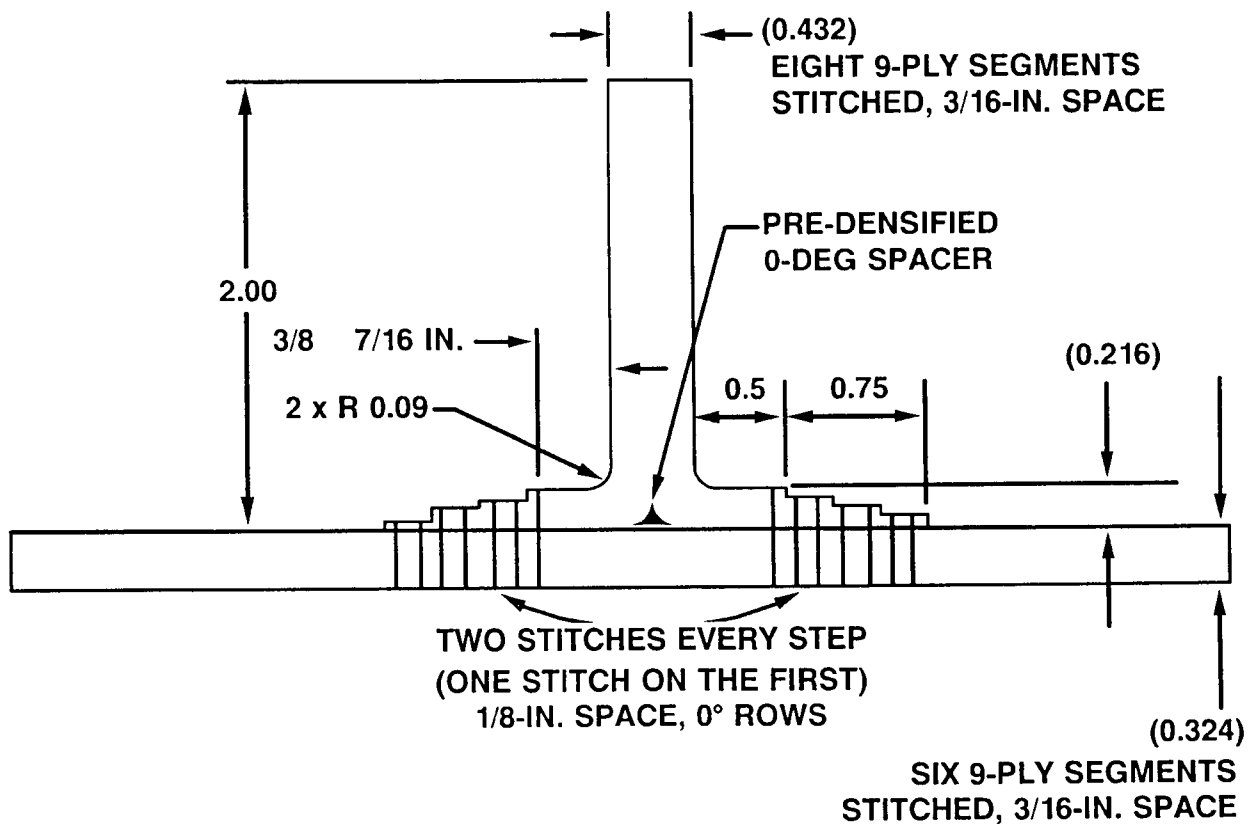
**SELECTED HARD SKIN DESIGN LIMITED TO 4,500 μ
STRAIN FOR DAMAGE TOLERANCE**

**STRAIN REDUCED IN PLACES TO 4,000 μ TO MEET
STIFFNESS TARGETS**

**STRAIN FURTHER REDUCED TO 3,750 μ TO ALLOW
BOLTED REPAIR PATCHES AT ANY LOCATION**

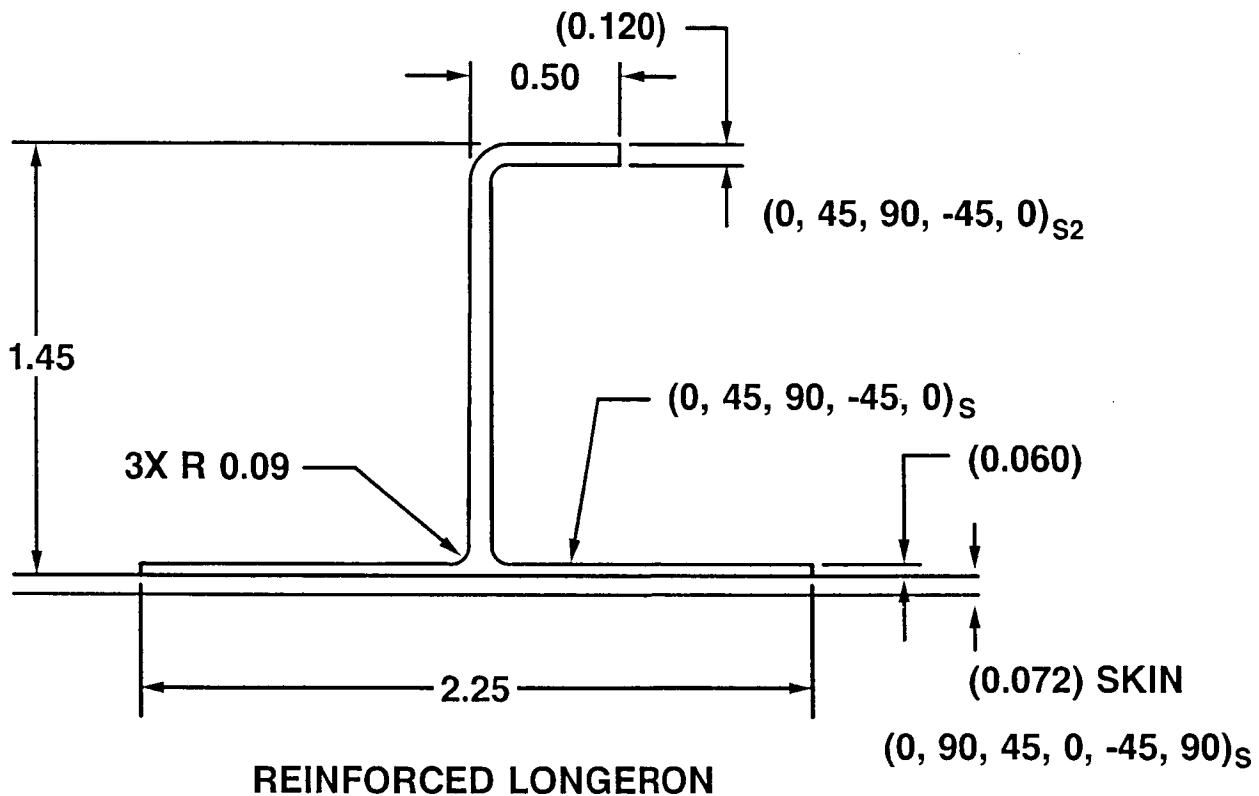
WING STIFFENER DESIGN

From the many studies and development tests performed, the stiffener selected for the wing design being considered is a basic stitched preform 9-ply balanced pattern arrangement from which stiffener and skin stacks are made. In the cross section shown, the vertical blade is stitched, the skin stack is stiffened, and then the blade flanges are stitched to the skin. It will be possible to do most of this automatically after discussion with equipment manufacturers.



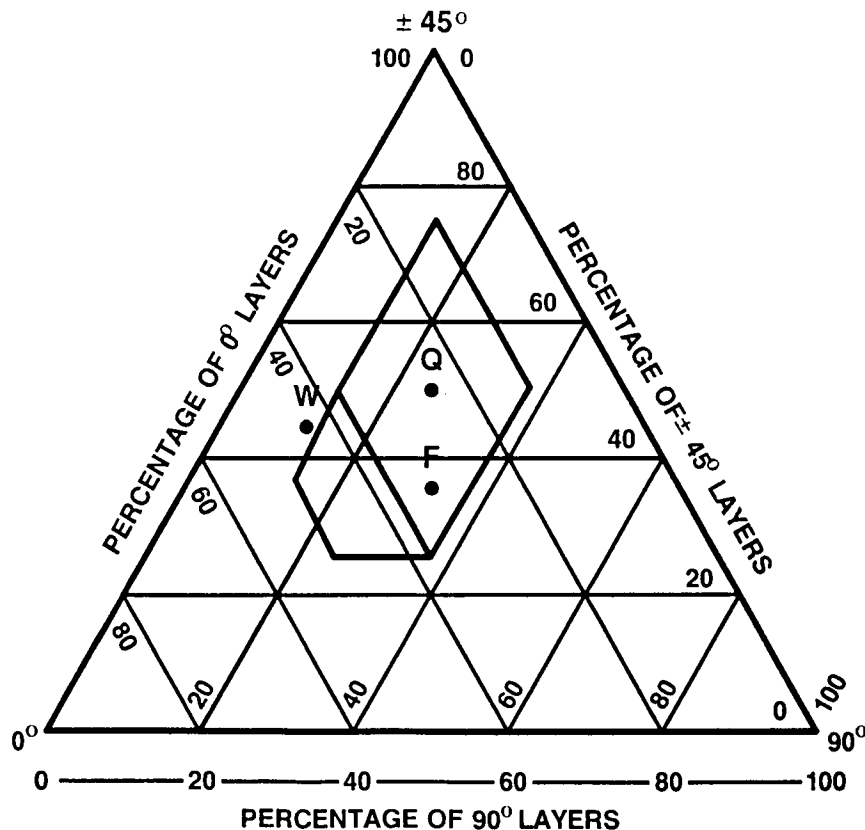
FUSELAGE STIFFENER DESIGN

From the many studies and development tests performed prior to the ACT program, the stiffener selected for the fuselage design is a "J" configuration. These stiffeners will be dry stitched in the vertical stem and "J" cap, and then stitched to the fuselage skin.



GUIDELINE FOR REPAIRABLE LAMINATES

A generalized design guideline in use for sometime at DAC constrains the percentage of fibers in each of the four directions (0, 90, +45, and -45) to fall between 12.5% and 37.5%. The fiber directions must be thoroughly interspersed to prevent the matrix from becoming the weak link in the laminate. These guidelines were set to allow good bolt load transfer behavior and did not necessarily apply to thin lightly loaded laminates or to laminates where no fasteners were required either in the original design or for repair. The chart extends the range slightly and permits, for example, the wing cover panels to increase the percentage of 0° fibers to 44.4%. This was desirable in meeting stiffness requirements.



COST DRIVERS

Since the early 1980's, Douglas has been focusing on the cost issue of composite components in three specific areas: non-recurring, recurring and ownership. During the 1970's, when we were making sizable components under the NASA sponsored Aircraft Energy Efficiency program, the initial focus was weight savings. Their weight savings goals were achieved, but at what price? When cost estimates were made for production, it was clear that something different had to be done in order to make the transition into production. For example, on the DC-10 rudder program, by a few internal system changes, tool variations the projected recurring costs could be reduced by 30%. The major drivers are shown in the following charts.

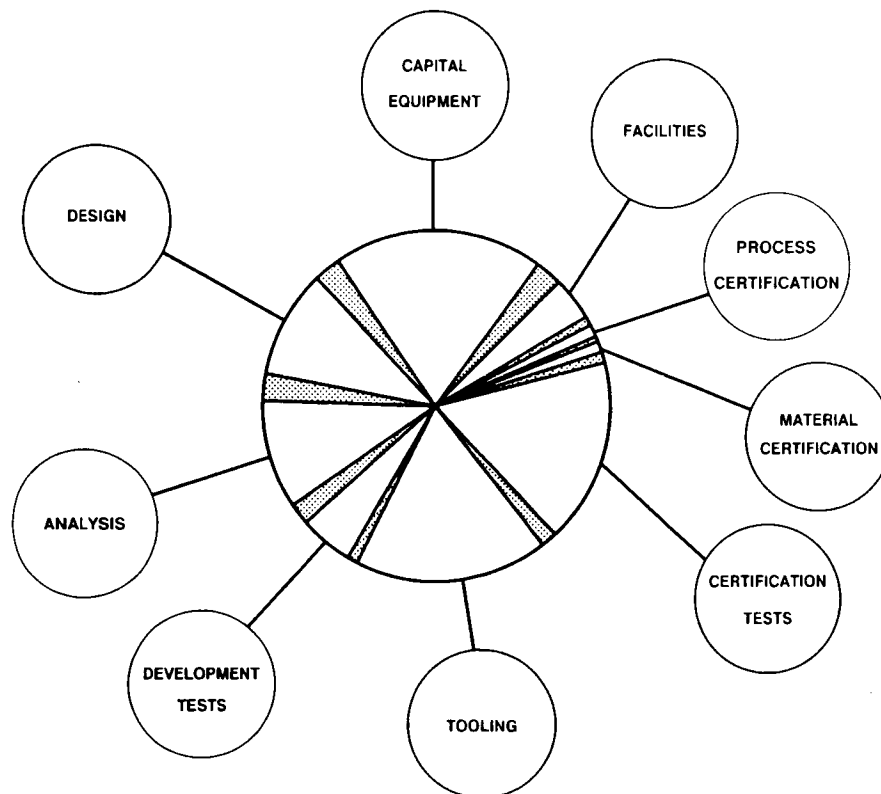
NONRECURRING

RECURRING

OWNERSHIP

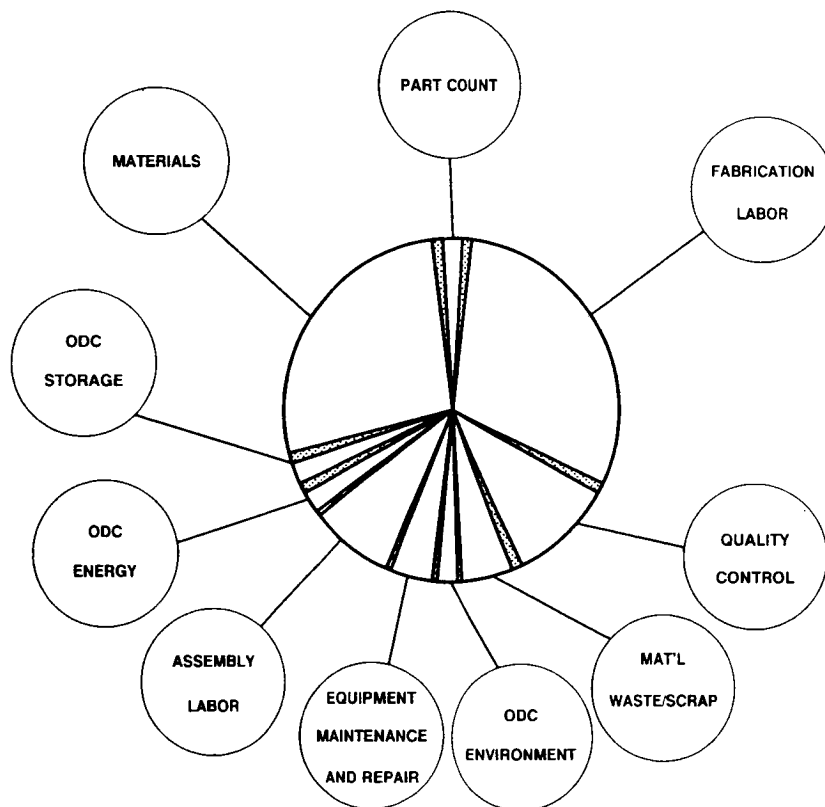
COST DRIVERS - NON-RECURRING

For non-recurring costs, an investigation was made to determine the percentage range of the various items that make up the total cost to focus on, which were the major contributors. The background data was from a number of programs and a range of parts from small to full assemblies. Both commercial and military components were included. Large percentage variables were identified in tooling and capital equipment. Tooling related to the complexity of the part being considered and the capital equipment variable depended on how the cost was distributed to various programs or how many units were to be considered in the spread. In the ICAPS effort, heavy emphasis will be focused on simplified design to reduce tooling costs and define the fabrication process to not require high cost equipment items.



COST DRIVERS - RECURRING

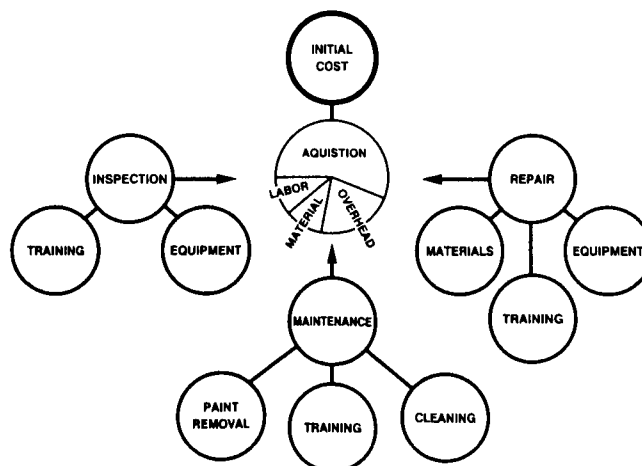
For recurring costs, the data show that there is a wide percentage range for the various elements from different data sources. It's clear that materials, fabrication, assembly, and quality control are the major cost drivers. On very small parts, the material cost is a high percentage in making the part. On a composite component made up of several parts, the material cost percentage is much lower. For ICAPS, the four major percentage areas are the ones on which the major focus is being addressed with significant reductions anticipated with the concept approach being taken. A majority of the other cost items will be reduced to some extent. As larger elements and subcomponents are fabricated, a specific set of percentages can be verified, and a cost relationship figure can be generated and compared to the state-of-the-art fabrication of the same component.



COST DRIVERS - OWNERSHIP

Although we have some carbon epoxy components flying on the DC-10 since June of 1976 and have accumulated over 55,000 hours on the high time units, we do not have a sufficient experience sample to draw specific conclusions at this time. Where we look at a transport that will have 40 or more years of service it's difficult to relate the inspection, maintenance, and repair history of only a few years.

In DOC data used by airlines, the cost of ownership in today's environment is approximately 50%. In ICAPS the major thrust is to develop the concept that would offer a 50% reduction in the cost of ownership for the composite components. As the percentage of composites increases, of the total operating weight empty there would be a significant effect to the operator DOC relationship. In the airlines DOC maintenance element, the structure represents half of this value utilizing composites that virtually eliminate corrosion and have a significant reduction in fatigue, there would be a further cost savings impact to the operator. On this figure we represent ownership as half and maintenance as the other half with regard to structure, and until we have more time to work with operators to develop cost impact trends, we will not connect the outside element to an operator cost pie chart.



SPECIFIC FOCUS OF ICAPS

This listing is what ICAPS is accomplishing to reduce the high cost drivers. A number of key parameters with respect to stitching have been investigated to optimize the process versus structural capability of the structure. Two new machines are being procured: one that will handle large widths for several processes and a computer controlled unit that will handle stiffener to skin stitching. The fabrication investigation covers two types of tools for RTM (resin transfer molding) in terms of vacuum or pressure impregnation. To compare processes for the fuselage, the Hercules advanced automated tow placement is being evaluated. New resins formulated for RTM are also being used. Of the thousand specimens tested, the data are being used for stitching parameter determination and structural mechanics methods improvement. As the larger components are fabricated, the cost data will be used to update the predictions that have been made to date. Each of these subjects is covered in further detail.

STITCHING DEVELOPMENT

STITCHING MACHINE PROCUREMENT

FABRICATION PROCESS TOOLS DEVELOPMENT AND RESINS

SUBCOMPONENT/COMPONENT TESTING

STRUCTURAL MECHANICS

COST DATA PROJECTIONS

POTENTIAL FOR STITCHING/RTM

Stitching has for a long time been considered to improve the through the thickness properties of laminated structure. When used with prepreg there was extensive fiber damage. The parts looked good, but the structural capabilities were degraded. With the development of unidirectional cloth with straight fibers, the probability of ply stacking and stitching was investigated. Structural testing showed substantial increase in damage tolerance capability with high residual strength approaching that of the toughened resins with high strength fibers.

Evaluations show that cost reductions could occur in many areas. Some are significant, others are not cost drivers but relate to facility requirements. As the design concepts were formulated, additional benefits were identified; i.e. near net shape stitched preforms, self-contained tool for RTM and cure, etc. With large high speed stitching equipment, scale-up to large aircraft structures is possible.

LARGE DAMAGE TOLERANCE INCREASE

LOW MATERIAL COST

LOW RECEIVING INSPECTION COST

LOW STORAGE COST

LITTLE AGING CONCERN

AUTOMATED NEAR NET SHAPE PREFORM

SELF-CONTAINED TOOL

LOW WORKPLACE ENVIRONMENTAL IMPACT

OPTIONAL FIBER PLY ORIENTATION

SCALE-UP CAPABILITY TO VERY LARGE STRUCTURE

STITCHING DEVELOPMENT

This is a listing of the various parameters that were considered and evaluated, and explained later as previously noted.

STITCH TYPE

- LOCK, CHAIN

STITCHING THREAD

- GLASS, KEVLAR

STITCHING PATTERN

- DENSITY AND DIRECTION

STITCHING TENSION

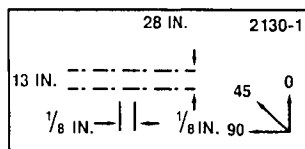
- NEAR NET SHAPE

COUPON/SPECIMEN TESTING

**FABRICATED 60 PANELS CUT INTO APPROXIMATELY
1,000 SPECIMENS FOR NASA TESTING**

STITCHING DEVELOPMENT TESTS

More than half of the tests planned in ICAPS are for stitching development. These are mostly done on quasi-isotropic laminates, which is close enough to practically used laminates in composition. One stitching parameter, whether stitch type, thread or pattern, is varied at a time. This slide shows the various stitch patterns chosen. Each panel was stitched accordingly, impregnated and cut into specimens. The goal of stitching development is to achieve the best balance of improved damage tolerance properties with minimum loss of basic tension, compression and stiffness properties.



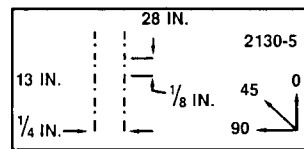
PANEL	SPACING	STEP	DIRECTION
-------	---------	------	-----------

2130-1	1/8 IN.	1/8 IN.	90
--------	---------	---------	----

2130-2	1/16 IN.	1/8 IN.	0
--------	----------	---------	---

2130-3	1/8 IN.	3/16 IN.	0
--------	---------	----------	---

2130-4	3/16 IN.	1/8 IN.	0
--------	----------	---------	---



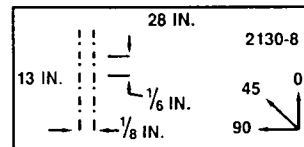
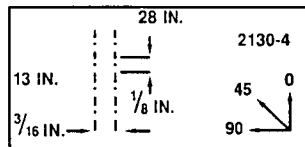
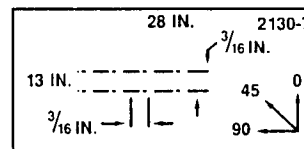
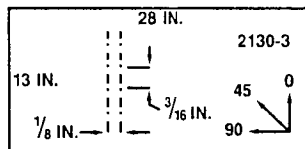
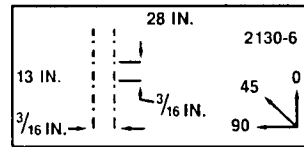
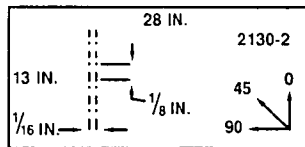
PANEL	SPACING	STEP	DIRECTION
-------	---------	------	-----------

2130-5	1/4 IN.	1/8 IN.	0
--------	---------	---------	---

2130-6	3/16 IN.	3/16 IN.	0
--------	----------	----------	---

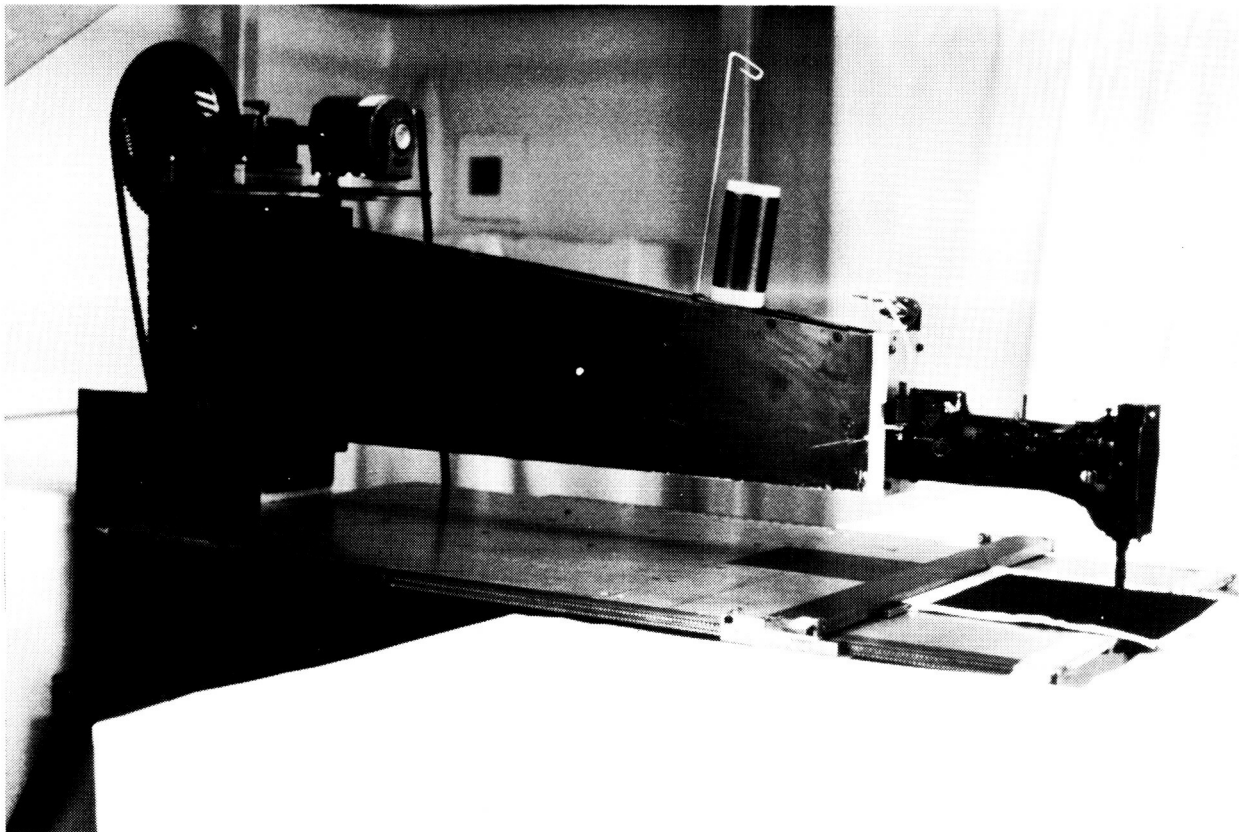
2130-7	3/16 IN.	3/16 IN.	90
--------	----------	----------	----

2130-8	1/8 IN.	1/6 IN.	0
--------	---------	---------	---



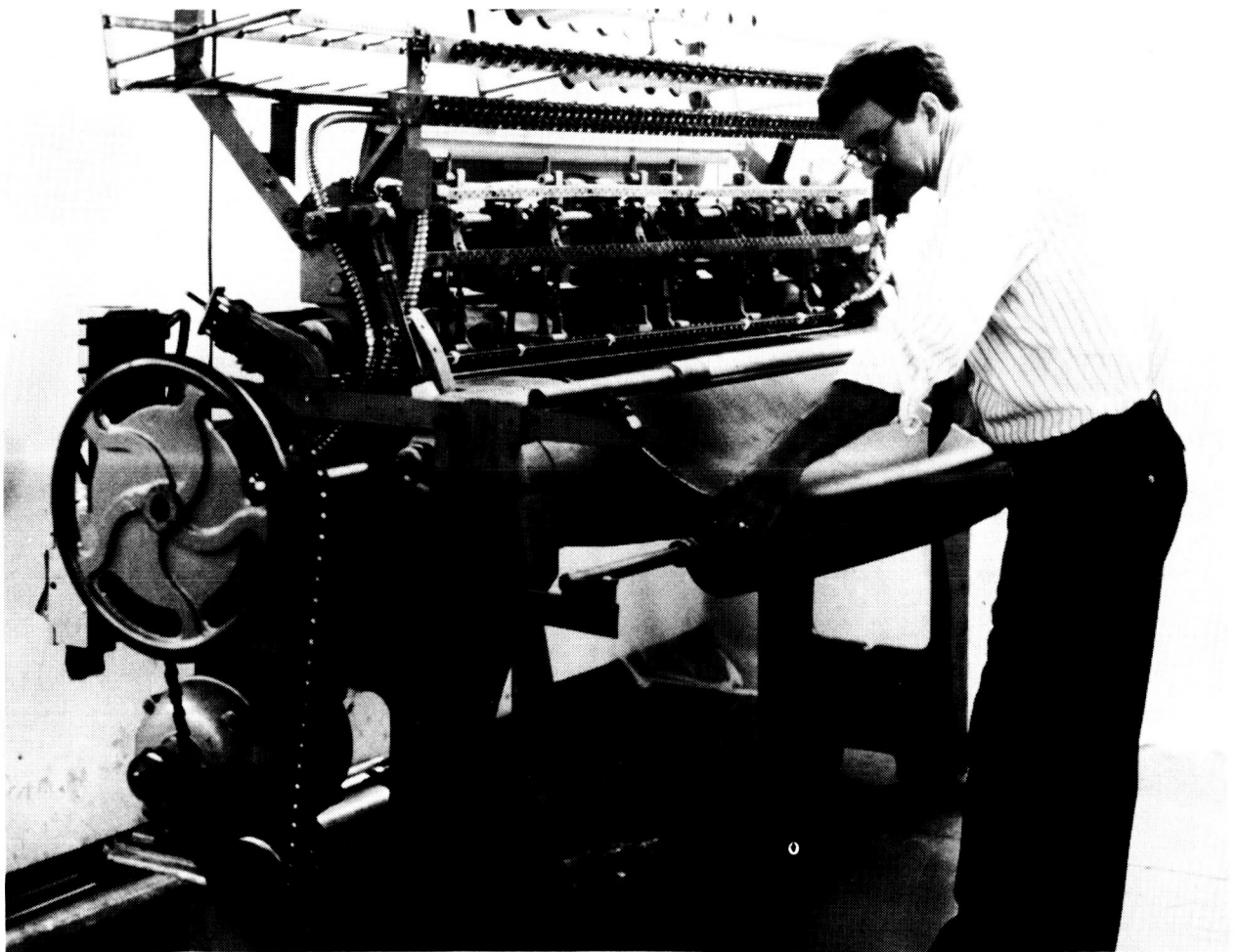
ORIGINAL SINGLE NEEDLE STITCHING MACHINE

All heavy density stitching development to this date has been on the manual control single needle 5' long arm machine shown in this photograph. Adjustment of stitch step and tension on the thread is available. The material to be stitched is secured in a holding frame and an adjustable guide rail controls the spacing of stitched rows. This machine is located at and operated by Ketema, Anaheim, California (formerly Textile Products, Inc.).



ORIGINAL MULTI-NEEDLE STITCHING MACHINE

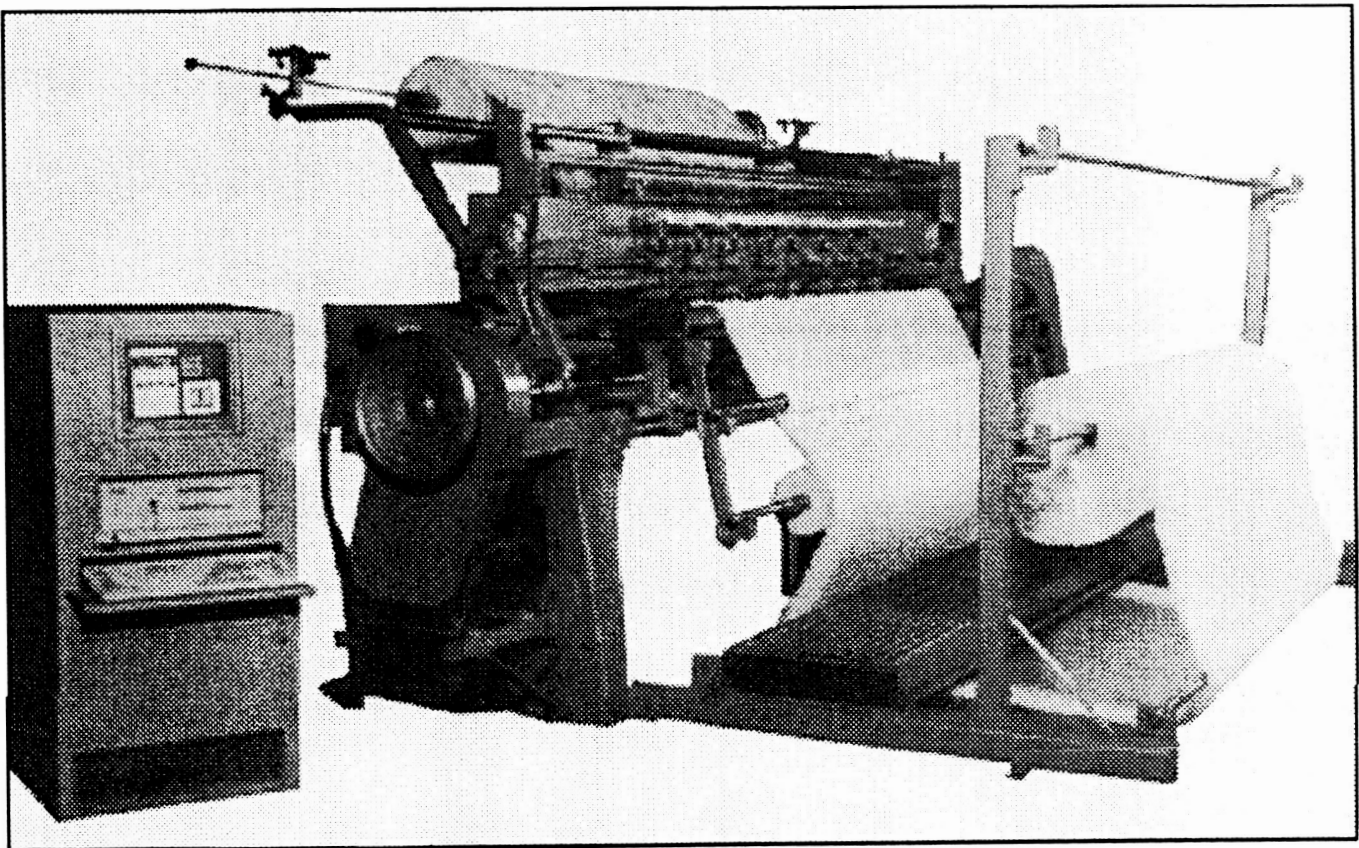
Light density stitching has been accomplished on this multi-needle machine at Ketema. The machine is 60" wide with 1" needle spacing and maximum thickness stitching of 10 layers of uniwoven fabric. The equipment does not have multi-feed rolls so individual layers of material were cut, stacked, and then passed through the machine.



NEW STITCHING MACHINE

The stitching machine selection for this program is a Pathe machine that is being modified to have up to twelve unidirectional roll feed to lightly stitch the fuselage skins and a more unidirectional roll feed to lightly stitch the wing preforms. The wing basic plies will be stacked and stitched together by the basic pattern selected. This machine is in the process of being checked out by stitching some of the subcomponent parts at the machine manufacturers.

PATHE MULTI-NEEDLE STITCHING MACHINE



BENEFITS OFFERED BY NEW STITCHING EQUIPMENT

The DAC ICAPS program features the automated stitching process to fabricate dry fiber near net shape stitched preforms. The development work completed to date to prove the structural benefits of the process (damage tolerance) has all been accomplished on a manual contour single needle long arm machine.

ICAPS will soon demonstrate the economic benefits of stitching that will become available with the new automated stitching equipment now being built for this project by Pathe.

This viewgraph shows

1. The description of the original machine, the computer control automated single needle machine, and the mechanical control multi-needle machines that are being purchased.
2. Identifies the assumed stitching speed for each machine. All machines are capable of operating at much higher rates. These rates are the assumed rates for a 1/4" thick preform and are conservative in all cases.
3. The estimated stitching efficiencies from observations on the original machine and from the experience of the automated machine builder.
4. Available penetration rate per minute is the assumed stitching rate times the efficiency factor times the number of needles.
5. The time to stitch one square foot with penetration density of 64 per square inch is the total penetrations per square inch ($64 \times 144 = 9216/\text{ft}^2$) divided by the penetrations per minute.
6. The time to stitch an 8'x12' uniform thickness panel is a multiple of step 5 above, times 96. Note that the current manual machine would require 24,576 minutes to stitch this skin where the new automated single needle machine would require 1248 minutes. This is a 95% reduction in time.

The multi-needle machine with 128 needles would require only 55 minutes to stitch this panel. This is a 95% reduction in time from the automated single needle machine.

The multi-needle machine with all 256 needles will require considerable testing before it can be considered for the application.

FABRICATION PROCESS FOR DEVELOPMENT AND RESINS

Two basic RTM processes and the automated tow placement process are being developed and demonstrated in the Douglas ICAPS program.

RTM

Vacuum impregnation and vacuum film infusion are being developed as a method of fabrication for the Douglas wing effort. This method of RTM utilizes either liquid or film resins depending on the resin processing characteristics and final mechanical properties.

Pressure impregnation is being developed to fabricate composite fuselage skins and longerons. This method of fabrication will rely entirely on liquid resin systems and in-tool curing techniques.

AUTOMATED TOW PLACEMENT

Finally, the automated tow placement process of Hercules is being demonstrated under subcontract to fabricate the same fuselage skin and longerons components being done under pressure RTM.

Completion of a subcomponent cost and performance evaluation (end of Phase A) will depict which process or combination of processes will be used for continued development in Phase B.

FABRICATION PROCESS AND TOOL EVALUATION

VACUUM IMPREGNATION

FILM INFUSION

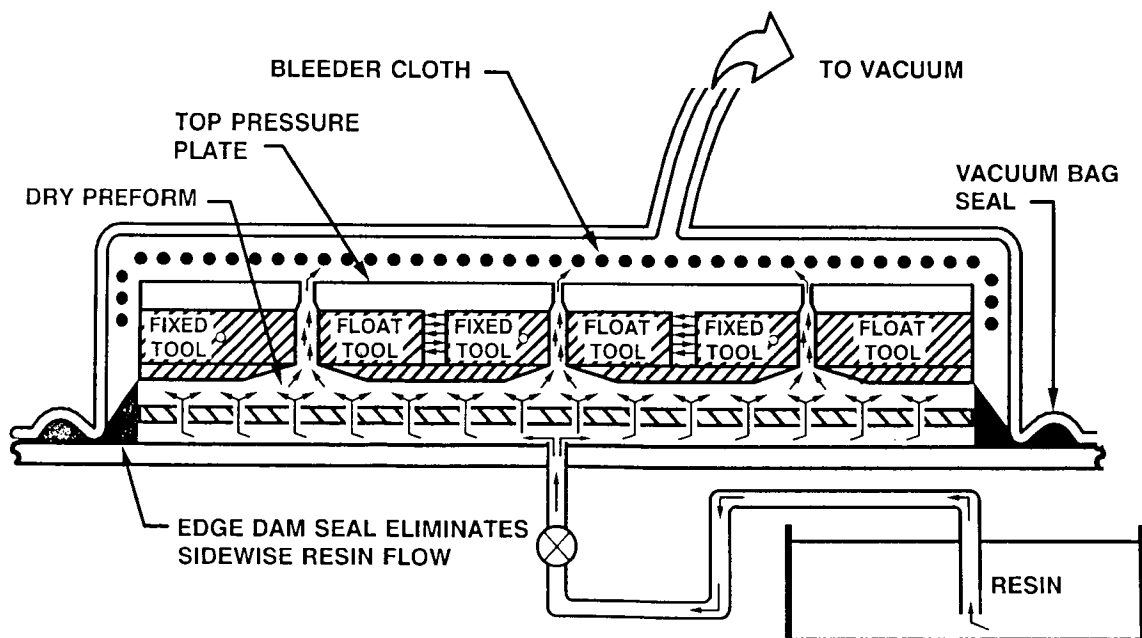
PRESSURE IMPREGNATION

AUTOMATED TOW PLACEMENT

VACUUM IMPREGNATION OF STIFFENED PANEL LIQUID RESIN INFUSION

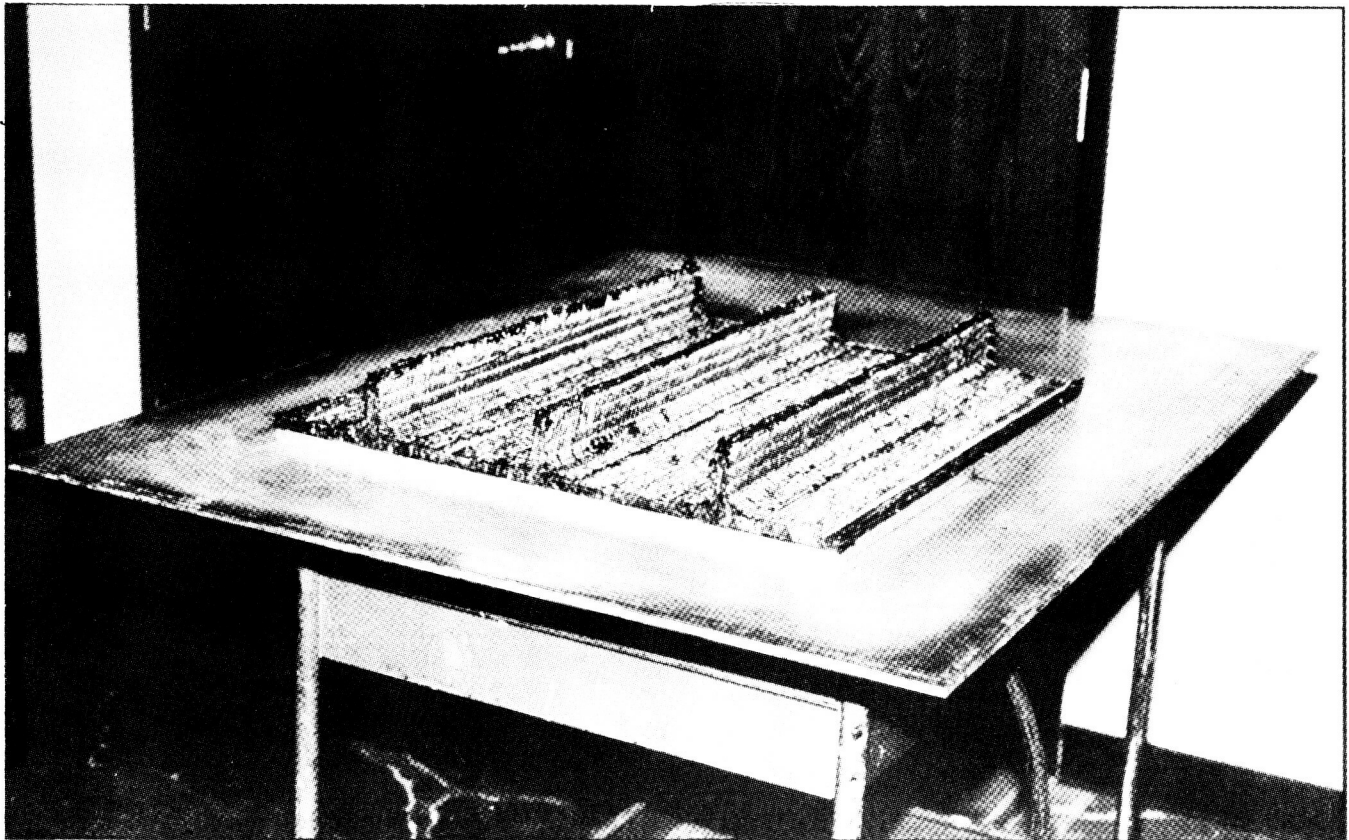
The complete process requires only vacuum source and either self heated tools or an oven.

Resin is mixed and degassed as required to remove trapped air. The tool is heated to desired temperature and vacuum is drawn on the system. The temperature varies for each resin system, for optimum impregnation and ranges from 150°F to 275°F. When the heat has stabilized, the valve is opened and the resin flows through the runners of a surface call plate, through holes in the runners that connect to the dry preform. The resin passes through the skin, up through the webs of the stiffeners, through holes in the upper pressure plate, and into the upper bleeder cloth. The temperature and resin gel time are coordinated so that the resin stops flowing and cures before it reaches the vacuum outlet line. Temperature may be raised, after resin gel, to a higher temperature to complete the cure cycle - all with only vacuum bag pressure.



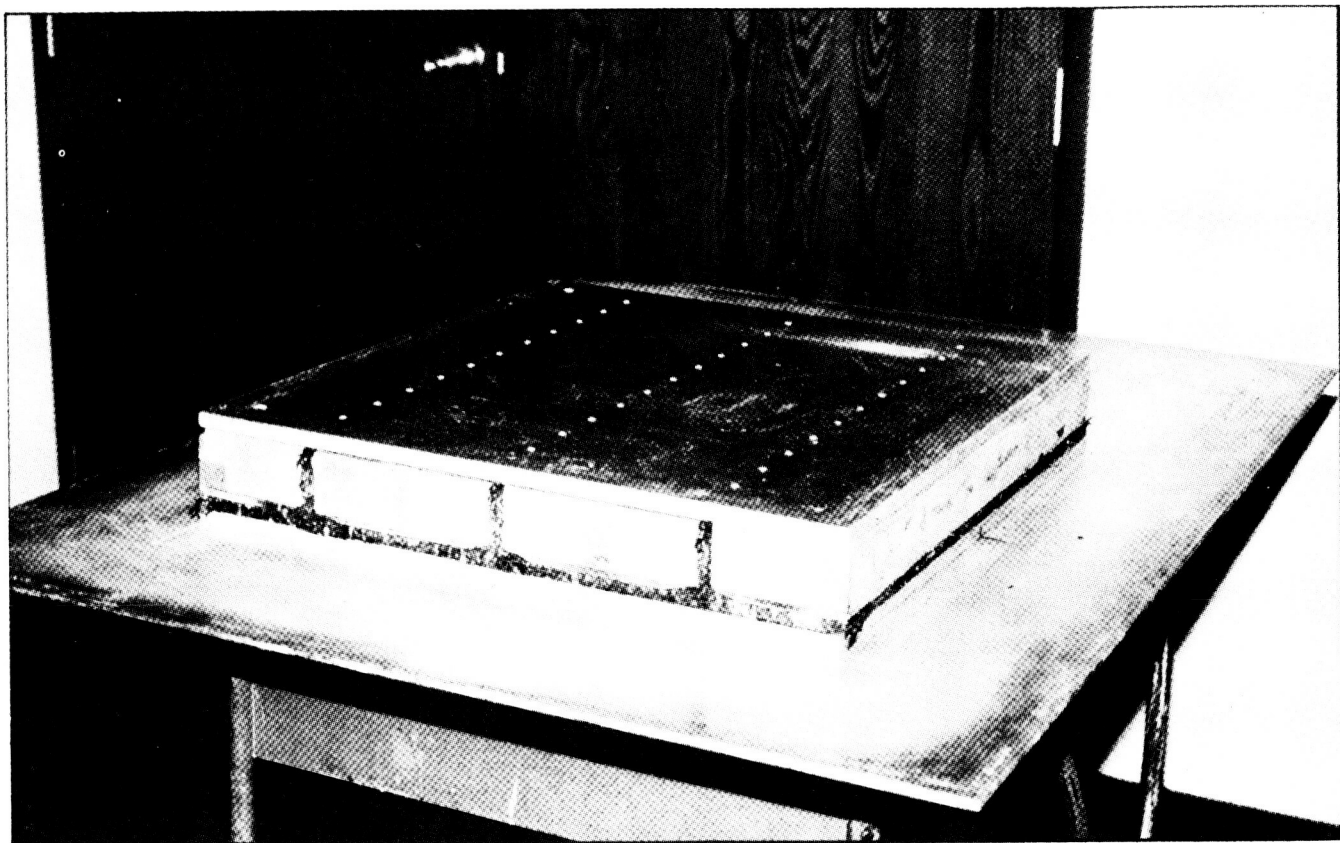
WING ELEMENT PREFORM

Douglas preforms are being developed with unidirectional graphite cloth being stitched into the three-dimensional shapes representing structural wing components. These structural shapes are then stitched directly to a stitched wing skin to give a complete wing skin assembly preform. This method of preforming has shown a great cost reduction in both layup and assembly of composite wing skins. Shown in this figure is a 3 blade stitched wing skin preform.



WING ELEMENT TOOLING VACUUM IMPREGNATION

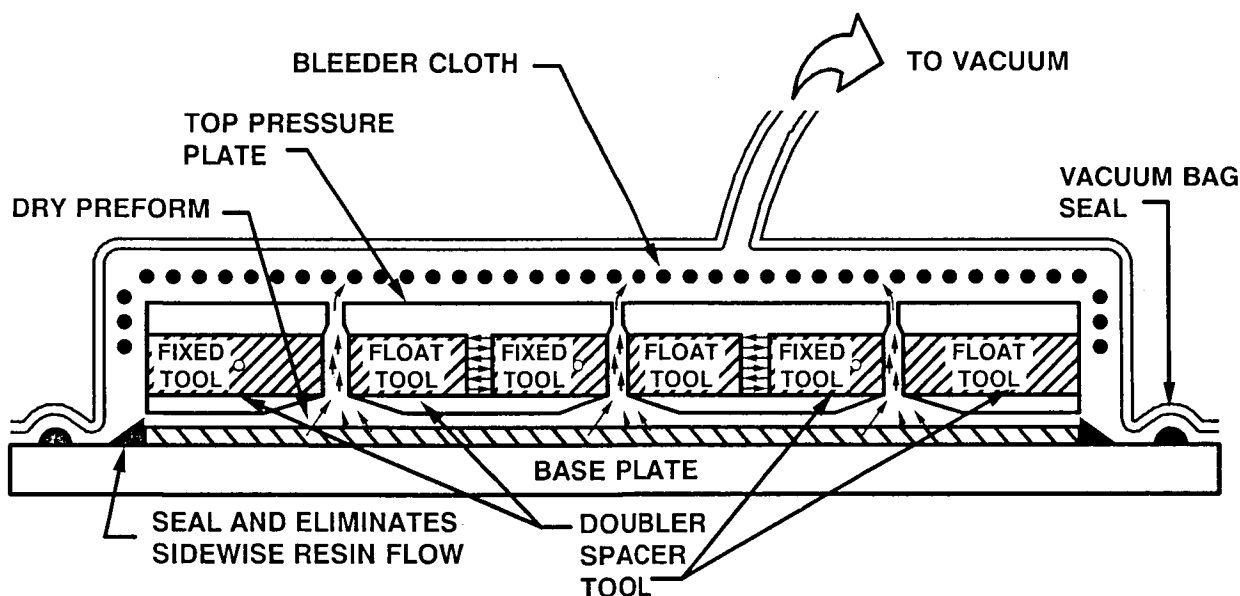
The tooling for vacuum impregnation of three blade stiffened wing elements consists of a set of machined aluminum blocks used to define the wing skin control with a set of matching flat tooling plates used to sandwich the preform/tooling blocks during impregnation. This entire assembly is then vacuum bagged while the resin is infused and cured in the preform.



RESIN FILM INFUSION OF STIFFENED PANEL

The complete process requires only vacuum source and either self heated tool or an oven.

Resin film of desired amount is placed on the surface of the tool. The dry preform is placed on the resin, the upper tools located in place, and enclosed in a vacuum bag. Heat is applied. The resin viscosity thins and the resin flows upward through the skin, the webs of the stiffeners, through the outlet holes in the upper pressure plate, and into the bleeder cloth where it gels. The amount of resin, the temperature, and the gel time are coordinated so that the resin will stop flowing and cure before it reaches the vacuum outlet line. Temperature may be raised after resin gels to a higher temperature to complete the cure cycle - all with only vacuum bag pressure.



NEW RESIN EVALUATION

In the continuing Douglas evaluation of new resin there were a considerable number investigated that were in liquid form suitable for the ICAPS program. From the past fifteen months, the selection was narrowed to three or four which are in the ICAPS specimen/coupon evaluation process. The objective is to narrow down to one or two for the component fabrication early next year.

DOW CHEMICAL CO.

TACTIX 695

SHELL CHEMICAL CO.

DRL 862

CIBA-GEIGY CO.

MATRIMID 5292 A/B (BMI)

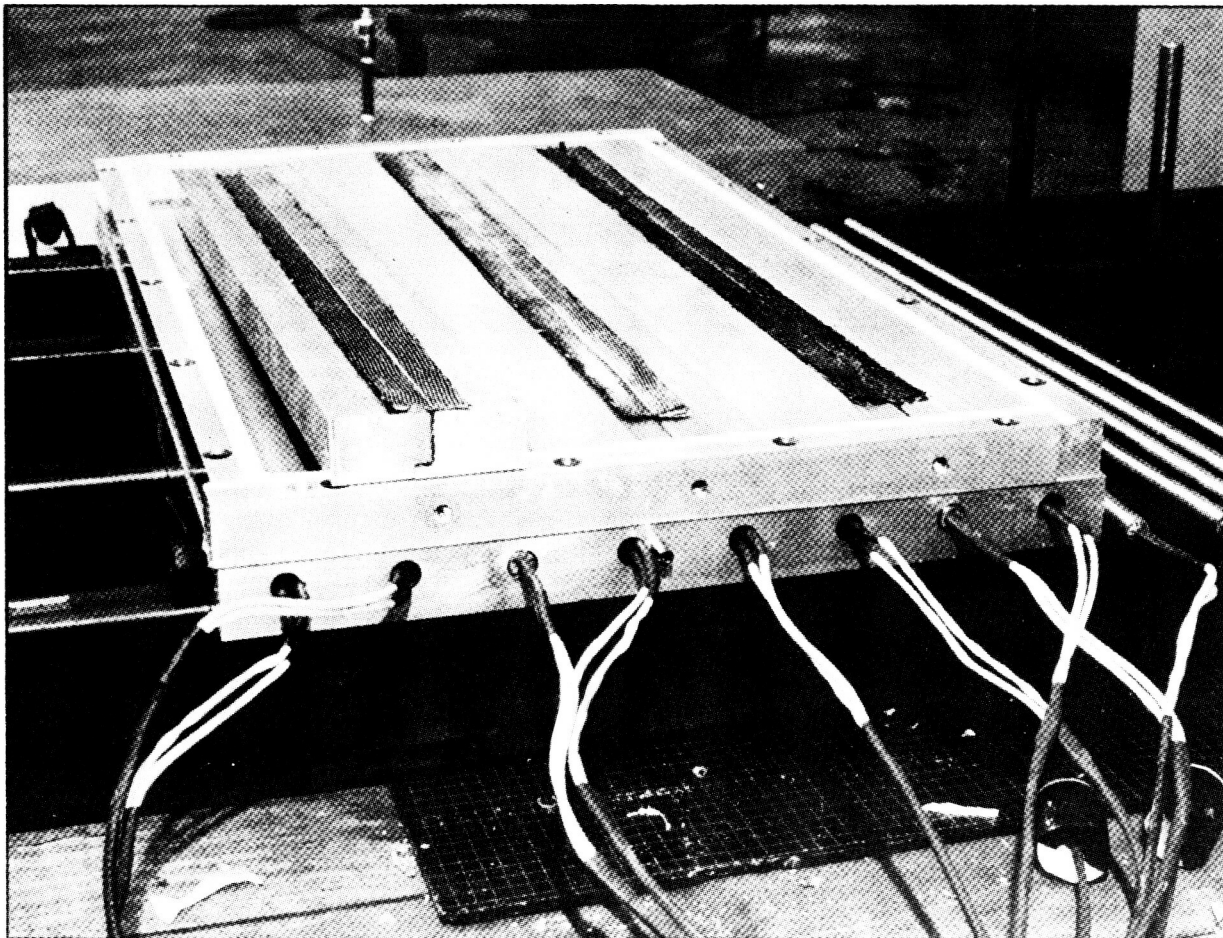
BRITISH PETROLEUM

E-905L

(OPEN)

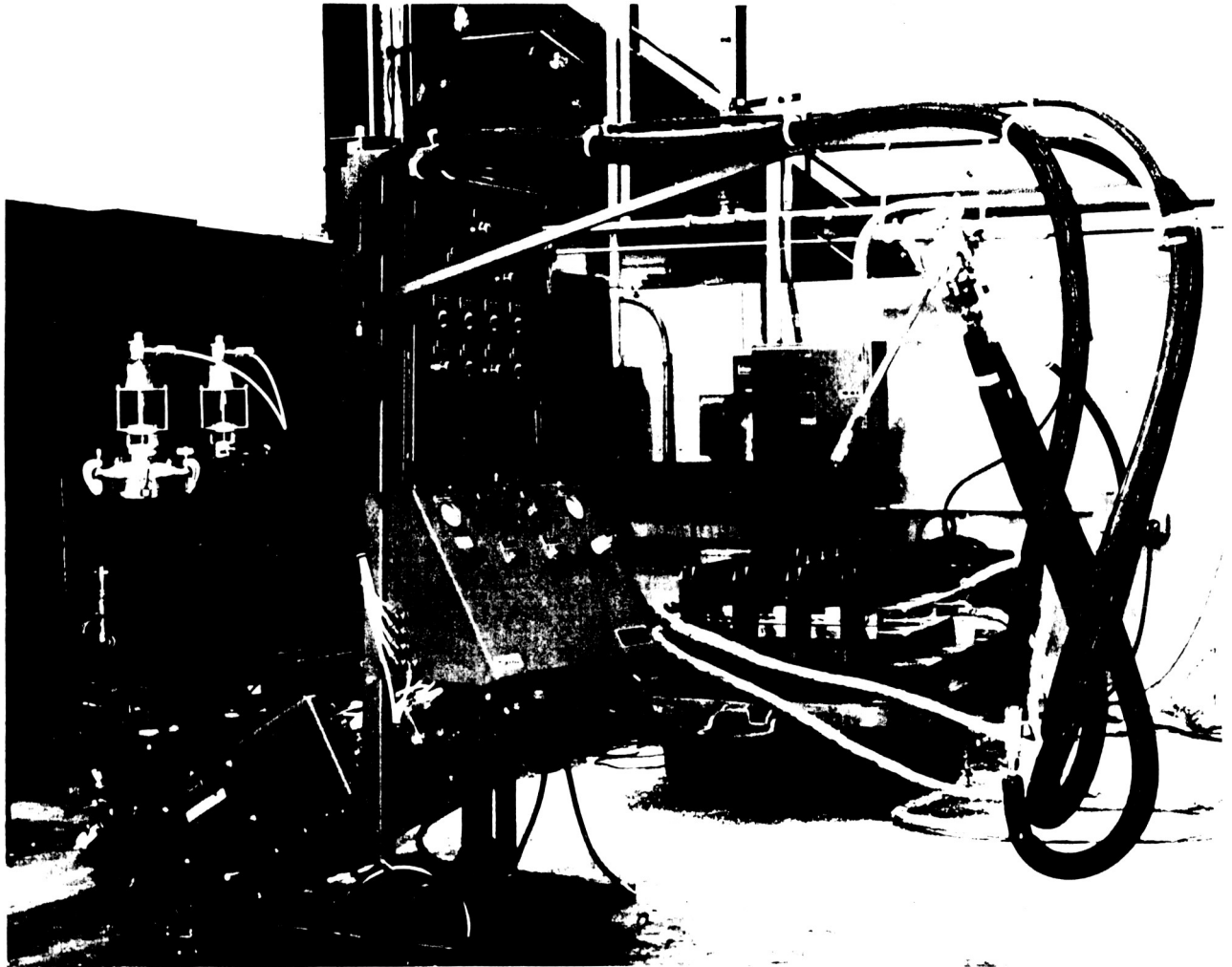
RTM FUSELAGE ELEMENT TOOLING

The pressure impregnation process is being developed for composite primary fuselage applications at Douglas Aircraft Company. This process is utilizing dry stitched preforms in combination with matched metal tooling and a positive displacement resin metering pump. The Douglas RTM fuselage element tool is shown in this slide.



DAC RTM MACHINE

All the pressure RTM development being done at Douglas Aircraft is being done with a liquid control multi flow-4 machine. This machine can handle one or two component resins that require pre-heat temperatures of up to 175°F. This machine will be used extensively in the RTM fuselage sub-component work to be done at Douglas during the remainder of Phase A of the ICAPS program.



PROCESS MODEL AND MONITOR

William & Mary College (W&MC) and Virginia Polytechnic Institute (VPI) are combining forces to create a process model and process monitoring system.

W&MC, under the direction of Dr. David Kranbuehl, has a FDEMS system that will record resin collation (as a preform is being impregnated along with resin viscosity and resin cure condition). A resin kinetics model is being developed to establish the relationship between DSC, viscosity, temperature, and time versus FDEMS measurement.

WILLIAM AND MARY COLLEGE DR. DAVID KRANBUEHL

PROCESS MONITOR

FDEMS SYSTEM

- RESIN LOCATION
- RESIN VISCOSITY
- RESIN CURE CONDITION

RESIN KINETIC MODEL

- DSC VERSUS VISCOSITY VERSUS TIME
VERSUS FDEMS RELATIONSHIPS
- CREATE RELATIONSHIP MODEL
- VERIFY MODEL PREDICTIONS

CURE MODEL AND MONITORING

VPI is conducting a porosity study of preforms and resin flow rates with temperature/viscosity/gel time restraints. VPI, under the direction of Dr. Al Loos, will use their data alone with the W&MC data to construct a process cure model. The objective of this model is to assess a new design, predict if the RTM system will work, and if so, specify a curing time/temperature cycle.

VIRGINIA POLYTECHNIC INSTITUTE (VPI) DR. AL LOOS

POROSITY STUDY OF PREFORMS

RESIN FLOW RATE

TEMPERATURE/VISCOSITY/GEL

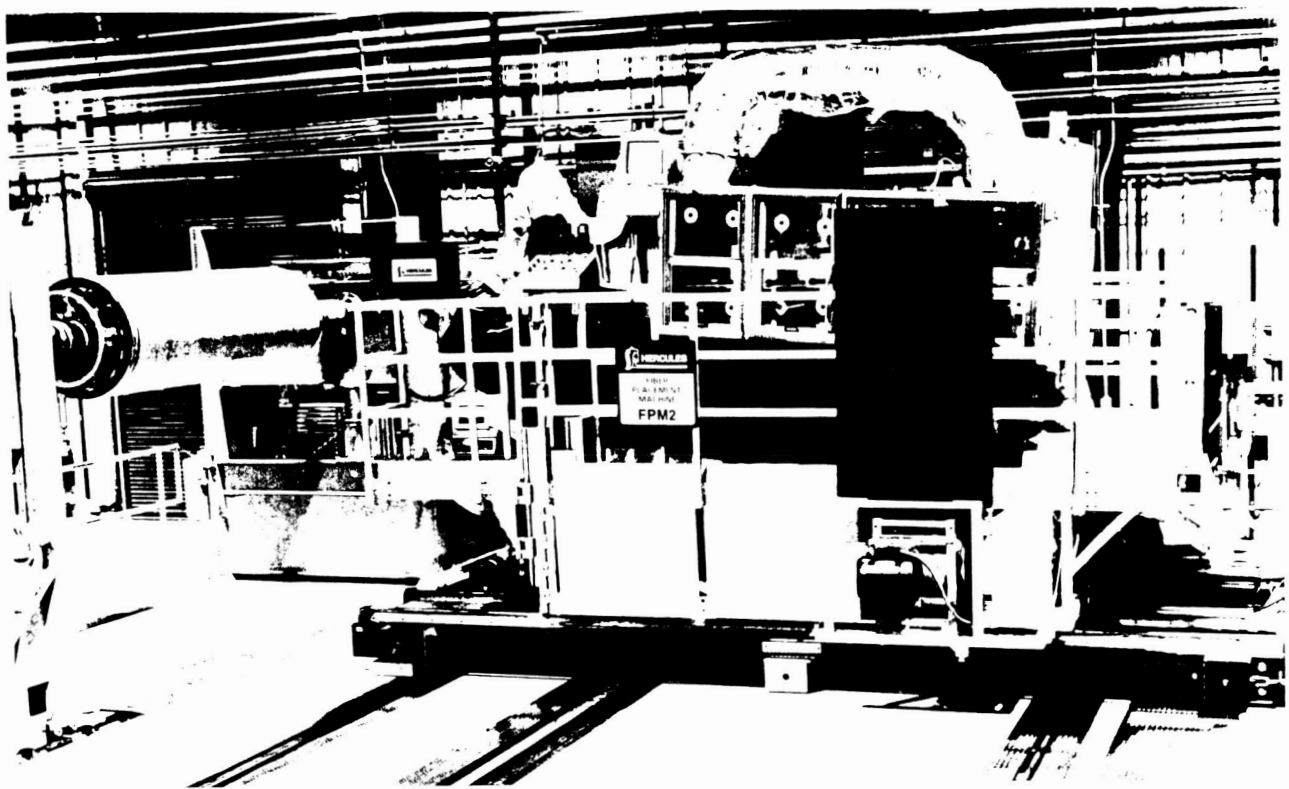
CREATE PROCESS PREDICTION CURE MODEL

- **VPI AND WILLIAM AND MARY DATA**

VERIFY MODEL PREDICTIONS

AUTOMATED FIBER TOW PLACEMENT

As part of the Douglas pressurized fuselage development, the automated fiber tow placement process is being evaluated in conjunction with the Douglas RTM fuselage effort. Hercules Inc. is fabricating element and subcomponent fuselage panels with their most advanced fiber placement machine in this Phase A effort. Shown below is a side view of the Hercules tow placement machine and a photo of the element panel fabricated earlier this year.



DEVELOPMENT TESTING

This is a summary of the wing and fuselage test articles being fabricated. The majority of the elements (smaller sizes) are fabricated and in test. The sub-components (larger sizes) are in the fabrication process.

WING (TEST ARTICLES - 15 TOTAL)

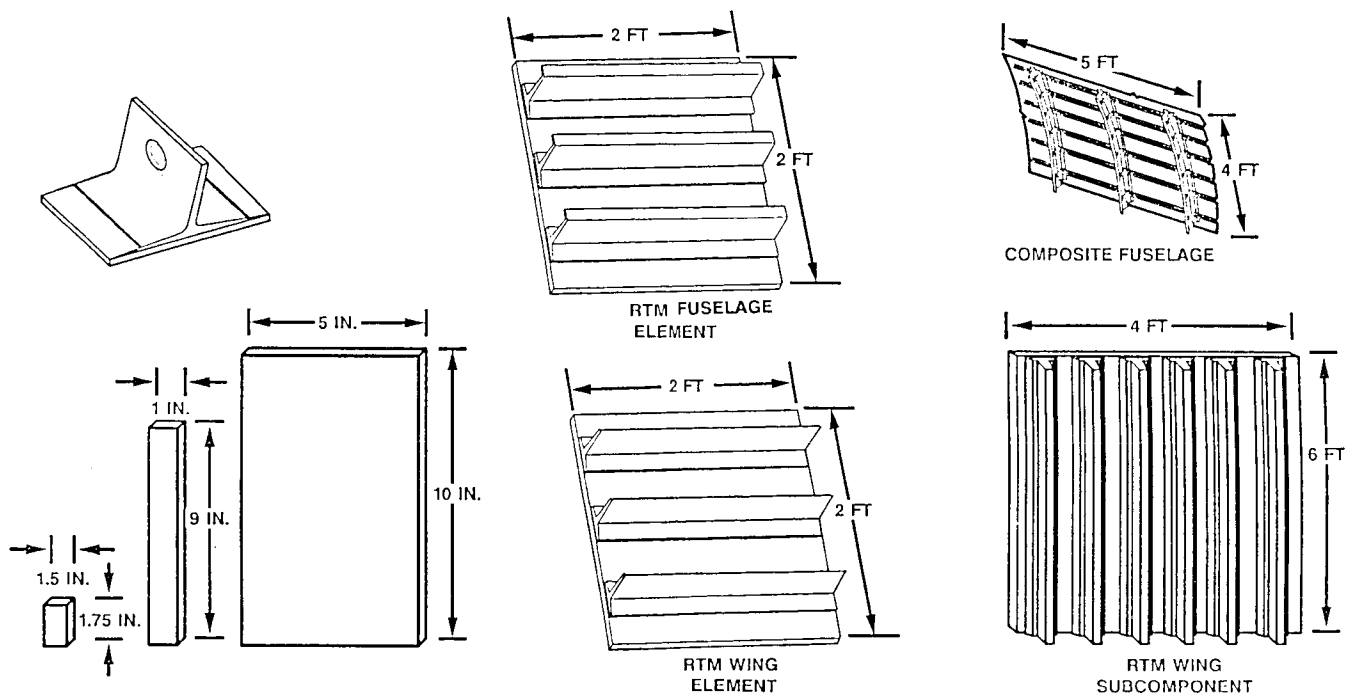
- **STRINGER PULLOFF**
- **THREE-BLADE STIFFENED PANELS (24 IN. X 21 IN.)**
- **SIX-BLADE STIFFENED PANELS (42 IN. X 60 IN.)**

FUSELAGE (TEST ARTICLES - 35 TOTAL)

- **LONGERON PULLOFF**
- **THREE J-STIFFENED PANELS (15 IN. X 21 IN.)**
- **SIX J-STIFFENED AND TWO-FRAME PANELS (48 IN. X 60 IN.)**

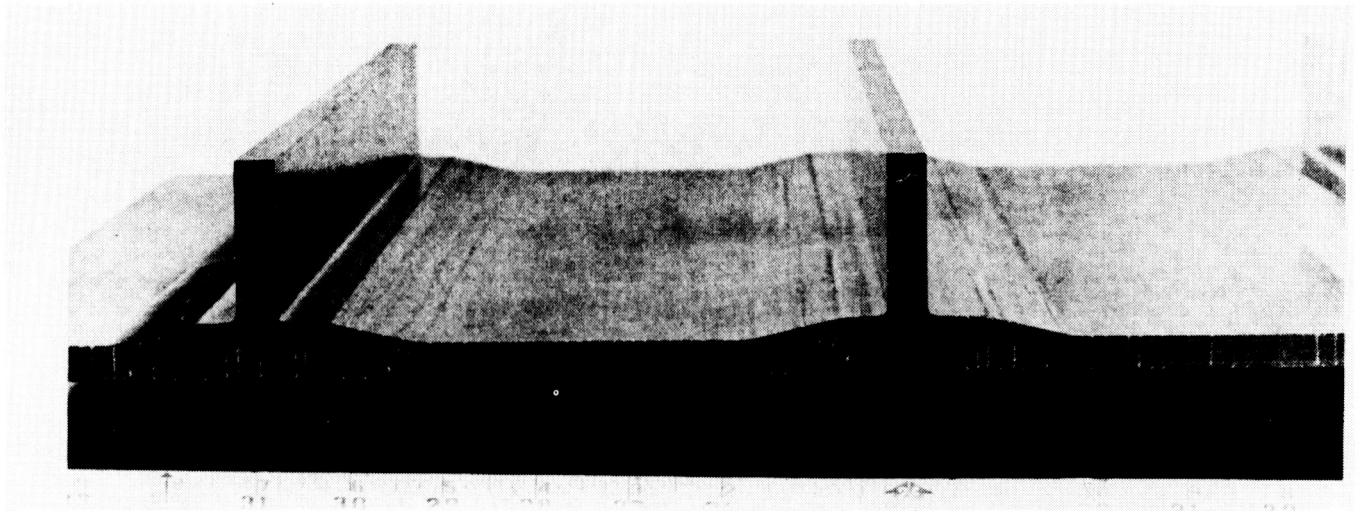
ELEMENT / SUBCOMPONENTS

This illustration shows the sizes of the various coupons, elements, and sub-components. The coupons were of thick and thin sizes to do development work for both fuselage and wing structures. When the elements were designed, they specifically focused on the J-stiffened panels for the fuselage application and the thicker blade stiffened panels for the wing application. The subcomponents are scale-up of the element test articles that were sized to fit the existing testing fixtures.



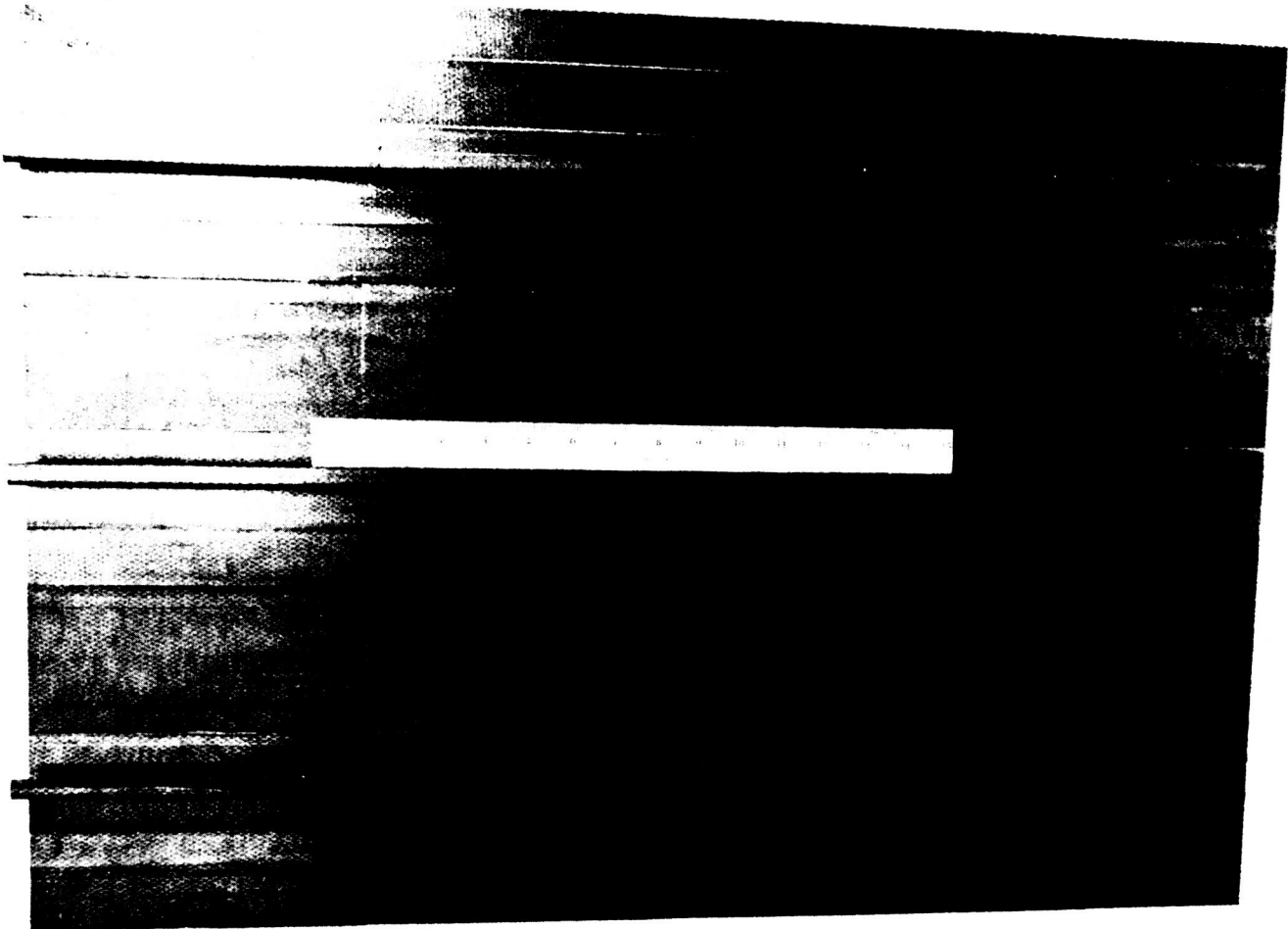
THREE BLADE WING PANEL

This photograph shows one of the three blade stiffened (element) wing panels fabricated for compression development testing. Panels of this type as well as coupons and test specimens using the current state-of-the-art resin and intermediate strength fibers have shown that the dry stitch preform fabrication concept structure yields strength after damage equivalent to the newer toughened resins and high strength fibers. This can be accomplished at a much lower material and fabrication cost.



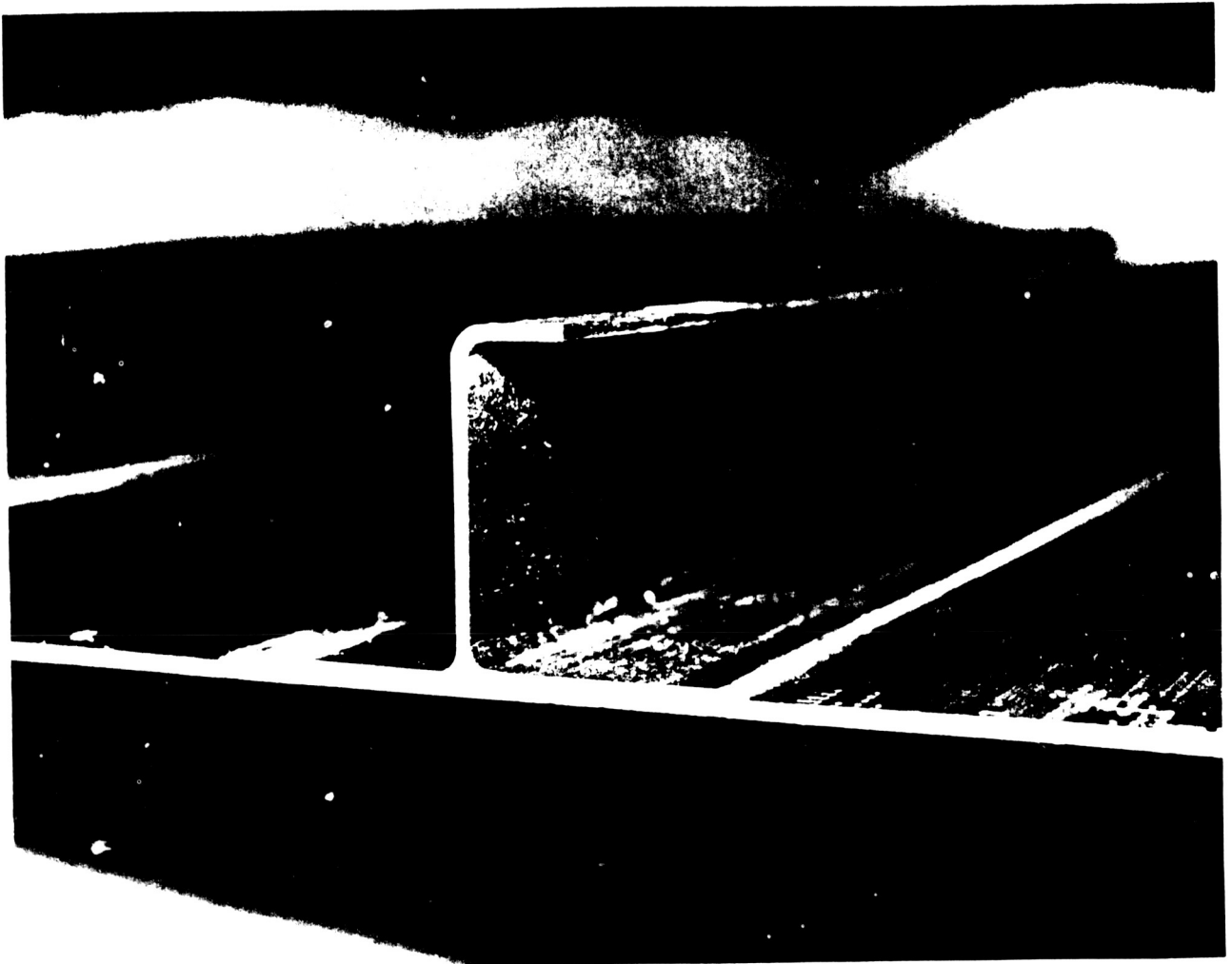
FUSELAGE "J" STIFFENED PANEL RTM

This photo represents a three "J" stiffened fuselage element panel fabricated by the pressure RTM process.



FUSELAGE "J" STIFFENED PANEL AUTOMATED TOW PLACEMENT

This is a cross section photo of a three "J" stiffened fuselage element panel fabricated with the automated tow placement process under subcontract to Hercules.



STRUCTURAL MECHANICS INVESTIGATION GOALS

As we introduce the innovative concept of Cost-Effective Resin Impregnated Stitched Preforms (CRISP), we need to investigate many new dimensions of composite structural mechanics. CRISP centers around two new approaches: stitching dry preforms and resin transfer molding (RTM in the general sense, including both vacuum and pressure processes). Both stitching and RTM alter the material properties to the extent that we need to modify the conventional laminate theory and composite design methodology. CRISP drastically improves composite damage tolerance performance under compression. Therefore we need to develop a new set of residual strength prediction tools for the design and application of stitched composites. There are more than a thousand tests at coupon, element, and subcomponent levels planned in ICAPS Phase A to validate our structural mechanics development.

**MODIFIED LAMINATE THEORY FOR STITCHED MATERIAL
DESIGN METHODOLOGY WITH STITCHED LAMINATES
RESIDUAL STRENGTH PREDICTION**

SUPPORTED BY MORE THAN 1,000 TESTS

MODIFIED LAMINATE THEORY FOR STITCHED MATERIAL

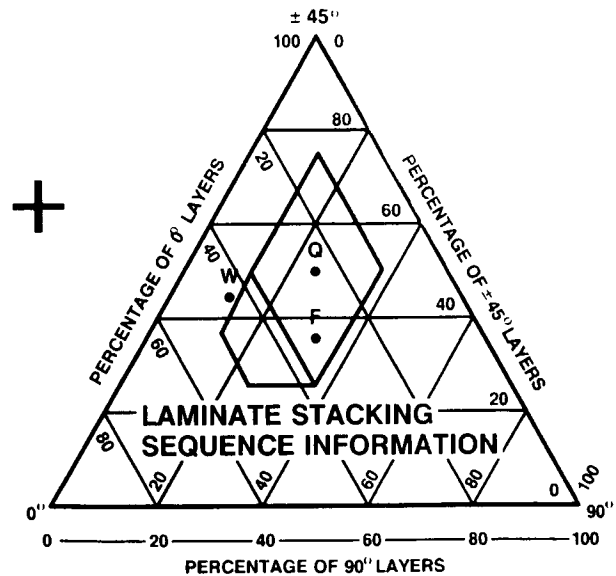
Stitched laminates have greatly improved through-thickness strength, which leads to higher compression after impact (CAI) strength, and in many cases, higher effective compressive strength due to the suppression of brooming. We are in the process of further quantifying these benefits of stitching. As stitching helps CAI and compression performance, it alters other in-plane properties, and our most important finding is that this property change is non-uniform. Stitching disturbs the fibers perpendicular to stitch-line the most, therefore causing more strength reduction in that direction. Further, the property change is not uniform through the thickness either and the surface plies are affected more. This causes more strength reduction in thin laminates than in thick ones. In essence, stitched laminates are treated as if they were hybrid materials -- the plies having their fibers parallel, 45° or perpendicular to the stitching lines, are modeled as different materials. Their strength and stiffness are added up using regular laminate theory.

LAMINA PROPERTIES OF

MATERIAL 1:	FIBER // STITCH
MATERIAL 2:	FIBER $\angle 45^\circ$ STITCH
MATERIAL 3:	FIBER \perp STITCH

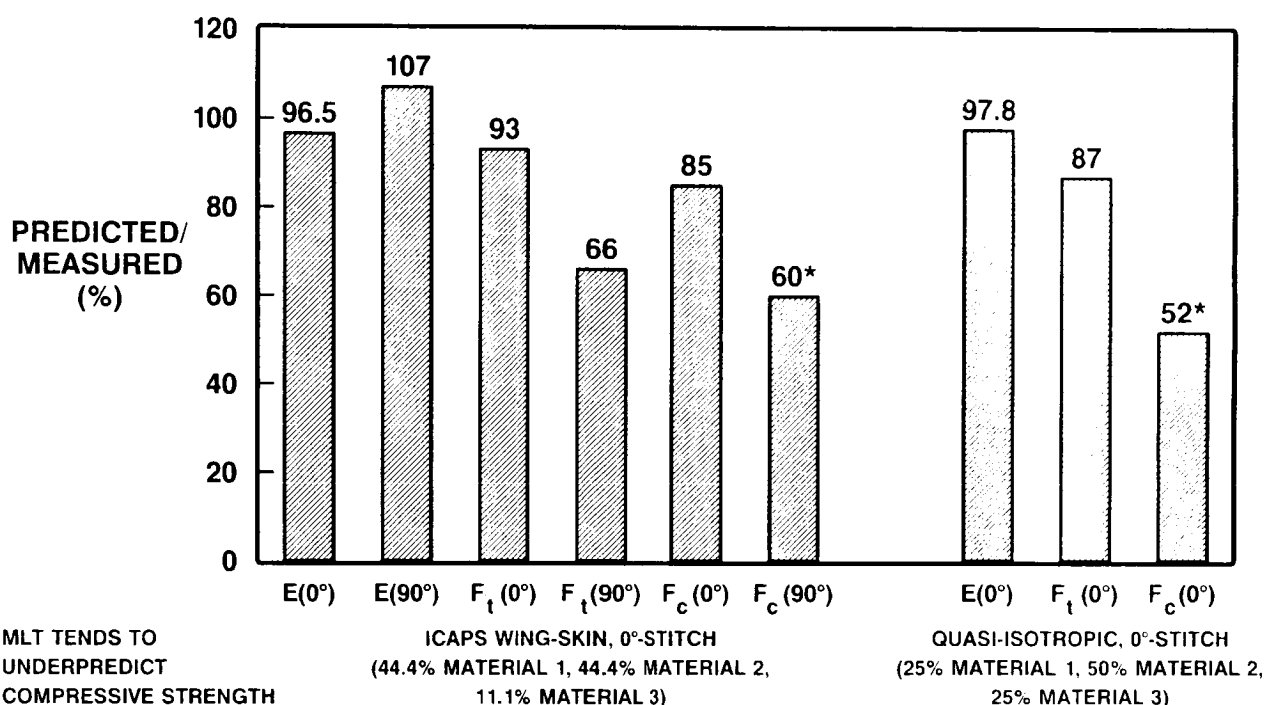
USE STITCHING PARAMETER TO
SORT OUT MATERIAL PROPERTIES
FOR EACH PLY, THEN

—————→
SUM UP STIFFNESS AND STRENGTH



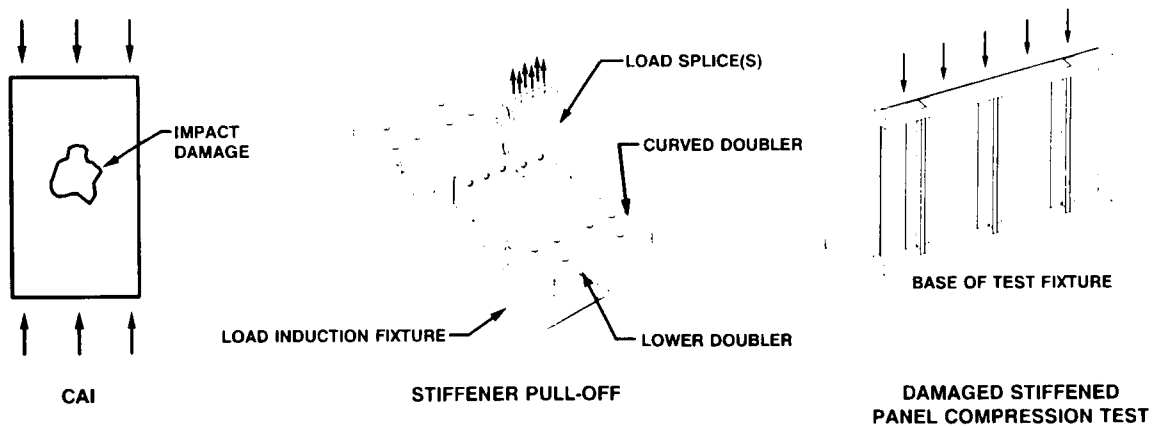
PREDICTION BY MODIFIED LAMINATE THEORY

The predictions shown in this slide are derived from a phenomenological theory modified for stitched laminates. Without any thickness correction factor, the model tends to under predict compression strength. A study is ongoing to determine if one extra factor is needed for the thickness effect. More tests are planned to study improved uniwoven material and thickness/stacking sequence combination effects.



RESIDUAL STRENGTH PREDICTION DEVELOPMENT

It is important to predict the ultimate strength (failure load) of damaged parts. Compression after impact (CAI) is probably the most common means of residual strength measure. However, large structures have redundant load paths built in them and do not lose the same percentage of strength with the same damage as the coupons. Also, most structures have stiffening members and stiffener-skin separation can be the failure mechanism. To estimate the ultimate strength of a stiffened part, this has to be accounted for in addition to buckling, crippling, and pure compressive failure. Stiffener pull-off tests will provide us with such strength data of stiffener-skin separation resistance for various material/process parts. We will use the CAI coupon and stiffener pull-off test results to establish impact damage modeling. Empirically matched "reduced stiffness and strength" parameters will be reduced and fed into finite element analyses. Element panel tests will be used to calibrate our prediction model parameters. The refined model will be used to predict the ultimate strength of damaged subcomponents.



ANALYSIS

- DAMAGE MODELING (REDUCED STIFFNESS AND STRENGTH)
- ULTIMATE STRENGTH PREDICTION ON DAMAGE PARTS (FINITE ELEMENT ANALYSIS WITH PARAMETERS OBTAINED FROM DAMAGE MODEL)

OTHER DEVELOPMENT TESTING

Since the ACT-ICAPS program has been initiated there have been several specific activities addressed to enhance the program results. Subcomponent fatigue testing will be accomplished prior to the Phase B components to determine if there are any issues that need to be addressed. Ply drop-off evaluation is being conducted to determine if the wing panel stacking sequence is acceptable. Validation of the splice joint is being made as well as thermal cycling of the stitched preform concept. Many components have over the years had varied compression failures related to the length between restraints called "brooming failure." This has been documented in numerous technical papers. A clarification of how stitching will affect these failure characteristics is being made. Additional damage tolerance tests are being conducted to cover additional impact force variables.

(DAC - NASA LANGLEY - UNIVERSITIES)

FATIGUE

PLY DROP-OFF CRITERIA

BOLTED JOINTS

THERMAL CYCLING

COMPRESSION FAILURE MODES

DAMAGE TOLERANCE

COST MODELING

For the wing program there are three large scale wing box evaluations for comparison of cost. The wing box size is 8 foot root chord, 5 foot tip chord with a 12 foot section of span representing in size the side-of-body section of a DC-9-30 wing. The three cost analyses are on a metal, conventional composite, and ICAPS composite version.

CONVENTIONAL WING DESIGN - METAL

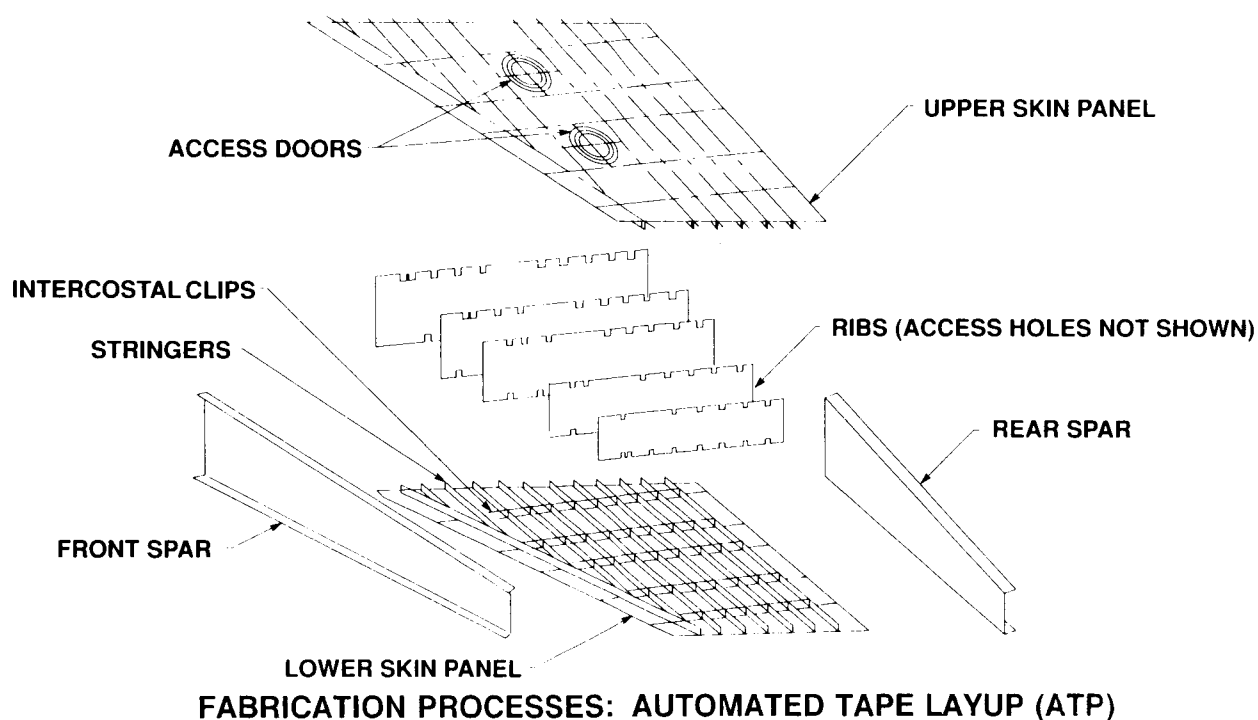
STATE-OF-THE-ART TOUGHENED RESIN WING - DOUGLAS

INNOVATIVE STITCHED DRY PREFORM WING DESIGN - ICAPS

STATE-OF-THE-ART COMPOSITE WING DESIGN

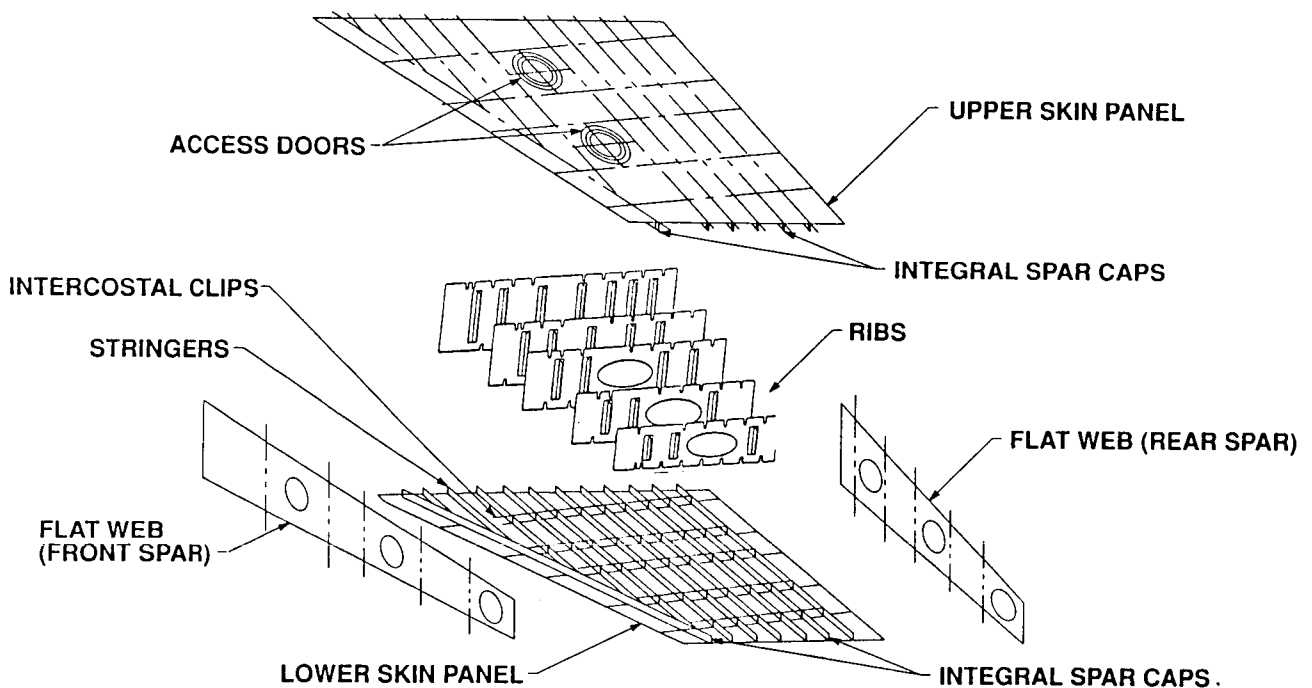
The Douglas composite wing program using toughened resin high strength fiber will consist of five ribs, two spars, and stiffened lower skins. The spars are typical spanwise "C" sections that will be mechanically fastened to the skins. Ribs will be flat with cutouts and stiffener. The cover skin thickness will taper by ply drip off and a blade stiffened cocured component. Rib shear clips will be secondarily bonded and fastened to the skins.

The component to be fabricated will have hand layup in many areas, but the cost model will search for and use the lowest cost fabrication concept (i.e. tape layup, filament/tow placement, etc.).



ICAPS WING BOX ASSEMBLY

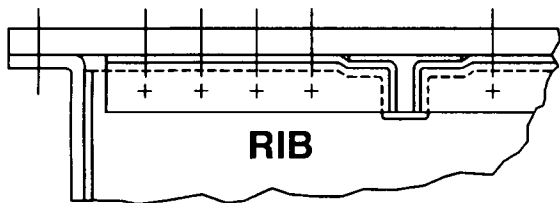
The ICAPS composite wing program will use dry stitched preform stiffened cover skins with stitched rib shear clips. Once again the ribs will be flat and nearly identical to the Douglas wing box ribs. The spars will be stiffened flat webs. The ribs and spar web will be mechanically fastened to the cover panels with shear fasteners with no tension fasteners through the cover skin. Savings in assembly and number are realized with this approach as well as future maintenance issues (i.e. fuel loads, etc.).



DESIGN DIFFERENCES

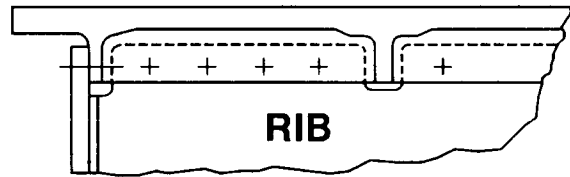
The significant difference between the state-of-the-art design and the ICAPS design is simplification and avoidance of problem issues that exist today. On the left there are mechanical fasteners joining the skin and spars that are in tension. A problem area develops when there are less than perfectly matched surfaces between the components. The ICAPS design avoids all fasteners through the cover skin as well as minimizing the number of fasteners. The ribs and spar webs are all stiffened flat members that are low cost minimum tool parts.

STATE-OF-THE-ART



UNTAPERED STRINGER FLANGES
C-SECTION SPAR
SEPARATE RIB CLIPS
MANY SKIN BOLTS

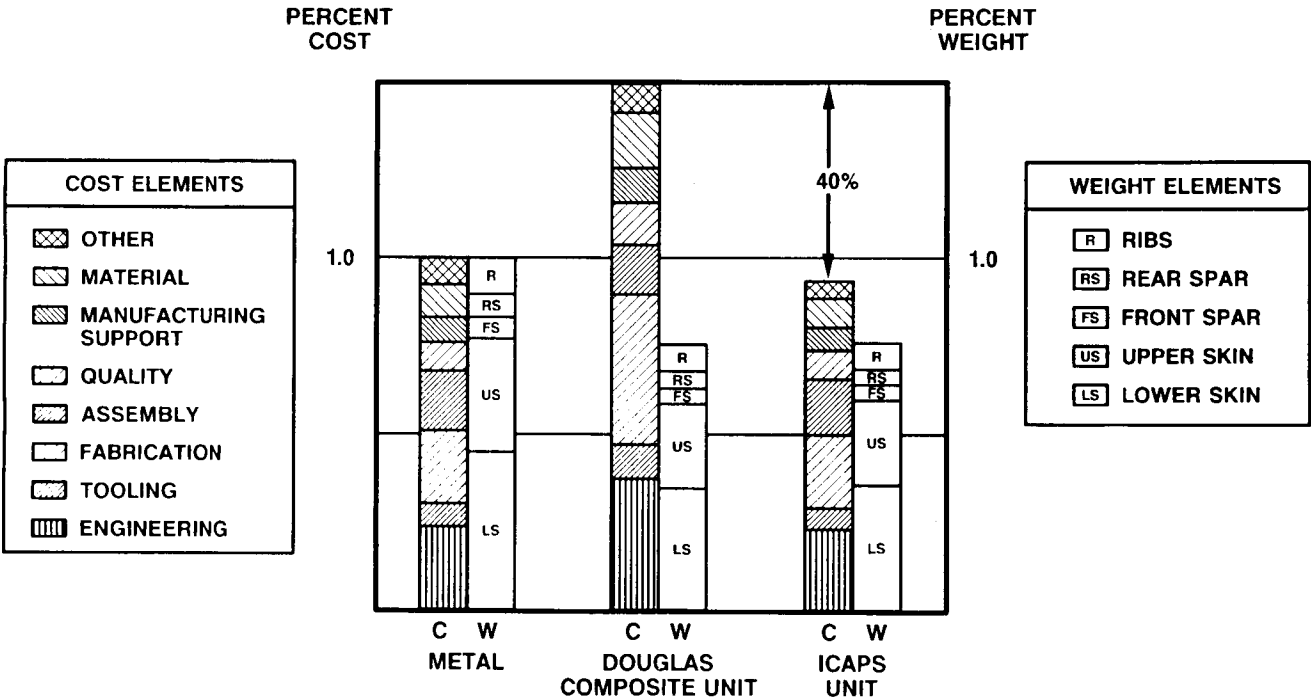
ICAPS



TAPERED STRINGER FLANGES
INTEGRAL SPAR CAPS
INTEGRAL RIB CLIPS
STITCHING - FEW SKIN BOLTS

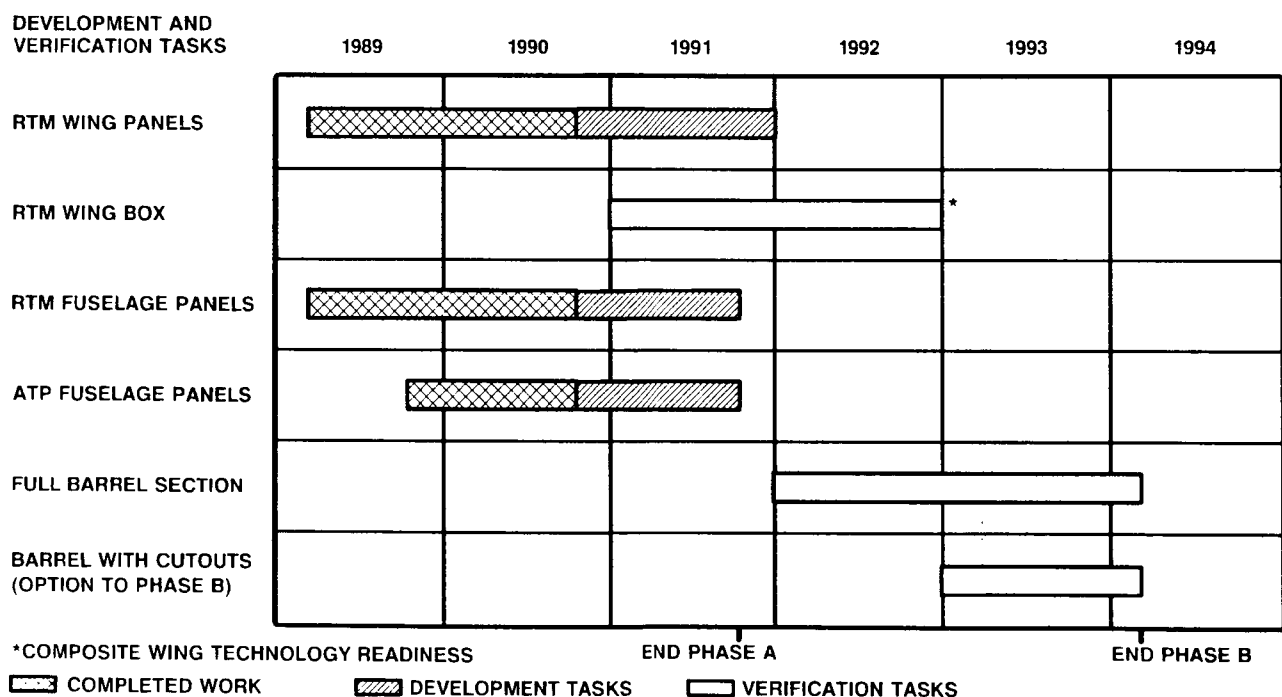
WING BOX COST DATA PROJECTION

The initial cost/weight projections for the three wing structural concepts are as shown. As additional data is generated from the elements, subcomponents and the two large scale box components, the analyses will be updated. The elements of cost data are listed as well as weight by component.



DEVELOPMENT AND VERIFICATION SCHEDULE FOR ICAPS

We are 19 months into the ICAPS program and have developed a considerable number of development tests focused at wing (thick laminate) and fuselage (thin laminate). Over the next year, we will be making and testing the large sub-component panels for both wing and RTM/tow placement fuselage panels. We will be initiating detail design on the RTM wing box so that the full box can be fabricated and structurally tested right after the Douglas wing box program. The full fuselage barrel design will depend on the selection evaluation of the RTM and tow placement test and cost data. The wing target dates are in agreement with the Douglas and ICAPS goals and objectives.



PRODUCTION STITCHING PREFORM PROCESS

This slide presents a pictorial step-by-step production process to make near net shape stiffened wing skin like dry fiber preforms. The basic design uses a 9-ply repeat pattern layers of fabric.

The uni-woven fabric is purchased with major direction of reinforcement fibers at 0°, at 45° and at 90°. Nine rolls of this material are placed in a feed system, passed through the multi-needle stitching machine and rolled and stored for later use. Stitching is light density 1" apart parallel rolls.

The next step is to unroll one 9 ply stitched pre-ply and cut the doubler buildups required for the skin.

Six of the 9 ply stitched pre-ply rolls (54 total ply) are positioned on the feed system and pulled to the multi-needle position of the machine. Doublers are placed in position on the 54 ply area and then the entire skin and doublers are stitched together with the desired high density stitch pattern.

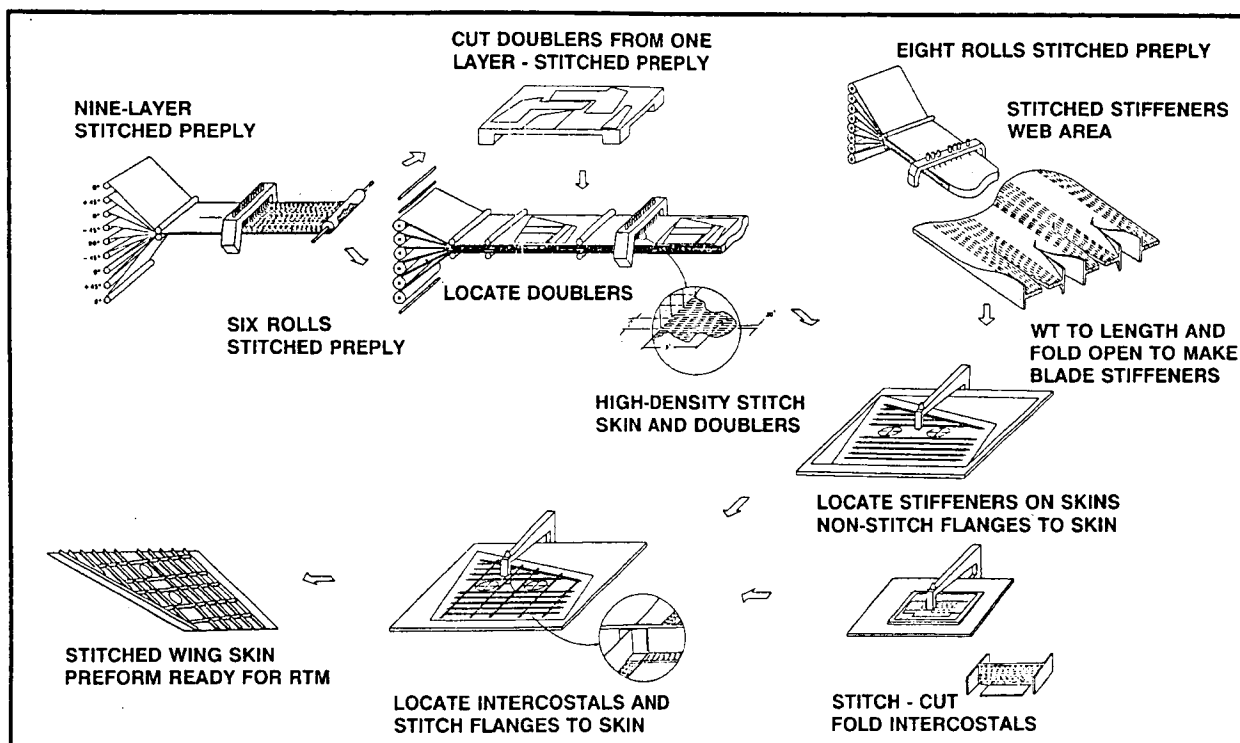
The stiffeners are made by stitching 8 nine ply stitched pre-ply material in areas of the web, only for each stiffener. The stitched sections are then cut to allow the web and flanges to be folded right and left ready for installation on the stitched skin.

The stiffeners are properly located and the flanges are stitched to the skin using an automated single needle machine.

The intercostals are cut from two stitched pre-ply layers, stitched in the web area on a single needle machine and flanges are folded for stitching to the skin. The intercostals are then located on the skin/stiffener detail and stitched in the skin flange area.

The dry stitched preform is now out to near net size and is ready for the RTM impregnation and cure process.

PRODUCTION STITCHING PREFORM PROCESS



SUMMARY

The goals and objectives of ICAPS are still the primary focus of the on-going effort. There have been a considerable number of accomplishments that indicate progress is being made in attacking the high cost drivers. The stitching development has selected specific parameters. New resins are in evaluation for the RTM process and Hercules has done an excellent job in providing the development panels on tow placement for fuselage application. The equipment for the RTM process monitoring has been ordered so that shortly we'll be able to go from the laboratory effort to VPI/W&MC to the shop floor in fabrication of the large subcomponent.

We have specific application targets and feel very strongly that we can accomplish the cost breakthrough we need to make it happen.

ACCOMPLISHMENTS

- **WING AND FUSELAGE SUBCOMPONENT DESIGNS**
- **DESIGN GUIDELINES FOR STITCHED/RTM COMPOSITES**
- **STITCHING AND ANALYSIS DEVELOPMENT TESTS 80% COMPLETE**
- **WING PANEL TOOLING DESIGNED**
- **FUSELAGE PANEL TOOLING COMPLETED**
- **ATP FUSELAGE PANELS FABRICATED**
- **HIGH-CAPACITY STITCHING MACHINES PURCHASED**

**TARGET OF OPPORTUNITY EXISTS FOR APPLICATION TO TRANSPORT
STRUCTURE IN MID-1990**

**STITCHING DRY PREFORMS/RTM OFFERS BREAKTHROUGH
IN AFFORDABLE MANUFACTURING**

ICAPS PROGRAM PROVIDES ENABLING TECHNOLOGY

ADVANCED TECHNOLOGY COMMERCIAL FUSELAGE STRUCTURE¹

L.B. Ilcewicz, P.J. Smith, T.H. Walker, and R.W. Johnson

Boeing Commercial Airplane Group

ABSTRACT

Boeing's program for Advanced Technology Composite Aircraft Structure (ATCAS) has focused on the manufacturing and performance issues associated with a wide body commercial transport fuselage. The primary goal of ATCAS is to demonstrate cost and weight savings over a 1995 aluminum benchmark. A 31 foot section of fuselage directly behind the wing to body intersection was selected for study purposes. This paper will summarize ATCAS contract plans and review progress to date.

The six year ATCAS program will study technical issues for crown, side, and keel areas of the fuselage. All structural details in these areas will be included in design studies that incorporate a design build team (DBT) approach. Manufacturing technologies will be developed for concepts deemed by the DBT to have the greatest potential for cost and weight savings. Assembly issues for large, stiff, quadrant panels will receive special attention. Supporting technologies and mechanical tests will concentrate on the major issues identified for fuselage. These include damage tolerance, pressure containment, splices, load redistribution, post-buckled structure, and durability/life.

Progress to date includes DBT selection of baseline fuselage concepts; cost and weight comparisons for crown panel designs; initial panel fabrication for manufacturing and structural mechanics research; and toughened material studies related to keel panels. Initial ATCAS studies have shown that NASA's Advanced Composite Technology program goals for cost and weight savings are attainable for composite fuselage.

INTRODUCTION

Technology advancements are needed to insure that the United States retains a majority share of the world market in transport aircraft. Composites have shown the potential to achieve improved performance (e.g., increased fatigue and corrosion resistance) and reduced weight relative to aluminum aircraft structures. However, higher costs associated with past composite structures remain an economic barrier to increased applications. A balance between cost and weight efficiency appears possible by integrating composite design, manufacturing, material, and structures technologies.

The application of affordable composite technology to transport fuselage is addressed in Boeing's program entitled Advanced Technology Composite Aircraft Structure (ATCAS). This program started on May 12, 1989. Assuming that all phases and options are funded, ATCAS is scheduled to be completed by the middle of 1995. The main ATCAS objective is to develop an integrated technology and demonstrate a confidence level that permits cost- and weight-effective use of advanced composite materials in future primary aircraft structures with the emphasis on pressurized fuselages.

An aft fuselage section directly behind the wing to body intersection is used for technology development and verification purposes in ATCAS. This section of fuselage, referred to as section 46, has many design details and associated technology issues that pose a staunch test of advancements in

¹ This work was funded by Contract NAS1-18889, under the direction of J.G. Davis and W.T. Freeman of NASA Langley Research Center.

composite primary structures. The design envelope (i.e., size, loads, and configuration constraints) chosen by ATCAS is based on preliminary data for section 46 of the 767-X (a current development program for an airplane 80% the size of a 747). The 767-X has a 240 in. diameter aluminum fuselage. The parallel efforts of 767-X and ATCAS provides an opportunity to completely evaluate cost and weight advantages of composites in the 1995 timeframe.

Keel, side, and crown areas of section 46 are being considered in the ATCAS program. Some manufacturing cost issues for this fuselage section are shown in Figure 1. Although many issues are common to the entire section, each area has unique problems that must be solved in order to achieve low costs. The complexity of design details such as window cutouts and section splices result in significant cost centers. Therefore, they are included in ATCAS studies to insure that overall low-cost composite technologies are adequately demonstrated. In order to save costs as compared to metals, the relatively high price of composite materials must be countered by innovative composite fabrication and assembly processes that minimize labor costs.

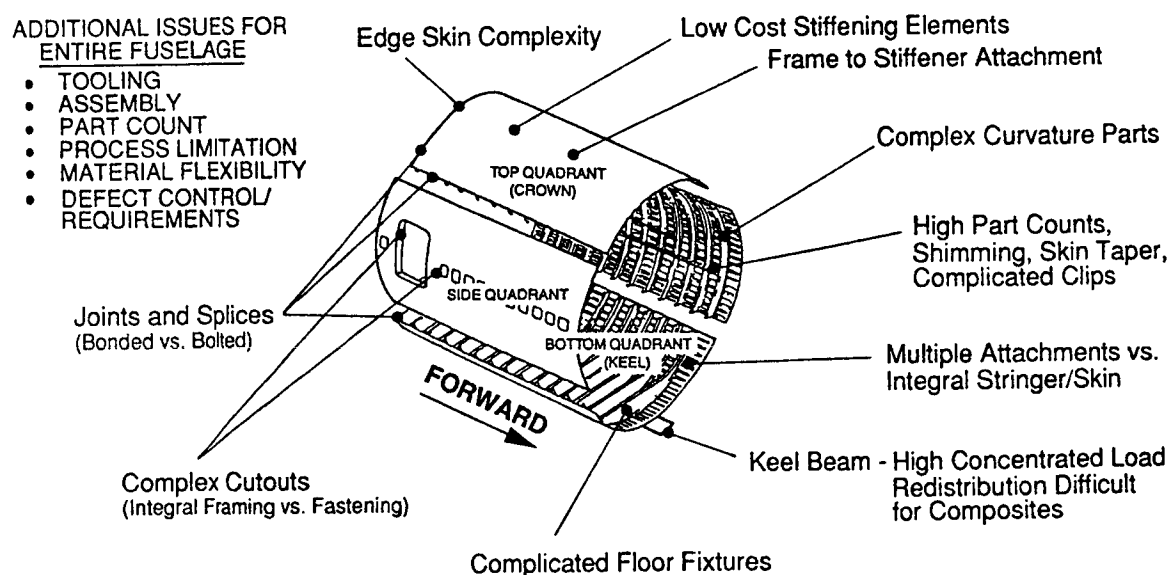


Figure 1: Cost Drivers for a Composite Fuselage

Many of the important composite structural issues, shown in Figure 2, are also unique to individual areas of the fuselage. Design of the crown is driven by tension loading. The side area is dominated by shear and pressure load redistribution around door and window cutouts. Keel design is driven by major load redistribution from the keel beam and combined loads dominated by axial compression.

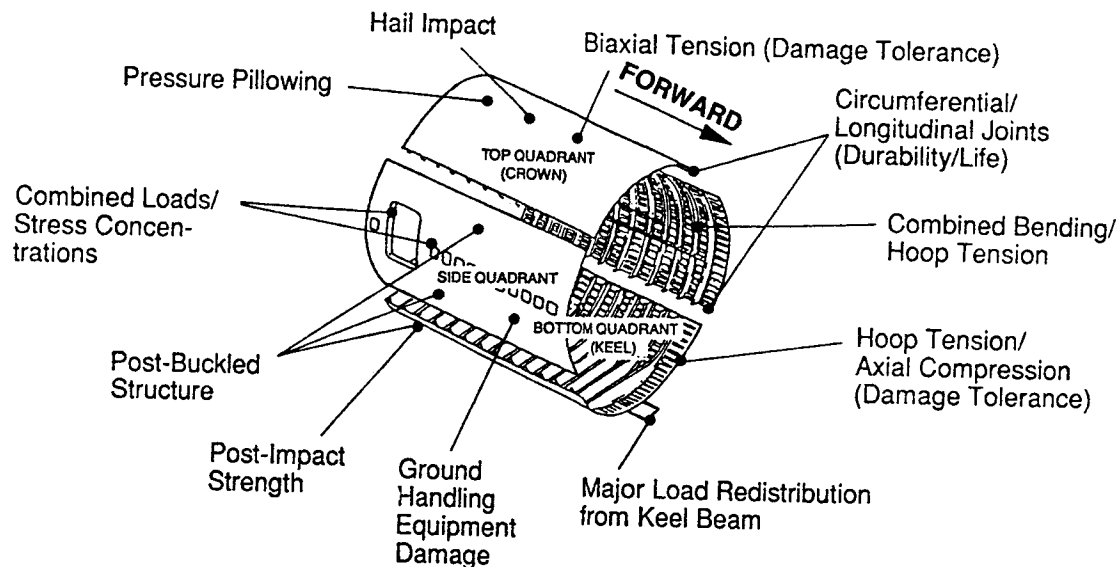


Figure 2: Structural Design Drivers for a Composite Fuselage

The remainder of this paper is broken into three main sections that overview the ATCAS program. The first describes the design build team approach. Baseline fuselage concepts and associated technical issues are described in the second section. Plans and progress to develop concepts and solve technical issues are presented in the final section.

DESIGN BUILD TEAM APPROACH

The greatest potential for saving cost and weight occurs in early phases of product development. Once the structural configuration is set, attempts to reduce weight or enhance manufacturing efficiency are traded against added costs associated with design changes. Past Boeing studies, indicating strong interactions between design details and manufacturing costs, led to a decision to consider assembled structure early in the ATCAS design cycle. The approach used for this effort is based on a design build team (DBT). The initial goal of the DBT is to identify composite design and manufacturing concepts that have a strong potential for cost and weight savings as compared to 1995 metals technology. An accurate estimate of the potential for cost and weight savings with a composite concept is established prior to the commitment for solving major technical issues.

The ATCAS DBT approach was derived by team members representing manufacturing, structural design, structural mechanics, materials, quality control, and cost analysis. As a result, each team member was given a sense of ownership in the ATCAS program. Early efforts revealed that the combined inputs from different disciplines was critical to identifying concepts with a potential for both cost and weight savings. Initial activities also indicated that the majority of work performed in support of a DBT occurs outside the group meetings used for coordination and review purposes.

Early developments by the ATCAS DBT prompted a need for an efficient method of studying candidate fuselage design concepts and manufacturing processes. Initially, 30 candidate fuselage

panel concepts were produced by design personnel. The number of concepts was increased from 30 to 159 during subsequent brainstorming sessions with the full DBT. Schedules would not allow cost and weight evaluations of all concepts. Instead, concepts were classified into the eight design families (see Figure 3) having common manufacturing characteristics. This allowed a more viable DBT approach in which a reduced number of concepts, representing chosen families, are evaluated for cost and weight efficiency. After identifying the best family for a given application, the cost and weight relationships of variables within that family are analyzed in greater detail.

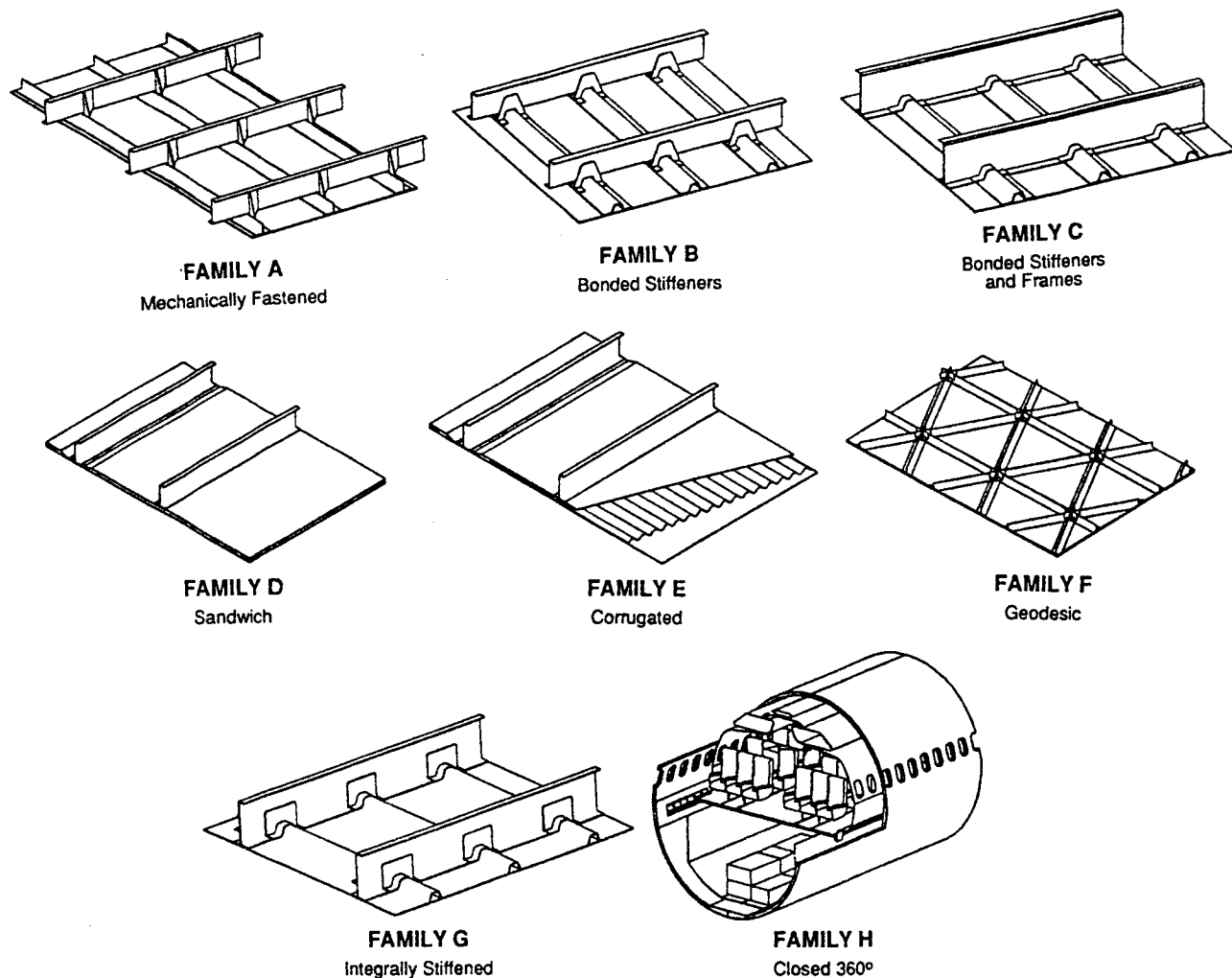


Figure 3. Representative Concepts From ATCAS Design Families.

Three steps are used by the ATCAS DBT to select, evaluate, and optimize fuselage concepts. The starting point is selection of baseline concepts as those design and manufacturing ideas having an apparent potential for cost and weight savings, combined with an acceptable risk. Technology issues are also identified during this phase of design, helping to focus early efforts in manufacturing, structural mechanics, and materials development. In the second step, referred to as global optimization, cost and weight savings are evaluated by performing detailed studies for the baseline and a limited number of alternative concepts. Global optimization effectively integrates manufacturing data into the design evaluation process. The final step, called local optimization, attacks cost centers and major technology barriers established during the first two design steps.

Figure 4 shows a flow diagram summarizing the global/local design optimization process. The cost estimating procedure for this effort uses detailed designs and fabrication/assembly plans. This facilitates cost and weight trades which consider enough details to select a cost-effective concept for further study. The ATCAS program is considering new material forms and manufacturing processes. Lack of sufficient data for these emerging technologies can reduce the accuracy of structural performance and cost predictions made during global optimization. Any uncertainties are noted and can influence the decisions made in this design step; however, the risk in selecting new technologies is minimized during local optimization which allows sufficient time to perform manufacturing trials, generate data bases, and complete more thorough analysis. Local design optimization addresses the critical cost centers, technology issues, and structural performance details. The goal of this DBT step is to minimize cost and weight, while insuring structural integrity.

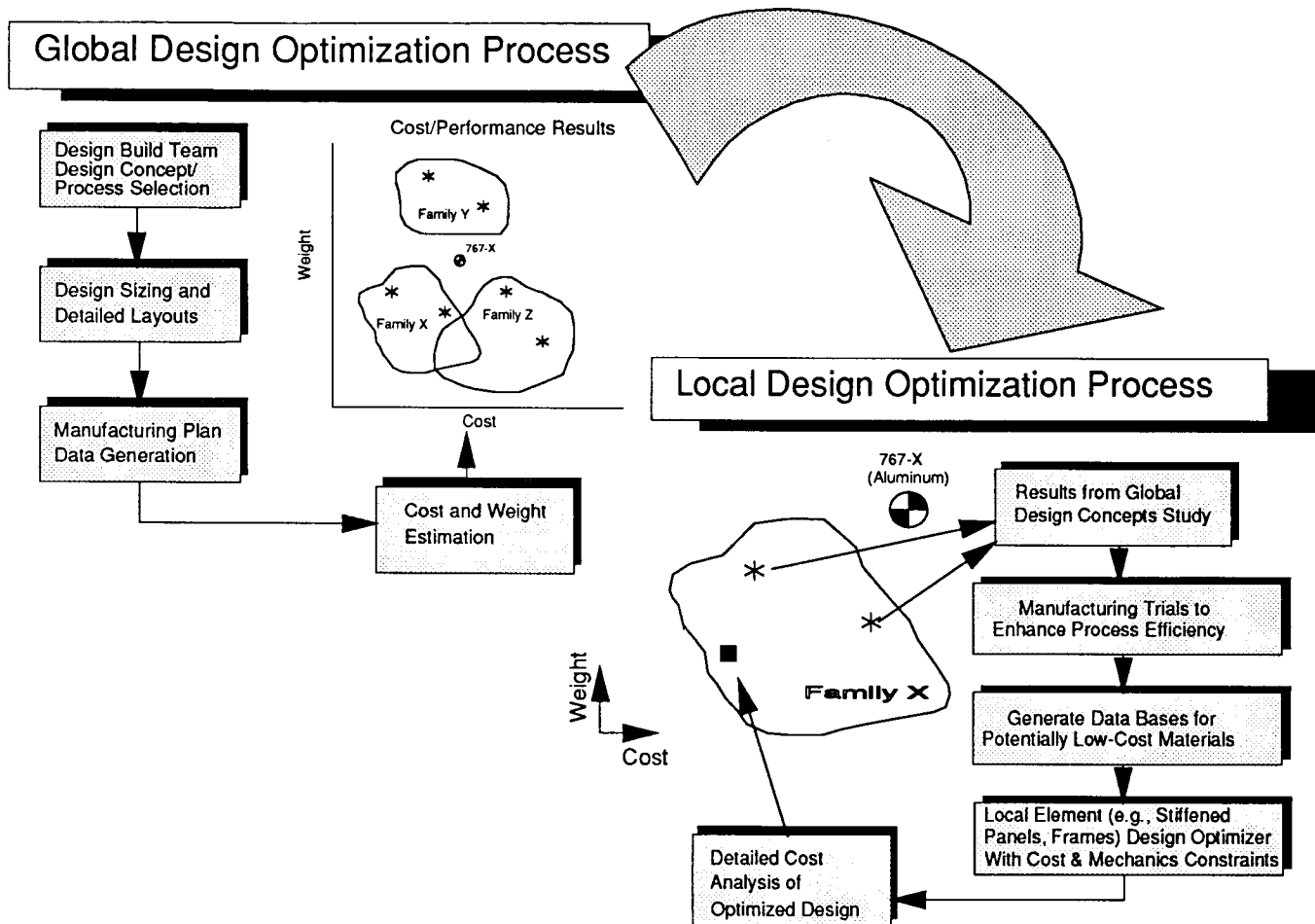


Figure 4. Global/Local Cost and Weight Optimization

BASELINE CONCEPTS

Baseline concepts have been selected for all areas of the aft fuselage section under study in ATCAS. The DBT selection rationale included several considerations. Critical manufacturing and performance issues were considered in selecting a design family that is compatible with structural details such as doors and the keel beam splice. Baseline manufacturing processes were selected to maintain cost efficiency with design details such as skin thickness tapers and curved frame geometries. Since the

scheduled completion date for crown global optimization coincided with baseline concept selection for the entire fuselage section, results from the former were used as an indicator of composite cost centers. The more detailed crown studies also helped to identify promising fabrication processes for skin, stiffener, and frame geometries. Finally, the only concepts considered were those judged to have a strong potential for large fuselage subcomponent manufacturing and test demonstrations by 1995.

Quadrant Panel Definitions

A quadrant manufacturing approach was selected for baseline panels. The four quadrant segments defined for the baseline fuselage section are shown in Figure 5. The quadrant concept is intended to reduce manufacturing costs in two ways. First, fuselage section assembly costs are lower than those of the metals benchmark due to a reduced number of longitudinal panel splices. Second, the quadrant concept is compatible with an advanced tow placement batch method for processing skin panels. As shown in Reference 1, crown trade studies projected this method of skin layup to be cost effective.

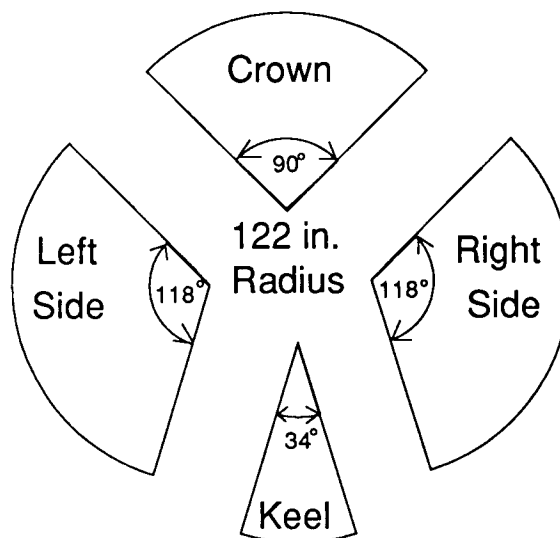
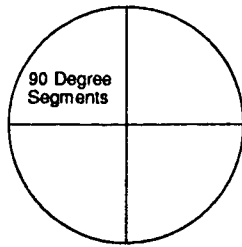


Figure 5. Exploded Circumferential View of Fuselage Quadrants. Note That Each Quadrant Panel is 30 ft. Long.

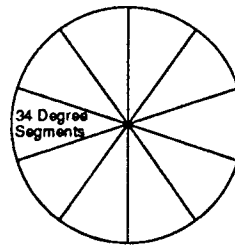
Differing arc lengths were chosen for each quadrant to accommodate the load conditions and specific design details for each area of the fuselage. Another goal was to select quadrants that minimize material waste of the batch process for advanced tow placing skins. The crown and keel quadrants were chosen as 90° and 34° segments, respectively. As shown in Figure 5, both crown and keel quadrants were symmetric about a vertical centerline to promote compatible skin gages on the right and left panel edges. The selection of a relatively small keel arc length was due to a cargo door location. Both side quadrants were large 118° segments, and include the cargo door, passenger doors, and window belt.

Figure 6 illustrates the number of manufacturing segments produced in a batch process for each fuselage quadrant. Crown and keel batch processes yield four and ten panels, respectively. Each crown or keel batch consists of uncured skin panels that are cut at the intersection of right and left edges. The side panel skin layup process required that both right and left sides be tow placed in the same batch. Each side panel skin design will have top and bottom edge layups that are compatible with the corresponding edge on the opposite side. For example, right top and left top panel edges will consist of the same thickness tailoring and layups that differ only in the sign of angle plies.

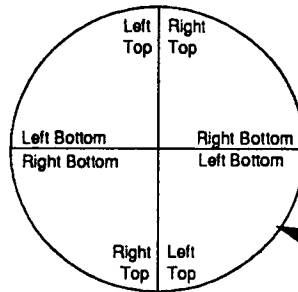
4 Crown Skin Panels
(Limited Amount of Thickness Tailoring)



10 Keel Skin Panels
(Large Amount of Thickness Tailoring)



2 Left and 2 Right Side Panels
(Thickness Tailoring from Top to Bottom and at Doors & Windows)



Larger Radius (160 in.)
to Yield 4 Panels
of Sufficient
Arc Length

Figure 6. Cicumferential View of Tow Placed Manufacturing Segments.

Figure 7 shows the automated tow placement work station for baseline skin panel manufacturing plans. Crown and side panel mandrels are illustrated, with the latter having a larger radius to accommodate four panels per wind. Note that both Figures 6 and 7 idealize tow placement mandrels as circular cylinders. Actual mandrel shape will accommodate design details. For example, a joggle at the edges of individual quadrant panels will be needed to allow for the geometry of longitudinal splices and cutting waste.

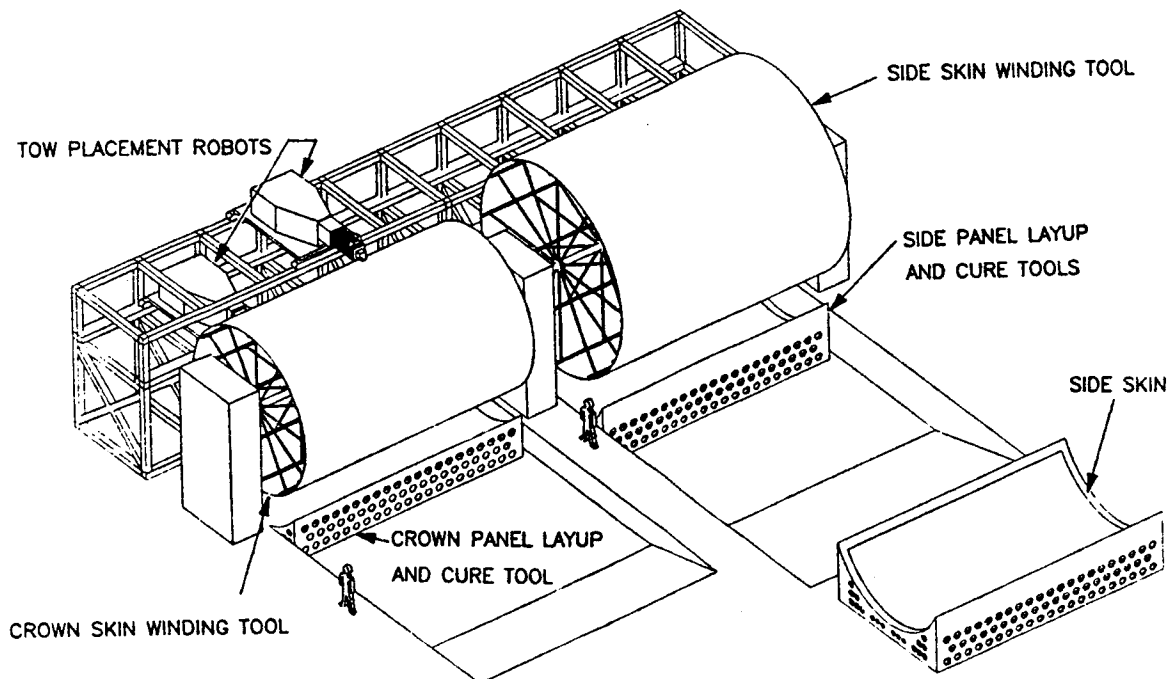


Figure 7. Automated Tow Placement Work Station.

Design Concept and Element Process Descriptions

A full factory flow from element fabrication through final assembly was envisioned to support baseline concept selection. Individual element processes are summarized in the following discussion. Mechanically fastened joints were chosen for splicing quadrants and section joining during final assembly. Additional features of the manufacturing processes appear in Reference 2.

Crown: Detailed cost and weight estimates from global optimization substantiated the baseline choice for the crown quadrant. Results from this effort are summarized later in this paper. A design concept from Family C (skin/stringer/frame with bonded stringers and frames) was chosen as the crown baseline. Figure 8 illustrates a representative area of the crown baseline quadrant. Frames are mouse-holed to avoid a complex bonding detail with the hat shaped stringers.

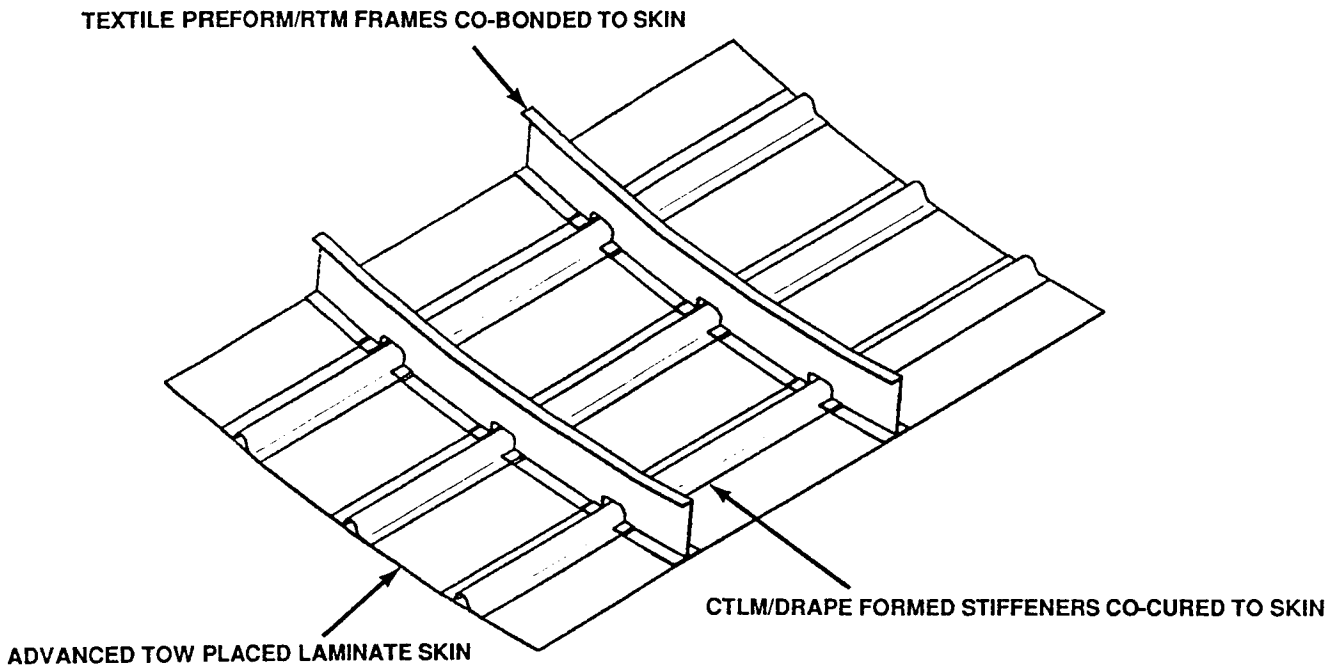


Figure 8: Crown Baseline Design Concept and Fabrication Processes.

Skin panels constitute the bulk of crown quadrant weight. Computer automated advanced tow placement was selected to layup the skins. The previous subsection gave some additional details on manufacturing multiple skin panels in a batch process.

Additional crown baseline elements include hat stiffeners and J frames. A contoured tape lamination machine (CTLTM), followed by a drape forming process was selected to layup and shape the hat stiffeners. Textile preforms in a J-shape and a resin transfer molding (RTM) process were chosen to form curved frames. The frames will have sufficient thickness to account for stress concentrations at the mouse-holes. Finally, the autoclave fabrication of full crown quadrant segments (≈ 192 in. by 374 in.) was envisioned as wet skin and stiffeners, cobonded with frames.

Window Belt (Side): A variation of design concepts from Family C (skin/stringer/frame with bonded stringers and frames) was chosen as the side panel baseline. The variation includes door and window design details. Figure 9 illustrates the window belt area of the side panel baseline. A skin/stringer/frame design family was chosen to facilitate design details at doors and windows.

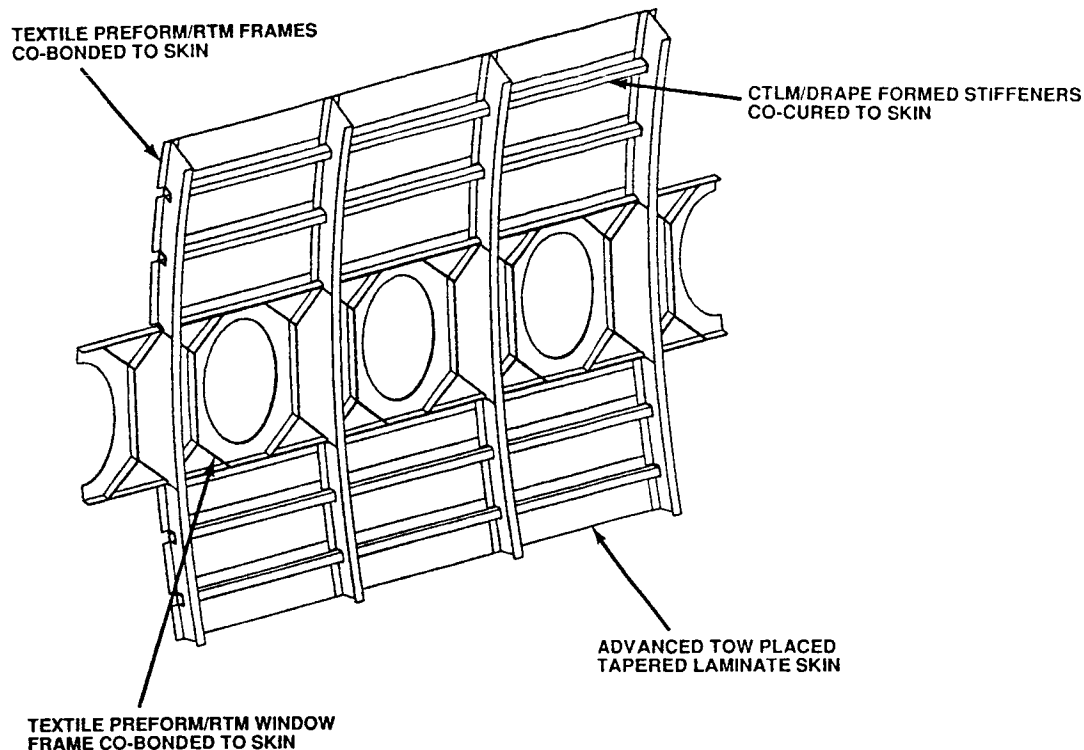


Figure 9: Side Baseline Design Concept and Fabrication Processes Near the Window Belt.

Skins for both side quadrants will also be produced in a batch tow placement. The skin thickness of side quadrants is close to minimum gage approaching the crown and relatively thick near the keel. Increased skin gages also occur locally near doors and windows. Automated batch processing and significant amounts of ply tailoring possible with the advanced tow placement method led to its selection for the side quadrant.

The same baseline processes and material forms were chosen for side panel stiffener and frame elements as were selected for the crown. The window and door frame design details were chosen to be textile preforms fabricated in an RTM process. Autoclave fabrication of full side quadrant segments (each side ≈ 251 in. by 374 in.) was planned to include wet skin and stiffeners, cobonded with frames (circumferential and window belt).

Keel: A variation of design concepts from Family D (sandwich) was chosen as the keel baseline. The variation includes a thick laminated plate to panelize the keel beam chords. The thick plate gradually transitions into a sandwich panel as axial compression loads decrease away from the section splice. The sandwich facesheets have tapered thickness in the transition zone. Figure 10 shows the heavily loaded end of the keel panel baseline near the section splice.

This innovative panelized concept was chosen for the keel quadrant baseline for several reasons. First, it avoids problems in fabricating and splicing two large composite keel chord members. Large fastener hole diameters needed to mechanically splice discrete composite chord members would cause a significant knockdown on the allowable strength. The panelized concept alleviates this problem to some extent. The blended thick laminate/sandwich construction also yields a constant gage panel that avoids problems in attaching frames and other elements to a skin/stringer design having skins with considerable thickness taper.

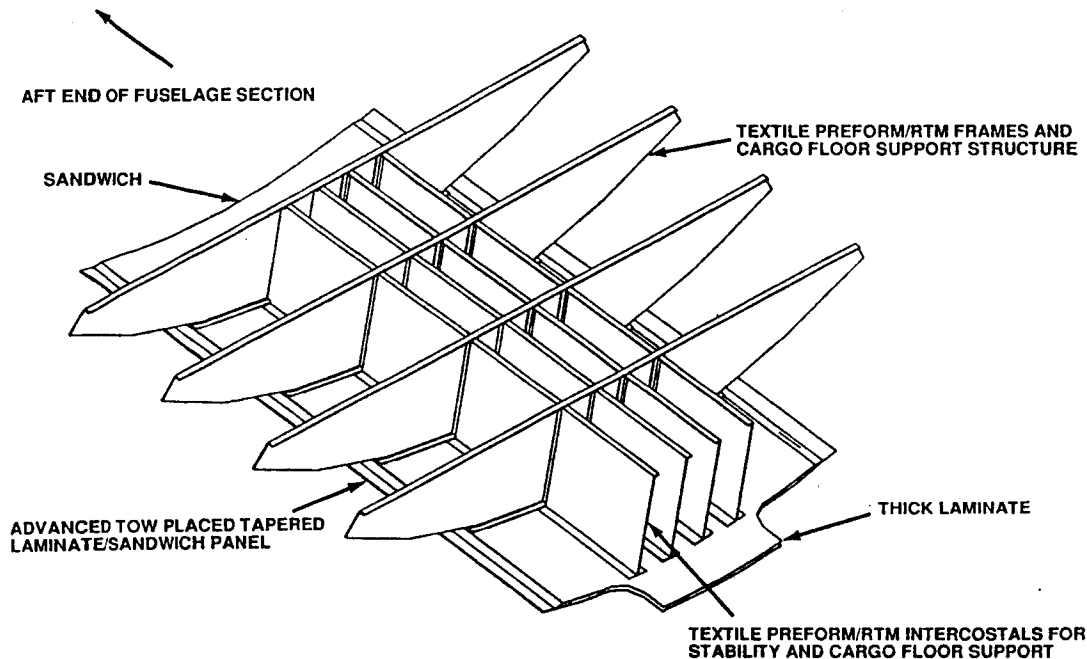


Figure 10: Keel Baseline Design Concept and Fabrication Processes.

Face skins for the keel panel will also be produced in a batch tow placement process. Again, automated batch processing and significant amounts of ply tailoring possible with the advanced tow placement method led to its selection for the keel quadrant. The sandwich core will be machined with a constant taper to keep the keel panel at a constant gage as laminate plies are dropped.

Keel baseline elements include intercostals and full-depth frames, both of which will be stiffened. These elements serve dual roles in overall panel stability and cargo floor support. Note that intercostals are discontinuous at the frames. Baseline material forms and processes for both these elements are textile preforms and RTM, respectively. Frames and intercostals will be mechanically attached to shear tied blade elements on the fully cured keel panel. These blade elements will be co-bonded to the keel panel at cure. Keel quadrant segments (≈ 72 in. by 374 in.) will each be small in comparison to side and crown panels; however, the weight per unit area will be relatively high.

Technical Issues

The most critical manufacturing issues associated with baseline concepts selected for ATCAS relates to final assembly. Crown and side panels have bonded stringers and frames, while the keel panel is sandwich with bonded frames. This eliminates element assembly steps and part count, but high bending stiffness of the baseline panels will limit attempts to deform them into shape prior to splicing. Figure 11 illustrates some of the problems on a diagram of the full baseline crown panel. Variations in locational tolerances of stringers and frames is critical to their alignment at circumferential and longitudinal splices, respectively. Overall panel warpage may also be an issue due to the local unsymmetric layups at bonded elements.

Another critical manufacturing issue is the quality control of quadrant panel fabrication processes. Quadrant panel cost benefits assume that large panels will not be rejected due to manufacturing defects. In order to avoid adding unnecessary costs to the manufacturing process, the panel fabrication quality required for acceptable performance must be understood.

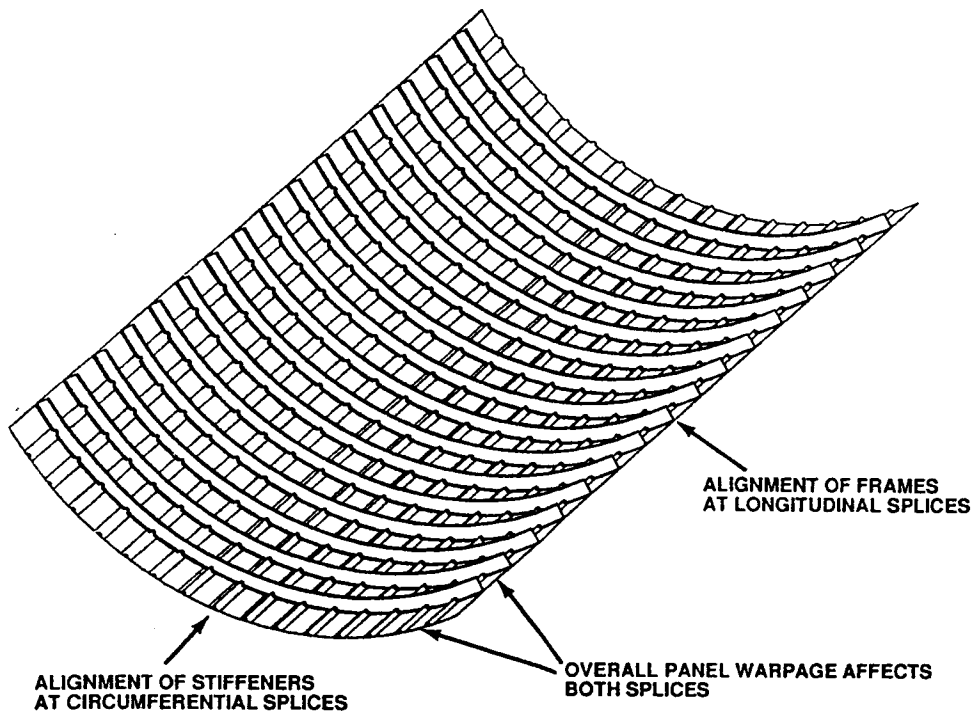


Figure 11: Assembly issues for the crown quadrant panel.

Crown: The fuselage crown area is the simplest quadrant in terms of design detail and manufacturing complexity. A smaller number of technical issues are also associated with the crown. Two critical manufacturing issues were discussed at the start of this subsection. Tension damage tolerance is the most critical structural issue for crown panels. Analysis and tests are needed to evaluate the effects of dynamic pressure release on tensile residual strengths following a through-penetration impact event (e.g., engine blade penetration). Other major issues for the crown baseline which will be addressed in ATCAS are listed in Reference 1.

Window Belt (Side): The fuselage side quadrants have considerably more design detail and manufacturing complexity than the crown. Many of the crown technical issues are also critical to side panel locations above the window belt. The two critical manufacturing issues that were discussed at the start of this subsection are of greatest concern for the side quadrants due to their size. The lower portion of side quadrants (i.e., approaching the keel) have considerable combined load interactions. The combined effects of axial compression, inplane shear, and hoop tension on damage tolerance need to be understood. Other major issues for the side baseline concepts which will be addressed in ATCAS are described in Table 1.

Keel: The aft fuselage keel quadrant poses one of the most difficult design challenges for applications of composites to transport fuselage (i.e., load redistribution of very high compression loads entering the fuselage shell at the keel beam attachment). It also has considerable design detail and manufacturing complexity related to the cargo bay floor. The critical manufacturing issues that were discussed at the start of this subsection are of particular concern for the baseline keel quadrant due to its high stiffness. Other technical issues listed for the crown and side quadrants are also critical to the keel. These include side issues number 5, 6, and 9 from Table 1 for circumferential frames. Note that loads affecting durability of keel frame to panel adhesive bonds differ from those in the crown. The 2 ft. deep baseline keel frames and intercostals also add manufacturing complexity to the textile preform and RTM fabrication processes. Other technical issues for the keel are given in Table 2.

Issue	Description
1.) Damage Tolerance of Pressure Loaded Panels With Large Penetrations	This issue involves failsafe load and damage conditions. The most critical damage geometries are expected to be slender notches oriented along the longitudinal axis (e.g., Reference 3). The effectivity of bonded frames as "tear straps" needs to be determined. The scenario of a penetration that severs a frame and skin must also be studied.
2.) Impact Damage Resistance and Tolerance of Stiffened Panels Near the Keel	Numerous in-service impact scenarios are possible in the lower portion of the side quadrant. These include stones, runway debris and ground handling equipment. Studies are needed to insure that the structure is resistant to damage occurring for the full range of impact events and to characterize damage for residual strength predictions. The effects of combined compression and shear loads representative of the lower side quadrant must be considered. An understanding of material, structural, and laminate variables affecting impact damage resistance and tolerance is needed to promote low-cost, robust designs.
3.) Shear Stability and Damage Tolerance Near Panel Cutouts Such as Windows and Doors	Window & door elements such as frames, door stops, and intercostals insure adequate strength and dimensional stability in areas of shear and pressure load redistribution. Design and fabrication of these elements must consider damage scenarios which complicate load paths. Current plans project window frame modules cobonded to the skin; however, potential debonding problems may require through-thickness reinforcement such as composite rivets for adequate performance.
4.) Efficient Laminate Thickness Tailoring at Door & Window Cutouts	An increase in laminate thickness near large cutouts such as windows and doors is required for stiffness, stability and strength. Since material tends to be a major cost center, it is desirable to understand the manufacturing options and mechanics issues that will enable thickness tailoring to save cost and weight.
5.) Fiber/Resin Distribution of Frames, Window and Door Design Details After RTM Processing	Performance, warpage, and additive dimensional tolerance control of complex geometries such as curved frames relates to fiber/resin distribution. These factors must be considered in seeking an answer to the scale-up issue of the element sizes feasible for RTM processes. Assuming a suitable cure cycle and tooling approach, the fiber/resin distribution of traditional tape and low materials is most strongly dependent on the prepreg operation. Receiving inspection tests add costs to these materials to insure prepreg of acceptable quality. Both resin infusion and part cure occur during RTM processing. Cost efficient methods of controlling the fiber/resin distribution and, hence, quality of RTM parts must be established.
6.) Handling and Storage of Cobonded Design Details Before & After RTMing	Methods of handling dry preforms must avoid distorting the textile weave pattern (e.g., fiber orientation) prior to cure. This includes the operation used to drape preforms into tools for RTM processing. After RTMed parts are cured, they must be stored to avoid surface contamination prior to cobonding with side quadrant panels.
7.) Nondestructive Inspection of Complex Window and Door Frame Detail Geometries	Methods for evaluating the quality of complicated part geometries (e.g., corner radii in window frame modules) need to be developed and demonstrated. Collaborative efforts with structural analysts is also required to determine the effects of defects and hence, support development of robust designs and quality control specifications. The approach established should ask the question of "what manufacturing quality is needed to insure performance standards?". This would avoid specifications that eliminate benign defects and add unnecessary costs to the fabrication process.
8.) Performance of the Frame Mousehole Design Detail	This design detail simplifies the skin/frame co-bonding operation but adds stress concentrations in frame and adjacent skin material that needs to be analyzed and tested. Higher stresses near the mousehole may lead to a need for additional frame material. Sufficient damage tolerance for skin penetrations located near the frame mousehole must also be established. Cost trades between reduced bonding labor and increased material needs to be understood to minimize total costs.
9.) Durability at Load Transfer Details (Bonded Elements and Mechanically Fastened Splices)	Durability of composite fuselage design details needs to be studied. Cyclic pressure load conditions are expected to drive the design of frame/skin adhesive joints. This pressure pillowing problem needs to address creep/fatigue interactions using analysis and tests. Combined cyclic load conditions also pose a significant problem for longitudinal and circumferential mechanically fastened joints. The combined loads include pressure and reversed inplane shear. The effects of environment and real time on damage accumulating in material surrounding the bolt hole will need to be considered.
10.) Skin Gage to Satisfy Hail Impact Criteria	Structural tailoring of the top of side panels is limited by the minimum skin thickness required to suppress visible hail damage. This avoids high repair costs for multiple-site impact damage caused by severe hail storms.

Table 1. Technical Issues for the Side Quadrants.

Issue	Description
1.) Impact Damage Resistance and Tolerance of Various Keel Panel Locations	The thick laminate/sandwich construction for baseline keel panels yield unique characteristics to consider in impact damage resistance and tolerance problems. Added laminate thickness has been shown to yield higher residual strengths for a given impact energy (Reference 4). However, the relatively small shell diameter to thickness ratio of a panelized keel and interlaminar stress redistribution due to many ply dropoffs may complicate the problem. The effects of combined compression/shear/pressure load conditions on post-impact residual strength need to be studied.
2.) Through Penetration Damage Tolerance of Various Keel Panel Locations	Failsafe constraints such as through-penetration damage may drive the design of various locations along the keel panel length. For example, added impact damage resistance at the thick laminate end of the panel may be such that ultimate load/barely-visible-damage criteria cause little strength reduction (note: this can occur when using a maximum impact energy as a threshold). Through-penetration damage tolerance will also have to consider the effects of combined compression/shear/pressure load conditions and ply drop-offs.
3.) Panel Stability With Major Compression Load Redistribution	There is likely coupling between residual strength, stiffness, and stability for a heavily loaded panel such as the baseline keel concept. Analysis and tests are needed to ascertain key variables affecting stability of the innovative keel design. Local eccentricities of a sandwich panel with internal ply drops and wedged core could be amplified by the presence of damage. The retention of frame-to-panel bond strength is crucial to stability along the panel length. Stability of the thick laminate at the forward end is also dependent on the effectiveness of intercostals for providing a side boundary condition.
4.) Process Cure Cycle for a Panel That is Thick Laminate On One End and Sandwich On the Other	A suitable cure cycle needs to be developed and demonstrated for the baseline keel concept. Traditional low density composite honeycombs are unable to withstand the high pressures needed to cure some toughened matrix materials. One solution to this problem is to precure laminate portions of the panel prior to adhesive bonding with the honeycomb core. This may prove costly and lead to adhesive bond problems if the precured thick laminate section is warped. Another solution is the use of foam core materials that are able to withstand pressures needed for cocuring with the laminate.
5.) Efficient Laminate Thickness Tailoring for Load Redistribution	Interlaminar stresses must be considered in selecting ply drop-off sequences as compression loads decrease from the forward to aft ends of the keel quadrant. Efficient processes such as automated tow placement that can drop plies with minimum material waste are sought. Analysis and test are needed to select materials best suited for the load conditions.
6.) Laminate Material Forms for the Baseline Keel	Strong trade-offs between performance and cost are anticipated by the DBT when attempting to select the optimum keel material. Crucial material characteristics include interlaminar shear load transfer, impact damage resistance, and through penetration residual strength. High interlaminar shear stresses near numerous ply drop-offs in the keel panel suggests a possible need for additional resin to enhance load transfer. This may be achieved by increasing overall towpreg resin content or locally adding adhesive at ply drops. A compliant, toughened adhesive is expected to work best for increasing both the interlaminar shear load transfer and impact damage resistance. The through-penetration damage tolerance also needs to be studied because it could conceivably drive the design of toughened materials.
7.) Core Material Form for the Baseline Keel	An impact damage resistant sandwich concept is needed for the keel baseline. Past work (e.g., References 3 and 5) have indicated an inherent weakness in traditional composite honeycomb and polymeric foam materials whereby impact causes significant damage that leads to the loss of facesheet stability and decreased compressive residual strength. Examples of improvements in impact damage resistance include higher density core materials and a foam with re-entrant cell structure (Reference 6). Other factors such as curvature and core/facesheet interactions also need to be studied.
8.) Thick Laminate Keel Panel Splice Heavily Loaded in Compression	Several technical issues need to be considered for heavily loaded mechanical joint attachments between thick laminates. Small fastener diameter-to-thickness ratios affect laminate bearing capability, and, due to typically low interlaminar shear moduli, will also increase fastener flexure. Large holes required to mechanically attach thick laminates directly affect bypass-dominated failures and are expected to change the bearing-bypass interaction.
9.) Repair of Thick Laminate/Sandwich Panels With Bonded Design Details	Repair is an issue at both ends of the baseline keel panel. Mechanical attachment of repair plates will be difficult for sandwich panel construction. Major repairs involving the base panel and portions of the full depth frames will also be laborious. Bonded repair methods for surface damage will need to consider difficulties in curing portions of thick laminates and sandwich panels in the field. New repair methods that can be performed more simply and with minimum cost are needed for thick laminate and sandwich panels.

Table 2. Technical Issues for the Keel Quadrant.

ATCAS SIX YEAR PLAN & PROGRESS TO DATE

Crown, keel, and side areas of the aft fuselage section will be studied in Phases A and B of the ATCAS program. These two phases span a five year time period ending in 1994. An optional addition to Phase B for fabricating a large pressurized panel test fixture and performing combined load tests is scheduled to occur from 1993 to 1995.

Figure 12 shows a timeline of the six main areas of development and verification tasks within the ATCAS program. Comprehensive schedules were created in each of these areas to integrate design, manufacturing, structures, materials, and test tasks. Crown, keel, and window belt areas will initially be studied separately because each has unique manufacturing and structural issues to be resolved. Efforts are spread such that the most difficult problems receive greater attention. For example, Figure 12 shows that 2.5 years are dedicated to crown panels, while keel studies will last a full 5 years.

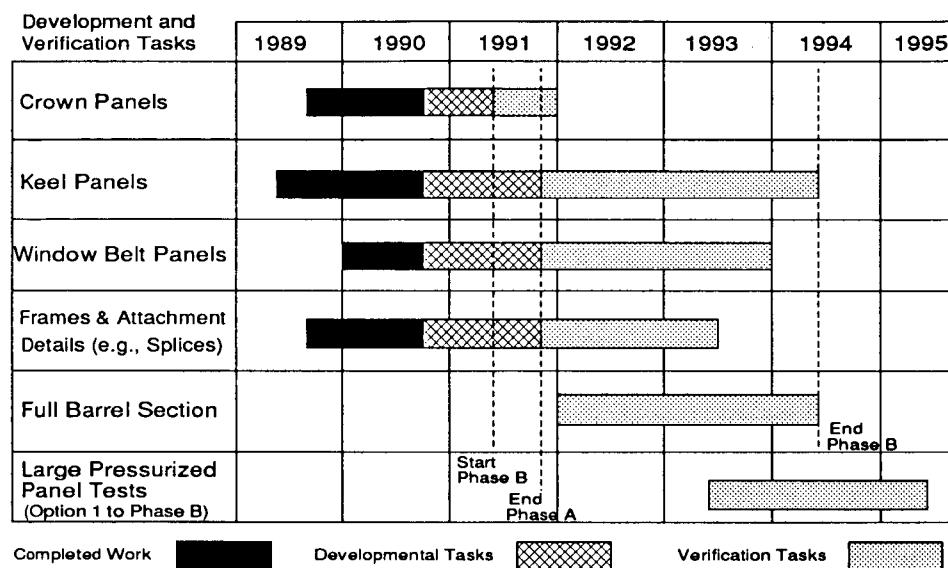


Figure 12. Development & Verification Timeline for ATCAS

Development and verification tasks for frames and attachment details support each quadrant. The final design optimization efforts with these elements and splices are left until the "Full Barrel Section" effort at the end of Phase B. This will promote assembly cost savings by striving for part commonality throughout all regions of the study section.

The three step DBT approach described earlier for achieving ATCAS cost and weight saving goals will be applied to each quadrant. Note that design activities for side quadrants are associated with the window belt timeline. The first step, baseline concept selection, has been completed for each quadrant. Global evaluation has been accomplished for crown panels and is currently underway for the keel quadrant. This second design step is scheduled to be completed for all quadrants by the end of Phase A, substantiating concepts chosen for verification tests with detailed cost and weight saving estimates. Local optimization (Step #3) has just begun for the crown and will be completed by early 1991. The time needed for local optimization varies for each quadrant depending on the engineering efforts required to overcome the associated technology barriers. For example, local optimization for the keel lasts more than 2.5 years.

There is considerable overlap in technology issues that need to be addressed for each quadrant. Fabrication, analysis, and testing efforts were scheduled to group common tasks. Figure 13, which is a modification of the ATCAS quadrant diagram (i.e., Figure 5), shows that many of the side quadrant technical issues will be addressed by crown and keel work tasks. The side panel manufacturing and test efforts will include windows, but not doors. Keel panel manufacturing and test studies will include compressive load redistribution approaching the forward end of the section but not the actual keel beam splice. Although doors and the keel beam splice are not included in ATCAS test and manufacturing hardware, both are considered in the design cost and weight estimates.

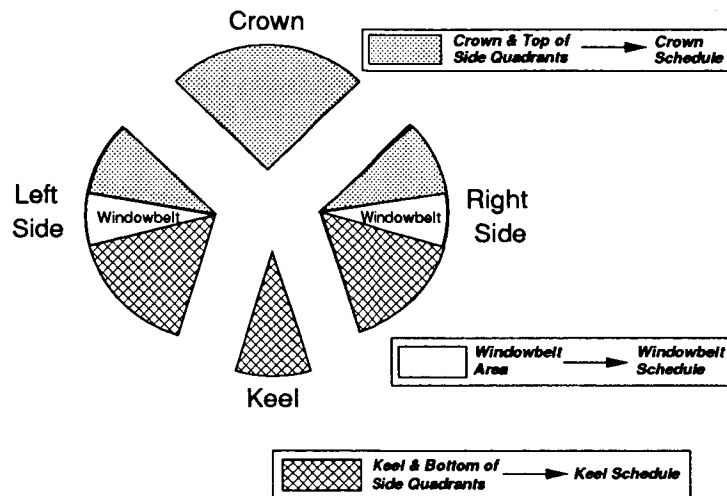


Figure 13. Schedules for Tracking Fabrication, Analysis, and Test Tasks

Industrial subcontractors and other Boeing groups play important roles in ATCAS. Early experiences suggest that the integration of diverse expertise from groups outside the immediate ATCAS team (Boeing Commercial Airplanes) is crucial to the development and verification of advanced technologies. Figure 14 shows groups that have supported ATCAS to date.

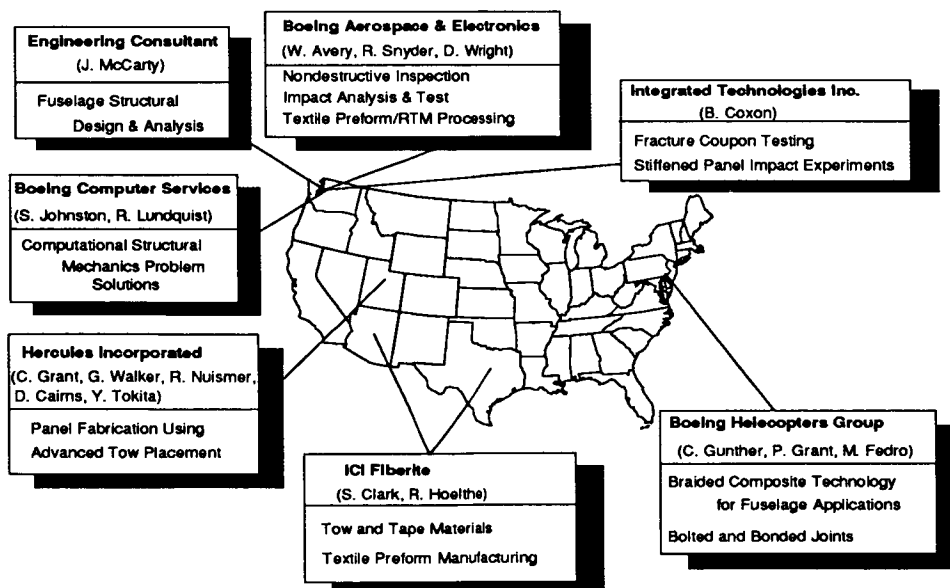


Figure 14. Other Boeing and Industrial Groups Supporting ATCAS

As shown in Figure 15, several university subcontracts have also been issued to support ATCAS. The approach taken to infuse universities in ATCAS has been beneficial to both parties. The Boeing/NASA ATCAS goal of advanced technology development complements the universities' engineering goal for improved education. Each university subcontract was defined to start with fundamental research and end with applications directly supporting work on a technical issue in ATCAS. The engineering tools developed at universities include analysis methods, test techniques, material characterization, and manufacturing developments. In return, the students education is supplemented with an understanding of fuselage technical issues and the opportunity to apply their research to a "real world" engineering problem. Secondary benefits from university infusion have included a cost-effective use of ATCAS funds, and budget for graduate student programs.

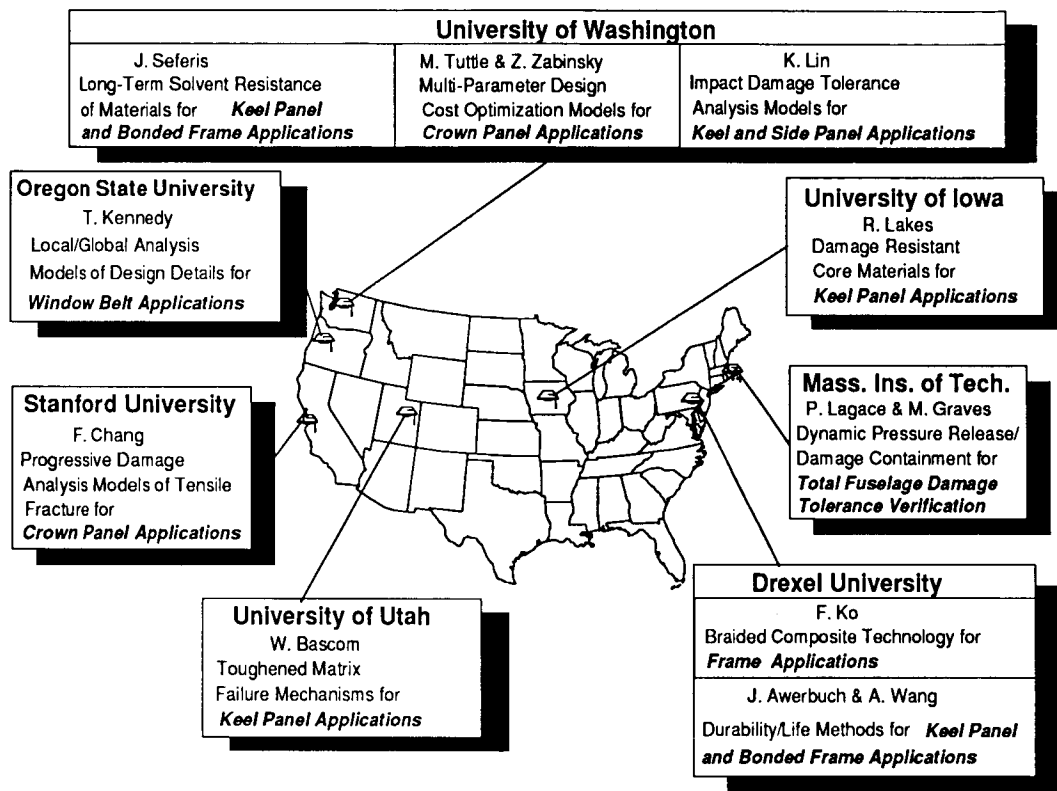


Figure 15. Integration of University Subcontracts in ATCAS

Crown Panels

Global Optimization: Crown panel efforts started in the fall of 1989. Most of the work performed to date supported the global evaluation of design and manufacturing concepts. Two designs from each of three families were developed for global optimization of the crown quadrant. Each design was sized considering multiple load cases, damage tolerance, and assembly design details. The three families were B, C, and D (see Figure 3 for family definitions). A detailed fabrication and assembly plan was developed for each design. These were used to estimate weight, material costs, and labor rates. Both recurring and nonrecurring (minus capital equipment) costs were estimated assuming specified groundrules (e.g., 300 shipsets at a rate of 5 per month). A synopsis of the results from global crown studies appears on the following paragraphs. A more complete account of this effort appears in Reference 1.

The two designs and manufacturing plans for each family varied material types, manufacturing processes, and structural details. This helped to establish a range of cost and weight variation for each family. Design trades within a family also yielded data on cost centers and variable interactions crucial to local optimization studies.

The majority of weight for all designs was in the skin where tension damage tolerance was found to drive skin thickness and layup of most of the crown panel area. Hail impact requirements also controlled the skin gage for the aft end of some panels. Stringer thicknesses were driven by reversed load stability requirements. Both skin and stringer gages near panel edges were controlled by joint bearing requirements.

Figure 16 shows the final results from global optimization. All composite crown designs studied were found to be cost and weight competitive relative to the metallic benchmark. Relative weights for composite designs ranged from 49% to 80% of the metal. The estimated relative manufacturing costs for composite concepts ranged from 99% to 139% of the metal. When considering an economically acceptable cost increase per unit weight savings (i.e., concepts to the left of the slanted solid line in Figure 16), all composite designs showed an advantage over the metal benchmark.

Aluminum costs were dominated by labor, while material and labor costs for composite designs were close to equal. Composite designs were competitive with the metal benchmark primarily because reduced assembly labor offset lower aluminum material costs. For example, a composite crown panel had 10,000 less fasteners than the metal counterpart. This relates to large composite quadrant panels with bonded elements for Family C.

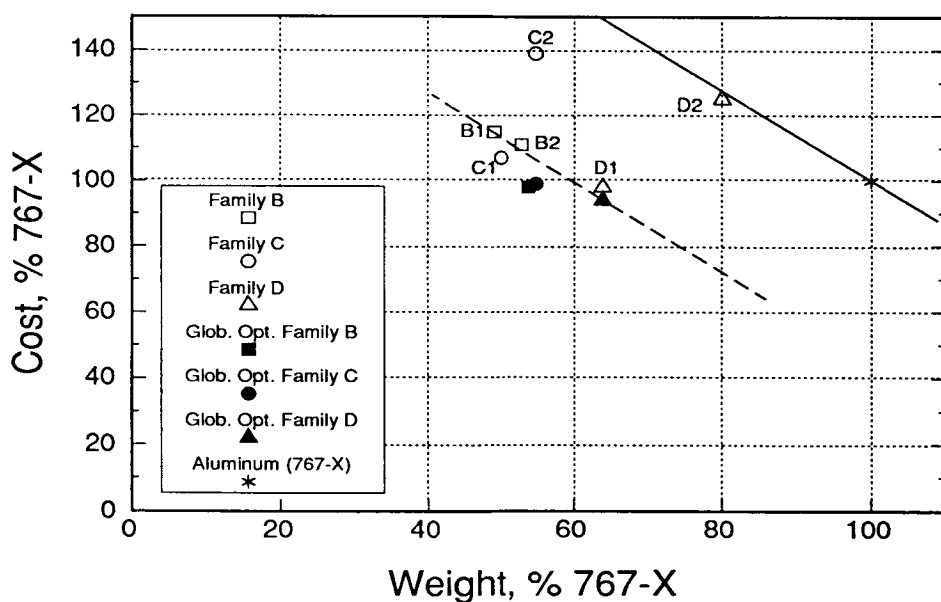


Figure 16. A Comparison of Results from Global Optimization Studies and the Metallic Benchmark.

Figure 16 also shows globally optimized family designs derived by mixing and matching the best features of concepts studied (e.g., cost-efficient materials and processes). The most promising family was selected based on results from this exercise and an evaluation of the potential for further cost and weight optimization. Globally optimized Families B and C were both found to be nearly equivalent in

cost and weight. Family D yielded a lower cost with some weight penalty (i.e., 94% the cost and 64% the weight of metal). The weight increase for Family D was not found to justify the cost savings. This is shown in Figure 16 where concepts to the left of the dashed line represent an acceptable cost increase per unit weight savings. Family C was chosen over Family B, despite greater manufacturing risk, due to good local optimization potential and bonded frames which may help damage containment.

Local Optimization: Local optimization of crown panels is currently underway. This task will further refine the design by attacking cost centers identified in global optimization. The most significant cost centers for crown panels were found to be skin, stringer, and frame fabrication; panel bonding (i.e., element subassembly, bagging and cure); and fasteners required for quadrant assembly and body join. The relative percentage of material and labor components of cost varied for individual fabrication and assembly steps. A rough estimate of the local optimization potential for composite crown panels indicated cost savings up to 25% (relative to the metallic benchmark) within the range of acceptable weight penalties.

The use of a high performance fiber to reduce skin weight was not found to be cost effective in global optimization of crown panels. This relates to the trade between a higher material purchase price and the costs saved from added performance capability. Attempts to reduce the composite material cost center for crown panels will include studies with graphite/fiberglass hybrids. The high tensile strength and low cost of fiberglass makes it a candidate for crown applications. The economically acceptable increase in weight per unit cost savings will be considered in this evaluation.

The relatively low aluminum material costs generally allow an effective trade of added weight for reduced labor. High composite material costs are expected to lead to relationships between cost and weight that differ from those of metals. A software design tool that includes cost and mechanics constraints is being developed by the University of Washington to support the optimization of crown panels (see Reference 7). Figure 17 shows this optimization tool schematically. Critical design variables are expected to include material type, stringer geometry, and laminate thickness.

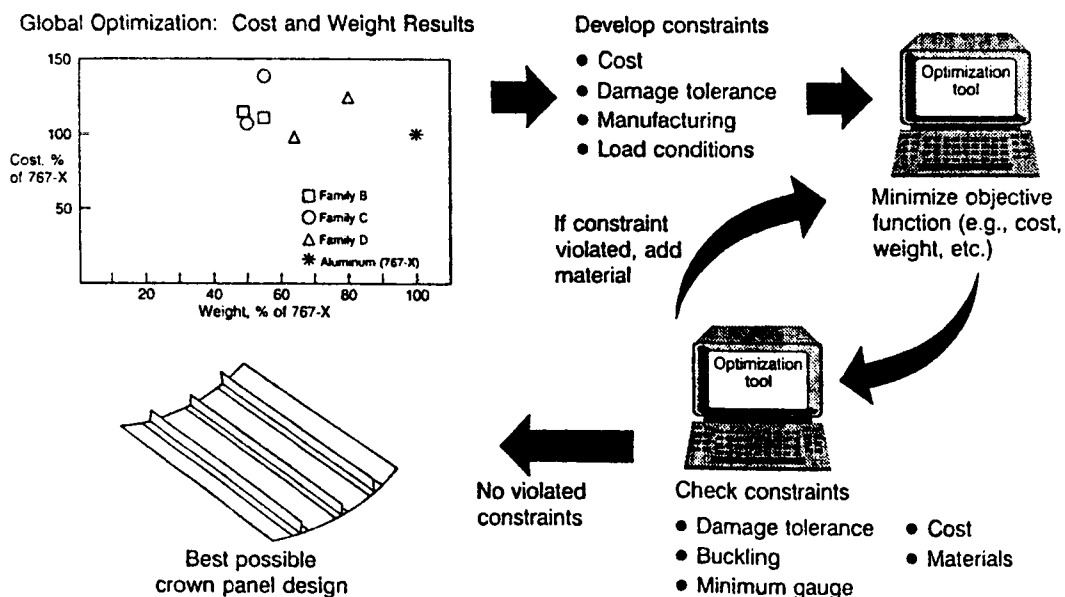


Figure 17. Local Crown Panel Optimization Tool

Several other factors will be considered to reduce cost in local crown optimization. These include the manufacturing approach to panel subassembly and the use of low-cost composite fasteners. Efficient processes for stringer and frame fabrication are also sought. Considerable costs were saved during global studies by envisioning batch processes for these elements; however, their costs were still high relative to the metallic counterparts. One potential cost savings may be in the use of tow placement rather than CTLM to layup stringer charges. This relates to projections that the future costs of prepreg tow will be less than that of tape. A continuous RTM process involving textile preforms may also be suitable for low-cost stiffening elements.

Analysis, Fabrication, and Test: Tension damage tolerance is the most critical performance issue for crown panels. Several damage tolerance analysis methods have been developed and implemented as mechanics constraints in the local optimization software shown schematically in Figure 17. These procedures, which utilize a characteristic dimension failure criteria, include the effects of pressure, panel curvature, bonded stiffening elements, and material anisotropy. Figure 18 plots typical results from residual strength analysis showing an interaction between pressure, panel curvature, and local bending stiffness. Pressure is shown to decrease residual strength due to local bending at the notch tip that increases the stress concentration. A sandwich panel construction alleviates some of the effects of pressure by increasing local bending stiffness. For this reason, a sandwich panel design was selected as a backup to the crown baseline.

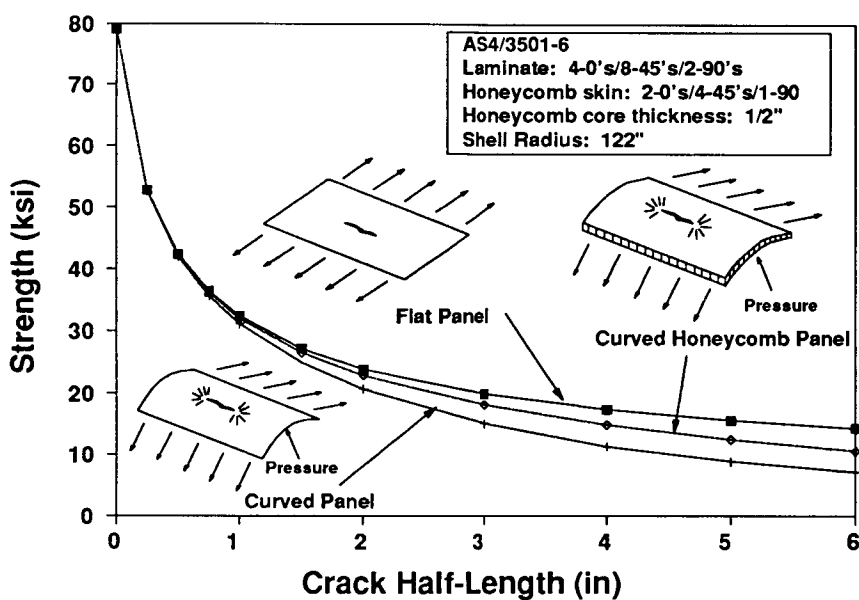


Figure 18. Predicted Tensile Strengths of Damaged Panels Subjected to Inplane and Pressure Loads

In addition to the simplified analysis described above for predicting tensile residual strength, a more complete progressive damage model is being developed at Stanford University. The Stanford models will be used during final test verification to evaluate the growth and accumulation of local damage that occurs prior to catastrophic failure. To date, progressive damage models have been developed to account for fiber breaks, matrix cracking, nonlinear shear behavior, and fiber/matrix splitting. Future enhancements will incorporate the effects of nonlinear longitudinal moduli, delamination, variable notch geometry, combined load conditions, and panel element geometries.

Advanced tow placement and the batch quadrant processing concept were shown to be efficient in detailed cost studies for crown skins. Tow placement layup costs were found to be on the order of 20% of the skin material costs. Since skin constituted the largest portion of panel weight, an efficient layup process helped to lower total composite crown costs. Advanced tow placement is ideally suited for the graphite/fiberglass hybrid concept being considered for reducing crown material costs. Tow-placed intraply hybrid panels can be fabricated without affecting process efficiency. Figure 19 shows one of the four graphite/fiberglass hybrid panels fabricated in ATCAS to date. Additional discussion of advanced tow placement manufacturing trials completed in ATCAS appear in the next section on keel panels.

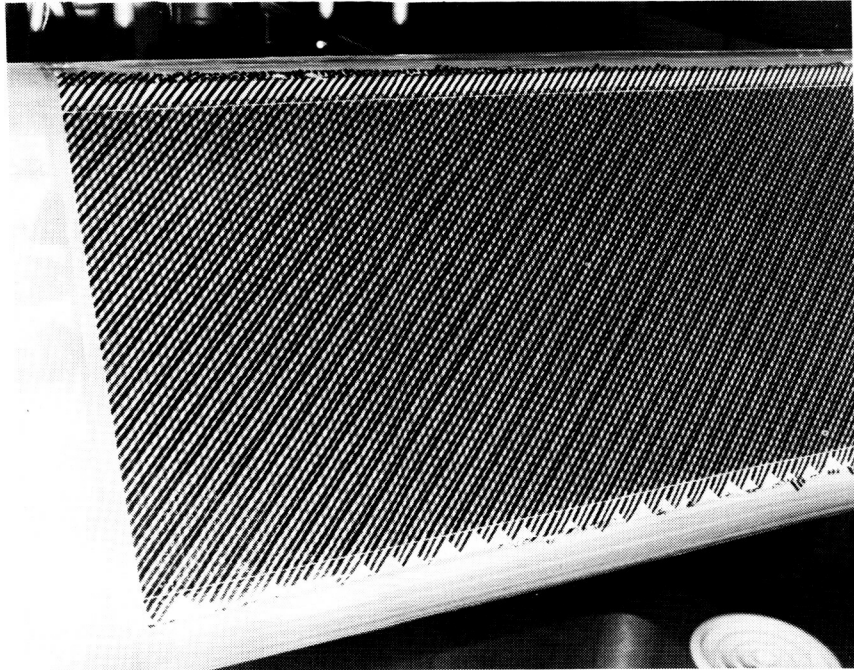


Figure 19. Tow Placed AS4/S-Glass Hybrid

Specimens cut from the hybrid panels will be used to evaluate notched tensile residual strength. The base material type in these studies is AS4/3501-6. Hybrid material and process variables under consideration include hybridizing fiber type (S-glass and T1000), percent hybridization (25% and 50%), and repeating unit tow width (0.35 and 1.1 in.). The screening test variables include notch type (hole, slit, and impact induced through-penetration) and notch size (0.25, 0.875, and 2.5 in.).

Plans and schedules in ATCAS are coordinated to yield test panels from process verification studies. Fabrication of crown panel demonstration hardware is scheduled for the first half of 1991. This effort will start with some tooling trials and end with the fabrication of several panels, the largest of which is 8 ft by 10 ft. Current plans will emphasize the baseline design (Family C, with bonded stringers and frames). If problems occur due to the complex bonding operation or insufficient tensile damage tolerance an alternate plan, involving sandwich panels with bonded frames, will be implemented.

Verification tests using stiffened panels (three to five stringer) that represent portions of the optimized crown design will occur during 1991. These will include (1) uniaxial panel stability tests for reversed load conditions (with and without critical impact damage), (2) impact trials to validate that minimum gage/hail requirements are satisfied, and (3) tensile damage tolerance tests (pressure, uniaxial, and biaxial) for various through-penetration damage scenarios.

Keel Panels

Aside from baseline concept selection, little keel design work has been completed to date. Initial keel work tasks have included analysis, fabrication, and tests to address some of the critical issues listed earlier. Specifically, issues number 1, 6, and 7 from Table 2 have been studied during the first 16 months of ATCAS. Results from these studies will support final material selection and detailed design. This subsection will summarize work on each of the three issues, followed by a description of the large keel hardware tests planned towards the end of ATCAS.

Designed Experiment for Fuselage Panel Impact Resistance: All quadrants of the fuselage have technical issues related to impact damage resistance. A test program was defined early in ATCAS to evaluate the effects of thirty two combinations of material, laminate, structural, and extrinsic variables on impact damage resistance. The experiment was designed to ascertain main effects with a minimum number of tests. Some of the details of this experimental design are described in Reference 8. The desire to integrate ATCAS tasks (e.g., manufacturing trials and test hardware) led to a more general plan for panel fabrication and usage than would have been required for impact screening alone. Figure 20 shows some of the manufacturing and performance issues addressed by this initial fuselage panel fabrication effort. Large panels were fabricated to study manufacturing scaleup issues such as low-cost tooling concepts in the presence of ply dropoffs.

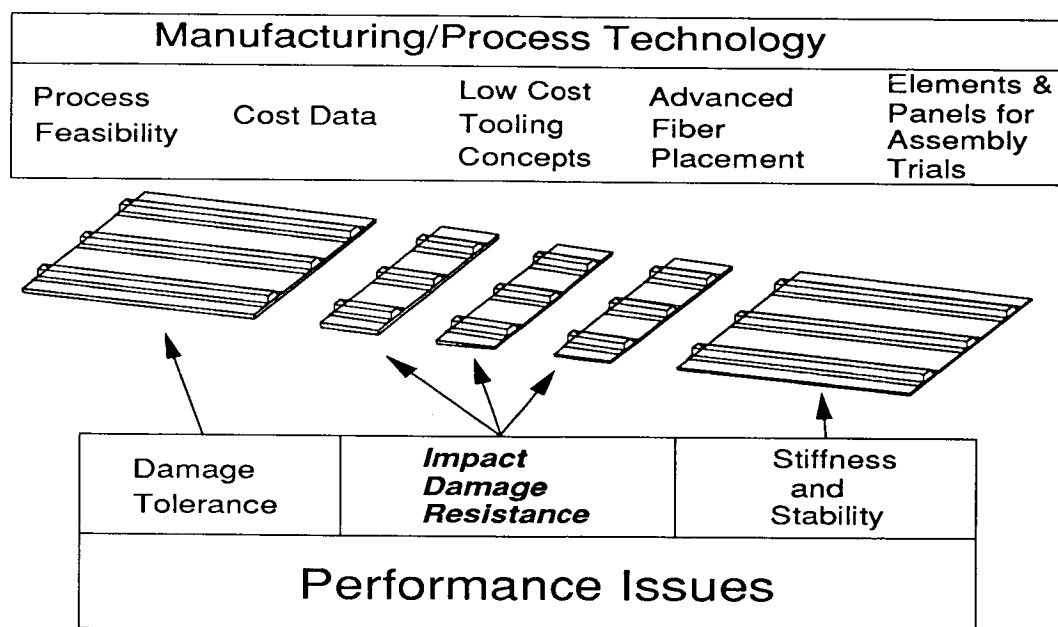


Figure 20. Multifunctionality of the Initial Fuselage Panels Fabricated for ATCAS

Sixteen 110 in long stiffened panels were fabricated to support the tasks shown in Figure 20. Each panel had thick (≈ 0.18 in.) and thin (≈ 0.089 in.) ends, with a central transition zone where 12 plies were dropped over a 10 in. length. Note that different portions of these panels were used to study baseline crown, keel, and side quadrant issues. The thick end provided data for the lower portion of side quadrants (i.e., below the windows). The thin end was used for the crown and the upper portion of side quadrants (i.e., above the windows). Finally, laminates in the transition region of the panel were used to fabricate sandwich panels that supported the keel baseline. All activities related to the fabrication of the sixteen stiffened panels were tracked on the keel schedule of ATCAS monthly reports, despite the relationships with other quadrants.

Eight of the sixteen panels were fabricated at Hercules Inc. using advanced tow placement. Figure 21 shows a photograph of one of the tow placed panels. All other panels were processed using tape material forms at the Boeing Company. Drape forming and low-cost rubber tools were used to facilitate fabrication of the hat stiffening element geometry at both companies.



Figure 21. Tow Placed Hat Panel

As discussed earlier, the most critical assembly issue related to cured panel warpage and locational tolerances for bonded elements. The approach used in ATCAS to solve this problem involves three steps. First, manufacturing demonstration hardware will be fabricated with design details. Second, cured panel imperfections will be experimentally measured. Figure 22 shows warpage measurements for one of the hat stiffened fuselage panels. Finally, a suitable analysis method will be developed to predict the warpage and perform sensitivity studies to select design variables that minimize potential assembly problems. Early developments supporting this final step included an ABACUS finite element model that predicted the shape and overall deflection shown in Figure 22 to within 5%.

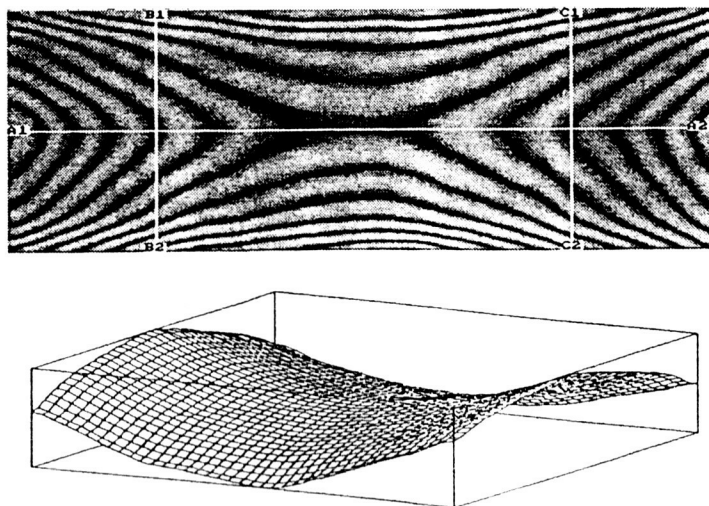


Figure 22. Panel Warpage Measurements Using a Moire' Technique

Toughened Material Models: Composite materials with compliant, resin-rich, interlaminar layers (RIL) tend to have improved interlaminar shear toughness and impact damage resistance. Both appear to be advantages for keel applications. Considerable efforts have been spent in ATCAS to develop analysis tools and generate data bases for toughened materials with RIL (see References 8-12 for more complete documentation).

Toughened materials studies have included (1) material property tests, (2) characterization of failure mechanisms, and (3) analysis method development. Some relationships with the RIL microstructure were found in each area. Mode II delamination toughness was directly related to RIL thickness; however, no such correlation was found to exist for mode I toughness (Ref. 11). The tendency for RIL to suppress delamination during an impact event has been found to lead to fiber failure as an alternate failure mechanism (Refs. 10 and 11). The presence of RIL was found to alter matrix crack resistance, reducing the in situ transverse strengthening effect observed with traditional composite laminates (Ref. 12). Not all analysis methods developed for materials with RIL required an accurate model of the microstructure. It was crucial to simulate the RIL for matrix crack predictions. However, accurate predictions of compressive strength after impact (CAI) were obtained without modeling the RIL.

Impact damage is expected to be a critical issue, particularly in the lower side and keel quadrants. Models have been developed and verified in ATCAS to predict CAI for different composite materials and laminate stacking sequences (Ref. 8-11). Laminate layups and specimen geometries used for material screening received special attention in ATCAS. Models were used to interpret results from experiments. For example, the effects of finite specimen width on CAI were eliminated with the help of analysis. Parametric analysis studies were used to identify key variables affecting CAI, resulting in recommendations for improved material screening procedures (Ref. 9). Figure 23 shows why it is crucial to screen materials over a range of impact energies and correct for specimen width effects.

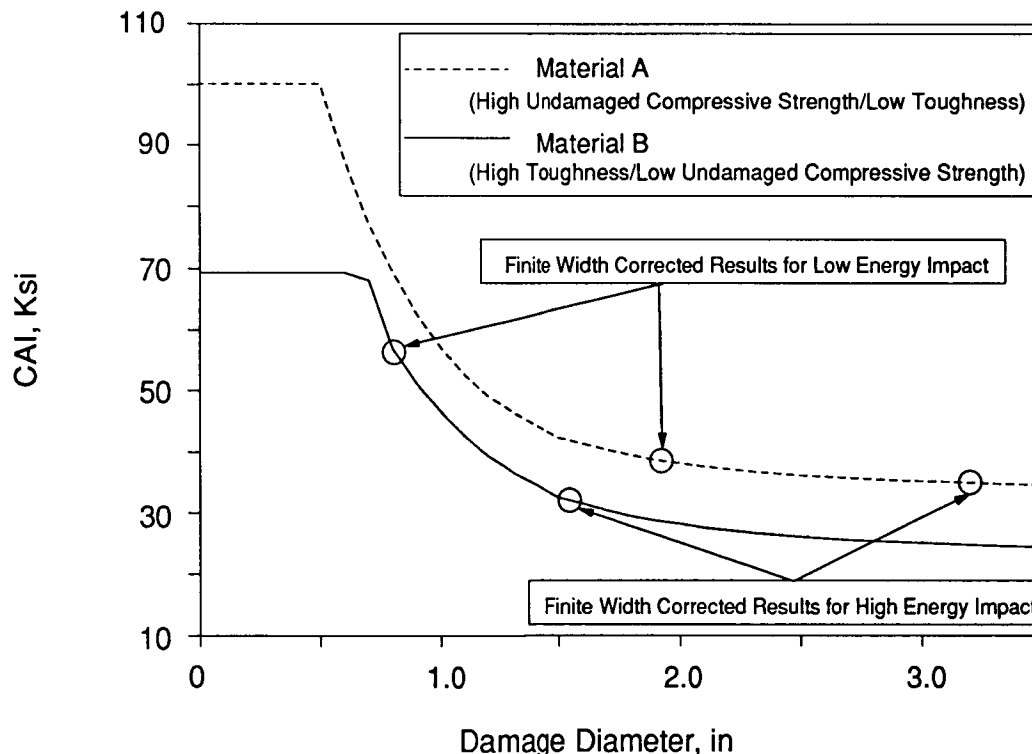


Figure 23. Theoretical Damage Tolerance Curves for Two Materials

Studies are underway in ATCAS to determine optimum fiber/resin combinations and resin contents (both intra and inter-laminar, see Ref. 11) from the standpoint of both cost and performance. Conceivably, lower cost fibers and higher resin contents may achieve the compression performance advantages of a RIL microstructure with reduced costs. The compressive failure strain was found to increase for toughened laminates having higher resin contents (Ref. 11). This attribute may be even greater when considering laminates with significant amount of ply dropoffs, characteristic of the keel baseline. Figure 24 shows that the ATCAS analysis methods developed for toughened materials are general enough to account for variations in resin content.

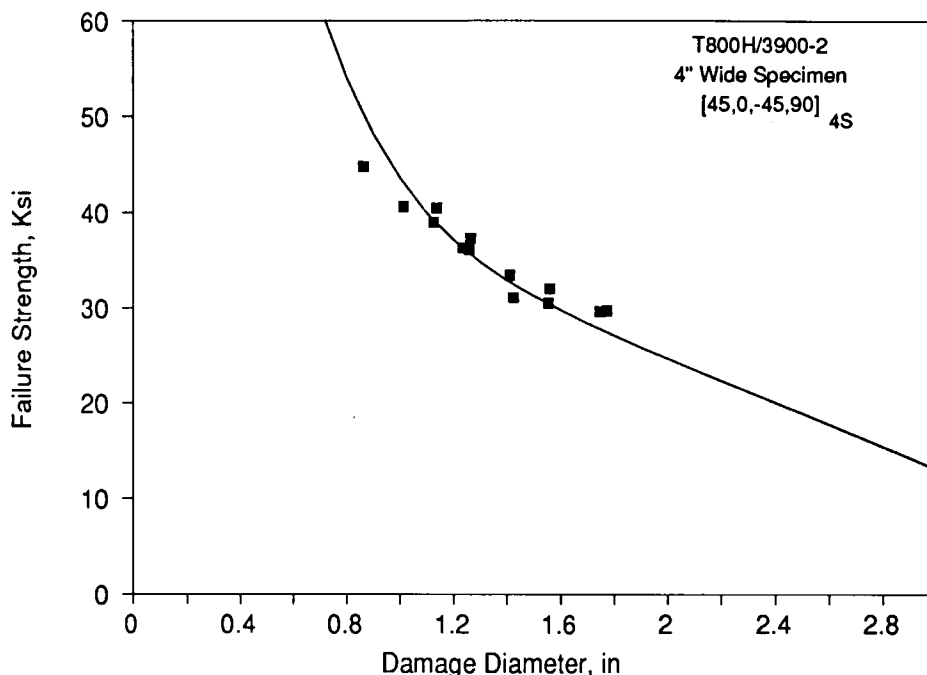


Figure 24. CAI Analysis and Experiments for a Toughened Material With Increased Resin Content ($V_f = 0.49$)

As shown in Figure 15, the development of toughened material models involves considerable interaction with universities. Two groups at the University of Washington are involved in the separate tasks of developing (1) methods to screen solvent resistance, and (2) general impact damage analysis models. The University of Utah is using microscopy to study relationships between toughened material microstructure and impact damage accumulation. Drexel University is involved with analysis and test characterization of the long-term durability of toughened materials, including environment and real time effects. Results from these studies will be presented in future ATCAS documentation.

Advanced Core Development: As discussed earlier (see issue number 7 in Table 2), damage resistant core materials are needed to facilitate the keel baseline concept. Considerable progress has been achieved in this area with the University of Iowa subcontract. Figure 25 shows a new class of sandwich core concepts which have potential advantages in fuselage applications. Advantages of the re-entrant cell structure which results in a negative Poisson ratio include high fracture toughness and indentation resistance for foam materials. One manufacturing advantage of the negative Poisson ratio is the ability to bend re-entrant foams and honeycombs into cylindrical shapes characteristic of

fuselage panels (note that traditional honeycombs tend to deform into a saddle shape under bending loads). Future work with this new material form will include scaleup of a suitable low-cost process; development of ultrasonic inspection procedures; and analysis/test studies on impact damage resistance, environmental sensitivity, and durability.

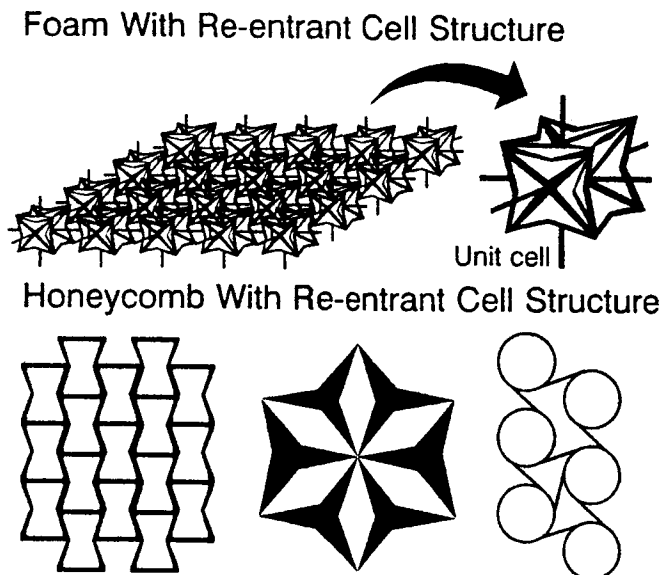


Figure 25. Advanced Sandwich Cores: Foam and Honeycomb

Large Panel Fabrication and Test Plans: A substantial portion of ATCAS funds addresses keel issues with manufacturing demonstration hardware and subcomponent panel tests. Several tests involving small panels (e.g., CAI with three stringer panels) are also planned. As with the crown, process demonstration studies yield panels for large verification tests. Combined compression/shear tests will be performed with curved panels (≈ 3.5 ft by 5 ft) representative of the lower side quadrant designs. A large curved panel (≈ 5 ft by 8 ft), representing the aft keel design, will be tested for damage tolerance in different combinations of compression and shear. Repairs will also be performed and verified with this panel. Finally, another large curved panel (≈ 5 ft by 8.5 ft) will be tested to validate the compressive load redistribution capability of the forward keel design. This panel will also be damaged, tested, repaired, and then tested to failure.

Window Belt Panels

Very little work has been performed in support of the window belt. A baseline concept was selected and the associated technical issues identified. Global optimization of the side quadrants will occur between March and October of 1991. Local optimization of the window belt lasts one year, ending in the fourth quarter of 1992.

As shown in Table 1, several issues (3,4,5,6, and 7) relate to RTM processing of the window frame detail. Manufacturing and supporting technology tasks have been initiated to address these issues. In particular, a request for proposals to fabricate RTM/textile window frame modules were sent to candidate manufacturers. Initial tasks will include coupon tests to determine basic material properties and the effects of defects for the window frame material form. Flat and curved window frame modules will be fabricated in the 1992 to 1993 timeframe to bond to window belt manufacturing hardware and test subcomponents. Analysis methods will be developed in an Oregon State University subcontract to

predict the overall performance of window belt panels. The effects of local design details (e.g., frame rib geometry) will be considered in this effort.

Panel and subcomponent tests will be used to verify the window belt design concepts. Included in the larger subcomponents is a curved panel (≈ 3.5 ft by 3.5 ft) with a central window cutout. This panel will be tested in hoop tension to evaluate the effect of cutout geometry and cutout-doubler configuration. Picture-frame shear tests (≈ 3.5 ft by 3.5 ft) will be conducted to verify the capability of the most promising window-belt concepts and the accuracy of predictions (load-redistribution and stability). The optimized window-belt configuration, including longitudinal stringers and simulated frames, will be tested under compression/shear loading to provide final verification of the design concept and analytical predictions. This panel (≈ 5 ft by 8 ft) will also address damage tolerance issues, including impact damage and loss of elements.

Frames and Attachment Details

Design development of frames and splices is integrally linked to other ATCAS efforts. Global optimization of these details will be accomplished with each panel quadrant. Local optimization will be performed in the "Full Barrel Section" effort, near the end of Phase B.

To date, the detail development has focussed on the crown quadrant (Ref. 1). These studies indicated that (1) curved frames have much higher weight-normalized costs than simpler geometries (e.g., skins); (2) braid/RTM processes are the most attractive for frame geometries; (3) recurring fastener costs can be significant, and (4) eccentricities at panel splices are a major fabrication issue. Significant efforts have been accomplished in addressing braided-composites variables and fastener costs.

Plans are in place to address other frame and splice issues. Mechanical joints data will be generated to support the splice design of new material forms selected for use in ATCAS (e.g., graphite/fiberglass hybrids and textile materials). Adhesives suitable for the frame-to-skin bond will also be evaluated. This assessment will include residual strength and durability tests. The latter will include sustained loads characteristic of cabin pressure. Robust splice plates that allow some locational tolerance mismatch between stringers or frames at panel joints will be designed and tested.

Braided Composites: Test plans have been developed to evaluate and compare properties of braided composites formed using two processes: (a) RTMing a thermoset matrix, and (b) consolidation of preforms with commingled graphite fibers and thermoplastic strands. Both two- and three-dimensional braids are being considered in this study. Data will be obtained for unnotched tension; open-hole tension, compression, and inplane shear; CAI; transverse tension and shear; bearing; and crippling. Analysis methods are being developed in parallel, to predict stiffness and strength of braided parts with known fiber architectures. Reference 13 gives additional details on progress to date.

Advanced Fasteners: By working with vendors, major fastener cost centers and potentially low-cost fasteners and/or installation methods have been identified. To date, spin-forming of graphite/thermoplastic rivets appears most attractive. Trial installations of the selected concepts and mechanical tests will be conducted to evaluate cost and strength performance.

Full Barrel Section

The primary objective of work associated with the "Full Barrel Section" timeline shown in Figure 12 is to complete work tasks which provide the degree of technology verification required to commit to development of a full scale barrel section (i.e., a potential Phase C option to ATCAS). The manufacturing steps for each quadrant of the aft fuselage will be optimized to minimize costs of a full barrel section. One of the main design activities will be to evaluate potential cost advantages of a 360°

concept from Design Family H. Local design optimization and verification tests will also be performed with frames, attachment details, and splices in attempts to minimize the number of parts. Any of the long-term research efforts with new material forms will also be completed by the end of ATCAS, allowing them to be included during full barrel design studies.

Large Pressurized Panel Tests

The optional addition to Phase B of ATCAS is scheduled to address dynamic aspects of pressure release following a through-penetration damage event. Additional studies of combined loads characteristic of fuselage bending will be coupled with the pressure release problem. Both analysis and test will be used to obtain solutions to these problems, resulting in additional verification on the damage tolerance of composite fuselage design concepts.

Three main analysis steps appear necessary. The first step involves a fluid flow analysis of pressure released through an opening in a curved panel. The second step is a mechanics problem to determine the stress state acting on the damaged composite structure due to a combination of dynamic pressure release and existing load state. Finally, verified failure criteria need to be developed which account for the combined effect of in-plane and out-of-plane load conditions. Some of the analysis development and coupon test verification for this effort will be performed under university subcontract by the Massachusetts Institute of Technology.

The full scale test fixture, illustrated in Figure 26, will be designed and fabricated to permit testing of large pressurized fuselage panels (≈ 6.5 ft by 10 ft). Flight conditions will be simulated by attaching a loading frame to a bulkhead. The loads will be reacted through another bulkhead which is attached to a strongback. The interface between the composite test panels and aluminum test hardware will be designed such that panel failure will not damage the test fixture.

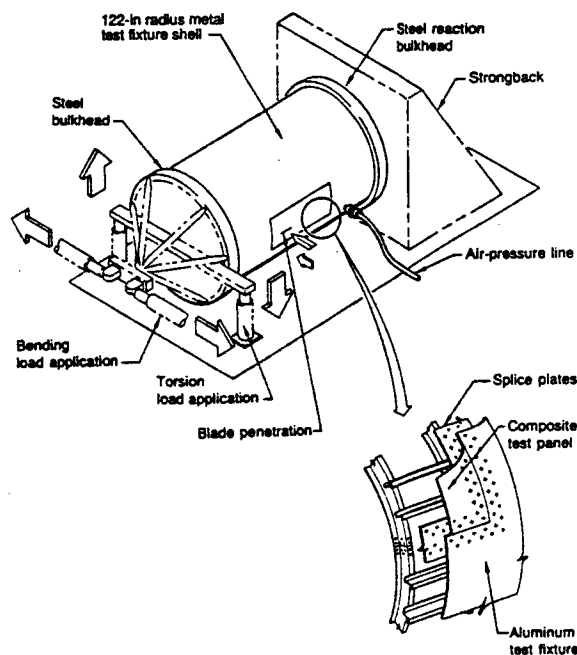


Figure 26. Pressurized Fuselage Damage Containment Tests

Four large panel tests are planned: (1) crown panel, (2) keel panel, (3) crown-to-side longitudinal splice, and (4) keel-to-side longitudinal splice. Each panel will be tested for multiple load conditions and damage scenarios prior to the large penetrating damage event.

SUMMARY

Keel, side, and crown areas of an aft fuselage section directly behind the wing-to-body intersection of a wide body aircraft are used for composite technology development and verification purposes in ATCAS. Boeing Commercial Airplanes Group is the prime contractor for the ATCAS program, with significant contributions also coming from other Boeing Groups, industrial subcontractors, and universities. Initial ATCAS efforts plan to develop composite technology that meet NASA Advanced Composite Technology goals for cost and weight savings, relative to 1995 metals technology. During the final years of the ATCAS program, work tasks are planned to provide the degree of technology verification required to commit to development of a full scale barrel section.

A design build team approach has been established to minimize manufacturing costs and structural weight. Three steps are used by the ATCAS DBT to select, evaluate, and optimize fuselage concepts. First, the DBT selects baseline concepts that appear to have a strong potential for cost and weight savings. This helps to focus early efforts in solving major technical issues. Second, cost and weight savings potential of the baseline and several alternate concepts are evaluated using detailed designs and manufacturing plans. This step has been termed global design optimization because it identifies cost centers associated with fabrication and assembly of the entire structure. Finally, the DBT attempts to reduce significant cost centers associated with the chosen concept. This third step has been termed local optimization because it addresses individual manufacturing steps and subcomponent design within the global cost constraints identified for the entire structure.

Four large quadrant panels (e.g., crown, 2 sides, and keel) were selected to minimize the number of panel splices and to take advantage of a low-cost batch process for fuselage skin layup. A skin panel concept with bonded stringers and frames, was selected for the crown and side quadrant baseline design concepts. Selection of this concept was justified by global design optimization studies for the crown, which indicated cost and weight savings potential. An innovative thick laminate/sandwich concept was selected for the keel panel. This choice was made to avoid anticipated problems with composites in fabricating and splicing a more traditional keel panel design. The major manufacturing and performance issues associated with baseline concepts were identified. Detailed cost estimates for side and keel baseline concepts will be performed in the following year.

All composite crown designs considered in global optimization studies indicated economic advantages over the metal benchmark in cost and weight trades. The most efficient composite crown designs were found to have 50% the weight and equivalent manufacturing costs. Composite concepts were competitive with the metal benchmark primarily because reduced assembly labor offset lower aluminum material costs. Cost savings on the order of 25% were projected for composite crown panels by attacking cost centers (e.g., using tow placed fiberglass/graphite hybrids to reduce material costs) in local optimization studies.

Considerable work was completed in addressing technical issues. A crown design tool that combines manufacturing cost and structural performance constraints with an optimization algorithm is near completion. Panels (e.g., 110 in. stiffened panels and intraply hybrid skin panels) were fabricated to serve multi-purposes in evaluating technical issues such as process feasibility, low-cost tooling concepts, impact damage resistance, and tension damage tolerance. Analysis methods were developed and experimentally verified for toughened composites in support of keel applications. These included post-impact compressive strength prediction. Data bases were obtained for manufacturing and performance evaluation of new material forms, including braided composites and sandwich core. Twenty technical papers, including seven in this proceedings, were published to document ATCAS work completed to date.

REFERENCES

- 1.) Walker, T.H., et al, "Cost Studies for Commercial Fuselage Crown Designs," First NASA Advanced Composites Technology Conference, NASA CP-3104, Part 1, 1991, pp. 339-356.
- 2.) Willden, K., et al, "Process and Assembly Plans for Low-Cost Commercial Fuselage Structures, First NASA Advanced Composites Technology Conference," NASA CP-3104, Part 2, 1991, pp. 831-842.
- 3.) Smith, P.J., Thomson, L.W., and Wilson, R.D., "Development of Pressure Containment and Damage Tolerance Technology for Composite Fuselage Structures in Large Transport Aircraft," NASA CR 3996, Contract NAS1-17740, August 1986.
- 4.) Horton, R., Whitehead, R., et al, "Damage Tolerance of Composites, Final Report," AFWAL-TR-87-3030, Vol. 3, May 1988.
- 5.) Rhodes, M.D., "Impact Fracture of Composite Sandwich Structures," AIAA/ASME/SAE 16th Structures, Structural Dynamics, and Materials Conf., May, 1975.
- 6.) Friis, E.A., Lakes, R.S., and Park, J.B., "Negative Poisson's Ratio Polymeric and Metallic Materials," J. of Materials Science, 23, 1988, pp. 4406-4414.
- 7.) Zabinsky, Z., Tuttle, M., et al, "Multi-Parameter Optimization Tool for Low-Cost Commercial Fuselage Crown Designs." First NASA Advanced Composites Technology Conference, NASA CP-3104, Part 2, 1991, pp. 737-748.
- 8.) Dost, E., et al, "Developments in Impact Damage Modeling for Laminated Composite Structures," First NASA Advanced Composites Technology Conference, NASA CP- 3104, Part 2, 1991, pp. 721-736.
- 9.) Ilcewicz, L.B., Dost, E.F., and Coggeshall, R.L., "A Model for Compression After Impact Strength Evaluation," Proc. 21st International SAMPE Technical Conf., 1989, pp. 130-140.
- 10.) Dost, E.F., et al, "The Effects of Stacking Sequence On Impact Damage Resistance and Residual Strength for Quasi-Isotropic Laminates," Presented at 3rd Symposium on Composite Materials: Fatigue and Fracture, Nov. 6-7, Buena Vista, Fla., ASTM, 1989.
- 11.) Grande, D., Ilcewicz, L., Avery, W., and Bascom, W., "Effects of Intra- and Inter-laminar Resin Content on the Mechanical Properties of Toughened Composite Materials," First NASA Advanced Composites Technology Conference, NASA CP- 3104, Part 2, 1991, pp. 455-476.
- 12.) Ilcewicz, L.B., et al, "Matrix Cracking in Composite Laminates With Resin-Rich Interlaminar Layers," Presented at 3rd Symposium on Composite Materials: Fatigue and Fracture, Nov. 6-7, Buena Vista, Fla., ASTM, 1989.
- 13.) Fedro, M.J., Gunther, C.K., and Ko, F.K., "Mechanical and Analytical Screening of Braided Composites for Transport Fuselage Applications," First NASA Advanced Composites Technology Conference, NASA CP- 3104, Part 2, pp. 677-704.

DESIGN, ANALYSIS AND FABRICATION OF THE TECHNOLOGY

INTEGRATION BOX BEAM

C. F. Griffin and L. E. Meade
Lockheed Aeronautical Systems Company

SUMMARY

Numerous design concepts, materials, and manufacturing methods were investigated analytically and empirically for the covers and spars of a transport wing box. This information was applied to the design, analysis, and fabrication of a full-scale section of a transport wing box.

A blade-stiffened design was selected for the upper and lower covers of the box. These covers have been constructed using three styles of AS4/974 prepreg fabrics. The front and rear T-stiffened channel spars were filament wound using AS4/1806 towpreg. Covers, ribs, and spars were assembled using mechanical fasteners. When they are completed later this year, the tests on the technology integration box beam will demonstrate the structural integrity of an advanced composite wing design which is 25 percent lighter than the metal baseline.

INTRODUCTION

Current applications of composite materials to transport aircraft structure, most of which are stiffness critical secondary structural components, have demonstrated weight saving from 20 to 30 percent. The greatest impact on aircraft performance and cost will be made when these materials are used for fabrication of primary wing and fuselage structures that are 30 to 40 percent lighter than their metal counterparts and have a reduced acquisition cost. Achievement of this goal requires the integration of innovative design concepts, improved composite materials, and low cost manufacturing methods.

In 1984, the Lockheed Aeronautical Systems Company began a program to develop engineering and manufacturing technology for advanced composite wing structures on large transport aircraft. The program was sponsored by the National Aeronautics and Space Administration (NASA) under contracts NAS1-17699 and NAS1-18888 and Lockheed Aeronautical Systems Company independent research and development funds.

The selected baseline component is the center wing structural box of an advanced version of the C-130 aircraft. The existing structural box, shown in Figure 1, is a two-spar multi-rib design, 440 inches long, 80 inches wide, and 35 inches deep at the crown. A preliminary design of a composite wing box was completed as were many design development tests. A full-scale section of the wing box was designed in detail, analyzed, and fabricated. This paper will summarize the major technical achievements of the box beam program.

It should be noted that some concessions as listed herein were made to reduce the cost of the program; the conclusions drawn thus far in this program are valid and achievable.

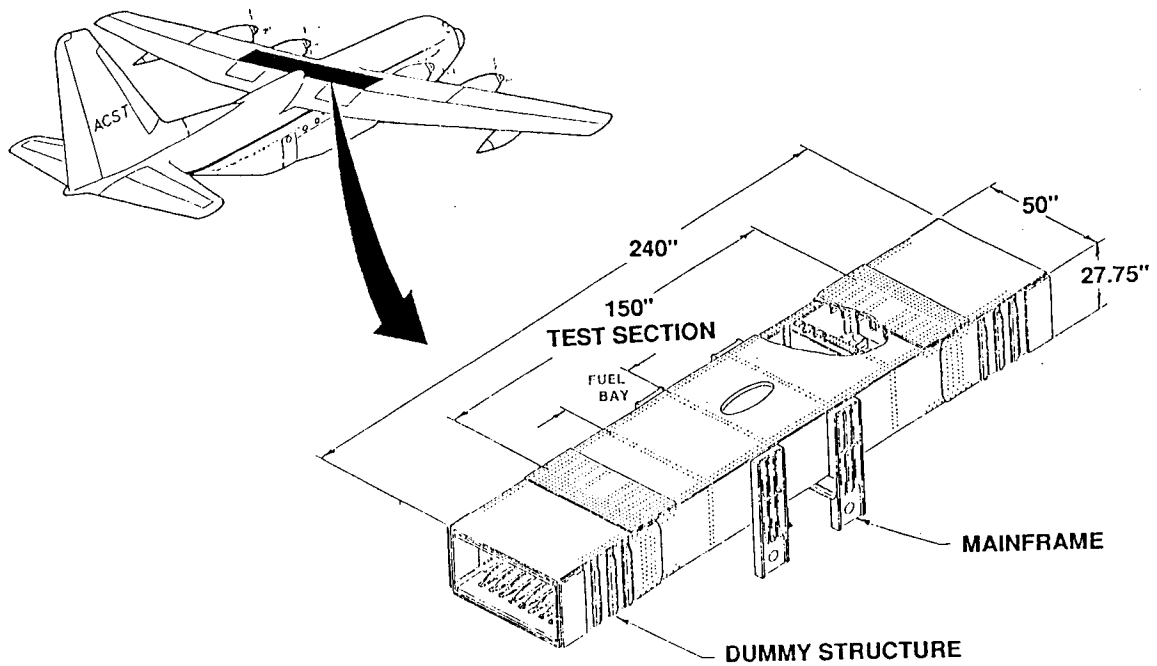


Figure 1. Technology Integration Box Beam

- Surface contour was eliminated
- Same tooling used for upper and lower covers
- L/E and T/E attachments were omitted
- Ribs were made of aluminum
- Cut-outs in the spars were omitted
- Stiffeners on spars were made of aluminum
- Constant sections were used
- Hand lay-up of hat-stiffeners, doublers, and C-channels was used
- Additional autoclave cycles were used for doublers
- Both spars were filament wound at once on common mandrel
- Aluminum access door hole doubler was bolted
- Spar/cover joint doublers were secondary bonded

BOX BEAM DESIGN AND ANALYSIS

GEOMETRY

The technology integration box beam, see Figure 1, represents a highly loaded full-scale section of the C-130 center wing box. The test section of the box is 150 inches long, 50 inches wide, and 28 inches deep. The test section contains a large access hole in the upper cover, wing box-to-fuselage mainframe joints, and center wing-to-outer wing joints.

DESIGN LOADS AND CRITERIA

The design loads for the box beam are based on the baseline aircraft requirements. Maximum ultimate loads are 26,000 lb/inch compression in the upper covers and 24,000 lb/inch tension in the lower covers. Ultimate spar web shear flow is 4,500 lb/inch. These loads are combined with the appropriate pressure loads due to beam bending curvature and fuel. The stiffness requirements for the wing were established to meet the commercial flutter requirements specified in FAR Part 25. Stated briefly, at any wing station the composite wing bending stiffness and torsional stiffness could not be less than 50 percent of the baseline wing, and the ratio of the bending to torsional stiffness must be greater than one but not more than four.

Structural requirements for damage tolerance considered civil as well as military criteria. Thus, the criteria used for this program requires the structure to have ultimate strength capability with the presence of barely visible impact damage anywhere within the structure. Barely visible impact damage is either the kinetic energy required to cause a 0.1 inch deep dent or a kinetic energy of 100 ft-lb with a 1.0 inch diameter hemispherical impactor, whichever is least.

COVER DESIGN

Design trade studies and structural tests were conducted on various configurations for the wing covers. Figure 2 describes several of the designs and presents results of compression tests on impact damaged panels. Based on these investigations and manufacturing cost estimates, the blade stiffened design was selected for the box beam.

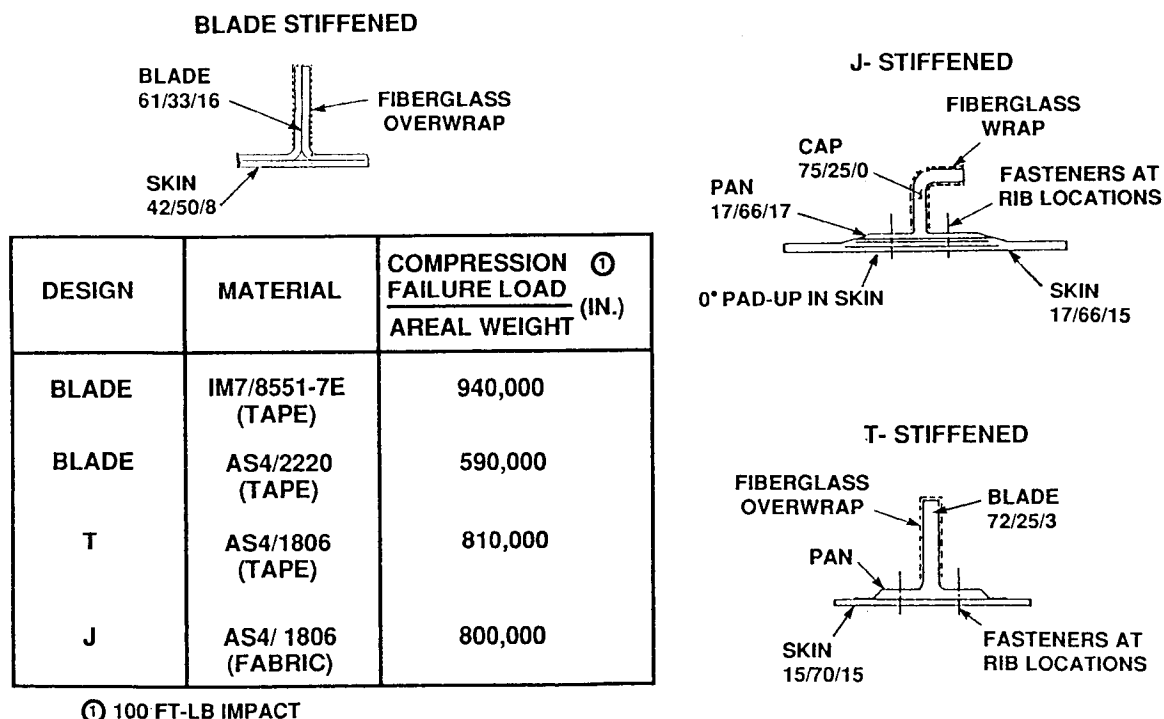


Figure 2. Wing Cover Designs

The lower cover design, shown in Figure 3, consists of back-to-back channels laid up on a skin laminate to form a blade stiffened panel. Note that the flanges of the channels contain additional 0 degree plies compared to the web thus resulting in a blade containing 67 percent 0 degree plies, 29 percent plus/minus 45 degree plies, and 4 percent 90 degree plies. The blades, which are spaced at 5 inches, are tapered in height to account for the increased axial loading from the outboard joint to the wing centerline. A constant thickness laminate containing 27 percent 0 degree plies, 64 percent plus/minus 45 degree plies, and 9 percent 90 degree plies makes up the lower skin.

The configuration of the upper cover, shown in Figure 4, is similar to the lower cover with the exception that the blades are slightly taller. Also, the central bay of the upper cover is reinforced by a hat stiffener which is terminated at each rib location. The cut-out in the upper cover is reinforced by an aluminum plate which is mechanically fastened to the cover laminate.

The chordwise splice of the composite covers to the aluminum load introduction box is accomplished with the double shear joint illustrated in Figure 5. Note, the bending stiffness continuity of the cover is maintained by inserting the aluminum splice Ts between the composite blades.

SPAR DESIGN

As with the covers, trade studies and subcomponent tests were conducted on various spar designs. Figure 6 shows the results of tests on stiffened shear panels manufactured using several different materials and methods. The results of these studies when combined with manufacturing cost estimates led to the selection of the T-stiffened channel configuration shown in Figure 7. The spar webs and caps are of constant thickness with the exception of the doublers located at the mainframe attachment and the spar splice locations. This spar was designed to be filament wound using AS4/1806 towpreg with unidirectional, bidirectional, and bias fabrics used for the spar cap inserts, and doublers. The stiffeners were made of aluminum for economy and were bolted and bonded to the spar web.

RIBS AND BOX ASSEMBLY

For the box beam, a J-stiffened skin configuration constructed of aluminum was selected for all of the ribs. As shown in Figure 8, a T-shaped shear tie connects the rib web and rib cap to the cover. All ribs will be mechanically fastened to the spar webs and covers. Also the spar caps are mechanically fastened to the covers using a double row of fasteners.

STRUCTURAL ANALYSIS

A detailed structural analysis was completed on the box beam using the methods shown in Figure 9. A three-dimensional finite element model was constructed and used to obtain internal loads for sixteen loads cases. Detailed two-dimensional models were used to analyze the cover chordwise joint, cover cut-out area, and the mainframe to spar joint. The compression stability of the covers was predicted using the PASCO code obtained from NASA. Several Lockheed computer programs were used to obtain local stresses and strains using the internal loads obtained from the NASTRAN models.

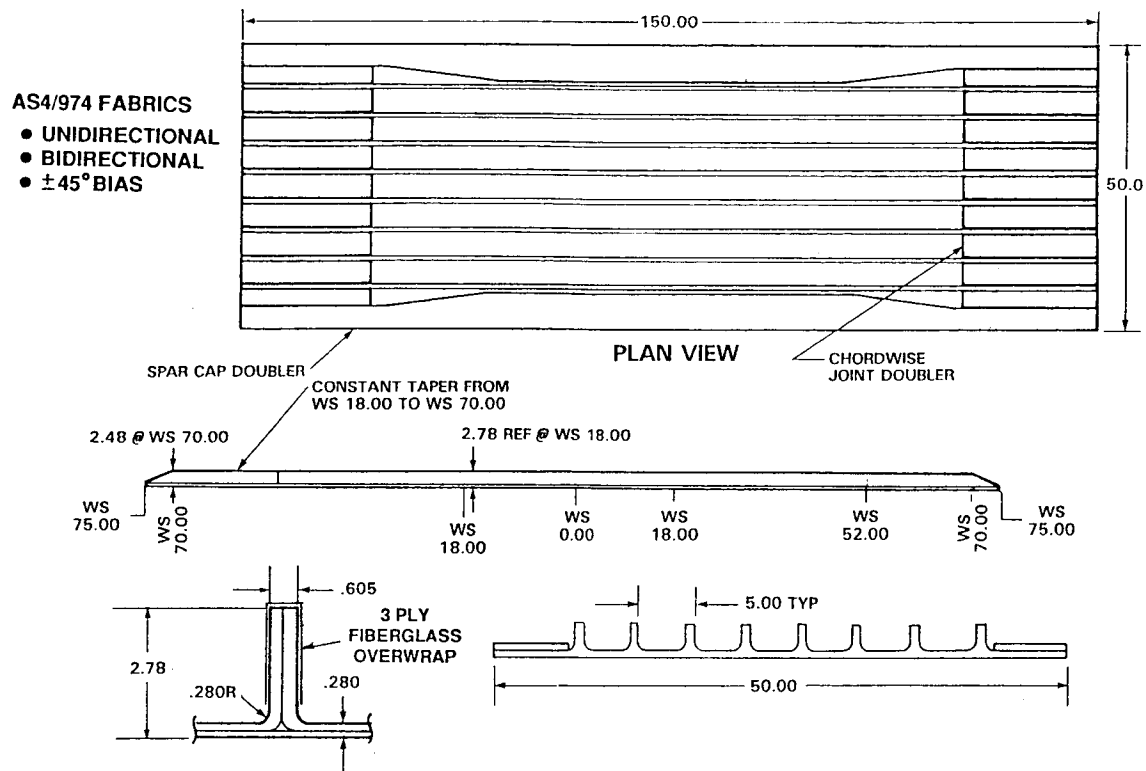


Figure 3. Lower Cover Box Beam Design

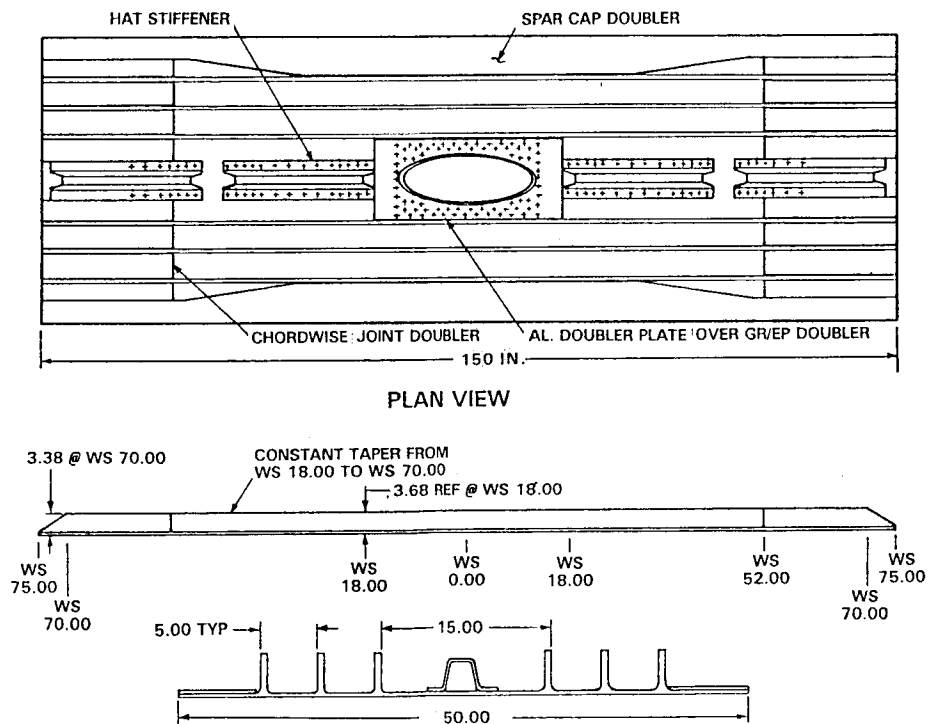


Figure 4. Upper Cover Box Beam Design

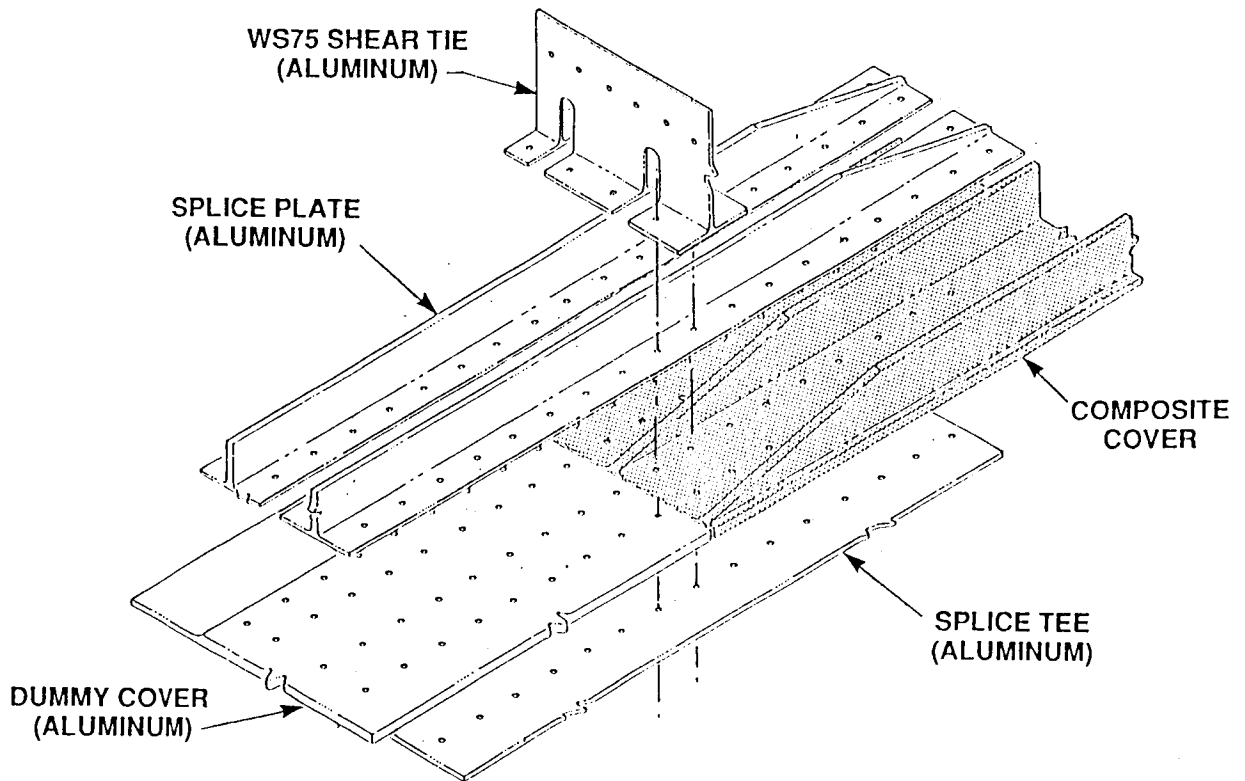


Figure 5. Cover Chordwise Splice

MATERIAL	MANUFACTURING METHOD	SHEAR FAILURE LOAD ^① AREAL-WEIGHT (IN.)
AS4/1806 FABRIC	HAND LAY-UP	410,900
AS4/1806 TOWPREG	FILAMENT WOUND	483,000
AS4/APC-2 TAPE	ROLL FORMED AND AUTO-CLAVE CONSOLIDATED	412,500
AS4/1806 FABRIC	HAND LAY-UP (POST BUCKLED DESIGN)	355,600

① 100FT-LB IMPACT

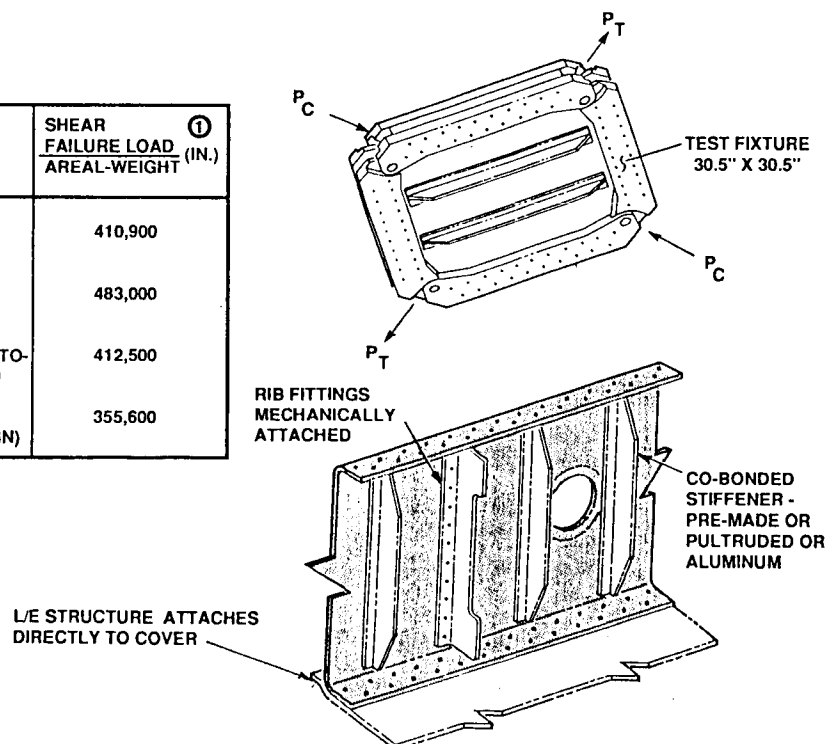


Figure 6. Wing Spar Designs

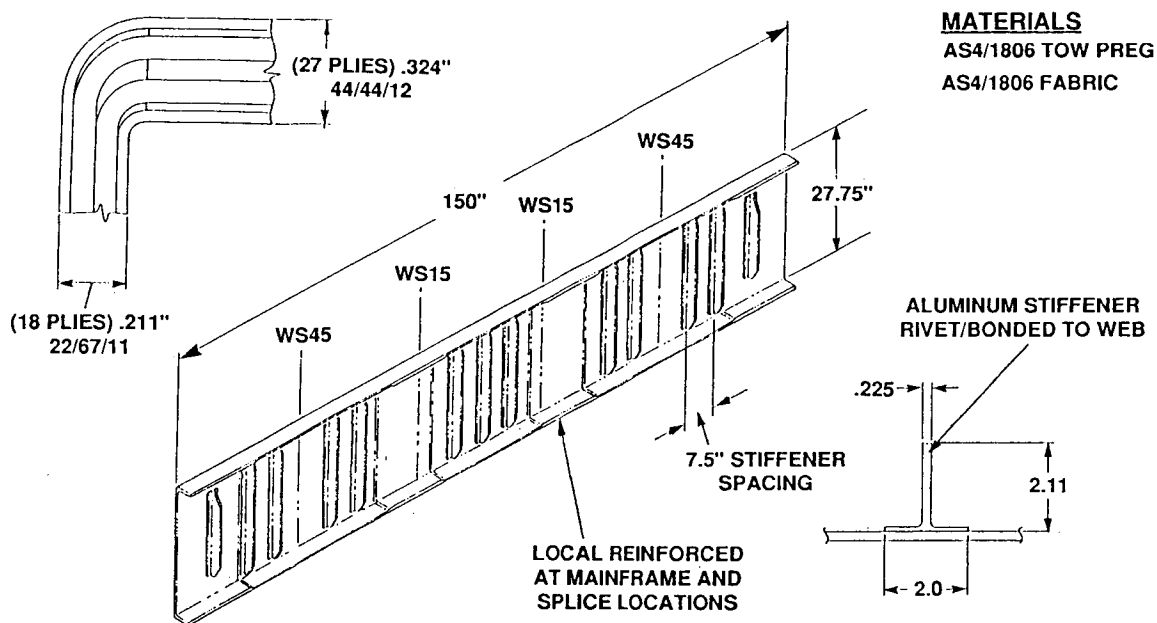


Figure 7. Spar Assembly

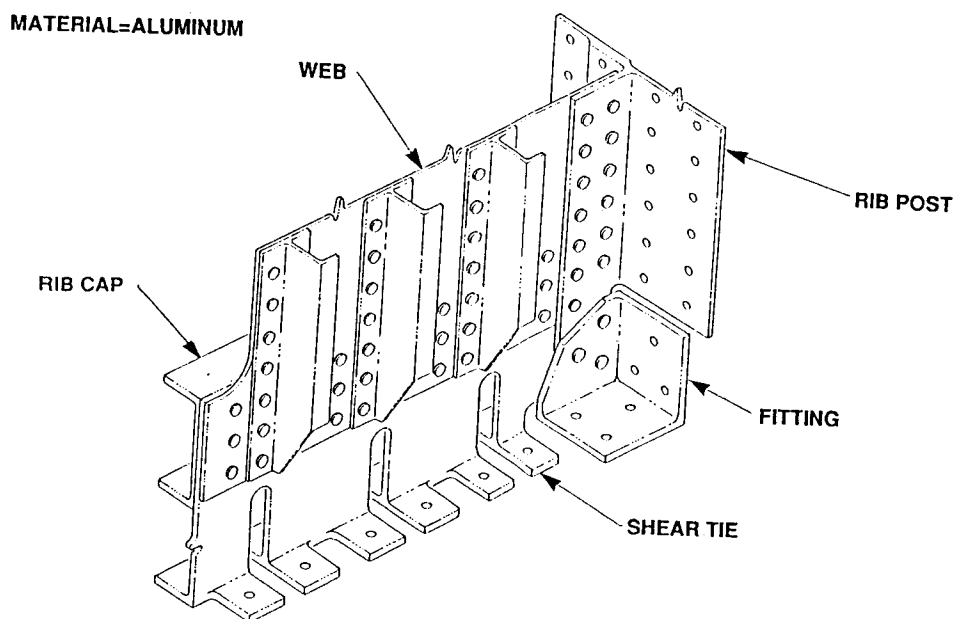


Figure 8. WS75 Rib

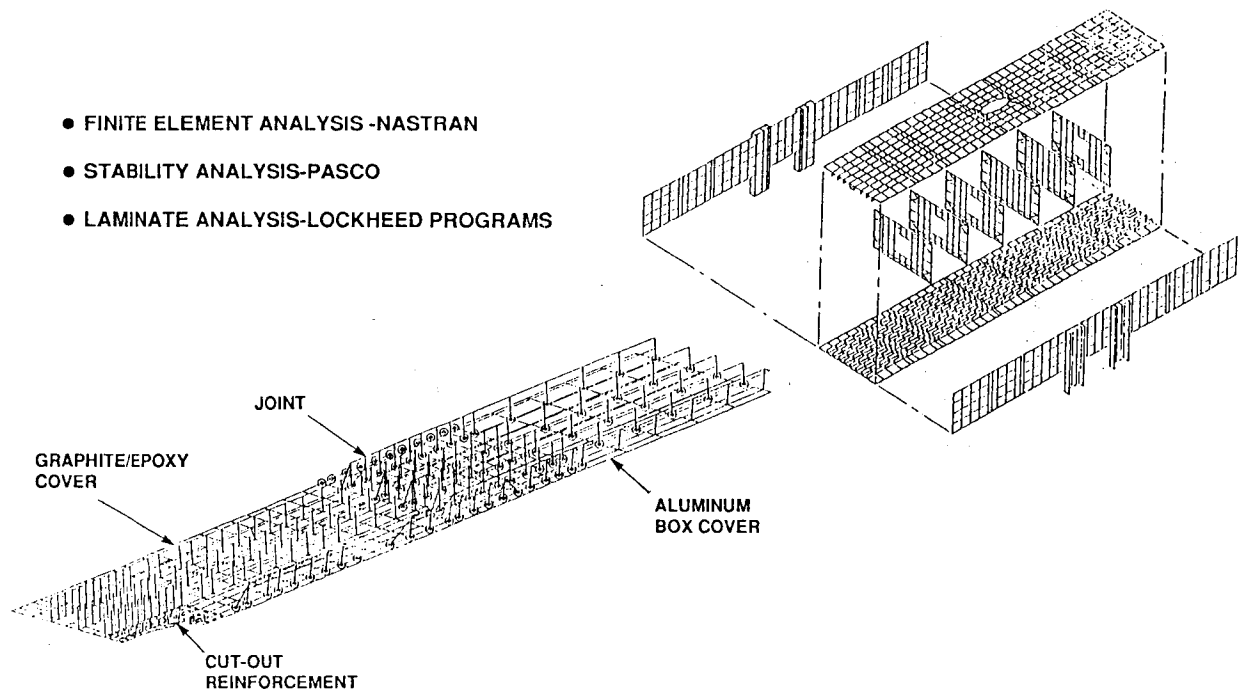


Figure 9. Structural Analysis Methods

Figure 10 presents the typical design allowables obtained for the AS4/1806 and AS4/974 fabric prepreg materials. These allowables were computed based on laminated tests, and in the case of the impacted laminate allowables, stiffened panel tests. Note that the allowable strain is plotted as a function of the percentage of plus/minus 45 degree plies within the laminate minus the percentage of 0 degree plies. This value is called the AML for angle minus longitudinal plies. For example, a quasi-isotropic laminate has an AML value of 25. The blade stiffener on the cover has an AML of -38 and the cover skin a value of 37.

Margins of safety were computed for numerous locations on the covers and spars using the applied strains and the design allowable strains. Several minimum margins of safety are presented in Figure 11. Both the upper cover and spar webs have a 0 margin of safety for the impact damaged condition. The lower cover and the spar cap are critical for bearing/bypass and net tension, respectively.

A preliminary design of a C-130 center wing box was completed using the design concepts and materials described for this technology integration box beam. Weights analysis indicated an overall savings of 25.4 percent compared to the metal baseline. The predicted spar weight savings was 35 percent and the cover was 28 percent. These weight savings could be improved if a higher modulus fiber such as IM7 were used in conjunction with the latest generation of toughened epoxies.

SPAR FABRICATION

The spars were fabricated by filament winding AS4/1806 towpreg onto a mandrel that when trimmed apart lengthwise produced both the front and rear spars at the

PLY LEVEL ELASTIC CONSTANTS		
PROPERTY	UNIDIRECTIONAL FABRIC	BIDIRECTIONAL FABRIC
0° TENSILE MODULUS (MSI)	17.70	9.70
90° TENSILE MODULUS (MSI)	1.47	8.80
0° COMPRESSION MODULUS (MSI)	17.00	9.70
0° INPLANE SHEAR MODULUS (MSI)	0.62	0.62
0° POISSONS RATIO	0.30	0.05

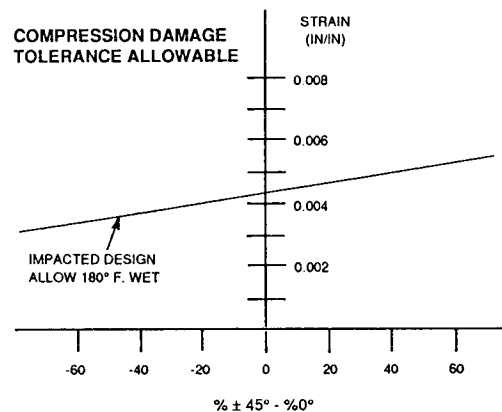
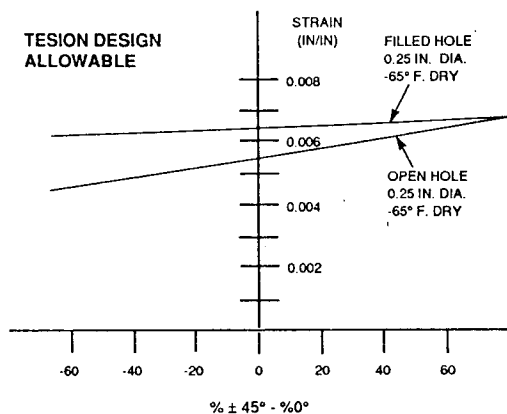
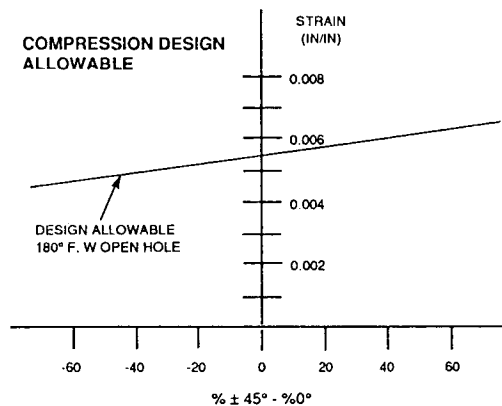
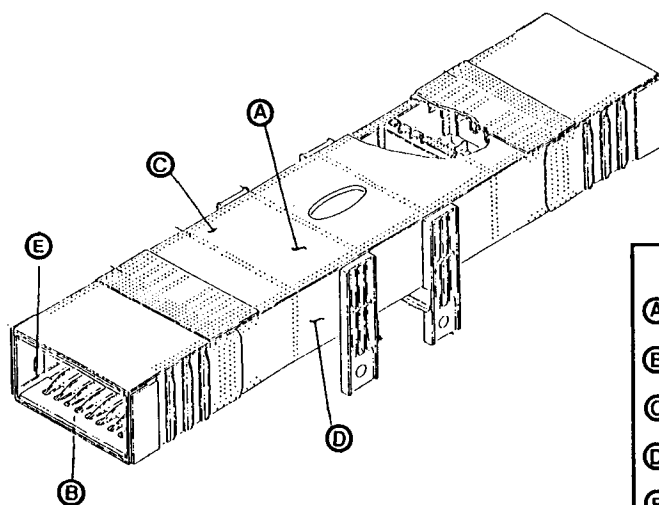


Figure 10. Design Allowables



LOCATION	M.S.	MODE
(A) UPPER COVER	0.00	CAI
(B) LOWER COVER	0.01	BRG/BYP
(C) UPPER COVER	0.04	BRG/BYP
(D) SPAR WEB	0.00	CAI
(E) SPAR CAP	0.05	NET TENSION

Figure 11. Minimum Margins of Safety

same time. Figure 12 shows the spars as filament wound and cured on the mandrel prior to removal. Figure 13 shows the two spars after separation. The aluminum stiffeners were fabricated, located on the spars, and drilled for fastener installation. The stiffeners were then phosphoric-acid anodized for bonding, adhesive coated with Hysol #9339 glass-microballoon filled adhesive and bolted and bonded in place. Figure 14 shows a spar with the stiffeners installed.

COVER FABRICATION

The covers were fabricated by separately laying-up C-channels, 64 tow stuffers and the skin laminate and then assembling the lay-ups for cure as shown in Figure 15. The C-channels were alternately laid-up on 'hard' mandrels and 'soft' mandrels to achieve both positive location of each blade stiffener and full fluid bag pressure during cure.

Note: 'Hard' mandrels were hollow aluminum mandrels formed into closed boxes by welding two Ls together. 'Soft' mandrels were U-shaped silicone rubber mandrels reinforced with included graphite fabric placed directly into the C-channel lay-ups to apply fluid pressure to the laminate while maintaining some stiffness for dimensional and shape control.

After laying up the skin laminate directly on the steel cover tool plate the center hard mandrel with its C-channel in place was positioned and pinned in place. (NOTE: Each hard mandrel, being aluminum to reduce worker handling weight, has a large difference in thermal expansion from the steel base; therefore, tooling pin holes were solid on one end and slotted on the other.) Next, a towpreg stuffer made of 64 tows was installed in the radius of the C-channel-to-skin joint. Then a soft mandrel C-channel layup was installed, another stuffer, another hard mandrel C-channel, etc., until the lower cover layup assembly was complete. Figures 16, 17, 18, and 19 show sequentially this layup process. A layer of FM 300 0.030 psf adhesive film is used between each layup interface. Thermocouples were installed, the tool corners padded, breather material applied, and the tool covered with the curing blanket which was sealed to the tooling base. The cover was then cured in the autoclave with 85 psi at 350°F for two hours. As seen in Figure 20, taken after unbagging and removal from the tool, the cover exhibited a curve which is due to differential shrinkage of resin at each blade stiffener location. This curve, however, is easily removed with moderate force at time of assembly with spars and ribs.

The cover has approximately four inches of trim excess on one end and 10 inches of excess on the opposite end which contains NDI standard flaws. This end will become the NDI standard for these panels after trimming to net size.

Additional material has to be added in a separate layup and cure cycle to serve as doublers for the load introduction box joint at each end of the covers. At the same time, spar cap doublers, separately laid up and cured, will be bonded on using FM 300 0.030 psf adhesive film. The hat stiffeners are to be installed on the cover with fasteners and micro-balloon filled paste adhesive, as were the stiffeners on the spars, in a bolted/bonded joint. After trimming the cover to final size, a 3-ply fiberglass layer overwrap will be installed with a vacuum cure at 250°F on the upstanding leg of each stiffener for damage tolerance protection as shown in Figure 2.

SPAR ASSEMBLY

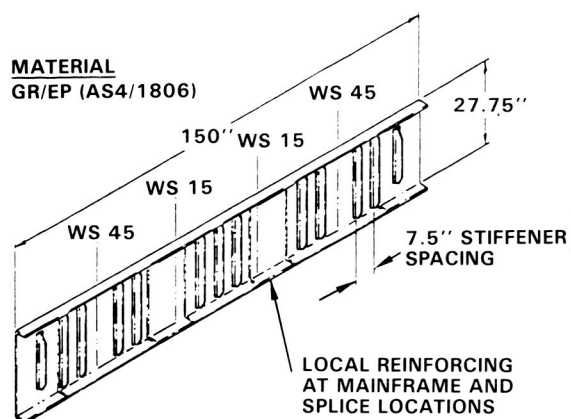


Figure 12. Spar Assembly

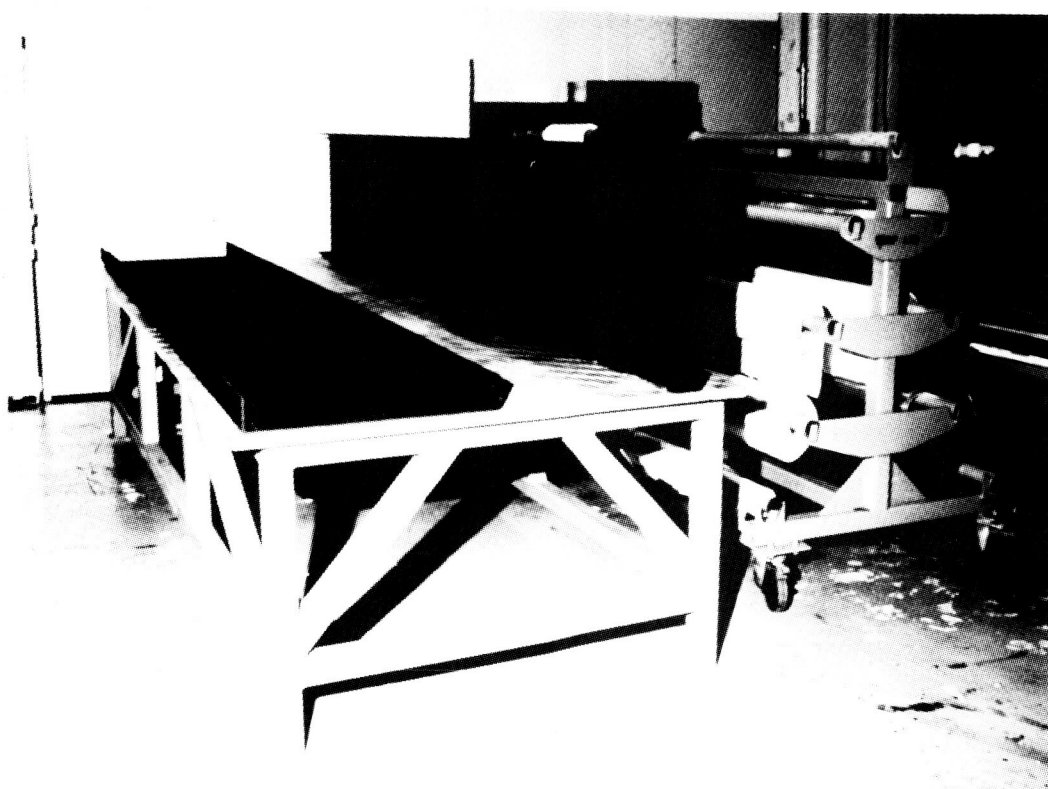


Figure 13. Two Spars



Figure 14. Spar Assembly

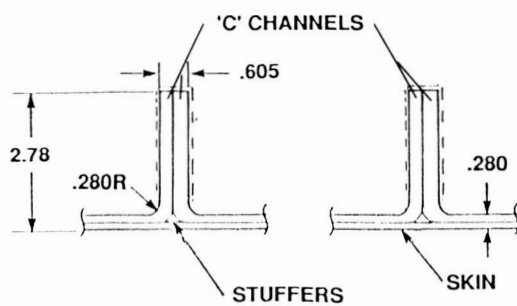
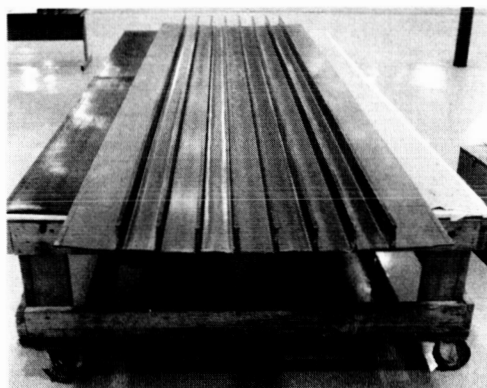


Figure 15. Skin Panel Layup Scheme

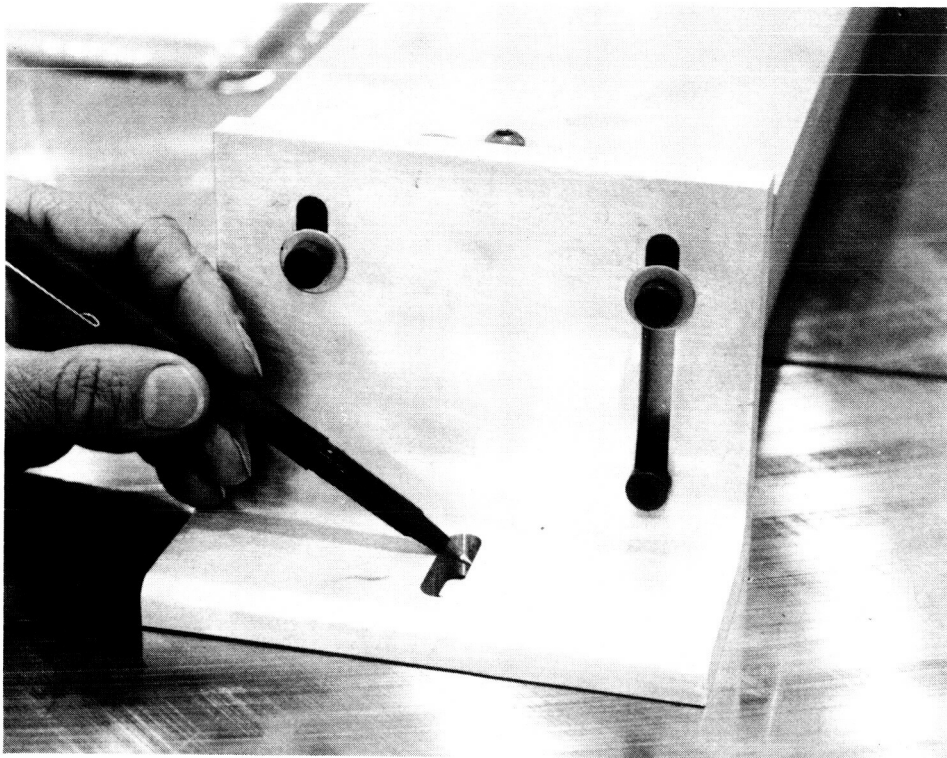


Figure 16. Solid versus Slotted Mandrel Tooling Holes

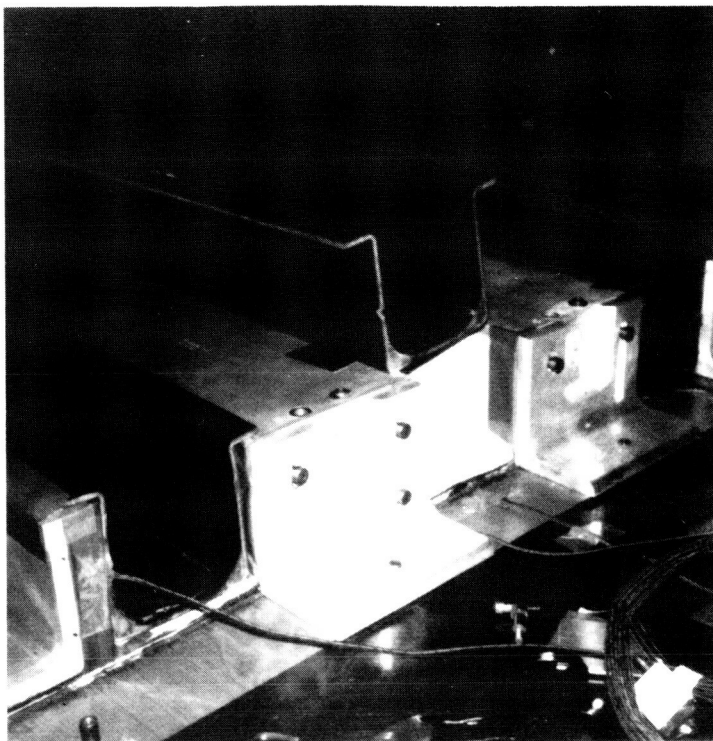


Figure 17. Soft Mandrel to be Inserted



Figure 18. Panel Ready for Bleeder



Figure 19. Bagged Lower Cover in Autoclave

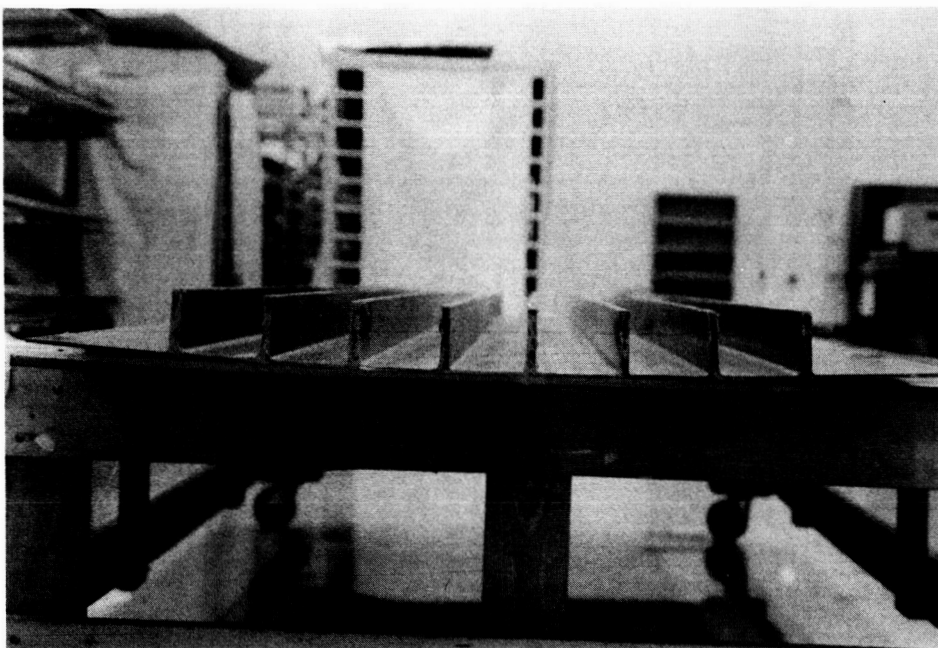


Figure 20. Curve in Panel Due to Blade Resin Shrinkage

RIB FABRICATION

The ribs being made of aluminum use standard aircraft assembly methods with mechanical fasteners as seen in Figure 21. An auto-fastener machine was used to install most of the rib assembly fasteners. Fastener locations were placed directly onto the part by using a mylar reproduction of the blueprint as an overlay.

BOX ASSEMBLY

The box assembly sequence will utilize assembly of the spar subassemblies with the rib subassemblies on a surface table using tooling knees initially for alignment and positioning. Once the spar-rib subassembly is assembled and squared, the covers will be joined to it and drilled using a Cybotec brand robot which will allow drilling of the cover-to-box holes without reaming. Although the box will not be sealed for fuel tightness, fasteners will be wet installed with corrosion inhibiting sealant where necessary to prevent corrosion between metal and composite surfaces. The box assembly includes an aluminum load introduction box extension on each end for testing. The test fixture is being fabricated under independent funding and will interface with the technology integration box beam via the aluminum box extension. Figure 22 details the assembly sequence of the box beam.

COST ANALYSIS

A detailed cost analysis compared a composite center wing structural box with an advanced aluminum version of the C-130 center wing box. The cost analysis evaluated the final technology integration box beam design, which was extrapolated to a full sized 80 by 440 inch wing box. The results demonstrate a potential 5 percent labor and material cost savings for a composite wing box compared to a new state-of-the art metallic design. Cost benefits are achievable in the current composite design concept through a reduction of labor costs; innovative design concepts result in less time required for fabrication and assembly operations. Also, automated manufacturing processes such as filament winding and pultruding have the potential to reduce costs. Estimated costs of the composite wing box, project recurring costs that will be incurred during a typical full-scale production program producing 200 ship sets of wing boxes. Figure 23 illustrates the cost breakdown for each major component as well as final assembly. Costs are distributed for both the advanced aluminum and composite wing box, illustrating relative costs of covers, ribs, spars, and assembly. Recurring production costs of the composite box are 95 percent of the baseline as a result of fewer parts in composite subassemblies and automated fabrication processes. Aluminum costs are based on actual C-130 cost history. Composite material costs are based on material vendors projections for material at high quantities. Fabrication costs, where possible, are generated from actual composite production experience. Where cost tracking data is not available, Value Engineering cost estimating methodology is used.

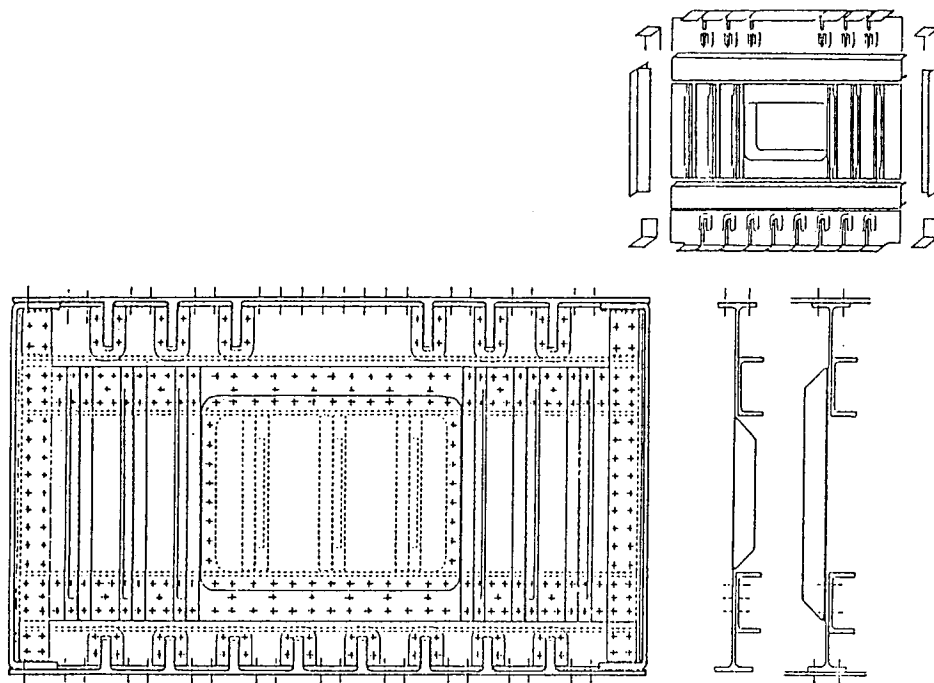


Figure 21. Rib Assembly

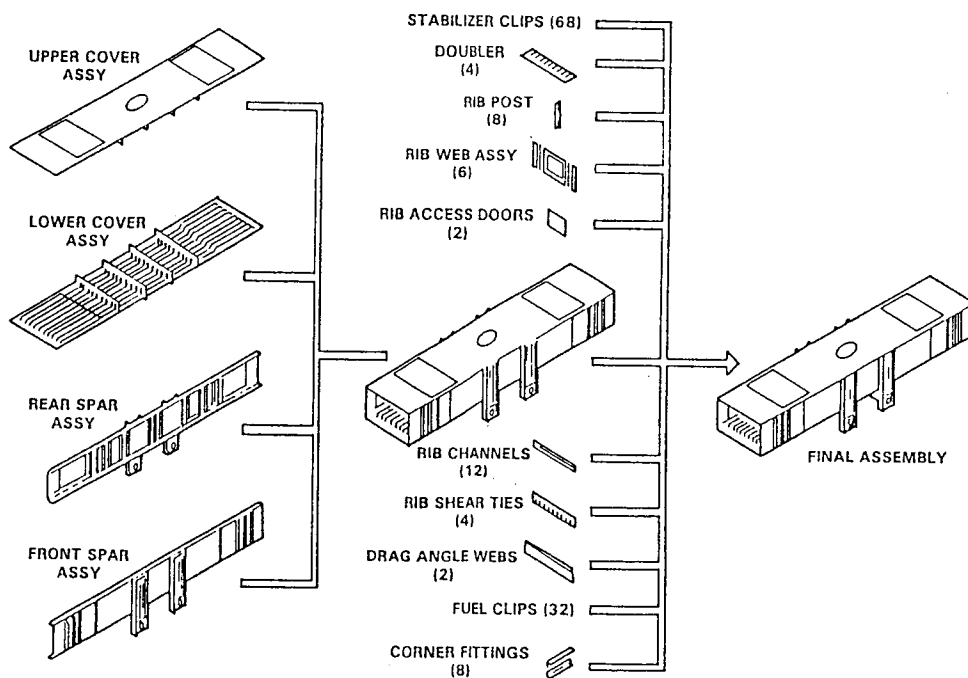


Figure 22. Task 5 - Box Beam Assembly Breakdown

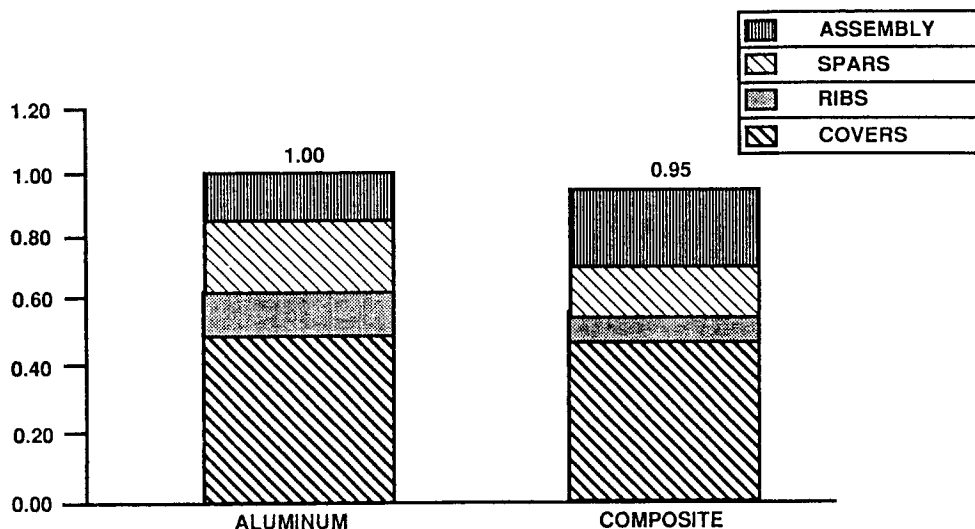


Figure 23. Wing Box Relative Cost Comparison Cost Breakdown

The covers comprise 49 percent of the total cost and account for 64 percent of the total weight of the wing box (reference Figure 24). A meaningful cost reduction could most easily be achieved through reducing costs associated with the covers. Assembly costs also have a considerable impact on costs, accounting for 25 percent of the total. Cost reductions for the spars and ribs will not result in an appreciable cost savings since their impact on total costs is only 10 percent and 16 percent, respectively.

Figure 25 further illustrates the total cost breakdown, showing material and labor costs separately. This provides a more specific means with which to target and assess cost drivers. Material costs for the covers stand out, accounting for 35 percent of the cost. Figure 26 shows a breakdown of material costs, demonstrating the significance of the cost of the covers as a percentage of total material costs. Approximately 74 percent of the total material costs is in the covers as shown. Material costs are based on projected costs estimated by vendors for graphite/epoxy prepreg at 10,000 pounds per year quantities. The plus/minus and minus/plus 45 degree knitted fabric is priced almost 87 percent higher than the uni-directional and 0/90 degree fabric. There is a potential for reduction in the former as the vendors have limited experience producing this material; consequently, their estimate may be conservative. A reduction in this price could have a significant effect on cover material costs as the plus/minus 45 and minus/plus 45 degree fabric accounts for 47 percent of the cover material costs.

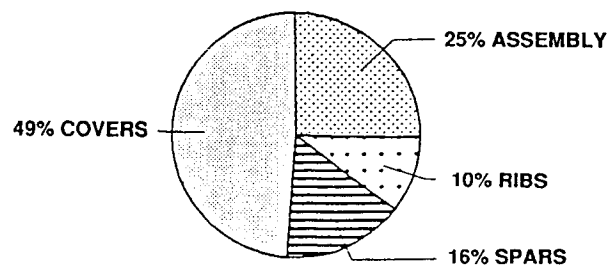


Figure 24. Total Cost Breakdown

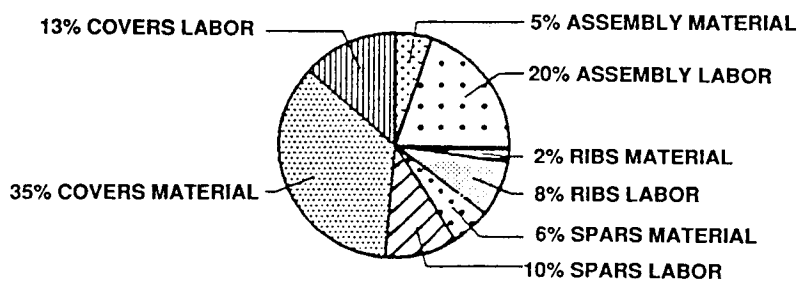


Figure 25. Labor Cost Breakdown

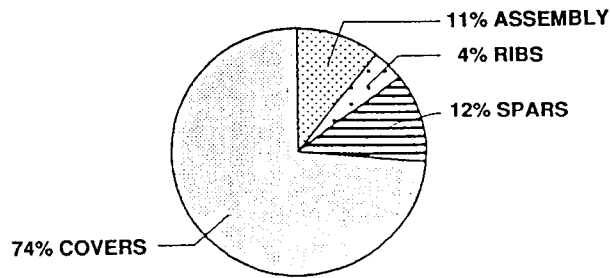


Figure 26. Material Cost Breakdown

Assembly costs are 25 percent of the total cost, 20 percent of which is assembly labor and 5 percent material. Assembly labor costs account for 39 percent of the total labor cost (reference Figure 27); assembly is labor intensive due to the necessity of a two-step drilling procedure required for graphite/epoxy composites to obtain acceptable holes. Improved composite drilling techniques/equipment or a reduction in the overall part/number of fasteners (see Figure 28) could significantly reduce the total costs. Material costs, at 5 percent of the total, are not a driver even though titanium fasteners are required.

Spar costs account for 16 percent of the total cost and probably represent an optimized design; the cost is based on a filament wound spar which significantly reduces the number of parts and fasteners, compared to a new metallic spar design. Further cost reduction is unlikely and would have a negligible effect on the total cost.

The ribs are only 10 percent of the total costs, 8 percent of that for labor. It is assumed that the skins and channels would be hand laid-up. Material costs are based on the same assumptions as the covers, and may be reduced; however, only 4 percent of the total material costs (reference Figure 26) is for the ribs. This is not an ideal target for emphasis on cost reductions.

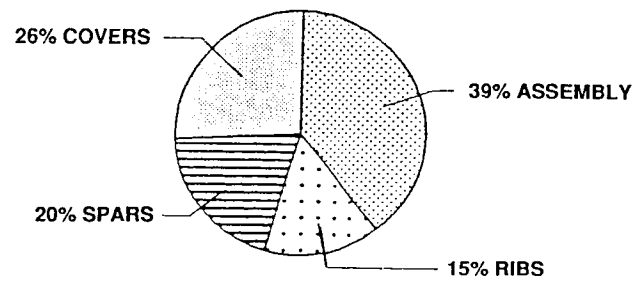


Figure 27. Labor Cost Breakdown

CONSTRUCTION TYPE	PARTS	FASTENERS
ALUMINUM "C130 CENTER WING" "FRONT SPAR"	160	3500
COMPOSITE SPAR	40	200

Figure 28. Part/Fastener Comparison

CONCLUDING REMARKS

The concurrent engineering approach used in this project has resulted in a wing box design which has a 25 percent weight saving and a 5 percent cost saving compared to the baseline advanced metal wing box. Incorporation of improved materials and the evaluation of alternatives to the bias fabrics could lead to further reductions in weight and acquisition costs. Spars were successfully filament wound, back-to-back on a common mandrel. Box covers were also successfully co-cured. These successful fabrication demonstrations point up still more lower-cost fabrication methods that could be incorporated in the future.

DESIGN AND MANUFACTURING CONCEPTS FOR THERMOPLASTIC STRUCTURES

Michael P. Renieri, Steven J. Burpo,
and Lance M. Roundy

McDonnell Aircraft Company
St. Louis, Missouri

SUMMARY

Results to date on the application of two manufacturing techniques, fiber placement and single diaphragm/coconsolidation, to produce cost-effective, thermoplastic composite (TPC), primary fuselage structure are presented. Applications relative to fuselage upper cover structure indicate potential cost savings relative to conventional approaches. Progress is also presented on efforts concerned with other design details which take advantage of thermoplastic composites such as fastenerless stiffener/frame attachments. In addition, results are presented on the development and verification testing of a composite lug analysis program which incorporates through-the-thickness effects.

INTRODUCTION

A major obstacle to widespread use of high performance composites in primary aircraft structures is the high cost of manufacture and assembly. Under NASA's ACT program, McDonnell Aircraft Company is investigating cost-effective, innovative techniques for the fabrication and joining of primary airframe structure using thermoplastic composite materials. MCAIR is teamed with Douglas Aircraft Company (DAC) under the ACT initiative in a program entitled Innovative Composite Aircraft Primary Structures (ICAPS).

Primary effort on the MCAIR portion of the ICAPS program has concentrated on developments relative to an advanced fighter fuselage section which are applicable to commercial vehicle structure. These include the application of two innovative manufacturing techniques, fiber placement and single diaphragm/coconsolidation to fabricate fuselage cover panels.

In addition to panel fabrication, elemental specimens are being fabricated and tested to address key design issues associated with the fuselage section such as pull-off strength of fastenerless frame attachment concepts and the performance of thick composite lugs. In support of the lug evaluation, an analytical program has been developed incorporating through-the-thickness effects.

GENERIC FUSELAGE SECTION

The advanced aircraft system selected for the fighter development effort was the Model 4629 ASTOVL design developed by MCAIR under the NASA-Ames sponsored U.S./U.K. ASTOVL Technology Development program. Based on representative

fuselage cross sections of the Model 4629 aircraft, a generic center fuselage structure, Figure 1, was developed as the primary structure demonstration component. While the fuselage structure contains design features particular to advanced ASTOVL aircraft, cost-effective fabrication techniques and innovative design concepts developed in this program demonstrate technology related to all emerging aircraft systems.

The generic center fuselage structure contains many challenging structural components:

- o Upper Cover
- o Tank Floor
- o Carry-Thru Bulkhead
- o Closure Bulkhead
- o Keel Webs
- o Frames
- o Inlet Ducts
- o Longerons

An upper fuel cell cover subcomponent was selected for design/analysis, fabrication, and structural testing for Phase A. The cover structure ties the upper longerons and bulkheads of the generic fuselage section together, and is a primary load carrying component for flight induced structural and fuel cell loading. The cover must be capable of a 255°F (110°C) operating temperature, have a limited number of fasteners on the outer moldline (OML), and resist hydrodynamic ram loading.

MATERIAL AND PROCESS SELECTIONS

Material

The material chosen was based on temperature requirements, solvent resistance, component design, manufacturing approach, and processing ease. Due to the 255°F design requirement, the baseline thermoplastic material selected was Imperial Chemical Industries' ITX (intermediate temperature crystalline), which has service capability to 300°F. The fiber selected was an intermediate modulus fiber produced by Hercules, IM7. ITX has processing characteristics similar to ICI's APC-2 (PEEK) system which is a mature resin that MCAIR has worked with extensively. In addition, AS4/APC-2 was selected for early forming studies due to availability and to verify analytical predictions for thick composite lugs.

Processes

Manufacturing processes were selected using a concurrent engineering approach. Processes were rated based on innovativeness, cost, risk, supportability, survivability, and weight. Two manufacturing techniques, fiber placement and single diaphragm/coconsolidation, were selected to fabricate subscale fuselage cover panels.

Fiber placement (FP), one of the more promising methods of fabrication, is the in situ consolidation of individual material layers using pressure and heat at the point of contact. This procedure eliminates the autoclave requirement and automates the material deposition process reducing significant cost elements in a typical composite production environment.

Secondly, MCAIR is evaluating a method that uses only a single upper diaphragm to form a skin and hat structure in one step. This process, single diaphragm/coconsolidation (SDCC), simultaneously consolidates the hat stiffened inner skin plies with the outer skin plies while coconsolidating the two yielding a high quality interface and reducing the number of process steps from three to one.

PRODUCIBILITY ANALYSIS

A producibility analysis was performed to determine the cost-effectiveness of the selected processes versus alternate approaches, Reference 1. Three material systems and five design options were considered for the cover. TPC materials are considered in three approaches: SDCC, fiber placement, and manual lay-up. The other two options include a manual lay-up of toughened bismaleimide (BMI) and a titanium superplastic formed diffusion bonded (SPF/DB) design.

The three approaches for thermoplastic composites include (1) SDCC in which a pressure box is employed to consolidate the outer skin while at the same time forming and consolidating the inner stiffened pan, (2) fiber placement, using a tow placement process over preformed hat stiffeners recessed into a fiber placement tool, and (3) a thermoplastic composite manual lay-up approach with autoclave consolidated unidirectional and comingled material forms. A traditional manual lay-up process was considered for the toughened BMI thermoset composite (TSC) design utilizing rubber mandrels and female tooling to produce a co-cured structure. In addition, the TSC design included stitching of the stiffeners to increase stiffeners-to-skin interface strength. A titanium superplastic formed/diffusion bonded design was the metal option. Diffusion bonding allows the economical creation of high performance hat stiffened skins without fasteners.

The analysis explored the impact of component complexity on producibility and cost. Two levels of complexity were considered. The fuel cell cover under development for this program is a single curved component. A producibility analysis of this generic cover was established to serve as a baseline. A complex, doubly curved version of the cover was also considered since OML fighter skins are typically complex surfaces.

High processing temperatures for thermoplastic composites (750°F, 385°C) impose two major fabrication constraints: (1) flexible rubber mandrels (for hat stiffener tooling) cannot be used since they are unable to survive the processing temperatures and (2) high temperature tooling is required instead of aluminum tooling. The influence of these constraints for both recurring and non-recurring costs was considered. Each fabrication approach listed above was evaluated in order to identify the best technique for both levels of complexity.

Recurring component costs were generated by summing material and labor costs for each step of process plans for each fabrication approach. Labor costs were burdened to include equipment/facilities costs. Non-recurring costs took into account tooling expenses, including any duplicate tooling required to produce the theoretical rate of 85 ship sets per year (600 aircraft total). Cost comparisons for this study were normalized; the least expensive simply curved approach is set equal to one with the cost of other options appropriately ratioed.

The cost study results for both complex and simply curved components showed that the SDCC approach was most cost-effective for the cover due to flat ply collation and short cycle times, Figure 2. TPC fiber placement was the next most cost-effective approach due to automated processing of the skin. Although TPC's are difficult to manually lay-up, this process is less expensive than TSC manual lay-up due in part to stitching requirements for TSC in order to increase hat pull off strength. Titanium SPF/DB and TSC were close in recurring cost due to the labor intensive operations required for these approaches. As expected, the recurring cost of fabricating complex structure was consistently higher than simple structure.

Non-recurring costs (tooling) for the five fabrication approaches showed that duplicate tooling requirements for TSC and TPC manual lay-up increase their respective tooling costs to a level comparable to the other fabrication approaches, Figure 3. Even with duplicate tooling, non-recurring costs for simply curved TSC and TPC are the least expensive options. Five-axis machining requirements for tooling on complex curved manual lay-up TSC and TPC approximately doubles their respective non-recurring costs. Although press forming and fiber placement tooling costs are identical for simply curved applications, a substantial cost increase is incurred in press forming versus fiber placement costs for complex curvature. This increase is attributed to difficult machining requirements (five-axis) for not only the press forming tool but also for the associated pressure box. High temperature matched metal steel tools must be supplied for the titanium SPF/DB approach resulting in the highest tooling costs of any approach.

SUBCOMPONENT DESIGN/ANALYSIS AND STRUCTURAL TESTS

Design loads for the upper cover subcomponent, Figure 4, were developed from maneuvering flight conditions consisting of a 9g symmetric steady-state pull-up (SSPU) for down bending, a -3g steady state pushdown (SSPD) for up bending, and 7.2g rolling pull-out (RPO) for combined vertical and lateral loads. All flight conditions are at sea level and 0.95 Mach. A 22.0 psi (ultimate) fuel pressurization load condition is also included.

Design loads were obtained at a fuselage station in the forward-center fuselage section at the most forward wing shear attach location. A hat stiffened skin of single curvature was sized for these loads. Various laminates were evaluated for static strength and panel stability. A finite element model of the cover was used to examine effects of combined loads and determine static deflections. Panel stability was determined using SS8 Anisotropic Curved Panel Analysis Program, Reference 2.

Two designs were developed for the upper cover. The first design, Figure 5, contains discrete hat stiffeners with a constant thickness skin. The second design, Figure 6, contains a constant thickness Inner Mold Line (IML) pan with a buildup under the stiffener in the OML skin. The first design will be utilized in the FP manufacturing process. The second design will be fabricated using the SDCC.

The laminate stacking sequences for the cover subcomponents represent the minimum necessary to sustain all flight load conditions, buckling constraints and fabrication requirements. Skin buckling occurs at 120% of design limit load, a requirement common in new fighter aircraft designs with composite mold line skins.

Planned structural testing of the subcomponents consists of compression static and fatigue loading. Static tests will be used to compare results of structural tests to analytical predictions, while fatigue tests will determine panel resistance to delamination modes of failure due to repeated loads.

ELEMENT DESIGN/ANALYSIS AND STRUCTURAL TESTS

Two structural areas of particular interest in the fuselage structure were selected for elemental evaluation. These are thick composite lugs and stiffener-to-skin joints.

Lug Elements

A method for predicting the static response of thick, highly loaded, composite lugs has been developed. Composite lugs provide a mechanism for the transfer of concentrated loads from one structural member to another. The most notable examples are lugs that transmit wing loads into bulkheads such as those present on the generic fuselage structures. The geometry of these lugs can vary substantially for different applications, and they may be required to carry in-plane as well as out-of-plane loads. In addition, effects such as pin bending may result in complex stress states through the thickness of a lug, even when it is subject to only in-plane loads.

The wide range of variables associated with this problem necessitates the use of an analytical method that is very flexible, both in the range of geometries and the types of load conditions that it is capable of analyzing. The complex through-the-thickness stress distributions that may develop require that the method also be capable of predicting three-dimensional stress fields. The finite element method is one such approach and was the method used in this development.

Laminated composite aircraft components are typically analyzed using plate elements that are based on classical laminated plate theory. These elements are simple to use since the geometry of the element can be defined in two dimensions, and they account for in-plane and out-of-plane loads. They are, however, restricted to the analysis of thin plates, which limits their usefulness for the analysis of thick lugs. The thin plate derivation permits

only linear variations in the in-plane stresses through the thickness of the lug, and out-of-plane stresses are assumed to be negligible.

At the other extreme, a thick lug can be modeled with three-dimensional solid finite elements. Using the approach, each ply can be modeled (one or more plies through the thickness of each element). These elements allow complete generality in defining the lug geometry and loads and are based on assumed three-dimensional displacement fields. Although models generated with these elements provide accurate results, their use is cumbersome and they require substantial computing resources. They are, therefore, not recommended for the type of parametric study that would be required to optimize a lug design.

The approach taken in this program was a compromise between the two methods described above. A subparametric laminated solid element based on cubic displacement functions was used. This element was developed in Reference 3 to study through-the-thickness stress fields that develop during low velocity impact events.

The geometry of this element is defined by four nodes in the X-Y plane, and the stacking sequence of the laminate under consideration, Figure 7. There are twenty-four degrees of freedom at each node. These degrees of freedom are the translations at the upper and lower surfaces of the laminate in each of the three coordinate directions and the derivatives of these translations with respect to each coordinate.

Using conventional finite element methods, the stiffness matrix for the element is generated by integrating the strain energy density over the volume of the element. The effects of stacking sequence are included by performing this integration numerically over the volume of each discrete ply and summing the results. This approach also allows the average strain in each ply and at each interface to be calculated once the translations and derivatives of the translations have been determined.

To account for pin bending effects, both the lug and the pin are modeled. The generation of these models is relatively simple since the geometry is defined in only two dimensions. The lug/pin contact is modeled by coupling lug and pin displacements in the radial direction. Since the extent of the contact area is not known a priori, the problem is solved iteratively. An initial contact area is assumed, loads applied, and displacements and reactions forces in the lug and pin calculated. The forces that develop between coupled points on the lug and pin are then investigated. If the force at a given point is compressive, the lug and pin remain in contact at that point; if tensile, the two separate. The model then analyzes the new contact area, and the contact forces are again investigated. This process continues until the contact area stops changing.

The converged displacement field is then used to perform a laminate analysis on an element by element basis. For each element, the average strain in a given ply is calculated by integrating the strain field over the volume of that ply contained in the element, and the average strain at an interface is calculated by integrating over the interface area. These strains are then used to calculate average ply and interface stresses within the element. Either stress or strain

may then be used in an appropriate failure criteria to evaluate the integrity of the element.

Advantages of this approach over existing finite element models are 1) model geometry is defined in only two dimensions, 2) three dimensional stress and strain fields are used, 3) the effects of the laminate stacking sequence are included, 4) both in-plane and out-of-plane loads are included, and 5) ply and interface stresses and strains are calculated. Although existing methods have some of these advantages, no other approach has all of them.

In order to verify the analytical code developed, three lug lay-ups and two pin diameters were chosen (Figure 8). Each lug has a different through-the-thickness stiffness distribution, but all have the same average in-plane stiffness. The lug with the smaller pin diameter was sized to fail in bearing, and the lug with the larger pin diameter was sized to fail in shear.

Based on sensitivity study results, four elements through the thickness were used for strength prediction of lugs. A comparison of bearing strain distributions at 40 kips predicted by models consisting of one, two or four elements through-the-thickness is shown in Figure 9.

The lug specimens were tested as shown in Figure 10. Test results and associated predictions for the lugs are summarized in Figure 11. Failure prediction in the critical elements was based on using a modified Hashin criteria. The 1.75 inch diameter holes exhibited a tensile fiber failure at the net section while the 1.0 inch diameter showed permanent yielding around the hole prior to shear bearing failure. Good correlation between test and prediction was obtained. The initial bearing failure load was determined by using axial strain data from the rosettes located 0.5 inches away from the edge of the hole. The load versus strain curve in Figure 12 shows that axial strain decrease associated with material failure ahead of the pin. Typical bearing and net section failure modes can be seen in Figures 13 and 14 for the 1.0" and 1.75" diameter specimens, respectively.

Frame Elements

The Y-section frame elements, Figure 15, will be fabricated and tested against a T-section of contemporary design. Both sections will be coconsolidated to a typical skin laminate during fabrication.

The Y-section was chosen for its potential formability in a diaphragm forming process and for its lower peel stress components. The effect of changing the angle of the Y-section is also being investigated. Two-dimensional finite element models of the T- and Y-sections were created for the purpose of defining the boundary conditions to be used in testing.

The fastenerless moldline Y-frame attachment element design is structurally simple, allowing it to be diaphragm formed and coconsolidated. Transverse tension strength for semicrystalline thermoplastic composites has been found to be appreciably greater than comparable thermosets. This property is expected to enhance the peel strength and survivability of the frame element and will be verified by our planned tests.

Test loads for the Y-sections will be introduced through an internal mandrel (Figure 16). This method alleviates possible failures other than those desired and allows for later design of several frame attach possibilities. Possible frame attachments include: amorphous bonding, resistance joining, adhesive bonding, coconsolidation, and mechanical fastening.

SUBCOMPONENT TOOLING AND MANUFACTURING

Tooling concepts for each cover design/manufacturing concept is discussed. Internal geometry of the hat stiffeners was designed to be similar to allow mandrel tools to be interchangeable.

The fiber placement manufacturing process consists of placing inverted roll formed hat stiffeners into an aluminum fiber placement tool. Aluminum mandrels will be placed in the hat stiffeners to prevent skin deflection during the fiber placement process. Tooling conceptual design is illustrated in Figure 17. Retainers are utilized to hold the stiffeners and mandrels in place during processing. The hat is positioned in the tool as shown in Figure 18. The hat flange is offset slightly above the aluminum tool to allow for adhesive and the first ply. Also, a heat blanket will be embedded into the aluminum tool that supports the preformed thermoplastic composites stiffeners. The blanket will provide a greater degree of temperature control where required. Following fiber placement of the skin, the panel will be trimmed and retainers removed. The mandrels will then be removed and the part prepared for nondestructive testing.

The SDCC concept is unique in that there is but one diaphragm, and the IML pan and OML skin are consolidated and coconsolidated during the diaphragm forming process. The SDCC tooling concept is illustrated in Figure 19.

The greatest risk in diaphragm forming over hat mandrels is the chance for bridging. To minimize this risk, the manufacturing and tooling team members utilized lessons learned criteria to optimize hat height, cap width, and skin thickness. Hat spacing was maximized to increase ply surface area between mandrels. The increased surface area will increase the force exerted to form the ply pack and prevent bridging. In addition, the mandrel will be fabricated with a slight radius (Figure 20). The gap between the mandrel, OML skin, and IML pan will be filled with a predetermined amount of unidirectional tow. This fillet area has the highest probability for bridging; however, with the unidirectional fillet, the pressure will be equally distributed to facilitate a quality consolidation.

A vacuum ring and a neat film layer will aid in ply pack location. The IML ply pack will be contained between the aluminum diaphragm and a layer of neat film. A vacuum ring surrounds the IML ply pack and vacuum draws the aluminum diaphragm to the upper surface of the IML ply pack and the neat film to the lower surface of the IML ply pack. The IML ply pack is then positioned correctly above the tool prior to application of heat and pressure. The neat film is coconsolidated between the IML and OML ply packs during the press operation. This will permit accurate location of the IML ply pack and aid in prevention of wrinkles.

Concepts for the subcomponent tool include machined steel weldment, cast bulk ceramic, machined aluminum, and a metal arc sprayed tool. A metal arc sprayed tool which can accommodate integral heating, faster cycle times, and low tool cost for production-type environments shows high potential.

ELEMENT TOOLING AND MANUFACTURING

Lug Elements

Tooling for the lug specimens consisted of simple project plates with steel dams positioned to allow for expansion during consolidation. The lug geometries and lay-ups that will be used were previously described in Figure 8.

The lugs were fabricated from AS-4/PEEK unidirectional tape. Eighteen 30" x 16" sublaminates panels of four different 30 ply lay-ups were consolidated in a hydraulic press. Six sublaminates were then stacked to form the three different 180 ply stacking sequences. The three stacking sequences were co-consolidated in the autoclave. The lug specimens were water jet cut from the panels and the holes reamed to final dimensions. Excellent consolidation was achieved in all lug specimens as evidenced by ultrasonic and photomicrographic inspections.

SDCC and Y-Frame Elements

An SDCC element verification tool (Figure 21) was developed which can incorporate either two hat mandrels or a single triangular mandrel to fabricate the Y-section frame elements. The hat dimension, spacing, height and width simulate the subcomponent design. The hat stiffener mandrels, located by pins, float on the unconsolidated skin. The inner skin is then formed over the mandrels in a press operation. The aluminum tools are readily extracted following forming.

To focus on the critical process variables and not on geometric complexities, element forming trials on the verification tool commenced with the Y-frame elements and will then proceed to the 2-hat section element. Scale-up is a very significant concern and is being considered in all the fabrication development activities.

Forming trials on the single "Y" configuration used one diaphragm to consolidate the upper ply pack with the lower plies. Initially full pressure (150 psi) was applied after the melt temperature of the ITX was reached but was maintained for only 5 minutes at which point the diaphragm ruptured. In spite of the short hold time the pressure was sufficient to fully consolidate the flat areas of the part and to form the material over the mandrel. The upper ply pack conformed to the mandrel surface very nicely, but the diaphragm rupture caused the outer ply to lift and bridge across the mandrel/skin intersection. The other plies remained in the formed condition, nesting closely to the mandrel, and showed excellent definition at the interface between stiffener web and lower skin.

Forming was next done below melt temperature because of anticipated problems where the two packs met each other beyond the stiffener area. For the next trial full melt temperature was achieved before pressurizing. Other changes to the setup included lengthening the mandrels to rest next to the ramp surfaces and widening the upper ply pack so it extended out to the ramp surfaces in all directions. This change required notches to be cut along the edge of the ply pack to prevent buckling and rupture of the diaphragm. Kapton tape was used to cover the notches for additional protection.

The next forming runs were performed with the noted changes and the diaphragm survived well up through 150 psi. Since the plies were above melt temperature, good consolidation was achieved between the upper and lower packs. The rupture occurred along the edge of the mandrel in a notch location that allowed the film to over elongate and burst. A large percent of the plies remained formed to the mandrel surface along its base. Only one ply lifted and bridged away from the radius area of the formed plies (Figure 22). The inside of the stiffener shape revealed very good contact between the plies being formed and the base of the mandrel even with loss of the diaphragm. Photomicrographs of the area show that the upper plies dragged the lower plies in toward the mandrel and formed wrinkles in the lower skin.

In an attempt to alleviate dragging of the base ply pack, the upper ply of the base pack was extended to run under the ramp areas of the tool. This change would maintain pressure on the top ply to allow slippage of the two ply packs without wrinkling. Also, a fiber glass cloth (picture frame), was placed around the ramp areas and over the mandrel to cover any areas that could potentially allow the diaphragm to rupture. During this run the diaphragm ruptured in a gap between the ramp and forming box causing incomplete forming of the element. However, less ply slippage was noted.

Due to the frequency of rupture of the UPILEX diaphragms, an aluminum (SUPRAL) diaphragm was selected for further trials. The aluminum diaphragm offers greater elongation capabilities not only at processing temperatures but also at temperatures below the melt temperature of the PEEK resin.

During the first run with an aluminum diaphragm, the pressure was applied at 550°F, (below the melt temperature of the thermoplastic resin). Applying the pressure at this low temperature allowed the lower plies to slip prior to a viscosity change of the resin. During this fabrication attempt, the top ply of the lower ply pack was extended beneath the forming ramps in an attempt to "lock" the ply in place, thus avoiding wrinkles. After applying pressure (120 psi) at 550°F, the temperature was increased to 750°F and held for 30 minutes.

The result was a stiffened panel with good surface quality but with bridging in the radius. NDT results revealed a porosity free part in the flat areas. However, photomicrographs revealed the lower ply pack wrinkled. Since the upper ply of the lower ply pack wrinkled and the ends were contained beneath the forming ramps, the ply obviously split between the fibers of this outer 45° ply.

Following review of the results of the run, two changes to the manufacturing process were identified to alleviate the wrinkling problem in the next run. The next attempt will incorporate a neat resin film between the two ply packs

to serve as a lubricant. This will reduce frictional forces to allow the two contacting plies to slip past each other. Another potential solution is to change the two contacting plies from 45 degrees to 90 degree orientations. This will increase the strength in the direction of slippage and reduce friction.

Blade Frame Elements

Using two aluminum block details a blade panel was hand laminated by bending and edge tacking each of seven plies with a soldering iron (Figure 23). The fillet was filled with thin strips (.30" to .90") of ITX unidirectional tape using a sharp cone tip on the soldering iron, Figure 24. A flat skin was preconsolidated and a strip grit blasted across the center where the blade attached (Figure 25). The two angles with fillet in place were inverted onto this skin, Figure 26, and vacuumed bagged to a project plate. There was a released UPILEX film between the angle plies (web) and the aluminum details. Upon consolidation (Figure 27) this configuration did not show acceptable c-scan results. The web area had many depressions in it that appeared to be oriented along the second ply down from the surface, i.e., normal to the surface ply fiber direction.

Outgassing from the release coated UPILEX and the lack of ears on the vacuum bag at the base (which may have prevented sliding of the blocks) were identified as probable causes for the poor consolidation. As such, a second blade was fabricated with no UPILEX on the tool details and with extensive ear folds in the vacuum bag. Nondestructive inspection of the second blade revealed porosity in the radius areas. Although the part quality was improved over the first blade, it was not the level desired. After a careful review of the part it was evident one of the tool details had slightly rotated during consolidation.

The consolidation tools are presently being modified to permit a positive control of the details. A trimetric view of the modification is shown in Figure 28. Keyways will be milled into the ends of the web details and fit to keys in the end plates. This modification will maintain the movement of the detail in the direction desired, thus maintaining constant and equal pressure across the part surfaces. In addition, an upper slotted plate will maintain minimum differential vertical displacement between the tooling blocks for the back-to-back L-sections which comprise the T-section.

CONCLUSIONS

Based on work to date, the following conclusions have been made:

- o Selection of the upper cover allows for the demonstration of two promising cost-effective manufacturing approaches, fiber placement and single diaphragm/co-consolidation, which have applications in a majority of the remaining generic fuselage section.
- o The producibility analysis indicated that the selected manufacturing approaches show potential for low cost fabrication of the upper cover. The accuracy of the analysis will be verified during subcomponent fabrication.
- o The use of an aluminum diaphragm during SDCC verification trials prevented diaphragm rupture due to increased durability and elongation properties compared to available polymeric films.
- o During SDCC pressure can be applied below resin melt temperature without fear of diaphragm rupture since aluminum diaphragms provide sufficient elongation at those temperatures.
- o Based on blade fabrication attempts, it is anticipated that control of the tooling movement through selected keyways will guarantee cap and web thicknesses and supply adequate pressure in the fillet area.
- o Quality, thick (1 in.) panels (for lug elements) can be successfully fabricated.
- o Abrasive waterjet cutting can be used to efficiently machine thick panels.
- o A lug analysis program capable of investigating through-the-thickness effects showed good correlation to experimental results.

REFERENCES

1. Hoffman, P.L.R. and Gibler, J.A., "Design for Manufacturing, Producibility Issues for Thermoplastic Composites," presented at SAMPE Spring Meeting, Anaheim, CA., April 4, 1990.
2. Wilkins, D.J., "Anisotropic Curved Panel Analysis," Report FZM-5567, Air Force Contract No. F33615-69-C-1494, May 1973.
3. Goering, J., "Initial Impact Damage of Composites," Material Science Corporation Report MSC TFR 1801/1207, March 1987.

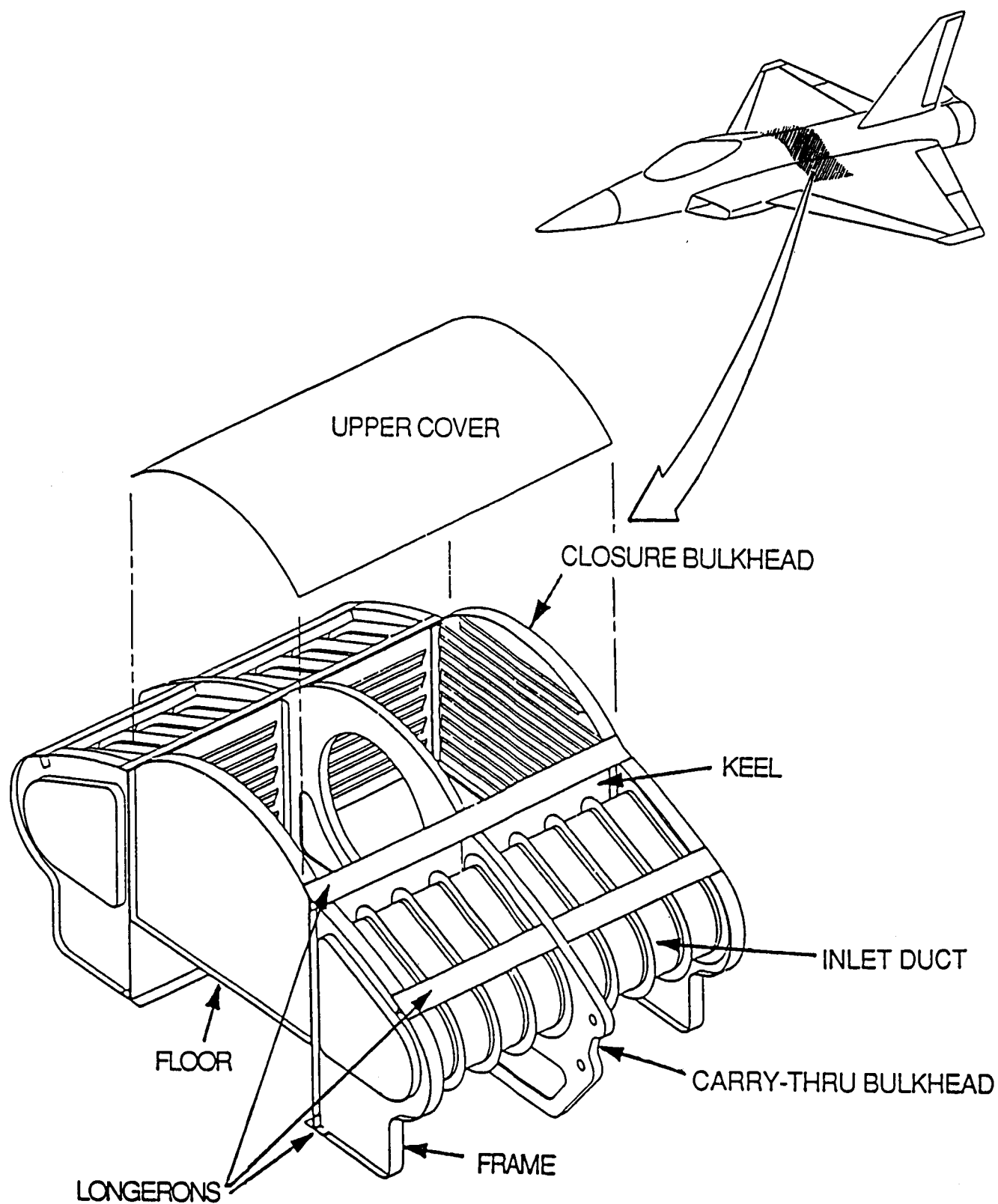


Figure 1 Generic Fuselage Section

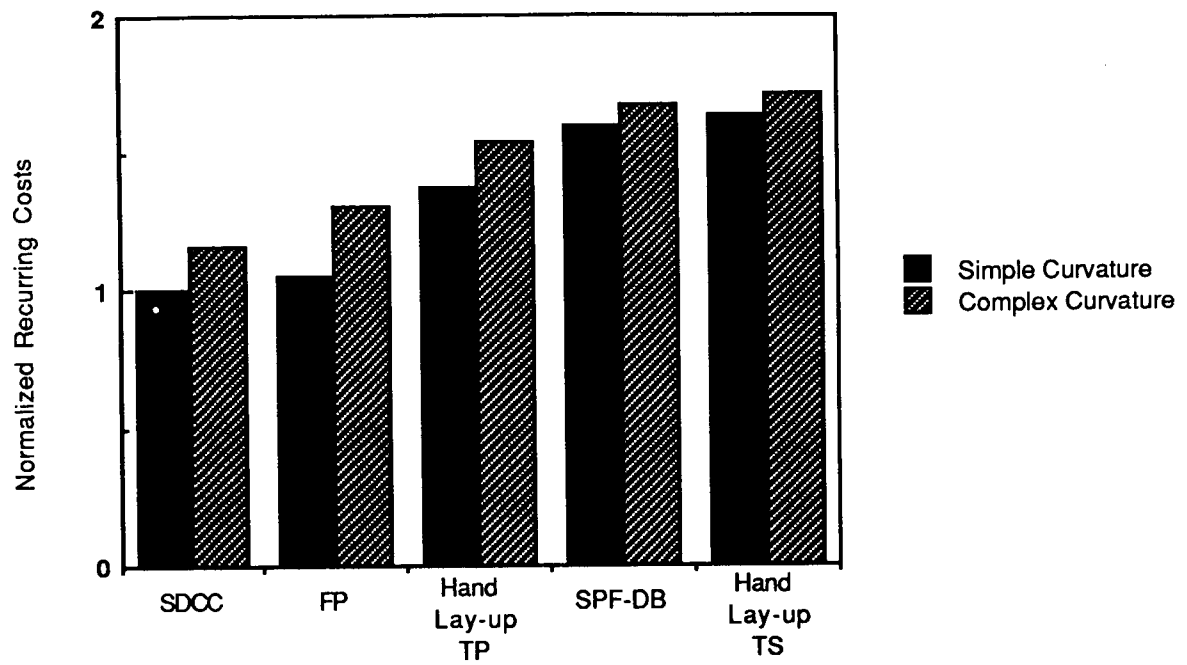


Figure 2 Recurring Cost Comparisons

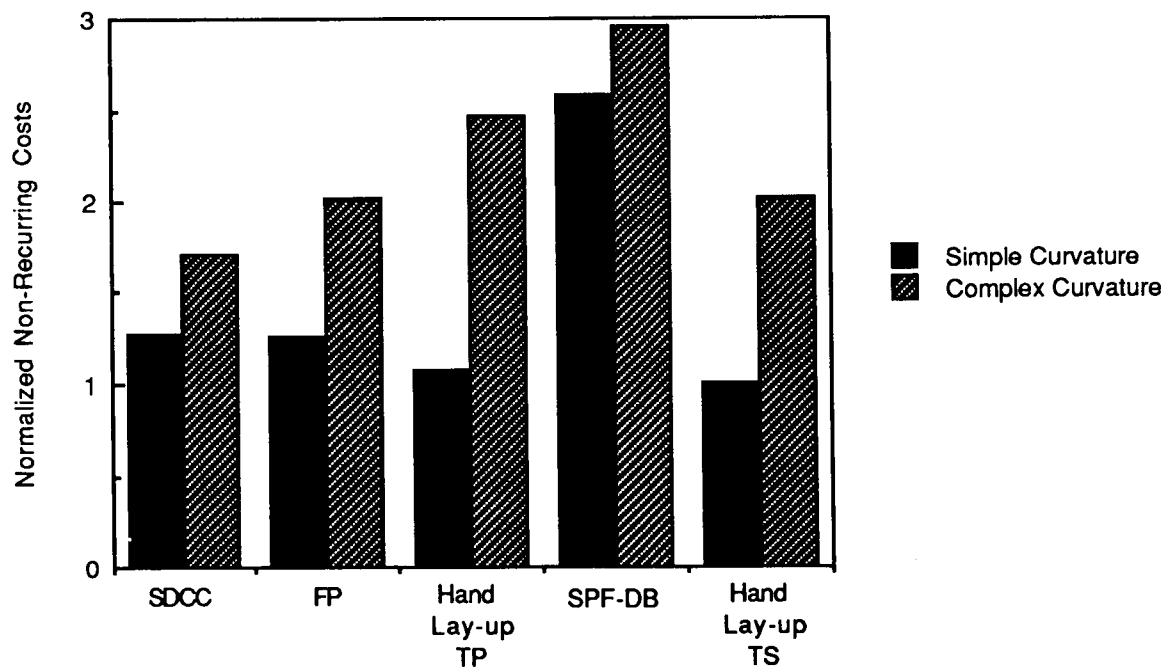
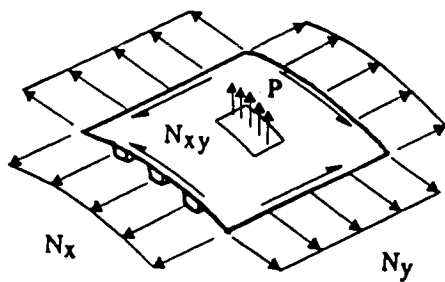
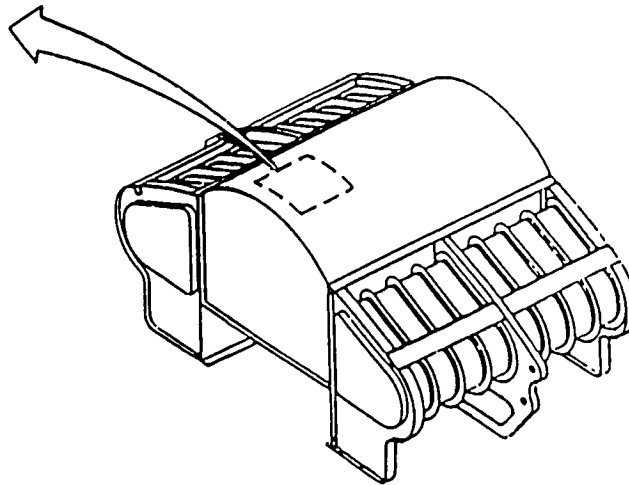


Figure 3 Non-Recurring Cost Comparisons



Phase A Subcomponent



Ultimate Loads

Condition	Nx (lb/in)	Ny (lb/in)	Nxy (lb/in)	P (psi)
SSPU, 0.95 MACH, SL, 9.0 g	2500	±100	0	1.0
SSPD, 0.95 MACH, SL, -3.0 g	-800	±100	0	5.0
RPO, 0.95 MACH, SL, 7.2 g	2000	±100	±500	5.0
Fuel System Over Pressure Malfunction	0	0	0	22.0

Figure 4 Subcomponent Designed for Actual Flight Loads

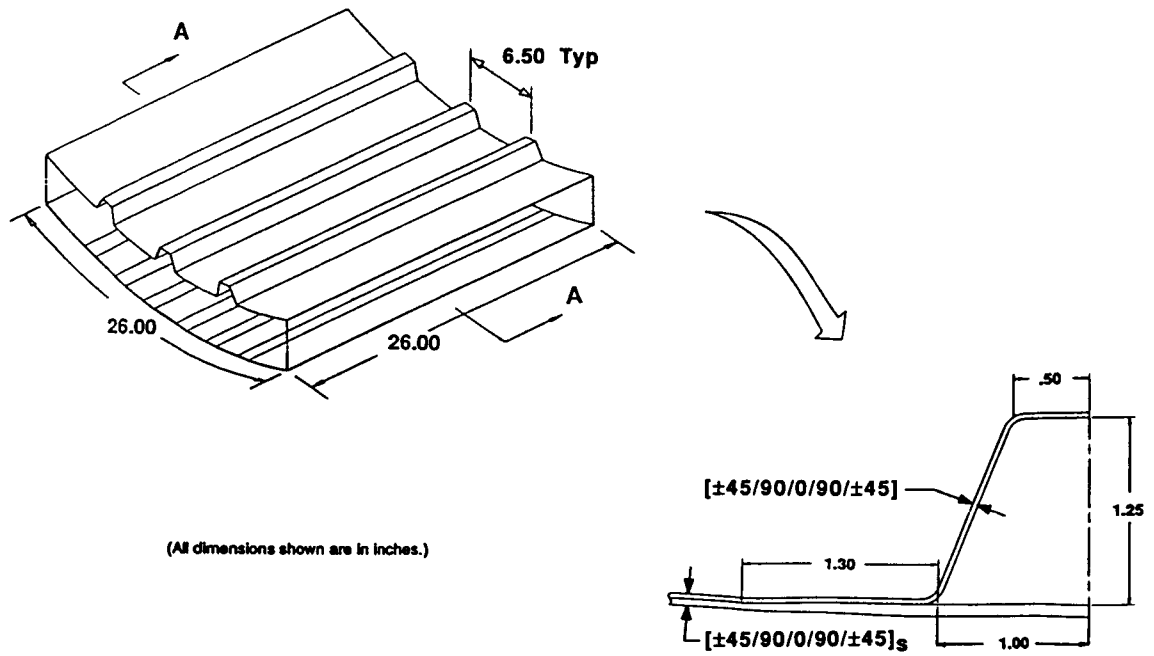


Figure 5 SDCC Subcomponent Configuration

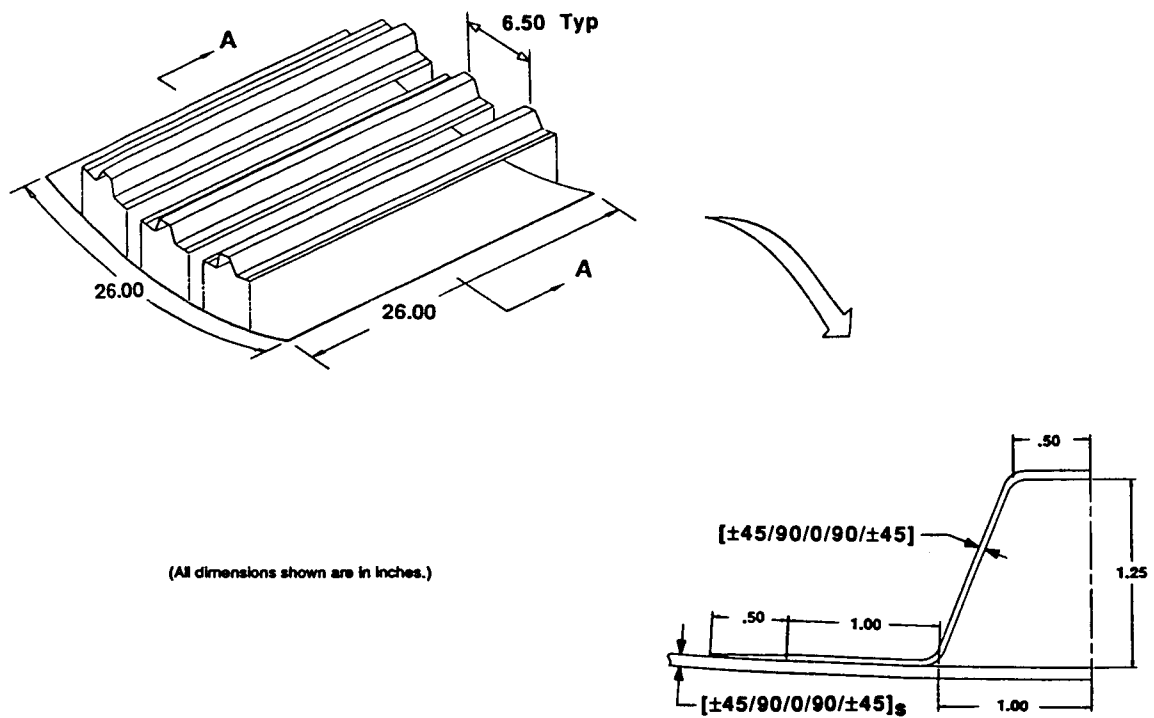


Figure 6 Fiber Placement Subcomponent Configuration

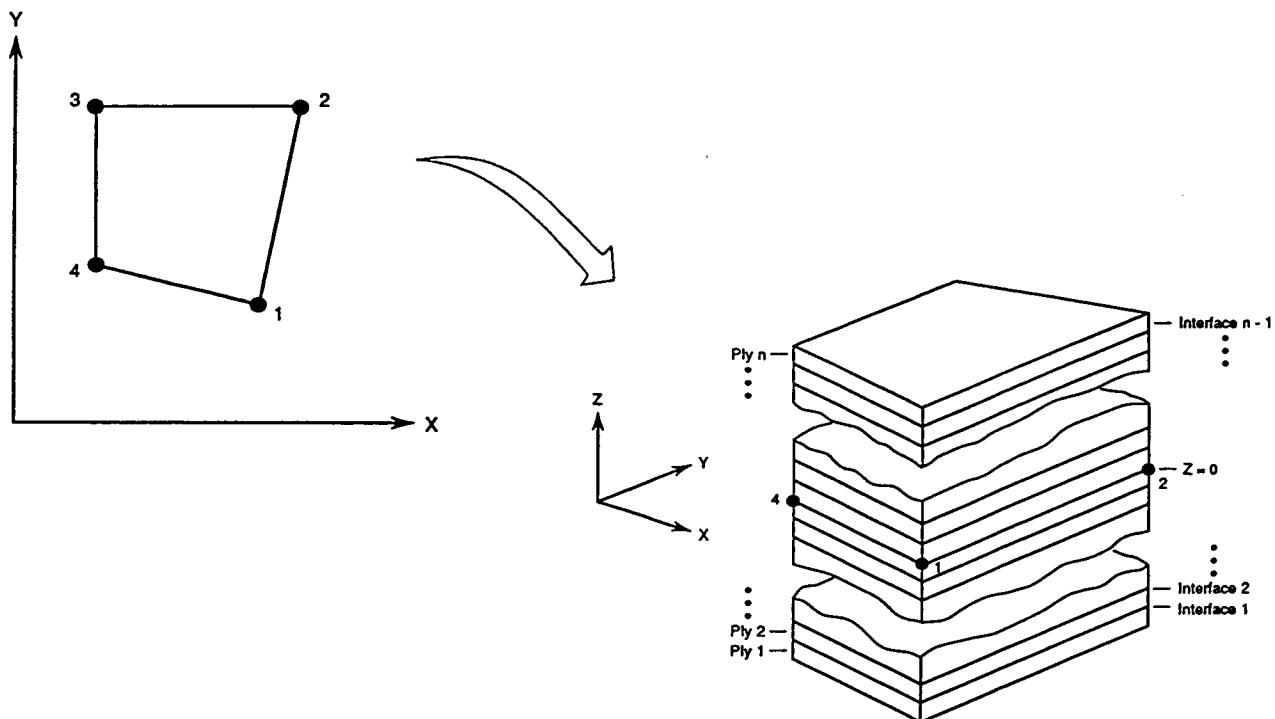
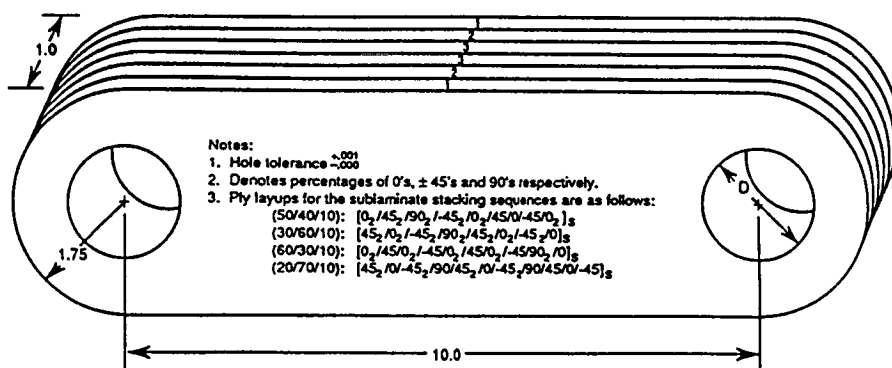


Figure 7 Subparametric Laminated Solid Element



Lug Specimens	Quantity Each	Hole Diameter ¹	Sublaminates Stacking Distribution ^{2,3}		
			Sublaminates 1	Sublaminates 2	Sublaminates 3
Static 1	4	1.00	(50/40/10)	(50/40/10)	(50/40/10)
Static 2	4	1.00	(50/40/10)	(30/60/10)	(60/30/10)
Static 3	4	1.00	(60/30/10)	(50/40/10)	(20/70/10)
Static 4	4	1.75	(50/40/10)	(50/40/10)	(50/40/10)
Static 5	4	1.75	(50/40/10)	(30/60/10)	(60/30/10)
Static 6	4	1.75	(60/30/10)	(50/40/10)	(20/70/10)

Figure 8 Lug Element Tests to Verify Analytical Methodology

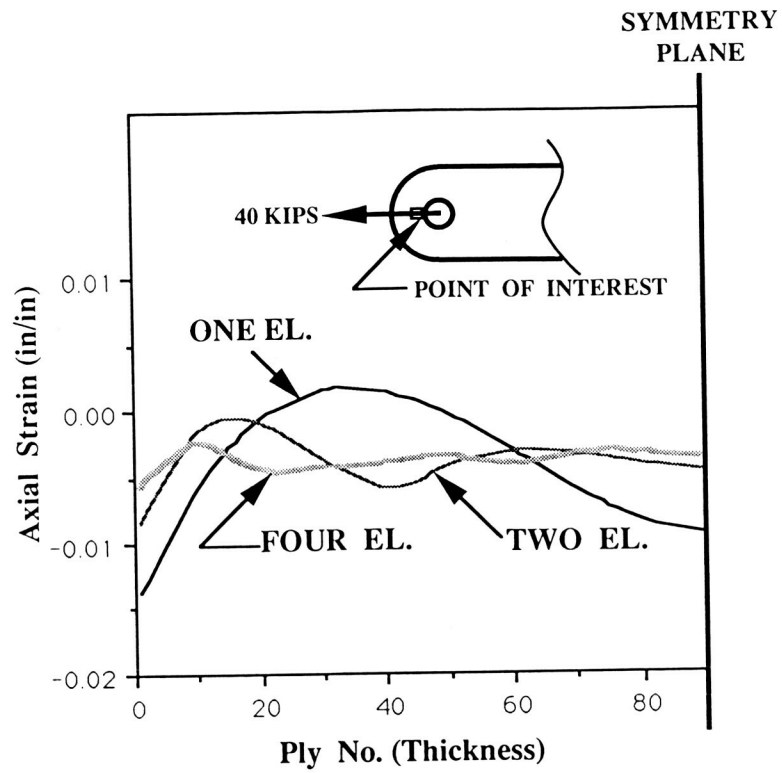


Figure 9 Convergence Study Indicates Four Elements Through-the-Thickness are Necessary

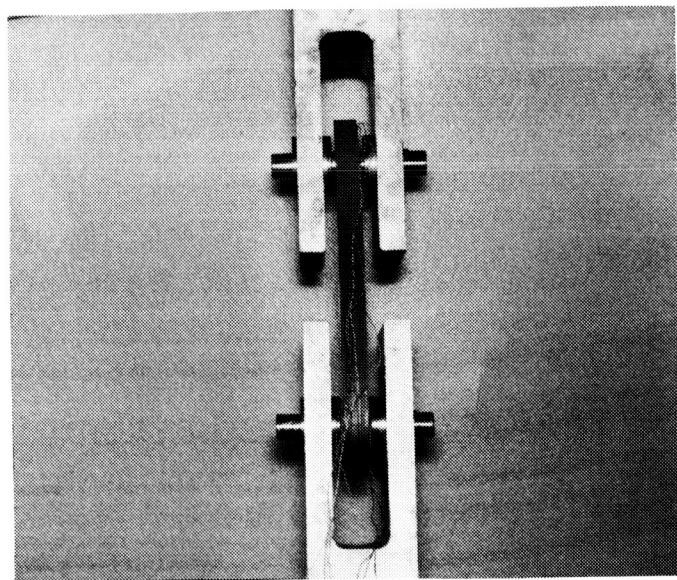


Figure 10 Lug Element Under Test

LUG Specimen	Quantity Each	Hole Dia. (inches)	Pred. Failure Load (kips)	Test Results (kips)
# 1	4	1.0	64.2	60.1 (76.7) *
# 2	3	1.0	65.9	62.3 (74.3) *
# 3	4	1.0	57.3	62.2 (74.7) *
# 4	4	1.75	66.9	69.3 **
# 5	4	1.75	66.5	68.7 **
# 6	4	1.75	61.5	66.8 **

* Initial Bearing Failure Load (Final Failure Load)

** Failure Load

Figure 11 Lug Test Results Showed Good Agreement to Predictions

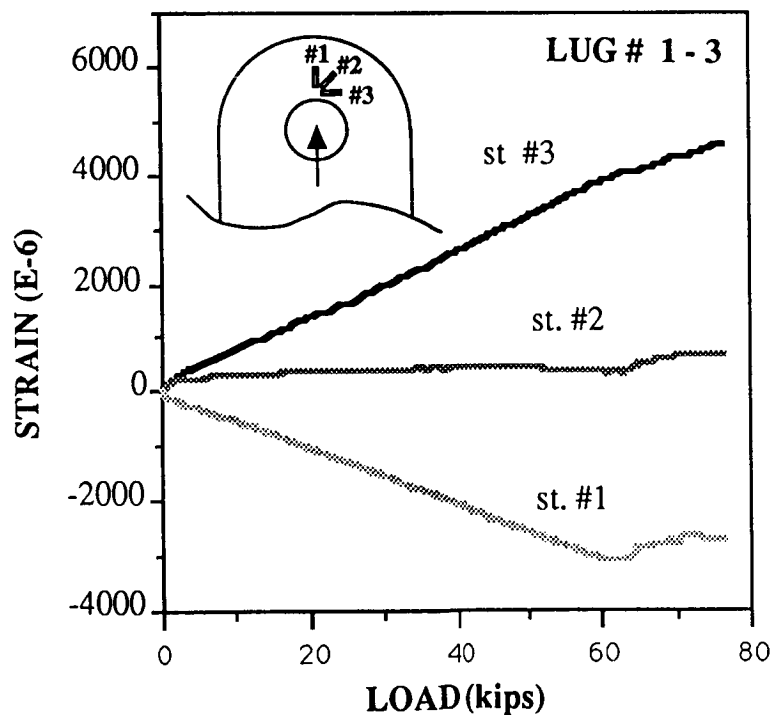


Figure 12 Strain Data Indicates Point of Bearing Failure

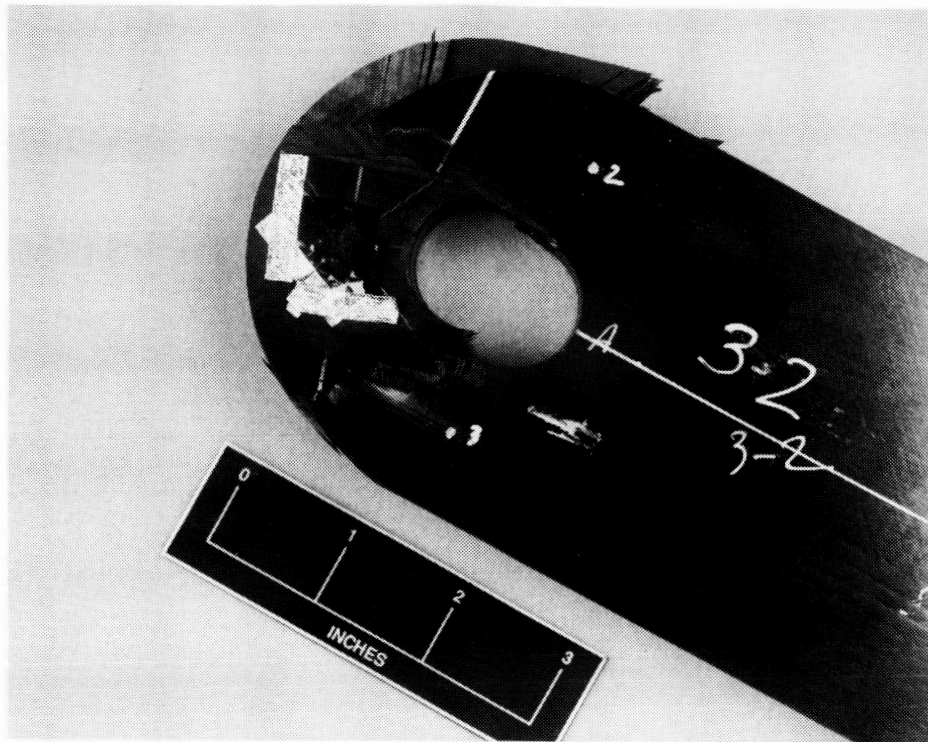


Figure 13 Typical Lug Bearing Failure

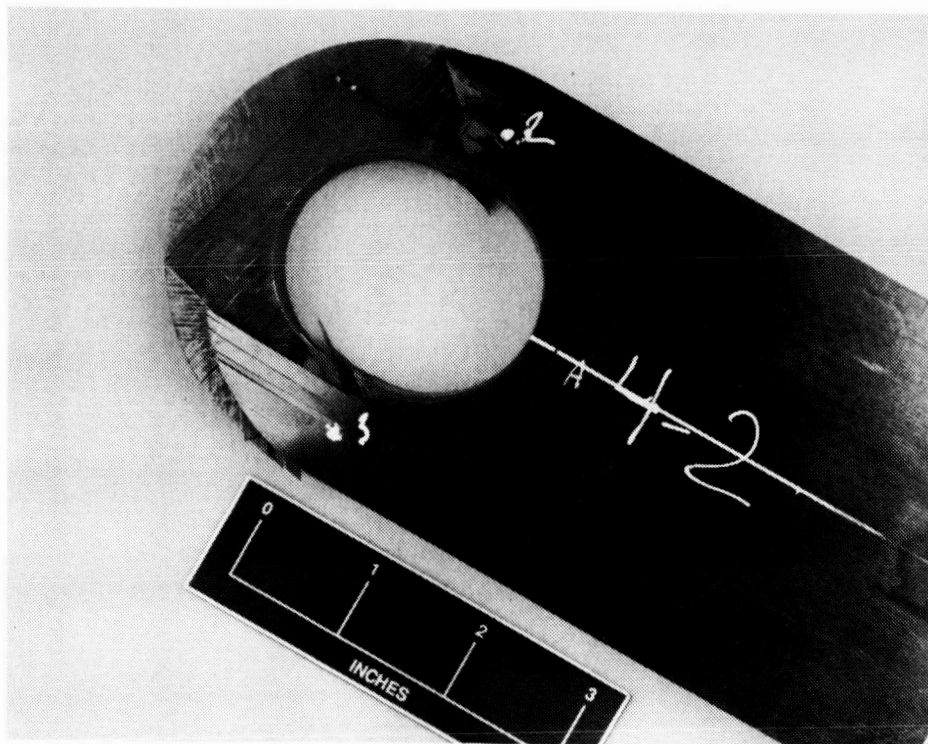
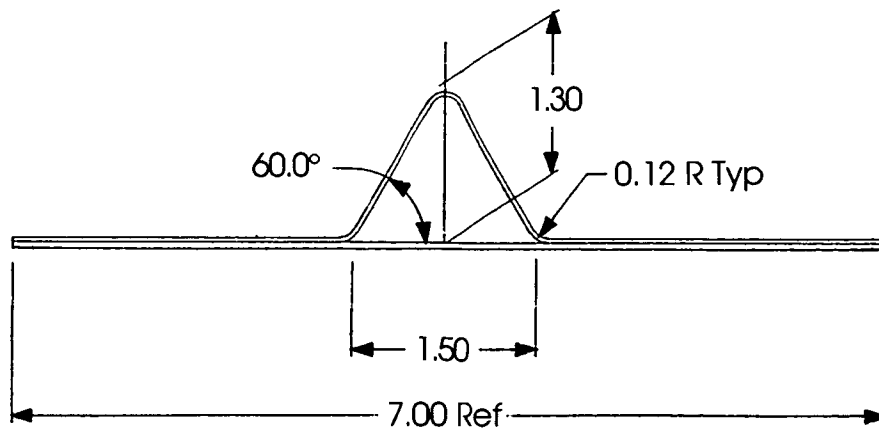
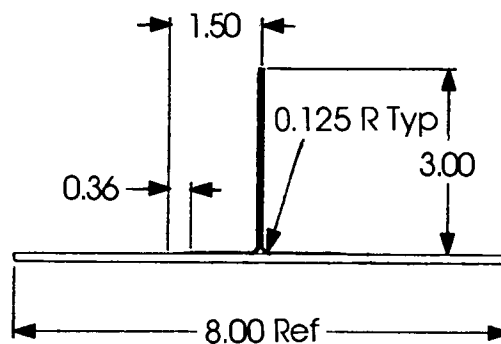


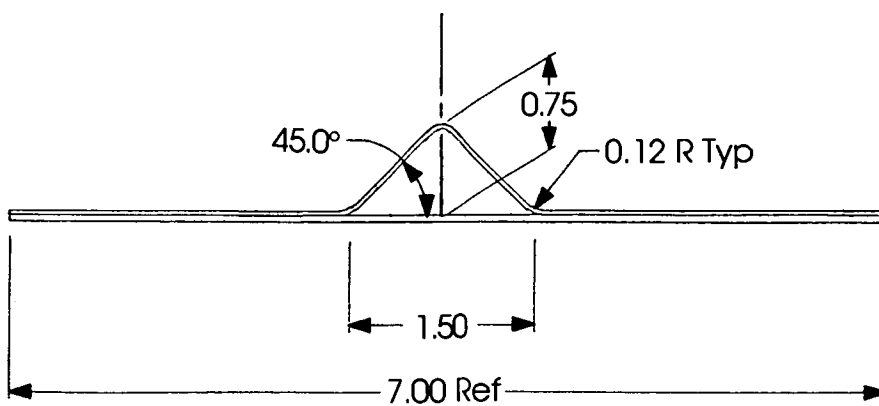
Figure 14 Typical Lug Net Section Failure



60° Y-Frame Specimen

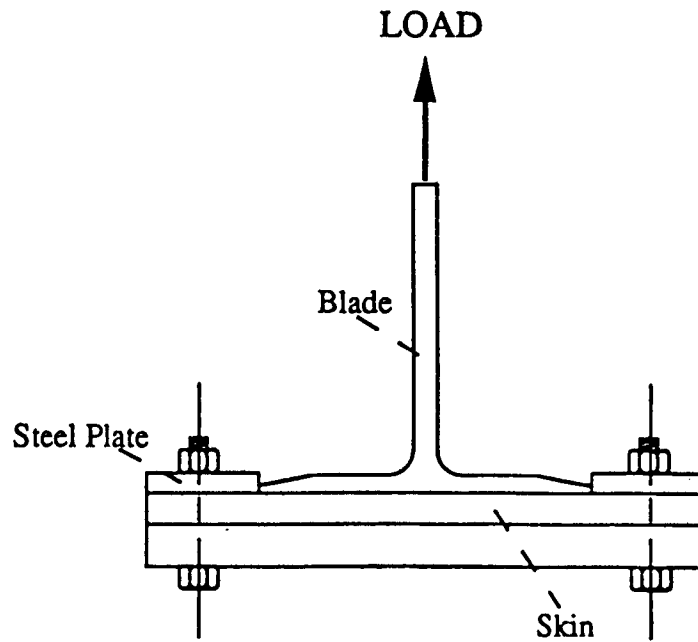


Blade Specimen



45° Y-Frame Specimen

Figure 15 Frame Element Test Specimens Will Determine Viability of Fastenerless Moldline Designs



Frame Configuration	Static	
	RTA	ETW*
Blade	3	3
Y($\alpha = 45$)	3	3
Y($\alpha = 60$)	3	3

* 255° F

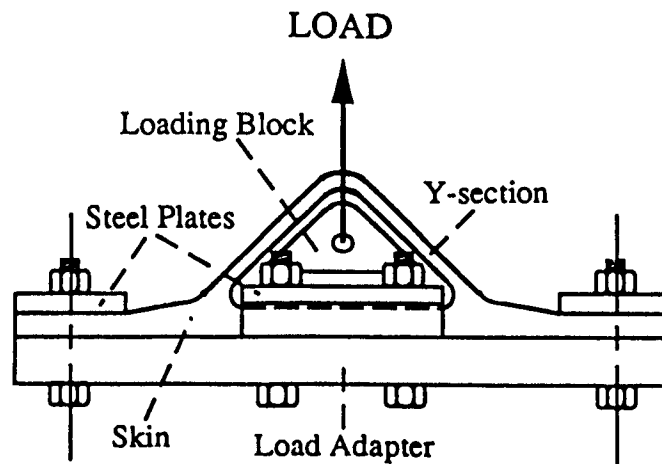


Figure 16 Pull-off Test Method Will Ensure Failure In Critical Regions

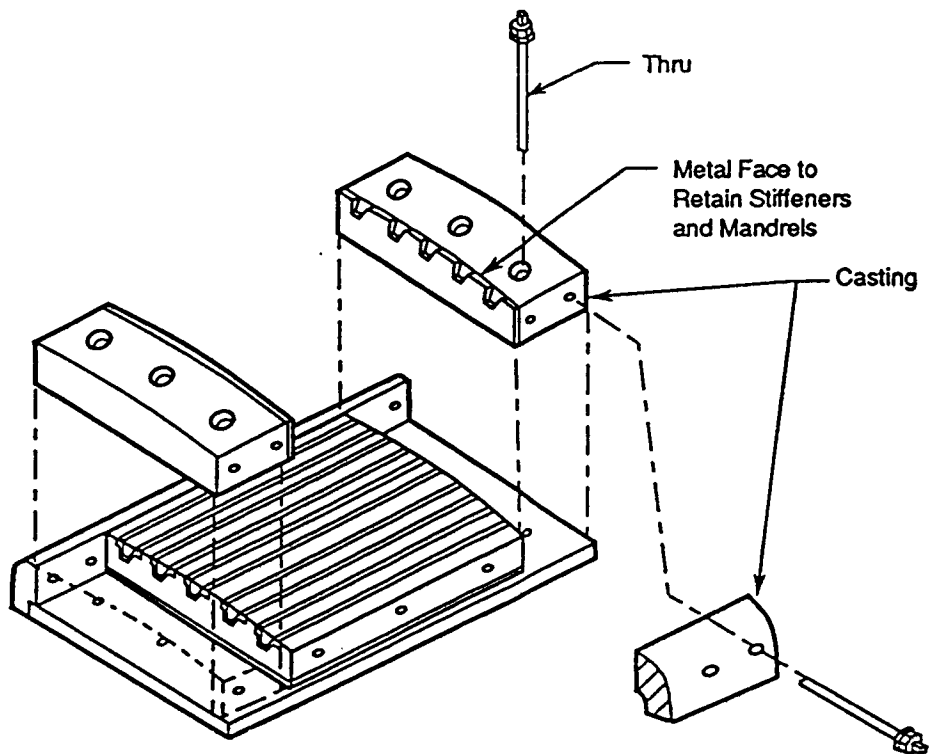


Figure 17 Fiber Placement Tooling Concept

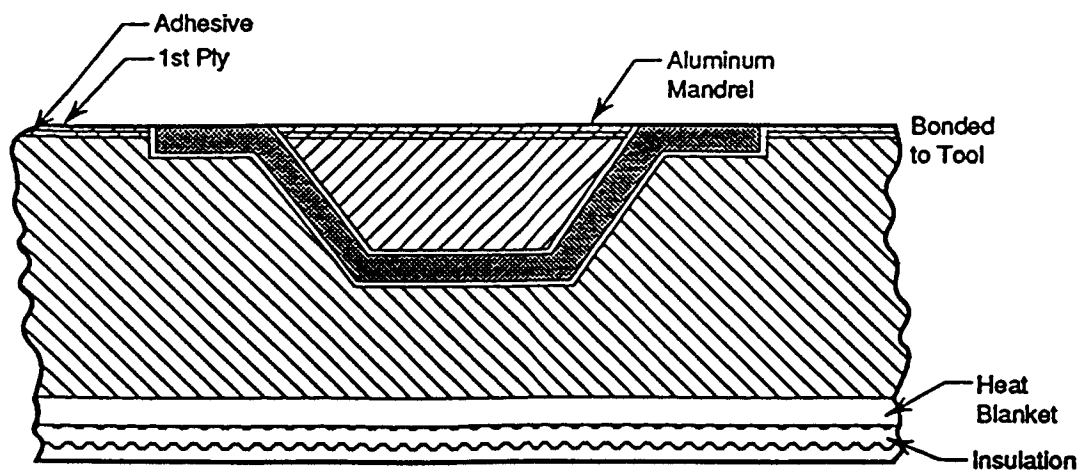
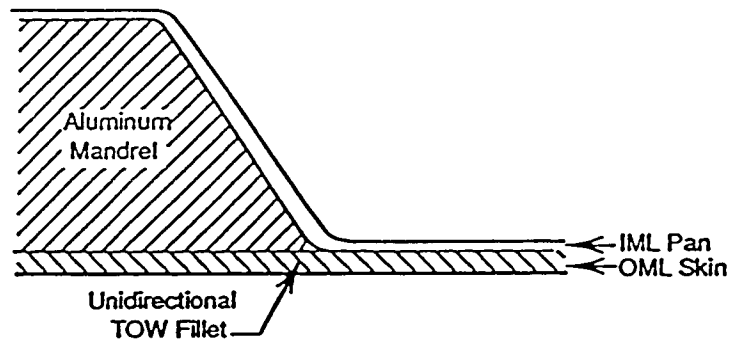
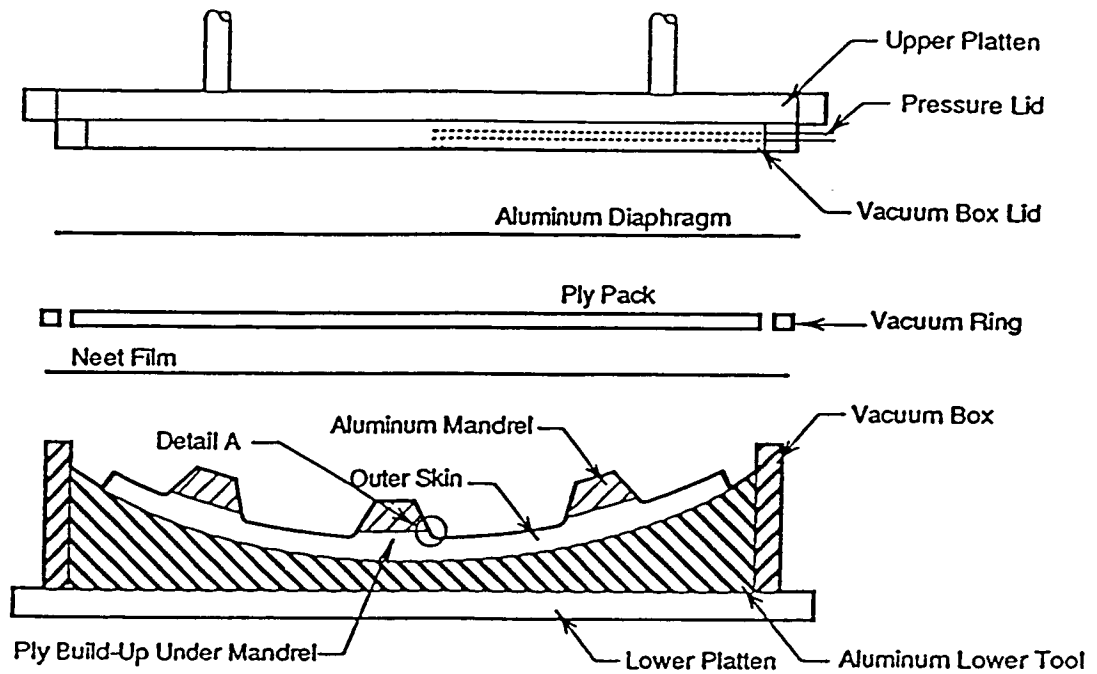


Figure 18 Hat Stiffener Embedded In Fiber Placement Tool



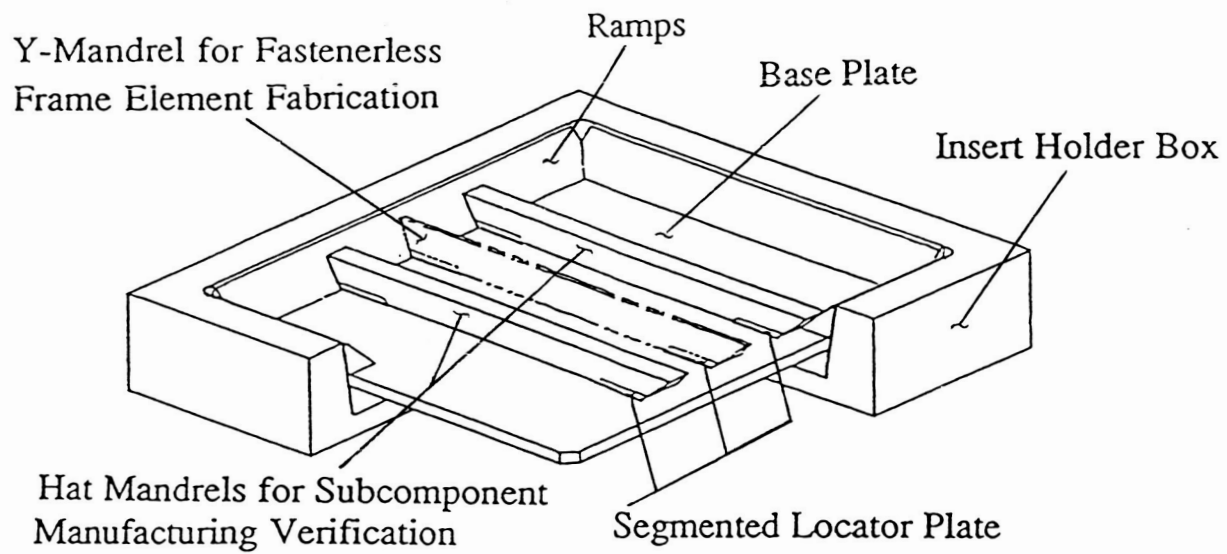


Figure 21 SDCC Element Tool

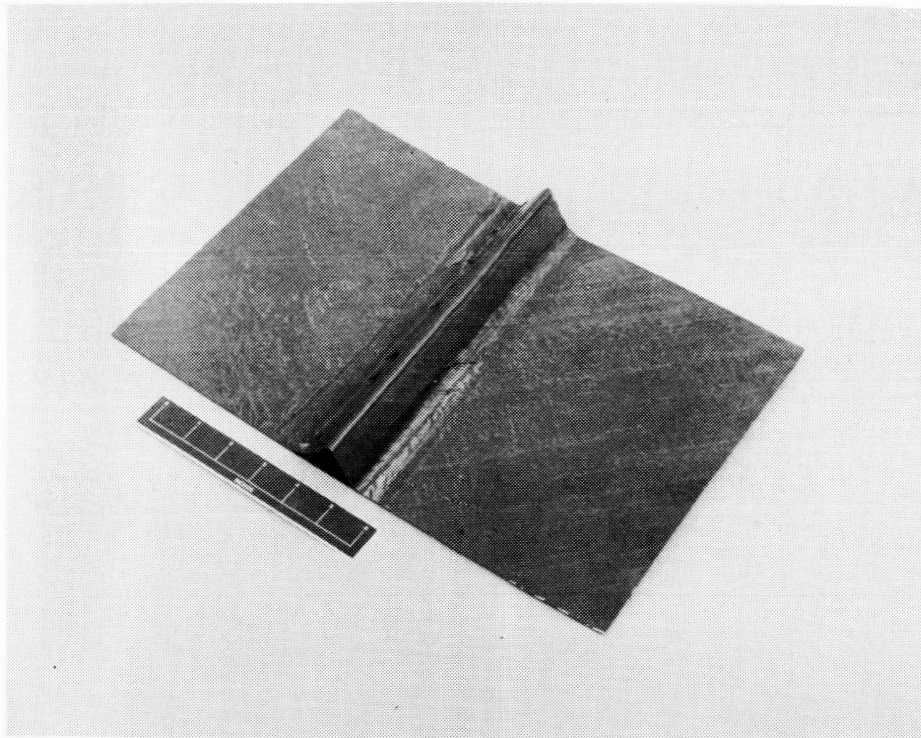


Figure 22 Initial Y-Frame Element Experienced Bridging in Radius



Figure 23 Blade L-Section Plies Hand Laid On Tooling Blocks



Figure 24 Tow Material Was Placed In Fillet Area

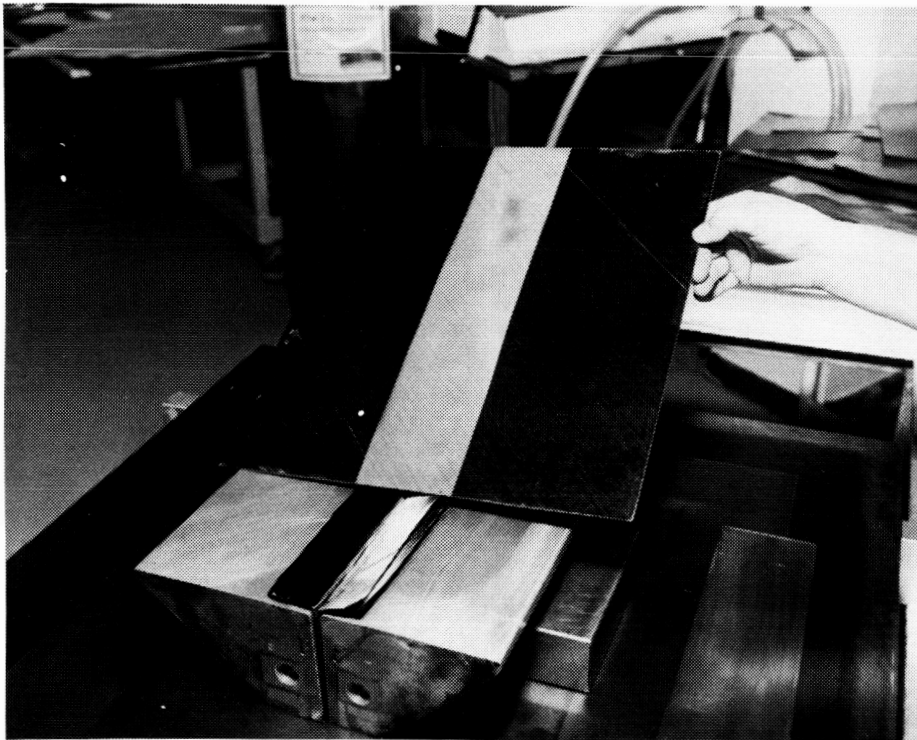


Figure 25 Base Plies Consolidated, Separated and Grit Blasted Prior To Assembly

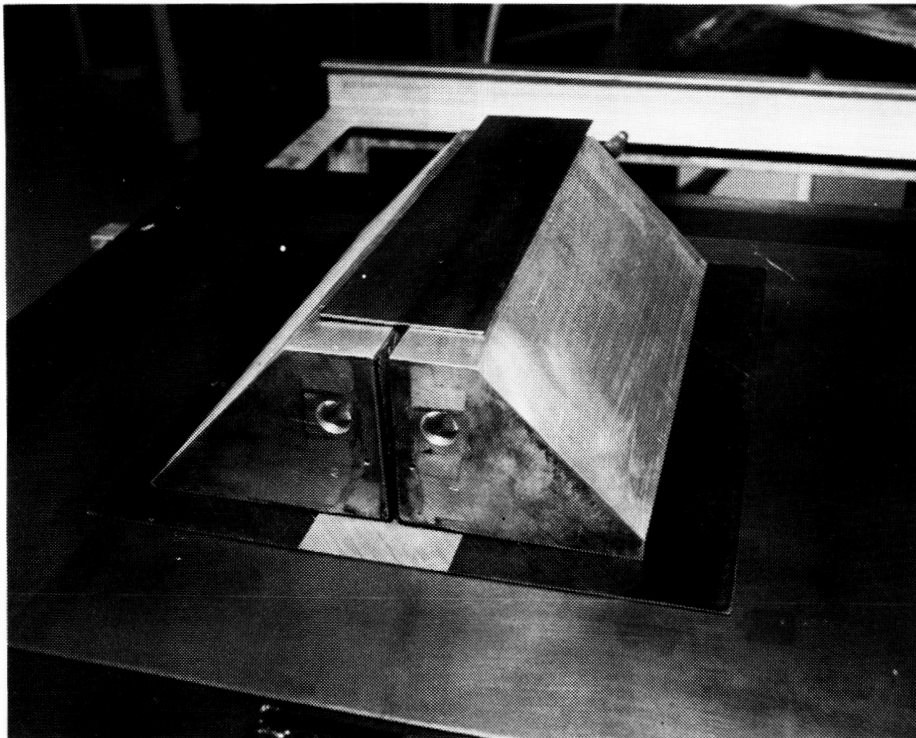


Figure 26 Assembly Prior To Autoclave Consolidation

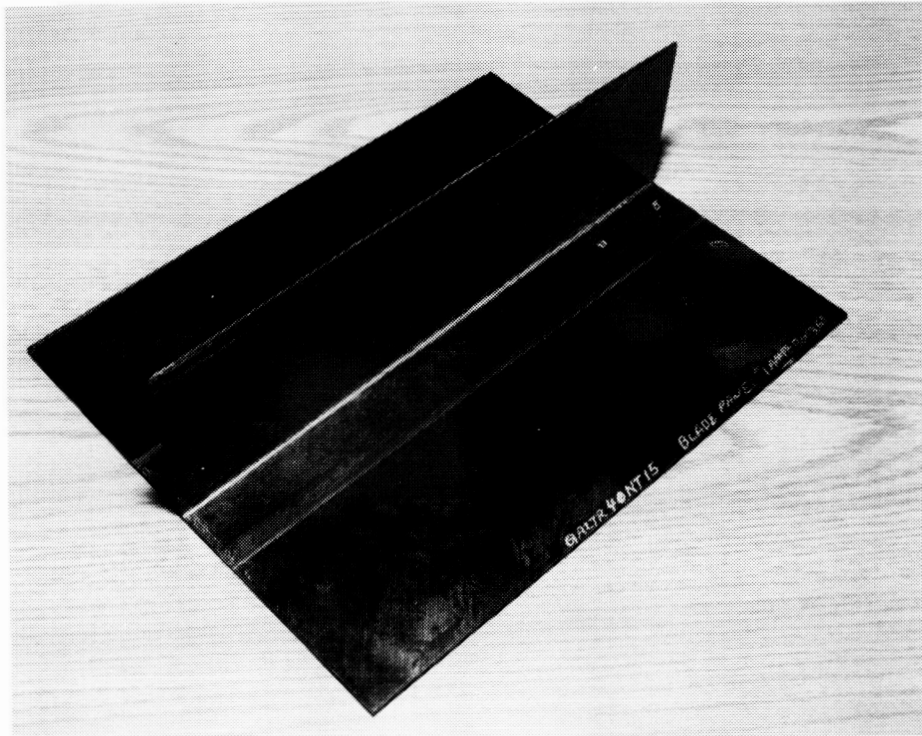


Figure 27 Intra Blade Elements Contained Porosity In Radius Due To Insufficient Pressure

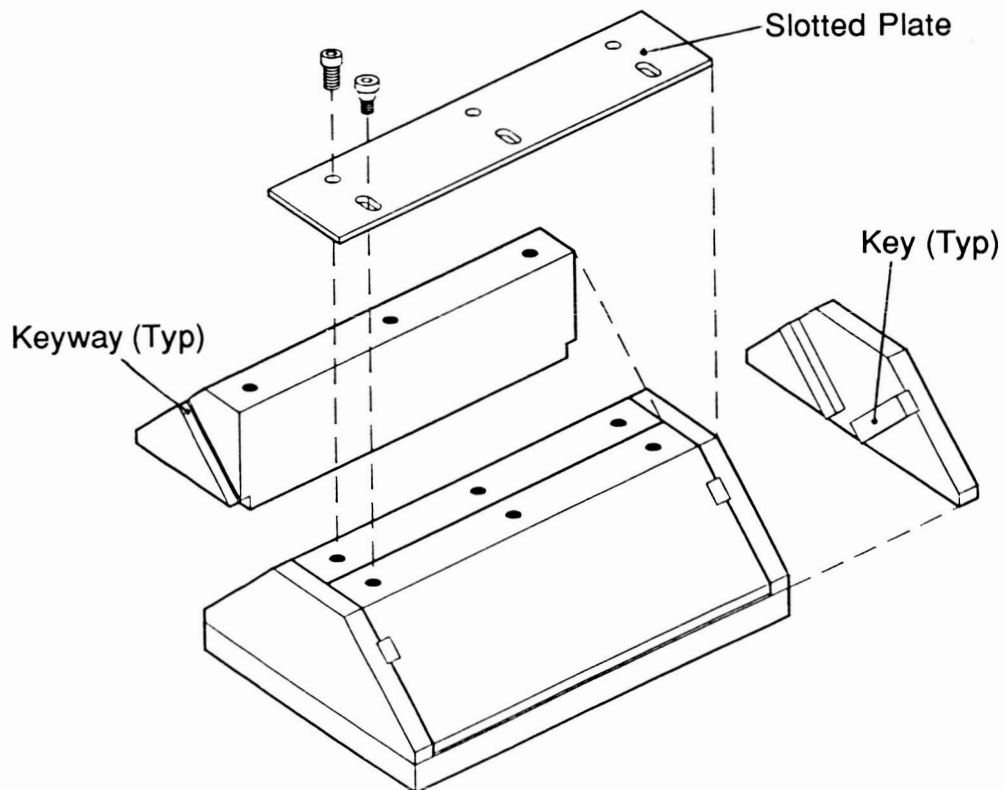


Figure 28 Modifications To Blade Element Tooling To Ensure Proper Pressure In Radius

STRUCTURAL EVALUATION OF CURVED STIFFENED COMPOSITE PANELS
FABRICATED USING A THERM-Xsm PROCESS

Christos Kassapoglou Albert J. DiNicola Jack C. Chou
Structures Research Section
United Technologies Sikorsky Aircraft
Stratford CT

Jerry W. Deaton
NASA Langley Research Center
Hampton, VA

INTRODUCTION

The use of composites in aircraft structures is often limited by material and manufacturing costs which, for some designs and applications, are prohibitively high. To increase the frequency of application of composites in primary airframe components alternative manufacturing processes are sought that reduce cost and/or enhance structural efficiency.

One alternative process involves the use of THERM-Xsm as the pressure transfer medium during autoclave curing. THERM-Xsm, a silicon-based flowable polymer which behaves like a liquid under autoclave pressure, transmits quasi-hydrostatic pressure to all contacting surfaces of the part to be cured. Once the autoclave pressure is relieved, THERM-Xsm reverts back to the powdery solid state and can be reused many times.

The THERM-Xsm process to be evaluated is depicted in Figure 1 and consists of (a) enclosing the tool and part to be cured by a set of frames that create a box, (b) pouring THERM-Xsm powder onto the part and filling the box, and (c) placing a vacuum bag over the box assembly. In this program, a separating non-porous film (Teflon) was placed between the part to be cured and THERM-Xsm powder to avoid any contamination.

The use of THERM-Xsm has two significant advantages over conventional manufacturing procedures. First, it eliminates complicated hard tooling since it guarantees uniform pressure transfer and thus good compaction at complex structural details (such as frame-stiffener intersections and corners). Second, it greatly simplifies vacuum bagging, since once the part to be cured is covered by THERM-Xsm powder, the vacuum bag need only conform to a relatively flat shape reducing significantly the number of pleats required.

A program is on-going at Sikorsky Aircraft to evaluate the structural performance of complex composite fuselage structures made with this THERM-Xsm process and to quantify the impact of THERM-Xsm on manufacturing labor hours and cost. The program involves fuselage panel optimization analysis, a building block test program where structural details representative of the full-scale article are analyzed and tested, and static and fatigue test/analysis of the full-scale test articles. The main results of this program are reported in this paper.

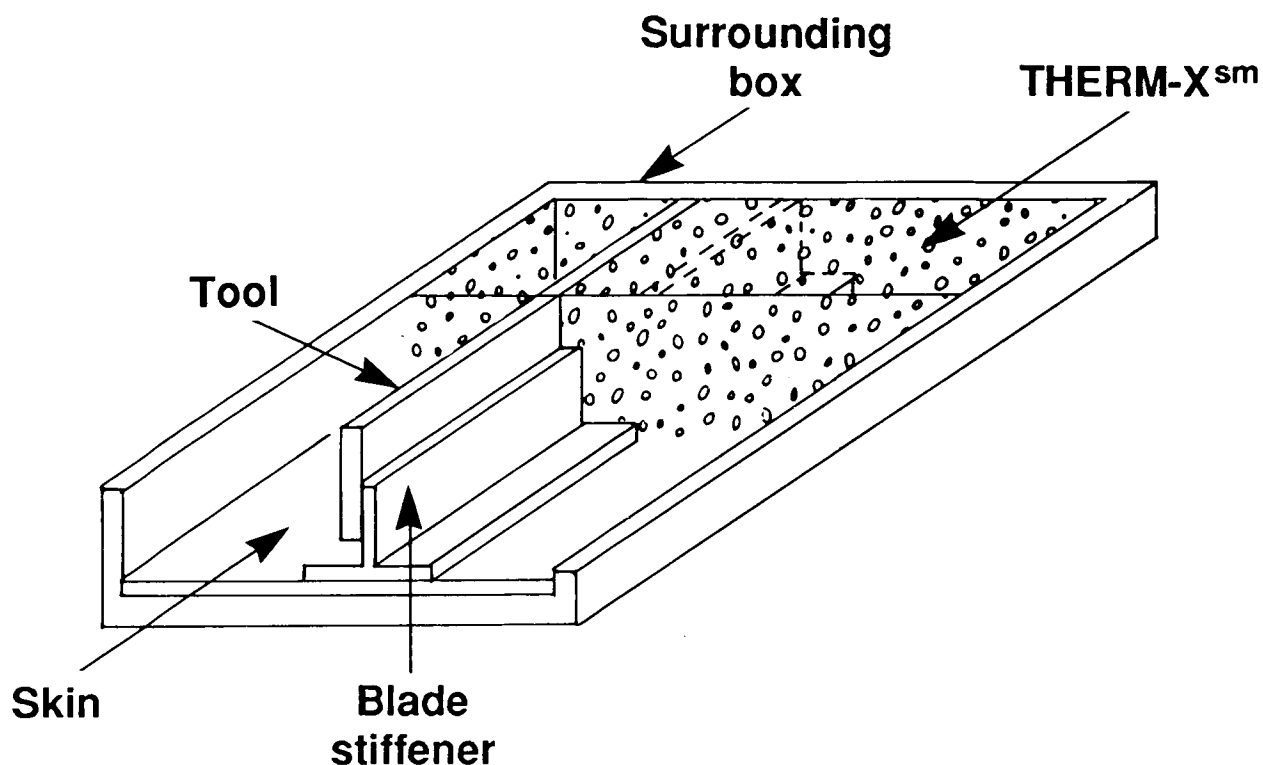


Figure 1. Illustration of THERM-Xsm Process

DESIGN SELECTION

An airframe construction representative of both helicopter and fixed wing structure was selected in order to demonstrate the general applicability of the results of this program. Several structural members were evaluated by estimating the impact of using THERM-Xsm versus conventional manufacturing. The most common detail with the largest cost savings due to THERM-Xsm processing, a curved panel with cocured frames and stiffeners, representing helicopter tailcone and fixed wing fuselage panels, was chosen (see Figure 2). The selection procedure is described in reference 1.

A simple method was developed to optimize the stiffened panel. In this process the skin thickness, frame, and stiffener spacing, and frame and stiffener area and moment of inertia were treated as variables and the weight and cost were minimized subject to loading constraints. The loading constraints were the following: (1) Applied loads were shear and compression (the latter along the stiffeners), (2) Panel failure occurred at a predetermined ultimate load, (3) Buckling of each bay and the panel as a whole occurred at a preselected load combination (fixed postbuckling factor), (4) No material used would be below minimum gage.

Panel failure of the postbuckled panel was determined as first-ply-failure of any of the structural members under the applied loads. A Tsai-Hill stress interaction criterion was used in conjunction with a maximum stress failure criterion. The latter was used to give an idea of the failure mode since, for first ply failure, a transverse tension failure of zero degree plies is very conservative. No such failure mode was noted.

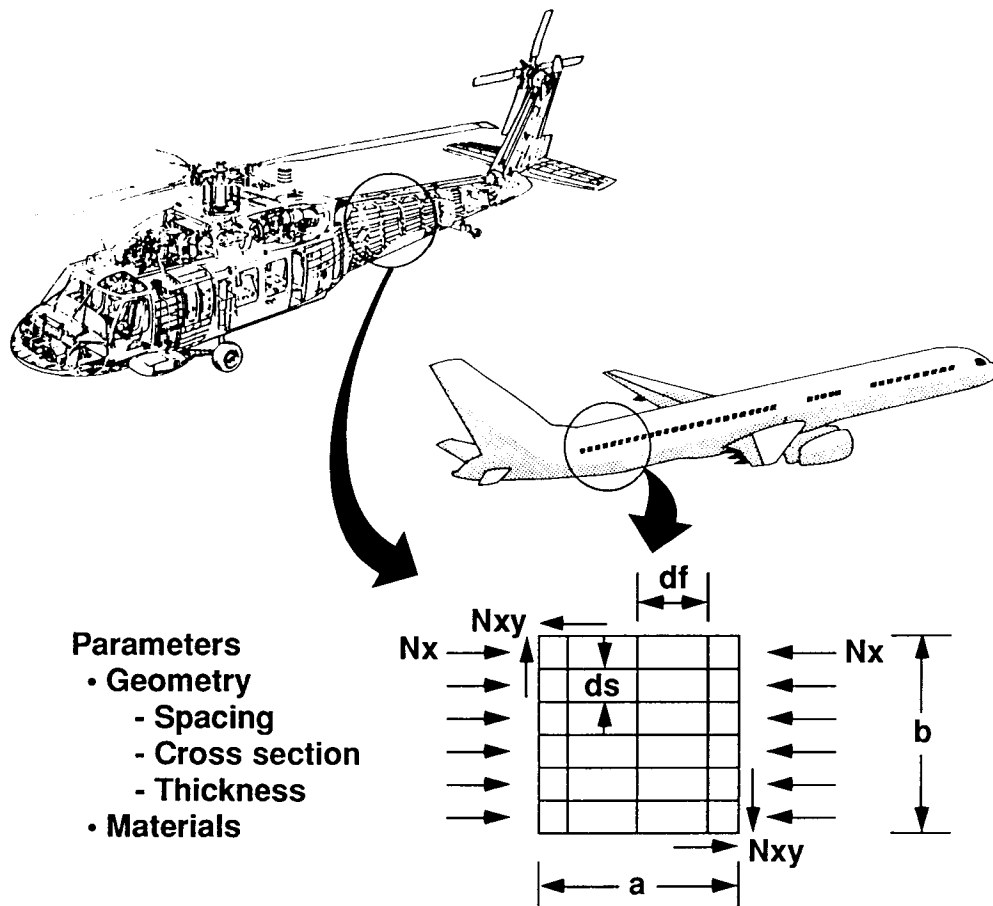


Figure 2. Stiffened Panel Usage in Aircraft Structures

The cost was a combination of material cost (\$50/lb for prepreg material) and labor hours (\$30/hr). Previous Sikorsky experience was used to estimate labor hours required and the effect of increasing stiffener and frame spacing on the total number of manufacturing labor hours. It was estimated that for each additional stiffener or frame, the manufacturing labor hours for the entire panel would increase by 13% for conventional manufacturing and 8% for THERM-Xsm processing. The 5% difference is due to the reduced bagging complexity of THERM-Xsm processing especially around intersecting members such as frames and stiffeners. For each panel configuration then, the cost was the sum of the raw material cost and the cost to manufacture that particular configuration. The latter comprised of manufacturing cost for the skin and the cost to fabricate the frames and stiffeners which took into account the 5% cost difference (per added frame or stiffener) between the two manufacturing approaches. For simplicity in the calculations, the panel was assumed flat and square with 30 inch sides.

The iterative optimization and sizing scheme was applied to various materials and loading configurations. This process is shown schematically in Figure 3. The cross-sectional area to spacing ratios for the stiffeners and frames (A_s/d_s and A_f/d_f respectively) are treated as independent parameters. These ratios are independently selected and the steps outlined in Figure 3 followed until convergence is reached and the panel weight is minimized. Then, another set of A_s/d_s and A_f/d_f values is selected and the procedure is repeated. The pair of

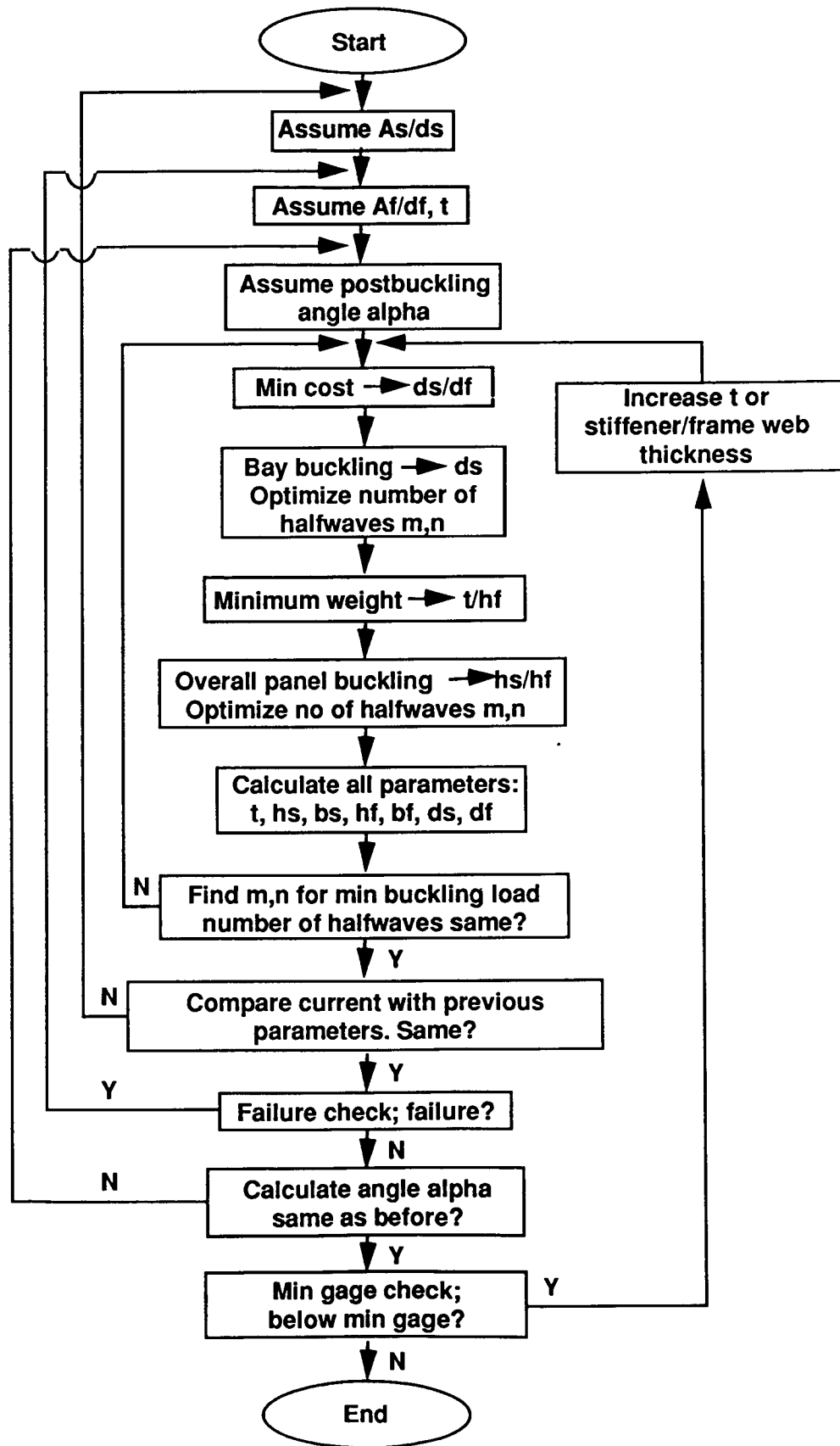


Figure 3. Stiffened Panel Optimization Procedure

The As/ds and Af/df value finally selected is the one providing minimum weight for all design variations.

A comparison of THERM-Xsm processing versus conventional manufacturing for typical helicopter tailcone and fixed wing fuselage loads is shown in Figures 4 and 5. For the helicopter tailcone configuration the ultimate loading design requirement was 250 lb/inch in compression and 250 lb/inch in shear (selected based on S-76 tailcone ultimate design loading). For the fixed wing configuration the ultimate loading was 2500 lb/inch in compression and 1250 lb/inch in shear corresponding to typical fuselage loads [2].

The (normalized) cost to manufacture stiffened panels for typical helicopter tailcones as a function of stiffener spacing ds is shown in Figure 4. The frame spacing df is determined by the optimization procedure (cost minimization equation) to be very nearly equal to $3.2 ds$. Two cost curves are shown, one for standard manufacturing and one for THERM-Xsm processing. For each geometry configuration, the cost is calculated as the raw material cost plus labor hours to manufacture based on previous Sikorsky Aircraft experience. It is important to note that the minimum cost configuration involves few frames and stiffeners ($ds = 5$ in.) of large area and moment of inertia and with thick skin, thus corresponding to a relatively high weight. For the loading considered here, the minimum weight configuration would be a minimum gage configuration (with minimum gage thickness for frame and stiffener webs) corresponding to a stiffener spacing less than 1 inch. Thus, the lightest configuration is labor intensive because it involves many stiffeners.

A tradeoff between weight and cost can then be established. At small stiffener spacings the panel weight is low but the manufacturing cost is high. At high stiffener spacings the cost is low but the panel weight is high. An equilibrium between the two driving quantities (weight and cost) can be found by considering the premium in dollars per pound (termed value of improved performance in Figure 4) the customer is willing to pay to reduce the structural weight by one lb. For example, for UH-60 (BLACKHAWK) helicopters, that value is \$750/lb.

In this context, since the minimum weight (still meeting the loading requirements) is that corresponding to a minimum gage design, any other acceptable configuration will have a potential weight penalty equal to the difference in weight from the minimum gage configuration. By multiplying this weight difference by the weight premium dollar value (termed here value of improved performance), an upward sloping curve (with increasing ds) is obtained that shows the weight penalty for each configuration translated to dollars. Various curves corresponding to different values of improved performance are shown in Figure 4.

The points of intersection of the weight penalty curves with the cost curves define optimum points, each corresponding to a different selection of manufacturing process and dollar value of improved performance. Any configuration away from the intersection points implies that for the particular manufacturing method selected, either the weight or the cost of the panel can be reduced and still meet the load requirements and the selected value of improved performance.

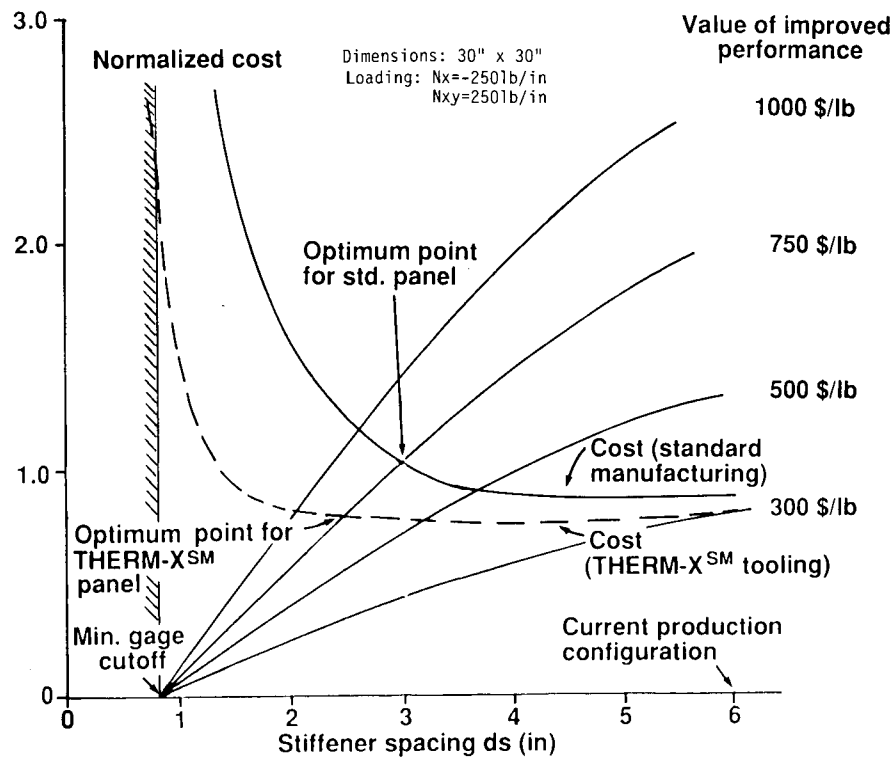


Figure 4. Determination of Optimum Geometry for Stiffened Panels in Helicopter Structures

STIFFENED PANEL OPTIMIZATION

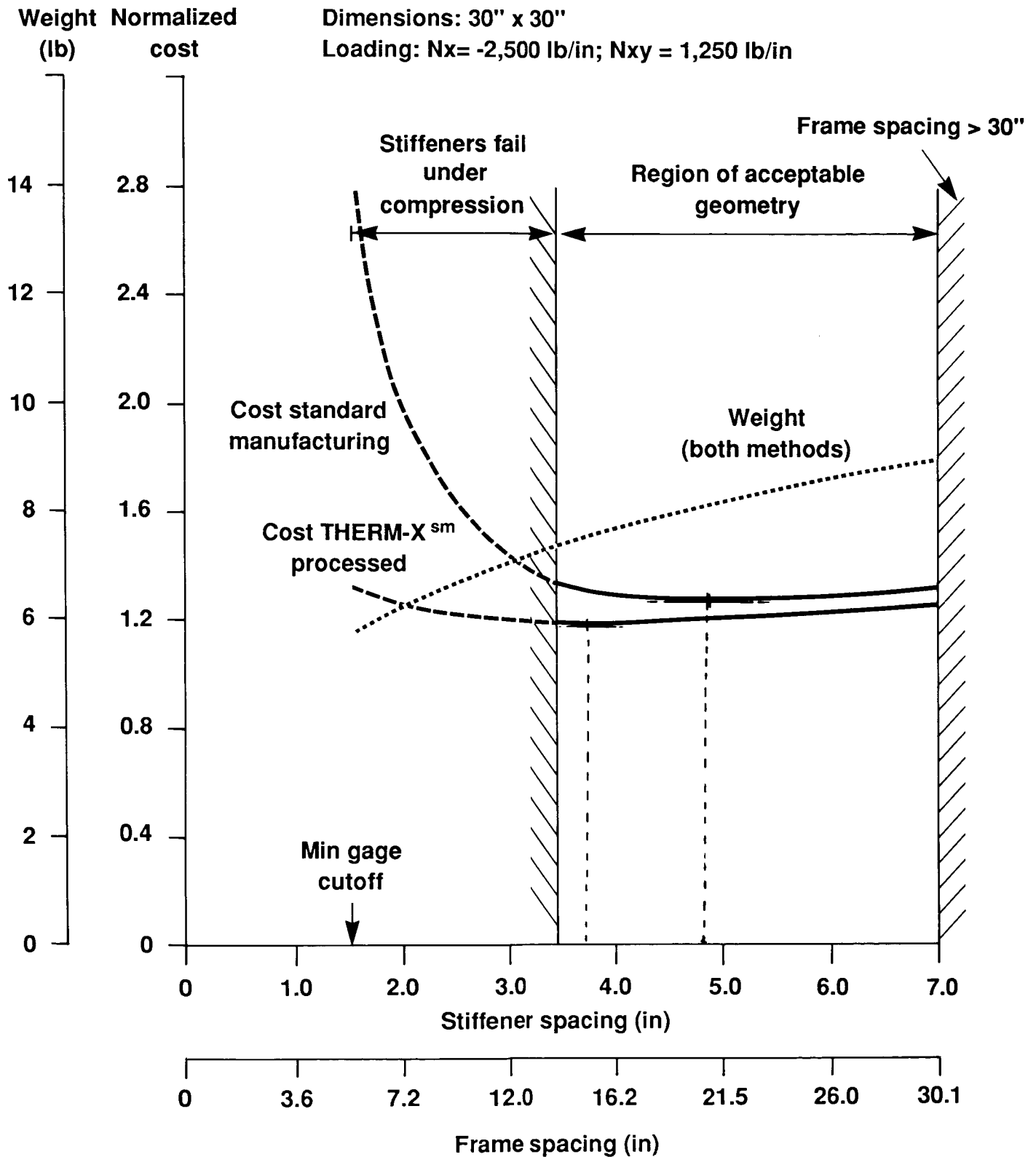


Figure 5. Determination of Optimum Geometry for Stiffened Panels in Fixed Wing Structures

The configuration selected for the full-scale article corresponds to a stiffener spacing of 6.5 inches. This corresponds to a value of improved performance of \$300/lb which was felt to be more representative of commercial fixed wing transport. At that spacing the THERM-Xsm process results in panels approximately 10% less expensive than conventionally manufactured panels. At smaller stiffener spacings (for higher values of improved performance) the savings can be as high as 22% (ds= 3 inches). It should be noted that these savings do not include savings in tooling. The THERM-Xsm process requires relatively simple tooling even for complex parts with cocured frames and stiffeners.

The effect of applied loading can be seen if Figure 4 is compared to Figure 5. In Figure 5, the optimization process was applied to panels with loadings representative of fixed wing transport fuselages. In this case, the minimum gage configuration is not attainable since the loading is high. The limiting factor at low stiffener spacings is the compression failure strength of the hat stiffeners assumed in this case to be 36000 psi which corresponds to the first ply failure load of a predominantly 45 degree stiffener web layup. This is shown by the left vertical curve at ds=3.5 inches.

Two cost curves are shown in Figure 5 much like the ones in Figure 4. In this case however, the weight change between the minimum weight configuration (at ds = 3.5 in.) and any other acceptable configuration is so small that the value of improved performance should be higher than \$10000/lb for the weight penalty curves to intersect the cost curves. For that reason, the weight penalty curves are not included. Instead, to show the tradeoff between cost and weight, the minimum weight of the panel for each value of stiffener spacing is shown as an upward sloping curve. The corresponding frame spacings are also shown in Figure 5.

Figure 5 suggests that the minimum weight configuration corresponds to ds=3.5 inches while the minimum cost configuration corresponds to ds=3.75 inches for THERM-Xsm processed panels and 4.75 inches for conventionally manufactured panels. The user will then have to make a choice on which configuration to select favoring either a minimum weight or a minimum cost design.

The conclusions can change significantly if the compression strength of the hat stiffeners is increased. That would move the left cutoff line to the left increasing the number of acceptable configurations. This would also increase the savings of the THERM-Xsm processed panels from approximately 6% (at ds=5 inches for example) to over 15% (at ds=3.0 inches).

As a final comment on the optimization study, the current approach does predict that the commonly used configuration of ds=6 inches and df=20 inches in aircraft structures is one of the acceptable configurations but corresponds to a higher weight configuration than can be attained with lower ds values. It should be borne in mind that the current process assumes a flat panel and neglects the stiffening effect afforded by curved panels. This effect would yield optimum configurations with ds values higher than currently predicted, thus closer to the commonly used value of ds=6 inches.

The configuration selected based on the optimization process (ds=6.5 inches, df=20 inches, Nx=-250 lb/in, and Nxy=250 lb/in at ultimate) was evaluated with a detailed test and analysis program that is described in the next section.

BUILDING BLOCK TEST PROGRAM

A representative sketch of the curved and stiffened composite panel under consideration is shown in Figure 6. In order to provide a basis for verification of predicting failure modes and the panel's ultimate load, the six building block tests also shown in the figure were performed prior to full-scale testing. Detailed results of these building block tests were reported previously [1]. Comparable, and often enhanced, strength and stiffness values were noted for THERM-XSM processed test specimens versus those conventionally manufactured, and excellent laminate quality control was attainable with substantially less effort. A summary of the data generated during the tests, which will verify analysis and assist in predicting ultimate load for the full-scale test, is presented in Figure 7.

Compression after impact tests were performed for the two damage regimes envisioned for the composite fuselage panel: low speed-high mass impact and high speed-low mass impact. The former is representative of "tool drop" style impact damage and the latter is characteristic of in-flight impact damage. Shear after impact tests were performed under low speed conditions only [1] since the trends of high versus low speed impact established for the compression specimens are expected to apply in this instance.

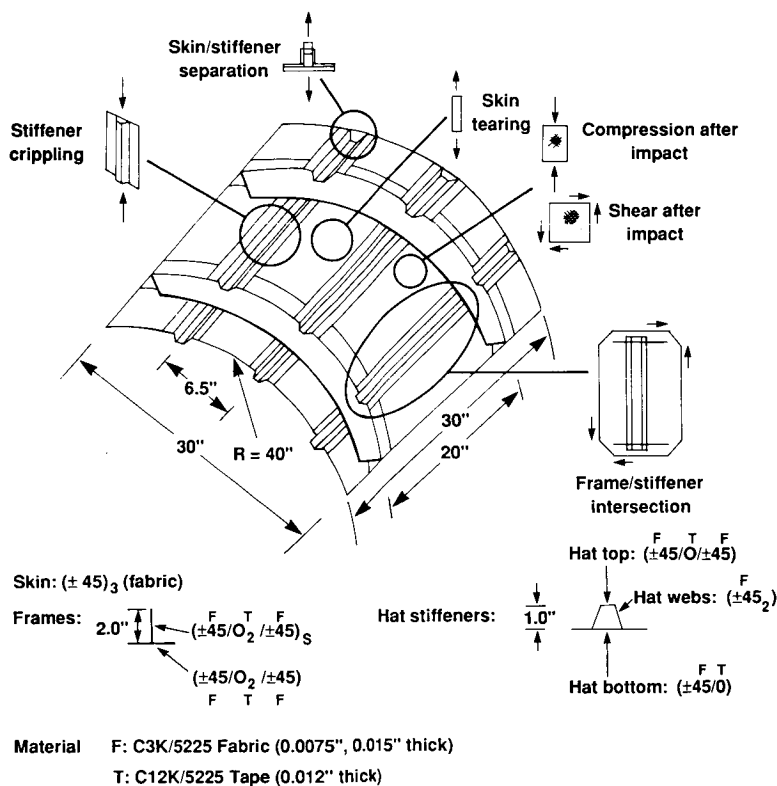


Figure 6. Building Block Approach and Full-Scale Article Configuration

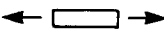
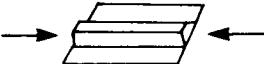
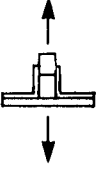
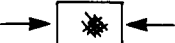
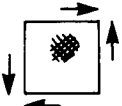
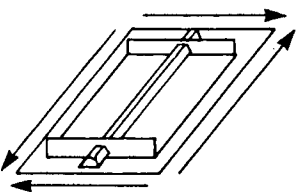
Building Block Evaluation	Configuration	Number Specimens	Results
Skin tearing		8	Tensile modulus: 10 MSI Tensile strength: 99 KSI
Stiffener crippling		6	Crippling strength: 14,628 PSI
Skin/stiffener separation		5	Pull-off strength: 90.5 lb/in
Compression after impact		10	Residual strenght vs impact energy and indentation at point of impact for high and low speed impact (See fig. 8-10)
Shear after impact		5	
Frame-stiffener intersection		3	Failure load at the intersection of the frame and Hat stiffener : 614 lb/in

Figure 7. Summary of Building Block Approach Results

A summary of the average normalized compression after impact (CAI) strength values is presented in Figure 8 for both velocity regimes and fabrication procedures. Conventional manufacturing appears to provide moderately superior CAI strength at both 600 and 1200 in-lb/in impact energies (15% and 3.3% respectively). The slight advantage afforded by conventional manufacturing was noted for both impact velocities. The underlying reason for the strength discrepancy is currently being investigated. The only significant difference between the two manufacturing methods, which may account for the residual strength discrepancy, is that the cure pressure for THERM-XSM processing is twice that used during conventional manufacture (100 psi versus 50 psi). More tests are needed to quantify these differences with statistical significance.

Internal damage resulting from impact as measured by ultrasonic C-scan is shown in Figure 9 for both fabrication procedures and velocity regimes. Consistent with other literature citations [for example references 3 and 4], the high speed impact event produced greater levels of internal damage than low speed impact for a fixed energy level. For 600 in-lb/in of impact energy, THERM-XSM processed specimens exhibited greater internal damage area (by 21%) whereas at 1200 in-lb/in of energy both fabrication procedures yielded similar amounts of internal damage.

There is evidence that indentation at the point of impact is an effective means to correlate a measureable quantity to resultant post-impact strength [1]. A comparison of average indentation for conventionally manufactured and THERM-XSM processed specimens is shown in Figure 10. Although indentation data for high speed impact of THERM-XSM panels were not available, the consistency of the data at hand indicates, irrespective of either velocity regime or manufacturing procedure, indentation may be a reliable way to predict resultant strength after impact.

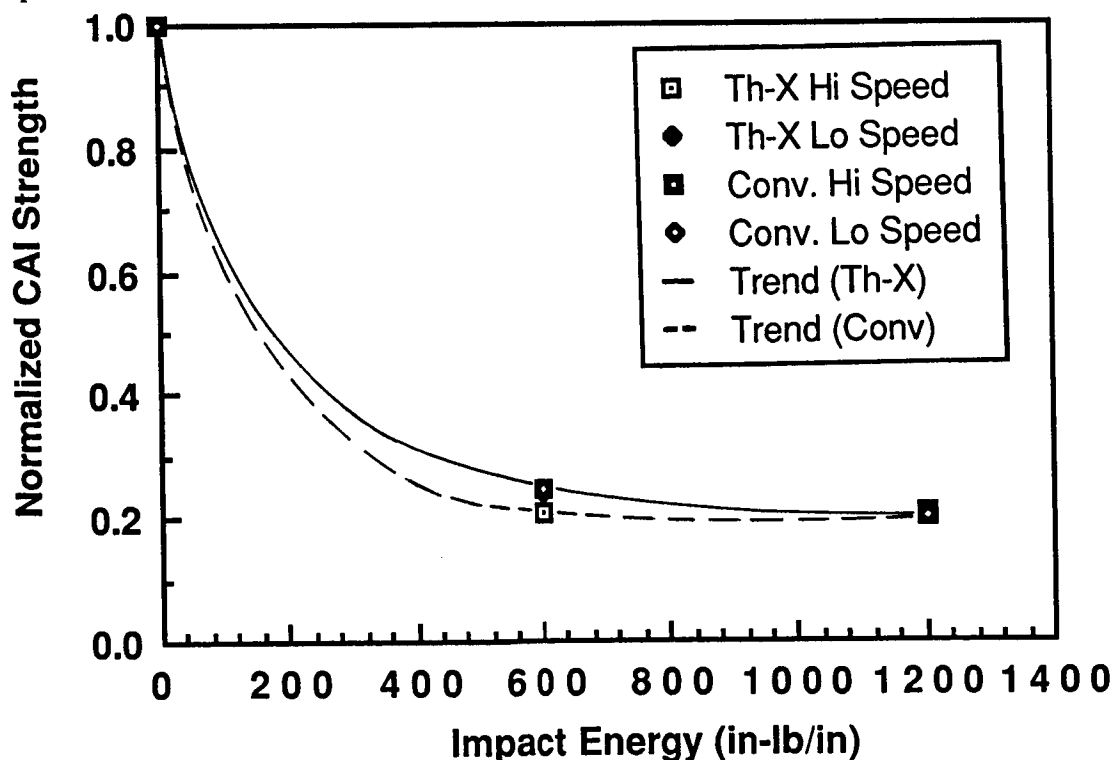


Figure 8. Compression after Impact Strength as a Function of Impact Energy

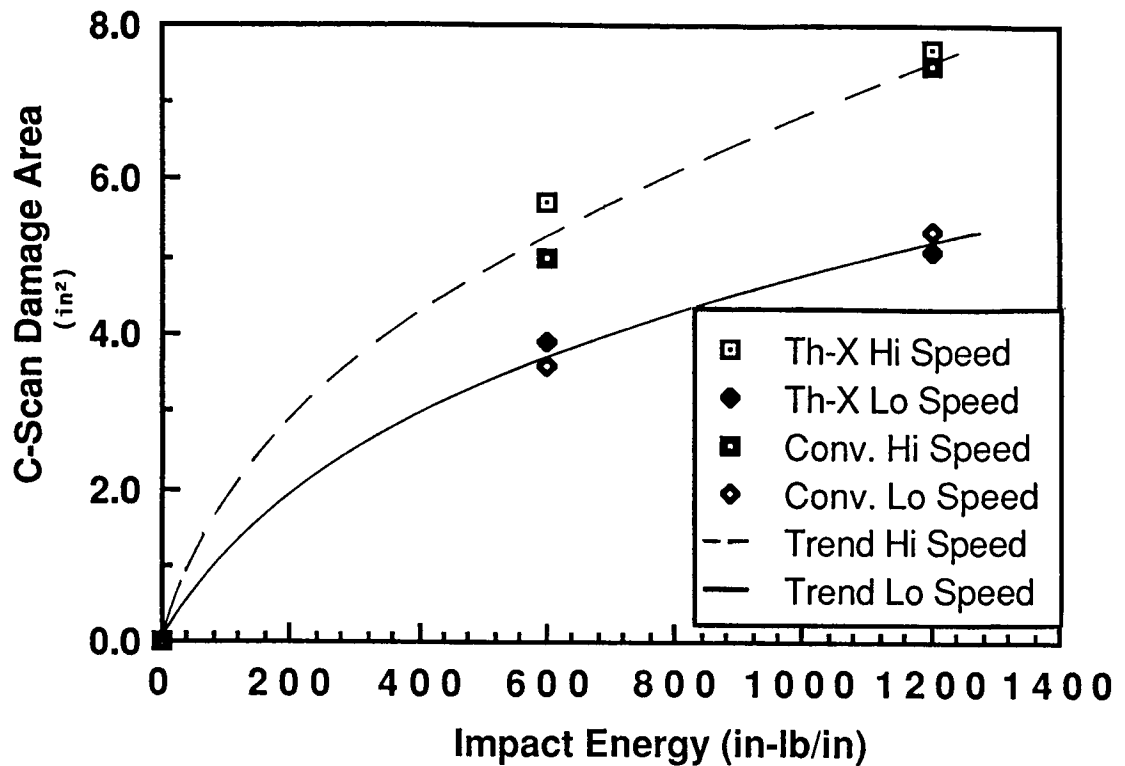


Figure 9. Variation of C-Scan Indicated Damage Area with Impact Energy

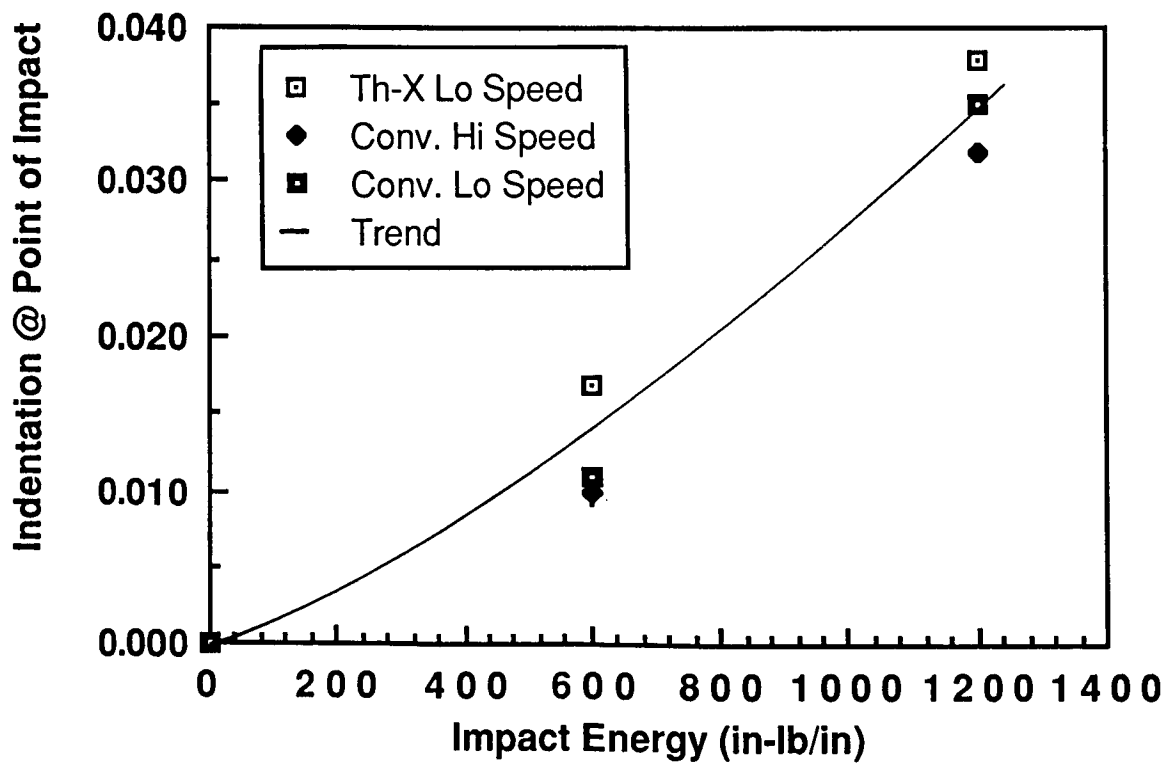


Figure 10. Indentation at Point of Impact as a Function of Impact Energy

Flat Frame/Stiffener Intersection Specimen

The frame-stiffener intersection specimen is used to provide experimental evaluation of failure mechanisms present in the full-scale article at the intersecting corners of frames and stiffeners, a link between flat and curved specimens, and to support corresponding analysis predictions.

The specimen is shown in Figure 11. It represents two bays of the full-scale curved stiffened panel. A closeup of a typical frame/stiffener intersection corner is shown in Figure 12. Excellent consolidation and radius definition is evident. Part quality around the shear tie which consists of the outer plies of the frame web cocured on the hat stiffener webs is also very high with accurate placement and contour definition. The layup of the skin, frames and stiffeners is identical to that of the full scale article as shown in Figure 6. Aluminum doublers 0.5 in. thick and 3.0 in. wide were used for load introduction fastened on three-ply graphite/epoxy doublers that were cocured with the specimen. The aluminum doublers formed a picture frame fixture for testing the specimens in shear.

The finite element model used is shown in Figure 13. One specimen end is loaded in tension (along a diagonal) and the opposite end is fixed. MSC NASTRAN SOL 66 geometric nonlinear solution was used to determine the buckling load and post buckling behavior of the panel. The model consists of 606 grid points, 576 CQUAD elements, and 3601 degrees of freedom.

Comparison of Test Results to Finite Element Predictions

The strain gage data obtained from the frame-stiffener intersection specimens was compensated for gage transverse sensitivity and percent reinforcement (resulting from gage bagging and adhesive material) following procedures recommended by the gage manufacturer (Micro-Measurements Division, Measurement Group Inc., Raleigh NC) and reference 5.

For the type of gages used (CEA-03-063UR-350) the transverse gage sensitivity is insignificant (only 1% change to the apparent strain). The percent reinforcement effect however, for the materials and layups used, ranges from 0.6% to 15.8% (depending on the gage installation such as back-to-back or single face, laminate thickness, and open face versus encapsulated gage configuration). The results reported below have this correction included wherever it is considered significant (more than 5%).

The strain gage locations (total of 18 rosettes) were chosen to give a detailed strain distribution throughout the specimen and in particular at skin bays and near the frame-stiffener intersections. Finite element predicted surface strains are compared to test results at various panel locations and load levels in Figures 14 through 17. The locations are (1) Hat Stiffener Center (Figure 14), (2) Frame-Stiffener Intersection Corner (Figure 15), (3) Bay Quarter Point (Figure 16), and (4) Bay Center (Figure 17). At low applied loads (except for the frame-stiffener intersection location) and high loads close to the failure load (in all cases), the finite element predictions are in very good agreement with the experimental results. At intermediate loads the correlation ranges from poor (bay center and frame stiffener intersection corner) to excellent (hat stiffener center and bay quarter point).



Figure 11. Flat Frame/Stiffener Intersection Specimen (Stiffened Side Overview)

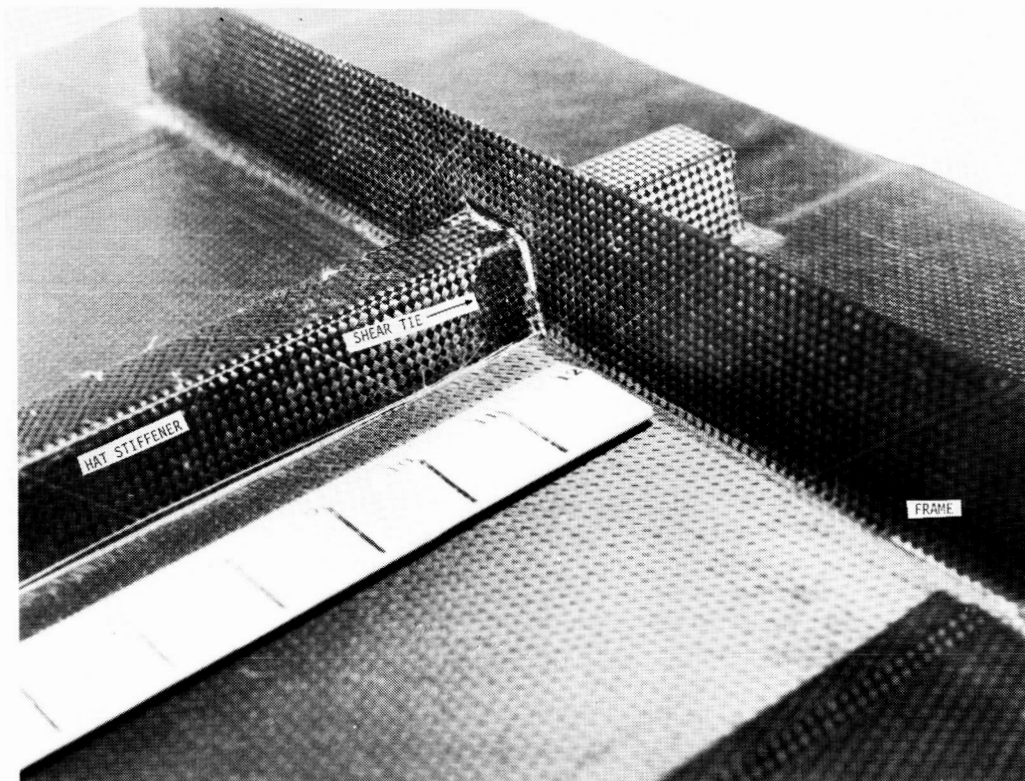


Figure 12. Frame-Stiffener Intersection Detail

The shadow moire method was used to monitor the out-of-plane displacements of the panel during the test. The first moire fringe pattern appeared at an applied load of 2600 lbs and is shown in Figure 18. The postbuckling mode shape just before the panel failure load of 20000 lbs is shown in Figure 19. The analysis of the photographs of the moire fringe pattern follows standard procedures outlined in the literature [6].

Typical experimental and analytical results for the out-of-plane displacement along the panel skin bay at the applied load of 16000 lbs is shown in Figure 20. The moire measured amplitude correlates well with the finite element prediction. However, the wavelength of the deflection mode shape is less than the finite element prediction. The discrepancy between finite elements and moire pattern data is attributed to local eccentricities of the specimen and resulting differences in load transfer.

The failure prediction for these specimens was obtained by determining the most highly loaded element in the finite element model and using the forces and moments on that element as input in a first ply failure criterion. That element coincided with the location where a crack initiated (near the bay corner) during testing. Using mean material allowables the failure prediction using a stress interaction criterion [7] is 26000 lbs of applied load. The corresponding B-Basis prediction is 22950 lbs. The test failure load (average of two specimens) is 21000 lbs (614 lbs/in). The failure predictions are based on allowables for conventionally manufactured parts and are off by 9 to 24% (B-Basis versus mean allowable predictions). There are two reasons for the discrepancy: (1) Loading of the first test specimen was stopped when the first

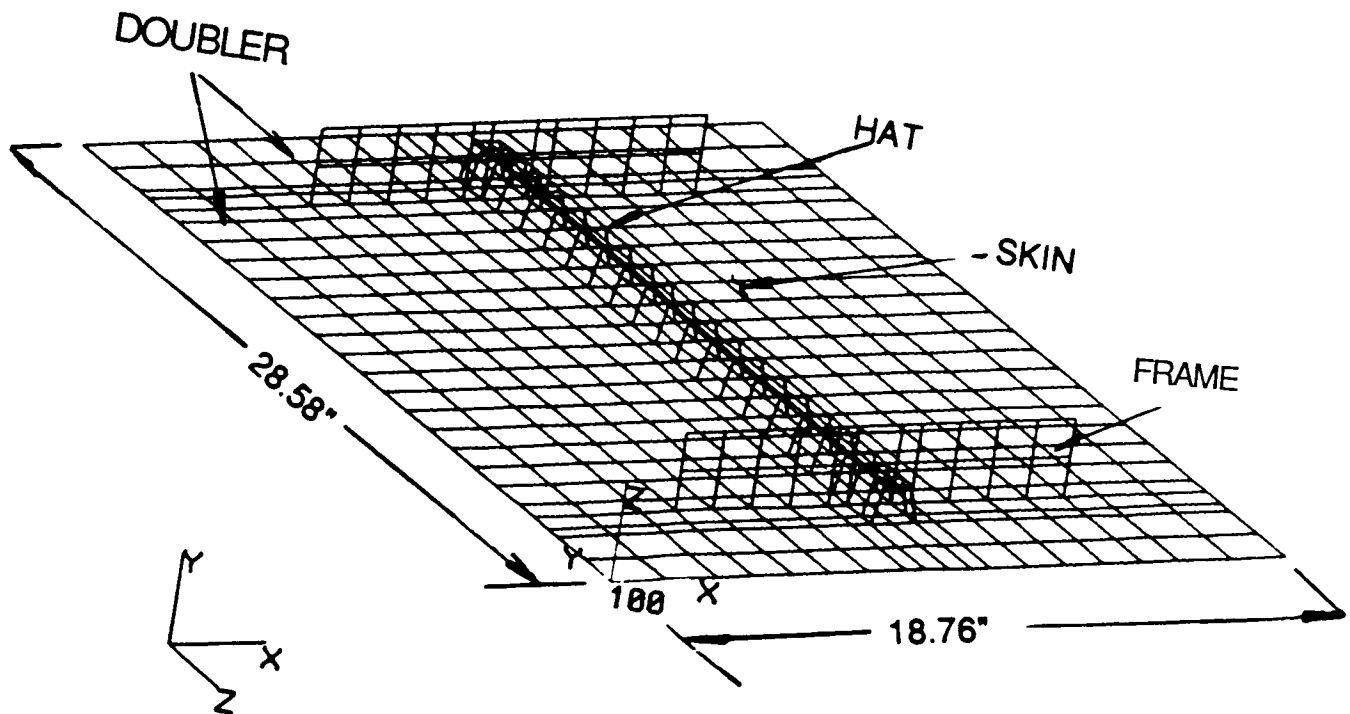


Figure 13. Finite Element Mesh for Frame/Stiffener Intersection Specimen

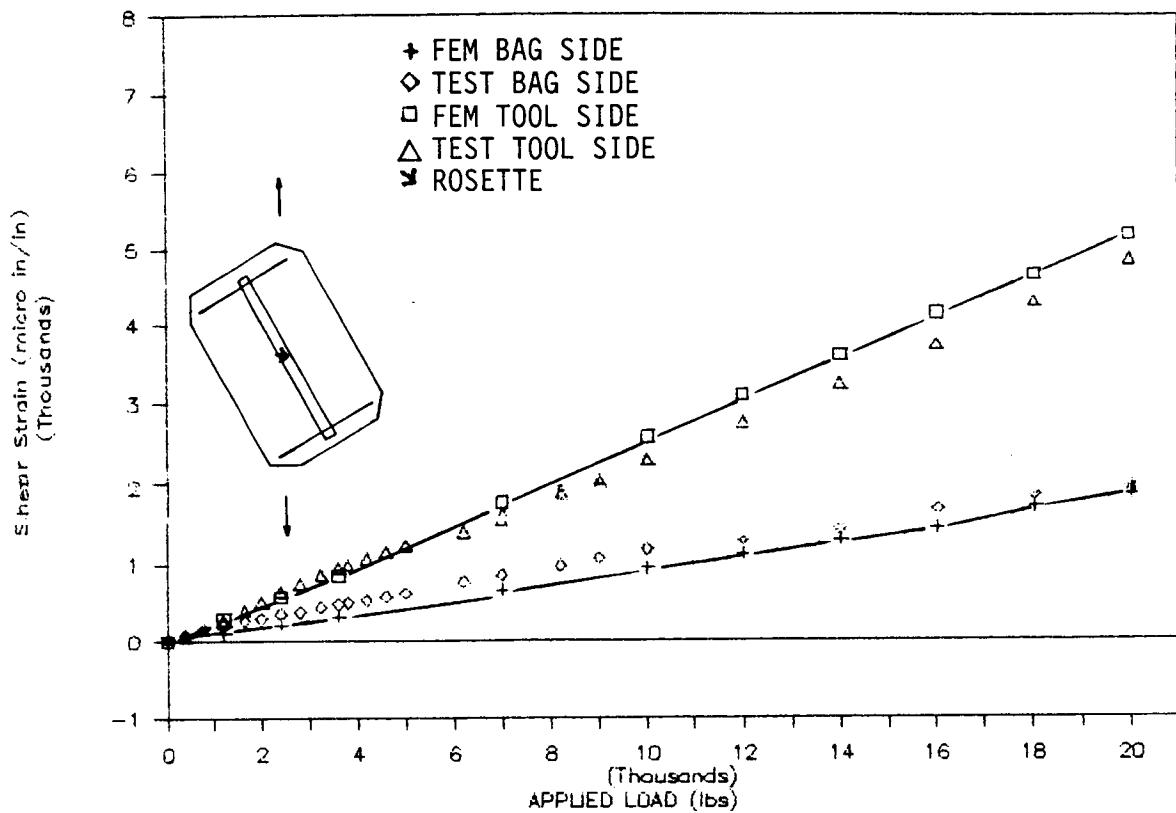


Figure 14. Comparison of Finite Element Predictions to Test Results at Hat-Stiffener Center (Shear Strains - Intersection Specimen)

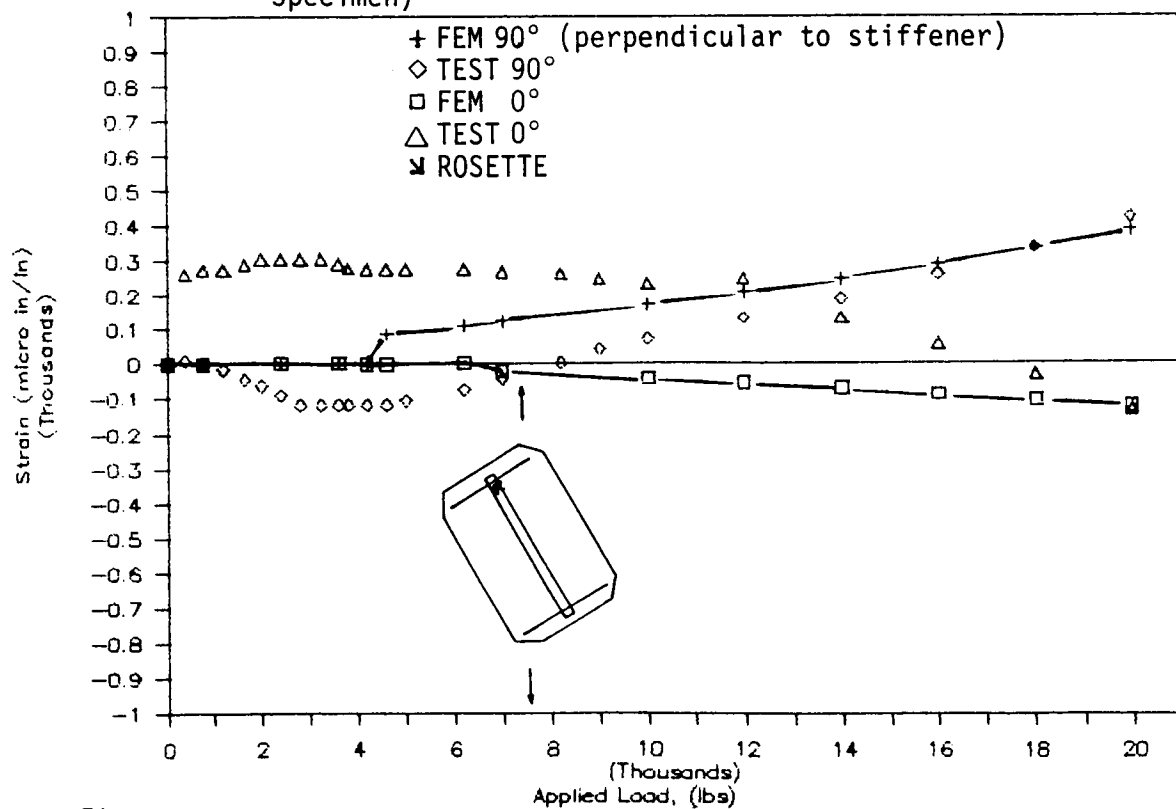


Figure 15. Comparison of Finite Element Predictions to Test Results at Frame/Stiffener Intersection Corner

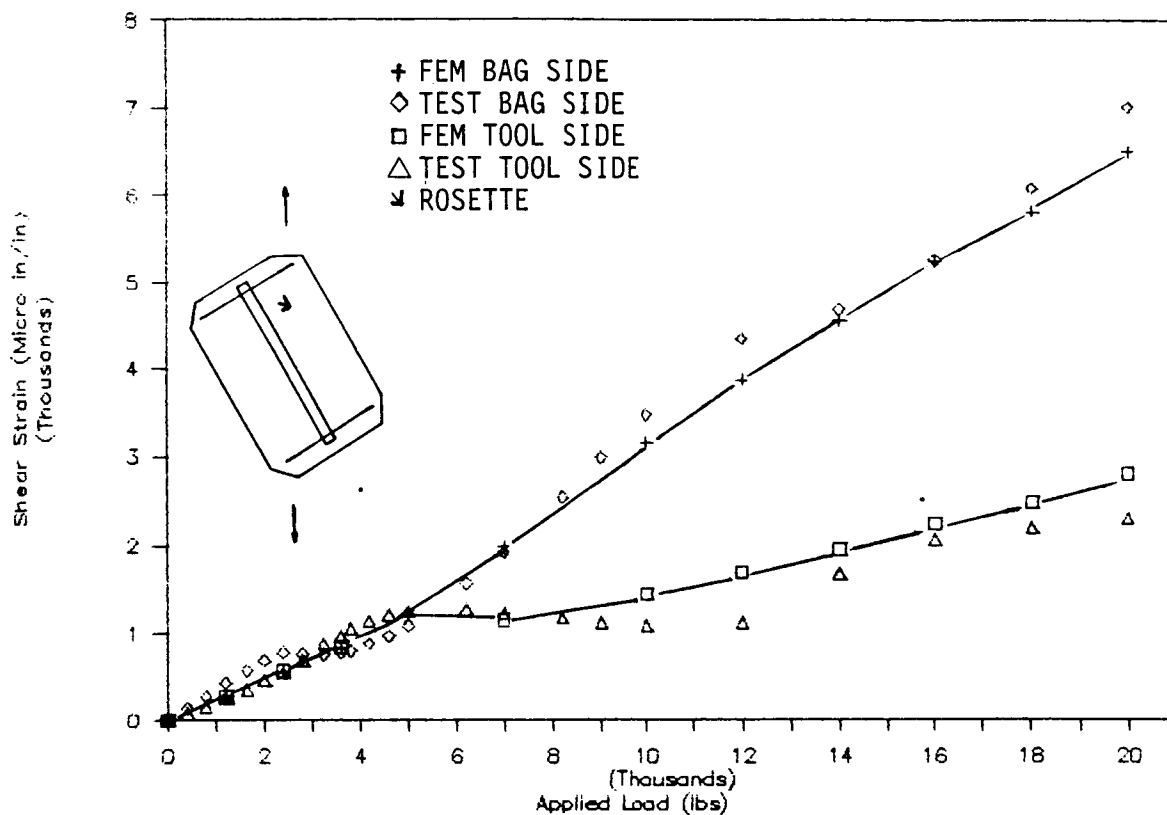


Figure 16. Comparison of Finite Element Predictions to Test Results at Bay Quarter Point (Shear Strains - Intersection Specimen)

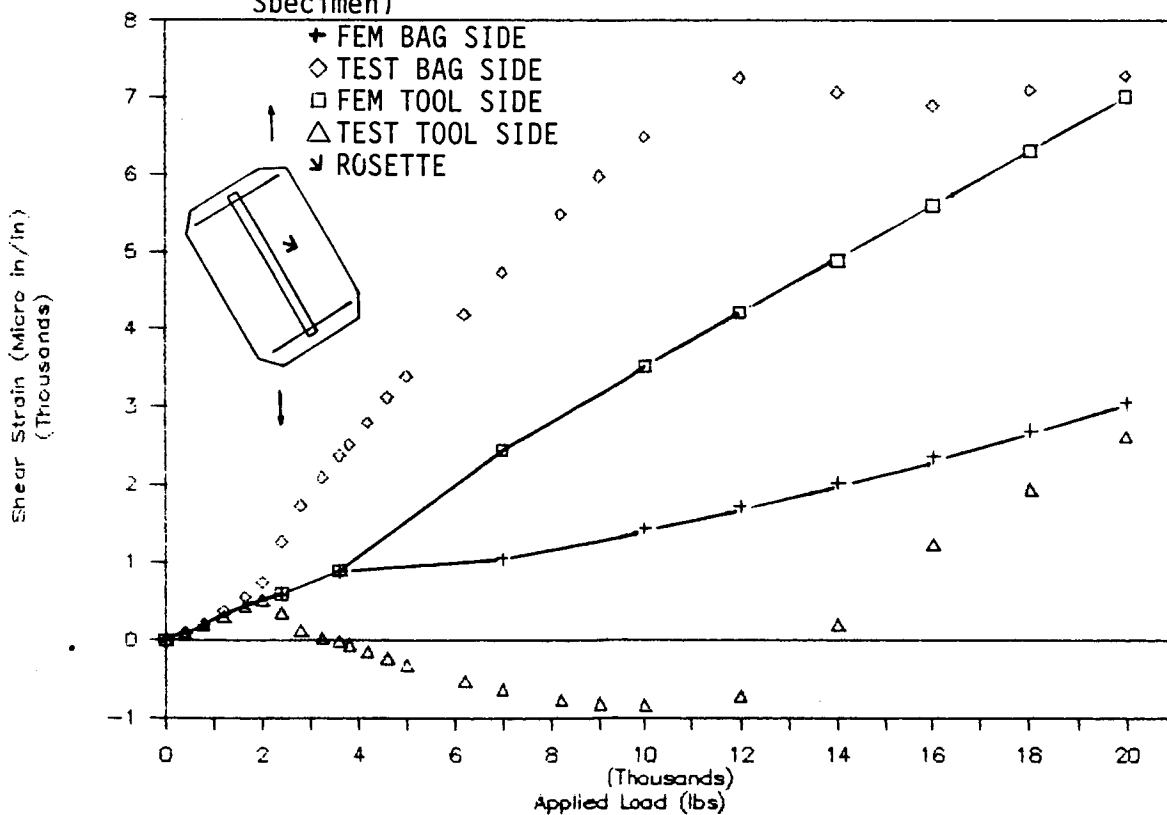


Figure 17. Comparison of Finite Element Predictions to Test Results at Bay Center (Shear Strains - Intersection Specimen)

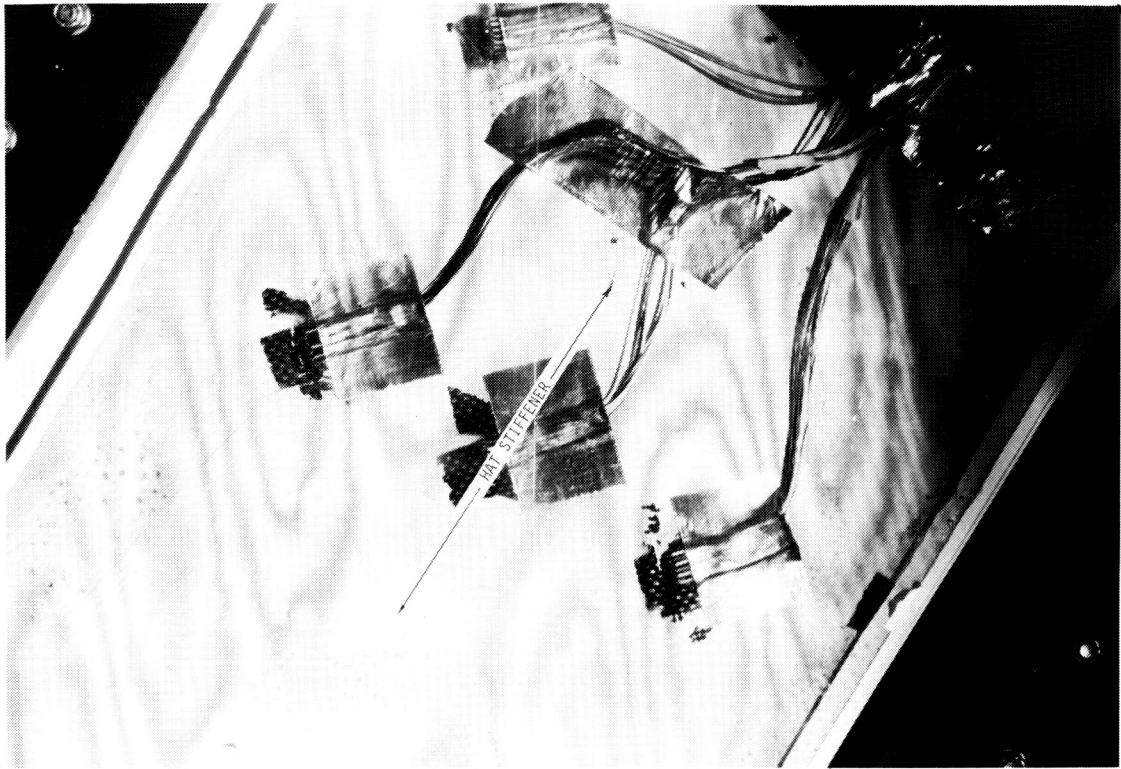


Figure 18. First Shadow Moire Fringes on Frame/Stiffener Intersection Specimen (2600 lbs)

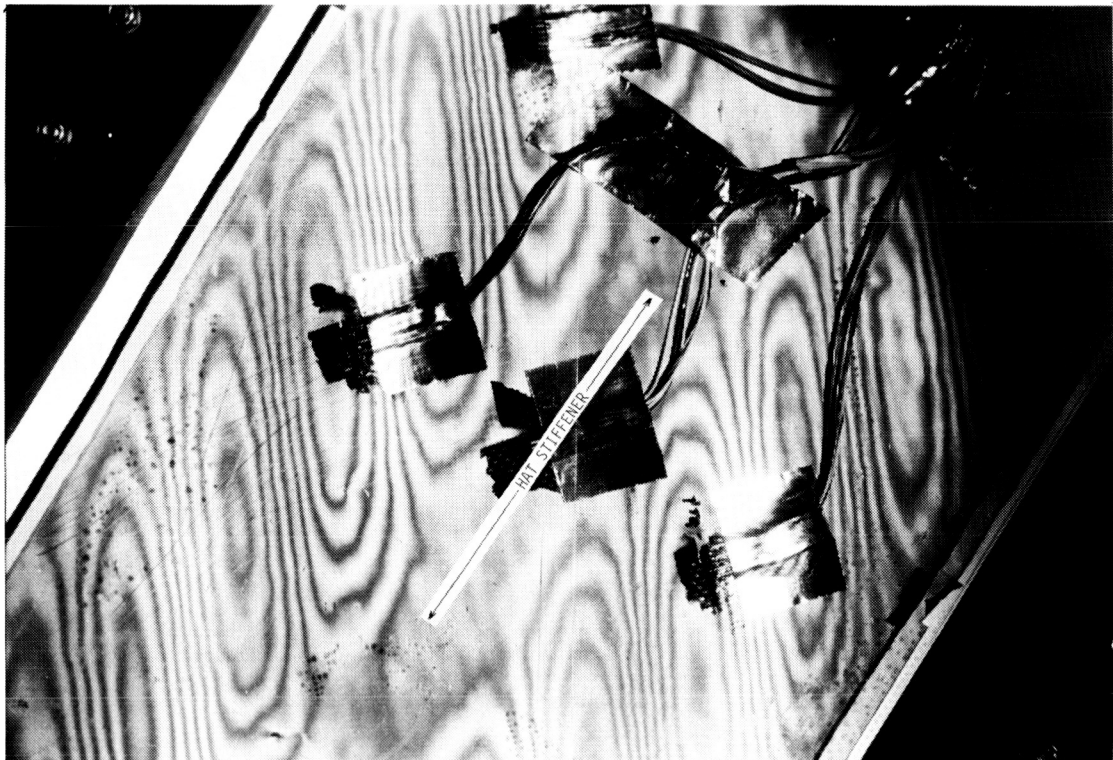


Figure 19. Shadow Moire Fringes Near Failure of Frame/Stiffener Intersection Specimen (20000 lbs)

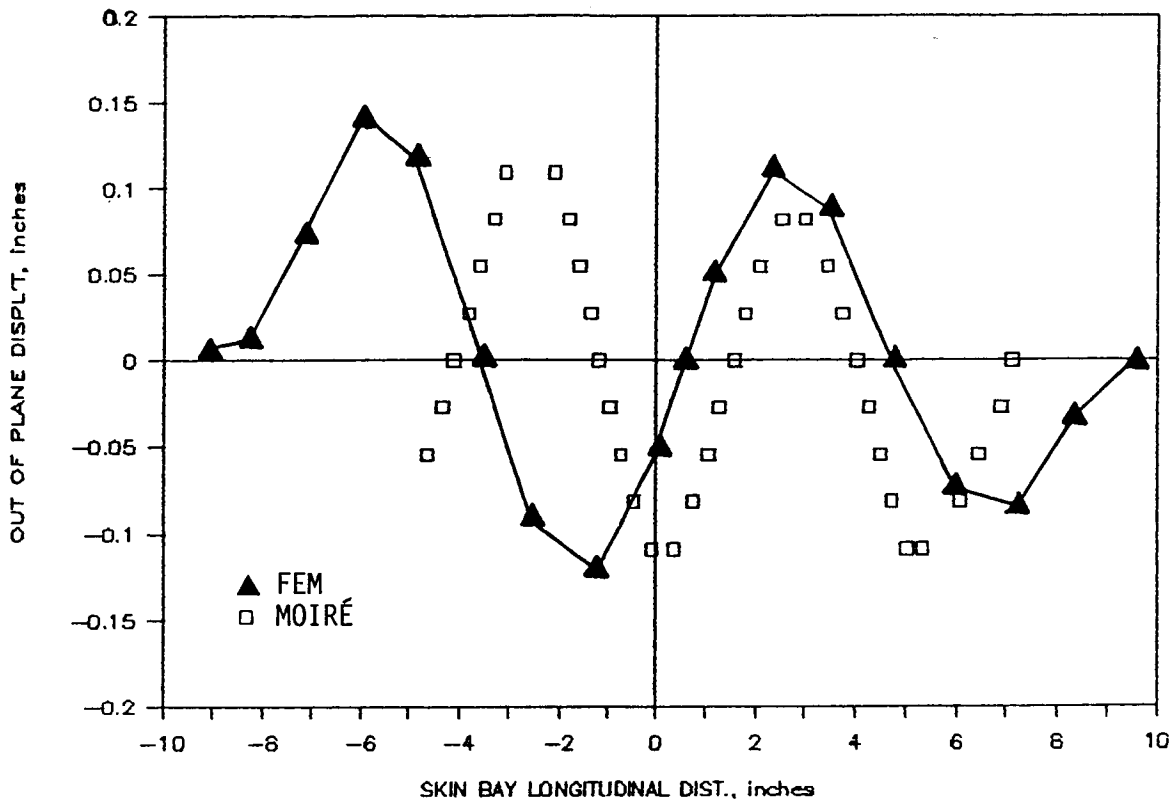


Figure 20. Comparison of Out-of-Plane Deflection Shape at Bay Center Along Stiffener Axis

cracks developed (at 20000 lbs) in order to see where failure started. The load capability may have been significantly higher as is indicated by the failure load for the second specimen (22000 lbs). Thus, the average test failure load of 21000 lbs may be conservative. (2) Based on post-test examination, final failure was determined not to result from corner cracking (that was noted in the specimen) but rather from high local strains in the vicinity of the root of the hat stiffener (near the frame/stiffener intersection) due to the buckled shape. This is verified by the shadow moire fringes (Figure 19), which do not cross the centerline of the specimen but stop where the stiffener webs meet the skin. The fringes, which indicate out-of-plane deflection, tend to come close together in the vicinity of the stiffener. This implies a large displacement gradient is present in this area and the associated high bending moments precipitated final failure. The existence and location of this high strain area was confirmed by the finite element analysis.

FULL-SCALE ARTICLE

The full-scale article (shown in Figure 6) was manufactured by laying up the skin in an aluminum tool that was surrounded by an aluminum frame similar to that shown in Figure 1. The hat stiffeners were laid up around teflon mandrels and placed in position on the skin. The frames were laid up on a specially made tool and then lowered into place in the assembly. Two aluminum cross members, one for each frame, were used to keep the frames in place during curing, in a manner similar to the tool shown in Figure 1. The outer web plies of the frames opened up to accommodate the hat stiffeners going through and

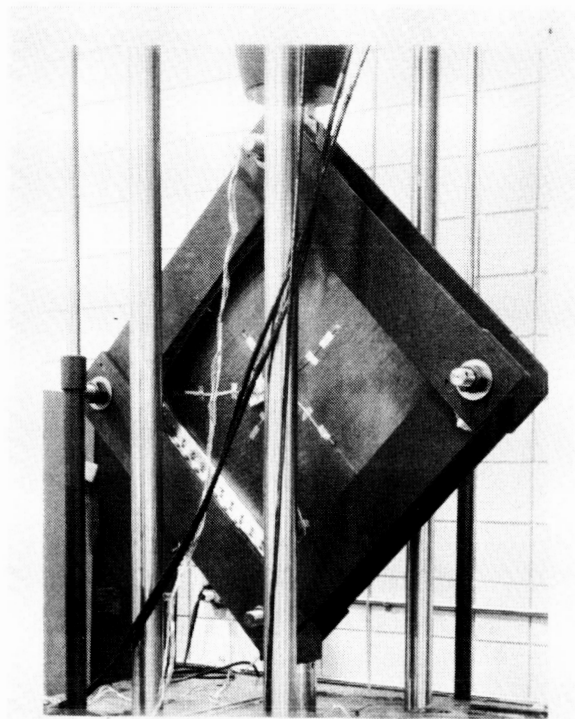


Figure 21. Full-Scale Test Setup

served as shear ties between frames and stiffeners. The top skin ply was placed last, covering all stiffener and frame flanges (embedded flange concept). The full-scale panel was tested in shear using a picture frame fixture (Figure 21). Axial load was applied to diagonally opposite ends of the fixture in order to introduce the desired shear loads through the structure. The finite element modelling procedures were the same as for the frame-stiffener intersection specimens. The model had 2530 nodes and 7590 degrees of freedom with 2424 CQUAD4 and 136 CBEAM elements.

A comparison of strain gage data near a frame/stiffener intersection (corner of outer bay) to finite element predictions is shown in Figure 22. The shear strain at a point inside one of the bays (quarter of the distance between the two hat stiffeners) is shown in Figure 23. The axial strain along the frame axis at the center of one of the outer bays is shown in Figure 24. In all cases, test and finite element analysis are in good agreement up to 10000 to 12000 lbs of applied load (postbuckling factor of about 3). The differences at higher loads are due to local failures that occurred (manifesting themselves with loud noises and sharp increases in the deflection gage measurements) and redistributed the load. These local failures were not modelled by the finite element model. The deflection pattern over the whole panel was monitored by shadow moire. In addition, a deflection gage positioned at the center of one of the two center bays was used to measure deflection locally. The out-of-plane deflection at that location is compared to the finite element predictions in Figure 25. For the same load, the deflections predicted by finite elements are 20-30% less than test results through panel failure.

Figure 25 shows that the bay buckling load predicted by finite elements is in excellent agreement with the test result of 4000 lbs (94 lbs/in). A more

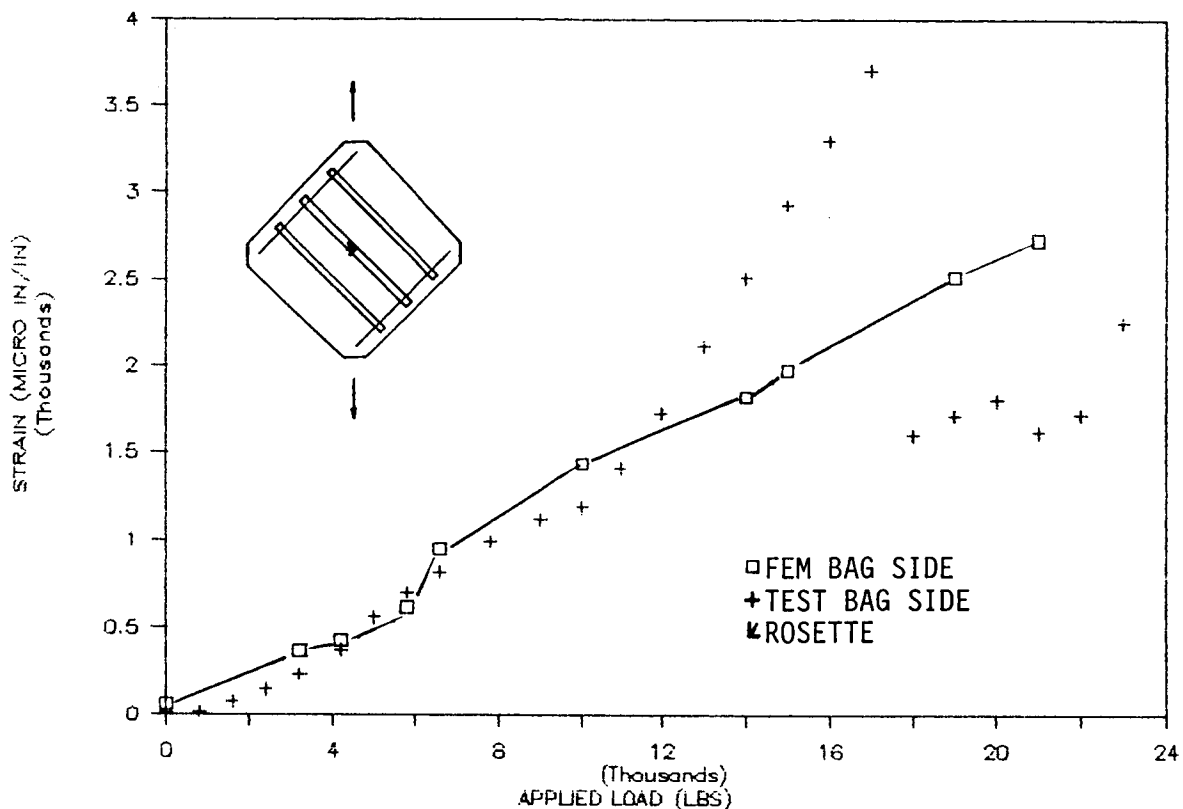


Figure 22. Comparison of Finite Element Predictions to Test Results at Hat-Stiffener Center (Shear Strains - Full Scale Panel)

detailed finite element analysis (up to buckling) with the same mesh but with smaller load increments showed the predicted bifurcation load to be 102 lb/in or 8% higher than the bifurcation load indicated by the deflection gage during test. It was a snap-through buckling where the skin, up to that point deflecting in the direction of the panel curvature, reversed direction with a jump in deflection of more than an order of magnitude. The average failure load of 23500 lbs (554 lbs/in) gives a postbuckling factor (failure load to buckling load ratio) of 5.9.

The failure progression as observed during test and inferred from examination of failed specimens was as follows: (1) Upon loading to 18000-19000 lbs, fiber cracking and matrix splitting were observed at one of the loaded corners of the specimen (see Figure 26 point 0). This is consistent with the starting crack observed during testing of the flat frame-stiffener intersection specimen and is at approximately the same location. Like the flat frame/stiffener intersection specimen, the crack on the full-scale article stopped after growing to a size of 3-4 inches. It is believed this crack initiated as a result of the test fixture pinching the lower corner of the specimen and served as a stress relief mechanism. The conjecture that this crack did not cause final failure was verified by the fact that each test specimen failed at significantly higher load, 4000-5000 lbs after the corner crack developed.

At 23000 to 24000 lbs of applied load, new fiber and matrix cracks were noted to initiate as a result of large displacement gradients caused by the buckled shape at the frame and hat stiffener intersection (see point F in Figure 26). These cracks, accompanied by some delamination, progressed from the

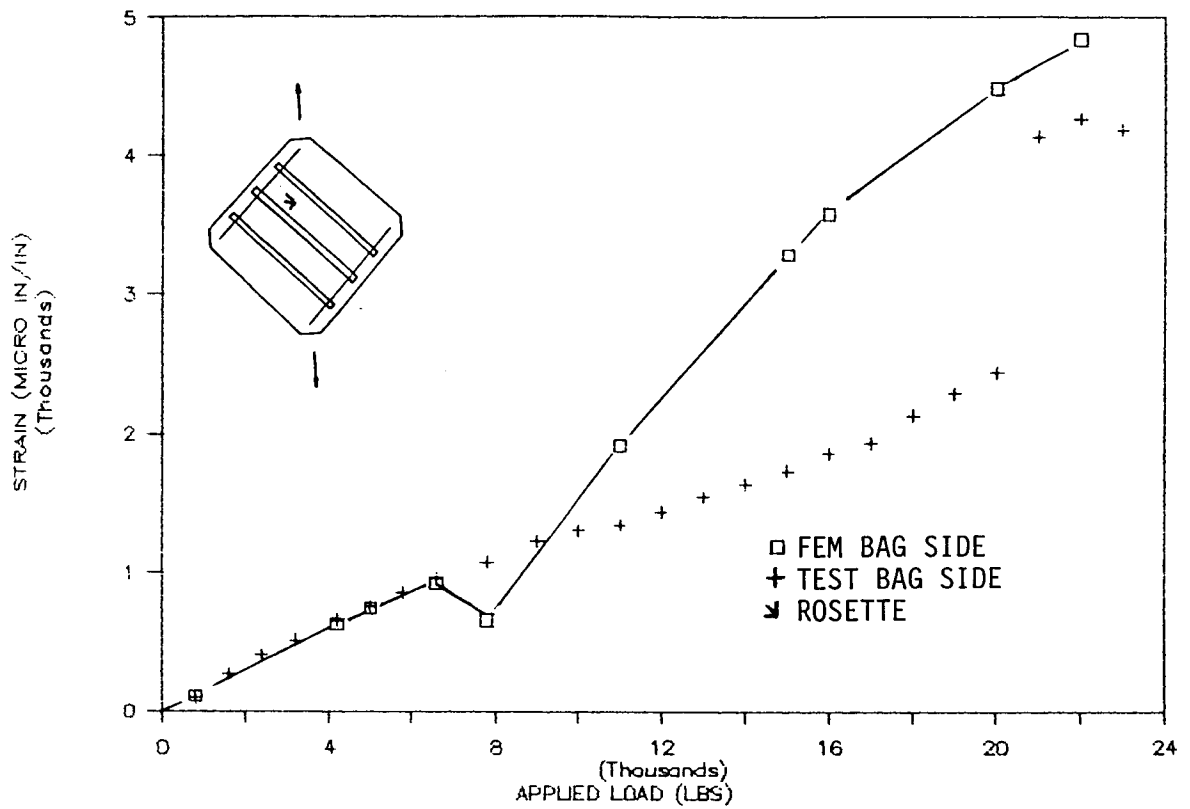


Figure 23. Comparison of Finite Element Predictions to Test Results at Bay Quarter Point (Shear Strains - Full Scale Panel)

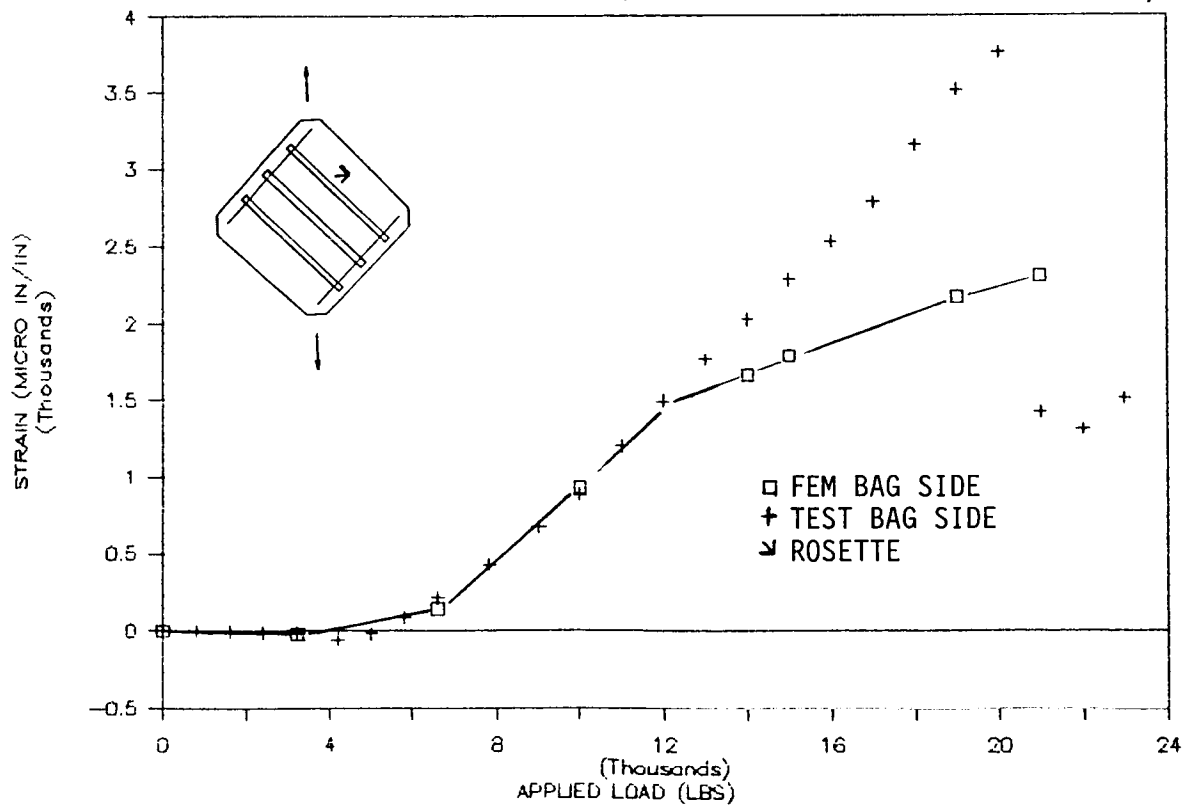


Figure 24. Comparison of Finite Element Predictions to Test Results at Bay Center (Shear along Frame Axis - Full Scale Panel)

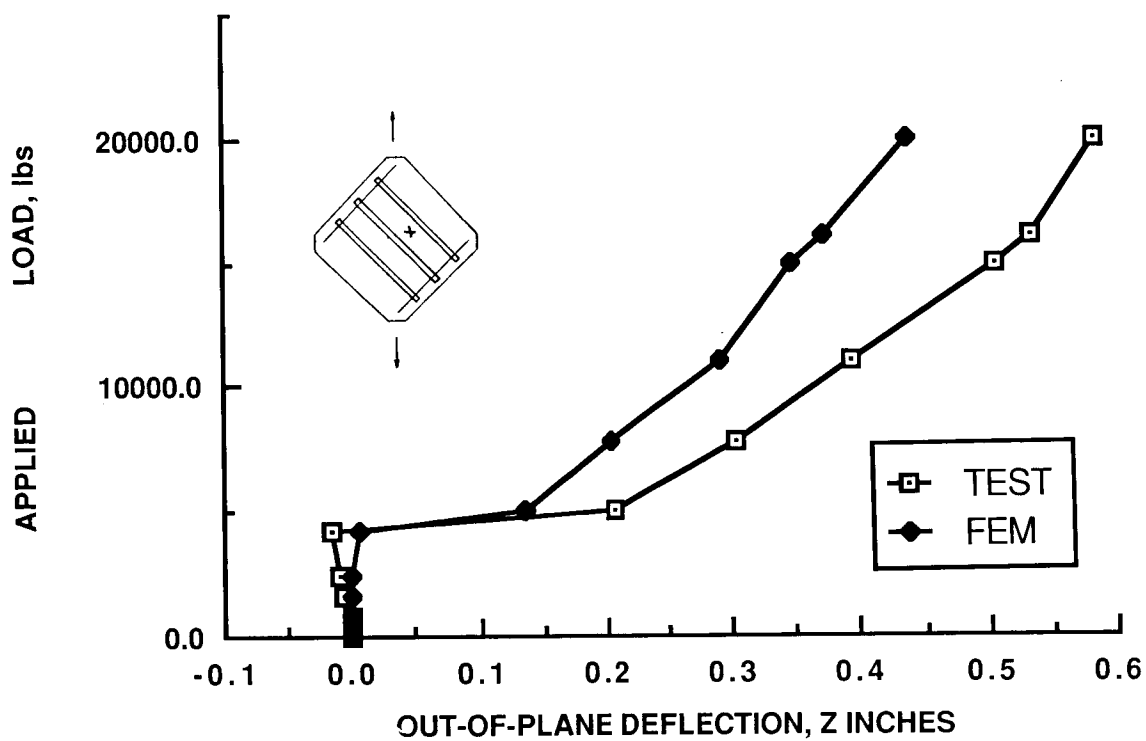


Figure 25. Load versus Deflection Plot at Bay Center (Finite Element Prediction and Test Measurement)

intersection along the edge of one of the hat stiffeners, propagated across the hat stiffener, and continued to final failure as marked by separation of the specimen into two large sections. The resulting fracture pattern is also shown in Figure 26. It should be noted that the flanges of the frames and stiffeners were embedded in the skin and no stiffener separation from the skin was noted. This is different from the common failure of these panels when the flanges are bonded directly on the skin (see for example reference 8) and shows that this configuration is effective in altering and delaying stiffener-to-skin failures in such panels.

Failure of the full-scale panels is predicted using the results of the flat frame-stiffener intersection specimens which showed very similar failure mode. As is shown in Figure 27, the shear strains at the bay center for the two specimens are very close to each other up to a load of 12000 lbs. At that point, the full-scale panel diverges probably due to a change in the mode shape that essentially reversed the buckling pattern. It is believed that the strains at the location where final failure started for both flat and curved specimens are similar and thus the loads (in lbs/in of shear) at which internal strains reach the material allowables should be the same for both types of specimen. The failure load for the flat specimen then should be a reasonable approximation to the full-scale article failure load. As already mentioned, the failure load for the full-scale article was 554 lbs/in which is 11% lower than the value of 614 lbs/in that the flat specimen failure would predict.

SUMMARY AND CONCLUSIONS

A program is on-going to evaluate the structural performance of composite fuselage structure fabricated using an autoclave THERM-XSM process. A building block approach is used to isolate failure modes and quantify load paths and failure loads for the full-scale article which is a curved skin panel with cocured hat stiffeners and frames with a tee-shaped cross section. Tests at the coupon and element level have shown that the THERM-XSM processed parts have comparable stiffness, strength, and failure modes. The only instant where the THERM-XSM processed parts showed moderate inferiority (up to 15%) to conventionally manufactured parts was in high speed-low impactor mass compression after impact test.

Finite element predictions of deflection shape and strains in the flat element level tests are in good agreement with test results except at some locations in the panel where at intermediate loads the test results suggest a difference in the postbuckled deflection shape.

The curved stiffened panel performed very well, exceeding the design ultimate load of 250 lbs/in by over a factor of 2 and failing at a postbuckling factor of 5.9. The finite element predictions are in good agreement with the test results up to a postbuckling factor of 3. At higher loads the test results suggest that local failures and changes in mode shapes took place that were not accounted for by the finite element analysis. The failure mode involved cracks starting at a frame stiffener intersection but no flange separations were noted (due to the use of embedded flanges) nor any shear tie failures. This suggests that failure is driven by in-plane skin failure in the vicinity of frame/stiffener intersections where stress concentrations will be present. More work is needed to better quantify this failure mode.

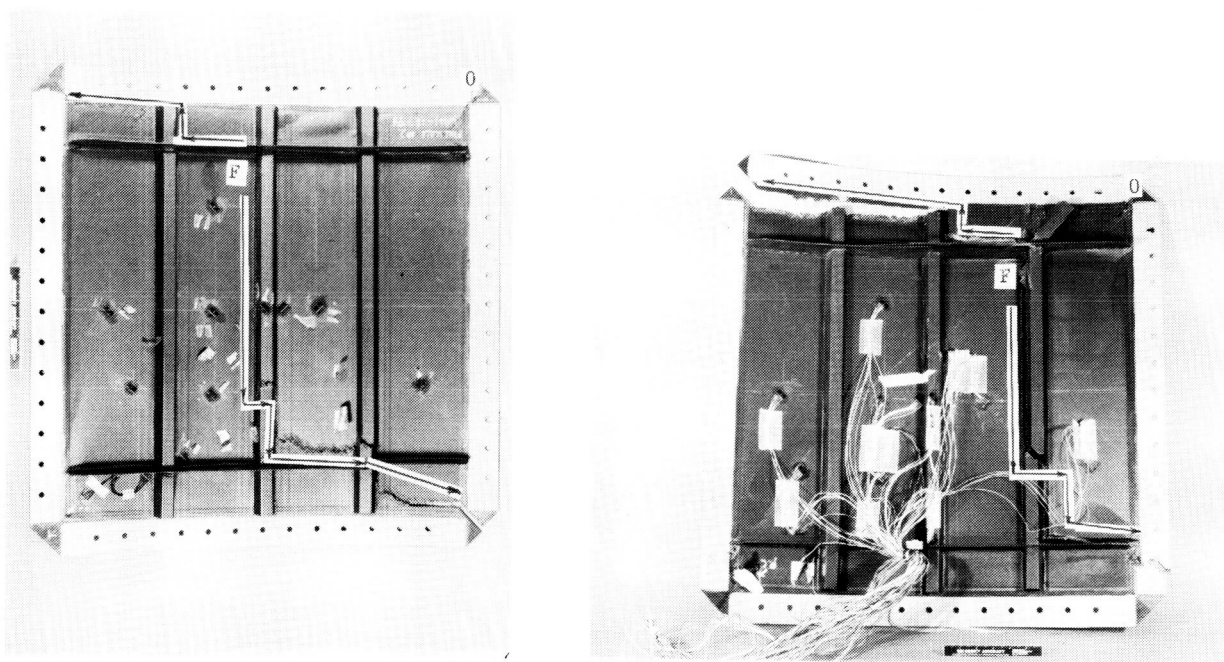


Figure 26. Failure Mode for First Two Full-Scale Tests

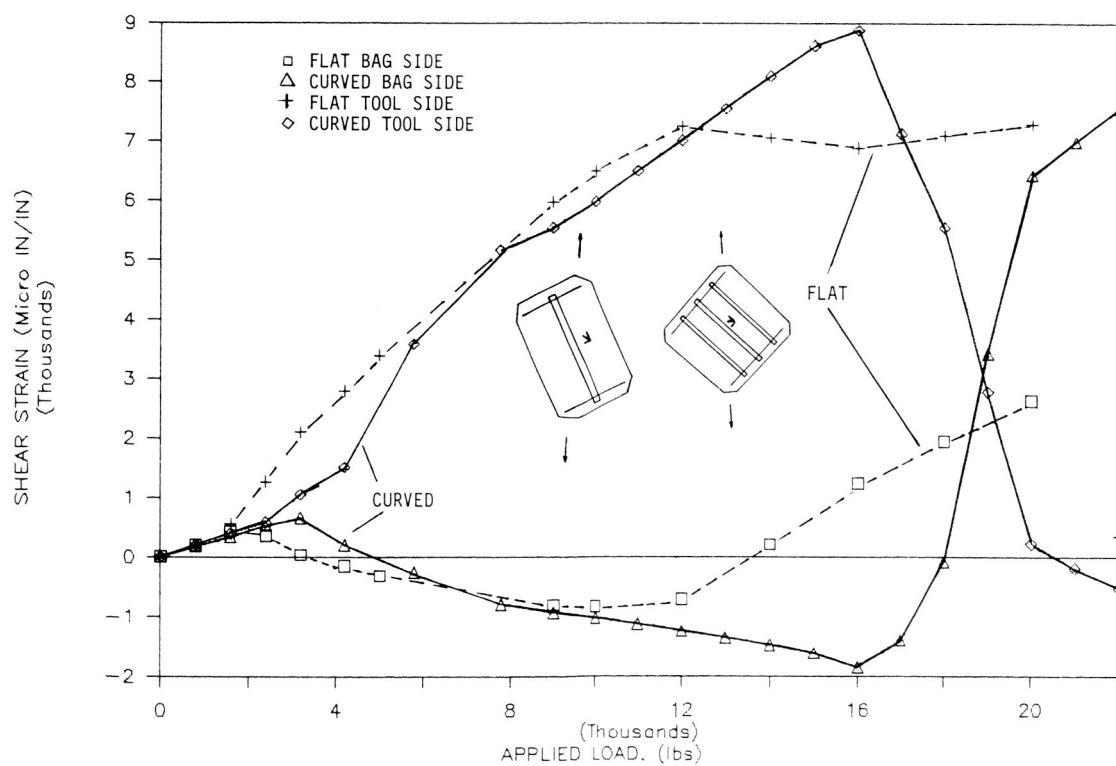


Figure 27. Shear Strain Comparison for Intersection and Full-Scale Tests (Bay Center)

Failure predictions for the curved panel can be obtained using the failure load from the flat element level test which had a similar failure mode. That prediction is 11% higher than the curved panel failure load.

The fact that the finite element analysis assuming the THERM-Xsm processed parts had the same properties as conventionally manufactured parts showed good agreement with test results up to the point where local failures and mode changes not accounted for in the finite element analysis became significant, suggests that undamaged THERM-Xsm processed parts are structurally equivalent to conventionally manufactured parts.

THERM-Xsm processing enables manufacture of high quality complex parts with corners and tight radii with minimum tooling and at low cost.

ACKNOWLEDGMENT

This work was performed under NASA contract NAS1-18799. Jerry W. Deaton is the technical monitor. The authors wish to thank S. Garbo, G. Schneider, and A. Dobyns for their comments and suggestions regarding failure of the stiffened panels.

REFERENCES

1. Kassapoglou, C.; DiNicola, A.J.; and Chou, J.C.: Structural Evaluation of Composite Fuselage Structure Fabricated Using a THERM-Xsm Process. Proceedings of 46th American Helicopter Society Forum, Washington DC, 1990, pp. 671-682.
2. Boeing Structural Test Components Presentation, Workshop on Common Structural Test Components for ACT, Newport News, May 1990.
3. Cantwell, W.J.; and Morton, J.: The Influence of Varying Projectile Mass on the Impact Response of CFRP. Composite Structures, vol 13, 1989, pp. 101-114.
4. Cantwell, W.J.; and Morton, J.: An Assessment of the Residual Strength of an Impact Damaged Carbon Fibre Reinforced Epoxy. Composite Structures, vol 14, 1990, pp. 303-317.
5. Error Due to Transverse Sensitivity in Strain Gages, M-M Technical Note TN-509, Micro Measurements Division, Measurement Group, Inc, Raleigh, NC, 1982.
6. Dally, J.W.; and Riley, W.F.: Experimental Stress Analysis, McGraw Hill, Inc, 1978, chapters 12.5 and 12.6.
7. Tsai, S.W.: Strength Characteristics of Composite Materials. NASA OR-224, April 1965.
8. Rouse, M.: Postbuckling and Failure Characteristics of Stiffened Graphite-Epoxy Shear Webs. 28th SDM Conference, Monterey CA, April 1987, AIAA paper 87-0733.

Noise Transmission Properties and Control Strategies for Composite Structures

Richard J. Silcox, Todd B. Beyer, and Harold C. Lester
NASA Langley Research Center

Abstract

A study of several component technologies required to apply active control techniques to reduce interior noise in composite aircraft structures is described. The mechanisms of noise transmission in an all composite, large-scale, fuselage model are studied in an experimental program and found similar to mechanisms found in conventional aircraft construction. Two primary conditions of structural acoustic response are found to account for the dominant interior acoustic response. A preliminary study of active noise control in cylinders used piezoceramic actuators as force inputs for a simple aluminum fuselage model. These actuators provided effective control for the same two conditions of noise transmission found in the composite fuselage structure. The use of piezoceramic actuators to apply force inputs overcomes the weight and structural requirements of conventional shaker actuators. Finally, in order to accurately simulate these types of actuators in a cylindrical shell, two analytical models are investigated that apply either in-plane forces or bending moments along the boundaries of a finite patch. It is shown that the bending model may not be as effective as the force model for exciting the low order azimuthal modes that typically dominate the structural acoustic response in these systems. This result will affect the arrangement and distribution of actuators required for effective active control systems.

Introduction

The expanded use of composite materials for primary aircraft structures is evidenced by the Boeing 360 and tiltrotor programs and new business aircraft. In commercial vehicles of this type as well as aircraft with conventional construction, the acoustic environment is an important element for passenger acceptance. Therefore, the understanding and control of the vibration and acoustic transmission properties of composite structures is an important element which will promote the widespread use of composites in large scale commercial aircraft. It is expected that the integrated nature of the composite skin with the frame, along with the decreased weight compared with conventional construction, will provide for less structural damping and potentially higher overall acoustic and vibration levels.

Although finite element models have now been developed for composite layered media, most of this work has been directed towards determining the static properties of structures. Little work has been done towards developing finite element methods for built-up structures responding to high frequency dynamic inputs. To date, finite element methods have not even found widespread use for conventional structures at frequencies applicable to noise annoyance. This is due to the complexity and cost of developing and running the required numerical models. Additionally, these numerical approaches provide little insight into the

structural/acoustic coupling mechanisms controlling the noise transmission process. A simpler approach that effectively models the gross shell motions and acoustic response is a more effective first step.

A number of simplified modal models have been developed that provide a basic understanding of the noise transmission mechanisms of aircraft structures.^{1,2,3} These techniques have successfully modelled the low frequency mechanisms of acoustic-structural coupling determined from experimental evaluations of simple fuselage models.^{4,5} These works have shown that the acoustic response of interior fuselage spaces is dominated by a limited number of low order spatial acoustic modes that are generally excited by off resonant response of the fuselage structure. These simple models do not take into account the anisotropic material characteristics of composite structures. However, it has been shown that the individual resonant structural and acoustical behavior of composite structures is similar to that of conventional isotropic structures at low frequencies.⁶ Therefore, these analytical modal models may be applied to composite structures with the qualification that the structural modelling may be less than realistic.

Passive noise control techniques have traditionally relied on stiffened structures or structural and acoustic damping to increase the transmission loss. The increased weight associated with these techniques can effectively offset the weight savings due to composite structures. Active control technology, however, has emerged as a realistic alternative for efficient control of the interior noise in propeller driven passenger aircraft. Flight tests^{7,8} and ground tests^{9,10} of active control systems have shown that a 10 to 15 dB attenuation of the global interior noise is attainable with either acoustic or vibration control sources. Experience with distributions of acoustic control sources has shown that large numbers of sources are required in order to provide control over a wide range of conditions and engine harmonics. The use of force inputs has provided nearly equally effective control with significantly fewer actuators. This reduction in number of actuators, however, requires more intelligent placement in order to couple efficiently into the range and order of structural acoustic modes encountered over the aircraft operational range.

Another aspect relating to active control is the type of actuator and sensor elements used to implement the active control system. In reference 9, 10 lb conventional shakers acting against their own inertial mass were used to generate the necessary control forces. This approach has obvious weight and force limitations on real aircraft. For this reason, piezoceramic elements are currently being evaluated for this application as they input strain energy directly into a localized region of the structure and their weight and cost are negligible.

The purpose of this paper is threefold. First, to illustrate the dominant mechanisms of noise transmission for a large-scale composite fuselage model. Second, to examine an approach for active noise control using piezoceramic actuators as demonstrated on an aluminum cylinder. And third, to present and examine two analytical models of piezoceramic actuators to apply either in-plane forces or bending moments to the structure. This work is part of a larger ongoing effort at Langley Research Center to apply active controls concept to ameliorate the noise and vibration environment of aerospace vehicles.

Experimental Configuration

In this section, two experimental efforts are outlined. The first describes a large scale composite fuselage structure excited by exterior acoustic sources. The shell and interior cavity responses are presented and discussed. The second describes a preliminary experiment in which piezoceramic actuators bonded to the side wall of an aluminum fuselage model were used to effectively control the interior noise due to a simple propeller model. This second experiment has led to a current interior noise control effort using similar transducers on the full scale composite shell described above.

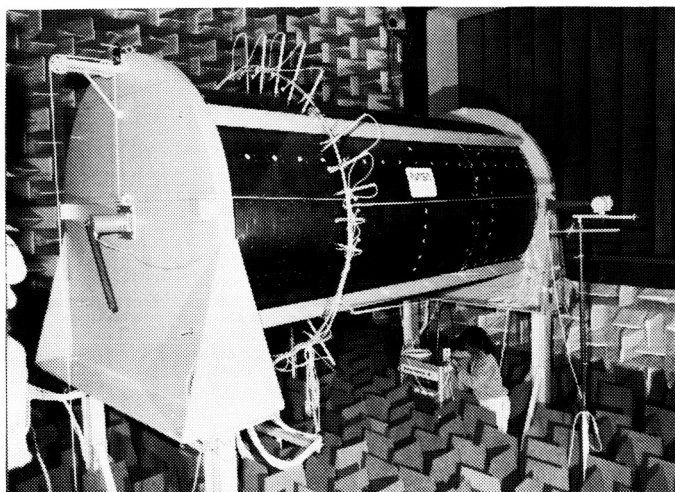


Fig. 1.- Composite cylinder in anechoic room.

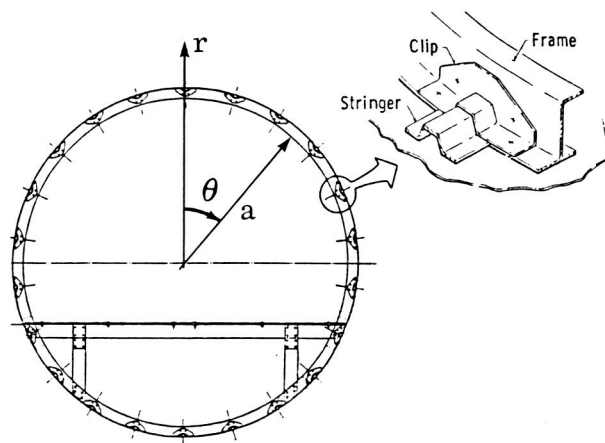


Fig. 2.- Cross section of composite cylinder.

Composite Cylinder Noise Transmission Tests

Figure 1 shows the test cylinder mounted on a stand in the large anechoic chamber of the Acoustics Research Laboratory at NASA Langley Research Center in Hampton, Virginia. This test configuration provided an environment for a comprehensive mapping of the exterior and interior sound fields in a free field environment.

The aircraft fuselage model used in the current study is a filament wound, stiffened cylinder 1.68 m in diameter and 3.66 m in length. The composite material of the cylinder shell consists of carbon fibers embedded in an epoxy resin. The ply sequence of the cylinder skin is $\mp 45/\mp 32/90/\pm 32/\pm 45$ for a total thickness of 1.7 mm. The cylinder is stiffened (longitudinally) by 22 evenly spaced composite hat-section stringers. The stringers pass through 10 composite J-section ring frames spaced 0.381 m apart. The ring frames and stringers are tied together with a clip and all elements of the fuselage are rivet-bonded together. A schematic of the cylinder cross section with detail of the stringer-frame geometry is shown in Figure 2. A 12.7 mm thick plywood floor is installed 0.544 m above the bottom of the cylinder. The supporting beams and posts for the floor are made from aluminum extrusions. An aluminum clip ties the floor to the shell at discrete locations. The plywood floor is bolted to the aluminum supporting beams. Rubber gaskets and silicon rubber sealant fill the gaps between the floor

edge and the cylinder structure in order to acoustically isolate the spaces above and below the floor. Additional details of the composite cylinder may be found in reference 11.

The cylinder endcaps were constructed from three layers of 32 mm thick particle board with a 3.2 mm wide groove cut out for the end of the cylinder to rest in. The endcaps are sufficiently massive so that any airborne sound transmission through them is negligible compared to the sound transmission through the cylinder sidewall.

The acoustic source used to excite the system was a point source located at $\theta=90^\circ$, $x=0.333\ell$ and $0.2a$ from the shell outer surface. The coordinate orientation is shown in Figure 2 with positive x into the paper. Here ℓ is the length of the cylinder, 3.66 m and a is the radius. The source was assumed to approximate a propeller noise with known temporal and spatial characteristics. The shell response was measured with an azimuthal array of 22 mini-accelerometers equispaced around a circumference at $x=0.333\ell$, the source plane. The interior pressure field was measured using six 12.7 mm condenser microphones mounted along a radius. These microphones could be traversed both azimuthally and axially such that a complete mapping of the interior acoustic field was obtained. The reader is referred to reference 12 for additional details.

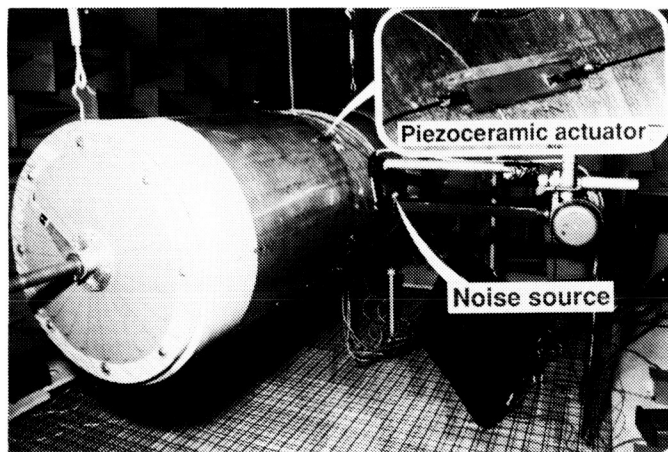


Fig. 3.- Photograph of experiment rig and piezoceramic actuator.

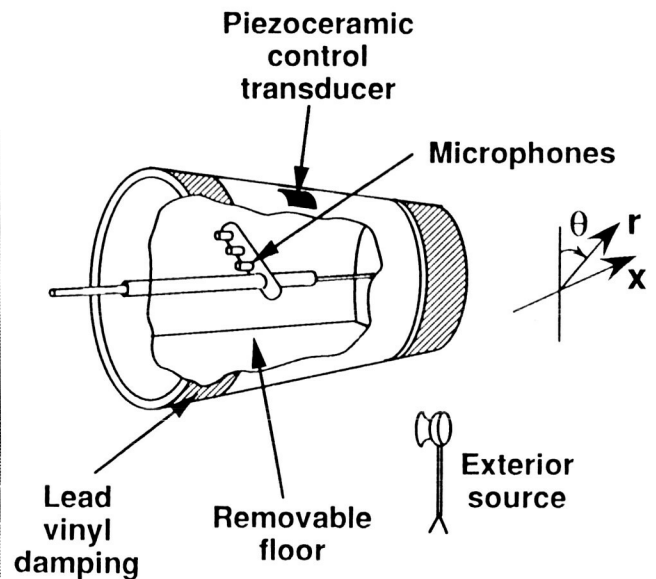


Fig. 4.- Schematic of aluminum cylinder test apparatus.

Interior Noise Control using Piezoceramics

Figure 3 is a photograph and Figure 4 is a schematic of the test arrangement of the second experiment consisting of an aluminum cylinder, 0.508 m in diameter, 1.245 m long, and 1.63 mm thick. The floor was 0.381 m wide and consisted of thin aluminum skin attached to a lattice structure. The cavity below the floor was filled with acoustic foam in order to inhibit acoustic resonances in this space which might complicate the system response. Propeller noise was simulated by a 60 W horn driver attached to a tapered horn whose outlet was

positioned 76 mm from the exterior of the cylinder. All tests were performed at single pure tone frequencies. The interior pressure field was measured by three 12.7 mm microphones mounted on a movable traverse. The results will be presented as sound pressure level contour plots located in the source plane. Additionally, the structural response was measured by an array of 24 uniformly spaced mini-accelerometers attached to the cylinder in the source plane. In order to simulate a free-field environment, the experiments were performed in an anechoic chamber at NASA Langley Research Center.

To generate control inputs, two bimorph piezoceramic actuators (see inset of Figure 3) of dimensions 50.8 x 12.7 x 0.51 mm were bonded to the exterior of the cylinder in the source plane at -90° and 45° (90° corresponds to the acoustic source location). A bimorph actuator has two co-located piezoceramic elements driven 180° out-of-phase in order to produce surface bending. A reference signal was used to drive the acoustic noise source and the same signal was passed through a two channel manually operated phase shifter. The control signals were then amplified, passed through transformers with a voltage gain of 7:1, and connected to each bimorph element. The experimental procedure was as follows: The exterior noise source was driven at the desired frequency and level. The amplitude and phase of each control signal (for some tests only one channel was used) were adjusted to minimize the interior sound levels at one and/or two error microphones located at fixed positions in the interior cavity. In practice, a computer based adaptive controller could be used to perform this function. However, the manual system used here was more convenient for the purpose of these tests. Once the error signals were minimized, the interior field was mapped using the traversing microphone array. The control signal(s) were then turned off and the interior noise of the primary field mapped.

Piezoceramic Actuator Models

In order to take effective advantage of any type of control actuator, reasonable analytical models must be developed and studied. Previous actuator models for plate and beam applications have assumed that the piezoelectric material occupies a small region of the total plate.¹³ With shells, however, the piezoelectric material has been assumed to occupy an entire layer of a multilayered shell.¹⁴ That is, simple piezoelectric actuator models for shell applications have not yet been developed. In the present work, two plate type actuator models are coupled to a finite length, isotropic cylinder model developed in reference 2. The displacement response of the cylinder and the interior acoustic pressure are expressed as modal expansions in the characteristic functions of each physical system. For more details on this model, the reader is referred to reference 2 which defines the response of a simple fuselage model due to adjacent acoustic point sources (simulating a propeller) and to a point force exciting the structure directly. In order to evaluate the effect of the piezoceramic transducer elements, extensions to reference 2 are currently being evaluated.

Two piezoceramic patch models have been formulated for active vibration/noise control of cylinders. These models, which are described below, represent adaptations of piezoceramic models previously developed for flat plate applications,¹³ where in-plane and bending (out-of-plane) deformations are uncoupled. Hence, these piezoceramic models are most likely valid only for patches whose dimensions are small relative to the radius of curvature.

The bending model simulates the effect of two out-of-phase piezoceramic patches attached on opposite sides of the cylinder wall. By driving the two piezoceramic patches out-of-phase, a normal stress distribution is produced which varies linearly through the thickness of the shell. This approximates a state of pure bending about the middle surface of the shell. However, some extensional deformation is produced since the out-of-plane and in-plane deformations in a shell are coupled due to curvature effects. The essence of the modeling involves replacing the piezoceramic patches by a uniform, line moment applied along the perimeter of the patch area. The amplitude of the moment is proportional to the piezoceramic supply voltage.

An in-plane piezoceramic model was also developed in which the adjacent patches are driven in-phase creating primarily an extensional deformation of the shell's middle surface. Again, because of coupling (due to curvature) some out-of-plane (bending) deformation of the cylinder is produced. It is this out-of-plane motion which couples with the interior acoustic space. With the in-plane piezoceramic model, the patch is replaced by a uniform, in-plane line force distribution applied along the patch perimeter. In this case, the force amplitude is proportional to the piezoceramic supply voltage.

Results

Results are presented in three sections. In the first section, representative shell and cavity acoustic responses will be used to illustrate the noise transmission characteristics of the composite fuselage model. The second series of results will illustrate the use of piezoceramic transducers as actuators on a simple aluminum fuselage model. Finally, predictions using the previously described analytical models for piezoceramic-patches will show the differences in the wave space mode spectra response of the shell model.

Composite Cylinder Response

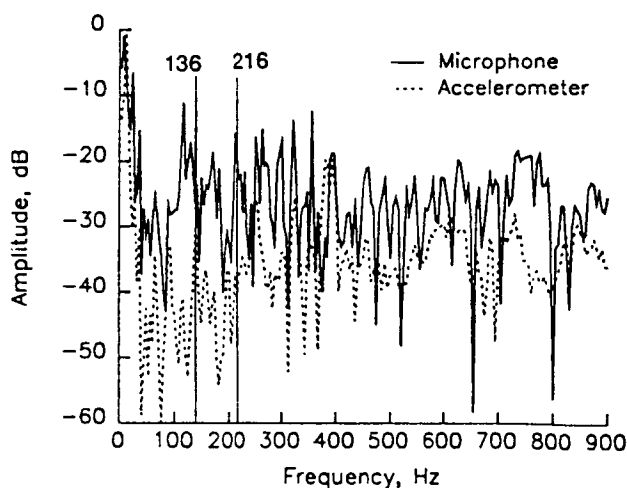


Fig. 5.- Typical interior pressure and shell acceleration spectra

Figure 5 compares the spectra recorded by an interior microphone (at $r=0.924a$, $\theta=-84^\circ$, $x=0.333l$) and an accelerometer on the exterior shell (at $\theta=-82^\circ$ and $x=0.333l$) of the composite fuselage model. These frequency response functions are measured with respect to a fixed microphone mounted at the source face. Both levels are then normalized to their respective individual peak levels. The exterior acoustic source used pseudo-random noise to excite a single acoustic monopole mounted $0.2a$ from the shell wall at $\theta=-90^\circ$ as discussed in reference 12. These frequency response functions indicate a strong modal response across the spectrum particularly for the interior pressure. The interior microphone response retains the sharp peaks out to the highest

frequency of 900 Hz. The accelerometer response begins to smooth out above 500 Hz indicating that the modal density is increasing such that individual modes no longer dominate the shell response. Note that the peaks of the vibration and acoustic responses do not in general coincide at many frequencies. At those frequencies at which they do correspond, a resonant shell response drives an off resonant acoustic response. There are however many strong acoustic responses that correspond to relatively weak shell vibration responses. These frequencies correspond to co-incidence frequencies where the spatial wavelength of an off resonant shell mode is nearly equal to that of a strongly coupled resonant acoustic cavity mode. Often, the shell mode that drives the acoustic response is not the dominant response in the shell. However, it is the one that most strongly couples to the acoustic cavity response. As will be shown, the acoustic cavity response is typically dominated by spatial distributions that correspond to individual modes of the interior cavity geometry.

Two cases representing typical coupling mechanisms will be examined in detail. These are noted in the frequency response functions of figure 5 as the two frequencies of 136 Hz and 216 Hz. At 136 Hz, the shell has a strong resonant response and forces an off resonant response of the interior cavity. At 216 Hz, the opposite is true, an off resonant shell mode couples strongly into a resonant cavity mode.

Figure 6 shows a plot of the shell vibration distribution plotted at 18 time increments over 1 cycle of vibration. This data is expanded from the 22 accelerometer measurements and illustrates the motion of the shell at 136 Hz. A strong modal response characterizes the upper cylinder response and corresponds with a structural mode defined in reference 6. The floor structure forces nodes at $\theta = \pm 110^\circ$ and the under floor response is reduced due to the

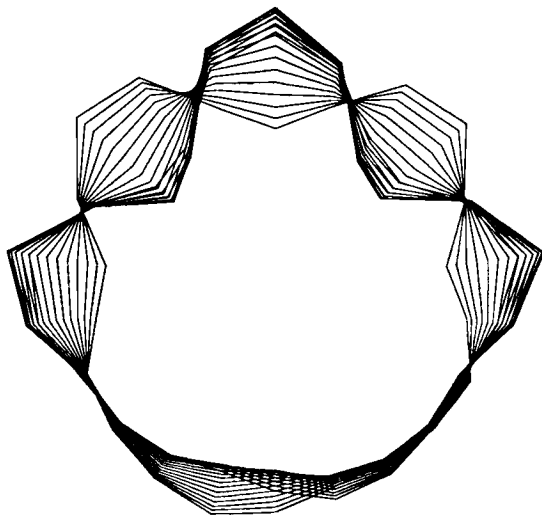


Fig. 6.- Shell vibration distribution for exterior monopole excitation of 136 Hz.

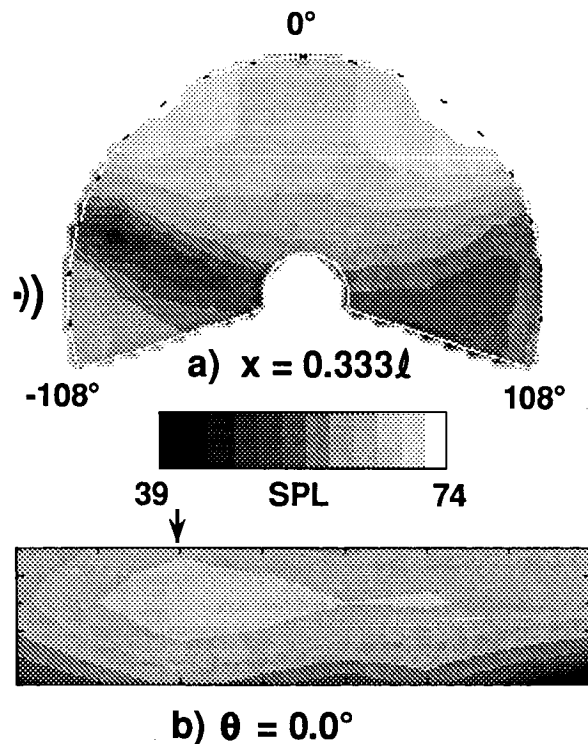


Fig. 7.- Interior cavity pressure distribution due to monopole excitation at 136 Hz.

stiffening effect of the floor and its supporting structure. This strong resonant response of the structure forces a relatively uniform interior response as illustrated by the pressure distributions of figure 7. Here, the pressure contours are plotted for the source cross section at $x=0.333\ell$ in figure 7a and an axial/radial distribution at $\theta=0.0^\circ$ in figure 7b. Because the excitation frequency does not correspond with any resonant cavity mode, the result is a combination of forced off-resonant responses. The overall interior cavity response is relatively uniform with the variations that do exist correlating with the shell vibration distribution.

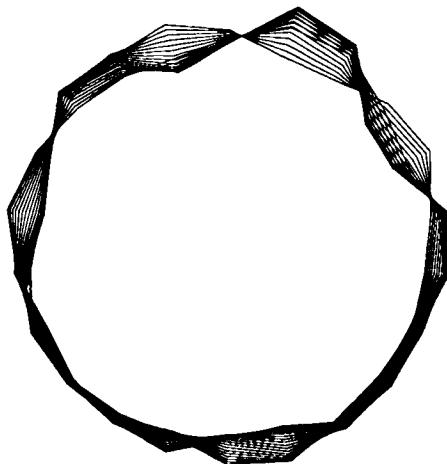


Fig. 8.- Shell vibration distribution for exterior monopole excitation at 216 Hz.

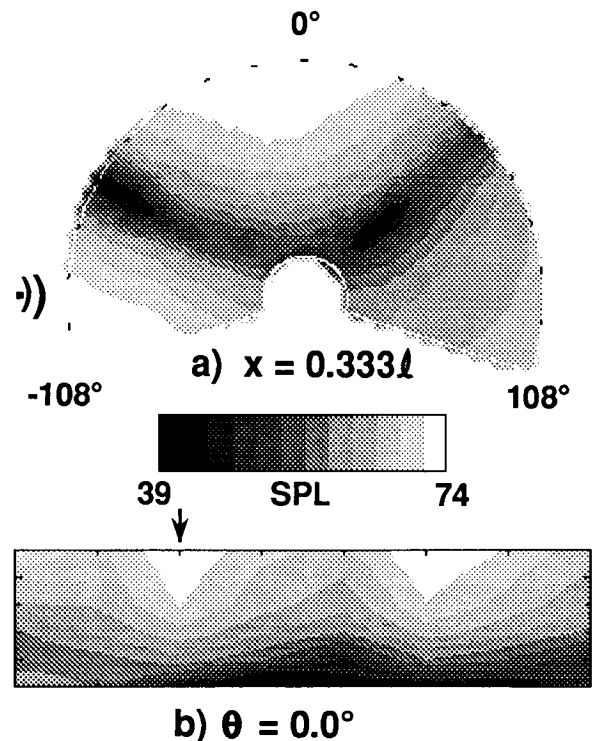


Fig. 9.- Interior cavity pressure distribution due to monopole excitation at 216 Hz.

The second coupled response condition is shown in figures 8 and 9. The shell response distribution is illustrated in figure 8 and is shown in correct relative scale to the accelerometer response at 136 Hz in figure 6. At this frequency, the shell is not responding in a resonant condition as evidenced by the magnitude of the response relative to figure 6 as well as the accelerometer spectra of figure 5. The shell vibration distribution does not correspond to any of the resonant modes of reference 6 and is thus inferred to be a combination of off-resonant modal responses. The interior acoustic response of figure 9 is, however, a strong resonant response. The microphone spectra of figure 5 illustrates a strong peak at 216 Hz and the cavity pressure distribution of figure 9 corresponds to a resonant acoustic mode of reference 6. The strong nodal lines in the source cross section of figure 9a illustrate the dominate behavior of this acoustic mode. The exterior source is in this cross section at $\theta=-90^\circ$ adjacent to the peak interior acoustic response. The axial/radial pressure contour shown in figure 9b is for $\theta=0.0^\circ$. This variation displays a $\cos(3\pi x/\ell)$ modal response. For this case, the acoustic pressure spatial distribution is not well correlated to the shell vibration distribution. This is due to the filtering effect of the structural acoustic coupling mechanism. Most of the shell vibration

modes couple poorly to the interior acoustic space. Only those modes that couple efficiently must be considered in any active control scheme. This simplifies the control task and makes it necessary to control only a limited number of interior cavity modes.

Active Control with Piezoceramic Actuators

Although active control results for a composite cylinder have not yet been obtained, an aluminum cylinder with the floor installed was excited at two frequencies that were characterized by a structural and an acoustic resonance. At 240 Hz, the structure is on a shell resonance and the acoustic field is being forced in an off-resonance response. This is similar to the condition for the composite cylinder at 136 Hz (figures 6 and 7). The interior acoustic pressure contour in the source plane cross section due to only the primary acoustic source is shown in figure 10a.

Using a single actuator located at $\theta = -90^\circ$ as indicated by the controller in figure 10b, the control input was adjusted to minimize the interior acoustic field as measured by the error microphone at $\theta = -90^\circ$ and $r = 0.925a$. The resulting controlled acoustic field is shown in the

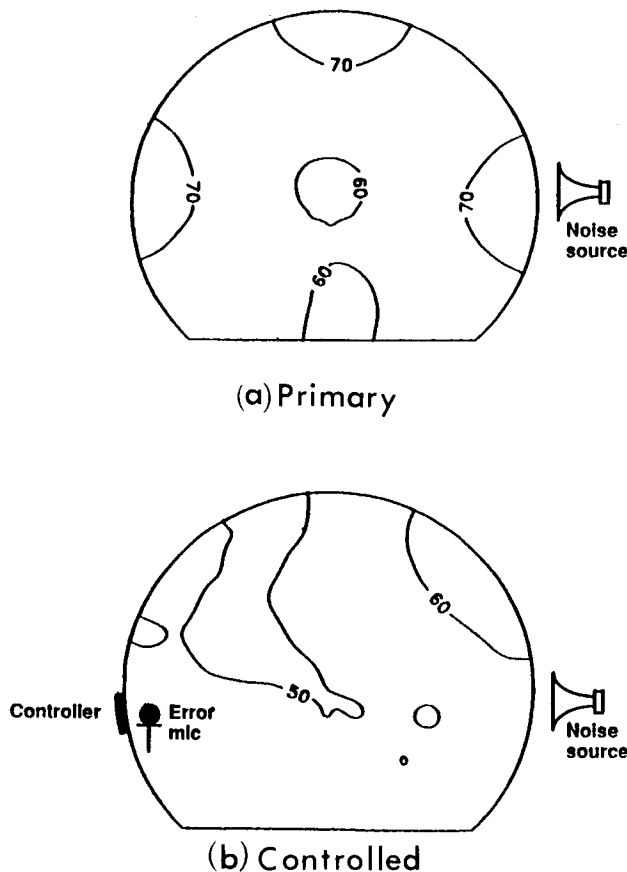


Fig. 10.- Interior sound pressure level for two source conditions at 240 Hz.

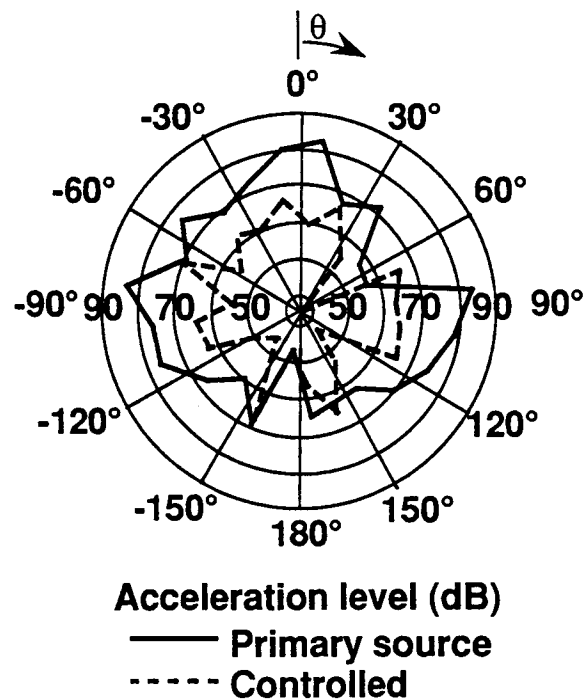


Fig. 11.- Shell radial acceleration distribution for two source conditions at 240 Hz.

contour plot of figure 10b. The peak acoustic levels are reduced on the order of 10 dB. This was also found to be the case for the out of source plane response with a consistent global reduction of about 10 dB.

Normalized shell acceleration levels in the source plane corresponding to the above primary and controlled conditions are shown in figure 11. The vibration response for the primary source alone is predominantly a distorted $\cos(2\theta)$ mode. The reduced response for the shell under the floor is thought to be due to foam damping packed under the floor. Compared to the vibration distribution for the controlled case, the single piezoceramic actuator is seen to reduce the vibration level by over 10 dB over most of the circumference. Only at a few isolated angles has the vibration level not been reduced. The residual response appears to be of a much higher azimuthal order. It appears that the controller has forced a significant reduction in the level of the dominant structural mode which is on resonance. This has produced a corresponding reduction in the forced acoustic response in the shell interior space.

The 687 Hz frequency of the second case corresponds to a cavity acoustic resonance as was the case for the composite cylinder in figure 9. The pressure contour arising from the primary acoustic excitation is shown in figure 12a. This antisymmetric mode has a strong nodal line aligned with the vertical radius and out-of-phase antinodes on either side as shown in this

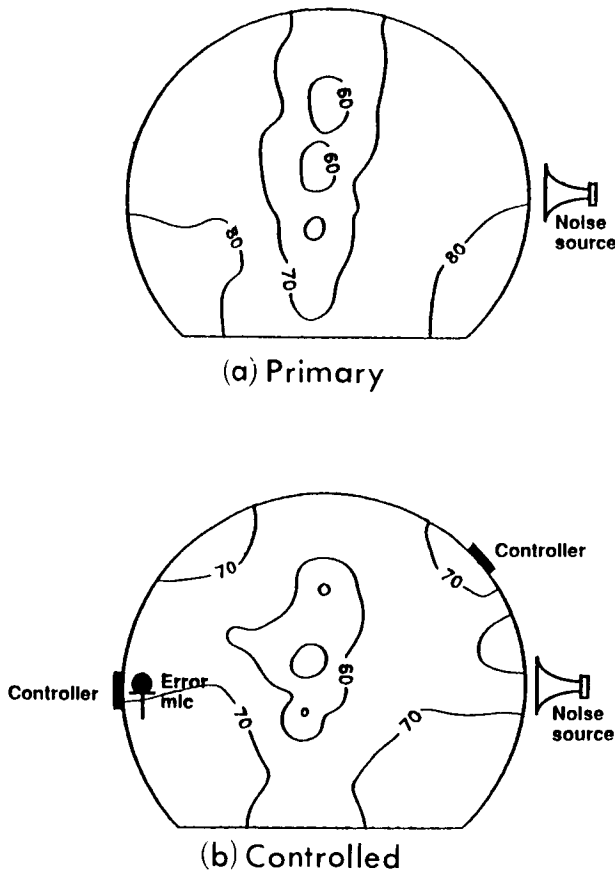


Fig. 12.- Interior sound pressure level for two source conditions at 687 Hz.

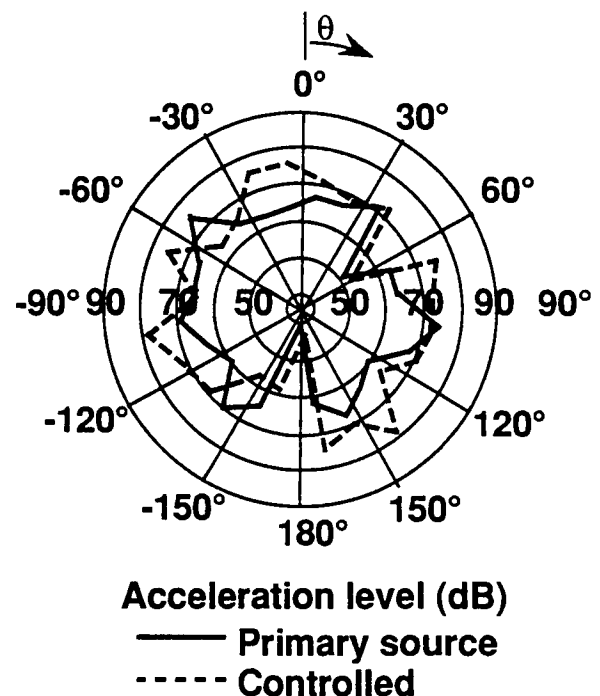


Fig. 13.- Shell radial acceleration distribution for two source conditions at 687 Hz.

source cross-section contour plot. For this case, control was exercised using both piezoceramic actuators placed at $\theta=-90$ and $\theta=+45$ degrees as noted in the contour plot for the controlled case of figure 12b. Peak reductions of 10 dB were obtained, although with somewhat less overall reductions. Again, however, reductions were obtained throughout the entire volume.

The normalized shell radial acceleration distribution corresponding to the previous primary and controlled cases is shown in figure 13. In this case, the dominant shell vibration motion does not couple effectively into the interior cavity space. One of several modes comprising the shell vibration however does couple effectively into the resonant cavity mode response. The effect of the controller is to couple effectively into this mode such that the overall interior pressure is substantially reduced. However, from figure 13, it is seen that the vibration levels in the shell have increased significantly. This increased motion of the shell does not effectively couple into the interior acoustics. This phenomenon may be taken as modal spillover, an effect of the limited number of control actuators and sensors allowing extraneous modes to be excited in the shell because they are not sensed by the error sensors. In cases such as this, distributed arrays of sources and sensors (on the shell) will be needed in order to control the overall shell response.

Piezoceramic Actuator Models

In this section, cylinder displacement modal response spectra are presented for each of the two piezoactuator models discussed previously. The results are for an aluminum cylinder having the same radius, length and thickness as the composite cylinder shown in figure 1. These results, though preliminary in nature, have implications in terms of the number and distributions of actuators as well as the input power to achieve control. This work is ongoing and illustrates the type of actuators currently under consideration.

The figures that follow are plots of the wave-space mode amplitude excited at 136 Hz for the radial displacement in a cylindrical shell due to different actuator models. The radial motion of the shell wall is the motion that couples with the interior acoustic pressure and is described by a $\sin(m\pi x/\ell) \cos n\theta$ variation. The in-plane motions of the shell only excite an acoustic response by coupling into the radial shell motion. The magnitude is plotted in gray scale normalized to the maximum level for each actuator vs axial mode order m on the horizontal axis and azimuthal order n on the vertical axis. Because the model actuator is geometrically located at the axial center of the cylinder ($x=0.5\ell$), no even axial modes may be excited. This is the reason that all modes with $m=0,2,4,\dots$ are identically zero in the results to follow.

Figure 14a illustrates the modal distribution produced by the bending piezoceramic actuator model. In this model, the actuator does not couple effectively into lower order azimuthal modes. The modes most effectively excited are low order axial modes of azimuthal order greater than 10. This is expected from the theory which shows the primary mode of response for low azimuthal order is an in-plane response rather than the out-of-plane radial response. Preliminary analysis indicates that the bending piezoceramic model couples most effectively with the higher-order axial and circumferential modes. Hence, the bending piezoceramic model may not be effective at low frequencies where the vibro-acoustic environment is dominated by the low-order cylinder modes. For this reason, an in-plane piezoceramic model was also developed.

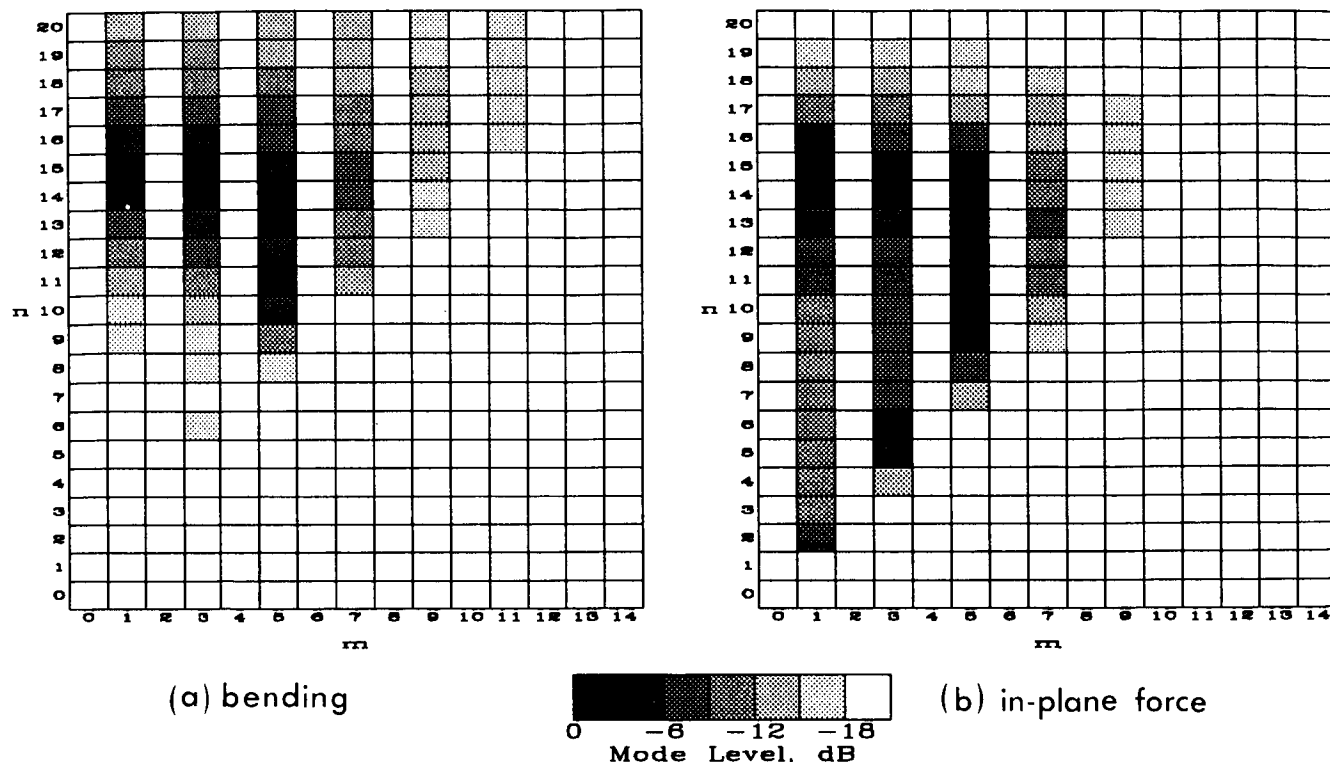


Fig. 14.- Modal amplitude distribution for two source models, $f = 136$ Hz.

Figure 14b shows the modal distribution excited by the in-plane piezoceramic model. The overall levels of the modes are down by a factor of 100 or greater. This is due to the shell being much stiffer in its in-plane response than in its radial or out-of-plane response. The low order azimuthal modes are responding in this case because the in-plane excitation is directly forcing the dominant in-plane response. These results indicate that the in-plane model will couple more readily with the lower order cylinder modes and therefore has the potential of providing better vibration and/or noise reductions at the lower frequencies. However, this is at the cost of reduced excitation efficiency, i.e. more control power is required.

In the above cases, the 63.5mmx38mm actuator subtends an angle of only 4.3° . Initial parametric studies show the bending model can excite lower order azimuthal modes by increasing the dimension of the actuator relative to the circumference of the shell. It is important to be able to excite these low order modes in order to couple effectively into the modes of the primary source that are creating the interior noise. In general, these actuators have been shown to provide effective excitation and by using distributions of tailored actuators, it is expected that effective control may be exercised.

Concluding Remarks

This paper has described an ongoing effort to apply active noise control concepts to affect the noise transmission of composite fuselage models. Results were presented for a built-up composite structure excited in vibration by an external acoustic source representing a propeller. An analysis of the shell response and interior acoustic cavity responses indicate that the noise transmission mechanisms are similar to that of metal construction and are two-fold. First, a resonant shell mode may force an off-resonant acoustic response. For this case, the control system may be designed to best advantage to control the dominant shell response. It may be expected that a minimization of either the shell response or the interior acoustic response will give equally good results. Second, an off-resonant shell mode excites a resonant acoustic mode. In this case, the shell modes most efficiently coupling into the acoustic response must be controlled. In general, the interior acoustic response must be minimized rather than the shell response. Minimizing the vibration response may even give rise to higher interior noise levels. Care must also be exercised in selecting and distributing the actuator elements. Finally, it has been shown that piezoceramic elements are effective transducers with many advantages over conventional force actuators. Additional work is required to model these actuator elements, but progress is being made in understanding the coupling mechanisms involved.

Bibliography

1. Lester, H. C.; and Fuller, C. R.: Active Control of Propeller Induced Noise Fields Inside a Flexible Cylinder. AIAA Journal, Vol. 28, No. 8, pp. 1374-1380, August 1990.
2. Silcox, R. J.; and Lester, H. C.: Propeller Modelling Effects on Interior Noise in Cylindrical Cavities with Applications to Active Noise Control. AIAA Paper No. 89-1123, April 1989.
3. Bullmore, A. J.; Nelson, P. A.; and Elliott, S. J.: Theoretical Studies of the Active Control of Propeller-Induced Cabin Noises. Journal of Sound and Vibration, Vol. 140, No. 2, pp. 191-217, 1990.
4. Silcox, R. J.; Fuller, C. R.; and Lester, H. C.: Mechanisms of Active Control in Cylindrical Fuselage Structures. AIAA Journal, Vol. 28, No. 8, pp. 1397-1404, August 1990.
5. Fuller, C. R.; and Jones, J. D.: Experiments on Reduction of Propeller Induced Interior Noise by Active Control of Cylinder Vibration. Journal of Sound and Vibration, Vol. 112, No. 2, pp. 289-395, 1987.
6. Grosveld, F. W.; and Beyer, T. B.: Modal Characteristics of a Stiffened Composite Cylinder with Open and Closed End Conditions. AIAA paper no. 86-1908, presented at 10th AIAA Aeroacoustics Conference, Seattle, WA, July 9-11, 1986.
7. Elliott, S. J.; Nelson, P. A.; Stothers, I. M.; and Boucher, C.C.: In-Flight Experiments on the Active Control of Propeller-Induced Cabin Noise. Journal of Sound and Vibration, Vol. 140, No. 2, pp. 219-238, 1990.

8. Dorling, C. M.; Eatwell, G. P.; Hutchins, S. M.; Ross, C. F.; and Sutcliffe, S.G.C.: A Demonstration of Active Noise Reduction in an Aircraft Cabin. Journal of Sound and Vibration, Vol. 128, No. 2, pp. 358-360, 1989.
9. Simpson, M.; Luong, T.; Fuller, C. R.; and Jones, J. D.: Full Scale Demonstration of Cabin Noise Reduction Using Active Vibration Control. AIAA paper no. 89-1074, April 1989.
10. Simpson, M. A.; Luong, T. M.; Swinbanks, M. A.; Russell, M. A.; and Leventhall, H.G.: Full Scale Demonstration Tests of Cabin Noise Reduction using Active Noise Control. Proceedings of InterNoise 89, Newport Beach, CA. December 1989, pp. 459-462.
11. Jackson, A. C.; Balena, F. J.; LaBarge, W. L.; Pie, G.; Pitman, W. A.; and Wittlin, G.: Transport Composite Fuselage Technology—Impact Dynamics and Acoustic Transmission. NASA CR 4035, December 1986.
12. Beyer T. B.; and Silcox, R. J.: Noise Transmission Characteristics of a Large Scale Composite Fuselage Model. Presented at AIAA 13th Aeroacoustics Conference, Tallahassee, FL, AIAA paper no. 90-3965, October 22-24, 1990.
13. Dimitriadis, E. K.; and Fuller, C. R.: Piezoelectric Actuators for Distributed Noise and Vibration Excitation of Thin Plates. Proceedings of the ASME 8th Biennial Conference of Failure Prevention and Reliability, pp. 223-233, Montreal, Canada, 1989.
14. Jia, J.; and Rogers, C. A.: Formulation of a Laminated Shell Theory Incorporating Embedded Distributed Actuators. ASME AD-vol. 15 Adaptive Structures, Book No. H00533, 1989.

Long Discontinuous Fiber Composite Structure - Forming and Structural Mechanics^{1*}

R. B. Pipes, M. H. Santare, B. J. O'Toole, A. J. Beaussart, D. C. DeHeer

Department of Mechanical Engineering and the Center for Composite Materials University of Delaware

R. K. Okine

E. I. du Pont de Nemours and Co., Inc.

Abstract

Cost effective composite structure has motivated the investigation of several new approaches to develop composite structure from innovative material forms. Among the promising new approaches is the conversion of planar sheet to components of complex curvature through sheet forming or stretch forming. In both cases the potential for material stretch in the fiber direction appears to offer a clear advantage in formability over continuous fiber systems. In the present study the authors have established a framework which allows the simulation of the anisotropic mechanisms of deformation of long discontinuous fiber laminates wherein the matrix phase is a viscous fluid.

The initial study focuses upon the establishment of micromechanics models for prediction of the effective anisotropic viscosities of the oriented fiber assembly in a viscous matrix. Next, the developed constitutive relation is employed through an analogy with incompressible elasticity to exercise the finite-element technique for determination of local fiber orientation and laminate thickness after forming. Results are presented for the stretch bending of a curved beam from an arbitrary composite laminate and the bulging of a clamped sheet.

Structural analyses are conducted to determine the effect of microstructure on the performance of curved beams manufactured from long discontinuous fiber composites. For the purposes of this study, several curved beams with ideal and non-ideal microstructures are compared for response under pure bending. Material parameters are determined from a separate microstructural analysis.

Micromechanics of Forming

Models for prediction of the effective anisotropic viscosities of an oriented assembly of discontinuous fibers (Figure 1) suspended in a power-law, viscous fluid with finite yield stress have been developed as summarized in Table 1. The present theory for the axial elongational viscosity is compared to a relation for non-dilute suspensions developed by Batchelor [1] in Figure 2. The Batchelor predictions are shown to be restricted to relatively small fiber volume fractions while the present theory was shown to be valid for volume fractions above 0.196. The models for both shearing viscosities are shown to satisfy the bounds at zero and maximum fiber volume fraction.

Results presented in Table 1 show the influence of power-law exponent upon each viscosity term as a function of strain rate. For finite yield stress of the matrix fluid, the effective yield stress of the assembly was determined for the two shearing and two elongational modes of deformation. Only in

^{1*} NASA Contract NAS1-18758 Program Monitor: Dawn Jegley

the case of longitudinal elongational mode did the effective yield stress differ from the matrix yield stress.

Fiber overlap length and geometry have been evaluated for their influence upon the effective elongational viscosity of an oriented fiber array. The results indicate that the developed relations are equivalent for both symmetric and asymmetric overlap geometries as shown in Figure 3. For variation in fiber length and overlap length within the assembly, an integral representation has developed and normalized frequency functions for fiber length and overlap length of zeroth and first order have been evaluated assuming independence of the two frequency distributions. Effective viscosity calculated for typical fiber length data shown in Figure 4 reveal that small percentages in long fibers can have a disproportionately large influence upon results as shown in Figure 5.

Two laminate theories have been developed for the prediction of the effective anisotropic viscosities of oriented discontinuous fiber assemblies suspended in a Newtonian fluid. The first theory is an analogy with classical laminate theory for elastic systems wherein the laminae are constrained to exhibit identical states of strain rate. Results presented in Table 2 for the pseudo laminate theory reveal that the highly anisotropic nature of the oriented fiber lamina is transferred to the laminate behavior. Indeed, laminates were constructed wherein the effective elongational viscosities are several orders of magnitude greater than the effective in-plane shearing viscosity, while other laminates were shown to possess effective in-plane shearing viscosity which greatly exceeded both effective elongational viscosities. The second theory allows individual lamina to be unconstrained by one another. In all the cases presented the values of effective viscosities of the laminates were greater for the constrained condition than for the unconstrained condition as shown in Table 3.

The influence of fiber orientation on elongational viscosity $\eta'_{11}(\theta)$ for the highly anisotropic lamina is shown in Figure 6 as a function of fiber aspect ratio (L/D). These results show that the viscosity of the lamina diminishes by three orders of magnitude for $\theta=1^\circ$ and $L/D = 10,000$. In Figure 7 the expected value of viscosity $\langle\eta_{11}\rangle$ for disoriented fibers is shown. Here the probability of fibers at orientation, θ is equal between $+\theta_1$ and $-\theta_1$. Again note that the apparent viscosity is a strong function of fiber misorientation.

Macromechanics of Forming

Consider the equivalent anisotropic constitutive relationship for the oriented fiber assembly described above in a state of plane stress:

$$\begin{pmatrix} \dot{\epsilon}_{11} \\ \dot{\epsilon}_{22} \\ \dot{\epsilon}_{12} \end{pmatrix} = \begin{pmatrix} \frac{1}{\eta_{11}} & \frac{1}{2\eta_{11}} & 0 \\ \frac{1}{2\eta_{11}} & \frac{1}{\eta_{22}} & 0 \\ 0 & 0 & \frac{1}{2\eta_{12}} \end{pmatrix} \begin{pmatrix} \sigma_{11} \\ \sigma_{22} \\ \sigma_{12} \end{pmatrix} \quad (1)$$

The (3 x 3) matrix in equation 1 can be inverted although the material is incompressible. The reciprocal stress/strain rate relation is

$$\begin{pmatrix} \sigma_{11} \\ \sigma_{22} \\ \sigma_{12} \end{pmatrix} = \begin{pmatrix} C_{11} & C_{12} & 0 \\ C_{12} & C_{22} & 0 \\ 0 & 0 & 2C_{66} \end{pmatrix} \begin{pmatrix} \dot{\epsilon}_{11} \\ \dot{\epsilon}_{22} \\ \dot{\epsilon}_{12} \end{pmatrix} \quad (2)$$

where

$$\begin{aligned} C_{11} &= \frac{4 \eta_{11}^2}{4 \eta_{11} - \eta_{22}} & C_{22} &= \frac{4 \eta_{11} \eta_{22}}{4 \eta_{11} - \eta_{22}} \\ C_{12} &= \frac{2 \eta_{11} \eta_{22}}{4 \eta_{11} - \eta_{22}} & C_{66} &= \eta_{12} \end{aligned} \quad (3)$$

In the present work we have followed the approach used in finite element analysis for viscoplastic forming of metallic material. Two differences between the case of a viscoplastic metal and a reinforced thermoplastic must be noted. First, the constitutive equation is linear for the composite material considered here, while a non-linear model is followed for metal forming to account for the high strain-rate dependence. Each step of the solution scheme is solved in one iteration for the composite material. The linear model is obviously a simplification of the problem. Average values of the anisotropic viscosities must be chosen in the range of values typical for the forming processes considered. The second difference is due to the anisotropy of the composite material. The flow

formulation and the finite-element discretization are perfectly valid for an anisotropic material. However, the fiber orientation change must be taken into account after each stage (time step) of the forming simulation, which corresponds to a small deformation. One can easily imagine that the fiber orientation in a sheet will not keep its initial direction, but will vary locally if the process involves large deformations. The solution scheme for the simulation of the sheet forming of a viscous, anisotropic material is as follows:

- Input: initial geometry and material parameters.
- Simulation:
 1. Solve for the velocity field " V " using the analogy to classical elasticity theory.
 2. Update the geometry by " $V\Delta t$ " where " Δt " is an appropriate time step.
 3. Update the local fiber orientation and the sheet thickness.
 4. Change the boundary conditions if new points come into contact with the mold surface.
 5. Repeat the process until pre-determined deformation is reached or until contact with mold is complete.
- Output at each step: components of stress and strain rate, updated geometry, thickness and fiber orientation distribution.

Implementation of the Plane Stress Formulation

One of the advantages of this method is the possibility of using existing finite element codes developed for elasticity to solve viscous creeping flow problems. Consider the case of the off axis tensile test shown in Figure 8 a. Results for deformed shape after 20 time steps are shown in Figure 8 b and corresponding fiber orientation in Figure 8 c. Consider the next the bending of a flat sheet of unidirectional material (Figure 9). The resulting deformed shape and fiber orientation are shown in Figure 9 b. Finally consider the bulging of a flat plate of 45° fiber orientation subjected to a lateral pressure shown in Figure 10. The results after 20 time steps and after 59 steps are shown in Figures 10 b and 10 c, respectively.

Forming Experiments

Curved C-channel structures have been manufactured from a planar, long discontinuous fiber laminate through a diaphragm forming process. The chosen diaphragm material is a superplastic aluminium alloy 2004. The long, discontinuous fiber laminates consist of a PEKK thermoplastic resin and PAN-based fibers, AS-4, that are approximately 2.2 inches in length.

To insure successful manufacture of the C-channel structure, two molding techniques were employed simultaneously. First, PEI films were placed between the composite and the diaphragm

material to act as a lubricating layer. For added flexibility, the PEI film can be used in joining thermoplastics by means of resistance welding. The second technique was to reduce the composite preform area, thus resulting in less excess material after molding. The size of the composite preform was found to influence the final shape and success of the structure.

The composite was isothermally formed at 390° C and was pressurized at 5 psi/min. (on average) with 5 minute dwells at 20 psi and 150 psi. The maximum pressure of 150 psi was maintained during cooling. Vacuum pressure between the diaphragms was held throughout the process.

The curved C-channel structures were manufactured from 8 ply, unidirectional laminates. Future studies will be performed using various stacking sequences and thicknesses to determine these parameters' effects on microstructure. The resulting components are shown in Figure 11.

Structural Micromechanics

The elastic properties of advanced composite materials depend strongly upon the orientations of the reinforcing components utilized. To better understand the structural performance of discontinuous fiber components the microstructural characteristics of formed parts must be determined. Toward this end, a study was conducted to evaluate two orientation parameters; relative fiber alignment and average fiber orientation.

Ideally, a ply of unformed fibrous composite sheet is unidirectional. However, processing limitations create sheets of the material that are not truly unidirectional. There will be some degree of fiber misalignment in a typical sample of unprocessed material.

During the manufacture of parts with discontinuous fiber material, some microstructural changes occur. The formation of curved components involves the forming of the originally flat material preform over a contoured surface. The fibers in the some portions of the material may tend to align themselves while fibers in other regions may become less aligned during the forming process. The local elastic properties are altered accordingly, producing a material with mechanical characteristics different than those of unformed sheets.

In order to determine the relationship between fiber alignment and mechanical properties, a computer program developed at the University of Delaware's Center for Composite Materials was employed [2]. The Sheet Molding Composites (SMC) program calculates the engineering constants of composite materials from basic input data.

The SMC program utilizes an aggregate model approach that reduces the composite material to a collection of typical reinforcing fiber regions and orientationally averages the properties of these regions. The relative alignment of these regions is described by a value known as Herman's orientation parameter f_p . Completely randomly oriented fibers produce a Herman's orientation of 0, while a value of 1 results from perfectly aligned fibers. In addition to the effective aspect ratio and Herman's orientation, the

program requires the mechanical properties of the fibers and matrix as input. These characteristics include elastic modulus, shear modulus, and Poisson's ratio. Fiber volume fraction of the composite material is also needed.

The parameter f_p is calculated in the following manner. The equation given below defines Herman's orientation as a function of a trigonometric average

$$f_p = 2 \langle \cos^2 \phi \rangle - 1 \quad (4)$$

where

$$\langle \cos^2 \phi \rangle = \int_0^{\pi/2} n(\phi) \cos^2 \phi \, d\phi \quad (5)$$

and ϕ is the orientation of the individual regions. Here $n(\phi)$ is the distribution function that describes the relative number of regions oriented at an angle ϕ with respect to the average fiber orientation. This function can be calculated for a particular sample with a histogram. N is assumed to be the total number of fibers counted and $N(\phi_i)$ is the number of fibers falling within $\phi_i \pm \Delta\phi$ of the average fiber direction. The value $\langle \cos^2 \phi \rangle$ can then be found from the following relation:

$$\langle \cos^2 \phi \rangle = \frac{1}{N} \sum_{i=1}^N N(\phi_i) \cos^2 \phi_i. \quad (6)$$

According to the supplier, the fiber volume fraction of the material samples studied was 0.60. In addition, the fiber length for these samples was given to be approximately 2 in. Using an average fiber diameter of 295 μin , an effective aspect ratio of 6780 was calculated.

An example of the estimation of Herman's orientation is summarized here. A micrograph of unprocessed material was analyzed and the histogram depicted in Figure 12 was obtained. A value of 0.997 was subsequently calculated for the Herman's orientation. Two samples of unprocessed sheet were analyzed, with an average Herman's orientation of 0.994. In addition, five samples of material formed into a spherical shell were examined. An average orientation parameter of 0.995 was found. The calculation of mechanical properties by the SMC program utilized the material parameters of PEKK resin and AS-4 carbon fibers. The relationship between relative fiber alignment and several material

properties is shown in Figure 13. The results show that relative fiber orientation has little effect on elastic properties in these unidirectional discontinuous fiber composites before and after processing.

In parts manufactured using a diaphragm forming process, the average fiber axes are not perfectly aligned with structural axes. Consequently the elastic properties of a given part vary depending upon local fiber orientation. It is necessary to determine structural engineering constants from the material properties of the composite and the average reinforcing fiber orientation. The most direct method of performing the transformation makes use of the compliance matrix of the material. The transformation matrix for the properties in the plane of the material is depicted below:

$$\begin{bmatrix} S_{11} \\ S_{22} \\ S_{12} \\ S_{66} \end{bmatrix} = \begin{pmatrix} m^4 & n^4 & 2m^2n^2 & m^2n^2 \\ n^4 & m^4 & 2m^2n^2 & m^2n^2 \\ m^2n^2 & m^2n^2 & m^4 + n^4 & -m^2n^2 \\ 4m^2n^2 & 4m^2n^2 & -8m^2n^2 & (m^2 - n^2)^2 \end{pmatrix} \begin{bmatrix} S_{xx} \\ S_{yy} \\ S_{xy} \\ S_{ss} \end{bmatrix} \quad (7)$$

Where the 1, 2 subscripts refer to the structural axes (the tangential and radial directions in the case of the curved beam) and the x,y subscripts refer to the material axes (x-being the local average fiber direction). Also $m = \cos \alpha$, $n = \sin \alpha$, and α is the angle between the average fiber axis x and the structural axis 1.

The structural engineering constants may then be determined by the following relations:

$$\begin{aligned} E_1 &= \frac{1}{S_{11}} & E_2 &= \frac{1}{S_{22}} \\ G_{12} &= \frac{1}{S_{66}} & \nu_{12} &= -\frac{S_{12}}{S_{22}} \end{aligned} \quad (8)$$

A typical curved part was manufactured in a diaphragm forming process as described in the previous section. A microstructural analysis was performed to determine the average fiber orientation at a number of points in the curved beam. Equation (8) was then used to calculate the the local material properties relative to the structural axes for use in a structural performance analysis.

Structural Macromechanics

The following analysis compares the relative performance of curved beams with several different microstructures based on a maximum stress failure criterion. The microstructures are chosen to be

representative of different manufacturing procedures. Efficiency of the structure is determined as the ratio of failure load to weight. No attempt was made to include the cost of manufacture or material.

Material heterogeneity is most prevalent in the web section; therefore analysis is conducted for a rectangular cross-section curved beam which represents the web of an I-beam, channel beam, T-beam, etc. Analysis shows that the principal stresses are in the radial and tangential directions for a beam loaded in pure bending and the maximum tangential stress can be several times greater than the maximum radial stress depending on the geometry. This indicates that the efficiency of a beam can be improved by orienting the majority of the fibers in the maximum load direction. Several beams have been produced by diaphragm sheet forming. Preliminary results show that the fiber orientation along the web of these beams is not quite tangential so that the material properties, relative to the beam coordinates, vary along the length of the beam. Figure 14 compares schematically the microstructures of unidirectional and quasi-isotropic curved beams made from stretching a straight beam and diaphragm forming processes with those made from a process which entails cutting a curved pattern out of a flat panel. Both an elasticity analysis and a finite element analysis are conducted to determine the effect of material heterogeneity on the stresses in the beam.

Elasticity Analysis

The analysis is conducted for a curved beam with heterogeneous material properties loaded in pure bending. Figure 15 shows the geometry of a beam loaded in pure bending where a and b are the inside and outside radii, r and q are the radial and tangential coordinates, M is the applied moment, R is the average beam radius, $R = (a + b)/2$, t is the beam depth and d is the distance from the beams centroidal axis. An important geometric parameter is the average radius to depth ratio, R/t .

The analytical solution is based on an elasticity approach similar to that found in Lekhnitskii [3] with the only difference being that the constitutive relation allows for material property variation in both the radial and tangential directions. The analysis is conducted by expressing the radial, tangential and shear stresses in terms of a stress potential, F . The details of this analysis can be found in [3] but the constitutive relation used here is

$$\epsilon_{ij} = a_{ik} \sigma_{kj}, \quad (9)$$

where

$$a_{ik} = \alpha_{ik} \cos(k \theta) r^{-n}$$

and a_{ij} are the elements of the compliance matrix, α_{ij} are the homogeneous material property base values of a_{ij} , r is the radius, and n and k are the degrees of heterogeneity in the radial and tangential directions respectively. The sign of n determines whether the beam is stiffer on the inside or the outside

radius; a negative value of n represents a beam which is stiffer on the inside, and a positive value of n represents one which is stiffer on the outside. Tangential heterogeneity can be represented by adjusting the value of k to match the frequency of the fiber waviness.

Finite Element Analysis

A linear finite element model is used to verify the results of the elasticity analysis. The model consists of 300 four node quadratic elements where the properties are input for each element to handle the material heterogeneity. The pure bending boundary conditions are applied by distributing the appropriate normal loads at the nodes along the straight edges. The results are within 8 % of the analytical results from the elasticity analysis.

Results

Stresses in the curved beams are affected by the geometry of the beam as well as the material heterogeneity. Figure 16 shows the relative shape of several beams with different radius to depth ratios, R/t . An R/t ratio of 25 or greater is typical of the curved beams used as primary structures in an aircraft fuselage. Figure 17 shows the effect of radial heterogeneity on the maximum radial stress for several different R/t values. The degree of radial heterogeneity, n , is varied from -2 to 2, where an n value of -2 corresponds to a 20% drop in stiffness from the inside radius to the outside and an n value of +2 corresponds to a 20% increase in stiffness. Figure 17 shows that for a radius to depth ratio of 1.0, the maximum radial stress is affected greatly by the value of n , but for an R/t value greater than 10.0, the degree of radial heterogeneity has no effect on the maximum radial stress. Figure 18 shows similar results for the effect of n on the maximum tangential stress. The degree of tangential heterogeneity, k , was found to have no effect on the stresses in the beam, but does have an effect on the deflection as well as the failure of the beam.

Maximum Stress Failure Analysis

The maximum stress failure criterion is used to compare the performance of beams made with the microstructures shown in Figure 14. The maximum tensile, compressive and shear stresses are determined for the beam and are compared to the corresponding ultimate loads of the material. The maximum moment to failure is determined by increasing the applied moment until one of the stresses exceeds the corresponding ultimate load. The moment to failure is determined for a beam with an inside radius of 3.5 inches, an outside radius of 4.5 inches and an included angle of 90° .

Several different unidirectional microstructures are compared; the first has tangentially oriented fibers, the second is the curved beam cut from a straight unidirectional panel, and the third has curved fibers, but not the same curvature as the beam. Data for this microstructure was taken from a part

produced by diaphragm forming. A beam with patchwork tangentially oriented fibers is also compared to the unidirectional microstructures. Two quasi-isotropic microstructures are also compared, one with axisymmetric fiber orientation as obtained from stretching a straight beam and another which represents a curved pattern cut from a quasi-isotropic panel. The analysis is conducted for an 8-ply lay-up so that the weight of all microstructures is the same. Table 4 compares the moment to failure of the different microstructures as well as the maximum deflection for a unit load. Unidirectional beams with non-tangentially oriented fibers result in considerable reduction of the moment to failure and a considerable increase of the maximum deflection. The two quasi-isotropic microstructures have virtually the same moment to failure and maximum deflection.

Conclusions

This paper briefly outlines a series of analyses that can be used to predict structural performance from basic processing information and material preform design for long discontinuous fiber thermoplastics. This information is important to the material manufacturer and the process designer as well as the structural designer. Although much needs to be added, these tools represent the basis for a truly integrated design methodology for composite structures.

References

1. G. K. Batchelor, "The Stress Generated in a Non-dilute Suspension of Elongated Particles by Pure Straining Motion," Journal of Fluid Mechanics, Vol. 46, part 4, 1971, pp. 813-829.
2. R. L. McCullough, G. J. Jarzebski, S. H. McGee, "Constitutive Relationships for Sheet Molding Materials," The Role of the Polymeric Matrix in the Processing and Structural Properties of Composite Materials," Plenum Press, New York, N. Y., (1983).
3. S.G. Lekhnitskii, Theory of Elasticity of an Anisotropic Body, Mir Publishers, Moscow, 1981

Table 1. Summary of Property Predictions

Term	Newtonian Fluid	Power-Law Fluid
η_{11}/η	$\frac{f}{2} \left[\frac{\sqrt{\bar{f}}}{1-\sqrt{\bar{f}}} \right] (L/D)^2$	$2^{-m} f \left[\frac{\sqrt{\bar{f}}}{1-\sqrt{\bar{f}}} \right]^m (L/D)^{m+1} \dot{\epsilon}_1^{m-1}$
η_{12}/η	$\frac{1}{2} \left[\frac{2-\sqrt{\bar{f}}}{1-\sqrt{\bar{f}}} \right]$	$2^{-m} \left[\frac{2-\sqrt{\bar{f}}}{1-\sqrt{\bar{f}}} \right]^m \dot{\gamma}_{12}^{m-1}$
η_{23}/η	$\left[1-\sqrt{\bar{f}} \right]^{-1}$	$\left[1-\sqrt{\bar{f}} \right]^{-m} \dot{\gamma}_{23}^{m-1}$
η_{22}/η	$4 \left[1-\sqrt{\bar{f}} \right]^{-1}$	$4 \left[1-\sqrt{\bar{f}} \right]^{-m} \dot{\epsilon}_2^{m-1}$
η_{23}/η_{12}	$2 \left[2-\sqrt{\bar{f}} \right]^{-1}$	$2^m \left[2-\sqrt{\bar{f}} \right]^{-m}$
η_{11}/η_{22}	$2^{-3} f \bar{f}^{-1/2} (L/D)^2$	$2^{-(m+2)} f \bar{f}^{-m/2} (L/D)^{m+1}$

Table 2. Apparent Laminate Viscosities, Laminate Theory

Laminate	$\bar{\eta}'_{11}/\eta$	$\bar{\eta}'_{22}/\eta$	$\bar{\eta}'_{12}/\eta$	$\bar{\lambda}'_{12}$	$\bar{\lambda}'_{21}$
$[0/90]_s$	1.04×10^6	1.04×10^6	4.48	1.52×10^{-5}	1.52×10^{-5}
$[0/\pm 45]_s$	6.96×10^5	2.32×10^5	3.48×10^5	1.0	3.33×10^{-1}
$[0/\pm 45/90]_s$	6.96×10^5	6.96×10^5	2.61×10^5	3.33×10^{-1}	3.33×10^{-1}
$[\pm 45]_s$	1.79×10^1	1.79×10^1	5.22×10^5	1.0	1.0

$$f = 0.6$$

$$L/D = 1000$$

$$\eta_{11}/\eta = 2.09 \times 10^6$$

$$\eta_{22}/\eta = 3.18 \times 10^1$$

$$\eta_{12}/\eta = 4.48$$

$$\mu_{11}/\eta = 2.09 \times 10^6$$

$$\mu_{12}/\eta = 1.59 \times 10^1$$

$$\mu_{22}/\eta = 3.13 \times 10^1$$

$$\mu_{66}/\eta = 4.48$$

Table 3. Constrained (LPT) and Unconstrained (UCT) Laminate Theory Results

Laminate	$\bar{\eta}'_{11}/\eta$ LPT UCT		$\bar{\eta}'_{22}/\eta$ LPT UCT		$\bar{\eta}'_{12}/\eta$ LPT UCT	
$[0/90]_s$	1.04×10^6	1.04×10^6	1.04×10^6	1.04×10^6	4.48	4.48
$[0/\pm 45]_s$	6.96×10^5	6.96×10^5	2.32×10^5	2.10×10^1	3.48×10^5	2.26×10^1
$[0/\pm 45/90]_s$	6.96×10^5	5.22×10^5	6.96×10^5	5.22×10^5	2.61×10^5	1.81×10^1
$[\pm 45]_s$	1.79×10^1	1.57×10^1	1.79×10^1	1.57×10^1	5.22×10^5	3.17×10^1

Table 4. Microstructural Comparison of Beams Loaded in Pure Bending

Fiber Orientation	Moment to Failure	Maximum Deflection
Unidirectional Tangential	1.00	1.00
Unidirectional Cut-out	0.39	1.14
Unidirectional Non-tangential	0.46	1.09
Unidirectional Patchwork	0.70	1.36
Quasi-isotropic axisymmetric	1.00	1.00
Quasi-isotropic Cut-out	0.97	1.00

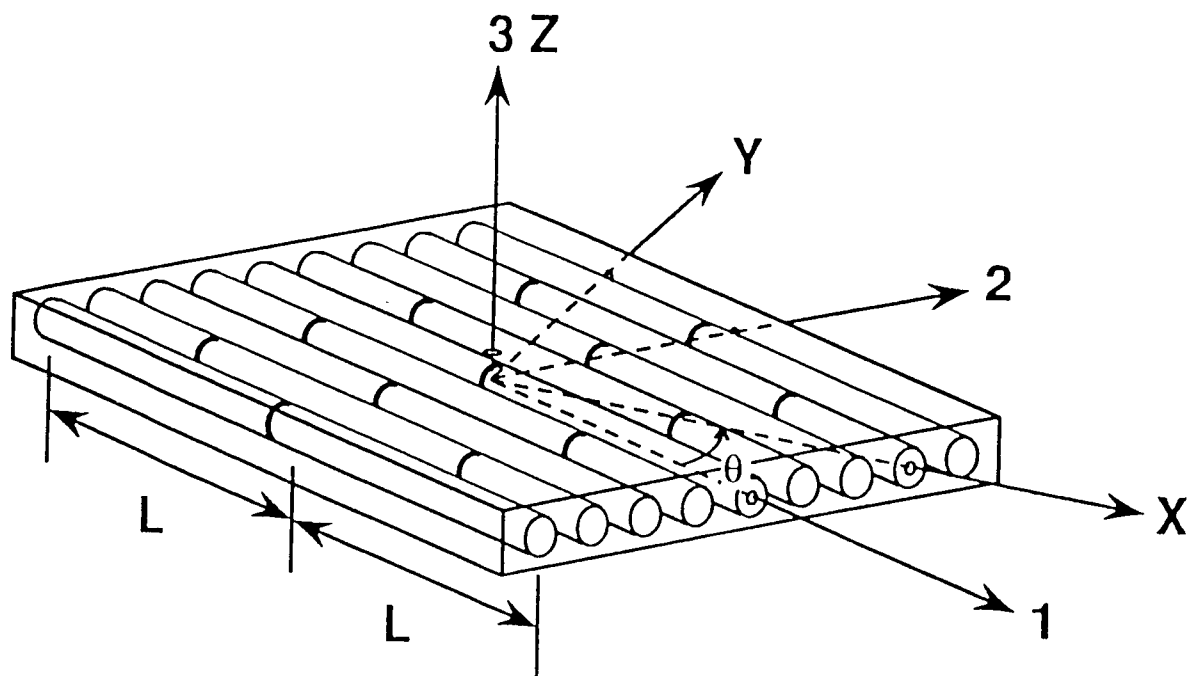


Figure 1. Oriented Fiber Assembly

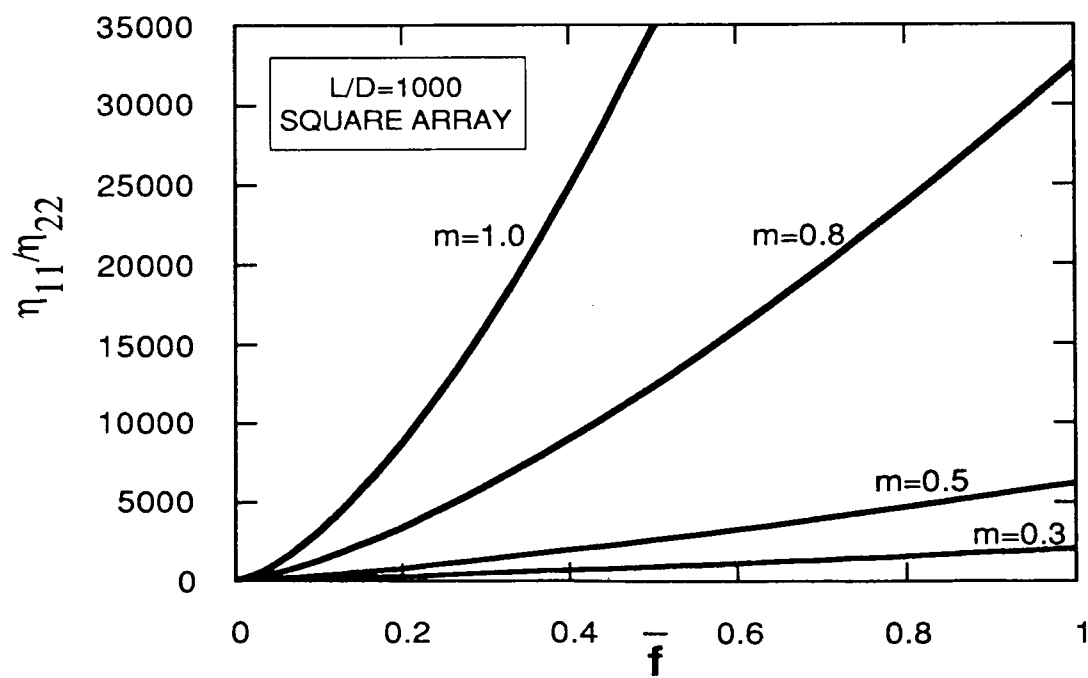


Figure 2. Ratio of Axial and Transverse Elongational Viscosities

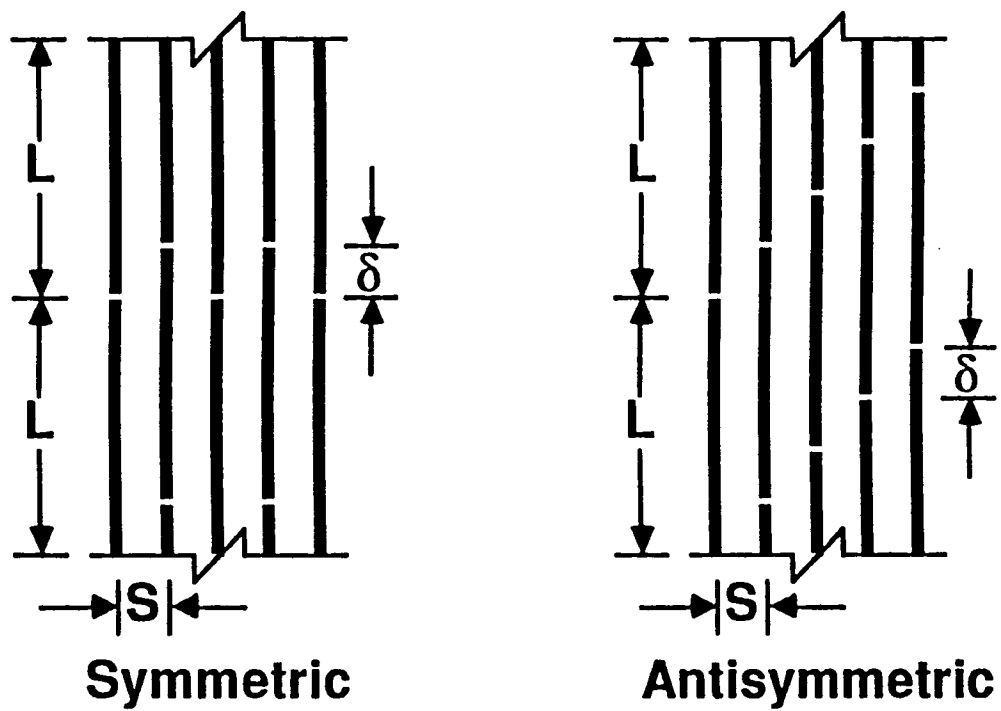


Figure 3. Overlap Length Geometry

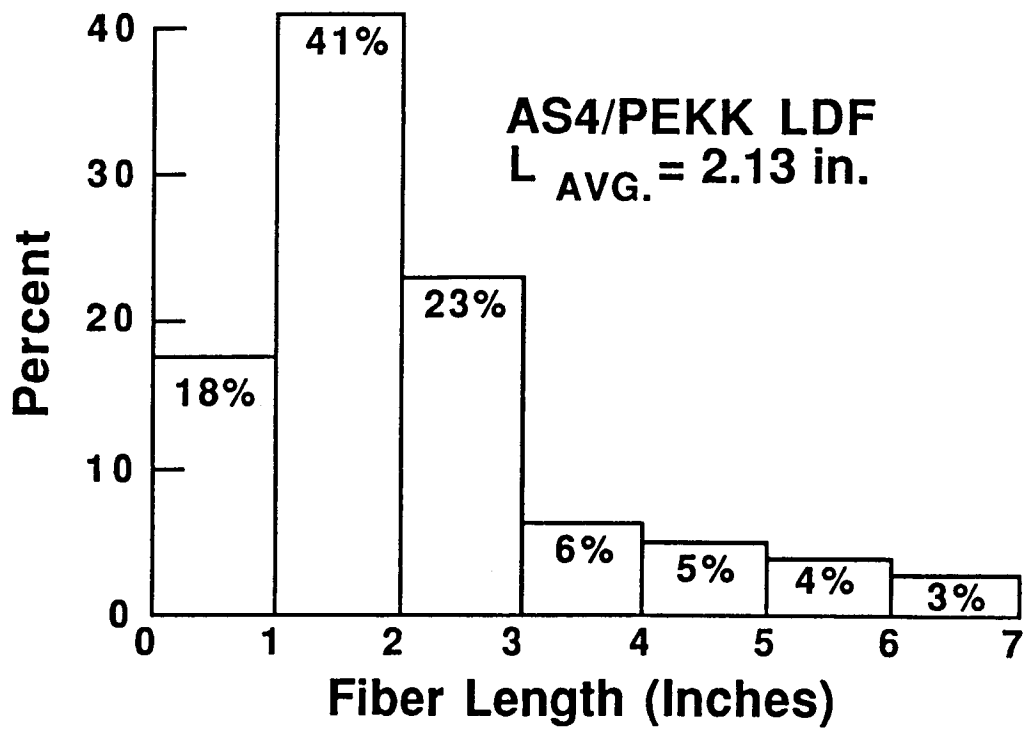


Figure 4. Fiber Length Distribution

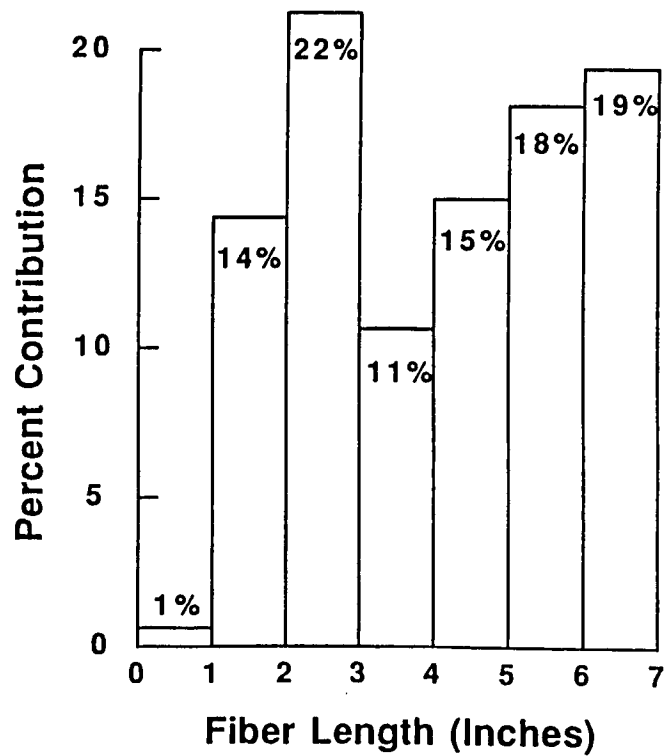


Figure 5. Fiber Length Contribution to Effective Viscosity

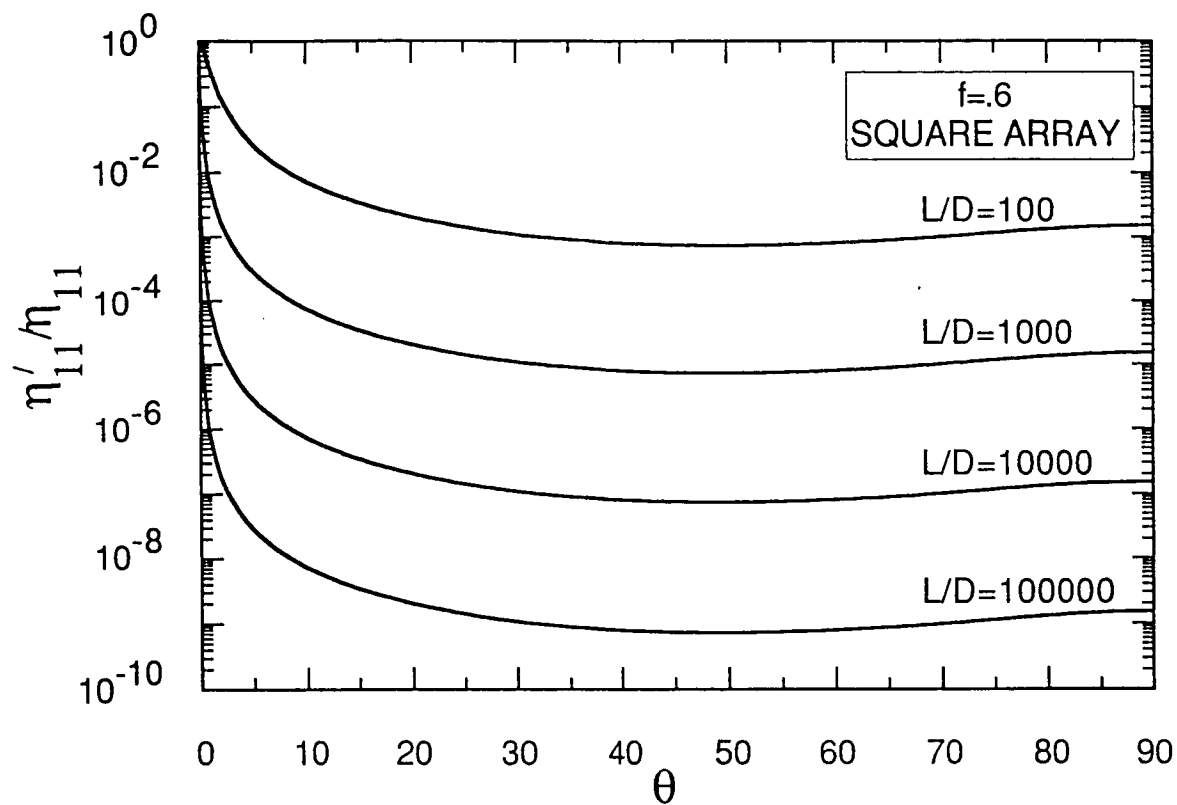


Figure 6. Influence of Fiber Orientation on Elongational Viscosity

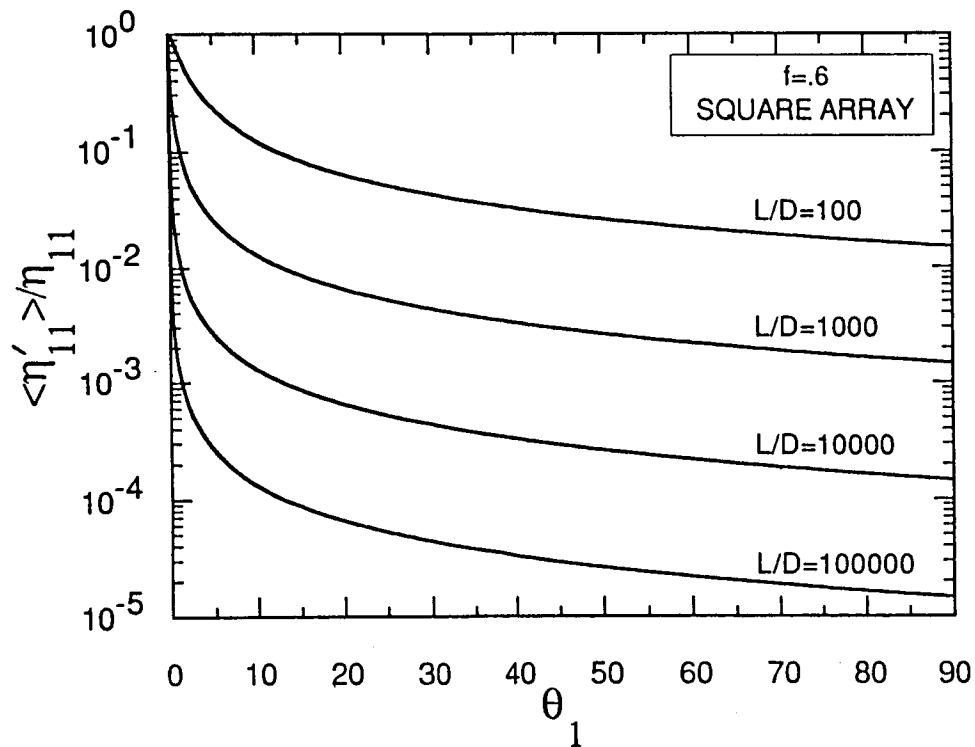


Figure 7. Effect of Orientation Distribution on Elongational Viscosity

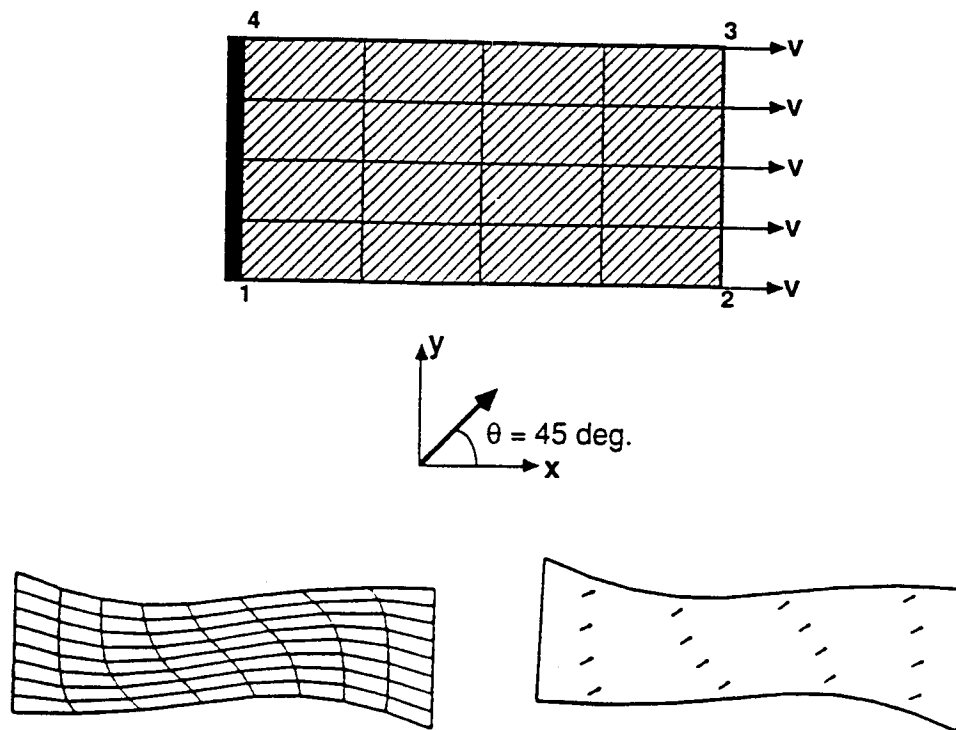


Figure 8. Off Axis Tension Test a) Problem Geometry b) Deformation After 20 Time Steps c) Fiber Orientation After 20 Time Steps

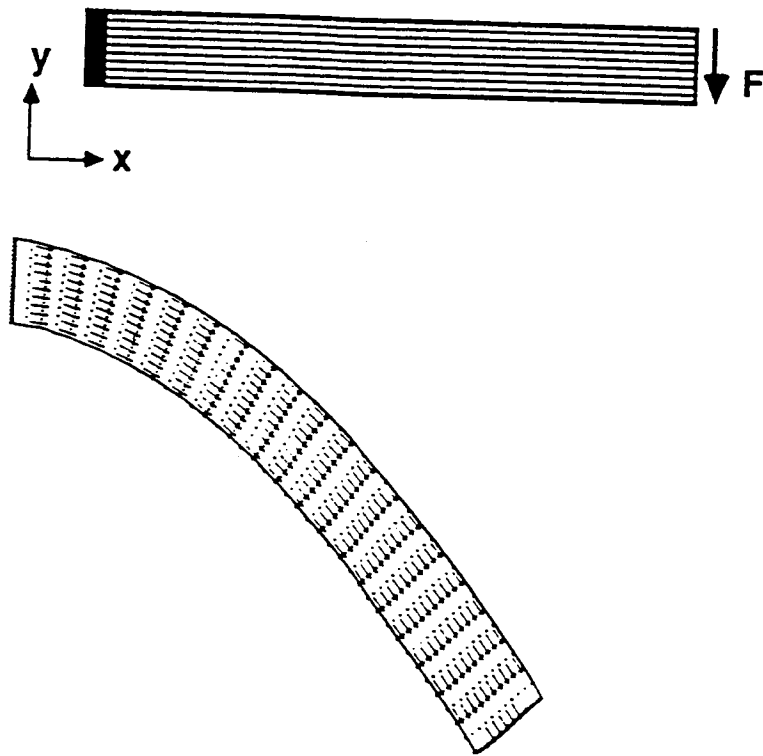


Figure 9. Bending of a Sheet of Unidirectional Material a) Problem Geometry b) Deformed Geometry

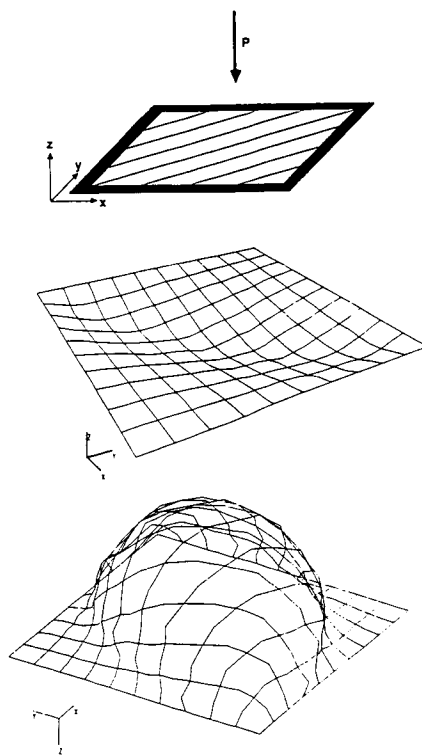


Figure 10. Bulging of a Clamped Sheet a) Problem Geometry b) Deformation After 20 Time Steps c) Deformation After 59 Time Steps

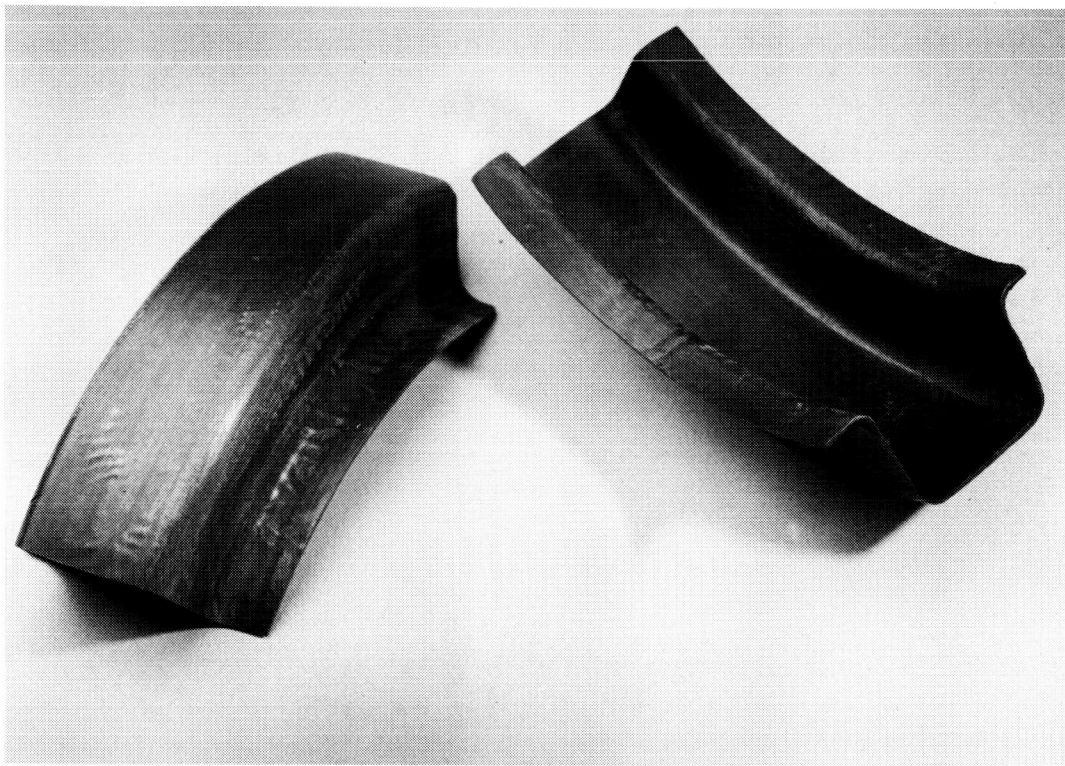


Figure 11. Diaphragm Formed Curved Beams

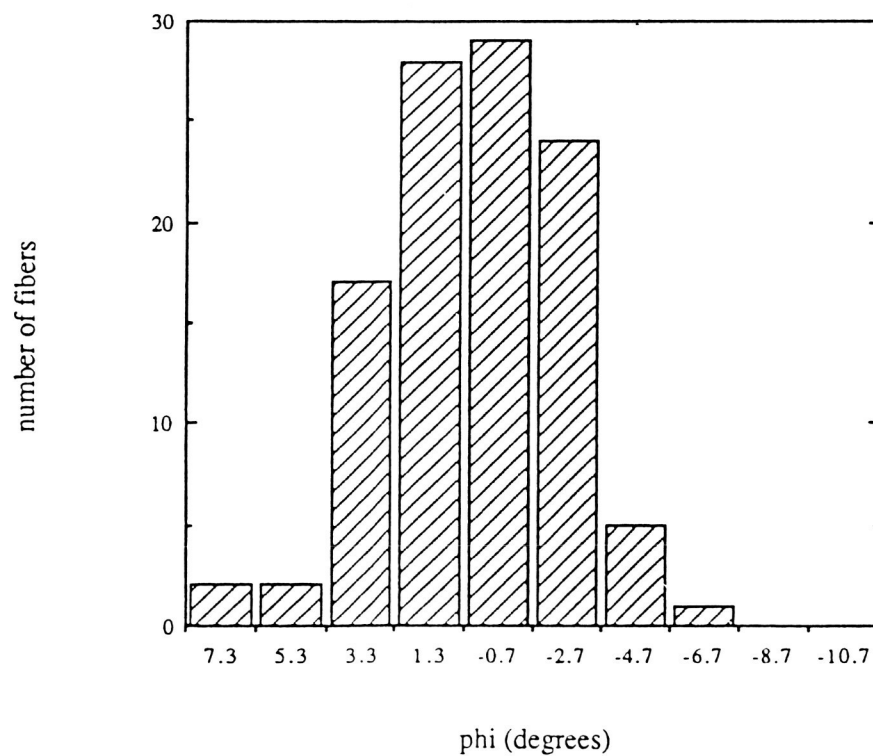


Figure 12. Fiber Orientation Histogram of Processed Material

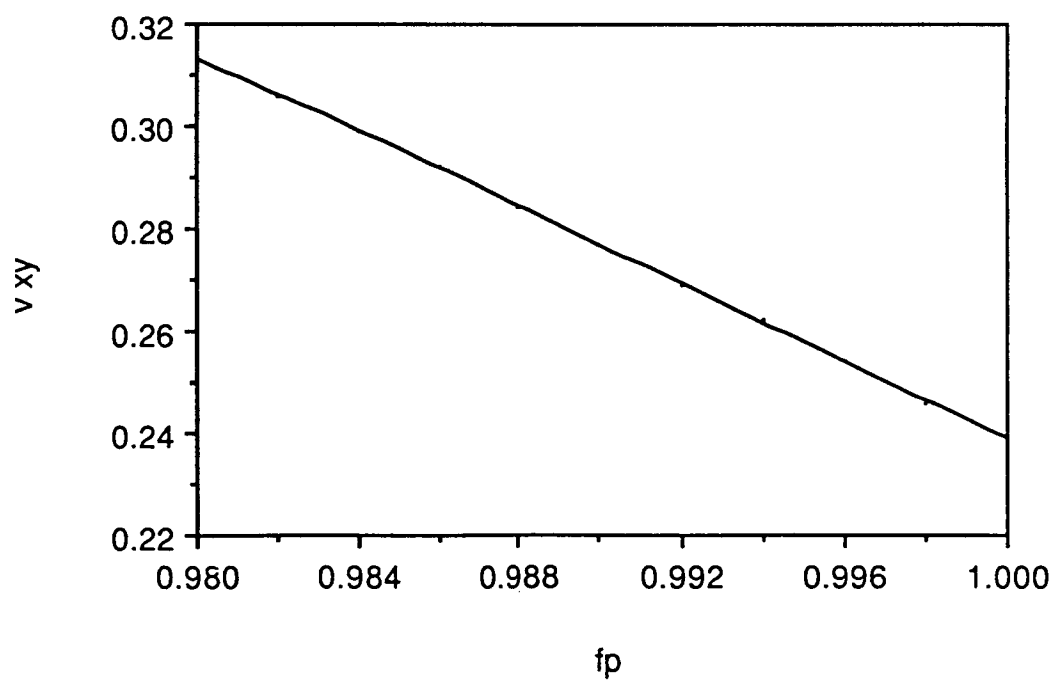
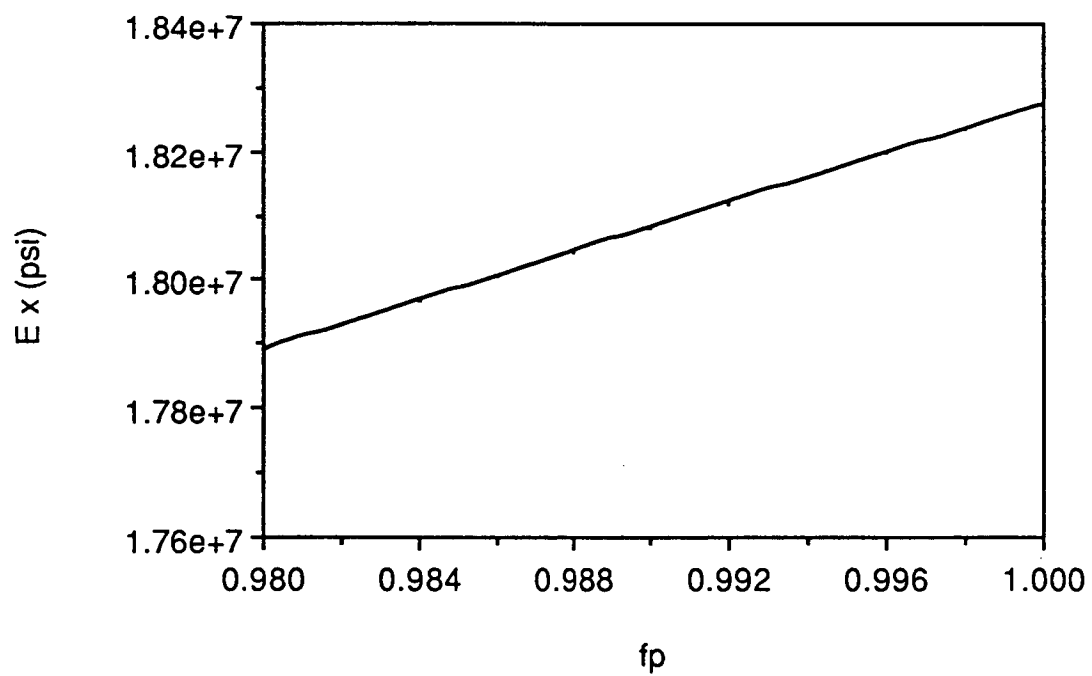


Figure 13. Material Properties vs. Relative Fiber Alignment

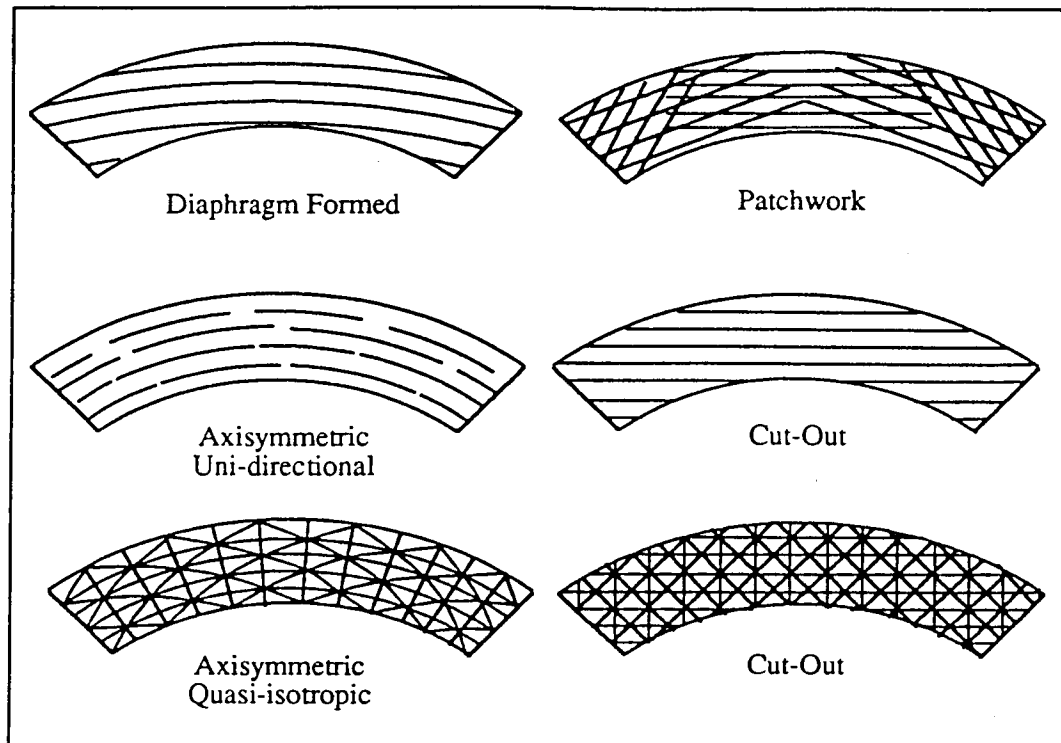


Figure 14. Comparison of Beam Microstructures

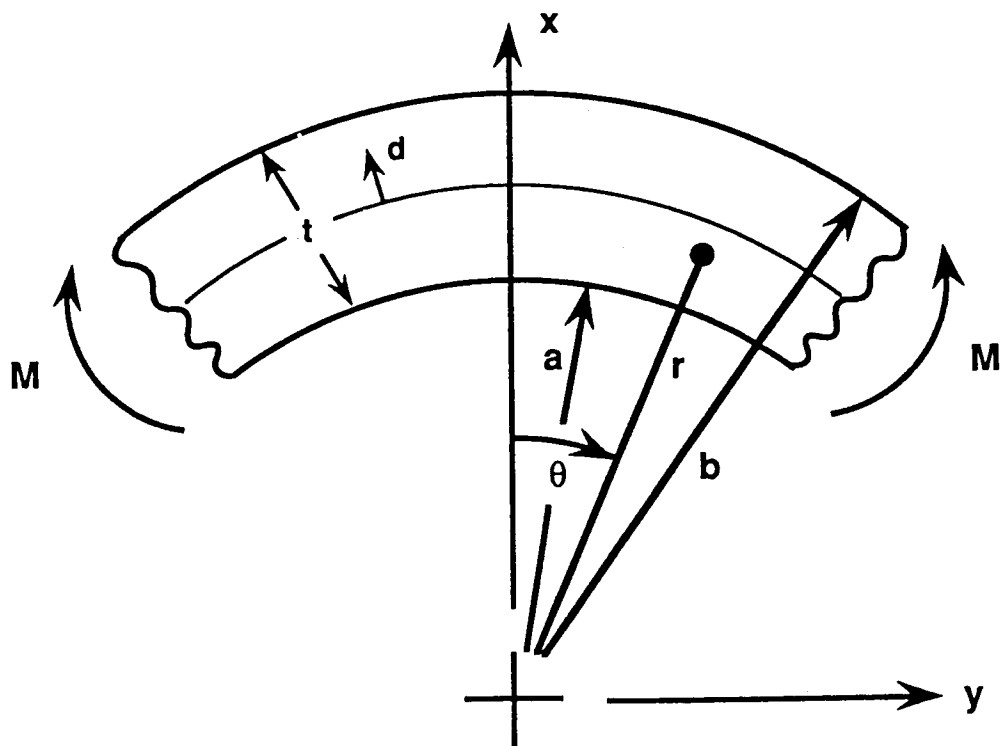


Figure 15. Pure Bending Load Case

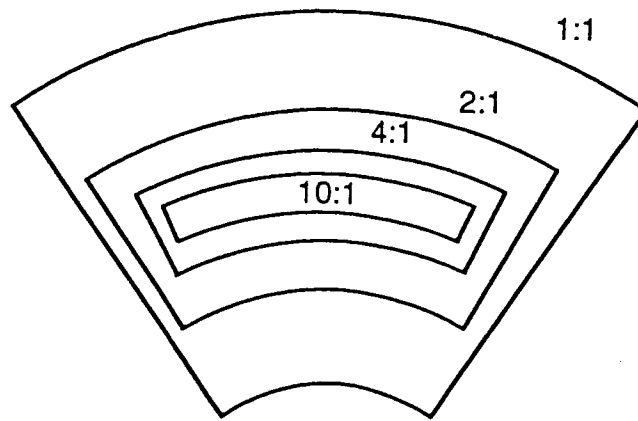


Figure 16. Comparison of Several Different Beam Geometries

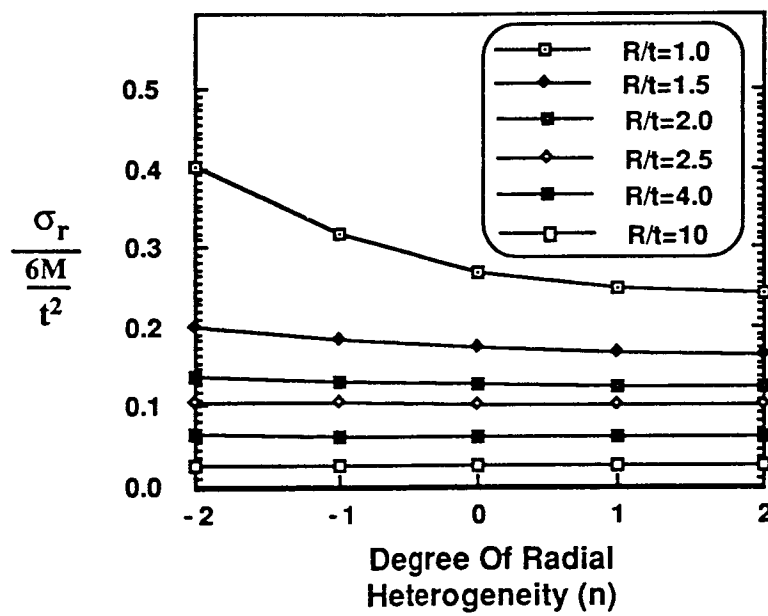


Figure 17. Maximum Radial Stress vs. Degree of Radial Heterogeneity

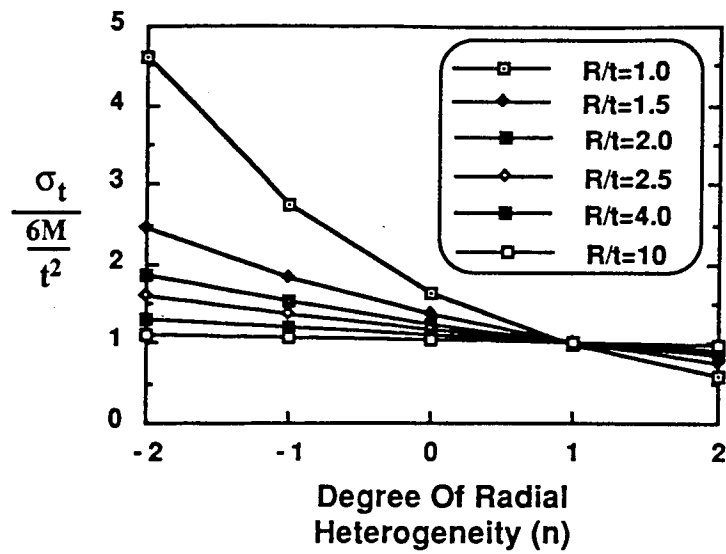


Figure 18. Maximum Tangential Stress vs. Degree of Radial Heterogeneity

**RESIN TRANSFER MOLDING
for
ADVANCED COMPOSITE
PRIMARY AIRCRAFT STRUCTURES**

**Alan Markus and Ray Palmer
Douglas Aircraft Company**

INTRODUCTION

Resin Transfer Molding (RTM) has been identified by Douglas Aircraft Company (DAC) and industry to be one of the promising processes being developed today which can break the cost barrier of implementing composite primary structures into a commercial aircraft production environment. The following paper will discuss the RTM process developments and scale-up plans Douglas Aircraft will be conducting under the NASA ACT Contract.

PROCESS DESCRIPTIONS

Resin Transfer Molding at Douglas Aircraft consists of two distinct methods of resin impregnation: 1.) Vacuum infusion and 2.) Pressure injection.

Figure 1 below describes the two forms of vacuum resin infusion being developed at Douglas. First is resin film infusion, in which a resin (film) is placed on the tool, the preform is placed over the resin, the entire assembly is vacuum bagged and oven cured according to the proper cure cycle for that resin system. The second form of infusion is liquid resin infusion. In this method, instead of placing the resin film on the tool, a porous distribution manifold is placed on the tool to allow the liquid resin to infuse the preform. As with the film infusion method, the entire assembly is vacuum bagged at 30 in mercury and cured at 350 degrees in an oven. (Note: Hard tooling can and often is used in place of vacuum bag.)

PROCESS DEVELOPMENT

VACUUM IMPREGNATION

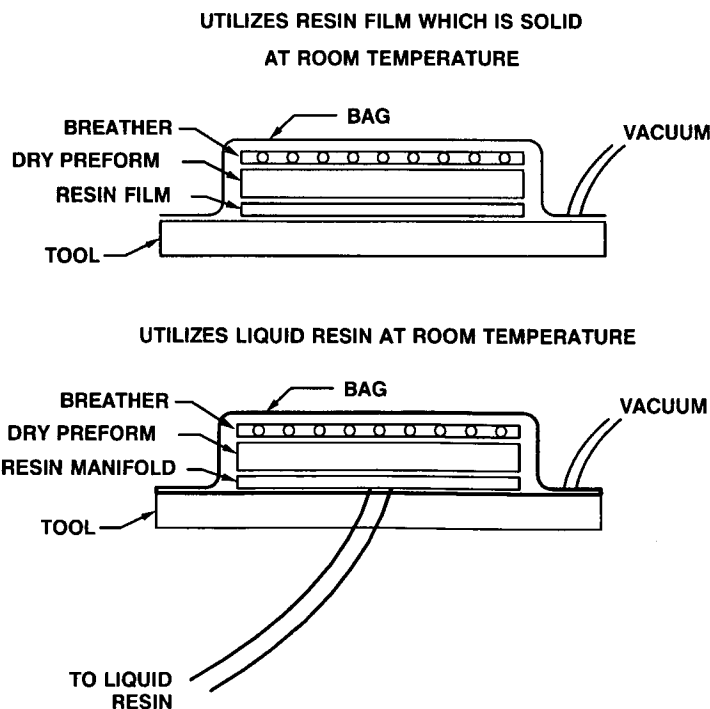


Figure 1

PROCESS DESCRIPTIONS

The second form of Resin Transfer Molding is pressure injection. As described in Figure 2 below, this process transfers liquid resins through a mix chamber into a compacted stitched preform contained within a matched metal tool. The tooling for this process is usually self-heated and requires some type of press or restraining fixture.

In the Douglas RTM development, the resin injection port is located at the center of the part allowing resin to flow directly into the preform, while venting occurs at locations deemed necessary by preform geometry (resin pressure of 40 psi is desirable). In the case of flat panels, venting usually occurs at each corner.

This type of process is currently being implemented into many automobile prototype manufacturing facilities.

PRESSURE IMPREGNATION

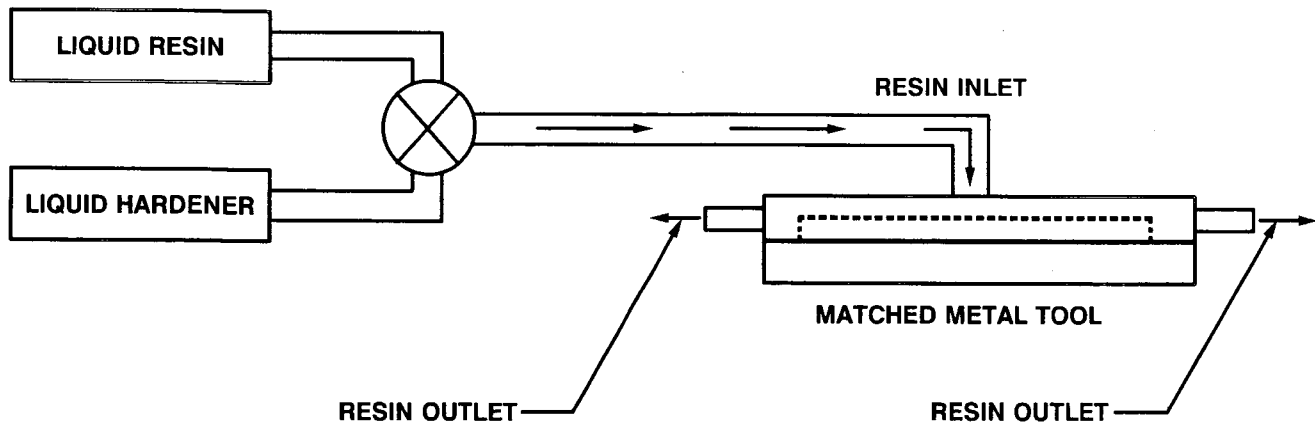


Figure 2

PROCESS OBJECTIVES

The objectives of Douglas' RTM development is to 1.) Exploit the benefits of RTM to maximum potential, 2.) Become cost competitive. Below is a list of the primary benefits RTM offers as a process (Figure 3).

RTM/STITCHING BENEFITS

LOW-COST MATERIAL SYSTEM (WITH PREMIUM DAMAGE TOLERANCE)

REDUCED ASSEMBLY COSTS (DUE TO STITCHING)

SHORTER PROCESS CYCLES

BUILT-IN QUALITY (REDUCED QUALITY INSPECTION COSTS)

GREATER CONTROL OF DIMENSIONAL ACCURACY

REDUCED FABRICATION COSTS (CUTTING, LAY-UP, PROCESSING)

INHERENT STRUCTURAL QUALITY

Figure 3

PROCESS OBJECTIVES

If all benefits of the RTM process are realized, significant advances can be made in the application of composite primary structure to commercial aircraft. Those benefits of most importance in leading to application are primarily cost related. Figure 4 below compares the Douglas funded 8' x 12' wing box fabricated with conventional materials and methods versus the NASA funded 8' x 12' wing box to be made by RTM. If full advantage of the stitching process can be realized, (stitching rib clips to skin) a cost savings of 48% is projected over the conventional box being fabricated by Douglas.

During wing box fabrication, detailed data will be compiled on material and labor costs. This data will provide a direct comparison between conventional and advanced composites fabrication. Obviously, a major issue is the cost of composite wing structure versus the cost of conventional aluminum construction. Attempts are underway to define aluminum costs at the wing box level. Another approach will involve wing cost models to project composite wing box costs to full scale wing structures.

RECURRING COSTS FOR 8 X 12 TEST BOX

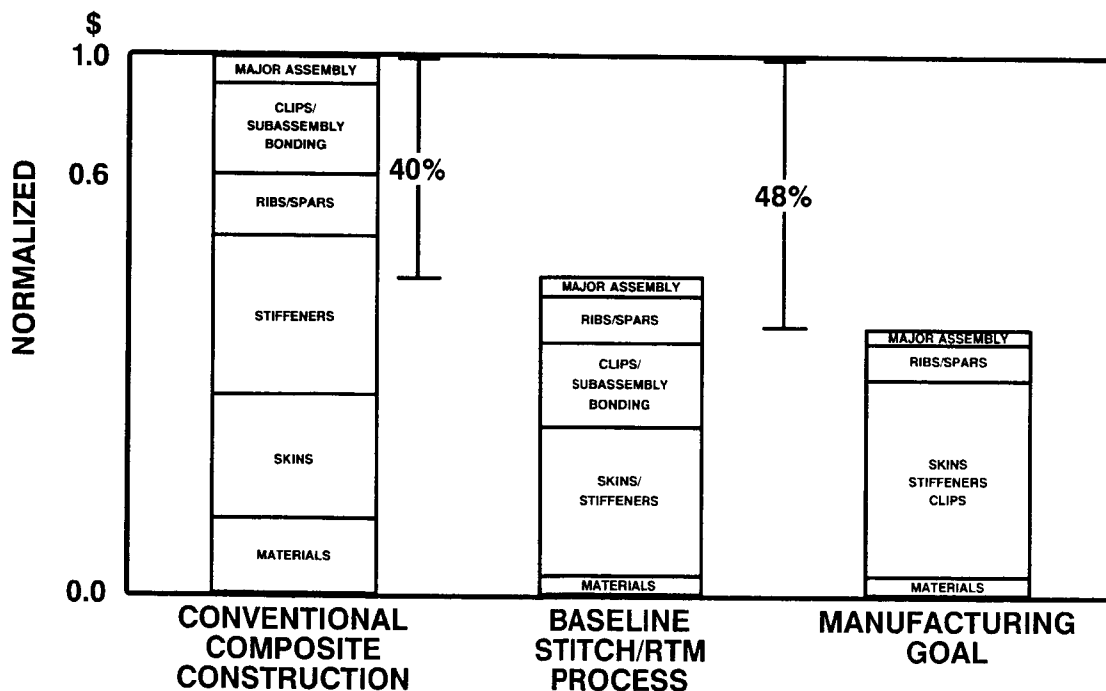


Figure 4

**MANUFACTURING DEVELOPMENT
for
COMPOSITE PRIMARY WING STRUCTURES**

WING SUB-SCALE TOOLING DEVELOPMENT

Effect of Preform

In developing a manufacturing strategy for the Douglas wing effort, it became clear that vacuum infusion with heavy density stitched preforms was a natural for this structure. The heavy density stitching gives the damage tolerance needed as well as the compaction necessary to utilize the vacuum impregnation minimum pressure process. Below in Figure 5, compaction studies run at Douglas indicate that the stitched preform gives 92% of what full compaction would be for 60% fiber volume. The real benefit of this is that the tooling for the structure can be greatly simplified. In fact, tooling is basically used for part volume definition only since no compaction or movement is required.

WING ELEMENT TOOLING DEVELOPMENT

EFFECT OF HEAVY DENSITY STITCHING ON TOOLING DEVELOPMENT

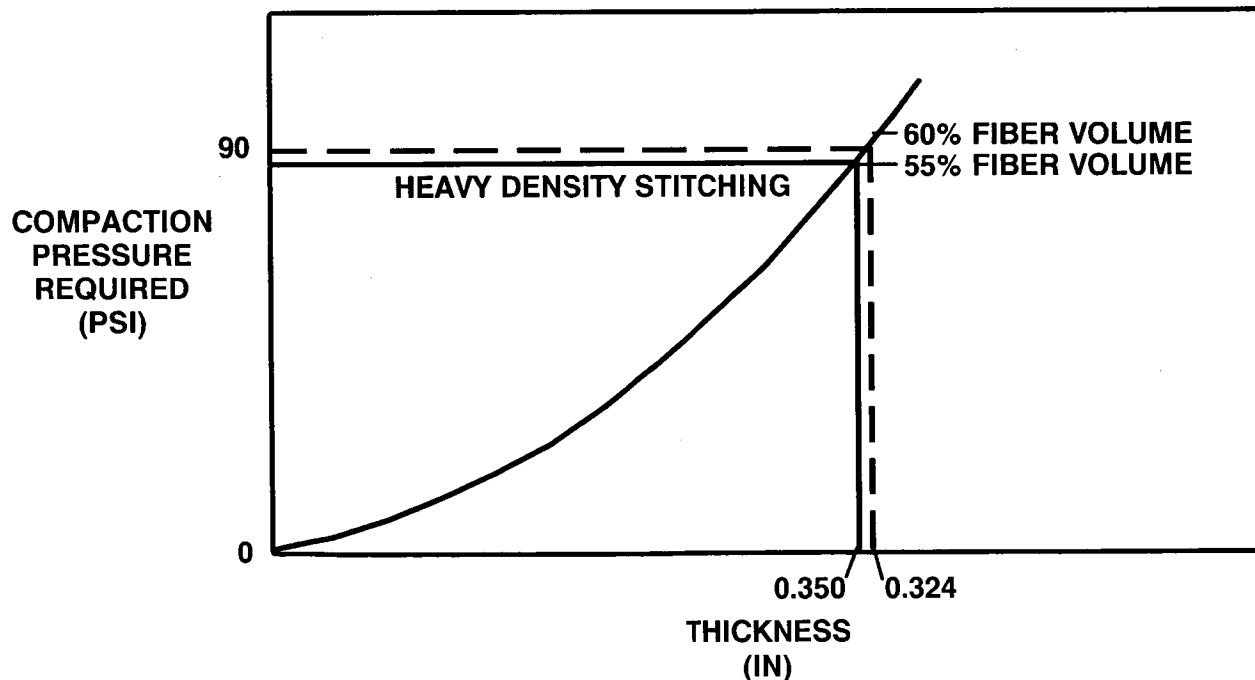


Figure 5

WING SUB-SCALE TOOLING DEVELOPMENT Tool/Process Definition

Douglas tooling for three stringer element wing panels is currently set up for both film resin infusion and liquid resin infusion. In Figure 6, on the left is a schematic of the film infusion tooling. As with the flat panel tool, the resin film is first placed on the tool, the preform and mandrels are then placed on the resin, and the entire assembly is bagged and cured according to the proper resin cure cycle. (Note: The current method of processing with 3501-6 film resins requires the use of an autoclave to insure proper wet-out.) In Figure 6 (right), the liquid vacuum infusion method is illustrated. In this case, the resin film is replaced with a porous distribution manifold that allows the liquid resin to uniformly permeate the preform. Once resin infusion is complete, the entire assembly is allowed to cure under vacuum bag pressure and oven heat only. (It should be noted that this tooling currently uses rubber expansion for compaction between stiffeners. In future tooling, this will not be necessary. Also, rigidized periphery tooling can be used in place of vacuum bag to hold tolerances of preform.)

WING ELEMENT TOOLING DEVELOPMENT

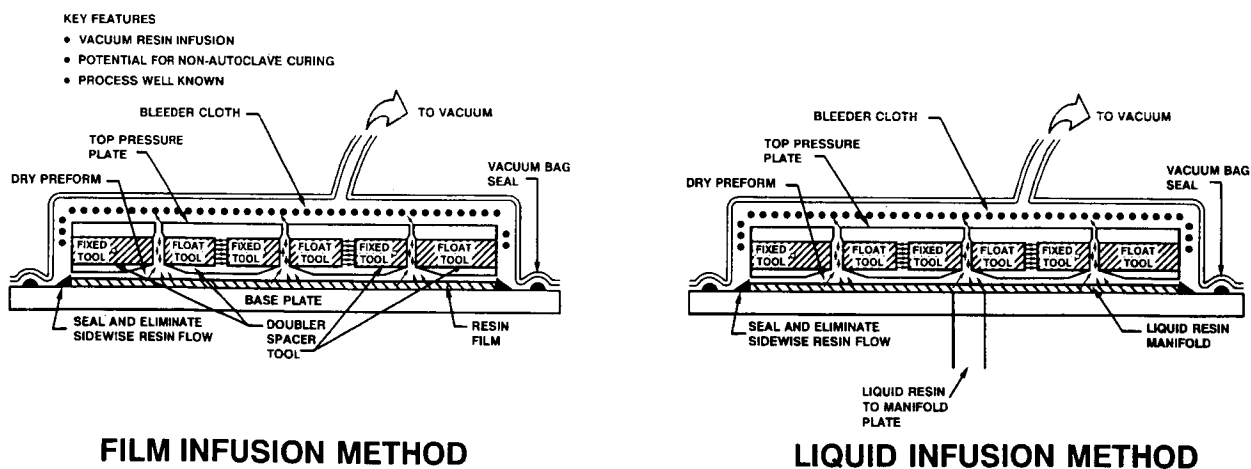


Figure 6

WING SUB-SCALE TOOLING DEVELOPMENT

Douglas Wing Vacuum Infusion Tool

Below in Figure 7 are photos of the preforms and tooling for wing element work. On the upper left is a heavy density stitched 3 blade wing element preform ready for resin infusion. Below to the right is the matched metal aluminum tooling assembled on the preform before vacuum bagging the assembly.

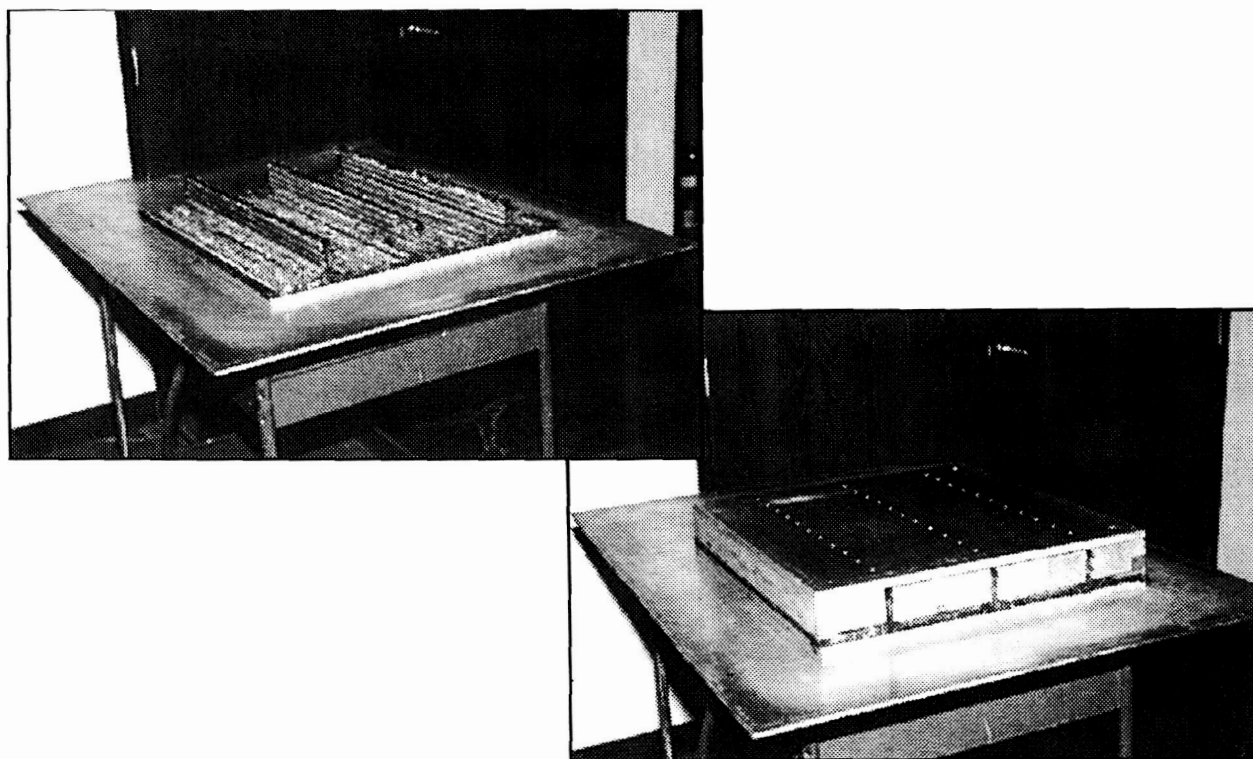


Figure 7

WING SCALE-UP TOOLING DEVELOPMENT

In scale-up of the vacuum infusion process, Douglas will select between liquid and film resin infusion. To date, the infusion process performs better with liquid resins rather than the film resins. However from a tooling scale-up perspective, the film resins are preferable. To utilize a film resin, it appears that a viscosity profile should be maintained well below 250 centipoise at 250 degrees F or below for between one and two hours.

In using such a film resin, the vacuum infusion tooling and process have a significant advantage in that both are currently well defined for scale-up. The primary development necessary is in selecting tool materials that satisfy classical tooling concerns (i.e., coefficient of thermal expansion, thermal mass/weight and cost.) The three Douglas concepts evaluated are shown in Figure 8. In evaluating each concept, expansion control for scale-up and cost were driving factors. The tooling concept selected by Douglas is the aluminum/graphite combination. While this aluminum/graphite concept is approximately 14% more costly than the all aluminum tool, the benefits in tooling tolerance control and scale-up outweigh the small cost penalties.

TOOLING CONCEPTS EVALUATED

VACUUM IMPREGNATION OF WING SCALE-UP ISSUES (SUBCOMPONENT)

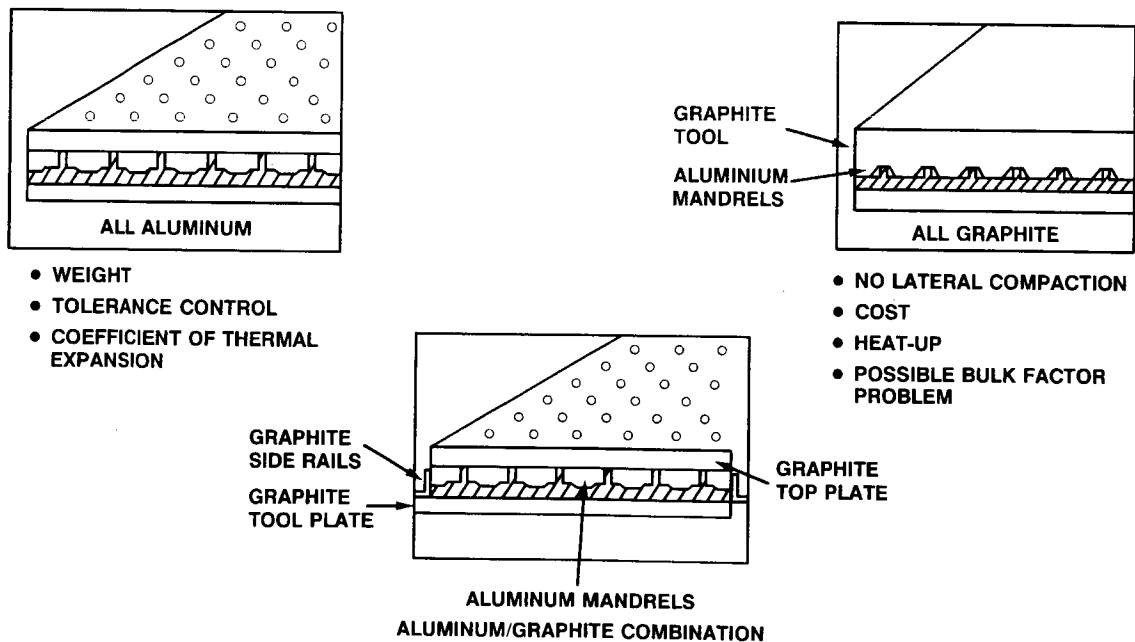


Figure 8

WING SCALE-UP TOOLING DEVELOPMENT

Shown to the right in Figure 9 is the tooling concept that will be used to fabricate 4' x 6' wing skin panels. This concept is a combination of graphite tooling plates with aluminum mandrels. This was chosen over an all aluminum tool because the graphite/epoxy tooling plate is better able to control tolerances, maintain resin bleed holes in proper location, and allow for possible integration of stitched rib to skin clips in future development. (Note: Resin bleed holes will consist of steel bushings potted into the graphite tooling plate to maintain hole dimensions and prevent excessive wear.) This aluminum/graphite tool once assembled is then placed in a restraining fixture as shown below on the left. A compaction pressure of 20-30 psi can be applied with a pressure bladder restraining fixture to squeeze excess resin out and insure a quality surface finish.

WING SUBCOMPONENT TOOLING CONCEPT AND PROCESS DEFINITION

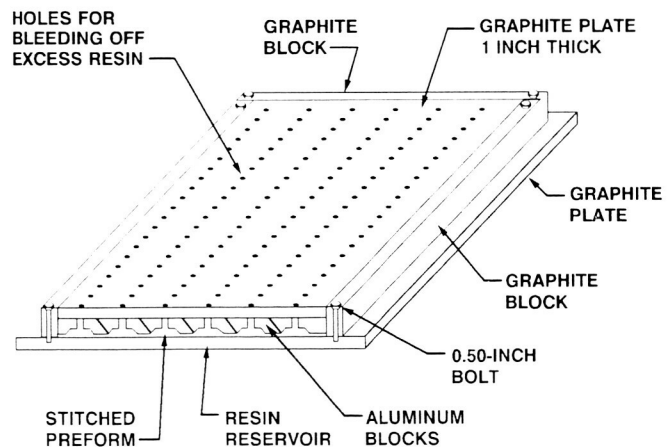
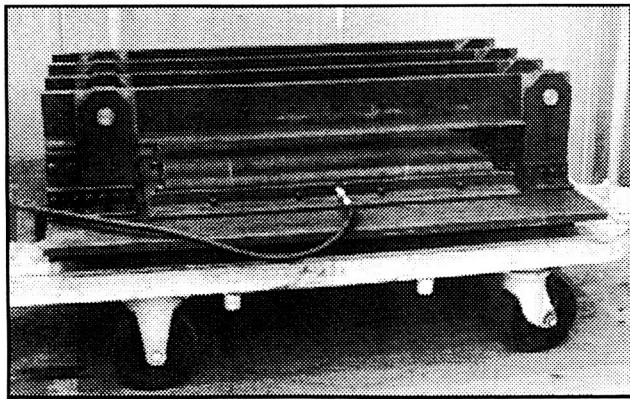


Figure 9

**MANUFACTURING DEVELOPMENT
for
COMPOSITE PRESSURIZED FUSELAGE STRUCTURES**

FUSELAGE SUB-SCALE TOOLING DEVELOPMENTS

Effect of Preform

In developing the pressure injection RTM process for thin fuselage structures, two critical points to tool design need to be considered up front. First is matched metal tooling needed for compaction pressures required to yield 60% fiber volume or the final desired thickness. (Compaction is needed due to the fact this preform is not heavily stitched.) In Figure 10, the chart on the left shows that approximately 48 psi is required to give the appropriate compaction pressure. This pressure becomes important when designing for tool rigidity and when pressurizing the tool with resin during fabrication. Another piece of information found on the chart is bulk factor. A 0.01 inch bulk factor is inherent in the preform. While this bulk seems small, in scale-up (i.e., multiple longerons) it does become additive causing tolerance problems for tooling. To circumvent these problems, the bulk factor must be accounted for in tooling. Figure 10 to the right illustrates both types of matched metal tooling being looked at by Douglas. First is a clamp/fit fixture used to eliminate bulk factor problem before assembly into a matched metal tool frame. The second tooling concept is a sidewall compaction matched metal tool that allows bulk factor and compacts after the tool is closed.

FUSELAGE ELEMENT TOOLING DEVELOPMENT

EFFECT OF PREFORM ON TOOLING DESIGN

BULK FACTOR

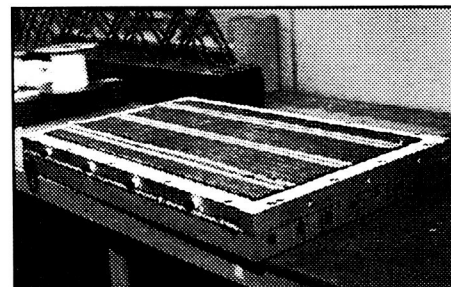
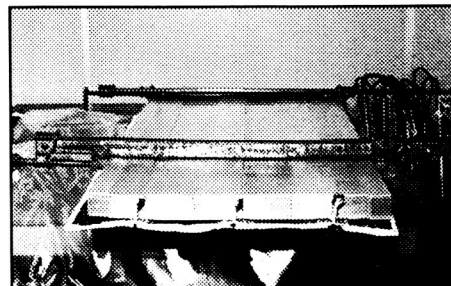
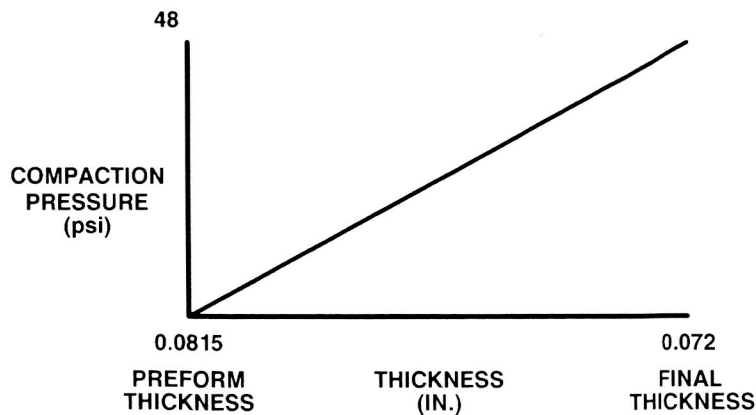


Figure 10

FUSELAGE SUB-SCALE TOOLING DEVELOPMENT

Effect of Preform

Another reason matched metal tooling is required for fuselage structure has to do with flexibility of the preform. Since the thickness of each "J" section longeron is only 0.072 inches, the preform will not maintain its required shape and orientation. In Figure 11 (left), preform flexibility is illustrated. Figure 11 to the right, shows the matched metal tool required to shape the longerons properly.

FUSELAGE ELEMENT TOOLING DEVELOPMENT

EFFECT OF PREFORM ON TOOLING DESIGN

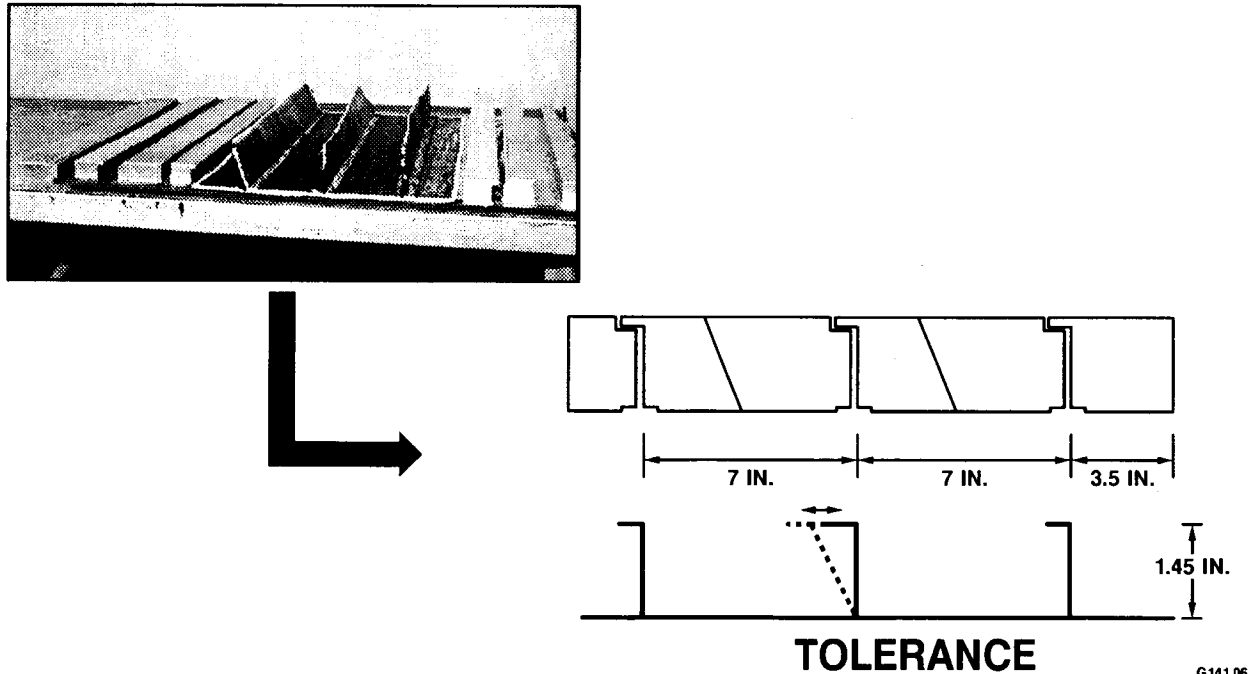


Figure 11

FUSELAGE SUB-SCALE TOOLING DEVELOPMENTS

Effect of Tooling Tolerances

In progressing from flat panels to stiffened structures, various unforeseen problems were encountered. While it was already known that resin injection pressures for thin preform were extremely high (125 psi), the effect of tooling tolerance had not yet been discovered. Figure 12 below, indicates that the resin pressure required to permeate a preform appears to follow some exponential form for very thin laminates. In examining the graph, note that as the thickness of the preform decreases, significant increase in the amount of pressure required to permeate the preform occurs. This result, translated to tool design, says that if tooling mandrel tolerances (for matched metal tools) are not extremely close, the resin flow profile expected may not occur. The resin will follow the path of least resistance to the exit vent, thus resulting in a part that is not fully impregnated. (This has only been found to present a problem in thin structures.)

FUSELAGE ELEMENT TOOLING DEVELOPMENT

EFFECT OF PREFORM AND TOOL TOLERANCES ON PROCESSING THIN STRUCTURES

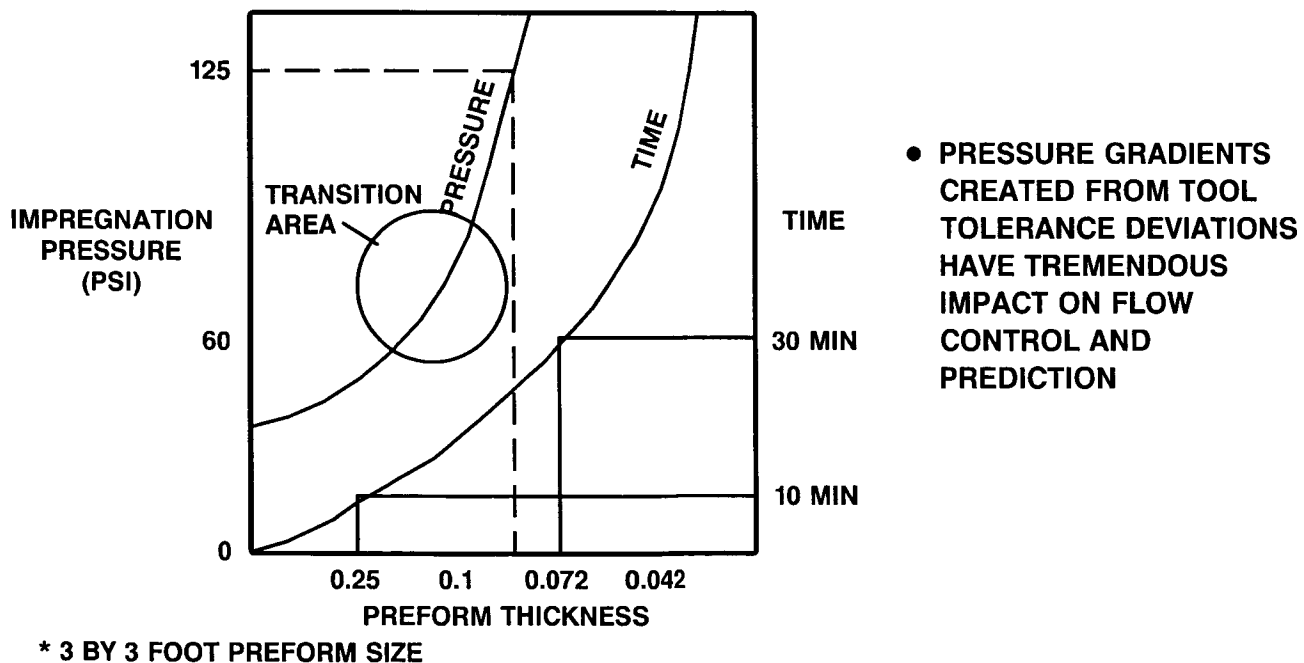


Figure 12

FUSELAGE SUB-SCALE TOOLING DEVELOPMENT

Douglas Fuselage RTM Tool

In developing the tooling for the sub-scale fuselage structure, strict attention was given to tool tolerances. All mating surfaces in the horizontal plane of the tool were blanchard ground to $\pm .005$ inch to aid in regulating resin injection pressures. This tool is constructed of aluminum, with self-heated calrod heaters and is clamped between I-beams to apply compaction pressure. The fabrication process is simply to inject resin into the skin at the center of the tool until resin appears at the corners, then inject the stiffeners until resin appears at the opposite vent at the other end of the tool. Resin pressure is maintained at 40 psi while the part is cured. See Figure 13 below.

FUSELAGE ELEMENT TOOLING DEVELOPMENT

ELEMENT TOOLING CONCEPT

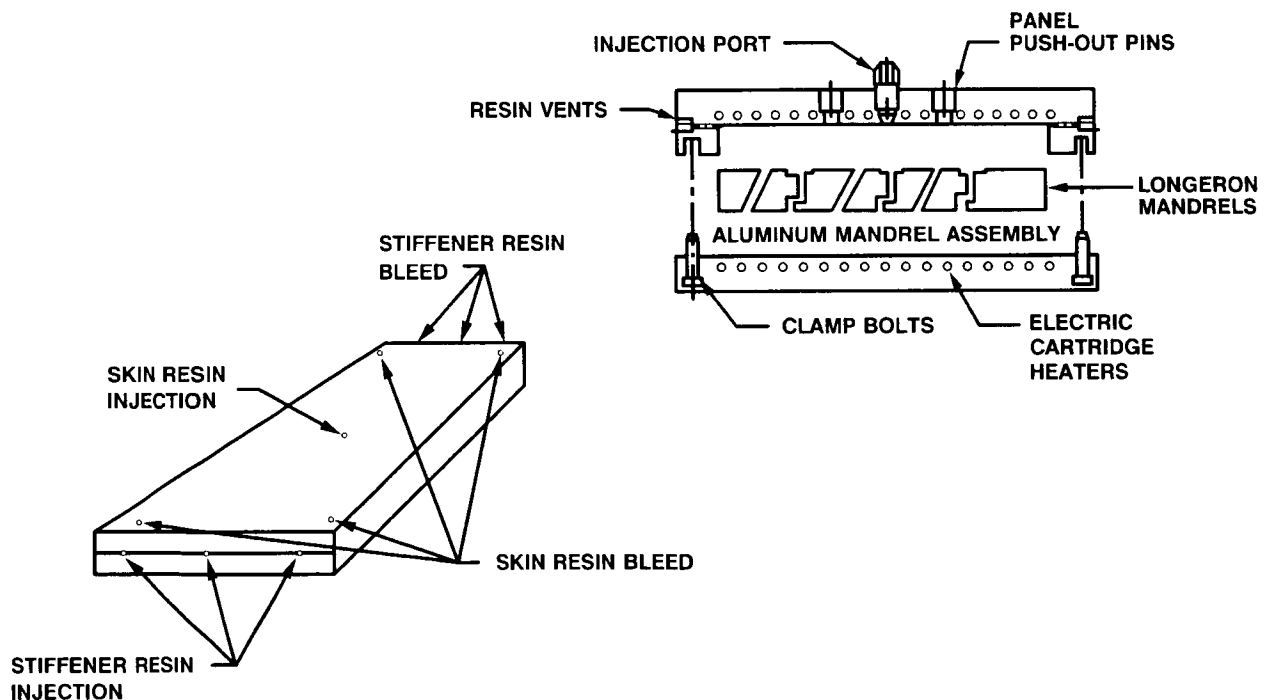


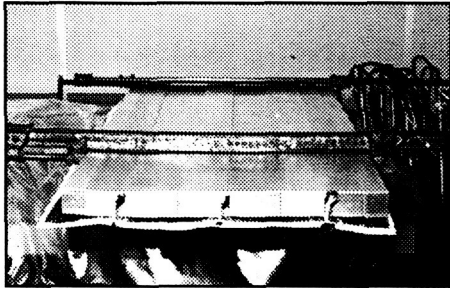
Figure 13

FUSELAGE SUB-SCALE TOOLING DEVELOPMENT

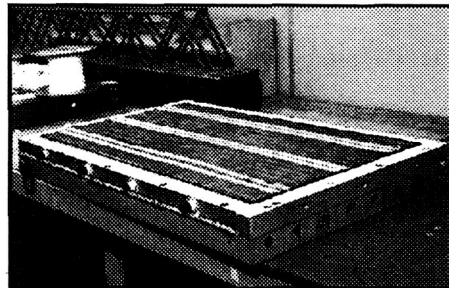
Figure 14 below shows the Douglas fuselage tool in various stages of fabrication. The upper left photo is a view of the clamp/fit tooling used to insert the preform and mandrel assembly into the matched metal self-heated containment tool shown on the upper right. Below is the entire tool assembly with heaters ready for final clamping from the pressure bladder restraining fixture.

FUSELAGE ELEMENT TOOLING DEVELOPMENT

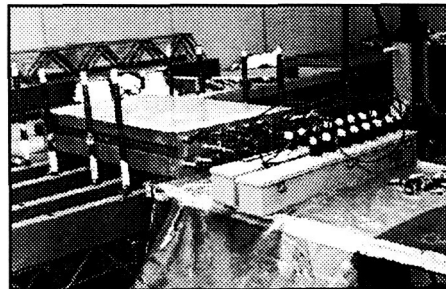
ELEMENT TOOLING



MANDREL ASSEMBLY



TOOL/MANDREL INTEGRATION



TOOL ASSEMBLY

Figure 14

FUSELAGE SCALE-UP TOOLING DEVELOPMENT

Major drivers in tooling scale-up development for fuselage as related to cost include tolerance control, tool heating and press/restraining fixture. In addressing these issues, numerous tool concepts were evaluated at Douglas. The best two are shown below in Figure 15. On the right of Figure 15 is a scaled-up version of the sub-scale fuselage tooling with minor modifications. These include use of flexible caul in place of a hard upper tool (to ease tool assembly), use of hot air convection heat system in place of calrod heaters (due to cost), and use of a dedicated restraining press with stainless steel inflatable pressure bladders (due to cost of large press). Below to the left is an alternate concept consisting of a one piece carbon/epoxy tool which is being considered to replace the mandrel concept if matched tool tolerances continue to be a problem in the resin injection cycle. (Note: A careful cost/performance study of the RTM composite fuselage panels will be done with duplicate panels being made by the Automated Tow placement process at Hercules. Data from this study will determine the manufacturing approach for Phase B fuselage development.)

PRESSURE IMPREGNATION OF FUSELAGE TOOLING CONCEPTS

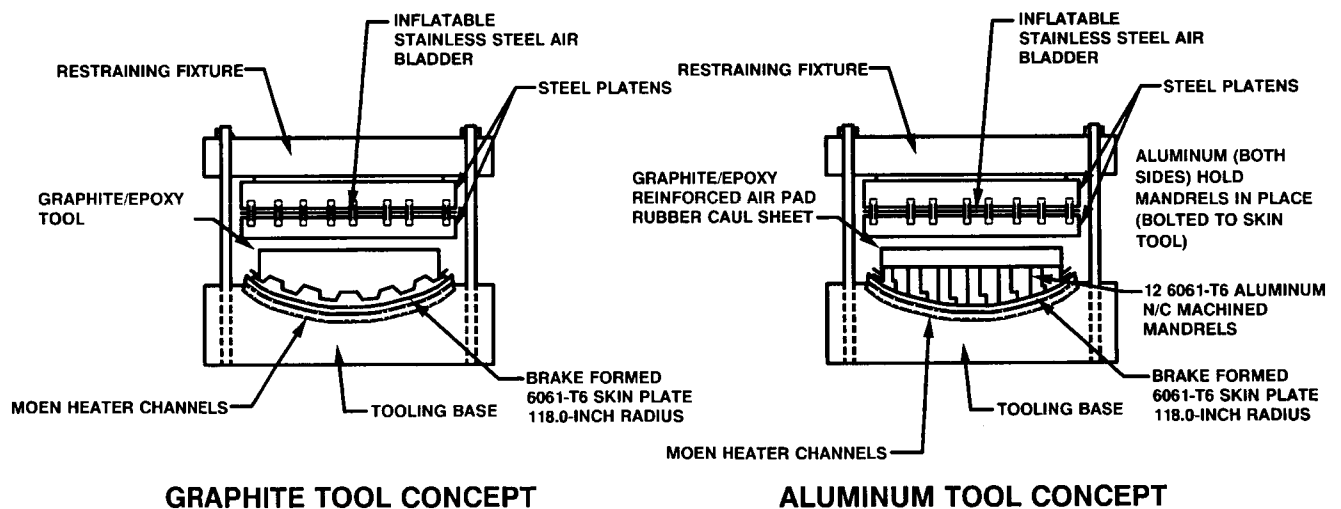


Figure 15

PRODUCTION UTILIZATION NEEDS

Tooling Scale-up to Production

In developing the tooling for the fuselage, it is clear that the OML tool surface and tool base are from a design perspective common for any tool concept Douglas may have. For this reason, an existing fuselage tool built under previous NASA contract will be modified to fit the RTM process being developed. Shown in Figure 16 is the size fuselage to be manufactured in Phase B and the existing tools to be used for the fuselage. This lower tool (similar to the tool base in Figure 15) will be used with the best concept for the upper tool portion and modified to include as much automation and heavy tool handling capability as possible.

Primary focus to date on fuselage has been the RTM fabrication development for fuselage quarter panel skins with "J" stiffener longerons. Therefore, to date, manufacturing development of other fuselage elements (clips, frames, floor beams, etc..) has not been addressed in detail.

PHASE B FUSELAGE DEVELOPMENT

FUSELAGE BARREL

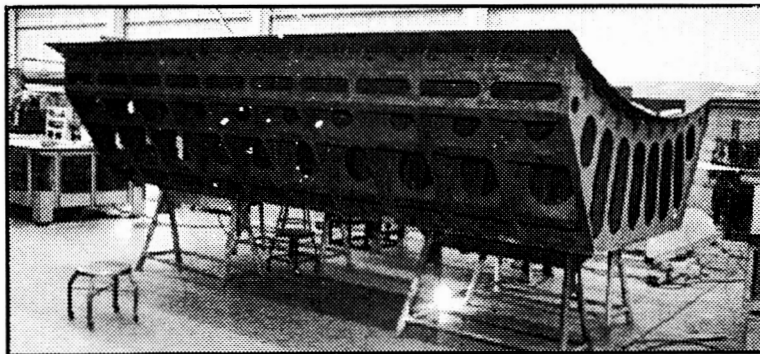
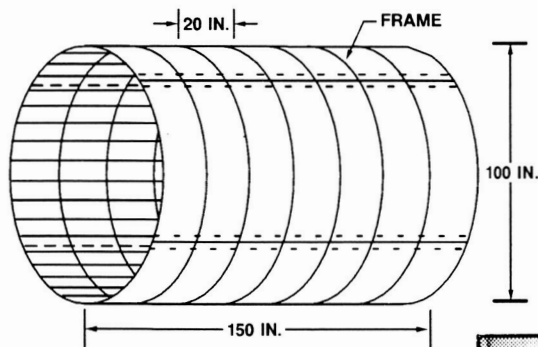


Figure 16

PRODUCTION UTILIZATION NEEDS In Line Process Monitoring

Process monitoring must ultimately become an integral part of the RTM process if it is to go to production. For this reason in line process monitoring with process modeling is part of a continuous Douglas funded improvement program and part of the NASA ACT program.

Figure 17 below illustrates the work being done under NASA contract with William and Mary College and Virginia Polytechnic and State University (VPI). In Figure 17 (above left) are the sensors being used by William and Mary College to generate kinetic relationships for various RTM resins. Below left are kinetic relationships for the Dow Tactix 138 resin. Figure 17 to the right represents permeability studies on stitched fabrics being done at VPI to begin modeling the RTM process. Shown in this chart are permeabilities for 54 ply wing skin lay-ups and 12 ply fuselage lay-ups.

PROCESS MONITOR / MODEL DEVELOPMENT

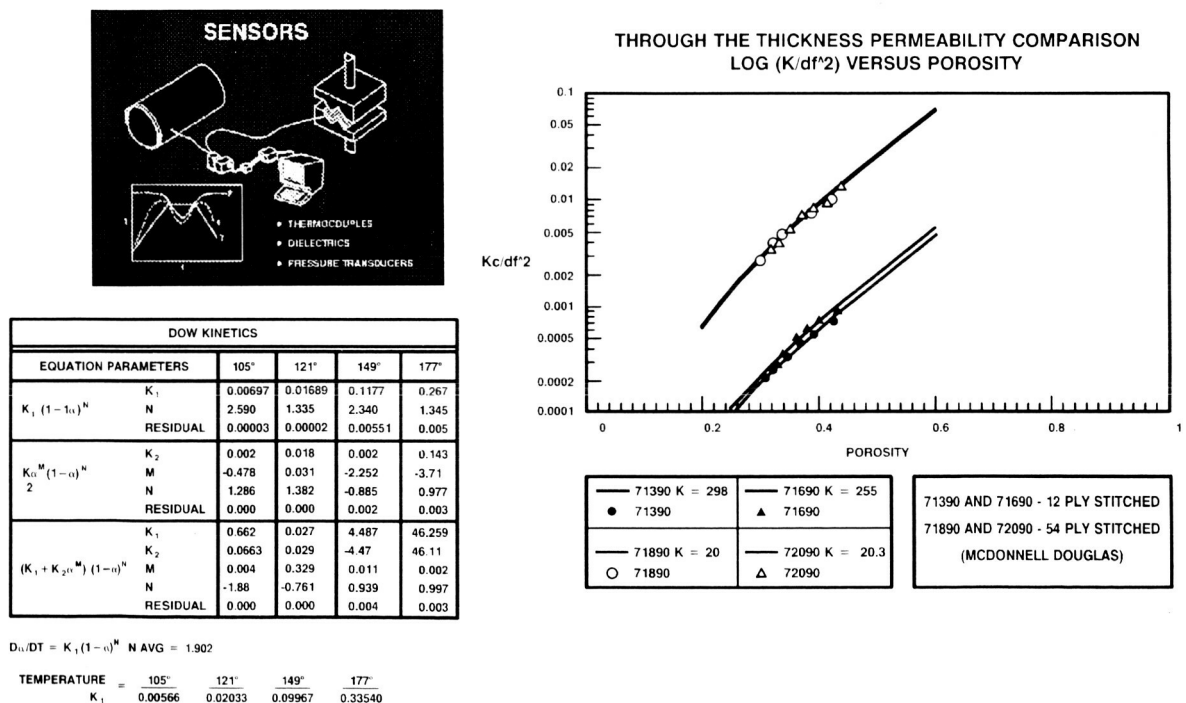


Figure 17

PRODUCTION UTILIZATION NEEDS

Future Factory

In looking forward, a futuristic factory must be envisioned that is equipped to handle the uniqueness of RTM fabrication concepts. At Douglas, we envision a close tie with major resin suppliers that will equip us with the capability of handling large quantities of liquid and film resins. In Figure 18 below, the resin storage is located within the building foundation for space conservation and system delivery purposes. Douglas also envisions 1.) the use of standard automated handling equipment to move preforms from automated stitching machines to the tools, 2.) state-of-the-art resin film laying equipment to calendar out resin on the tools, and 3.) hydraulically controlled tools with in line process control to supply complete process control from a central control point.

PRODUCTION NEEDS

ADVANCED FACTORY CONCEPT

KEY FEATURES

- IN-GROUND RESIN STORAGE
- HYDRAULIC-CONTROLLED VACUUM-TIGHT TOOL CAVITIES
- COMPLETE AUTOMATED CONTROL OF STITCHING AND CURE OPERATIONS

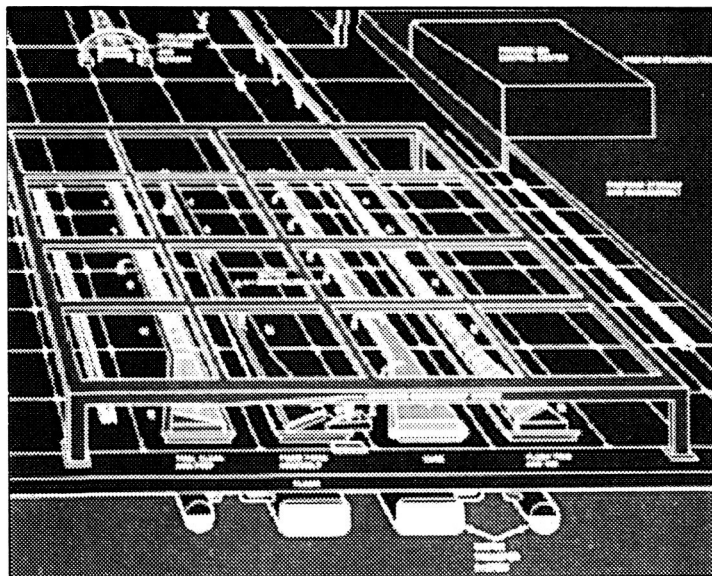


Figure 18

CONCLUSIONS

1. Thru-thickness vacuum infusion process well suited for large wing structures
2. Projected cost savings of 48% for RTM composite wing over conventional technology composite wing
3. Resins currently acceptable for vacuum infusion not meeting 3501-6 mechanical property standards
4. Resin requirements:
 - a. Film form resin desirable
 - b. Less than 100 centipoise resin viscosity
 - c. Less than 250 degrees F resin infusion temperature
 - d. Resin infusion time of 1 hour or more
 - e. Resin capable of oven cure under vacuum bag desirable
 - f. 3501-6 composite laminate properties desirable
5. Scale-up tooling costs for pressure RTM is cause for concern
6. Tooling and preform integration critical to success of pressure RTM
7. Fuselage cost/performance comparisons of Automated Tow Placement versus pressure RTM are key to design/manufacture of full scale Phase B fuselage barrels
8. Advanced RTM factory will require multi-industry participation to succeed

CONSOLIDATION OF GRAPHITE/THERMOPLASTIC TEXTILE PREFORMS FOR PRIMARY AIRCRAFT STRUCTURE

J. Suarez and J. Mahon
Grumman Aircraft Systems
Bethpage, New York

Abstract

The use of innovative cost effective material forms and processes is being considered for fabrication of future primary aircraft structures. Processes that have been identified as meeting these goals are textile preforms that use resin transfer molding (RTM) and consolidation forming. The Novel Composites for Wing and Fuselage Applications (NCWFA) program has as its objective the integration of innovative design concepts with cost effective fabrication processes to develop damage-tolerant structures that can perform at a design ultimate strain level of 6000 micro-inch/inch. In this on-going effort, design trade studies were conducted to arrive at advanced wing designs that integrate new material forms with innovative structural concepts and cost effective fabrication methods. The focus has been on minimizing part count (mechanical fasteners, clips, number of stiffeners, etc.), by using cost effective textile reinforcement concepts that provide improved damage tolerance and out-of-plane load capability, low-cost resin transfer molding processing, and thermoplastic forming concepts. The fabrication of representative Y spars by consolidation methods will be described. The Y spars were fabricated using AS4 (6K)/PEEK 150g commingled angle interlock 0/90-degree woven preforms with ± 45 -degree commingled plies stitched using high strength Toray carbon thread and processed by autoclave consolidation.

INTRODUCTION

The Novel Composites for Wing and Fuselage Applications (NCWFA) Program is performed by the Grumman Aircraft Systems Division of Grumman Corporation and its subcontractors, Textile Technologies, Inc., and Compositek Corporation, under the sponsorship of NASA Langley Research Center, Hampton, Virginia 23665-5225. Mr. H. Benson Dexter is the NASA/LARC Contracting Officer Technical Representative.

Background

The full weight savings and life cycle cost savings potential of state-of-the-art composites have not been achieved because of design strain levels limited by the materials LOW

- Damage tolerance
- Fracture toughness
- Notch strength
- Out-of-plane strength

and HIGH

- Material cost
- Manufacturing cost

We need

- Novel material forms
- Design strain levels of 6,000 + micro in./in.
- Cost effective manufacturing concepts

PROGRAM OBJECTIVES

The overall objective of the NCWFA program is to integrate innovative design concepts with cost effective fabrication processes to develop damage-tolerant primary structures that can perform at a design ultimate strain level of 6000 micro-inch/inch.

- 1) Develop optimum wing design concepts with high performance fiber architecture to achieve
 - Improved damage tolerance and durability
 - High notch strength
 - Increased out-of-plane load capability
- 2) Develop integrally stiffened fuselage bulkhead concepts that
 - Eliminate skin/stiffener separation failure modes
 - Minimize fabrication cost
- 3) Explore textile processes to achieve affordable integral skin/stiffener structures by automated
 - Weaving
 - Knitting
 - Stitching
- 4) Explore RTM and consolidation/forming hybrid Gr/TP fiber forms for cost-effective fabrication of primary wing and fuselage components
- 5) Conduct tests to validate structural performance and correlate test results with analytical predictions.

PROGRAM TASKS

The program is divided into five major tasks: Task 1 – Wing Design Concepts; Task 2 – Fuselage Bulkhead Design Concepts; Task 3 – Wing Spar-Rib Intersection Design Concepts; Task 4 – Design and Fabricate a Generic High Strain Wing Torque Box Component; and Task 5 – Structural Test of the Wing Torque Box Component. The work reported here was accomplished in Task 1.

Task 1 - Wing Design Concepts

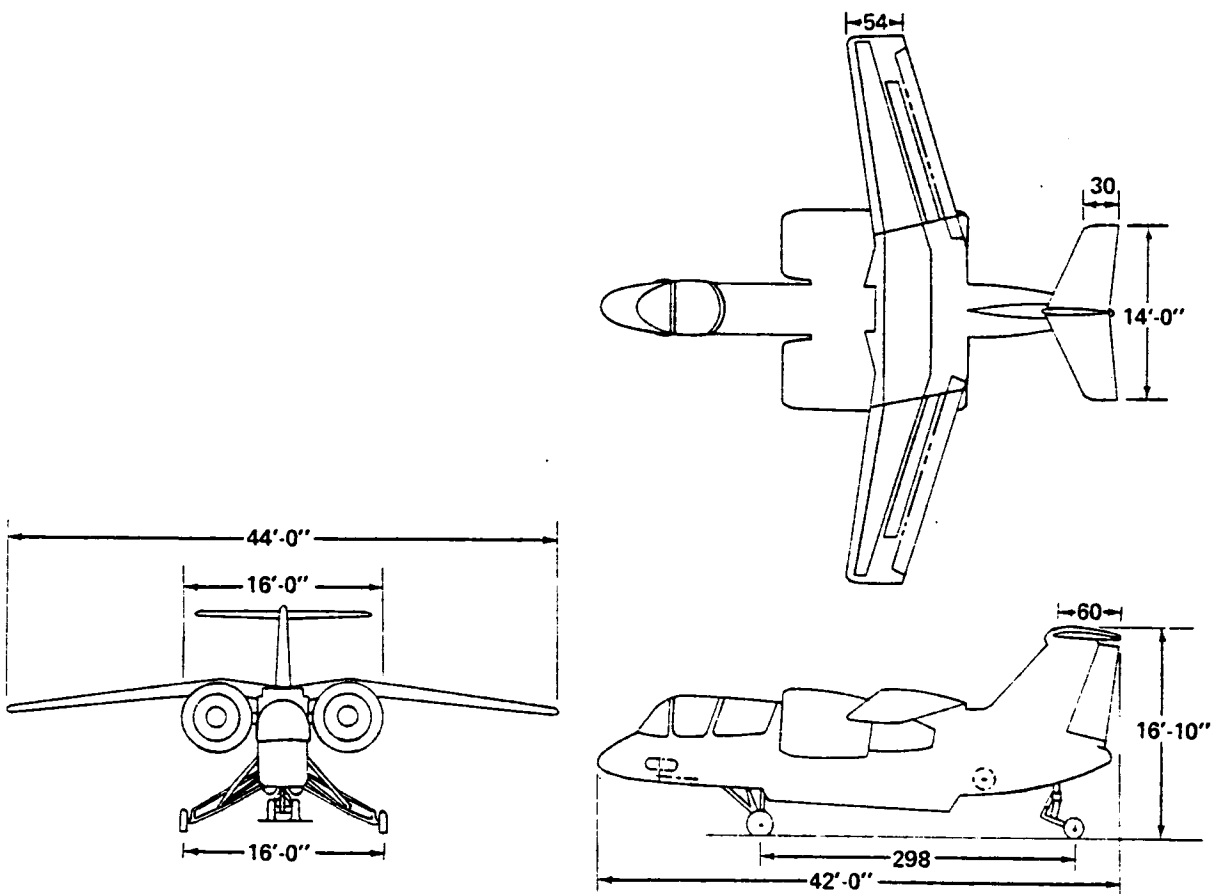
Design Trade Studies:

- Baseline, VSTOL 698-420
- Generate advanced wing designs using innovative structural concepts (target weight savings of 50%)
 - Multi-directional weavings (fiber form architecture)
 - Stitching
 - Softening strips
 - Compliant laminates
 - Integral cover to substructure
 - Crack arrestment strips
 - Y, blade and hat stiffeners
 - Spread 0° covers
 - Discrete cap covers
- Newer/emerging materials:
 - Fibers ($E > 40$ msi, $F > 600$ ksi)
 - Commingled yarns
 - Powder-based resin matrices
 - Toughened TS and TP resin matrices
- And cost effective processes (target cost savings of 25%):
 - RTM
 - Autocomp
 - Consolidation forming

BASELINE AIRCRAFT

The baseline aircraft selected for this program is a subsonic patrol VSTOL aircraft, Grumman design 698-420. This design is a high-wing, T-tail, turn-tilting nacelle configuration which combines both power-plant and control vanes immersed in the fan stream.

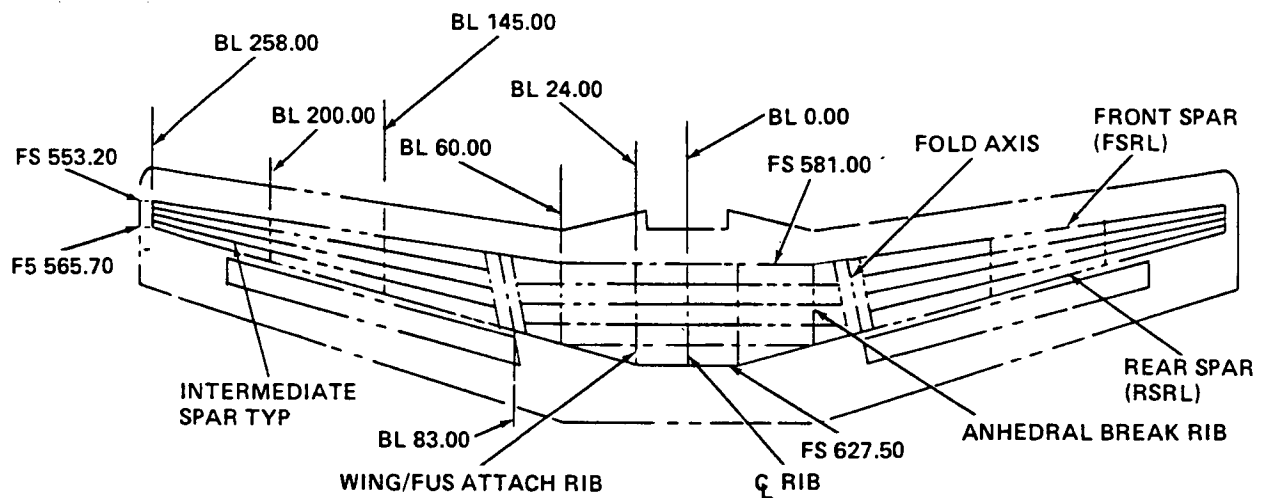
BASELINE SUBSONIC PATROL V/STOL SEA CONTROL CONFIGURATION



WING STRUCTURAL CONFIGURATION

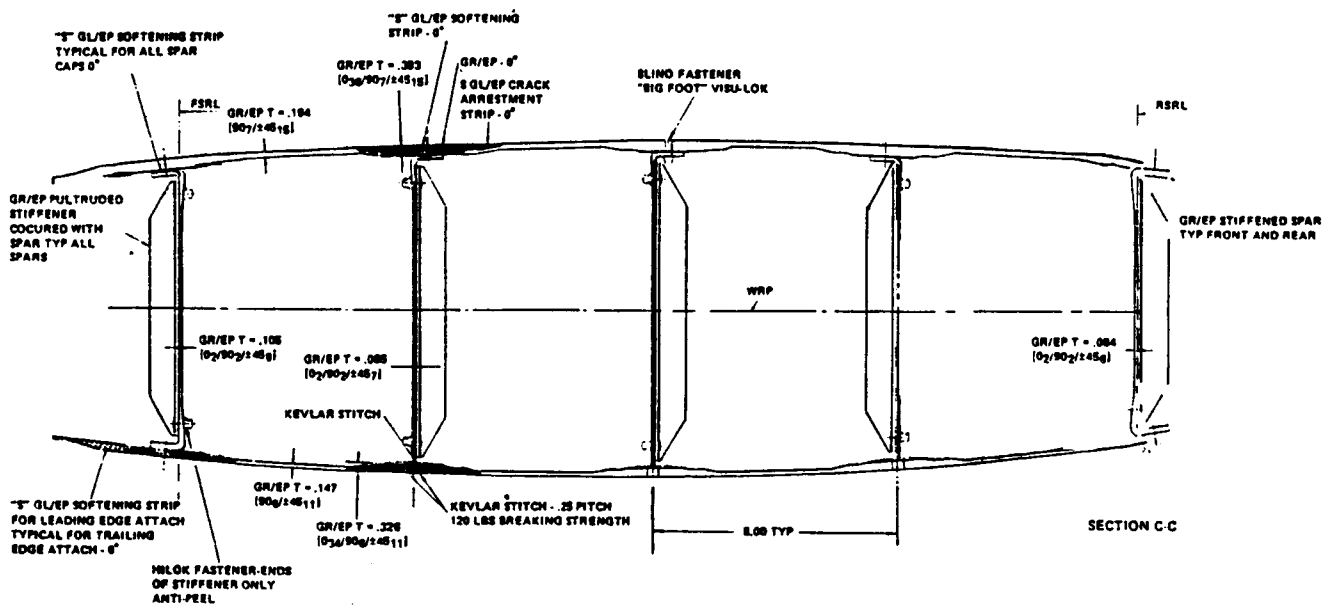
The structural configuration for the wing is shown below. The wing has a span of 44 ft and a fold span of 16 ft and is sized to allow installation of the conformal radar. The thickness ratio is 14% at the root and 12% at the tip with a maximum depth of 14.4 in. at the centerline. Fuel is carried in the wing box from fold-joint to fold-joint. Roll control in conventional flight is provided by spoilers mounted on the rear beam.

Five-Spar Wing Box Configuration



WING BASELINE CONFIGURATION

Consistent with the structural arrangement, design requirements, and advanced composite wing design technology, a baseline wing configuration was established from previous design efforts on the High Strain Wing Program. The upper and lower covers are Gr/Ep laminates, working to a design ultimate strain level of approximately 6000 micro-in./in., and include Gl/Ep for softening strips and crack arrestment strips (for damage tolerance). The substructure consists of a front, rear, and three intermediate spars. The spar webs are flat angle-stiffened Gr/Ep laminates, with the intermediate spars integrally co-cured and stitched (with kevlar) to the lower cover. Gr/Ep sinewave ribs were used, except at the wingfold and tip where titanium and Gr/Ep plain panels were used, respectively.



STRUCTURAL CONCEPTS

In achieving the objectives of the NCWFA Program, composite design concepts incorporated into the baseline wing have been studied. These can be classified into two categories: multi-spar and multi-rib. The structural arrangement considered spar/stiffener orientation, spar/stiffener spacing, and rib pitch. The structural geometry was varied to achieve a least weight/cost cross section of detail structural elements.

Structural Concepts Trade Studies, Wing Torque Box Structures

- Torque box covers
 - Flat monolithic (unbuckled)
 - Discrete cap (unbuckled and buckled)
 - Lumped spar cap (buckled)
 - Isolated discrete cap (buckled)
- Hat stiffened (unbuckled and buckled)
- Tee stiffened (unbuckled and buckled)
- Wye stiffened (unbuckled and buckled)
- Blade stiffened (unbuckled and buckled)
- Spar webs
 - Shear resistant
 - Stiffened web (unbuckled and buckled)
 - Sinewave Shear Resistant
- Spar caps
 - Angle
 - Tee
 - Wye
- Rib webs and caps
 - Similar to spars

Structural Concepts

Structural Sizes/Weight Derivation

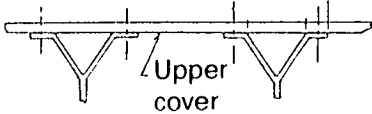
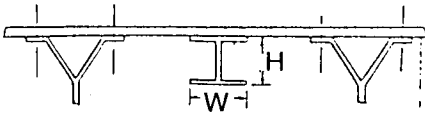
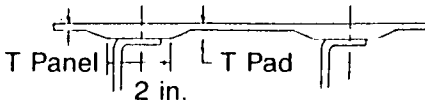
- Minimum weight design of each concept considered derived to compare concepts on a common basis
- Structural sizing/weight analysis performed using multi-station-wise basis
- Appropriate analytical methods used to determine least weight geometry & thickness to satisfy strength/stability and stiffness for each component/concept considered
- Analytical methods yield geometry/thickness that represent upper limit to efficient use of structural material from which theoretical weights are derived
- Non-optimum factors (NOFs) applied to theoretical weights to project realistic assembly weights
- NOFs derived from previous composite programs/studies account for weight penalties associated with
 - Load introduction
 - Build-ups around cut-outs
 - Fasteners
 - Ply transition and smoothing
 - Variation in laminate thickness and density

MULTI-SPAR CONCEPT

Our multi-spar concept was derived from previous studies, which indicated a five spar configuration to be the most efficient from both a weight and cost standpoint. A total of 15 ribs was used in our arrangement.

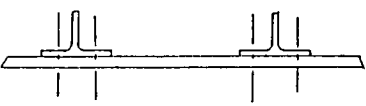
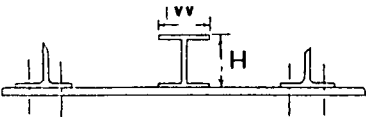
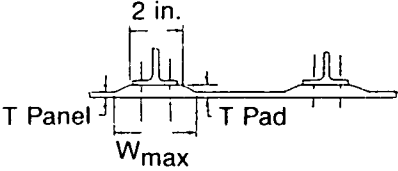
Two types of wing cover configurations were evaluated which have the potential of successfully increasing the working strain to levels at least 50% higher than those of the baseline. The two types evaluated were plain panel-spread and discrete cap. The first type, plain panel-spread, is essentially a monolithic skin of approximately constant thickness at any chordwise cut. In addition, the laminate consists of the same family of lamina orientations (0° , 90° , $\pm 45^\circ$) at any point. The second type, discrete cap, utilizes a skin of two distinct laminate orientations. Between spars, the skin panel consists of a high strain to failure laminate of 90° and $\pm 45^\circ$ layers. The absence of 0° layers, in this panel has two additional advantages: first, for a given thickness it will possess a higher resistance to buckling loads; and second, the laminate's EA (extensional stiffness) is very low as compared to the total section, resulting in a lesser axial load applied to the unsupported segment of skin. At each spar 0° layers are added to the panel laminate resulting in a local pad. The 0° layers provide the axial filament control to the laminate and carry the preponderance of axial load. Located over the spar, the high loads are rigidly supported, minimizing any instability problems.

Structural Concepts Upper Cover Configurations

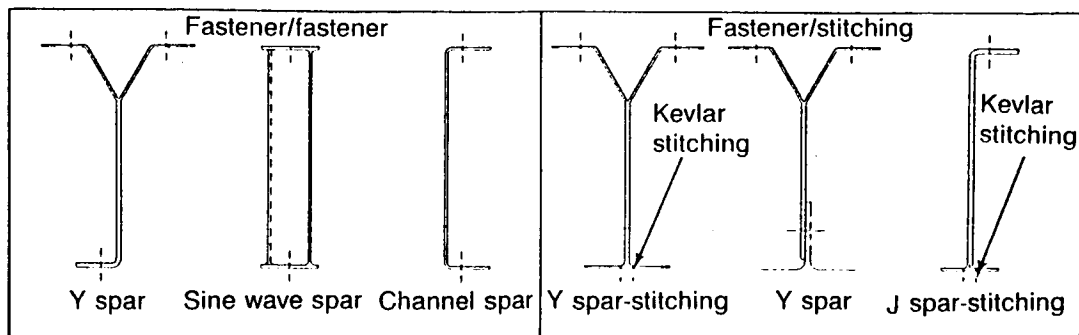
	Advantages	Disadvantages
<p>Spread zero upper cover (with "Y" intermediate spars)</p> 	<ul style="list-style-type: none"> • Least cover fab cost • Very efficient comp cover when combined with Y spar • Easily repaired • Good battle damage tolerance due to multiple load paths 	<ul style="list-style-type: none"> • Max rows of fasteners – assy cost impact • High strain concentration – fasteners through laminate with high % of 0-deg plies • Damage tolerance totally material dependent • Excessive S/S shear carrying material
<p>Spread zero upper cover with integral "I" stiffner</p> 	<ul style="list-style-type: none"> • Minimizes number of spars • Reduced assembly costs • Good battle damage tolerance due to multiple load paths 	<ul style="list-style-type: none"> • High strain concentrations – fasteners through laminate with high % of 0-deg plies • Damage tolerance totally material dependent • Difficult to repair
<p>Discrete cap upper cover</p> 	<ul style="list-style-type: none"> • Most efficient comp cover design for multi-spar configuration • Min number of substructure attachments • Excellent damage tolerance due to multiple load paths & compliant laminates 	<ul style="list-style-type: none"> • Increased laminate tailoring • High strain concentration factor – fasteners through laminate with high % 0-deg plies • Difficult to repair

Structural Concepts

Lower Cover Configurations

	Advantages	Disadvantages
<p>Spread zero lower cover</p> <p>– Tee & angle spar support</p> 	<ul style="list-style-type: none"> • Least cover fab cost • Very efficient comp cover when combined with Y spar • Easily repaired • Good battle damage tolerance to multiple load paths 	<ul style="list-style-type: none"> • Max rows of fasteners – assy cost impact • High strain concentration – fasteners through laminate with high % of 0-deg plies • Damage tolerance totally material dependent • Excessive S/S shear carrying material
<p>Lower cover with integral “I” stiffener</p> 	<ul style="list-style-type: none"> • Minimizes number of spars • Reduced assembly costs • Good battle damage tolerance due to multiple load paths 	<ul style="list-style-type: none"> • High strain concentrations – fasteners through laminate with high percent of 0-deg plies • Damage tolerance totally material dependent • Difficult to repair
<p>Discrete cap lower cover</p> 	<ul style="list-style-type: none"> • Most efficient comp cover design for multi-spar configuration • Min number of substructure attachments • Excellent damage tolerance due to multiple load paths & compliant laminates 	<ul style="list-style-type: none"> • Increased laminate tailoring • High strain concentration factor-fasteners through laminate with high % 0-deg plies • Difficult to repair

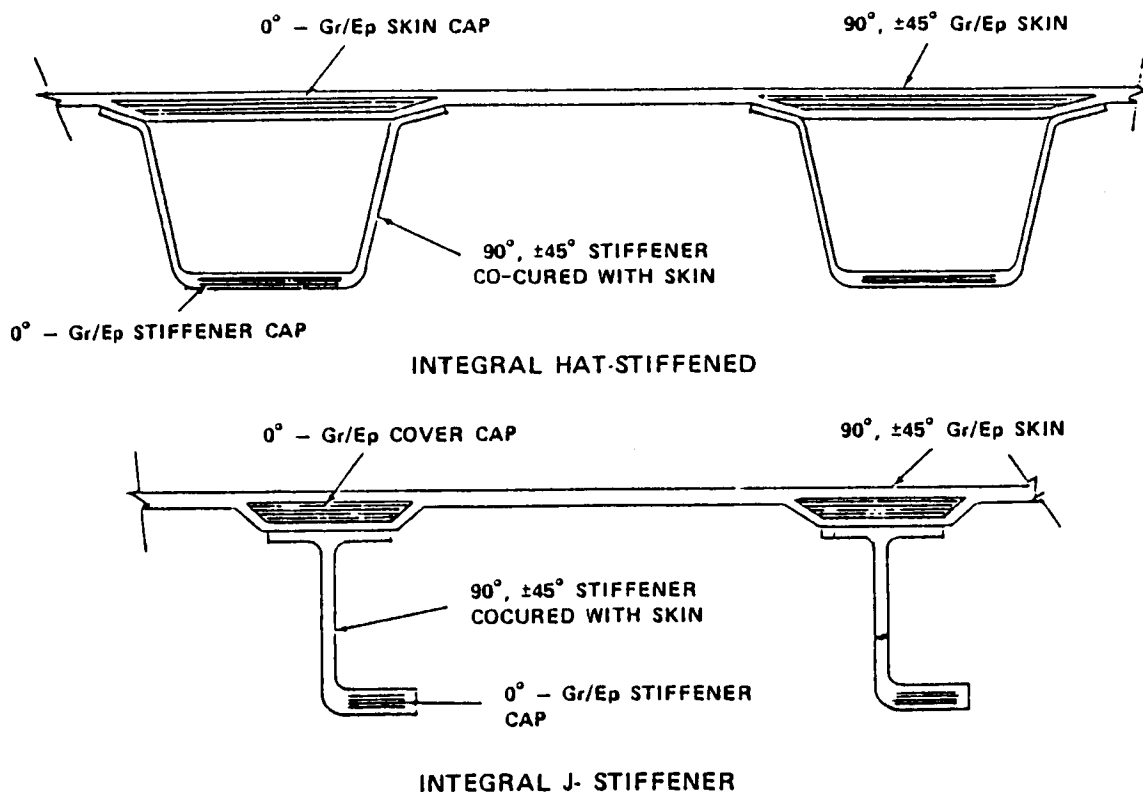
Spar Design Concepts



MULTI-RIB CONCEPTS

In general, subsonic patrol aircraft wings are relatively thick where strength/stability conditions govern. Consequently it is of interest to investigate cover configurations in which load-carrying material in the cross section is redistributed so as to achieve increased flexural stiffness over that of the relatively uniform thickness cross-section multi-spar cover designs. This concept leads to the consideration of longitudinal stiffening systems as an integral part of the cover itself. The integral hat and open J stiffener configurations were considered in the study and are illustrated below in combination with the skin. The designs were sized for all combinations of stiffener pitch equal to 4, 5, 6 and 7 in. and rib spacing equal to 15, 20, 25 and 30 in. Because of relatively high structural efficiency and potential ease of manufacture, stiffeners parallel to the front spar were selected as the preferred stiffener orientation.

Cover Concepts, Multi-Rib



MATERIAL-ORIENTED DESIGNS WEIGHT SUMMARY

For the baseline wing and the various material-oriented high strain wing concepts, theoretical cover and substructure weights were derived analytically on a multi-station basis utilizing t's generated for the various forms of construction. To account for such weight items as penalties associated with load introduction, attachments, cutouts, variations in laminate thickness and density, the theoretical weights are multiplied by an empirically determined "non-optimum factor", thereby yielding a realistic assembly weight.

A weight breakdown of the multi-spar design, for both material systems (IM7/8551-7A and G40-800/F584 Gr/Ep), and multi-rib design (IM7/Tactix 123 Gr/Ep) is shown below. The multi-rib design concept consists of four hat stiffeners outboard of the fold, seven inboard and twenty-five ribs at a 25-inch pitch.

The weight savings generated by these concepts show significant improvement over the baseline. The multi-spar design, using G40-800/F584, provided a savings of 543 lb, or 42% of the metal torque box weight of 1233 lb. The multi-rib design, using IM7/Tactix 123 Gr/Ep, yielded a 541 lb savings or 41% of the metal torque box weight.

Weight Breakdown for Selected Wing Designs (Material-Oriented)

COMPONENT	BASLINE WING TORQUE BOX (LBS)	MULTI-SPAR IM7/8551-7A (LBS)	MULTI-SPAR G40-800/F584 (LBS)	MULTI-SPAR (CONCEPT C) HAT-STIFFENED (LBS)
UPPER COVER	293.80	258.30	246.20	266.60
• BASIC INTERSPAR COVER	240.50	223.90	211.80	266.60
• SOFTENING STRIP PENALTY (0° GL/EP)	2.60	---	---	---
• DAMAGE TOLERANCE PENALTY (0° GL/EP)	10.60	---	---	---
• DAMAGE TOLERANCE PENALTY (+45° GL/EP)	0.00	---	---	---
• SPAR CAPS (INC WRINKLING PENALTY)	40.10	34.40	34.40	
LOWER COVER	224.10	192.40	182.70	185.70
• BASIC INTERSPAR COVER	187.20	175.30	165.60	185.70
• SOFTENING STRIP PENALTY (0° GL/EP)	2.20	---	---	---
• DAMAGE TOLERANCE PENALTY (0° GL/EP)	8.00	---	---	---
• DAMAGE TOLERANCE PENALTY (+45° GL/EP)	1.50	---	---	---
• SPAR CAPS (INC WRINKLING PENALTY)	24.90	17.10	17.10	---
FRONT SPAR (SYNCORE STIFF)	88.60	73.80	73.80	98.80
REAR SPAR (SYNCORE STIFF)	36.00	32.90	32.90	40.10
INTERMEDIATE SPARS (SYNCORE STIFF)	110.00	101.80	101.80	---
	52.20	52.20	52.20	96.60
RIBS				
	806.20	711.40	689.60	687.80
TOTAL TORQUE BOX	---	94.80	116.60	118.40
WEIGHT SAVINGS OVER BASELINE % SAVINGS	---	11.80	14.50	14.70

COMBINED MATERIAL/CONFIGURATION CONCEPTS

After completing the material-oriented design concepts, our efforts were directed toward developing combined material/configuration concepts. This involved the use of Y-spars and Y-stiffeners to support the covers. For the upper cover, the following concepts were studied:

- 1) Spread 0° supported by 5 or 6 Y-spars
- 2) Isolated discrete cap supported by 5 or 6 Y-spars
- 3) Isolated discrete cap supported by integrally cured Y-stiffeners

The basic philosophy in using intermediate Y-spars is that they reduce panel widths and required thickness on the upper cover. Although an increase in weight is expected for the intermediate spars, the weight savings produced by the upper cover will adequately compensate for it, and yield an overall weight savings.

The same loading conditions that sized our previous spar concepts were used to size the Y-spar configuration. For all Y-spar designs, the angle was set at 120° to provide equilibrium and balance. The distance between the legs of the Y-spar at the attachment to the upper cover depends on the spar spacing. To obtain the maximum benefit from the Y-spar configuration, the fastener spacing is half the spar spacing.

G40-800/F584 tape was used for the upper and lower covers and 3-D IM7/Tactix 123 and 3-D commingled AS4/PEEK 150G weave was utilized to size the Y-spars. For the multi-spar concepts, only the intermediate spars were designed with the Y configuration. The SynCore-stiffened design was used for the front/rear spars.

The corresponding lower cover design configurations were as follows:

- 1) Spread 0° supported by 5 or 6 Y-spars
- 2) Isolated discrete cap supported by 5 or 6 Y-spars
- 3) Spread 0° supported by blade stiffeners.

MATERIAL- AND CONFIGURATION-ORIENTED DESIGNS

Weight Summary – Similar to previous design concepts, the theoretical weights, derived for the material/configuration concepts, were multiplied by an empirically determined non-optimum factor, to yield a realistic assembly weight. The table below shows a weight breakdown of the multi-spar designs (spread 0° and discrete cap) and multi-rib design. The weight savings generated by these concepts show significant improvement over the baseline. The multi-rib design, using G40-800/F584 with Y stiffeners, provided the greatest savings (573 lbs. or 46% of the metal torque box weight of 1233 lbs.)

Weight Breakdown for Selected Wing Designs (Material & Configuration Oriented)

COMPONENT	BASELINE WING TORQUE BOX (LBS)	MULTI-SPAR (SPREAD 0°) (LBS)	MULTI-SPAR (DISCRETE CAP) (LBS)	MULTI-SPAR (Y-STIFFENED) (LBS)
UPPER COVER	293.80	182.80	191.50	215.50
• BASIC INTERSPAR COVER	240.50	169.00	177.70	215.50
• SOFTENING STRIP PENALTY (0° GL/EP)	2.60	---	---	---
• DAMAGE TOLERANCE PENALTY (0° GL/EP)	10.60	---	---	---
• DAMAGE TOLERANCE PENALTY (±45° GL/EP)	0.00	---	---	---
• SPAR CAPS (INC WRINKLING PENALTY)	40.10	13.80	13.80	---
LOWER COVER	224.10	207.00	186.60	208.90
• BASIC INTERSPAR COVER	187.20	200.20	179.80	208.90
• SOFTENING STRIP PENALTY (0° GL/EP)	2.20	---	---	---
• DAMAGE TOLERANCE PENALTY (0° GL/EP)	8.00	---	---	---
• DAMAGE TOLERANCE PENALTY (±45° GL/EP)	1.50	---	---	---
• SPAR CAPS (INC WRINKLING PENALTY)	24.90	6.80	6.80	---
FRONT SPAR (SYNCORE STIFFENED)	88.60	73.80	73.80	98.80
REAR SPAR (SYNCORE STIFFENED)	36.00	32.90	32.90	40.10
INTERMEDIATE SPARS (Y-SPARS)	110.00	159.00	159.00	---
RIBS	52.20	52.20	52.20	96.60
TOTAL TORQUE BOX	806.20	707.70	696.00	659.90
WEIGHT SAVINGS OVER BASELINE	---	98.50	110.20	146.30
% SAVINGS	---	12.20	13.70	18.10

CONCEPT EVALUATION

Each design concept was rated in terms of the following parameters: weight, risk, manufacturing and production costs, durability/damage tolerance, repairability, inspectability and operation and support costs.

With the concept rating forms, along with layouts, engineers from different disciplines were able to rate the various novel composites wing concepts. These disciplines included Advanced Materials and Manufacturing, Tooling, Design/Structural Analysis, Quality Control and Reliability/Maintainability. The results are incorporated in the following table, for the multi-spar and multi-rib concepts. The Total Score column represents the total of each discipline's score for that parameter. The Average Score column represents the Total Score divided by the No. of R (rating disciplines), which is four in all cases. For example, for the first parameter, Weight, Concept I received scores of 100, 125, 125, 100, from the four disciplines, which resulted in a Total Score of 450 and an Average Score of 113 (450/4). The sum of the Average Scores then represents the rating for that particular concept.

Concept Evaluation, Multi-Spar Concepts

PARAMETERS	WEIGHTING FACTOR	CONCEPT I			CONCEPT II			CONCEPT IV			CONCEPT V		
		IM7/8551-7A SYNCORE-STIFFENED			G40-800/F584 SYNCORE-STIFFENED			G40-800/F584 SPREAD 0°/Y-SPARS			G40-800/F584 DISCRETE CAP/Y-SPARS		
		TOTAL SCORE	NO. OF R	AVG SCORE	TOTAL SCORE	NO. OF R	AVG SCORE	TOTAL SCORE	NO. OF R	AVG SCORE	TOTAL SCORE	NO. OF R	AVG SCORE
WEIGHT	25	450	4	113	700	4	175	575	4	144	675	4	169
RISK	10	300	4	75	300	4	75	240	4	60	240	4	60
MFG RDT & E AND PRODUCTION COSTS	18	552	4	138	528	4	132	552	4	138	552	4	138
DURABILITY AND SURVIVABILITY	14	378	4	95	364	4	91	378	4	95	406	4	102
REPAIRABILITY	15	435	4	109	435	4	109	405	4	101	420	4	105
INSPECTION/ACCESS	10	290	4	73	290	4	73	220	4	55	220	4	55
OPS & SUPT COSTS	8	224	4	56	224	4	56	236	4	59	236	4	59
SUM OF AVG. SCORES				659			711			652			688
R90-4125-007													

CONCEPT SELECTION

The relative closeness of the ratings for Concepts II, V and VI, and subjective nature of the evaluation make them virtually equivalent. However, continued effort will be directed towards Concepts V (Multi-Spar: Y-Spar) and VI (Multi-Rib: Y-Stiffened), since they represent the latter stages of development and the most potential to attain the program's goals.

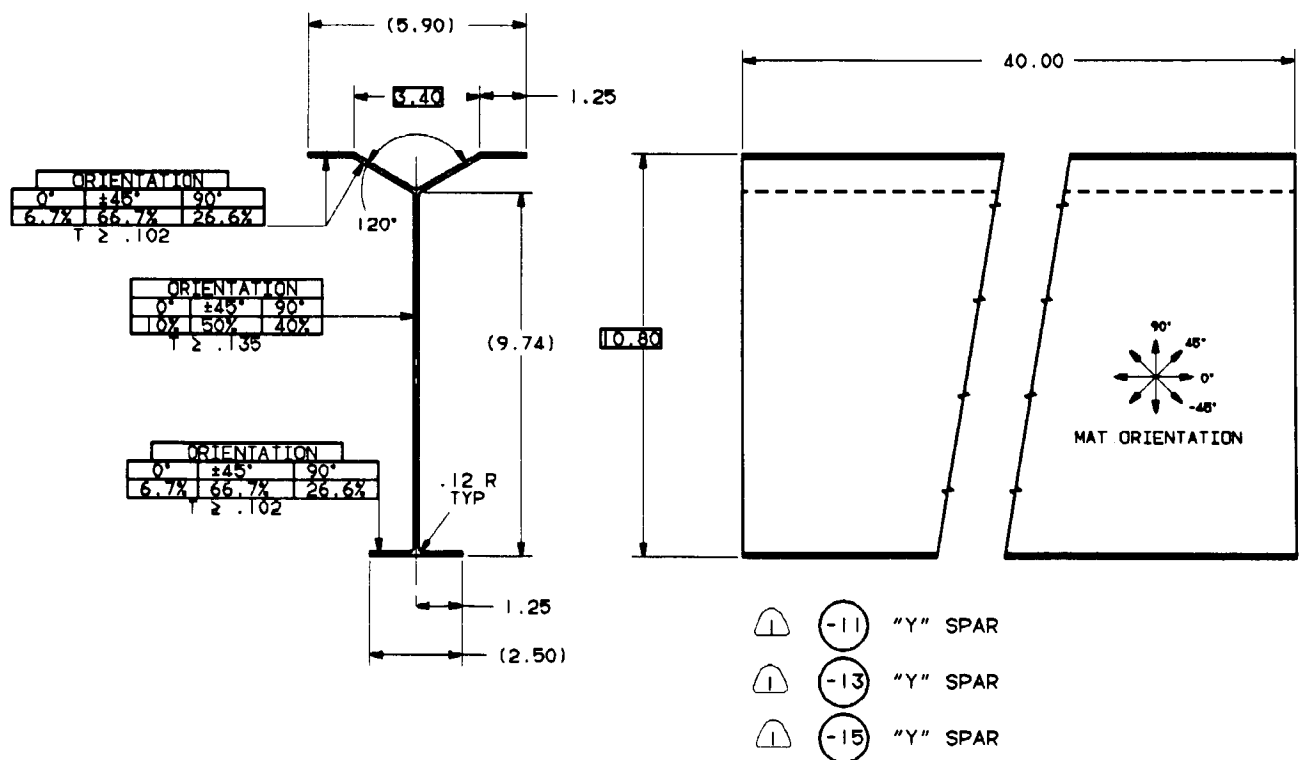
Concept Evaluation, Multi-Rib Concepts

PARAMETERS	WEIGHTING FACTOR	CONCEPT III			CONCEPT VI		
		IM7/TACTIX 123 HAT-STIFFENED			IM7/TACTIX 123 Y-STIFFENED		
		TOTAL SCORE	NO. OF R	AVG SCORE	TOTAL SCORE	NO. OF R	AVG SCORE
WEIGHT	25	700	4	175	925	4	231
RISK	10	250	4	63	250	4	63
MFG RDT & E AND PRODUCTION COSTS	18	456	4	114	480	4	120
DURABILITY AND SURVIVABILITY	14	406	4	102	364	4	91
REPAIRABILITY	15	405	4	101	390	4	98
INSPECTION/ACCESS	10	260	4	65	250	4	63
OPS & SUPT COSTS	8	245	4	61	212	4	53
SUM OF AVG. SCORES				681			719

DESIGN, ANALYSIS, FABRICATION AND TEST OF Y-SPARS

- Y-spar representative of intermediate wing spar segment in size, complexity and load carrying capability (shear flow of 1,015 lb/in. in 5-spar wing configuration)
- Three 40-in. Y-spar preforms woven by Textile Technologies, Inc. on NASA Jacquard loom using angle interlock fiber architecture
 - Commingled AS4(6K)/PEEK 150g Tows
 - 0/90-degree weave and ± 45 -deg fabric stitched with Fiberglass/Toray H.S. thread
- Demonstrate structural integrity of Y-spars
 - Two Y-spars destructively sectioned
 - Mechanical & physical properties tests
 - Standard for ultrasonic NDI
 - One Y-spar tested in four-point beam bending

**Commingled AS4/PEEK 150G
Y-Spar Configuration
D19B8220-13**



MANUFACTURING EFFORT OVERVIEW

- Commingled AS4/PPS 0°/90° I-Beams
 - Design and fabrication of woven commingled AS4/PPS 3-D I-Beam preforms
 - Consolidation/forming of I-Beam preforms
 - NDI and dimensional analysis of I-Beams
- Commingled AS4/PEEK 150g Y-spars
 - Design and fabrication of woven commingled AS4/PEEK 150g Y-spar preforms
 - Consolidation/forming of Y-spar preforms
 - NDI and dimensional analysis of Y-spars
 - Structural test of Y-spar

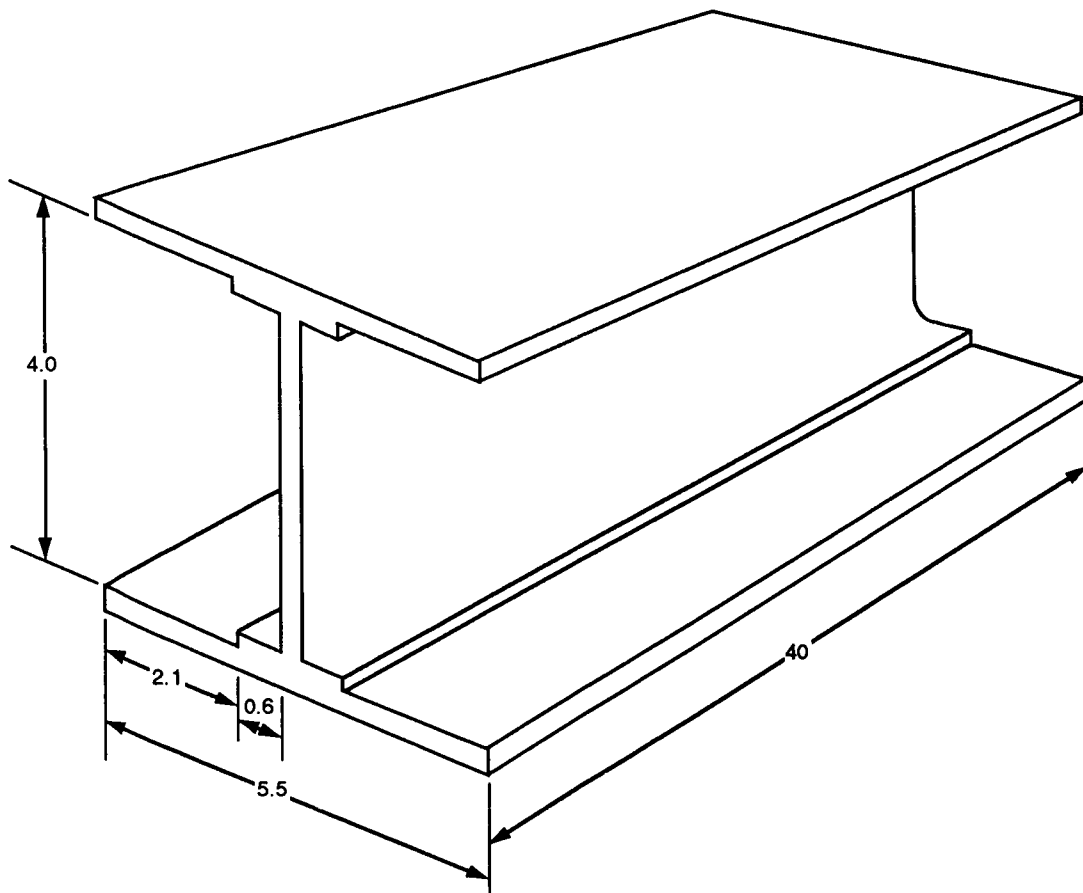
COMMINGLED AS4/PPS 0°/90° I-BEAMS

Textile manufacturers at present cannot weave 3-D preforms with 0°, 90° and $\pm 45^\circ$ fiber reinforcement orientations. Preforms with fibers oriented 0°/90° to each other are woven to provide 3-D carcasses. Plies of fabric are then stitched to these carcasses in 45°/135° orientations to provide preforms which when consolidated will provide structural parts.

A series of woven commingled AS4(3K)/PPS 0°/90° I-beam carcasses were consolidated to provide processing data for these intermediate preform configurations. Emphasis was placed on the consolidation characteristics of these material forms and resultant percent fiber volume values. It was realized that the structural properties of the consolidated 0°/90° I-beams were minimal (without 45°/135° reinforcement); therefore testing for physical properties was emphasized in these processing studies.

Textile Technologies, Inc. (TTI) was requested to weave three I-beam preforms using commingled AS4/PPS fiber. The 3-D preforms were to be fabricated using commingled tows with a 60/40 graphite fiber to PEEK 150g filament volume ratio. The 0°/90° preforms were to be configured to accommodate the following target dimensions after consolidation: length – 40 in., cap width – 5.5 in., and web height – 4.0 in. The thickness of the web was to be 0.072 ± 0.006 in. The web flanges were to be 0.60 in. wide and 0.036 ± 0.003 in. thick.

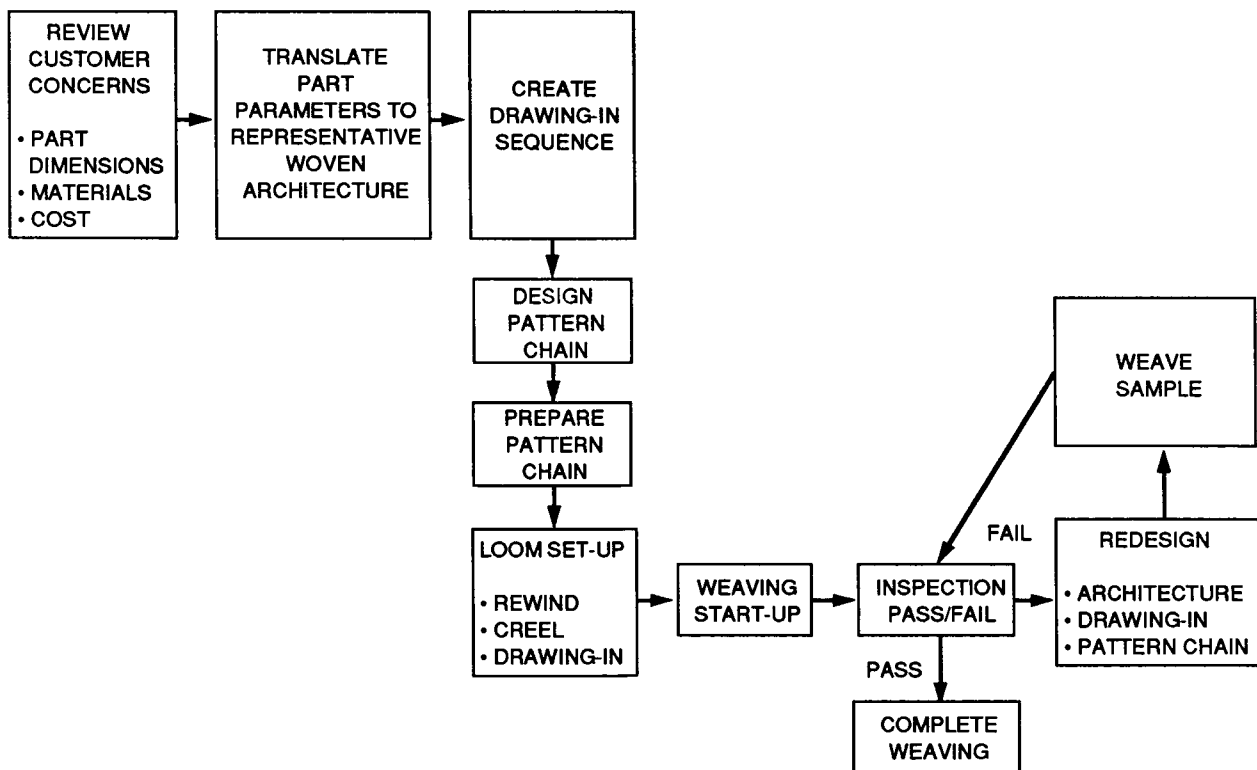
Woven Commingled AS4/PPS 0°/90° I-Beam



DESIGN METHODOLOGY

TTI reviewed configuration and material requirements plus cost concerns for the proposed commingled AS4/PPS I-beam. These customer requirements were then translated into an architecture for a woven 3-D preform which upon consolidation would yield a structure meeting design specifications. Preparation of a preform architecture is supported by the use of the interactive computer program Framework. This computer program permits the textile designer to rapidly determine the effect of fiber mix on the final thickness and fiber volume in given areas of the woven structure.

The loom is set up to accommodate the weaving requirements of the preform architecture. (A Jacquard loom was used to fabricate the commingled AS4/PPS preforms.) A series of trial weaving runs are then performed. Following each operation the appearance, dimensions and weight of the preform are evaluated. Based on these determinations the preform architecture is refined as necessary to produce an acceptable part. Since 3-D weaving is not an exact science this design/manufacturing iteration may have to be performed a number of times.

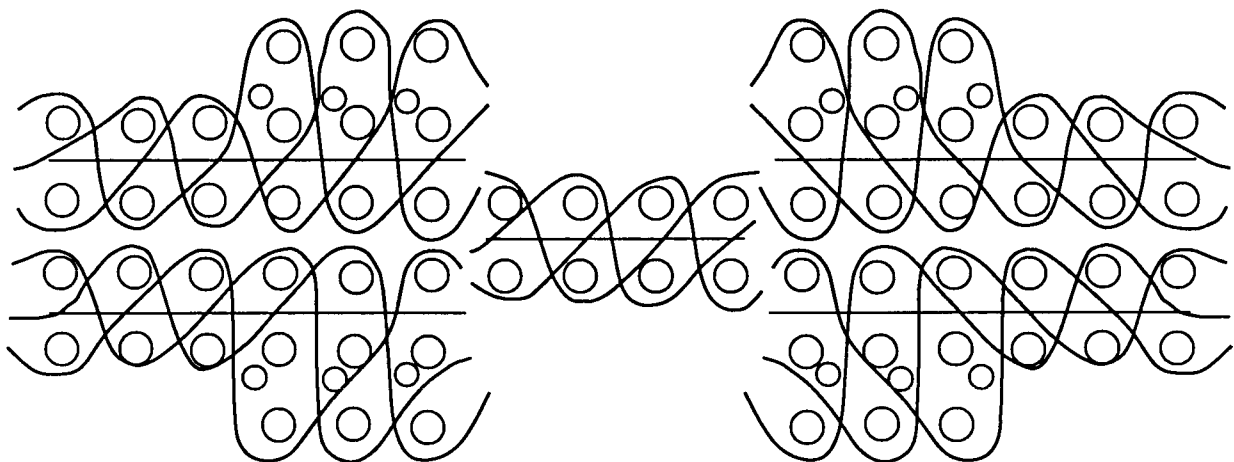


WOVEN PREFORM ARCHITECTURE

The architecture of a given preform shows the relative orientation of the fibers used to build that fabric part. In the case of the commingled AS4/PPS I-beam preforms, three fiber types (by function) were used: fill, stuffers and warp weavers. The stuffers are continuous, non-crimped fibers, installed in the same direction as the interlaced (with the fill fibers) warp weavers.

The architecture for the commingled AS4/PPS 0°/90° I-beam describes fiber configurations in the web and caps of the I-beam. The stepped area in the I-beam cap is also shown.

Architecture of Woven Commingled AS4/PPS 0°/90° I-Beam



	TOWS	THK
○ FILL	4	.040"
— STUFFERS	8	.064" (EXCEPT IN WEB SECTION)
~ WARP WEAVERS	4	.040"

MATERIAL: AS4 (3K)/PPS COMMINGLED

FRAMEWORK

Consolidated Thickness Spread Sheet

The Framework is an interactive computer program that predicts the thickness of a consolidated preform based on the physical characteristics of the fibers used by the weaver in the fill and warp directions of the preform. These inputs are identified by an asterisk in the Framework shown for the web of the I-beam preform. They are end count (fiber ends per in.), denier (grams per 9000 meter) and fiber density. In the case of the I-beam web, a thickness of 0.060 in. and a percent fiber volume of 62.8 percent were predicted for the consolidated part.

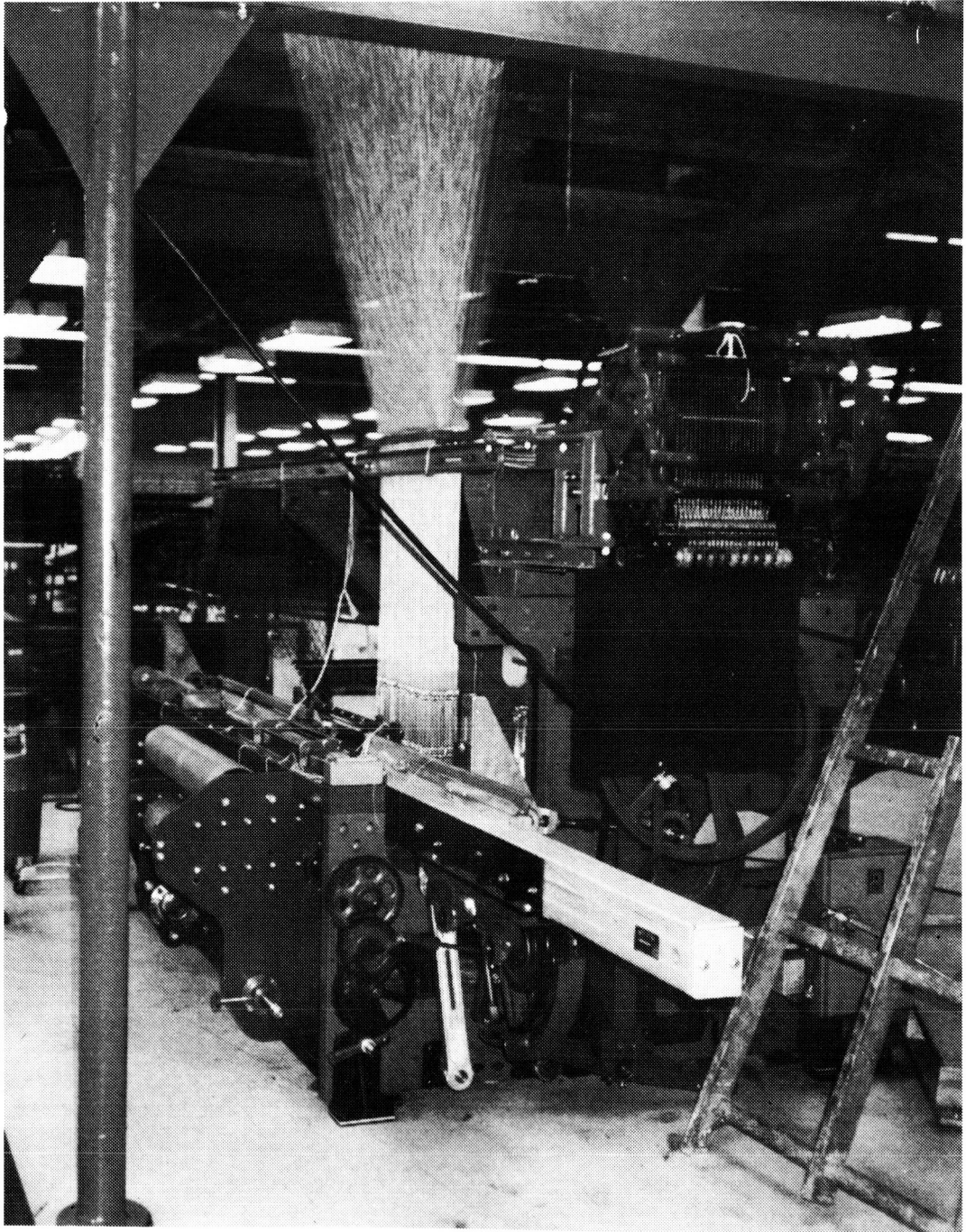
Consolidated Thickness Spread Sheet Woven Commingled 3-D AS4/PPS I-Beam

HYBRID YARN FABRIC			FIBER	RESIN	TOTAL	
I-BEAM WEB						
WARP	* END COUNT (ENDS/IN)		128	128		
	* MANUFACTURER		HERCULES	BASF		
	* PRODUCT CODE	AS-4,3K	PPS			
	* DENIER (GR/M)		1963	900	2863	
	YIELD (YDS/LB)		2276	4965	1561	
	* DENSITY (GR/CC)		1.73	1.34	1.58	
	AREAL WEIGHT (GR/SQ M)		1099.1	503.9	1603.1	47.24
	THICKNESS (MILS)		25.0	14.8	39.8	^OZ/SQ YD^
	VOLUME FRACTION (%)		41.9	24.8	66.7	
	WEIGHT FRACTION (%)		45.7	21.0	66.7	
FILL	* END COUNT (ENDS/IN)		64	64		
	* MANUFACTURER		HERCULES	BASF		
	* PRODUCT CODE	AS-4,3K	PPS			
	* DENIER (GR/M)		1963	900	2863	
	YIELD (YDS/LB)		2276	4965	1561	
	* DENSITY (GR/CC)		1.73	1.34	1.58	
	AREAL WEIGHT (GR/SQ M)		549.6	252.0	801.5	23.62
	THICKNESS (MILS)		12.5	7.4	19.9	^OZ/SQ YD^
	VOLUME FRACTION (%)		20.9	12.4	33.3	
	WEIGHT FRACTION (%)		22.9	10.5	33.3	
TOTAL FABRIC	AREAL WEIGHT (GR/SQ M)		1648.7	755.9	2404.6	70.85
	THICKNESS (MILS)		37.5	22.2	59.7	^OZ/SQ YD^
	VOLUME FRACTION (%)		62.8	37.2	100	
	WEIGHT FRACTION (%)		68.6	31.4	100	
	DENSITY (GR/CC)				1.58	

JACQUARD WEAVING MACHINE

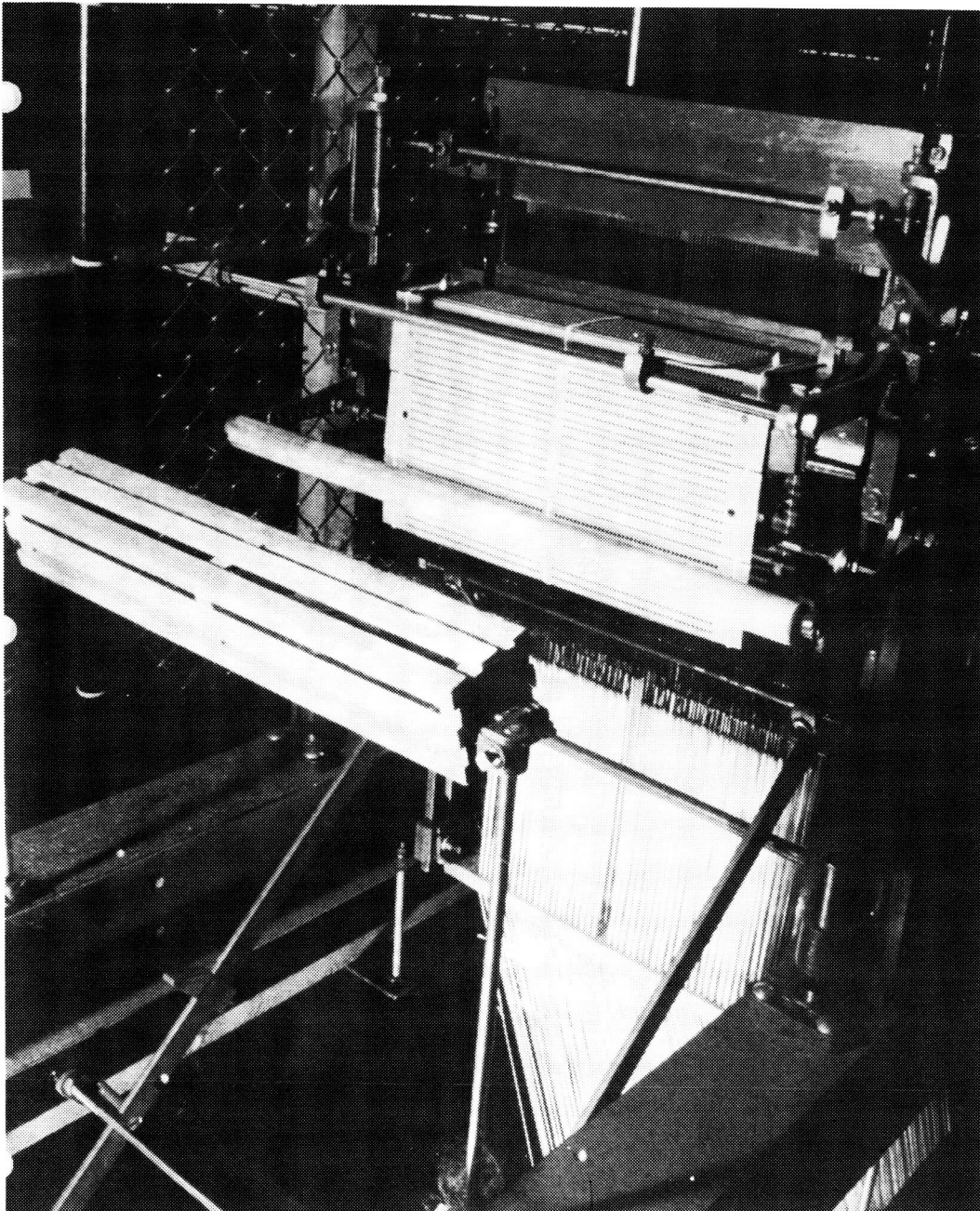
This machine was purchased by TTI under NASA Contract NAS 1-18385. The machine features a mechanism which permits individual control of every yarn weaving across the width of a given fabric or preform. With a Jacquard head, weaving possibilities become infinite. It is this capability that permits the weaving of 3-D preforms.

The NASA machine has a 2500 warp end capability.



JACQUARD CARDS

Punched cardboard cards convey the fabric design or preform architecture to the Jacquard loom. The cards operate much like the rolls of perforated paper which control the operation of player pianos. The cards determine whether or not warp yarns are raised or lowered to accommodate the insertion of a fill yarn.

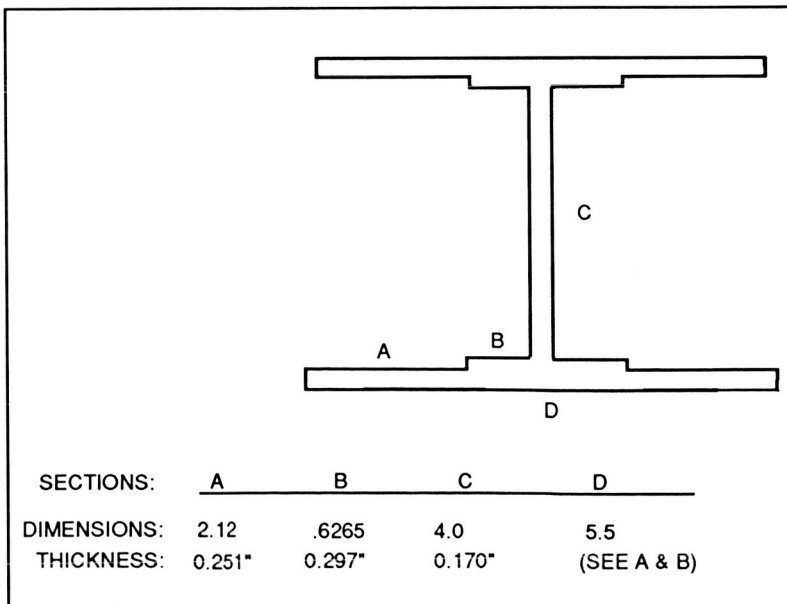
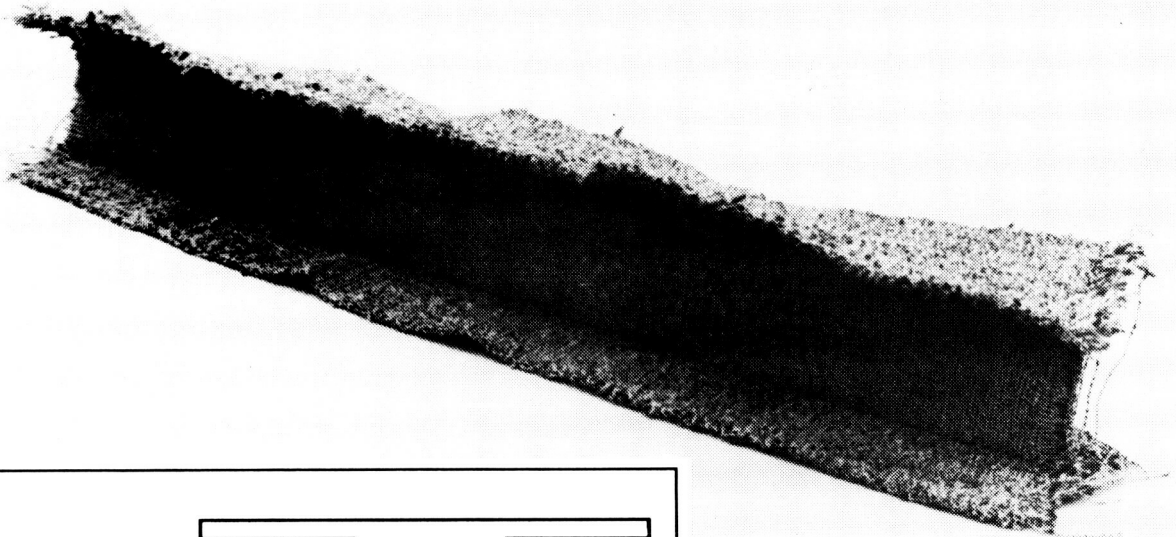


WOVEN COMMINGLED PREFORM

Three 40 in. (length) woven commingled AS4/PPS 0°/90° preforms were received from TTI. The visual appearances of the preforms were satisfactory; no floaters were detected in either the cap or web of the preform and the parts were tightly woven. (A floater is a warp weaver that has relatively long distances between successive interlacing fill yarns.)

The average thickness dimensions of the preforms were as follows:

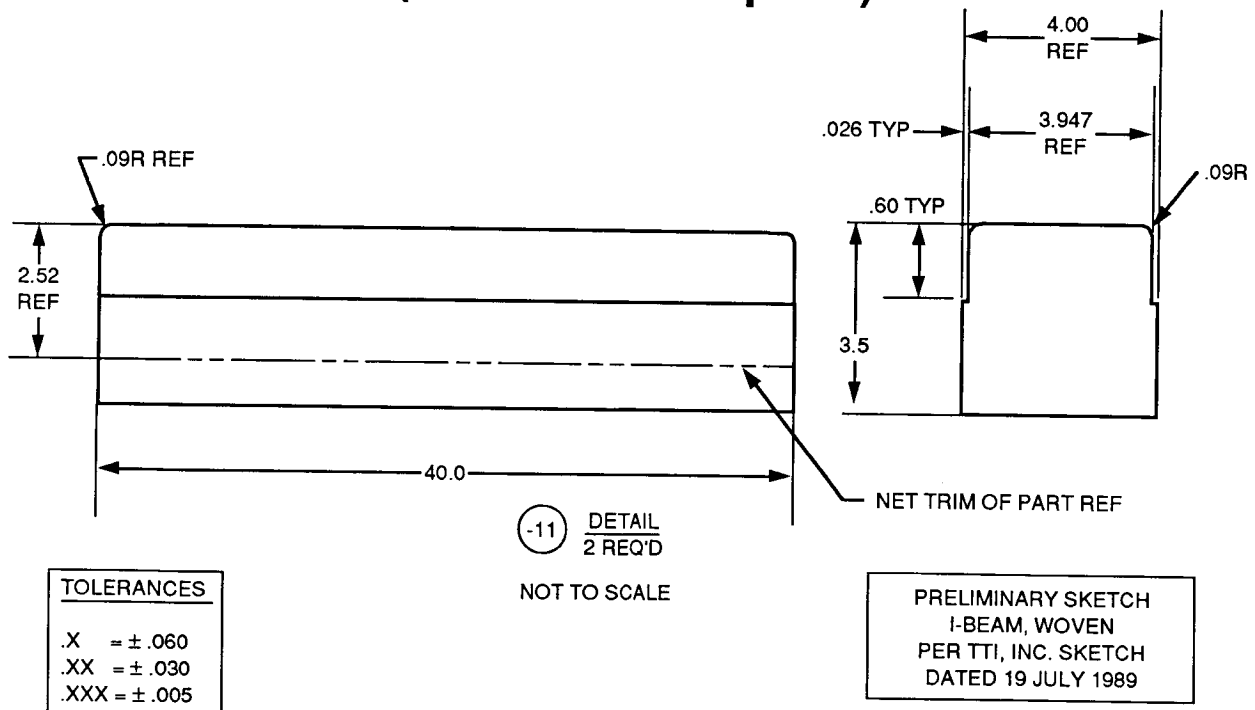
Web: 0.627 in.
Outer Cap: 0.1251 in.
Inner Cap: 0.297 in.



CONSOLIDATION/FORMING MANDRELS

It was decided to consolidate/form the commingled AS4/PPS I-beam preforms using matched monolithic graphite mandrels. The male tools would insure achievement of the required web height and thickness plus optimum forming/consolidation of the steps on the inner surfaces of the I-beam caps. Flat 0.125 in. thick aluminum caul plates were selected for use in consolidating the I-beam caps against the underlying monolithic graphite mandrels.

I-Beam Consolidation/Forming Tools (Monolithic Graphite)

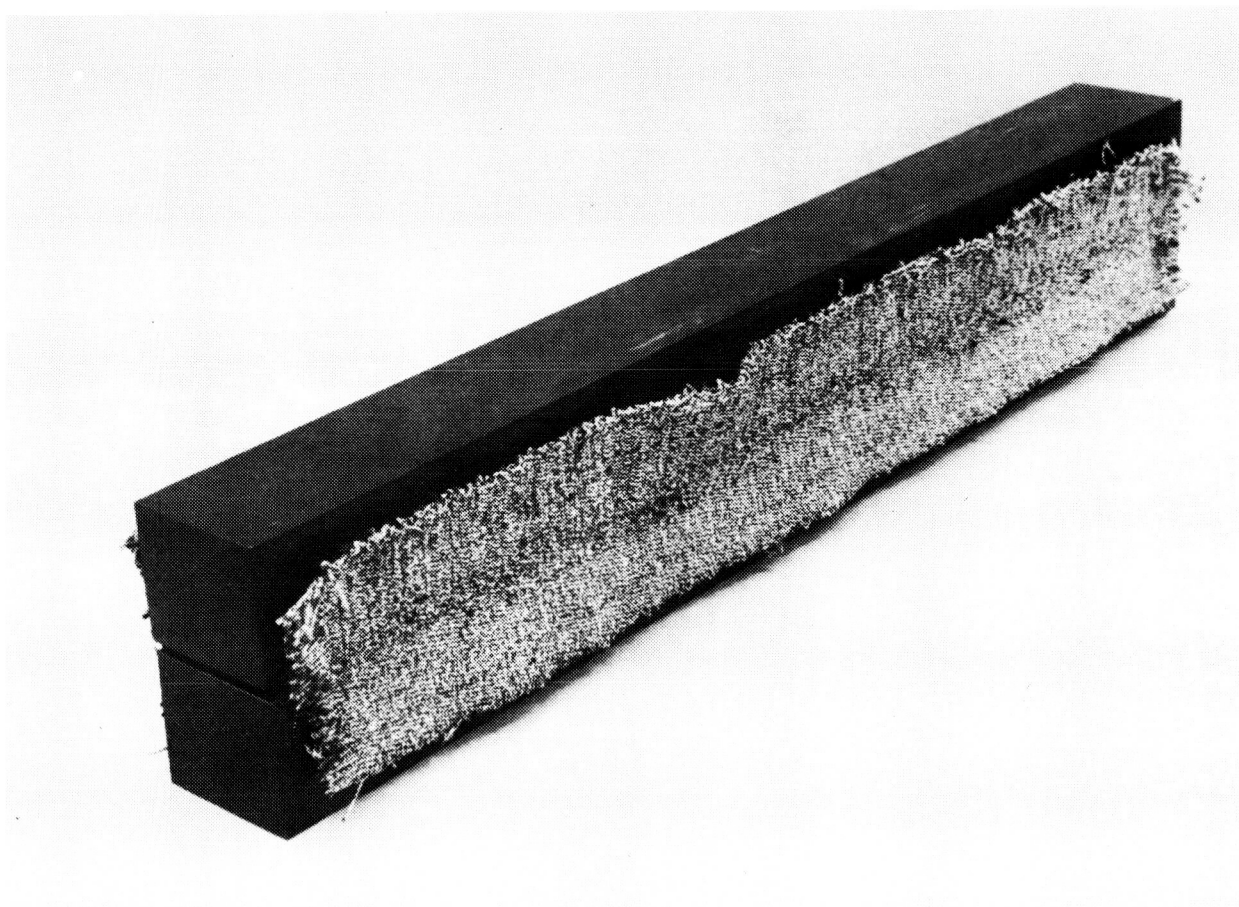


MONOLITHIC GRAPHITE TOOLING

Monolithic graphite was chosen as the material of construction for the tooling mandrels. The coefficient of thermal expansion (CTE) for this material ranges from 1.5 to 2.0×10^{-6} in./in./°F. This value compares favorably with the commonly used CTE range for Gr/Ep composite laminates, 1.0 to 1.5×10^{-6} in./in./°F. (The CTE value for consolidated woven 3-D commingled AS4/PPS 0°/90° structure is presently not available.) Corresponding CTE ranges for competitive tooling materials such as aluminum, steel and nickel alloy are 13.0 - 13.6 , 6.1 - 6.7 , and 6.6 - 7.4×10^{-6} in./in./°F, respectively. The thermal conductivity of monolithic graphite is greater than that of steel and nickel tool alloys (68 vs 26 and 34 BTU-ft/ft²-hr-°F, respectively) but less than that of aluminum alloy (68 vs 117 BTU-ft/ft²-hr-°F). Aluminum tool alloys, however, are not useful at temperatures above 700°F whereas monolithic graphite tools can be reliably utilized at temperatures up to 1000°F .

Monolithic graphite tools also have exceptional resistance to thermal shock at high temperatures due to the material's low CTE, high thermal conductivity, high tensile strength and relatively low modulus of elasticity.

Finally, monolithic graphite is very machinable and tools with precise tolerances (<0.003 in.) and smooth surfaces (<10 rms) may be cost effectively manufactured.

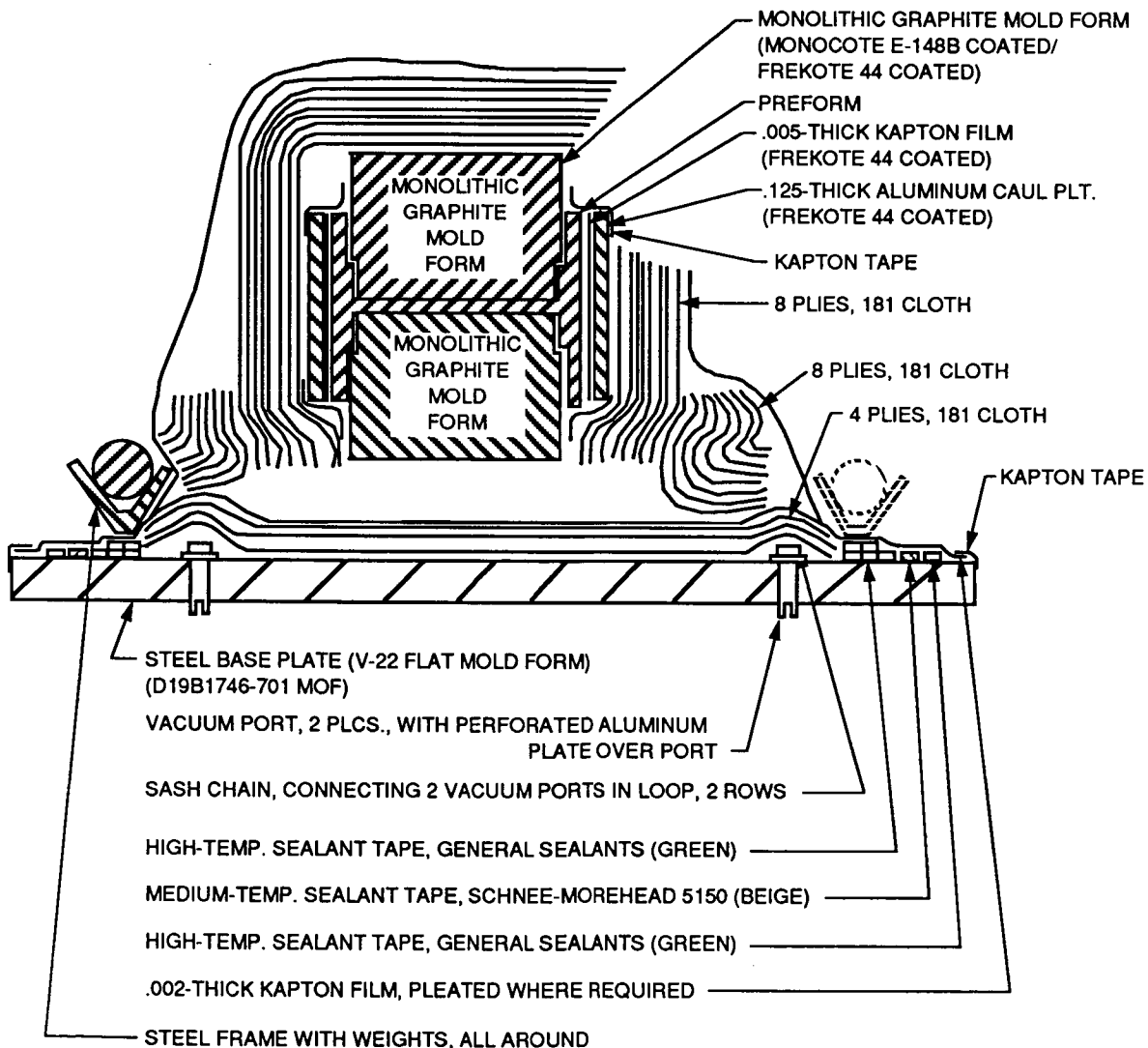


AUTOCLAVE VACUUM BAG ARRANGEMENT

The commingled AS4/PPS I-beams were consolidated using an autoclave/vacuum bag procedure. The workpiece (I-beam preform installed between matched graphite mandrels) was installed on a steel base plate. The workpiece was vacuum bagged to the baseplate using Kapton film material. A weighted steel frame, in combination with medium and high temperature sealant materials, was used to provide a vacuum tight bag over the workpiece.

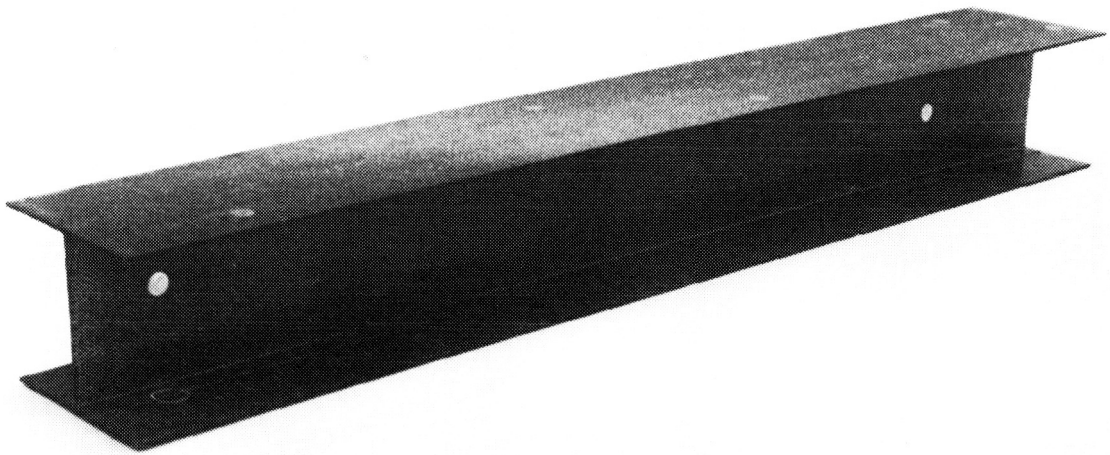
The commingled AS4/PPS preforms were consolidated for 30 minutes at 630°F and 200 psi.

Woven Commingled AS4/PPS 0°/90° I-Beam Autoclave Vacuum Bag Arrangement



CONSOLIDATED I-BEAMS

The autoclave/vacuum bag consolidation procedure for I-beam -1 was unsatisfactory. The graphite mandrels hung up and did not properly close on the web of the preform. As a result, this I-beam did not pass ultrasonic or dimensional inspection. The layup procedure for the workpiece and the vacuum bagging arrangement were refined to ensure optimum closure of the forming dies. I-beam preforms -2 and -3 were subsequently consolidated to provide I-beams that were acceptable with respect to ultrasonic and dimensional NDI. The trim drop-off from each of the I-beams was used to provide coupons for percent fiber volume analysis and edge photomicrographic inspection. Edge photomicrographic inspection indicated that I-beams -2 and -3 were free of porosity. The average percent fiber volume for these structures was approximately 57 percent.



- Ultrasonic Inspection: No Defects
- Edge Photomicrographic Inspection: OK
- Percent Fiber Volume: 57%
- Final Web Thickness: 60% That of Preform

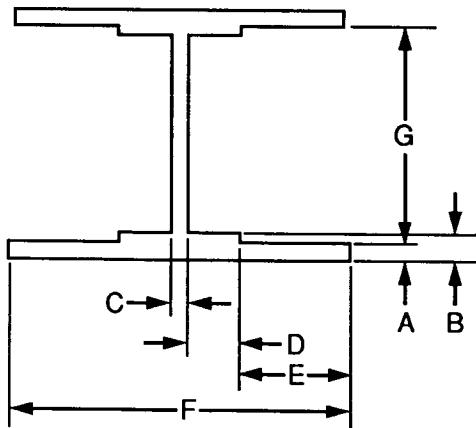
TARGET, PREFORM AND FINAL PART DIMENSIONS

Target, as received preform and final consolidated dimensions are presented for each of the three I-beams. Emphasis is placed on final web thickness since a specific target value was given to TTI, i.e., 0.072 ± 0.006 in. As expected, the web thickness of I-beam -1 was unacceptable, 0.115 in. The web thicknesses of I-beams -2 and -3, however, were acceptable, i.e., 0.065 and 0.074 in., respectively.

Average percent consolidation values for the web and cap areas of the preforms are presented for I-beams -2 and -3. (Percent consolidation equals preform thickness – consolidated thickness divided by preform thickness multiplied by 100.) The average percent consolidation value for the webs was 56.5 percent.

The 56.5 percent consolidation value was used in the shimming operation for consolidation/forming of the AS4/PEEK 150g Y-spar preforms.

Woven Commingled AS4/PPS I-Beam Target, Preform & Final Part Dimensions



	TARGET (IN.)	PREFORM (IN.)	CONSOLIDATED I-BEAMS			PERCENT CONS. (%)
			1 (IN.)	2 (IN.)	3 (IN.)	
A	>0.084	0.251	0.112	0.112	0.102	59.4
B	>0.120	0.297	0.144	0.140	0.144	51.5
C	0.066 -0.078	0.170	0.115	0.065	0.074	56.5
D	0.6	0.6	0.6	0.6	0.6	—
E	>2.0	2.2	2.2	2.2	2.2	—
F	>5.0	5.6	5.6	5.6	5.6	—
G	4.0	4.0	4.0	4.0	4.0	—

COMMINGLED AS4/PEEK 150G Y-SPARS

Three 40 in. (length) commingled AS4/PEEK 150g Y-spars are being fabricated by the autoclave consolidation of woven/stitched preforms. Cap details will be mechanically attached to the Y-spars to provide elements suitable for destructive testing.

Y-spar 0°/90° carcasses were woven by TTI using their Jacquard loom. Sewing Machine Exchange, Inc. (SMX), a TTI subcontractor, stitched woven commingled AS4/PEEK 150g fabric in 45°/135° orientations to the carcasses to provide woven/stitched 3-D Y-spar preforms.

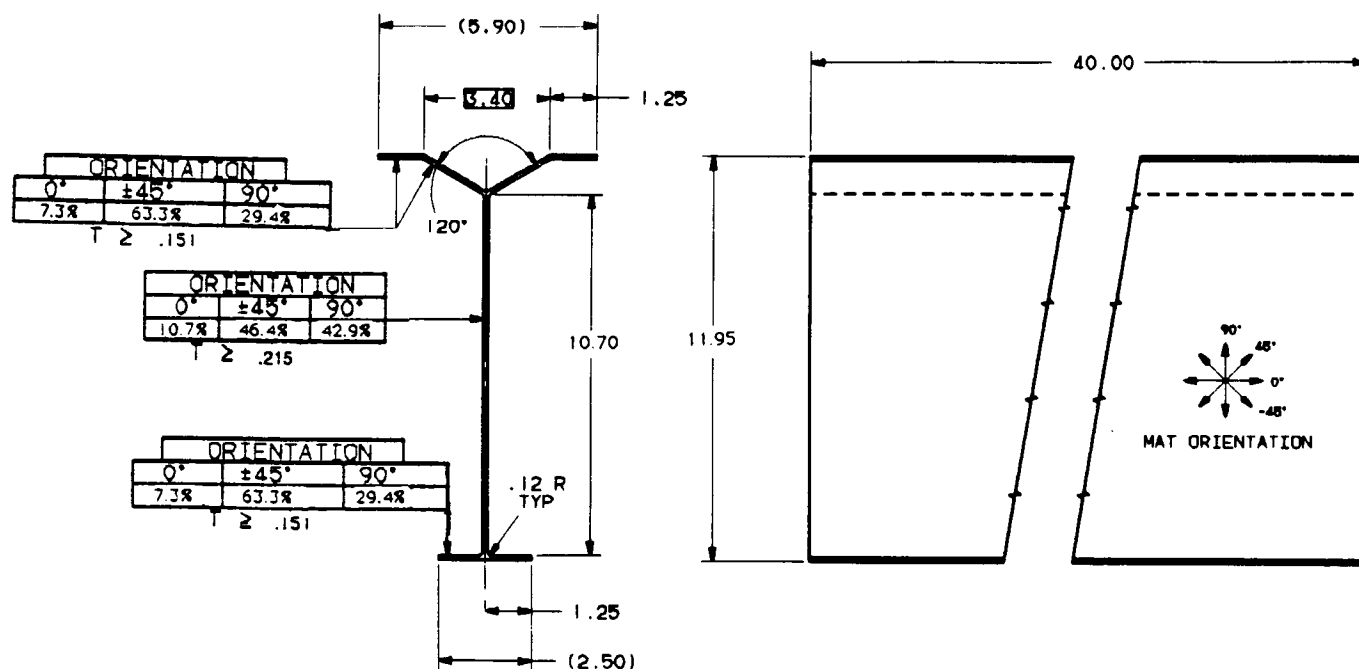
The Y-spar preforms are being sequentially consolidated by Grumman using vacuum bag processing in an autoclave. Grumman is presently evaluating non-autoclave consolidation procedures which have the potential to be more cost effective than the baseline process. These innovative processes include thermoforming and the Therm-X process. Since the primary goal of our program is to provide reliable engineering data and since a limited number of Y-spars are to be fabricated, it was decided to use the low risk autoclave process. Furthermore, the autoclave process had already been demonstrated by the successful consolidation of the commingled AS4/PPS I-beam preforms.

The Y-spar preforms are being sequentially consolidated using the following approach. The first Y-spar will be inspected using ultrasonic NDI and dimensional analysis. The Y-spar will be destructively sectioned and reinspected using dimensional and micrographic analysis. Design/Manufacturing/Quality Control personnel will review these data and refine the consolidation procedure accordingly. The second Y-spar will be consolidated and the above review process will be repeated. The third Y-spar will be consolidated using the refined process and then destructively tested using four-point beam bending.

COMMINGLED AS4/PEEK 150G Y-SPAR CONFIGURATION

TTI provided three woven/stitched commingled AS4/PEEK 150g Y-spar preforms which upon consolidation would meet modified configuration requirements of D19B8220-13. The percent fiber volume of the consolidated preforms was to be 60 percent.

Commingled AS4/PEEK 150G Modified Y-Spar Configuration

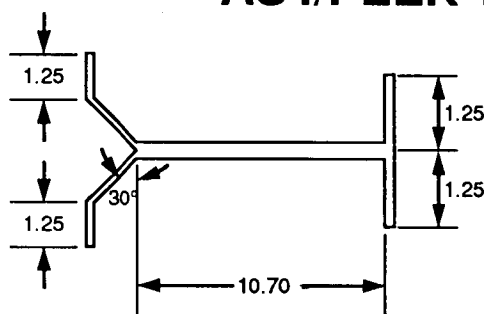


ARCHITECTURE OF PREFORMS

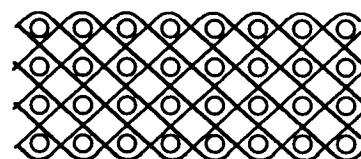
The architecture of the woven commingled AS4/PEEK 150g 0°/90° preforms is presented below. The preform webs consist of 76.59 percent fill yarns, 19.14 percent warp stuffers and 4.25 percent through the thickness warp weavers. The preform flanges consist of 75.00 percent fill yarns, 18.75 percent warp stuffers and 6.25 percent through the thickness warp weavers.




The critical dimension for the preforms was the web height as measured from the radius of the 90-degree flange to the radius of the Y-flange, i.e., 10.70 in. This dimension was made important by the decision to use male mandrels for consolidation of the preforms. Web and flange thicknesses were to be such that upon preform consolidation to a 60 percent fiber volume, modified D19B8220-13 target dimensions would be achieved. A 55 percent consolidation value was expected.

Architecture of Woven Commingled AS4/PEEK 150G 0°/90° Preform






WEB SECTION



WEB SECTION	
	FILLING
	WARP
	THROUGH-THE THICKNESS

YARNS/ INCH	% FIBER BY WEIGHT
72	76.59
18	19.16
4	4.25

FLANGE SECTION

	FILLING
	WARP
	THROUGH-THE THICKNESS

36	75.00
9	18.75
3	6.25

FLANGE SECTION



MATERIAL TYPE: AS4/PEEK 150G
COMMINGLED YARN

FRAMEWORK **Consolidated Thickness Spread Sheet - Web**

The Framework print-out for the web of the commingled AS4/PEEK 150g 0°/90° Y-spar preforms is shown below. The 27 ends/in. end count for the warp fibers was composed of 22 warp stuffers and 5 through-the-thickness weavers. The denier value for the AS4 and PEEK 150g fibers making up the tows used in the warp and fill directions were 3927 and 1800, respectively.

Target thickness and percent fiber volume values for the consolidated web were 0.071 in. and 61.0 percent, respectively.

Woven Commingled 3-D AS4/PEEK150 G 0°/90° Y-Spar Web Preform

HYBRID YARN FABRIC			FIBER	RESIN	TOTAL	
WARP	* END COUNT	(ENDS/IN)	27	27		
	* MANUFACTURER		BASF	BASF		
	* PRODUCT CODE		AS-4 6K	PEEK		
	* DENIER	(GR/M)	3927	1800	5727	
	YIELD	(YDS/LB)	1138	2482	780	
	* DENSITY	(GR/CC)	1.80	1.29	1.60	
	AREAL WEIGHT	(GR/SQ M)	463.8	212.6	676.4	19.93
	THICKNESS	(MILS)	10.1	6.5	16.6	^OZ/SQ YD^
	VOLUME FRACTION	(%)	14.3	9.2	23.5	
	WEIGHT FRACTION	(%)	16.1	7.4	23.5	
FILL	* END COUNT	(ENDS/IN)	88	88		
	* MANUFACTURER		BASF	BASF		
	* PRODUCT CODE		AS-4	PEEK		
	* DENIER	(GR/M)	3927	1800	5727	
	YIELD	(YDS/LB)	1138	2482	780	
	* DENSITY	(GR/CC)	1.80	1.29	1.60	
	AREAL WEIGHT	(GR/SQ M)	1511.7	692.9	2204.6	64.96
	THICKNESS	(MILS)	33.1	21.1	54.2	^OZ/SQ YD^
	VOLUME FRACTION	(%)	46.7	29.9	76.5	
	WEIGHT FRACTION	(%)	52.5	24.1	76.5	
TOTAL FABRIC	AREAL WEIGHT	(GR/SQ M)	1975.5	905.5	2881.0	84.89
	THICKNESS	(MILS)	43.2	27.6	70.8	^OZ/SQ YD^
	VOLUME FRACTION	(%)	61.0	39.0	100	
	WEIGHT FRACTION	(%)	68.6	31.4	100	
	DENSITY	(GR/CC)			1.60	

FRAMEWORK **Consolidated Thickness Spread Sheet - Flange**

The Framework print-out for the flange of the commingled AS4/PEEK 150g 0°/90° Y-spar preforms is shown below. The 15 ends/in. end count for the warp fibers was composed of warp stuffers and through-the-thickness weavers. The denier value for the AS4 and PEEK 150g fibers making up the tows used was again 3927 and 1800, respectively.

Target thickness and percent fiber volume values for the consolidated 0°/90° Y-spar web carcass were 0.036 in. and 61.0 percent, respectively.

Woven Commingled 3-D AS4/PEEK150 G 0°/90° Y-Spar Flange Preform

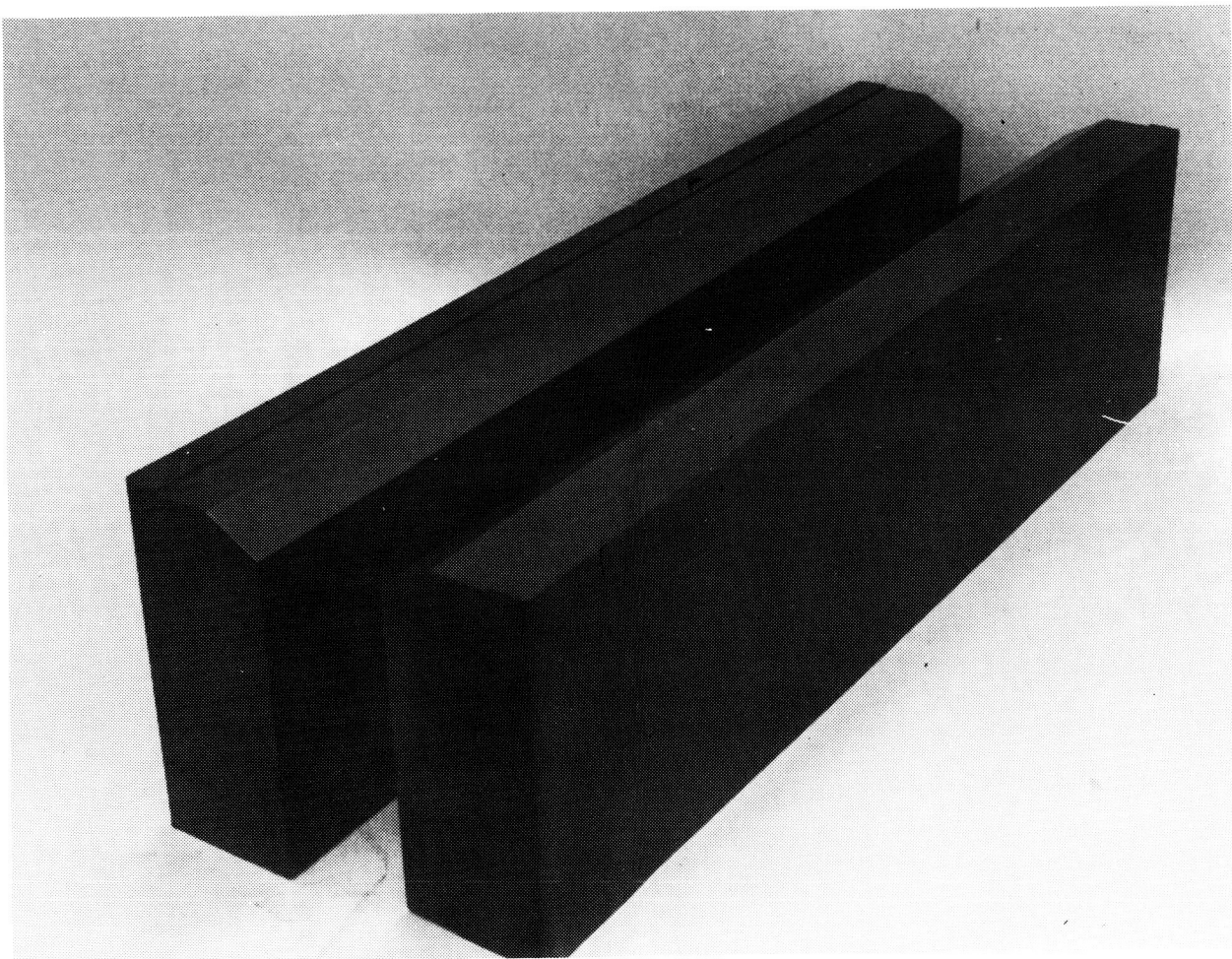
HYBRID YARN FABRIC			FIBER	RESIN	TOTAL	
WARP	* END COUNT	(ENDS/IN)	15	15		
	* MANUFACTURER		BASF	BASF		
	* PRODUCT CODE		AS-4 6K	PEEK		
	* DENIER	(GR/M)	3927	1800	5727	
	YIELD	(YDS/LB)	1138	2482	780	
	* DENSITY	(GR/CC)	1.80	1.29	1.60	
	AREAL WEIGHT	(GR/SQ M)	257.7	118.1	375.8	11.07
	THICKNESS	(MILS)	5.6	3.6	9.2	^OZ/SQ YD^
	VOLUME FRACTION	(%)	15.5	9.9	25.4	
	WEIGHT FRACTION	(%)	17.4	8.0	25.4	
FILL	* END COUNT	(ENDS/IN)	44	44		
	* MANUFACTURER		BASF	BASF		
	* PRODUCT CODE		AS-4	PEEK		
	* DENIER	(GR/M)	3927	1800	5727	
	YIELD	(YDS/LB)	1138	2482	780	
	* DENSITY	(GR/CC)	1.80	1.29	1.60	
	AREAL WEIGHT	(GR/SQ M)	755.9	346.5	1102.3	32.48
	THICKNESS	(MILS)	16.5	10.6	27.1	^OZ/SQ YD^
	VOLUME FRACTION	(%)	45.5	29.1	74.6	
	WEIGHT FRACTION	(%)	51.1	23.4	74.6	
TOTAL FABRIC	AREAL WEIGHT	(GR/SQ M)	1013.5	464.6	1478.1	43.55
	THICKNESS	(MILS)	22.2	14.2	36.3	^OZ/SQ YD^
	VOLUME FRACTION	(%)	61.0	39.0	100	
	WEIGHT FRACTION	(%)	68.6	31.4	100	
	DENSITY	(GR/CC)			1.60	

CONSOLIDATION/FORMING MANDRELS

It was decided to consolidate/form the commingled AS4/PEEK 150g Y-spar preforms using matched monolithic graphite mandrels. Monolithic graphite tooling was chosen because of the good performance of the mandrels used to consolidate the previously discussed commingled AS4/PPS 0°/90° I-Beams.

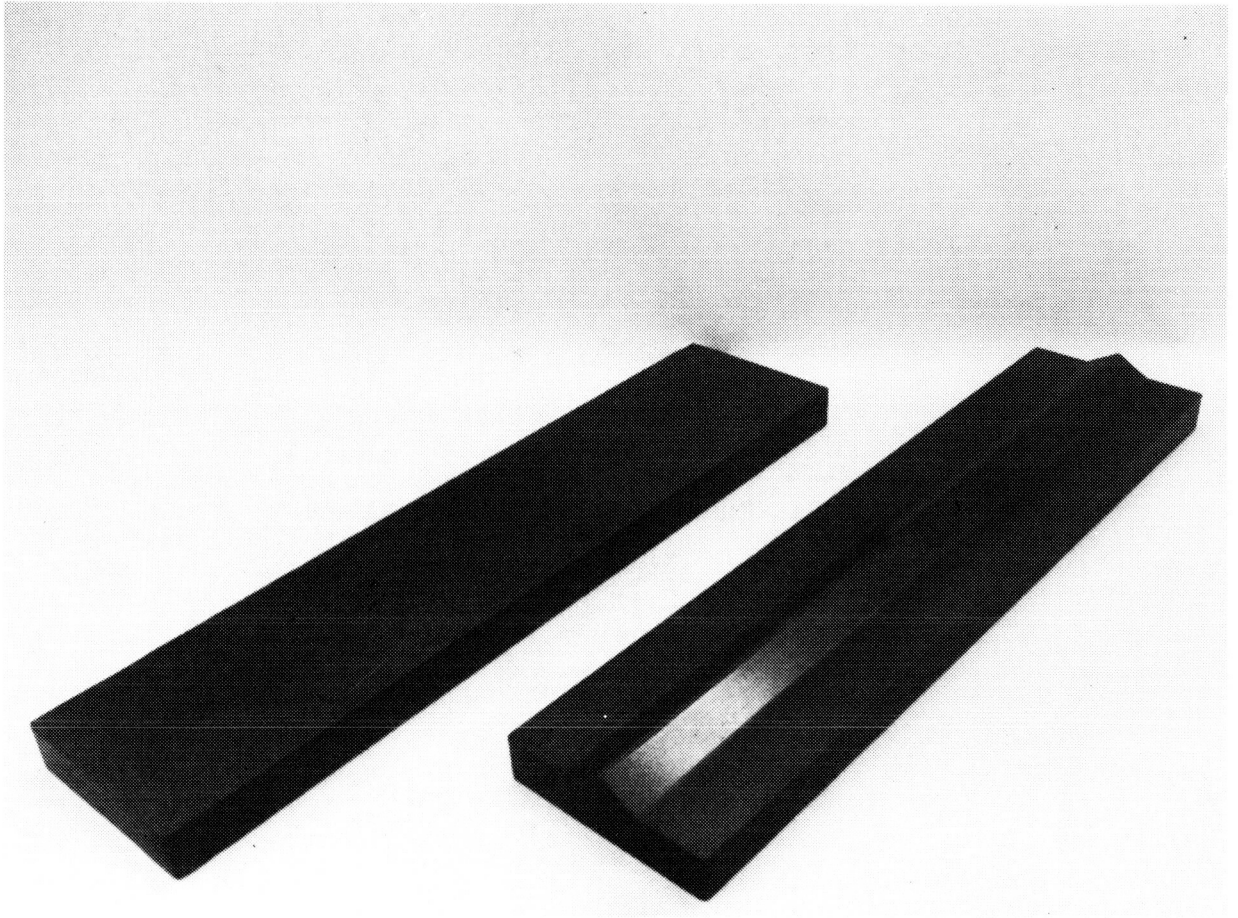
It was recognized that these mandrels are bulky and would act as heat sinks during autoclave consolidation of the Y-spar preforms. An optimum tooling approach would be to use integrally heated and cooled monolithic graphite mandrels. The cost of this type of tooling for the consolidation of three Y-spars was inconsistent with the scope of the subject program. It was considered more cost effective to use the relatively less expensive solid graphite tools with relatively longer autoclave consolidation cycles.

The figure below shows the matched monolithic graphite mandrels fabricated by Coast Composites, Inc. The tools are configured to accommodate Y-spar preforms with a web height of 10.70 in.



UPPER AND LOWER BASE PLATES

Monolithic graphite upper and lower base plates were provided to ensure optimum consolidation/forming of the Y and 90-degree flanges.



WOVEN 0°/90° Y-SPAR PREFORMS

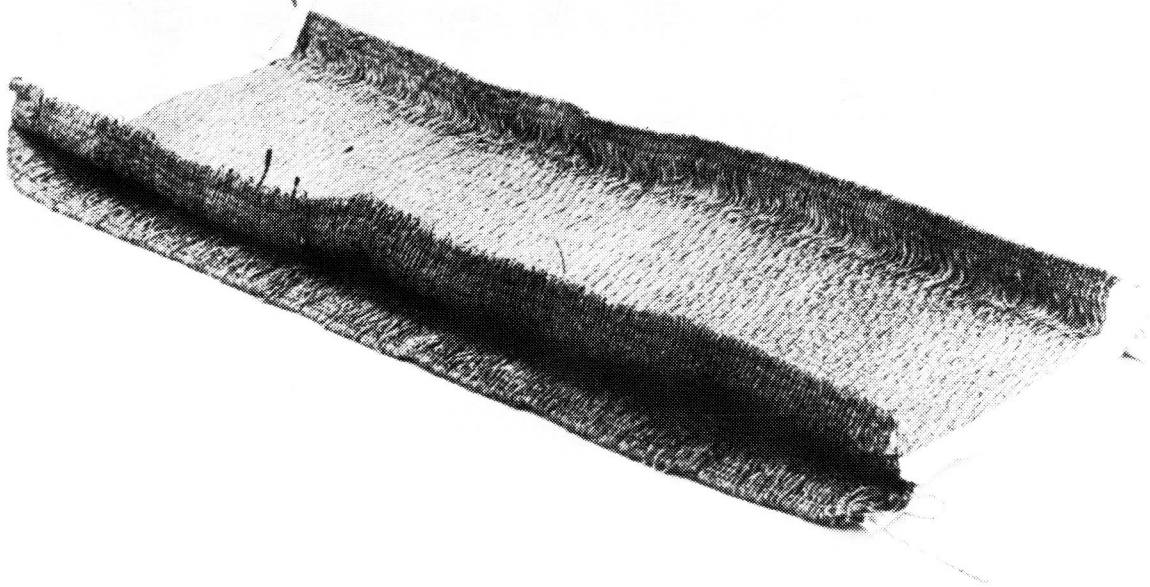
Three sections of 0°/90° Y-spar preforms (each in excess of 40 in. long) were woven by TTI using the web and flange architectures previously described. A shorter section of 0°/90° Y-spar preform was also provided for physical and mechanical properties characterization testing.

Visual inspection of the 0°/90° Y-spar carcasses revealed the presence of floaters (maximum length 2.5 in.) in the radii of the Y and 90-degree flanges. The floaters were due primarily to the use of 12K tows and the requirement that only 5 percent of the fiber reinforcement be used in the Z direction of the preform. The length and number of floaters could be reduced significantly by the use of 3K tows which would provide more fiber ends per in. (but at increased cost) in the Z direction to tie down the Y direction fibers. The percentage of fiber reinforcement in the Z direction could also be increased but with a corresponding reduction of in-plane mechanical properties.

Potential reduction in mechanical properties of the consolidated Y-spar due to the presence of floaters in the radii of those elements was minimized by the subsequent stitching operation for installation of 45°/135° fabric reinforcement.

The radii of the preforms (with 45°/135° fabric reinforcement located on the 0°/90° Y-spar carcasses) were stitched with three rows of stitches using an 1/8 in. row spacing. The remainder of the preforms were stitched using a cross hatch pattern with 1/4 in. row spacings.

The floaters are visible in the radius of the section of 0°/90° woven preform shown in the figure below.



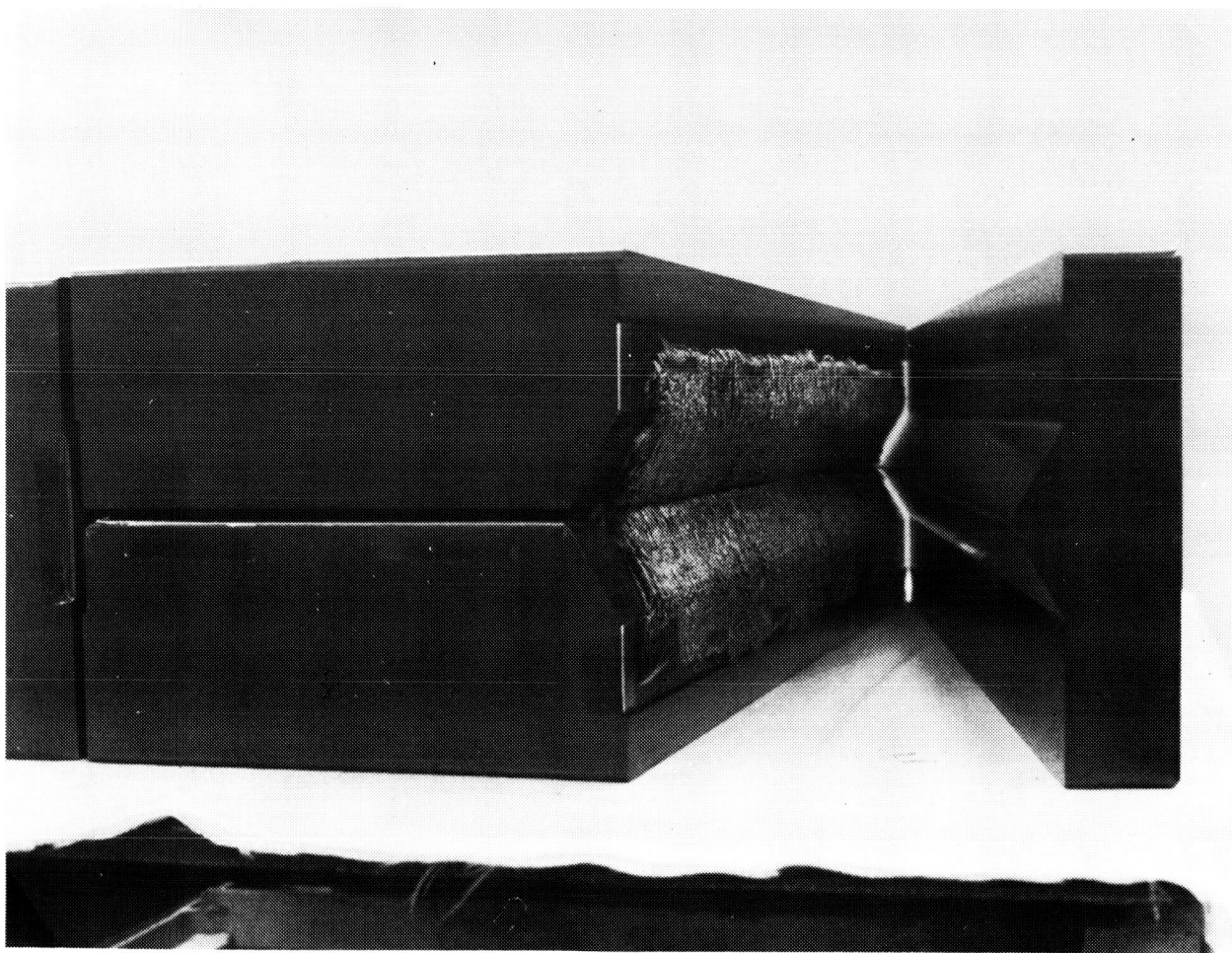
CONSOLIDATION OF SECTION OF 0°/90° Y-SPAR PREFORM

A section of woven commingled AS4/PEEK 150g 0°/90° Y-spar preform was consolidated for 120 minutes at $720 \pm 10^\circ\text{F}$ and 200 psi in an autoclave. The section of preform was consolidated using the monolithic graphite tooling and the autoclave/vacuum bag process previously described for the commingled AS4/PPS 0°/90° I-beams.

The consolidated section of woven AS4/PEEK 150g 0°/90° Y-spar preform was visually excellent. A 16 in. (0° direction) by 6 in. section of the Y-spar web was cut and inspected using ultrasonic NDI. The section of Y-spar web was free of sonic discrepancies. The average thickness of the consolidated panel was 0.140 in. Based on an as-received web thickness of 0.340 in., the percentage reduction in preform thickness was 58.5 percent.

Resin content and fiber volume determinations for the consolidated panel were

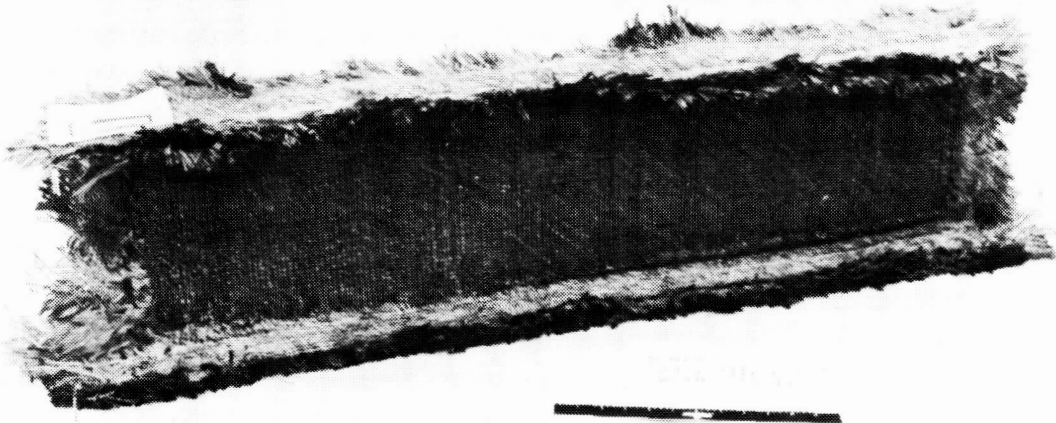
Percent Fiber Volume:	55.8%
Percent Resin Volume:	43.6%
Percent Void Volume:	0.6%



WOVEN/STITCHED Y-SPAR PREFORM

Required 45°/135° fabric reinforcement was stitched to the woven 0°/90° commingled AS4/PEEK 150g Y-spar carcasses by SMX. As stated earlier, the preform was stitched using a cross hatch pattern with a row spacing of 1/4 in. In the radius areas, however, three rows of stitches were installed with a row spacing of 1/8 in.

It was intended that the preform be stitched using only Toray T-900-100 50A carbon fiber; SMX, however, required the use of fiberglass loops in combination with the carbon fiber thread in the radii and flanges of the preform. The carbon stitching equipment was too large to be conveniently used for the Y-spar flanges. In addition, this equipment lacked the sensitive feeding characteristics required for the flange stitching operation. Ultimately, the Y-spar preform flanges were stitched manually.



**CONSOLIDATION OF
Y-SPAR PREFORM S/N-1
Near Net Trimming**

D19B8220-13 Y-spar Preforms S/N -2 and -3 will be fabricated using the procedures to be described for Preform S/N-1.

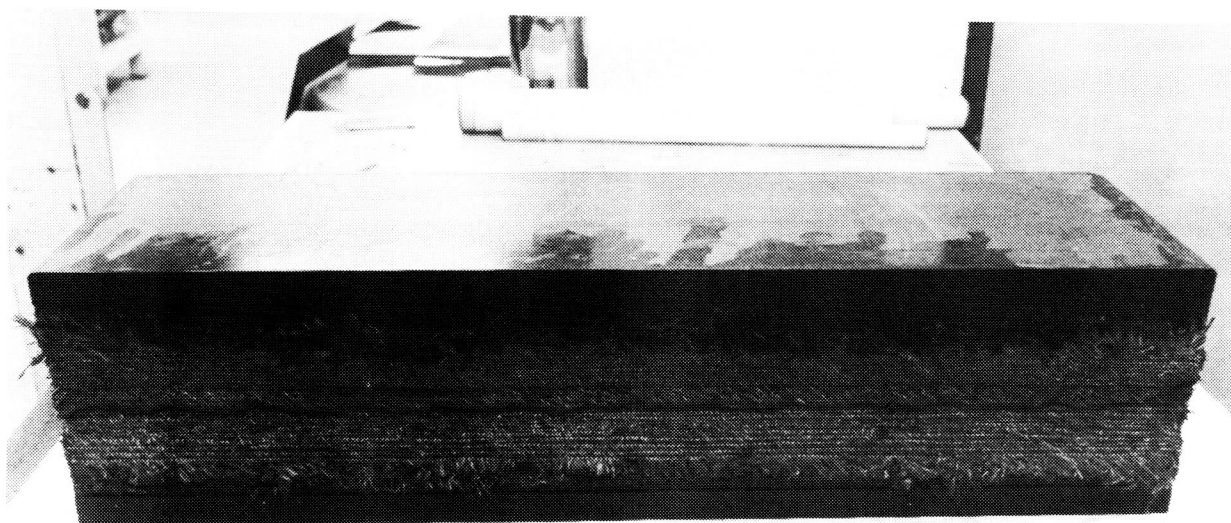
Preform S/N-1 was installed on one of the tool mandrels and manually trimmed to near net dimensions using scissors.



INSTALLATION OF Y-SPAR PREFORM BETWEEN TOOLING MANDRELS

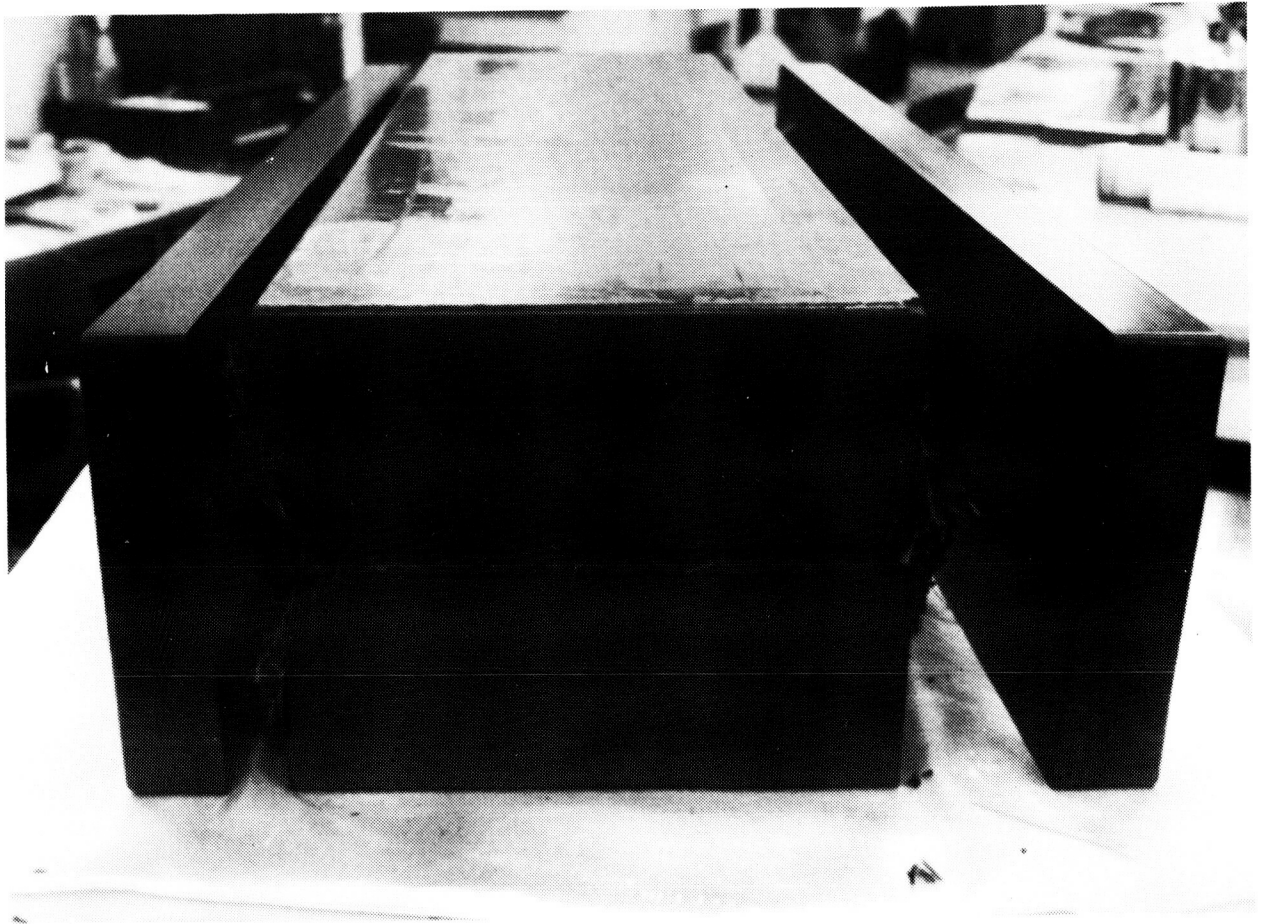
The Y-spar preform is installed between the matched monolithic graphite mandrels. The mandrels are undercut to accommodate the flanges of the Y-spar preform. The width of each of these undercut surfaces is oversize with respect to the final trim of the corresponding Y-spar flange.

The 90° flange of Y-spar Preform S/N-3, as shown in the figure below, has been trimmed to a near net dimension that accommodates that of the tool but is larger than the final dimension of the consolidated Y-spar.



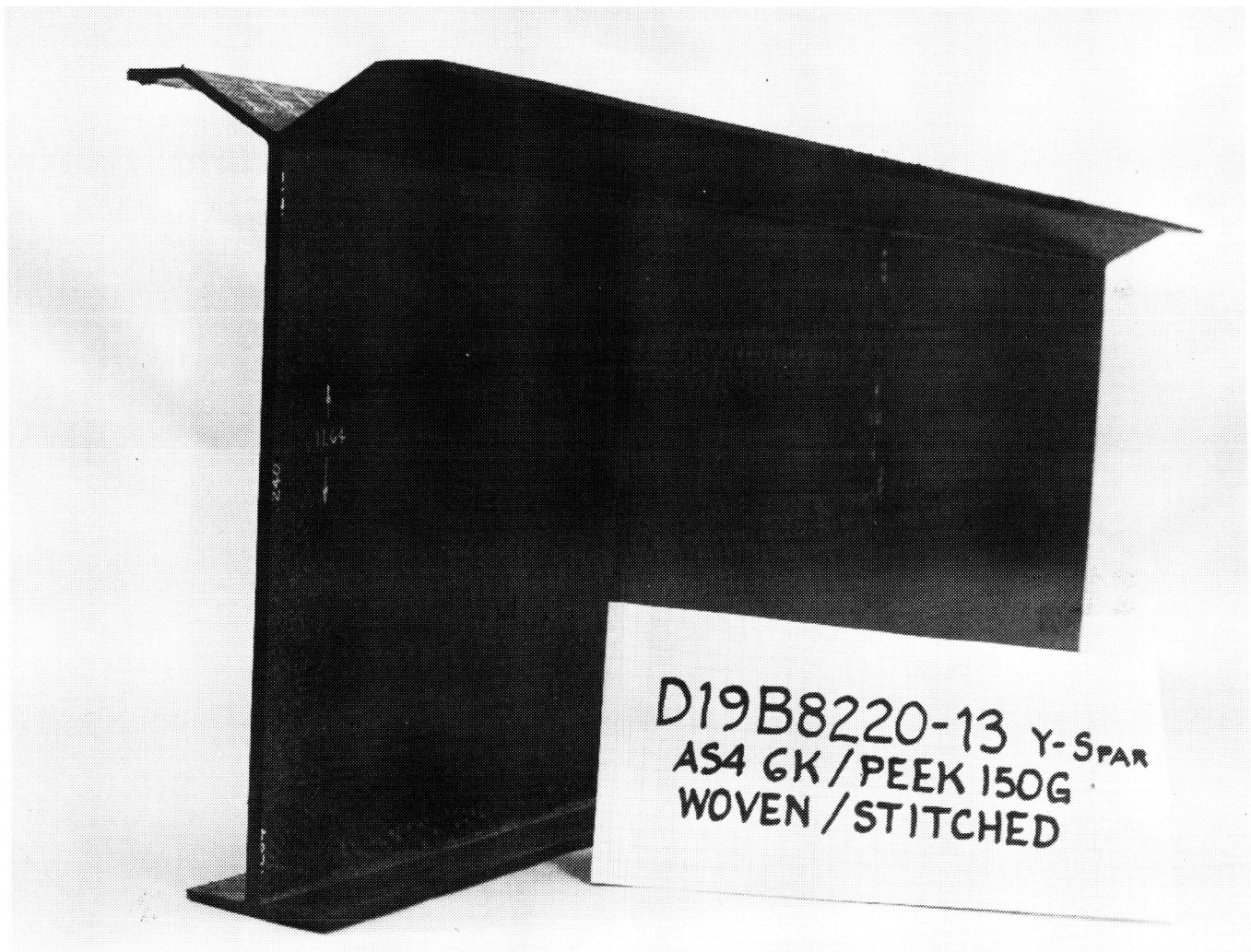
INSTALLATION OF UPPER AND LOWER TOOLING PLATES

The near net trimmed Y-spar preform is installed between the matched mandrels. As shown in the figure below, the mandrels are positioned on the autoclave table so that the web of the part is parallel to the surface of the autoclave table. The upper and lower closure plates are then placed against the outboard surfaces of the preform Y and 90° flanges.



CONSOLIDATED (TRIMMED) Y-SPAR

The consolidated commingled AS4/PEEK 150g woven/stitched Y-spar was consolidated for 4 hours at $720\pm 10^{\circ}\text{F}$, 160 psi fluid pressure plus full vacuum bag pressure. The prolonged hold at elevated temperature was required to accommodate the relatively large mass of the monolithic graphite mandrels which acted as heat sinks. In production, integrally heated and cooled tools would be used in combination with cold-wall autoclave procedures to provide a low-cost consolidation methodology. The high-temperature autoclave run was performed without any processing difficulties. The consolidated Y-spar was visually acceptable. Tap testing indicated a satisfactory consolidation.

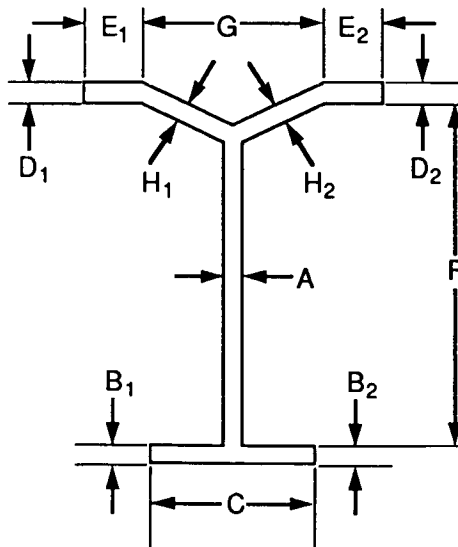


TARGET, PREFORM & FINAL PART DIMENSIONS OF WOVEN COMMINGLED 3-D AS4/APC-2 Y-SPAR 1

The results of a preliminary dimensional inspection (the Y-spar will be sectioned to provide in-depth dimensional analysis) are presented below. Target values for the consolidated oversize Y-spars were provided by TTI. These values are estimates based on corrective inputs to their Framework computer program to accommodate the greater mass of AS4 fiber used to fabricate the Y-spar preforms. (The Framework is an interactive computer program that predicts the thickness of a consolidated preform based on the physical characteristics of the fibers used in the fill and warp directions of the preform.) The table also provides initial preform thickness values and corresponding consolidated thickness measurements. Comparison of the last two measurement groups permitted calculation of percent reduction in preform thickness values.

Target values for the web (A) and outer sections of the Y-spar flanges (D₁ and D₂) were essentially realized by the consolidated structure. Target values for the inner sections of the Y-spar flanges (H₁ and H₂) and the 90° flanges (B₁ and B₂) were not achieved. Indeed, the consolidated thicknesses for the two inner Y-spar flanges were considerably different (0.170 vs 0.158 in.) indicating that the corresponding side mandrel may have hung up during consolidation. Percent consolidation values for these flanges support this hypothesis (H₁ vs H₂, 53.6 vs 60.2% and D₁ vs D₂, 58.2 vs 64.5%).

Woven Commingled 3-D AS4/APC-2 Y-Spar S/N-1 Target, Preform & Final Part Dimensions



MR90-4125-034

	TARGET (IN.)	PREFORM (IN.)	CONS. Y-SPAR (IN.)	CONS. (%)
A	0.215	0.463	0.242	47.7
B ₁	0.151	0.381	0.134	64.8
B ₂	0.151	0.350	0.127	63.7
C	2.50	2.74	2.50	N/A
D ₁	0.151	0.366	0.156	58.2
D ₂	0.151	0.397	0.141	64.5
E ₁	1.25	—	0.90	—
E ₂	1.25	—	1.00	—
F	11.65	—	11.65	—
G	3.40	—	3.34	—
H ₁	0.151	0.366	0.170	53.6
H ₂	0.151	0.397	0.158	60.2

COST STUDIES FOR COMMERCIAL FUSELAGE CROWN DESIGNS¹

**T. H. Walker, P. J. Smith, G. Truslove, K. S. Willden,
S. L. Metschan, C. L. Pfahl**

Boeing Commercial Airplane Group

ABSTRACT

Studies were conducted to evaluate the cost and weight potential of advanced composite design concepts in the crown region of a commercial transport. Two designs from each of three design families were developed using an integrated design-build team. A range of design concepts and manufacturing processes were included to allow isolation and comparison of cost centers. Detailed manufacturing/assembly plans were developed as the basis for cost estimates.

Each of the six designs was found to have advantages over the 1995 aluminum benchmark in cost and weight trade studies. Large quadrant panels and cobonded frames were found to save significant assembly labor costs. Comparisons of high- and intermediate-performance fiber systems were made for skin and stringer applications. Advanced tow placement was found to be an efficient process for skin layup. Further analysis revealed attractive processes for stringers and frames. Optimized designs were informally developed for each design family, combining the most attractive concepts and processes within that family. A single optimized design was selected as the most promising, and the potential for further optimization was estimated. Technical issues and barriers were identified.

INTRODUCTION

During the 1970s, high fuel prices dictated a focus on reduced weight in aircraft design. The lower fuel prices in recent years, in conjunction with a highly competitive aircraft marketplace, have forced airframe manufacturers to consider the affordability of weight savings. Past applications of composite materials have demonstrated their ability to reduce weight, but typically at significantly higher costs.

The relative lack of experience with composite materials results in increased risks in both cost and performance. Boeing, therefore, requires potential composite applications to not only have significant weight savings, but also to have costs less than or equal to aluminum alternatives. NASA has also recognized the need for affordability and funded the Advanced Composite Technology (ACT) program, with the objective of developing the technology required for cost-effective application of composite materials to primary aircraft structures. The specific goals of the program are to obtain 25-30% cost savings and 40-50% weight reductions from current airframes for a resized all-composite airframe.

The emphasis of Boeing's Advanced Technology Composites Aircraft Structures (ATCAS) contract, funded under the ACT program, is on pressurized commercial transport fuselages. The approach is to

¹This work was funded by Contract NAS1-18889, under the direction of J. G. Davis and W. T. Freeman of NASA Langley Research Center.

develop and demonstrate innovative composite fuselage structural concepts that are cost and weight effective. Boeing selected the fuselage section immediately behind the wing box and main-landing-gear wheel well area for this technology development and verification effort. The 767-X development airplane, targeted for production in 1995, was selected as the metal benchmark to provide a comparison with state-of-the-art aluminum technology.

Recurring labor is a major cost center in metal aircraft structure, due primarily to the low raw material costs. The large amount of assembly required in aluminum structure results in assembly activities accounting for nearly half the recurring labor costs, as shown in Figure 1. This, combined with indications of strong interactions between design details and manufacturing costs, led to a decision to consider assembled structure during concept selection. Manufacturing and cost personnel were included in the design team to ensure these areas were addressed early in the design cycle, where changes have the largest impact. The design-build-team (DBT) process, which is discussed more fully in Reference 1, involves detailed cost- and weight-sensitivity studies (referred to as "global optimization") to determine the best overall design concept. These studies are followed by "local optimization," which includes subcomponent and element tailoring within the selected design concept.

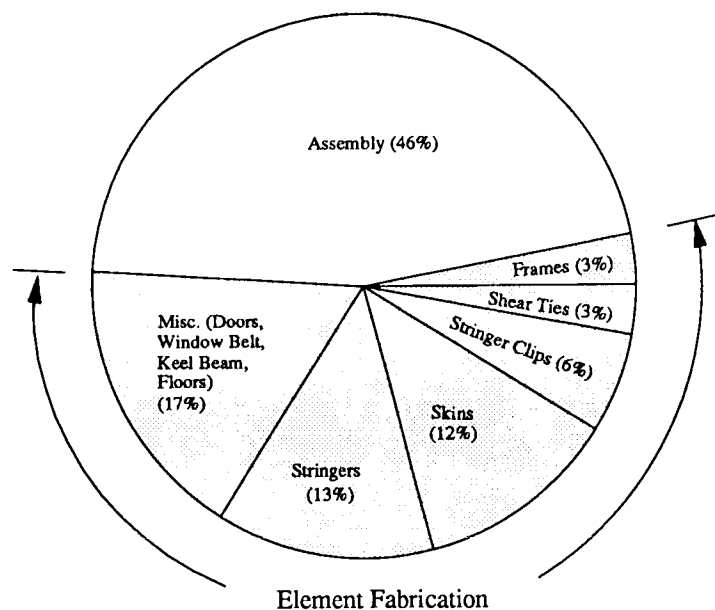


Figure 1: Recurring Labor for a Typical Boeing Metallic Aft-Fuselage

The study section of the fuselage was divided into four quadrant panels: crown, keel, left side, and right side. Each of these panels was treated separately. This paper addresses the detailed cost and weight studies of the global optimization process for the crown quadrant panel, which was accomplished during the period of January 1990 through July 1990.

COSTING PROCESS

An industrial engineering approach was used to develop cost estimates of each design concept. The completed design layouts contained information needed to generate detailed manufacturing plans. These plans defined each individual process required to fabricate and assemble the finished quadrant panel, and the tooling, labor, and recurring material requirements to support each. In-house historical data and vendor-supplied estimates were used to define machine capabilities, process limits, process-based material utilization rates, materials costs and labor for individual operations. Process variables, such as learning curves, and shop variances, were also developed from historical and vendor-supplied data. Detailed costs for each operation were then generated and summed to provide various levels of cost visibility.

In developing manufacturing plans and cost estimates, an automated factory was assumed for definition of equipment and tooling. Reduction of part handling and the combination of operations were significant considerations. Estimates were based on a production run of 300 airplanes at a rate of 5 per month. Costs for materials were based on only this 31 ft. crown panel at these production rates. Labor rates of \$100 and \$75/hr. were used for recurring and non-recurring labor, respectively; 1995 dollars were used in all cases. Capital equipment costs were not included.

DESIGN DEVELOPMENT

Design Conditions

Designs developed for this study were sized to loading conditions representative of the baseline metallic fuselage. Hoop and axial damage tolerance, Euler stability, and bolted joint strength were all considered. A minimum gage of 10 plies (0.074 in.) was used to minimize repair requirements after severe hail storms.

Predictions of damage tolerance strength were made using a method based on References 2 and 3, and Boeing-internal studies. Analysis of crown configurations using this method indicated that "failsafe" tension damage tolerance conditions are more critical than "ultimate" or "safe-flight" conditions. An axially oriented 8 in. narrow slot in conjunction with a hoop tension loading of 1260 lbs./in. was used for the hoop damage tolerance. A circumferentially oriented 8 in. narrow slot in conjunction with an axial tension load distribution, ranging from 2900 to 3600 lbs./in. on the forward end and from 1400 to 1800 lbs./in. on the aft end, were considered for axial damage tolerance.

"Ultimate" tension loads were used for determining joint strength. The ultimate hoop loading is 2200 lbs./in. The ultimate axial loads range from 5400 to 6800 lbs./in. on the forward end and from 2700 to 3500 lbs./in. on the aft end.

Column stability was determined with ultimate compressive loading. These axial loads range from 2300 to 2700 lbs./in. on the forward end and from 1100 to 1400 lbs./in. on the aft end.

Design Families

Early developments by the ATCAS DBT prompted a need for an efficient method of studying candidate fuselage design concepts and manufacturing processes. Initially, 30 candidate fuselage panel concepts were produced by design personnel. The number of concepts was increased to 159 during subsequent brainstorming sessions. Schedule constraints would not allow cost and weight evaluations of all concepts. Instead, concepts were classified into eight design families, each having common manufacturing characteristics.

Three of these families are permutation of the skin/stringer/frame concept, with differing amounts of cocuring and cobonding of individual elements. Two families are variations on sandwich construction with circumferential frames. Other families include geodesic stiffening, integrally stiffened skins, and continuous 360° fuselage concepts.

Crown Designs

Three families were selected for consideration in the crown panel studies, based on their perceived potential for cost- and weight-effectiveness. Family B is a traditional skin/stringer/frame geometry, with the stringers cobonded or cocured to the laminate skin. The frames are mechanically attached to the stiffened panel. Family C is also a skin/stringer/frame geometry, with both the stringers and frames cobonded or cocured to the laminate skin. Family D is a sandwich geometry, with cobonded frames to provide hoop stiffening.

Two designs were developed from each of these three families. In developing the concepts, cost-minimization was a major consideration. In addition, a range of concepts for each element (i.e., skins, stringers, frames) was included within and across the design families to isolate costs.

Table 1 itemizes the important features of the two Family B designs. The major differences are (1) the skin and stringer materials, (2) the stringer geometry and fabrication process, and (3) the frame fabrication process. Design B1 uses IM6²/3501-6³ for the skins and drape-formed hat stringers. The frames for this design are compression-molded fabric. Design B2 uses AS4⁴/3501-6 for the skins and pultruded non-tapered blade stringers. The frames are fabricated by resin-transfer-molding (RTMing) braided preforms.

		Design B1	Design B2
Skin	Mat'l, Form Mfg. Process	IM6/3501-6, Tow Batch Tow-Placement	AS4/3501-6, Tow Batch Tow-Placement
Stringers	Shape Mat'l, Form Mfg. Process	Hat IM6/3501-6, Tape CTLMDrape Form	Blade AS4/3501-6, Prekitted Tape Pultrusion
Frames	Shape Mat'l, Form Mfg. Process	Z AS4/3501-6, Fabric Compr. Molded	Z AS4/DPL862 ⁵ , Braid Batch RTM (4)

Table 1: Major Features of Family B Designs

²IM6 is a graphite fiber system produced by Hercules, Inc.

³3501-6 is a resin system produced by Hercules, Inc.

⁴AS4 is a graphite fiber system produced by Hercules, Inc.

⁵DPL862 is a resin system produced by Shell Oil Corp.

Table 2 compares the two designs of Family C. The primary variables between the two concepts are (1) the stringer geometry, (2) the frame geometry, and (3) the frame manufacturing process. In Design C1, the hat stringers are constant-height and thickness-tapered. The frames for this design are manufactured using braid/RTM technology, and the frame flanges are bonded to the skin and entire stringer cross section. In Design C2, the hat stringers are constant-thickness and height-tapered. The frames are fabricated from a long discontinuous fiber (LDF⁶)/PEKK using a stretch forming operation. The frame flanges bond only to the skin and attached stringer flanges. "Mouse-hole" cutouts in the frame at the stringer-frame intersections allow the stringers to pass through.

		Design C1	Design C2
Skin	Mat'l, Form Mfg. Process	IM6/3501-6, Tow Batch Tow-Placement	IM6/3501-6, Tow Batch Tow-Placement
Stringers	Shape Mat'l, Form Mfg. Process	Thickness-Tapered Hat IM6/3501-6, Tape CTLM/Drape Form	Height-Tapered Hat IM6/3501-6, Tape CTLM/Drape Form
Frames	Shape Mat'l, Form Mfg. Process	Contoured-Flange J AS4/DPL862, Braid Batch RTM (16)	Mouse-Holed J AS4/PEKK, LDF Stretch Form

Table 2: Major Features of Family C Designs

The major features of the two Family D designs are shown in Table 3. Primary differences include (1) the skin material, (2) the panel edge concept, and (3) the frame manufacturing process. Design D1 features AS4/3501-6 skins, with a ramped-down panel edge. The frames for this design are fabricated using braid/RTM techniques. IM6/3501-6 is used for Design D2 skins. A square-edge panel concept is employed, and the frames are manufactured using a dry-fiber pultrusion process.

		Design D1	Design D2
Skin	Mat'l, Form Mfg. Process	AS4/3501-6, Tow Batch Tow-Placement	IM6/3501-6, Tow Batch Tow-Placement
Core	Shape Form Thick., Density	Ramped-Edge Aramid Honeycomb 0.5 in., 4 lb./ft ³	Square-Edge Aramid Honeycomb 0.5 in., 4 lb./ft ³
Frames	Shape Mat'l, Form Mfg. Process	J AS4/DPL862, Braid Batch RTM (2)	J AS4/3501-6, Raw Mat'ls Dry-Fiber Pultrusion

Table 3: Major Features of Family D Designs

⁶LDF is a trademark of E. I. du Pont de Nemours & Co.

RESULTS

From the design studies conducted, several generalizations can be made concerning design drivers. Tension failsafe damage tolerance controls the majority of the panel in all designs. Stringer thicknesses are determined by Euler stability considerations. Skin and stringer thicknesses at the edges of the panels are controlled by the fastener bearing requirements. Minimum gage requirements affect the skin thicknesses near the aft (lightly-loaded) end of the panels.

Figure 2 illustrates the approximate weight breakdown observed in the six design concepts. The stiffened panel (skin and stringers, or sandwich panel) accounts for 70 to 80% of the total crown quadrant weight. In the skin/stringer designs, the skin is approximately 50% of the total, and the stringers 20%. In both concepts, frames account for 10 to 15%, and the splices 5 to 10% of the total weight.

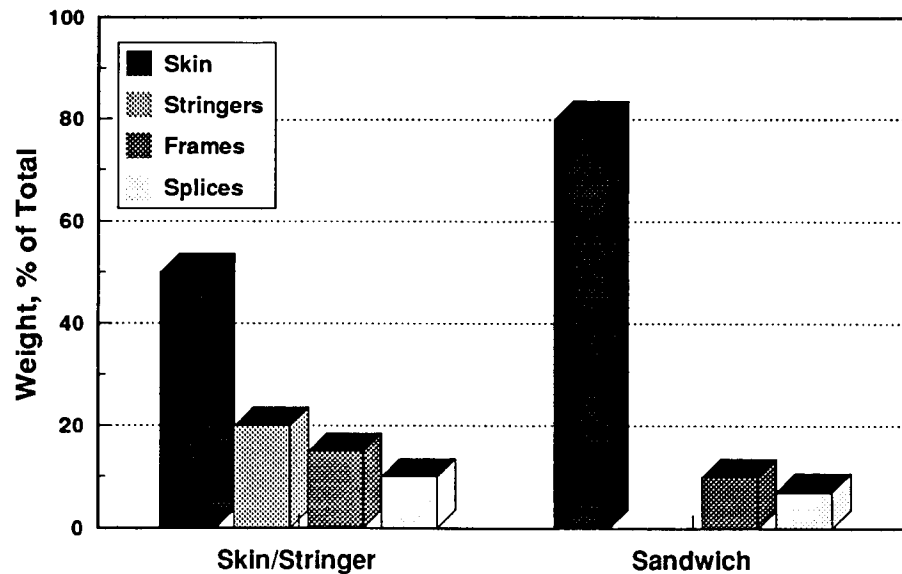


Figure 2: Approximate Weight Breakdown of Crown Designs

Figures 3 through 5 illustrate cost results specific to Design C1, but they reflect trends inherent to all the designs. The relationship between recurring and nonrecurring costs are shown in Figure 3. Recurring costs comprise approximately 75% of the total costs and are divided nearly equally between material and labor.

In Figure 4, the recurring and nonrecurring costs are each separated into fabrication, panel bonding, and assembly/installation costs. About half of the nonrecurring costs are related to element fabrication (e.g., skins, stringers, frames, etc.), with costs relating to bonding and assembly operations comprising the other half. In contrast, approximately 70% of the recurring costs are related to element fabrication, with the remainder related to bonding and assembly operations.

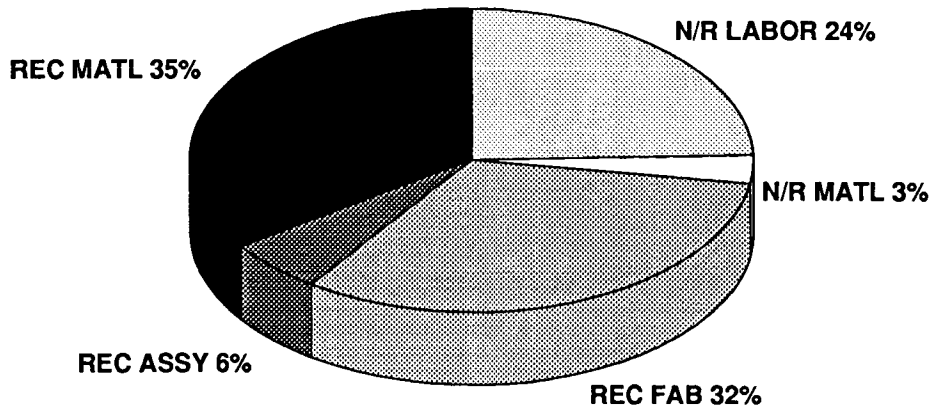


Figure 3: Recurring and Nonrecurring Costs of Design C1

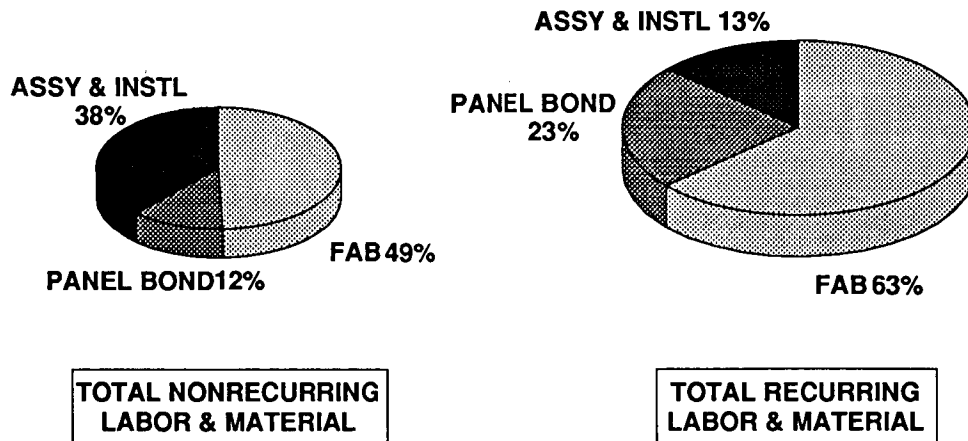


Figure 4: Breakdown of Recurring and Nonrecurring Costs of Design C1

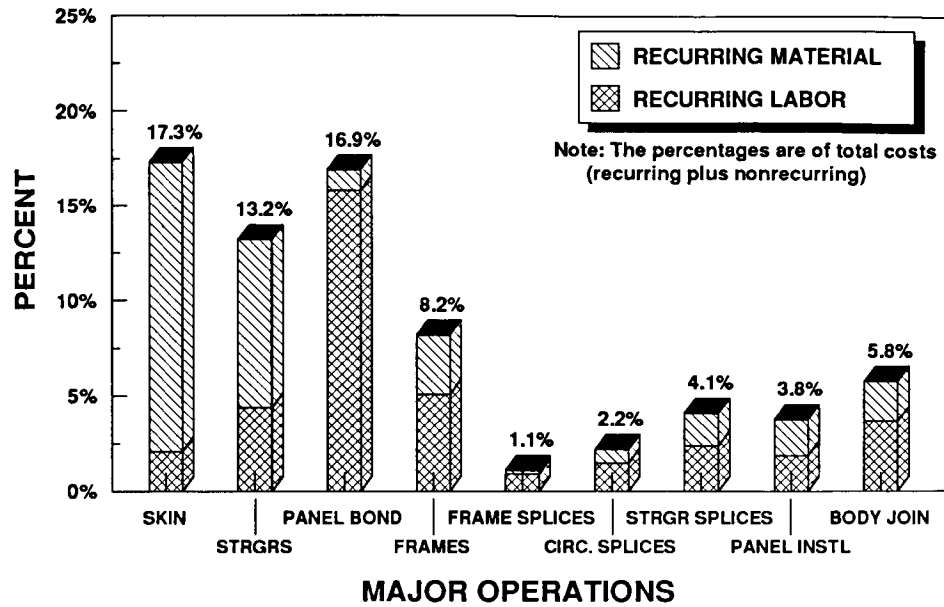


Figure 5: Design C1 Recurring Costs by Major Operation

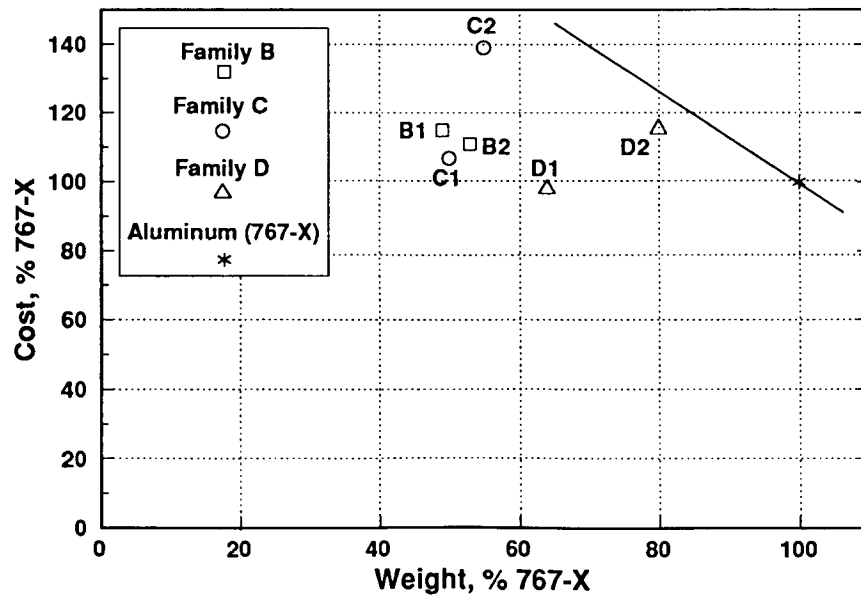


Figure 6: Crown Design Cost/Weight Results

The recurring material and labor costs for each major manufacturing step are shown in Figure 5. The most significant recurring cost centers are (1) the fabrication of the skin, stringers and frames; (2) the panel bonding operation; and (3) fasteners required for installation.

A comparison of the cost/weight results, normalized to that of the 767-X aluminum baseline, is contained in Figure 6. The costs, in general, are within 100 to 120% of the baseline value, with Design C2 being the notable exception. The skin/stringer concept weights are approximately 50 to 60% of the baseline, with the two sandwich concepts (i.e., Designs D1 and D2) being somewhat higher.

The sloped line through the 767-X baseline point in Figure 6 represents a typical performance value of weight. This value is the amount that customers are willing to pay for reduced weight, and therefore is a measure of the life cycle costs of this weight. All designs falling on a single line parallel to this are of equal value. Those designs falling below this line are more desirable, and those falling above, less desirable. As shown, all composite concepts, although not optimized, are more attractive than the aluminum baseline. Note that two of the designs (i.e., Designs C2 and D2) are less attractive than the other four composite designs.

ANALYSIS OF RESULTS

Cost Comparisons

As shown in Figure 2, structural weight is dominated by that of the skin. All designs studied used advanced tow placement and a quadrant panel batch process to layup the skin plies (see Ref. 1). This process was found to be cost efficient in several ways. First, large quadrant panels minimize labor costs for final assembly (see costs for panel installation and body join in Figure 4). As shown in Figure 1, assembly labor is significant for metal structure. Another advantage to advanced tow placement in a batch quadrant process is the relatively low percentage of recurring labor costs. Finally, prepreg tow is projected to be a low-cost material form in 1995 (e.g., \$25/lb. for AS4/3501-6 tow prepreg).

Since the stiffened panel is a major cost and weight center, the impact of the fiber system used in these locations is of extreme interest. In all designs, either AS4/3501-6 or IM6/3501-6 material was used for the skins and stringers. An analysis of the cost trends involved in replacing IM6 fibers with AS4 is shown in Figure 7. The bars in this graph show the ratio of AS4 to IM6, with the adjacent bars addressing the behavior observed in the skins and the stringers. The lower performance of the AS4 fiber system results in a 10 to 15% weight penalty due to added material. However, the cost per pound of the AS4 is significantly lower, ranging from 55 to 65%, depending on the material form (i.e., tow or tape). The final material-cost ratio is the product of these two values, and is in the 70% range. Additional recurring labor costs, which are incurred due to the increased number of plies, are not included in this analysis. However, even when they are included, the cost advantages of AS4 clearly outweigh its performance penalty, for these applications. A performance value of weight in excess of \$130/lb. would be required to select the IM6 system, significantly higher than normal values.

Similar results are seen in an analysis of the sandwich designs. In Design D1 and D2, a hard (0°-dominated) AS4 concept and a soft IM6 ($\pm 45^\circ$ -dominated) concept are used, respectively. Additional studies of soft AS4 and hard IM6 concepts indicate that, while the hard concept is slightly more cost effective than the soft concept, the large cost reductions are gained by changing to the less expensive AS4 system.

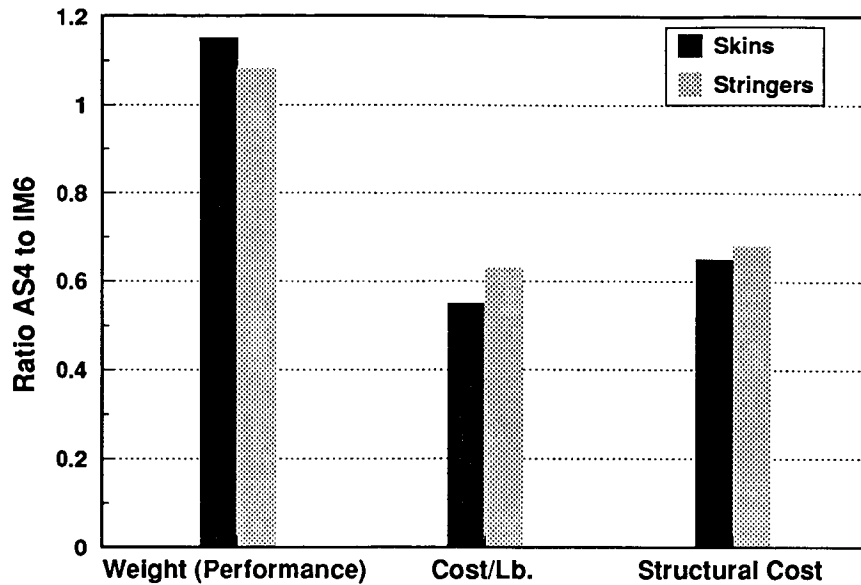


Figure 7: Comparison of AS4 and IM6 Fiber Systems

A comparison of stringer fabrication processes is contained in Figure 8, which illustrates the costs per pound of each stringer design. The pultrusion process used on the Design B2 blade stringers results in cost of \$175/lb. primarily due to the cost of the pre-kitted prepreg material form. The hot-drape-formed hat stringers of Designs B1, C1, and C2, are less costly on a per pound basis (\approx \$110/lb.), although recurring labor was higher than the pultrusion process. In a modified Design B1, where AS4 material is substituted for IM6 (including additional plies to meet the performance requirements), the cost per pound is reduced to approximately \$75/lb.

Several interesting conclusions result from this comparison. First, the pultrusion process is inherently more efficient than tape laminating with hot-drape-forming, but the material costs must be reduced to approximately \$30 to \$40/lb. for the end product to be a viable option. This suggests that dry fibers with an in-line resin wetting process is likely required. Secondly, material is a major cost center in stringer fabrication. Further reductions could possibly be obtained for the drape-formed stringers by switching from a tape form to prepreg tow in fabricating flat charges for draping.

The frame manufacturing process used for each design is the primary variable for which costs can be isolated. Costs per pound are shown in Figure 9. The stretch-formed LDF (Design C2) and the compression-molded fabric (Design B1) designs both result in relatively high costs (\$212 and \$170/lb., respectively). The LDF frames are purchased as finished parts, so their costs are considered as recurring material costs. Because of this, the major cost centers of this process cannot be identified. High recurring labor costs for the compression-molded fabric frame are due to hand layup of the fabric charges. The costs per pound of batch processed braided/RTM frames exhibit a considerable range. This is attributed to the number of frames in a batch process, with the costs reducing from \$160 to \$90/lb. as the quantity of frames fabricated in a single operation increase from 2 to 16. The \$126/lb. costs of the dry-fiber pultrusion concept (Design D2) is lower than all other concepts, except the 16-at-a-time batch RTM process.

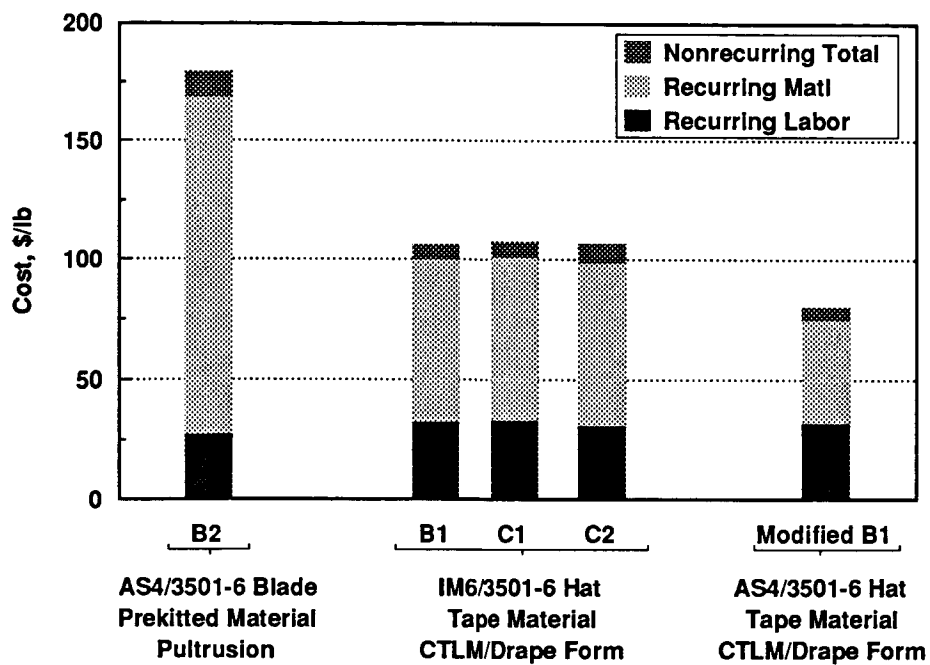


Figure 8: Cost Comparison of Stringer Fabrication Processes

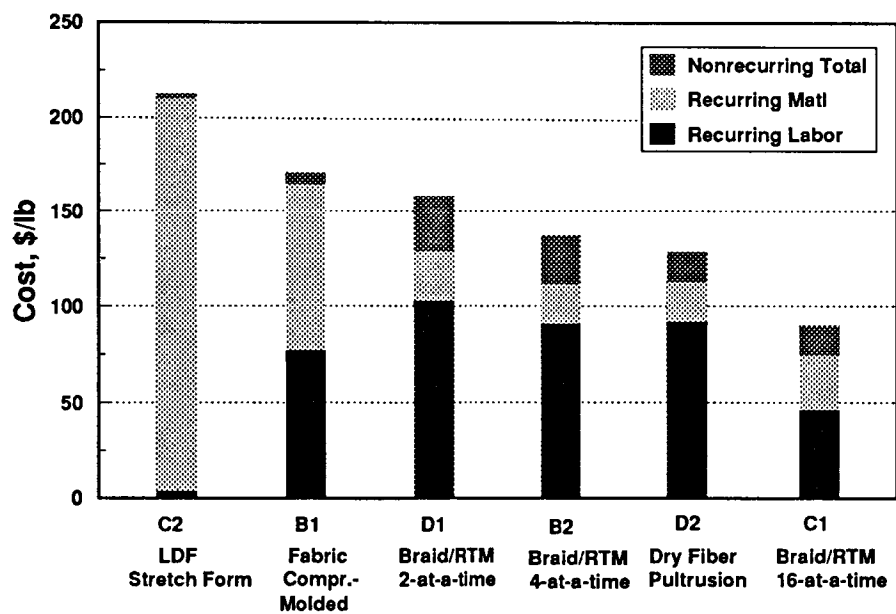


Figure 9: Cost Comparison of Frame Fabrication Processes

Global Optimization

After understanding the cost estimates derived for individual design concepts, an "optimum" design within each family was developed. Efficient materials, fabrication process, and element design concepts that are included in the six designs described above, were combined to provide the most cost- and weight-efficient crown panels for each design family. This process was significantly less formalized than the original cost estimates but was necessary to provide a basis for determining the best design.

The globally optimized Family B design is primarily the hat-stiffened concept from Design B1. The skins, stringers, skin splices and stringer splices are all converted to AS4/3501-6. The thickness of the skins and stringers are increased by 2 plies and 1 ply, respectively, to maintain adequate damage tolerance. The braided/RTM Z-section frames from Design B2 are used, although it is assumed that the frames are RTMed 16-at-a-time. The results of the study show that this design concept is 98% of the cost of 767-X baseline concept and 54% of the weight.

The globally optimized Family C design is a slight modification of the continuously bonded frame concept of Design C1. The skin, stringer, and associated splice materials are converted to AS4/3501-6, with 2 plies and 1 ply being added to the skin and stringers, respectively, for damage tolerance requirements. The J-section frame with the contoured outer flange is maintained without modification, since it already assumes an RTM batch process of 16-at-a-time. The results of the study show that this design concept is 99% of the cost of 767-X baseline concept and 55% of the weight, nearly identical to those for the globally optimized Family B design.

The globally optimized Family D design is close to that of Design D1. The only modification is the cost-efficient frame batch process that RTMs 16 frames in one process. The skins are a hard AS4/3501-6 concept. The ramped edge of the quadrant panel is maintained, although it has not been established as clearly superior to the square-edge design. The results of the study show that this design concept is 94% of the cost of 767-X baseline concept and 64% of the weight.

Selection Rationale

The cost and weight results of the globally optimized designs for each family are shown in Figure 10 with the original results. The Family B and C costs and weights are nearly identical, both being approximately equal in cost and 50% of the weight of the 767-X. The sandwich design (Family D) is slightly less costly, yet significantly heavier than either of Families B or C. The sloped line through the Family B and C designs reflects a typical performance value of weight. When this is considered, Family D is clearly not an optimum design concept.

For all concepts, damage tolerance requirements control much of the design. It was therefore a major consideration in choosing the baseline crown concept for further development in local optimization. In all designs, it is assumed, based on limited existing data, that additional skin padding (i.e., tear straps) are not required for tension damage tolerance. Since longitudinally oriented cracks appear to be the more critical condition, the Family B concept seems to be at most risk from this assumption. Families C and D have integrally bonded frame flanges to provide some crack stopping capability, where Family B has no such features. Family D design appears to be at least risk, since the sandwich construction increases the local bending stiffness at the crack tip, which in turn reduces the localized bending stresses. Significantly higher strengths are realized in sandwich construction for pressure loads with the 8 in. crack size considered for the failsafe condition.

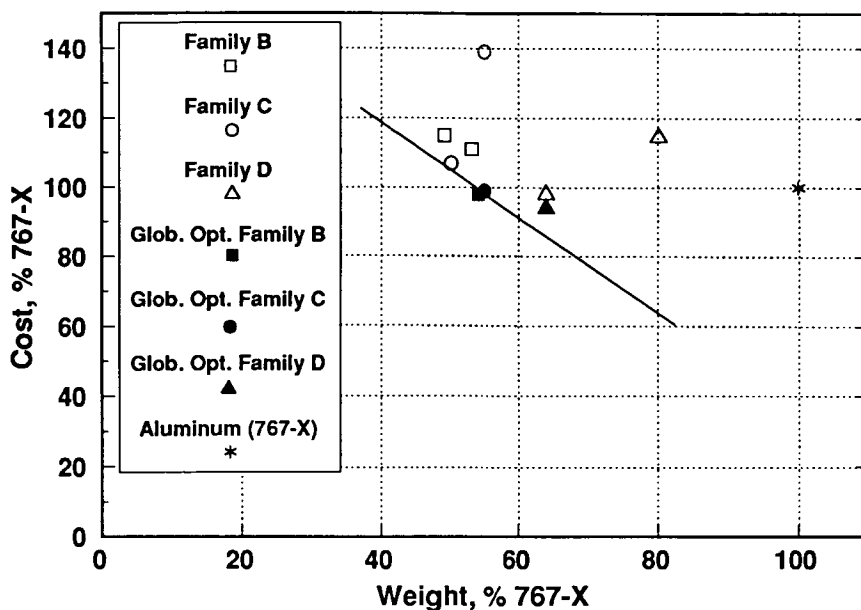


Figure 10: Globally Optimized Designs

Manufacturing risk was also a significant consideration in selecting the baseline concept. Family B has the lowest perceived risk, since manufacturability of a mechanically fastened concept has been previously demonstrated, although on wing/empennage-type structure. The Family C manufacturing risk was judged to be the highest. Both Families C and D carry substantial risk associated with joining very large, stiff sections to other quadrants and to other body segments. High local stresses can be induced by forcing compatibility between warped panels. The overall stiffness of these built-up designs magnifies the localization of these high stresses. The Family C design, however, has additional complexity of splicing the stringers at the body-join operation. Maintaining the very small locational tolerances required for these splices at both ends of a very long panel adds additional risk.

Family C was selected as the baseline crown concept. It demonstrates excellent cost/weight performance, clearly superior to Family D. Its manufacturing risk was judged to be higher than that of Family B, but it also carries significantly less performance (i.e. damage tolerance) risk.

Due to damage tolerance uncertainties in both Families B and C, Family D was selected as a backup to the baseline. This provides a fall-back position if the apparent cost/weight performance erodes as additional data on damage tolerance becomes available, or if the manufacturing concerns of Family C cannot be overcome.

Local Optimization Potential

The local optimization process provides the opportunity to further refine the selected concept within the cost constraints defined by global optimization. Material, geometric and laminate variables affecting cost and weight are considered in the local optimization, as well as improvements in the manufacturing processes. An effort was made to evaluate the magnitude of the potential cost/weight changes that might occur during that process.

The use of less costly materials will be assessed, especially in the skins and stringers, where the majority of material resides. Fiberglass, which exhibits a very large strain-to-failure, appears attractive as a low-cost material for use in the skins and stringer flanges, where tension damage tolerance is an important consideration. Intraply hybrid concepts using S-glass and AS4 material could provide similar residual strength as compared to an all AS4 concept, resulting in a cost savings and a weight increase. This intraply hybrid concept is also ideally suited for the efficient tow-placement process. Other reductions in material cost may be realized by using dry-fiber pultrusion processes in the stringers, and by tow placing the stringer charges for hot-drape-forming.

Major geometric variables to be considered include stringer spacing, frame spacing, stringer height and width, and frame height and width. Major laminate variables include ply orientations and stacking sequences. A software design tool that incorporates cost and structural mechanics constraints with an optimization algorithm is being developed to support studies on the effects of material, geometric, and laminate variables.

Several manufacturing improvements provide opportunities for cost savings. Tow placement efficiency rates can be increased by simply enlarging the current band width or using multiple tow placement heads. These technologies are considered to be low risk and could conceivably increase rates up to 100%. A major cost center is the process for locating and bagging the quadrant assembly for subsequent curing. The technology of form-fit reusable bagging offers significant cost savings by reducing locating-tooling, recurring material costs, rejection rate, and assembly/bagging labor.

Panel splicing provides additional opportunities for improving both cost and weight. Composite fasteners and rivets may be able to reduce the recurring fastener costs. Stringer splicing at the fore and aft ends of the quadrant is also a major concern for Family C. Splice concepts that do not require precise stringer alignment are attractive as a method of reducing the cost and risk in this area.

The potential cost and weight improvements in the local optimization process are shown in Figure 11, along with similar potential for the aluminum baseline design. These aluminum improvements relate primarily to breakthroughs in assembly technology, including high-speed robotic fastening. The broader width of the composite potential is an indication of the wider range of materials and other variables available in the local optimization process. The cost-reduction potential appears to be significantly greater for the composite design than for the aluminum baseline.

TECHNICAL ISSUES AND BARRIERS

The most critical manufacturing issue associated with both the Family C (skin/stringer, bonded frame) and Family D (sandwich) concepts is the effect of locational tolerances and panel warpage on final assembly. Quadrant panel designs have high local stiffness due to bonded stringers/frames or sandwich construction. This stiffness magnifies panel fitup and stringer splicing difficulties.

Another critical manufacturing issue is the control of fabrication processes to yield quadrant panels of acceptable quality. Quadrant panel cost benefits assume that large panels will not be rejected due to manufacturing defects. Further refinement of the designs will include robust designs and processes which minimize potential problems due to fabrication anomalies.

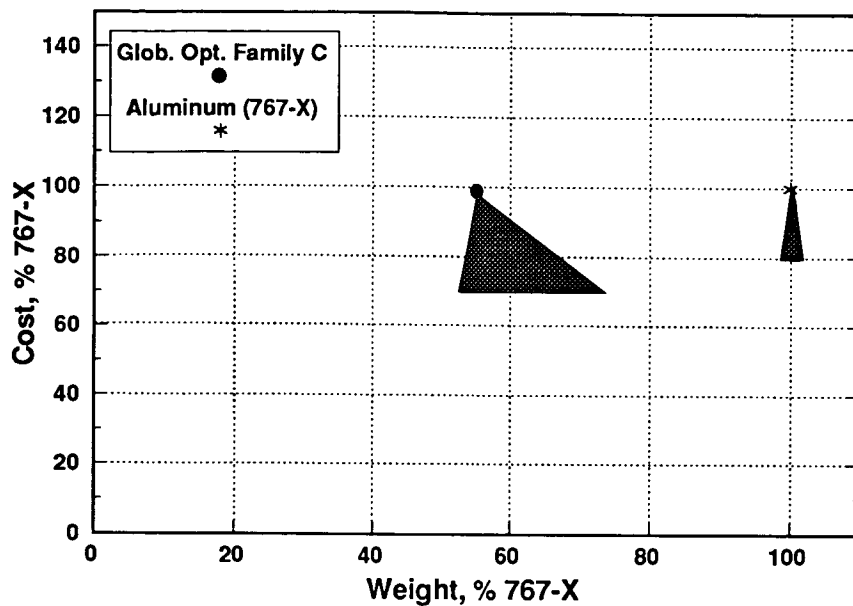


Figure 11: Local Optimization Potential

Several critical performance issues require further understanding to ensure adequate performance and properly refine the design. These include:

1. *Hoop tension damage tolerance of panels with large penetrations.* The most critical damage geometries for hoop loading are expected to be slender notches oriented along the longitudinal axis (Reference 3). The effectivity of bonded frames as "tear straps" needs to be determined. The scenario of a penetration that severs a frame and skin must also be studied.
2. *Axial tension damage tolerance of panels with large penetrations.* The critical damage geometries for axial loads are expected to be slender notches oriented along the circumferential axis and severing a stringer. Both hoop and axial tension damage tolerance in the crown are expected to yield lower strengths for unidirectional loading cases since the Poisson effect reduces ply stresses for the biaxial tension case (Reference 4). However, the complex stress distribution near a hard point could be most severe.
3. *Axial compression stability of panels with and without damage.* Euler stability and post-buckled performance of the panel must be demonstrated with and without damage.
4. *Minimum skin gage required to satisfy hail impact criteria.* Structural tailoring in the crown is limited by the minimum skin thickness requirement used to suppress visible damage due to severe hail storm conditions.
5. *Fiber/resin distribution of frames after RTM processing.* The performance, warpage, and dimensional tolerance control of complex geometries such as curved frames is expected to relate to fiber/resin distribution. Cost efficient methods of controlling the quality of RTM parts must be established.
6. *Performance of the stringer/frame intersection.* The intricate bond concept, with the frame bonded to the entire stringer cross section, requires precise alignment of all parts. The mouse-

hole concept alleviates some of the alignment concerns, but adds an additional stress concentration in the frame. Sufficient damage tolerance for skin penetrations located near the intersection must also be established.

7. *Durability of design details (cobonded frames and mechanically fastened splices).* Cyclic pressure load conditions are expected to drive the design of frame-to-skin adhesive joints in the crown. Creep/fatigue interactions must be addressed. Potential bond-surface contamination, resulting from poor handling, can also affect the durability of the frame-to-skin bond. Combined cyclic load conditions also pose a significant problem for longitudinal and circumferential mechanically fastened joints. The effects of environment and real time on damage accumulating in material surrounding the bolt hole will need to be considered.

CONCLUSIONS

Several conclusions can be drawn from the above studies. First, and most important, composite designs can be developed for fuselage crown applications that are significantly more attractive, from a cost and weight perspective, than current aluminum concepts. Composite designs that are approximately equal in cost and half of the weight of aluminum designs are possible.

Recurring costs account for approximately three-fourths of the total crown panel costs, with material splitting this amount nearly equally with fabrication and assembly labor. Element fabrication (i.e. skins, stringers, frames), panel bonding, and fastener costs are the major recurring cost centers.

Batch advanced tow placement layup of quadrant skin panels was found to be cost-efficient for all designs studied. Large quadrant panels minimized assembly labor costs by reducing the number of splices; however, manufacturing concerns about panel warpage and element locational tolerances need to be addressed in future work.

In the crown applications considered, high performance fibers, such as IM6, do not appear to justify their increased cost when compared with intermediate performance fibers, such as AS4. This conclusion cannot be generalized to other applications.

Drape forming of flat uncured charges appears to be an efficient method of stringer fabrication. Automated methods to create the flat charges from either tape or tow are important. Pultrusion also appears attractive for stringer fabrication, but only using a dry-fiber method.

Resin-transfer-molding of braided preforms is an effective method for fabricating body frames. Batch-RTMing provides significant cost advantages as the number of frames per operation increases. Dry-fiber pultrusion also has potential for this type of structure.

A stiffened panel design concept with cobonded frames was selected for future studies that address additional cost and weight savings. The local optimization potential of this design was judged to be greater than that of aluminum designs. This relates to the larger number of composite design variables and the relative maturity of aluminum technology.

Damage tolerance is the primary technical issue to be resolved for crown applications. Several issues required further understanding to ensure adequate structural performance and allow proper optimization. These issues include bonded and bolted joint durability, panel stability with large damage, and the effects of fiber-resin distribution in RTM parts.

REFERENCES

1. Ilcewicz, L. B., et al, Advanced Technology Commercial Fuselage Structures, First NASA Advanced Composites Technology Conference, NASA CP- 3104, Part 1, 1991, pp. 127-156.
2. C. C. Poe, "A Unifying Strain Criterion for Fracture of Fibrous Composite Laminates, Engineering Fracture Mechanics, Vol. 17, No. 2, pp. 153-171, 1983.
3. Chang, S. G. and J. W. Mar, "The Catastrophic Failure of Pressurized Graphite/Epoxy Cylinders Initiated by Slits at Various Angles", AIAA Paper 84-0887, Submitted at 25th Structures, Structural Dynamics, and Materials Conference.
4. Smith, P. J., L. W. Thomson, and R. D. Wilson, "Development of Pressure Containment and Damage Tolerance Technology for Composite Fuselage Structures in Large Transport Aircraft," NASA CR 3996, Contract NAS1-17740, August 1986.

A Unified Approach for Composite Cost Reporting and Prediction in the ACT Program

W. Tom Freeman
NASA Langley Research Center

Louis F. Vosteen and Shahid Siddiqi
Analytical Services & Materials, Hampton, VA

Abstract

The Structures Technology Program Office (STPO) at NASA Langley Research Center has held two workshops with representatives from the commercial airframe companies to establish a plan for development of a standard cost reporting format and a cost prediction tool for conceptual and preliminary designers. This paper will review the findings of the workshop representatives with a plan for implementation of their recommendations.

The recommendations of the cost tracking and reporting committee will be implemented by reinstituting the collection of composite part fabrication data in a format similar to the DoD/NASA Structural Composites Fabrication Guide. The process of data collection will be automated by taking advantage of current technology with user friendly computer interfaces and electronic data transmission.

Development of a conceptual and preliminary designers' cost prediction model will be initiated. The model will provide a technically sound method for evaluating the relative cost of different composite structural designs, fabrication processes, and assembly methods that can be compared to equivalent metallic parts or assemblies. The feasibility of developing cost prediction software in a modular form for interfacing with state of the art preliminary design tools and computer aided design (CAD) programs will be assessed.

Introduction

Boeing Commercial Airplane (BCA) Group and Douglas Aircraft Corporation (DAC) use approximately 400,000 pounds of composites per year in spoilers, rudders, elevators, doors, and other secondary structure. The rate of application of composites to empennage, wing, and fuselage commercial airframe primary structure has been disappointingly slow. Composite materials are an obvious choice for performance optimization, corrosion resistance, and fatigue suppression, but before a bold leap toward more extensive use of composites can be expected in commercial applications, accurate cost prediction methods and confidence that production costs can be predicted accurately must be demonstrated. The Advanced Composite Technology Program's goal is to establish design concepts, develop manufacturing approaches, and demonstrate the structural integrity and cost effectiveness of innovative low cost composite assemblies, providing confidence for production commitment to primary structure by the turn of the century.

The need to unify cost reporting and prediction methods for the Advanced Composites Technology (ACT) program has been identified by industry participants during program reviews. Accurate cost prediction is considered a high priority issue to assure a valid comparison of cost effective structural concepts, material forms, and assembly methods being developed by the participants. The Structures Technology Program Office (STPO) has hosted two workshops with representatives from the commercial airframe companies to define

- (1) a standard cost tracking and reporting format, and
- (2) a development plan for a conceptual and preliminary design cost prediction model.

The preliminary design process has been identified as the most critical period of opportunity for substantial cost reduction during an airframers hardware production cycle. Boeing has experienced that 70% of airplane fabrication costs are fixed by the time the design is frozen and that the influence of engineering on fabrication cost reductions is significantly reduced once the design is completed. Concurrent engineering interdisciplinary teams are emphasizing cost evaluation at the early stages of the development cycle in the preliminary design process. The advent of CAD/CAM on powerful work stations provides the designer with the possibility of including cost as a complementary variable in the design process. A comparative cost algorithm, which can function purely as an engineering design tool to evaluate different design concepts, would be exceptionally valuable to concurrent engineering teams. As part of the overall NASA effort to improve the economic viability of composite structures, the STPO plans to implement two activities related to composite costs:

1. Reinstitute and automate the collection of composite part fabrication costs in a format similar to the DoD/NASA Structural Composites Fabrication Guide (Fab. Guide) (Ref. 1).
2. Determine the feasibility for development of a universally accepted academically rigorous theoretical method for predicting the relative cost of different composite structural designs in the preliminary design process.

The NASA-Industry Workshops

The first workshop on cost reporting and prediction (Ref. 2) was held in Norfolk, VA in December 1989. The purpose of the workshop was to

1. Determine the procedures currently used by the industry to predict the production cost of composite components and to determine if there was a need to develop or modify existing methodology to account for new composite manufacturing processes such as tow placement, resin transfer molding, and filament winding.
2. Establish a uniform procedure for reporting the costs of parts developed in the ACT program.

Participants at this workshop were divided into cost reporting and cost prediction committees and concluded that

1. Development of standard cost reporting and prediction methodologies were desirable.
2. Each company would identify representatives to serve on a steering committee to draft a plan.

3. The STPO should strive for implementation of unified reporting and prediction methods by the last quarter of 1990.

The second workshop (Ref. 3) was held at Douglas Aircraft Corporation in Long Beach, CA in February 1990. The purpose of the second workshop was to

1. Establish standard forms for cost collection and reporting.
2. Establish written requirements for a conceptual and preliminary designers' cost prediction model.

Participants at this workshop were divided into cost reporting and cost prediction committees and requested to report their recommendations to STPO by July 15, 1990. L. E. Meade (Lockheed Aeronautical Systems Co.), chairman of the cost reporting group, indicated that representatives of the three commercial companies agreed that the Data Abstraction Form developed for the Fab. Guide adapted to a Lotus 123 spreadsheet format would be an acceptable form for the ACT program.

G. Swanson (BCA), chairman of the cost prediction group, prepared a committee report (Ref. 4)* with the following recommendations:

1. NASA should take an active role in updating the composites data base with current state-of-the-art cost data and manufacturing processes. A "subscriber" approach, wherein contributors to the data base would have access to it, was suggested as one approach for obtaining data in addition to the ACT program participants' hardware cost results.
2. NASA should ensure that the data base be kept current with long term support.
3. NASA should develop a producibility guide to assist design-build teams in making decisions on a design concept. This document would supply information on selected manufacturing processes and provide information to the designer on types of design details to avoid that would adversely affect cost. At the same time, large cost drivers would be delineated. An implementation plan to address CAD interfaces would be required to accompany the development of the producibility guide.
4. NASA should establish standard material costs (including future costs) to be used for comparative costing studies and include them in the data base.

Cost Tracking and Reporting

As part of the ACT program, various airframe manufacturers will be designing and fabricating composite components that are more cost effective than previous composites or equivalent aluminum structure. The components, of various sizes, will be made using low cost and automated fabrication processes. In order to assess the cost effectiveness of the designs and their fabrication processes, cost information must be acquired on the fabrication process. As noted above, the workshop committee suggested that the form originally developed for the Fab. Guide included all the essential information and was familiar to the industry. Most Government programs on composite

*(Letter Report. See Ref. 4)

structure development during the 1970's and the early 1980's included requirements for the completion of the "Fabrication Guide Data Abstraction Form". The effort to collect fabrication information ended about 1983. More recent contracts have not had that requirement.

In revitalizing the data collection activity, STPO will attempt to automate and simplify the process. A standard, unified cost collection Data Abstraction Form will be implemented via a software module that easily allows the relevant manufacturing data to be collected and formatted for subsequent inclusion in a fabrication cost data base.

The proposed cost tracking program will proceed in two stages:

1. The procedure for entering data will be standardized to a user friendly software interface which is MS-DOS®, Macintosh™, and UNIX™ compatible.*
2. A data base with an appropriate data base management system (DBMS) will be established to store the existing fabrication data as well as data acquired in the current programs. The DBMS will be selected so that the data base can be easily updated and sorted to provide a variety of forms, charts and graphs. The data base will be accessible to companies that contribute fabrication data.

The first task is essentially an evolution in the technology of the Fab. Guide Data Abstraction Form (DAF). Interactive software will be developed to run under MS-DOS, Macintosh, or UNIX systems. The software will be "intelligent" enough to prompt the user for only required input, and present the user with a flow diagram of a composite structure manufacturing process. Figure 1 shows the hierarchical structure of the DAF. The diagram will be displayed to the user and boxes

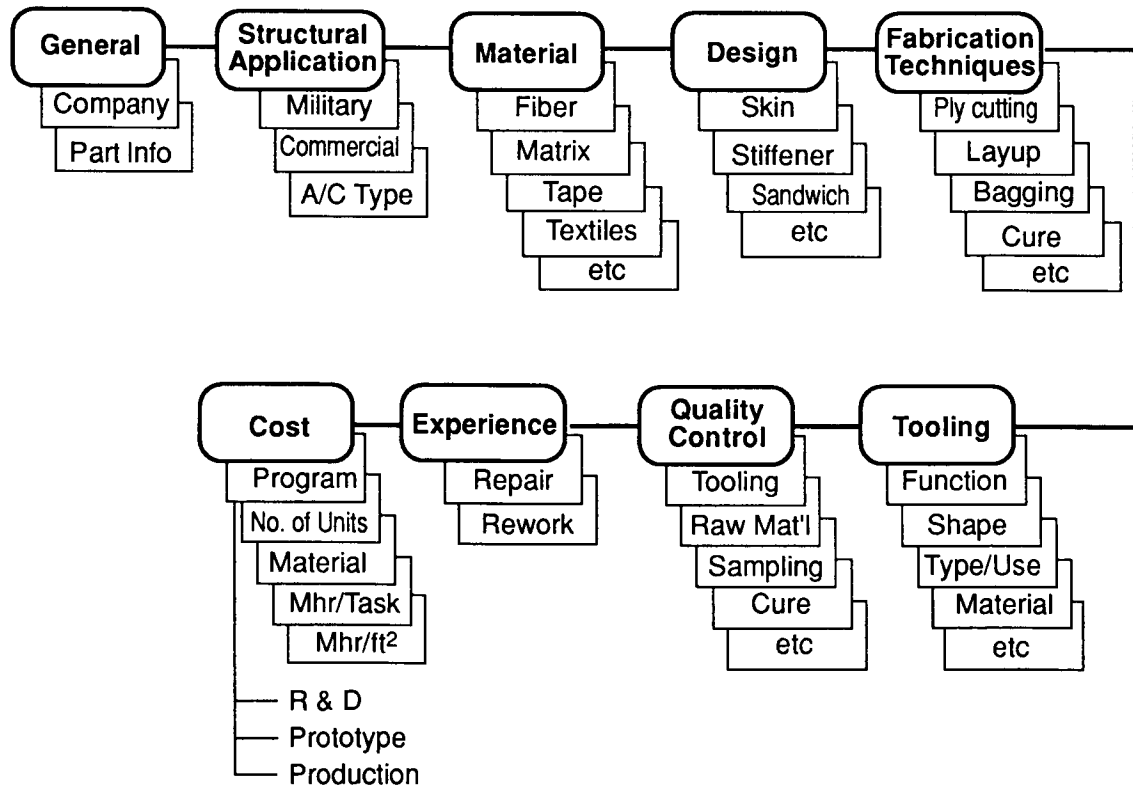


Figure 1. - Hierarchical structure of data abstraction form.

will serve as menus and “buttons” that allow the user to move directly to any section of the form. Figure 2 shows screen images of a demonstration version of a portion of the data input form which runs under HyperCard™* on the Macintosh. The program is configured so that the cursor moves to the next appropriate field after input has been entered.

The figure consists of four separate screen images arranged in a 2x2 grid, each representing a different screen of an automated data abstraction form. Each screen features a navigation menu at the bottom with buttons for General, Application, Material, Part, Fab Tech, Cost, Experience, QC, and Tooling.

- Top Left Screen:** Contains fields for Company, Division, Recorder (with sub-fields for Last Name, First Initial, Org/Dept, and Phone Number), and Date Recorded (Mo/Da/Yr). It also has radio buttons for Commercial and Military.
- Top Right Screen:** Features two columns of radio buttons: Fibers (Carbon, Kevlar-490, E-Glass, S-Glass) and Matrix (Epoxy, Polyimide, Thermoplastic, Polyester). It includes input fields for Fiber Diam (mils) and Fibers per tow (K), and radio buttons for Material Form (Tape, Sheet, Broadgoods) and Fabric Style.
- Bottom Left Screen:** Displays a list of radio buttons under the heading "Application & A/C Type": Transport, Helicopter, Executive/Jet, Executive/Prop, and GA.
- Bottom Right Screen:** Shows two columns of radio buttons: Platform (Rectangular, Square, Trapezoidal, Triangular, Irregular, Round) and Cross Section (Rectangular, Square, Trapezoidal, Triangular, Airfoil, Round). It also includes input fields for Dimensions (Max width, Max length, Max Thickness, Wetted area).

Figure 2. - Screen images of automated Data Abstraction Form.

After the software form has been filled out, the user will have the option of electronically transmitting these data to a NASA host mini-computer via an electronic mail system, by calling an 800 number to log in directly, or by mailing a disc.

Another software module that will be resident on the host computer will be a data input parser (checker). This will verify that the user inputs are within “reasonable” and “acceptable” ranges. Once developed, this software could be made available directly to the user. It will also be available for interactive use when the data is directly transmitted to the host computer. Companies will not interface with the data base directly, but only with a host data collection file. Data will be entered into the data base by NASA only after the source and the acceptability of the data are verified.

The last software module that will be developed will be one which allows a user to interface with the fabrication cost data base in a “read only” mode. A user friendly interface is envisioned that will allow the user to extract information based on specified queries such as “provide the labor hours required for manufacturing hat stiffeners of any composite material by all manufacturing processes.” A schedule for the development and distribution of the data abstraction form and the establishment of the data base is given in figure 3.

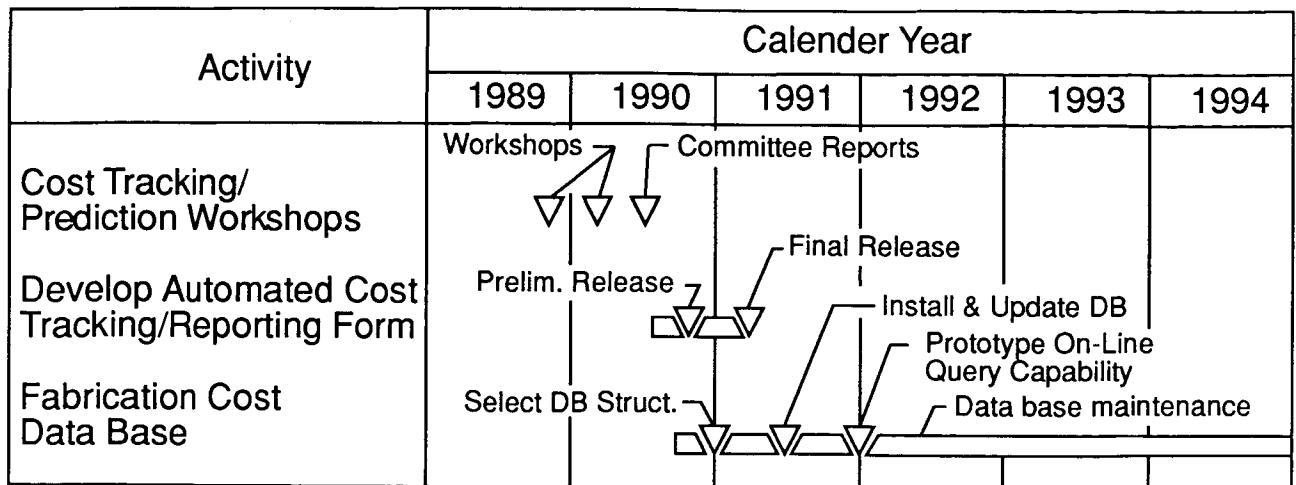


Figure 3. - Fabrication cost data base development.

The selection of a DBMS requires careful attention in order to ensure that it is both user friendly and versatile. The user interface must be structured so that the user will not have to learn and understand details of the data base structure in order to access it and obtain information from it. A survey will be made of the DBMS packages available on the market with the following attributes:

1. Wide acceptance/use in the field.
2. UNIX based or demonstrated on a number of platforms.
3. A demonstrated MS-DOS and Macintosh interface capability.

For the future, one can envision including additional information in the data base such as tables of available material forms and their current costs, manufacturers' property data, digitized drawings and images of parts, contractor reports, video images, audio reports, etc.

Composite Cost Prediction

"All costs are based on facts that may or may not be true" (Ref. 5). The word "cost" has a variety of meanings to different disciplines. Designers, accountants, estimators, managers, manufacturing engineers etc. are interested in different levels of detail and economic conditions that imply a numerical value to the term "cost". Often price is confused with cost. This lack of uniform, concise description of the elements and time-valued rate constants that make up recurring cost, nonrecurring cost, etc. leads to confusion and debate. Unifying the way the composites community represents hardware cost for composites and metallics is perhaps as much a communication problem as it is a demanding engineering challenge. This program will determine the feasibility of establishing theoretical cost functions that relate geometric design features to summed material cost and computed labor content in terms of process mechanics and physics.

Figure 4 provides a flow chart form of the detailed cost bookkeeping elements that should be considered when comparing composite aircraft cost to a metallic equivalent. The ability to fabricate very large one piece composite structure to eliminate thousands of fasteners in equivalent aluminum hardware requires assembly level cost estimating to establish a fair comparison during preliminary design. The exceptional fatigue life and resistance to environmental degradation of composites should be considered since they provide favorable maintenance and supportability comparisons.

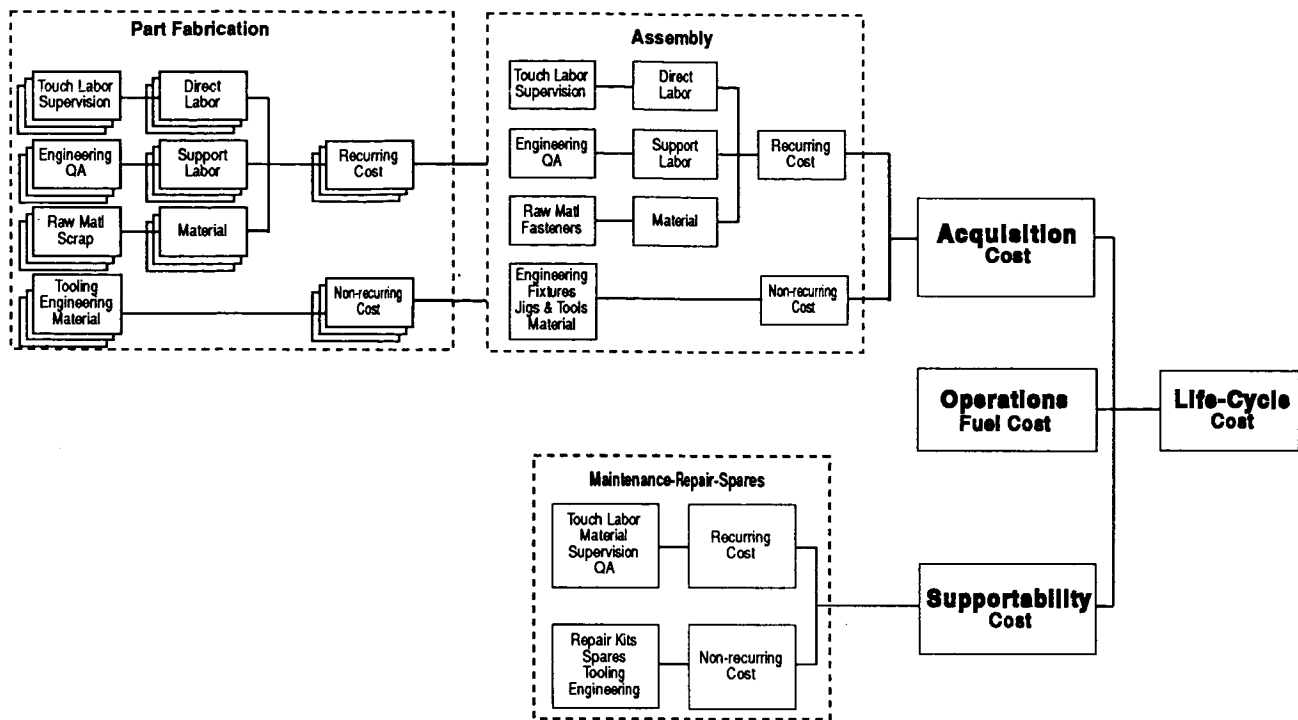


Figure 4. - Detailed cost bookkeeping elements.

Large weight savings associated with extensive use of composites in wing and fuselage structure would result in significant fuel savings over the operational life of each aircraft. Ideally the designer should be aware of the cumulative effects of operational and supportability cost savings, but his influence on lowering the acquisition cost generally dictates the success of a replacement part or new design being committed to a production application.

STPO's objective in attempting to develop a designer's cost model is not to replace company accountants or estimators, or to develop more efficient bookkeeping tools, but rather to develop a cost model to provide the designer with a user friendly tool that relates cost to terms the designer normally uses. The cost related issues a designer can influence usually are related to selections of materials, tolerances, simple versus complex shape or geometry, and process dependent features that contribute to automation potential and tooling complexity. The designers model should provide definitive assistance in identifying the cost implications of these choices, but it should not be expected to replace the professional cost analyst that has to interpret company policy and historical pricing practices. Managerial decisions affecting actual program costs related to availability of land, unused company facilities, future labor rates, return on investment, etc. are not issues the designer can be expected to consider. The primary goal for a design-with-cost model is to provide the designer with a producibility data base and theoretical cost model that relates a new composite design to an equivalent aluminum structure using elements of the design process that the designer can realistically influence.

Figure 5 illustrates the standard methods used for cost/price estimating. Variations of these methods are used routinely by estimators and price analysts to forecast or compare the relative value of materials, automated processes, and projects. Figure 6 shows four state of the art cost models used for estimating composite hardware program requirements. The current state of the art models

Estimating Methods	Technique	Resource Category
Parametric	<ul style="list-style-type: none"> Correlates design and historical cost data Estimates applicable at the component and subsystem 	Conceptual Preliminary design
Factors	<ul style="list-style-type: none"> Used when details of item are not available Compares new item to a prior similar item and then factors historical cost 	Conceptual Preliminary design
Analogous	<ul style="list-style-type: none"> New item very similar to a current item in production. Specific analogies are drawn as the basis for defining the cost of the new item 	Conceptual Preliminary design
Trend Analysis	<ul style="list-style-type: none"> Use historical production trend data to estimate future production costs 	Conceptual Preliminary design
Identical Units	<ul style="list-style-type: none"> Actual cost of the item is known. Units are in production for other applications. 	Design Development Production
Detailed	<ul style="list-style-type: none"> Estimates accomplished by defining tasks, characteristics, manhours, material costs for specific work packages These types of estimates are based on previous detailed labor/material history 	Design Development Production

Figure 5. - Summary of estimating methods.

<ul style="list-style-type: none"> An interactive spread sheet to include cost Starts with basic part of a simple form then adds: <ul style="list-style-type: none"> Palate of manufacturing methods Builds up discrete parts to give airframe structure
Advantages: <ul style="list-style-type: none"> Allows both metal and composite technologies
Disadvantages: <ul style="list-style-type: none"> Requires a mainframe and does not have user friendly data base or CAD interface

(a). - Battelle Manufacturing Cost/Design Guide

<ul style="list-style-type: none"> A detailed breakdown of the production process into its component parts based on a time and motion study conducted in 1976
Advantages: <ul style="list-style-type: none"> A data base of limited production processes for Al and composites Each production process is based on the average labor time, average productivity factor, QC, etc.
Disadvantages: <ul style="list-style-type: none"> Requires a mainframe and does not have a user-friendly data base or CAD interface

(b). - Northrop ACCEM & FACET

<ul style="list-style-type: none"> Lotus 123 spreadsheet models for many composite processes
Advantages: <ul style="list-style-type: none"> Production methods compared & evaluated on the basis of cost of materials, scrap, QC, tolerances, & overhead Econometrics module available
Disadvantages: <ul style="list-style-type: none"> Can only handle parts, not assemblies

(c). - MIT/IBIS model.

<ul style="list-style-type: none"> A commercial model with nation-wide subscribers Resident on a mainframe
Advantages: <ul style="list-style-type: none"> Includes extensive mathematical methods for manufacturing cost estimation Includes standard risk models
Disadvantages: <ul style="list-style-type: none"> Requires a highly expert user with a large training time investment Code and equations practically unavailable

(d). - GE PRICE model

Figure 6. - State of the art cost estimating models used for composite structures.

used to estimate the cost of composite fabrication for hand layup and automated tape laying are the ACCEM (Ref. 6) and FACET (Ref. 7) programs. Northrop developed the ACCEM program in 1976 based on a time and motion study of different composite material manufacturing processes. Equations were developed to estimate recurring composite part manufacturing costs. FACET has been developed as a Fortran language mainframe computer program that evolved from ACCEM with updated Air Force project data bases. New material forms and manufacturing processes that can be evaluated for production of the most cost effective structure are considered in the MIT/IBIS model (Ref. 8). These spreadsheet models estimate individual cost elements and enforce consistent accounting assumptions. The G.E. PRICE H (Ref. 9) model is very complex and requires extensive training with terms and concepts that best suit the needs of a cost analyst or accountant.

The Boeing, Douglas, and Lockheed workshop participants all currently use a preferred composite fabrication cost estimating methodology. Boeing estimators rely heavily on the G.E. PRICE Model, the only model that cost analysts from all three companies use routinely. Lockheed uses both ACCEM and FACET and has developed parametric equations based on in-house fabrication experience. Douglas is developing an expert system model based on the GURU (Ref. 10) artificial intelligence program and in-house experience. None of the current cost models used by the airframers contain information on newer fabrication processes (e.g. RTM, pultrusion, filament winding, braiding and stitching). All of the available composite cost models appear best suited for fabrication experts, and none are independently used by designers. The tools that are available are not suitable for preliminary and conceptual designers who will not spend their time filling out forms and collecting material or process specific data that must be input to existing cost models. Modifying existing models has been considered. Establishing accounting consistency with Lotus 123 (or equivalent) spreadsheet forms and contractually requiring all ACT program participants to uniformly report with these forms has been discussed. Holding an additional workshop to develop unified equations, factors, and standard constants to be used in the G.E. Price model also has been considered. The major concern for these approaches is that designers will not use a tool that is unfamiliar and unrelated to the design process. If a cost estimating system is to be useful to the designer, and helpful in the selection of design concepts with their associated fabrication processes, the system must be relatively transparent to the designer. A model for designers must be structured to have input that can be coupled directly to a preliminary design module. Such input relates cost to panel thickness, stringer spacing, stiffener height, laminate ply orientation stacking sequence, etc.

The primary thrust of the designers' cost model development would be to use a first principles approach to establish building block unit cell elements (e.g. prepreg tow, 12" prepreg tape, cloth, etc.) that represent different material forms, and to use basic principles (mechanics, dynamics, physics, etc.) to describe labor content in terms of machine feed rates, accelerations, and material deposition efficiencies that characterize processes and the effectiveness of automation. Modeling concepts of cost per inch, materials cost per cubic inch, and layup man hours per square inch for a unit cell representative of each material form are concepts that would suit the designers' needs. Engineers customarily express cost comparisons as \$/pound or man-hours/pound. Ratioing comparisons with respect to geometric properties and dimensions of length, area, or volume would provide a means of incorporating geometric complexity in the comparison. Complexity factors determined as theoretical relations for radii of curvature, degree of double curvature, tight dimensional tolerances, number of stiffening elements, etc. would provide equations to uniformly express theoretical cost of materials and labor for simple or difficult to fabricate designs. The designer employs laminated plate theory to sum lamina properties that are experimentally determined through the thickness of a

laminate to develop smeared stiffnesses that account for ply orientation and stacking sequence. A similar approach for treating cost as a lamina material property (\$/square inch) that's summed through the thickness, accounting for material length associated with part topography and process dependent scrap of off angle plies, would allow development of a totally theoretical cost representation. Panels could be designed to calibrate the labor content of automated processes by measuring man hours per square inch to apply lamina to a simple and complex shape mandrel providing process dependent coefficients similar to the lamina modulus measurements now used to evaluate composite materials.

Assemblies could be considered by describing the material and man hours associated with fastener installation and added structural joint complexity. A metallic structural part or assembly cost could be used for comparison to provide ratios (index of value) that nondimensionalize the cost representation and remove issues of proprietary labor rates, time value of money, etc. Initial efforts should concentrate on recurring costs which are most amenable to a detailed breakdown and are directly related to design features. Recurring costs should be a function of the physical description of the part and the fabrication process related to the part. As the term "recurring costs" implies, these costs are incurred for every part made and should be consistent from part to part. Since the recurring cost elements of a fabrication process are amenable to a time and motion study, equations can be developed that predict cost from material volume, part geometry and the physics that describes the time and resources required to perform each step of the of construction, machining, and assembly with fasteners or adhesives. This approach would provide designers with an technically sound, academically rigorous, and universally accepted model to describe a theoretical material cost and labor content for comparison of their designs. These models could be calibrated with actual corporate experience to provide bounds of theoretical versus actual process efficiencies. Ideally the model can be a module to existing design software that will compute cost from the geometric features derived from design software, geometry generator programs and, eventually, CAD programs. Such a model would allow the designer to use cost equations as minimization functions in optimization models now used in designing to minimum weight. Figure 7 provides a flow chart for a prototype designers' theoretical cost optimizer concept with emphasis on the data base elements that must be developed.

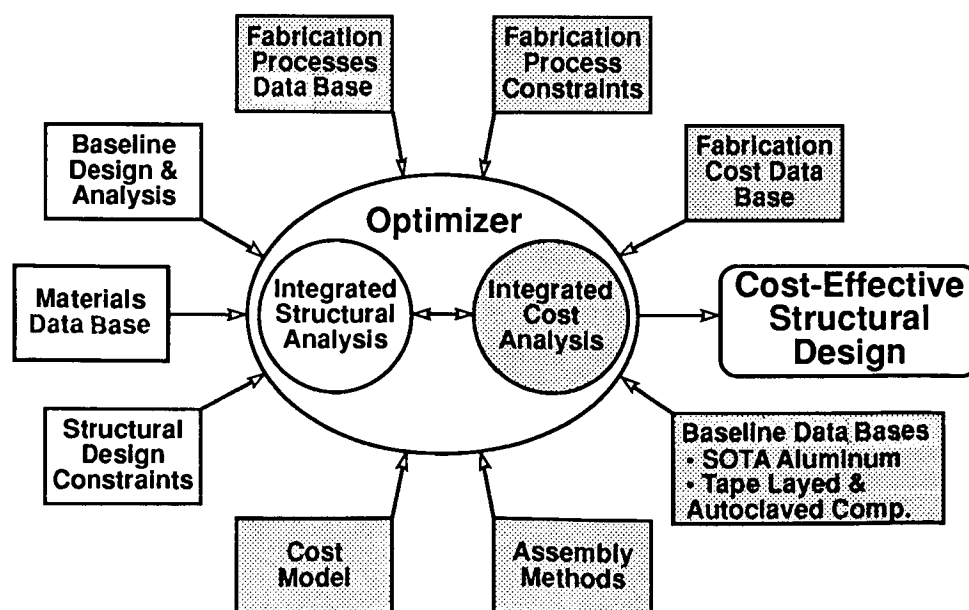


Figure 7. - Optimization of design process with cost as a design variable.

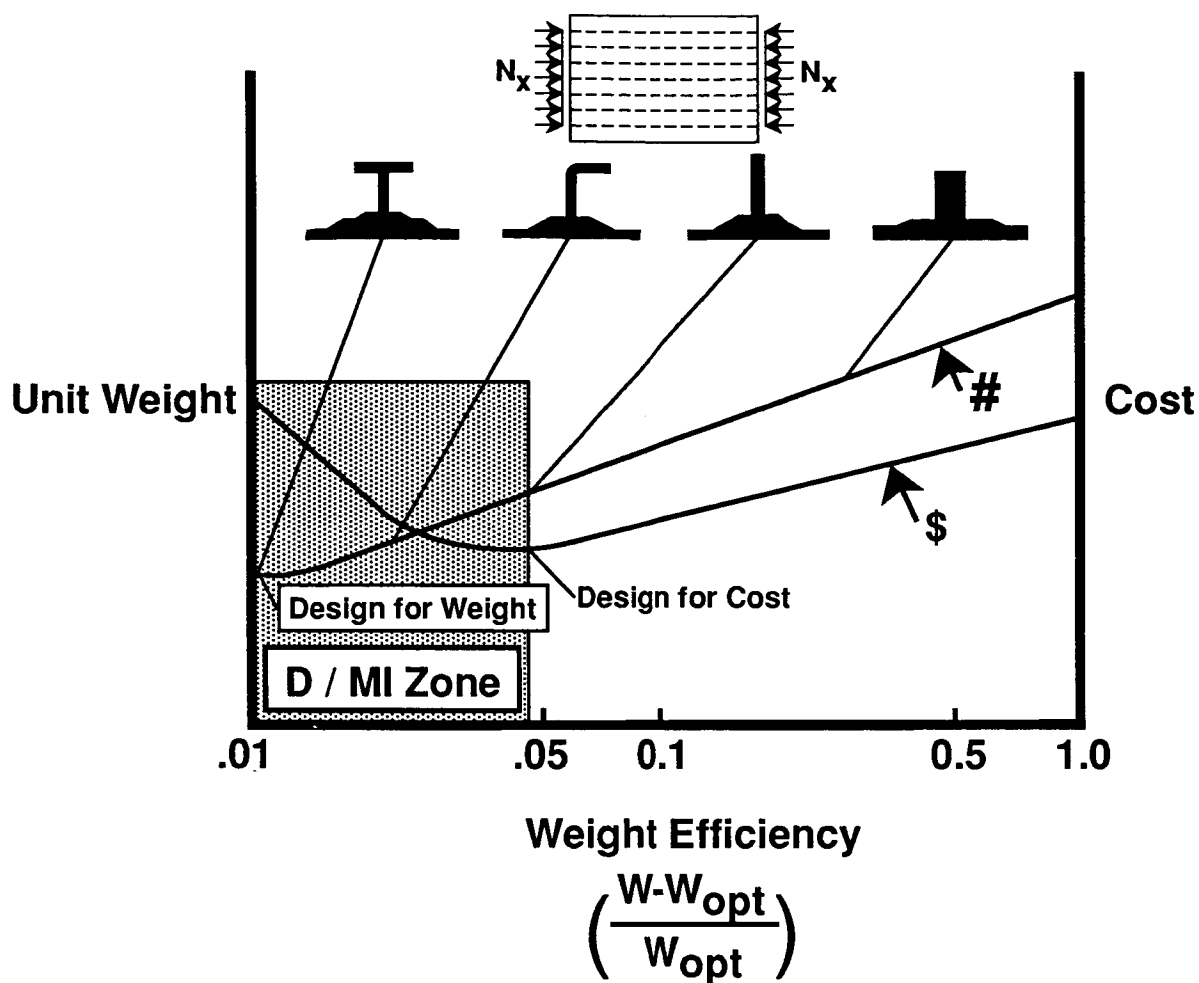


Figure 8. - Influence of design/manufacturing integration (D/MI).

The designers' cost model must have sufficient fidelity to distinguish between concepts if the concepts have significantly different costs. This fidelity implies the need for adequate detail in both the description of the part and the associated cost methodology. Figure 8 provides a schematic of the results of the design-with-cost process for a simple stiffened skin compression panel. The influence of design concept on cost and weight is the product of this process. The D/MI zone permits the designer the opportunity to increase weight efficiency with cost as a primary variable. A cost methodology that sums the cost of each element of the fabrication process and allows for parallel as well as serial operations may be required to achieve the needed fidelity. Figure 9 shows a flow chart for manufacturing an elevator including panel, rib, and spar details. Developing equations representing economic relationships in terms of energy, power, thermodynamics, mechanics, process physics, etc. for each step would sum to a theoretical cost for performing each operation. Statistical bounds applied to each operation could establish theoretical maximum and minimum cost values. One model concept would be to treat cost as a control theory or chemical engineering process problem where time dependent cost functions were inputs to be integrated through process steps to completion as a part or assembly. Participants in the ACT program will be generating cost data related to new processes and the state of the art for manufacturing large composite structures, providing the required data base to formulate a theoretical cost model approach and the coefficients and constants necessary to calibrate or verify the model.

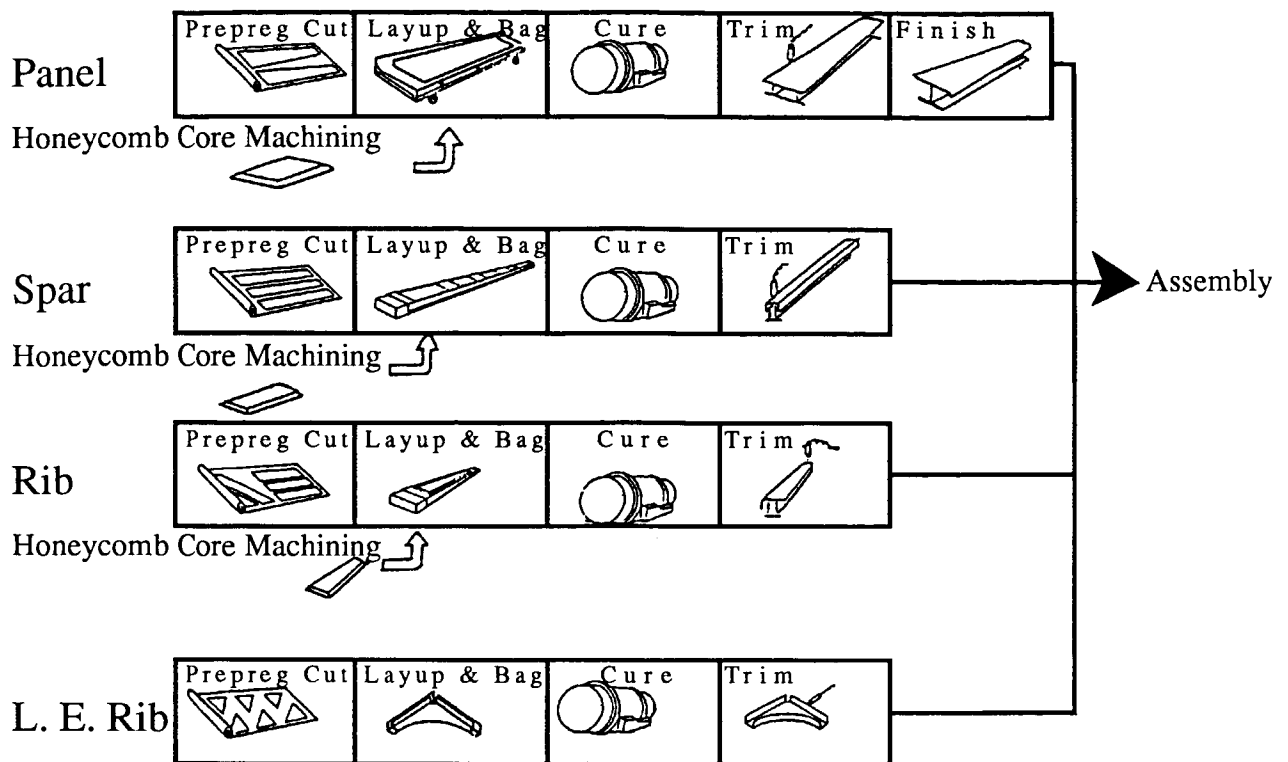


Figure. 9 - Elevator manufacturing flow.

Nonrecurring costs are important since the need to build new tooling often adds large start up expenses to a project. Tooling costs should be considered because they vary according to the selected design concept or fabrication process and are therefore an element of cost that is directly related to design. Tooling cost should be predictable in relation to the physical, dimensional and geometric complexity of the part to be made. Tooling costs are a function of the production rate and the total number of parts to be made. A program that includes tooling costs should have the flexibility to consider changes in production rate and the total number of units over which the costs of tooling will be amortized. The feasibility of a theoretical tooling cost model related to tool material type and geometric complexity of the part to be made will be evaluated.

Conclusions

The remarkable advances in computer hardware and commercial software technology have led to low cost data storage and sophisticated data base management systems. These developments make it economically feasible to track the cost history of numerous projects and provide the historic opportunity for bringing cost into the preliminary design process as an engineering variable.

Recommendations of the cost reporting and cost prediction workshop committees will be implemented by

1. Continuing an established task with AS&M to develop an electronic data base that will unify formatting and automate the collection of composite part fabrication costs provided by ACT program participants. A "subscriber" approach, wherein contributors to the data base would have

access to it, will be implemented. The data base will include standard material costs (including future costs) for consistent comparative costing studies. The database will be kept current through the duration of the ACT program and methods for long-term maintenance will be considered.

2. Development of an academically rigorous model for predicting the cost of different composite designs during the preliminary design process will be initiated. This effort will include development of a producibility guide (a manufacturing data base software module) to provide the designer with information on selected manufacturing processes and types of design details that adversely affect cost. Large cost drivers will be identified and software approaches to couple the data base to design optimization and CAD interfaces will be pursued.

References

1. Meade, L.E., "DoD/NASA Structural Composites Fabrication Guide-3rd Edition", pages A7-A15, Volumes 1-2, Air Force Wright Aeronautical Laboratories, 1982. **Presented.**
2. "First Workshop on Cost Tracking and Prediction", Structures Technology Program Office-NASA-LaRC, Norfolk, Va., November 30-December 1, 1989. **Presented.**
3. "Second Workshop on Cost Tracking and Prediction", Structures Technology Program Office-NASA-LaRC, Long Beach, CA., February 21-22, 1990. **Presented.**
- *4. Swanson, G., Cost Model Recommendations, Letter Report-dated July 13, 1990, "Second Workshop on Cost Tracking and Prediction", Structures Technology Program Office-NASA-LaRC, Long Beach, CA., February 21-22, 1990.
5. Davis, H.V., LASC Present Approach To Cost Tracking, "First Workshop on Cost Tracking and Prediction", Structures Technology Program Office-NASA-LaRC, Norfolk, Va., November 30-December 1, 1989. **Presented.**
6. LaBlanc, D.J., "Advanced Composites Cost Estimating Manual", AFFDL-TR-76-87, WPAFB, August 1976.
7. Meade, L.E., "DoD/NASA Structural Composites Fabrication Guide"-Final Administrative Report, AFML-TR-82-4137, Air Force Wright Aeronautical Laboratories, 1982.
8. Krolewski, S. and Gutowski, T., Economic Comparison of Advanced Composite Fabrication Technologies, 34th International SAMPE Symposium, Reno, Nevada, April 1989. **Presented.**
9. PRICE H™ Reference Manual, Price Systems, General Electric Co., Dayton, Ohio, 1988.
10. Cost/Benefits Analysis System User's Guide Ver. 2.0, Advanced Program Development, Douglas Aircraft Company, March 21, 1989.

* MS-DOS® is a registered trademark of Microsoft Corporation, Macintosh™ and HyperCard™ are trademarks of Apple Computer, and UNIX™ is a trademark of AT&T Bell Laboratories.

F-15 COMPOSITE ENGINE ACCESS DOOR⁺

Ramaswamy L. Ramkumar
Northrop Corporation, Aircraft Division

James C. Watson
McDonnell Aircraft Company

SUMMARY

This paper presents a summary of the successfully concluded Phase I of the two-phase Design and Manufacture of Advanced Thermoplastic Structures (DMATS) program. It addresses the design, manufacture and validation testing of a thermoplastic F-15E forward engine access door and includes lessons learned during the concurrent product and process design development phases of the program.

INTRODUCTION

The F-15 forward engine access door is moderately sized (42 in. x 38 in.) with a contour curvature that varies from gentle to relatively severe. The door is a built-up, channel stiffened, titanium structure on the F-15C/D and a superplastically formed/diffusion-bonded (SPF/DB), hat-stiffened titanium structure on the F-15E (Figure 1).

The F-15 door is located approximately eight feet aft of the main landing gear, directly underneath the engine compressor section. The component requires structural integrity and durability in a high temperature (300°F) and severe acoustic (156 dB max.) environment. Due to its location, the door is impacted with runway debris and is removed frequently by maintenance personnel during routine maintenance. Engine equipment located above the door includes the main oil tank and fuel filter; thus the door is exposed to aircraft fluids. The door is a secondary structure and is loaded primarily in shear.

+ Work reported in this paper was performed in Phase I of an ongoing Northrop/WRDC contract F33615-87-C-5242, titled "Design and Manufacture of Advanced Thermoplastic Structures". Ms. D. Carlin and Ms. T. B. Tolle are the WRDC technical monitors.

Major longerons located inboard and outboard of the door carry the majority of the fuselage bending loads. Air loads are relatively low (3.75 psi). The door structure contains two non-structural service doors for oil and fuel filter service. When open, the door is attached to the surrounding structure by two metal gooseneck hinges.

MATERIAL SELECTION

Thermoplastic matrix composite (TP) material selection for the F-15E forward engine access door was dependent primarily on the maximum continuous service temperature the structure is exposed to during aircraft operations. Recorded flight temperatures for the critical speed and altitude show a maximum temperature of 280°F. Therefore, a material system with a 300°F service temperature was deemed adequate to meet temperature requirements.

Originally, Imperial Chemical Industries' (ICI) AS4/HTX was selected as the material system for the door. The AS4/HTX material's 350°F service temperature met the temperature requirements, had the necessary mechanical/physical properties, and was available. However, micro-cracking and processing problems that occurred during trial manufacturing runs led to the withdrawal of the HTX material system from the program.

ICI's AS4/ITX was subsequently selected to replace AS4/HTX. The AS4/ITX material's 300°F service temperature met the temperature requirements for the door, and it had mechanical properties comparable to AS4/HTX. The processing characteristics of ITX are significantly better than those of HTX, and no micro-cracking was identified in the parts.

TP DOOR DESIGN

The initially selected coconsolidation concept for the TP F-15E door was finally replaced by an amorphous-bonded structure containing autoclave-consolidated outer mold line (OML) and diaphragm-formed inner mold line (IML) skins (see Figure 2). To facilitate diaphragm forming of unidirectional TP, the hat stiffeners on the TP door are shallow and the bend radii of the hat stiffeners (at the corners of the bays) are generous. The two nonstructural service doors were redesigned to be

compression molded using chopped AS4/HTX tape. Due to the difference in the stiffener cross-sectional geometry between the titanium and the TP access door, all attachment and reinforcement hardware were redesigned to fit the TP hat stiffeners on the door. This included changes to the aluminum hinges for the service doors and the titanium gooseneck hinges that attach the access door to the aircraft. The gooseneck hinges were also designed to permit adjustment during installation. Two brake-formed sheet metal parts attach the hinge to the hat stiffener (Figure 3). This allows for manufacturing tolerances in the hat-stiffener geometry.

The OML and IML skin layups result in a laminate design that is a series of five-ply symmetrical sublaminate. The individual components (OML and IML skins) are symmetrical to reduce fabrication-induced warpage. Also, the ply build-ups in the OML skin are symmetrical to reduce warpage, and ply drop-off spacings are no smaller than 0.1 inch to enhance performance and producibility. Titanium fasteners were used, and all non-titanium metallic hardware were isolated from the composite door through the use of non-metallic shims.

The door was designed to fit to an existing metal substructure. Therefore, the edge distance (E) on the peripheral Milson fasteners was only two fastener diameters (D). To obtain an allowable bearing stress for an E/D of 2, bearing tests were performed. An allowable ultimate bearing stress of 40 ksi was determined from the test. In order to meet the bearing stress requirements, the door thickness around the edges was increased to 35 plies.

The door was designed to buckle below limit load and operate in the postbuckling range as an additional weight savings measure. The SS8 computer code was used to predict the initial buckling of individual door bays. Assuming that the hat stiffeners provide clamped supports, the center bay was found to be critical at an initial buckling load of 319 lbs/in shear flow. Therefore, at a maximum shear load of 850 lbs/in, the postbuckling ratio was 2.66.

The nonstructural service doors were designed using chopped AS4/HTX material (Figures 4 and 5). The basic shape of the service doors remained similar to the current aluminum service doors. However, because of the difference in material properties between aluminum and chopped AS4/HTX, the thickness of the door was resized to withstand air pressure and handling loads. Material properties for chopped AS4/HTX were determined from test results.

Amorphous bonding of AS4/ITX skins with polyetherimide (PEI) was shown to have strengths equivalent to coconsolidation. This is

because PEI is a low melt temperature thermoplastic material with matrix properties compatible with thermoplastic materials including PEEK and ITX. A typical amorphous bond process has one 0.005 inch PEI ply consolidated to the joining surface of each detail during the consolidation of the details. When the two details are joined together, two additional 0.005-inch PEI plies are inserted between the details to effect joining/subassembly. The resultant consolidated bondline is typically 0.010 inch thick.

Based on the results from two subcomponent tests, a design change was made to install fasteners around the hats in the amorphously bonded door full-scale assembly (Figure 6). This was required because of the inconsistency in the bondline quality, resulting in a premature failure during one of the subcomponent tests. However, a second subcomponent went to 150% of the design ultimate load, with no failure in the bond region. Therefore, the fasteners were installed as a safety precaution since a reliable database on amorphous bonding was not available. The fastener pattern design for the door (see Figure 6) uses 4D and 6D spacing, depending upon the proximity to highly stressed areas. The fasteners chosen were 3/16 inch tension head hi-loks with self-aligning washers and collars.

MANUFACTURING PROCESS DEVELOPMENT

Significant technical challenges were encountered in transitioning from the preliminary manufacturing processes at the initiation of the program to the processes that were eventually applied on the flightworthy TP F-15 engine access doors. The challenges were posed by material-, design-, tooling- and equipment-related issues, and are summarized in the "Lessons Learned" section of this paper. The manufacturing processes used for the "production" TP doors are described below:

Fabrication of AS4/ITX IML Skin

Diaphragm forming, using an SPF aluminum diaphragm, was chosen as the manufacturing process for the IML skin because of the proven ability of this process to fabricate high quality, complex, efficient composite parts (Figure 7). The skin was fabricated in a press on a female carbon/ceramic tool. Dual diaphragms were utilized to maintain location of the ply pack during forming.

Fabrication of AS4/ITX OML Skin

Autoclave consolidation was the selected manufacturing process for the OML skin (Figure 8). Diaphragm forming in a press with a contoured vacuum frame was recommended for a future production scenario and was used in the cost analysis for the fabrication of the OML skin. The fabrication process consisted of envelope bagging on the OML carbon/ceramic tool utilizing an aluminum caul sheet. Processing parameters were set as close as possible to those used in the diaphragm forming process. The caul sheet was roll-formed to the approximate contour of the OML tool.

Amorphous Bonding of AS4/ITX OML and IML Skins

The IML skin and the OML skin initially had one layer of PEI film coconsolidated on the bonding surface. These surfaces were cleaned prior to bonding using cheesecloth and isopropyl alcohol. The OML skin was then placed on the OML tool. Twelve layers of dried .005 inch PEI film were placed over the skin to ensure the filling of any gap due to IML/OML mismatch. The IML skin was then placed on top of the PEI film layers and envelope bagged to the OML tool. The periphery of the part was periodically taped with high temperature tape to allow air to escape and to control PEI squeeze-out. To aid in air/gas removal, fifteen 0.040-inch diameter holes were drilled at strategic locations through the IML skin into the bondline. Amorphous bonding was effected during a 45 minute hold at 20 psi and 575°F. A 3-5°F/minute cool down was used to minimize any resulting thermal stresses.

TESTING AND TP DESIGN VALIDATION

An extensive test program was conducted to validate the TP F-15 door design. Results of the test program were used to evaluate the flightworthiness of the door. A building block approach was used, as evidenced by the testing of elements, subcomponents, and finally the full-scale door.

One full-scale production door (without hardware, access doors, or finishes) was subjected to structural verification testing consisting of static, spectrum fatigue, and residual strength

tests. All tests were performed under room temperature ambient (RTA) conditions. The door, to be structurally qualified for flight test, had to meet the following test criteria:

- (1) No delaminations or disbonds occur that result in permanent set of the composite material at or below 100% design limit load (DLL). No yielding or fracture of the the composite material at or below 100% DLL. Disbonds between the hat and the skin would be allowed if the disbond were arrested by the fasteners placed around the hats.
- (2) The door must survive two (2) lifetimes of spectrum fatigue loading (1 lifetime = 8000 spectrum flight hours).
- (3) After completing two lifetimes of spectrum fatigue testing, the door must reach 150% DLL with no catastrophic failure.

The full-scale door was subjected to shear loading using a picture frame arrangement. The shear loads applied were based on loads taken from the F-15E aft fuselage finite element model. This shear load is slightly lower than the original 850 lb./in. shear that the door was designed to.

Before the door was tested, a baseline ultrasonic A-scan and C-scan were performed. The door was A-scanned after being subjected to the limit load and during the fatigue tests to determine if any nonvisible damage had occurred. A C-scan was taken of the door after the ultimate test was performed to determine the extent of the damage.

The full-scale AS4/ITX F-15 door test was successful. Test results validated the TP door design and established its capability to withstand 100% DUL after two lifetimes of F-15 fatigue loading.

LESSONS LEARNED

The Phase I effort described in this paper culminated in the successful delivery of flightworthy TP F-15 forward engine access doors to the U.S. Air Force. However, the path to success was punctuated by challenges, some of which could not be overcome, in technology areas that included materials and processes, manufacturing technology, tooling technology, processing equipment and structural design. A summary of the lessons learned is presented below:

Materials

- (1) Materials-related challenges faced on the DMATS program included high melt viscosity, narrow processing window and limited reprocessability. The last issue (limited reprocessability) was primarily introduced by long process cycles, due to a lack of rapid heating/cooling capability in the processing equipment. Consequently, the preferred assembly process for the OML/IML skins was changed from coconsolidation to amorphous bonding.
- (2) Selected Phase I TP materials (AS4/HTX and AS4/ITX) were only available in the unidirectional tape (UDT) product forms. This posed a forming challenge for the complex-contoured, stiffened IML skin. The use of a Kapton/Upilex polyimide film in Northrop's diaphragm forming press setup increased diaphragm rupture occurrences at forming pressures in excess of 100 psi. But, the IML skin did not completely form at 100 psi, exhibiting small regions of "bridged" plies. This necessitated the use of the SPF aluminum diaphragm in MCAIR's diaphragm press setup, and the application of a 200 psi forming pressure. If drapeable AS4/HTX and AS4/ITX product forms had been available, forming of the IML skin and the concurrent OML/IML coconsolidation could have been demonstrated on the program.

Manufacturing Processes

- (1) Diaphragm forming of small flightworthy F-5 and T-38 details had been established by Northrop as a producible and cost-effective process prior to the DMATS Phase I effort. However, the scaleup of this process to the F-15 door IML skin was a major challenge. The replacement of the polyimide diaphragm by the SPF aluminum diaphragm, and the use of a 200 psi forming pressure, overcame the IML skin forming challenge and resulted in a producible process.
- (2) Autoclave consolidation of the gently contoured F-15 door OML skin, using an envelope bagging technique, required the use of a caul sheet to eliminate wrinkles.
- (3) The use of a washaway mandrel to coconsolidate the OML and IML skins was successfully demonstrated on the program, though its application was considered risky due to the complexity in the final OML/IML cross-sectional cavity shape

compared to the simple hat cross section in the preliminary design.

- (4) The implementation of the amorphous bonding process was challenged by three factors: (a) the unknown interlaminar (bondline) properties for the ITX/PEI combination; (b) the lack of dimensional control of the IML and OML bonding surfaces, due to the design of the forming tools for the preliminary coconsolidation process; and (c) the use of a low amorphous bonding pressure (20 psi) to eliminate the need for washaway IML cavity mandrels. Significant process development efforts were expended to accommodate these factors, and to establish the reprocessability of the amorphous bonding operation to eliminate any PEI/moisture-induced porosity in the bondline.
- (5) Compression molding of the oil and fuel filter service doors, using AS4/HTX offal, was successfully demonstrated on the program.

Tooling

- (1) The complex pan-stiffened F-15 door IML skin design and the high processing temperature (700-800°F) requirement for TPs, established the need for a match in the coefficient of thermal expansion (CTE) between the tool and the part. Though only partially successful in the reported effort, a matched CTE tooling concept that lends itself to rapid forming is essential for successful application of TPs to composite structures.
- (2) Polyimide diaphragms (Kapton and Upilex) were barely adequate for processing AS4/ITX under 720-750°F, 100 psi conditions. SPF aluminum alloy diaphragms performed very well and withstood a 200 psi forming pressure at 720-750°F.
- (3) For the F-15 door details, the forming tools were designed to control the OML side of the OML skin and the IML side of the IML skin, based on the original coconsolidated assembly concept. This created a mismatch between the bonding surfaces when the coconsolidation process was replaced by amorphous bonding, requiring a variable thickness of PEI along the bondline and raising the issue of bond strength variation with PEI thickness. Had the OML and IML tools controlled the bonding surfaces, this issue may not have arisen.

Equipment

- (1) The diaphragm forming process is unique to TP applications, and has only been demonstrated in a press setup for small parts. Transitioning this process to the F-15 door application required considerable equipment development efforts at Northrop and MCAIR. In extending the process to larger primary structural parts, the capability to adapt existing high temperature (>800°F) autoclaves to this process is essential.
- (2) The feasibility of economically rapid forming TP parts has been established in many programs. However, the development of large rapid thermoforming equipment has been slow.

Design

- (1) A concurrent design development effort was successfully demonstrated on the program and contributed to the selection of the preliminary coconsolidated F-15 door concept, and its change to the final amorphous bonding process. However, the use of developmental materials, manufacturing processes and tooling concepts, and the ambitious Phase I schedule constraints, forced the concurrent design development effort to falter at times and accept too many changes without the necessary supporting data.
- (2) In transitioning from the preliminary design (uniform thickness OML and IML skins) to the final design (multiple drop-offs, local doublers, etc.), producibility was partially sacrificed in favor of structural performance, and a large weight reduction (39%) over the baseline SPF/DB titanium door was aimed for. This played a major role in introducing drop-offs and local build-ups, and in changing the assembly process from coconsolidation to amorphous bonding. The program demonstrated that considerable cost and weight savings are realizable with TP designs, but these have to be achieved without compromising producibility.

CONCLUSIONS

Phase 1 of the DMATS program was concluded very successfully with the structural qualification/design validation of the TP F-15E engine access door via full-scale static and fatigue tests and the delivery of flightworthy TP doors.

For the selected F-15E engine access door application, the TP design developed and validated on this program was projected to yield significant weight (39%) and cost (25%) savings over the SPF/DB titanium production doors. The viability of using TP materials in secondary structures, and their potential for primary structural applications, was established beyond doubt. Lessons learned from this Phase I effort are being incorporated into ongoing Phase II tasks to identify cost-effective primary structural applications for thermoplastic matrix composites.

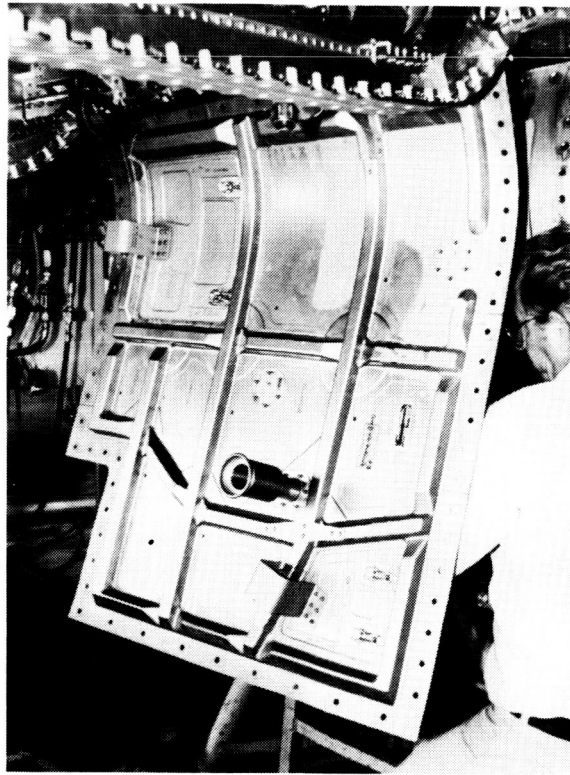


Figure 1 F-15E SPF/DB Titanium Door

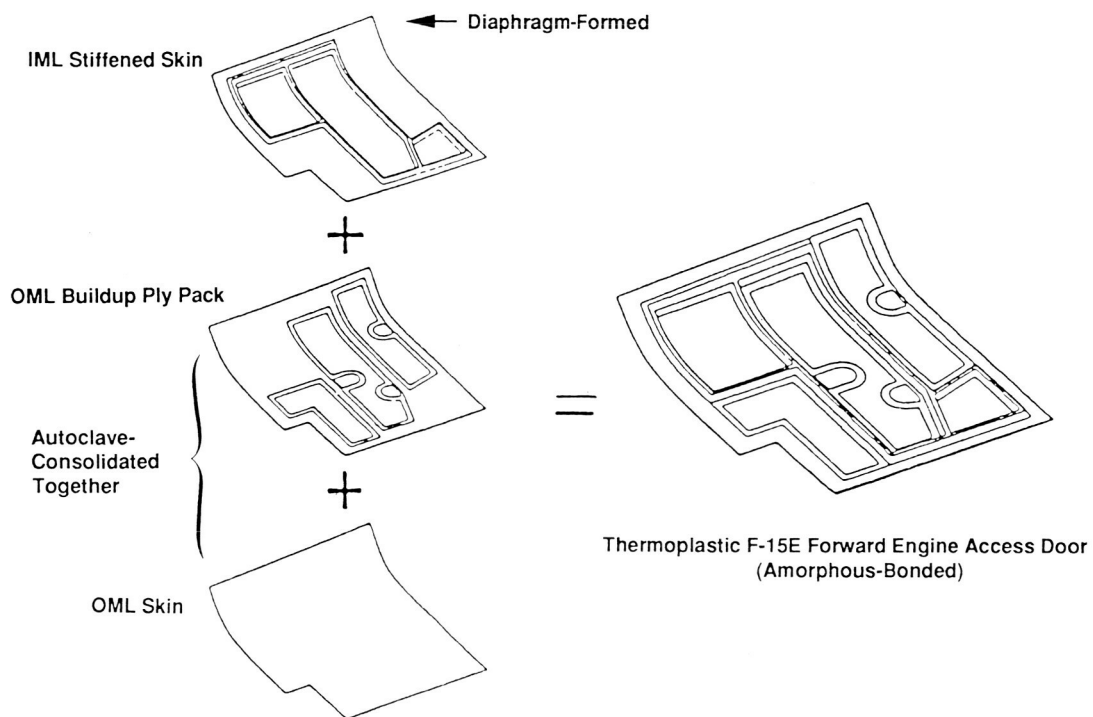


Figure 2 TP F-15 Engine Access Door Design

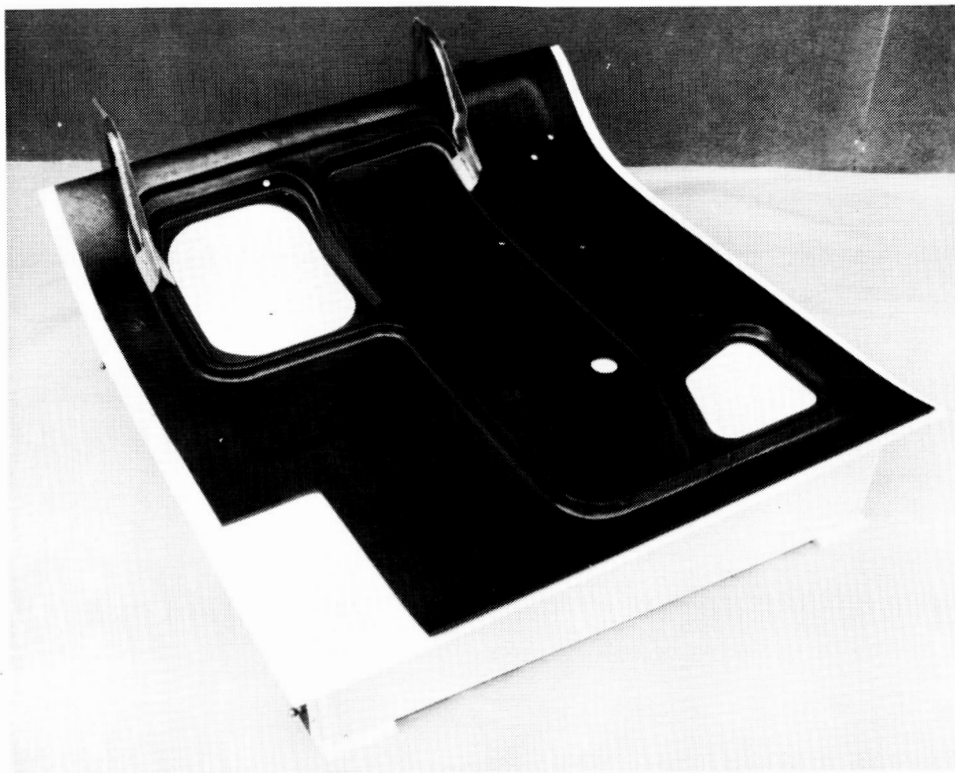


Figure 3 Redesigned Gooseneck Hinges

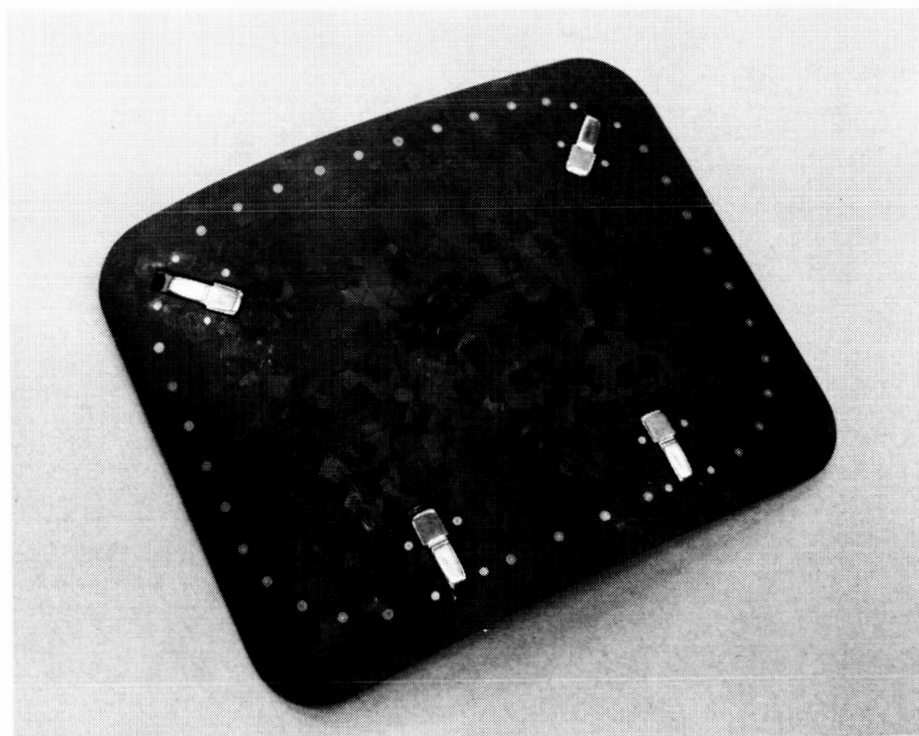


Figure 4 OML Side of the Compression Molded AS4/HTX Oil Service Door

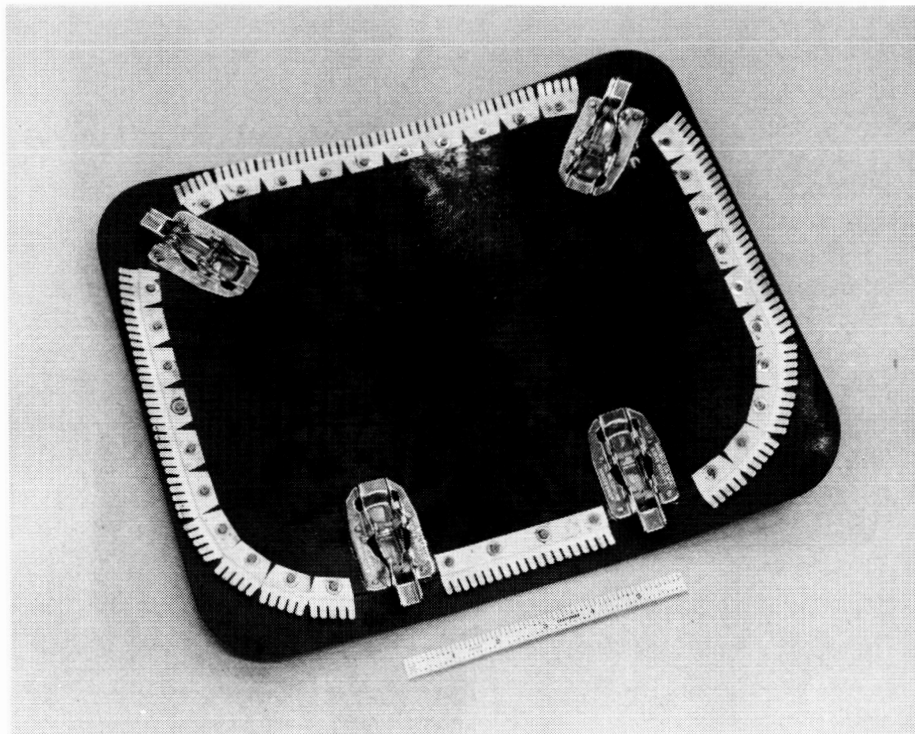


Figure 5 Electromagnetic Interface (EMI) Fingers on the IML Side of Oil Service Door

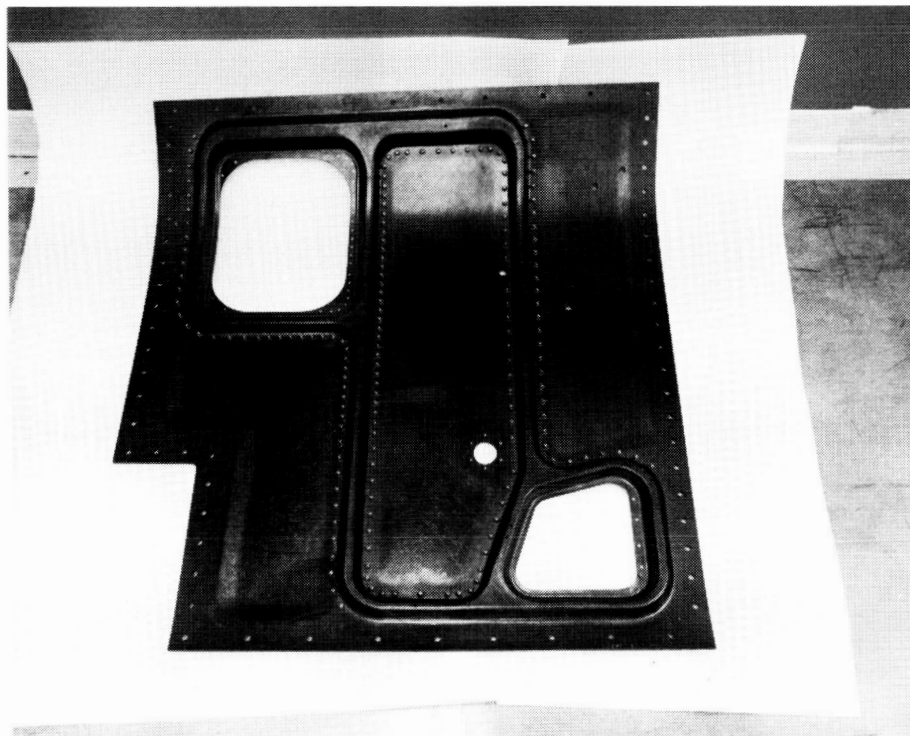


Figure 6 Fastener Pattern for Amorphous Bonded F-15 Door

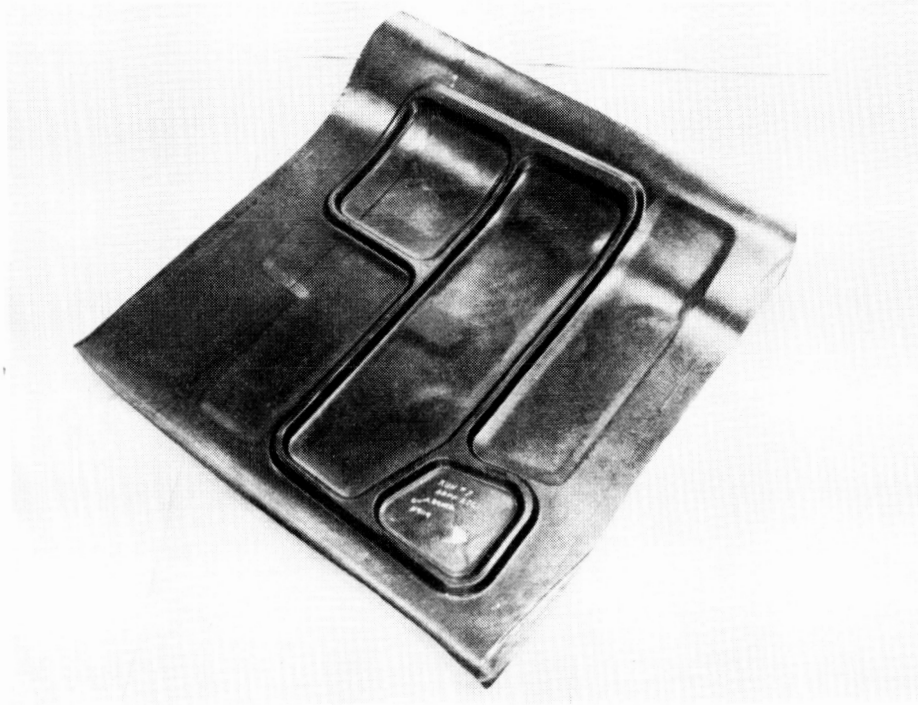


Figure 7 Diaphragm Formed F-15 Door IML Skin

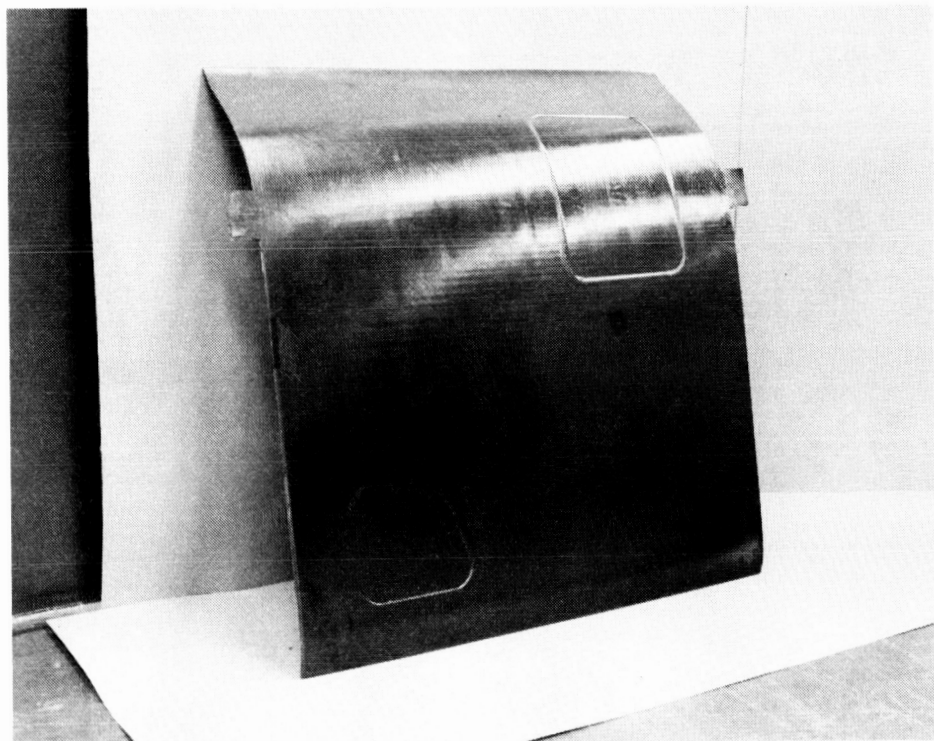


Figure 8 Autoclave Consolidated F-15 Door OML Skin

FABRICATION OF THE V-22 COMPOSITE AFT FUSELAGE USING AUTOMATED FIBER PLACEMENT

Robert L. Pinckney

Boeing Helicopters, Philadelphia, PA

SUMMARY

Boeing Helicopters and its subcontractors are working together under an Air Force Wright Research and Development Center (WRDC)-Manufacturing-Technology Large-Composite Primary Structure Fuselage program to develop and demonstrate new manufacturing techniques for producing composite fuselage skin and frame structures. Three sets of aft fuselage skins and frames have been fabricated and assembled, and substantial reductions in fabrication and assembly costs demonstrated.

INTRODUCTION

Advanced composite structures are lightweight, strong, stiff, and resistant to fatigue and corrosion. These features make composites highly attractive for major applications in military and commercial aircraft. Currently, industry is producing a number of secondary structure applications, and a significant amount of R&D effort is being expended to further develop engineering and manufacturing technology for wing primary structure. To maximize the benefits derived from using composites on aircraft, there is a need for a corresponding level of development activity on fuselage primary structure.

The Boeing Company, in a team effort with other major companies, conducted a WRDC sponsored program entitled "Manufacturing Technology for Large Aircraft Composite Primary Structure (Fuselage)." This program addressed the need to establish manufacturing capability to produce primary composite fuselage structure for large aircraft at predictable and reasonable cost. The program objective was to establish and validate low cost manufacturing methods for efficient production of such structure which could be applied to a variety of future aerospace systems.

The Boeing team effort combined the technical skills, automation technology, resources, and production experience of six companies in a concerted effort to achieve maximum cost-effectiveness in composites fuselage manufacturing. While Boeing had primary responsibility for carrying out the program, five other companies participated in Phase I and II. They were

Northrop Corporation
Hercules, Inc.
Teledyne-Ryan Aeronautical
Rohr Industries, Inc.
Xerkon, Inc. (formerly Proform, Inc.)

In order to evaluate various manufacturing methods and assure incorporation of the latest state-of-the-art technology in advanced composite manufacturing, the six-member team produced manufacturing test hardware during the first two phases of the program.

Innovative tooling and manufacturing methods were used to fabricate the test hardware. These test components were compared for manufacturing cost, quality, strength, and weight. The methods found to be superior were selected to fabricate full-size verification and demonstration hardware in Phases III and IV.

The planned down selection at the program decision point led to the start of Phase III in September 1985 with the team narrowed to Hercules, Teledyne-Ryan, and Xerkon.

A pictorial overview of the program test and demonstration components is shown in figure 1.

MANUFACTURING CONCEPTS

The manufacturing concepts selected for the production demonstration of the V-22 aft fuselage were those developed by the Hercules, Teledyne-Ryan and Xerkon Companies. Hercules fabricated the one-piece aft fuselage skin with its 157 cocured stiffeners on a male mandrel using their multiaxis fiber-tow placement machines.

The Xerkon Company

The Xerkon Company fabricated the J-section stiffener preforms and two of the five fuselage frames using their dry-fiber stitching and resin infusion processes. Teledyne-Ryan fabricated the remaining three frames using their press molding (Quadrapress®) system. Design changes were made to accommodate each of the new manufacturing and material forms as required. Changes were validated by means of detail stress analysis and predicted fuselage dynamic responses.

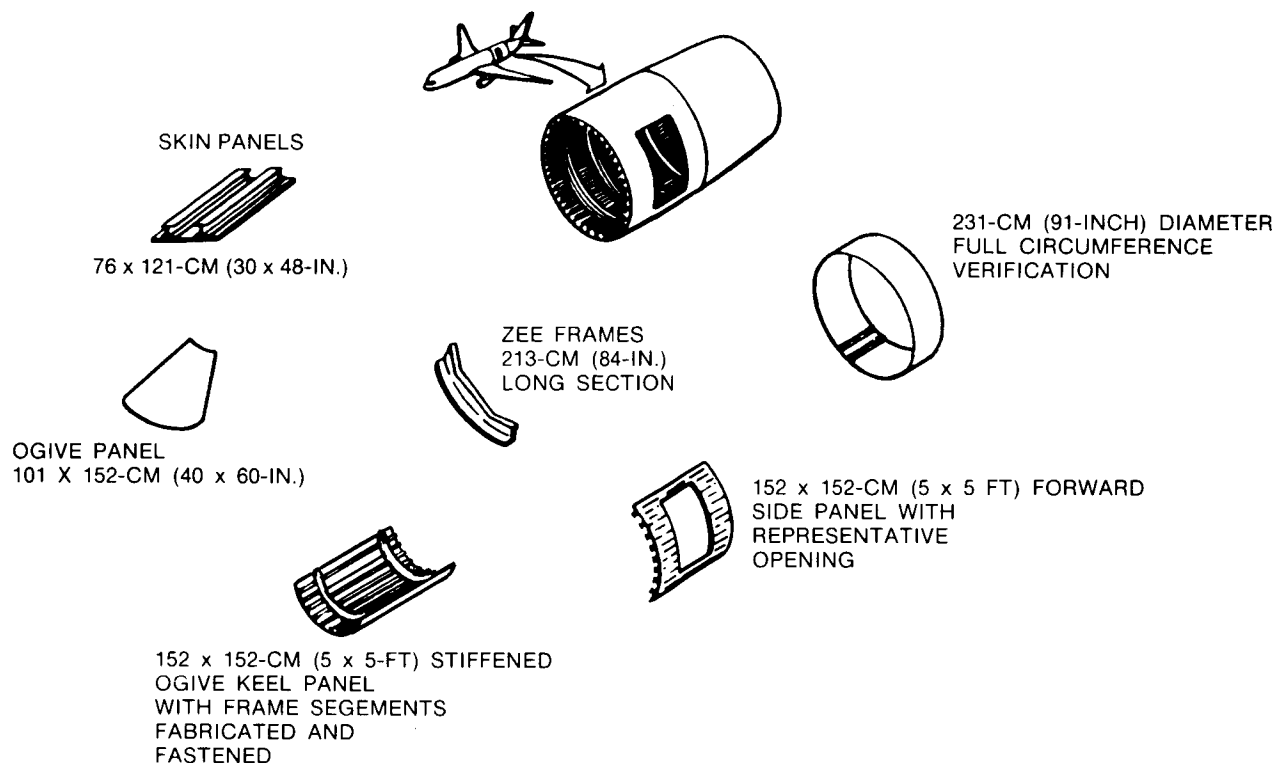
The Xerkon Company replaced square weave fabric and unidirectional tape preimpregnated materials with dry fiber tows stitched into preformed shapes for the frames and stiffeners. The preforms were then impregnated with epoxy resin and cured in integrally heated and cooled, closed molds using their Autocomp® process. A high degree of automation in the stitching process was employed. Robotic tool loading and final part trimming was developed, figure 2.

Teledyne-Ryan

The Teledyne-Ryan Company fabricated the three forward frames required for final aft fuselage assembly using their Press Cure Quadrapress® technique. No major design changes were required to utilize the press cure system rather than the more conventional autoclave cure technique; however, the fabric material forms, splice areas and other design details were changed to reduce layup hours. The use of 60-inch wide, 5 harness weave, 13-mil thick carbon fiber fabric significantly reduced preform layup time.

The use of graphite fiber-epoxy tooling inserts to transport, load, and unload the frame components to and from the curing press allowed the press platens to be maintained at a constant temperature of 182°C (360°F) thus appreciably reducing the cure cycle time. In addition, the frame configurations were such that the three individual frames could be nested and simultaneously cured during one press cycle. The tooling configuration is shown in figure 3 and a press load of cured frame sections in figure 4.

PHASE I & II LARGE FUSELAGE SECTION



PHASE III & IV V-22 AFT SECTION

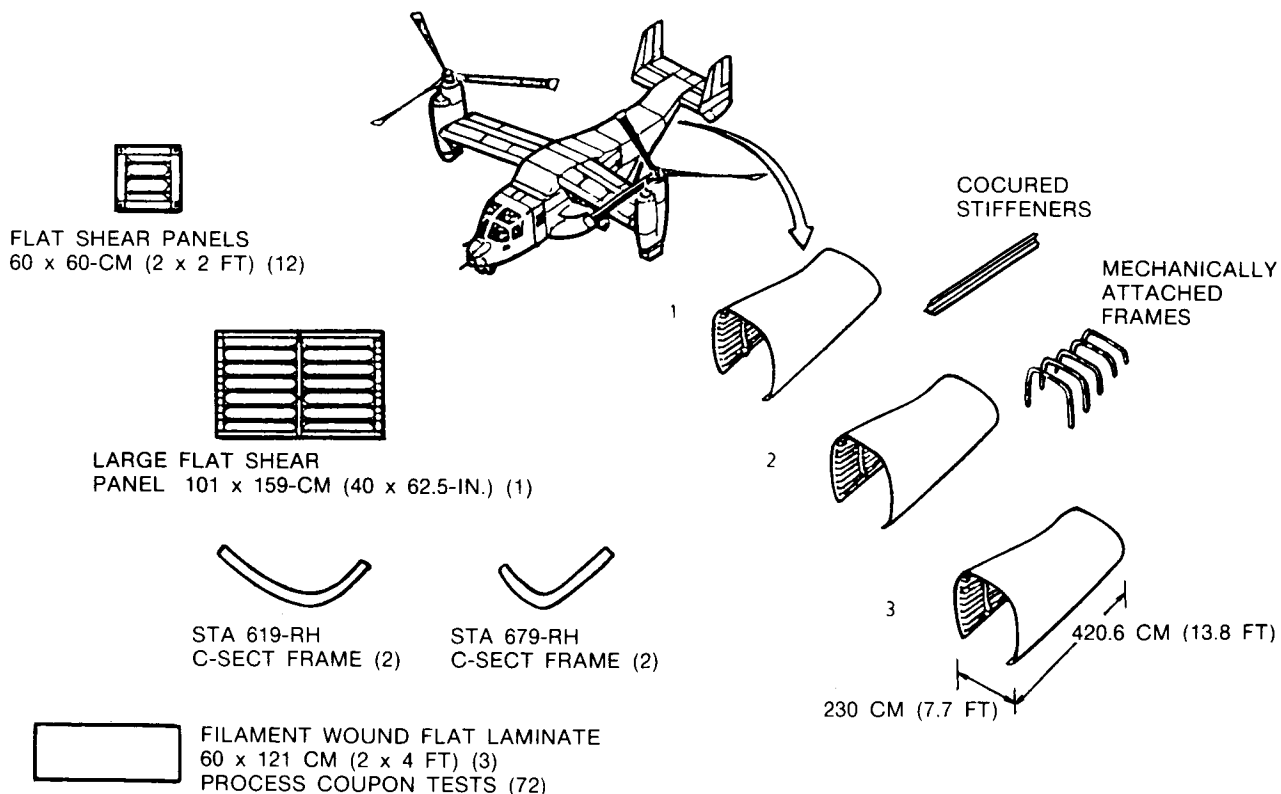


Figure 1. Program Test Components

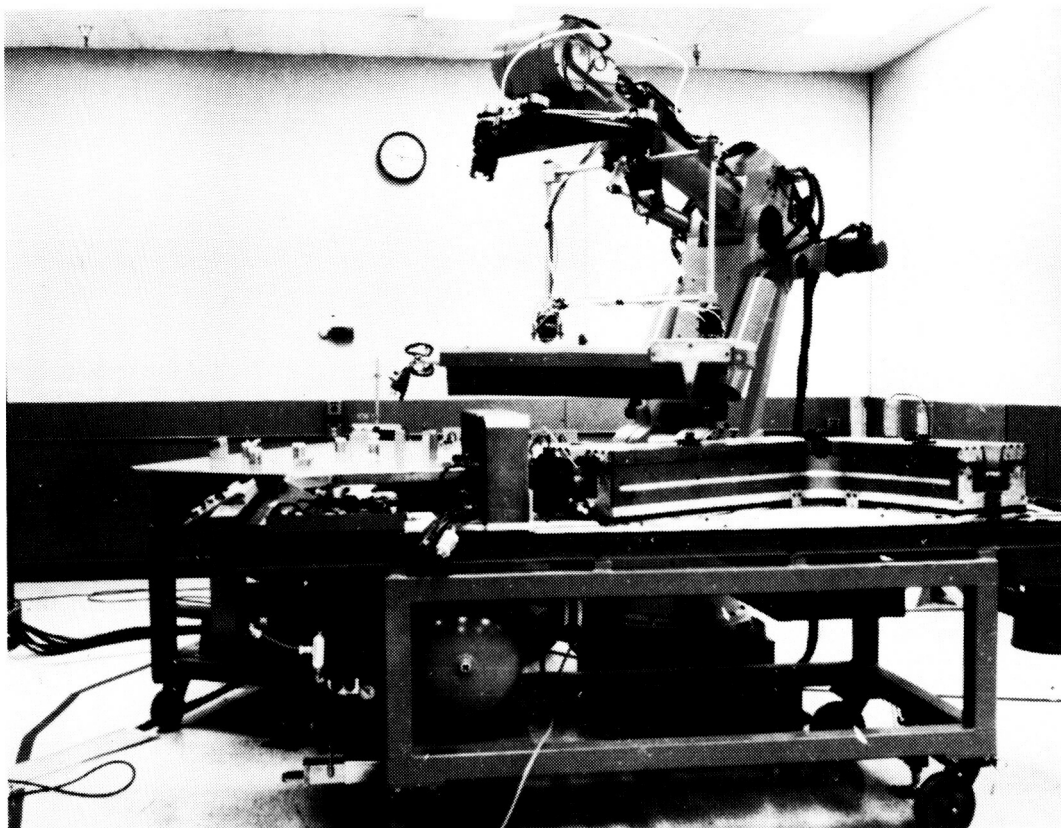


Figure 2. Robotic Handling of Center Tool Section



Figure 3.



Figure 4.

The Hercules Company

The Hercules Company; using CADAM data, tooling master models, and technical assistance supplied by Boeing; designed and fabricated the necessary tooling to produce the V-22 aft fuselage shells using their multiaxis fiber tow placement machines. Fiber tow placement offers reduced cost through automated, multitow placement (up to 32 tows of prepreg simultaneously onto a variety of tool geometries). Thickness and fiber angle control and in-process compaction, using the lowest projected cost material form, are key elements of this technology. Sectional, internal tooling provides precise detail part location, internal mold line (IML) control, and allows internal doubler pads and stiffeners to be cocured to the skin. Following autoclave curing of the part, the tooling is disassembled from within providing a single unit fuselage section. This results in the elimination of assembly joints and fasteners, and reduces the part count from eight sections to one.

The fiber placement machines utilize a computerized mathematical model of the part to generate a fiber path of a specified width, thickness, and orientation and to control cut and add functions. The software and hardware provide synchronization control and movement. The material delivery system processes, delivers, and compacts the prepreg tow material on the mandrel as demanded by part geometry.

Tooling for fiber tow placement must meet the following three requirements: It must form and apply pressure to all of the internal details of the finished part; it must have a center shaft to enable it to be rotated in the fiber placement machine; it must be able to withstand the pressure and temperature of repeated cure cycles; and it must be capable of being removed from the finished part interior.

Fiber tow placement offers many improvements over hand layup which contribute directly or indirectly to cost savings. Tow width control allows for nonstandard ply thicknesses which optimizes part design while maintaining constant band width. Gaps and overlaps are kept within a tolerance of 0.75 mm (0.030 inch). Constant ply thickness can be maintained by adding or dropping tows as the part changes cross section. Tow and band cut/add features reduce material scrap to as low as 5% by placing the material only where required. Fiber placement also utilizes prepreg tow which is projected to be the lowest cost material form available.

During the fiber tow placement process, a conformable roller rides directly on the part or tool to deliver the tow material while providing in-process compaction. This minimizes the need for intermediate compaction steps. The placement head flexibility allows fiber placement on convex and concave surfaces. The delivery head delivers individual tows as a flexible band to minimize material distortion. This flexibility provides fiber angle control which allows for fiber placement of non-geodesic shapes. There are no limits on the winding angle. Purely axial (0 degree) plies can be readily placed with this process.

Hercules currently has two fiber placement machines (FPM). FPM1 is a 6-axis, development machine which has been in use since 1982. This machine was used to manufacture the first three V-22 aft fuselage sections. FPM2 is a production rated, 7-axis, fiber placement machine to be used for production programs and to fabricate the final deliverable V-22 aft fuselage section. Figure 5 shows a typical FPM2 setup with an explanation of the various axes of motion.

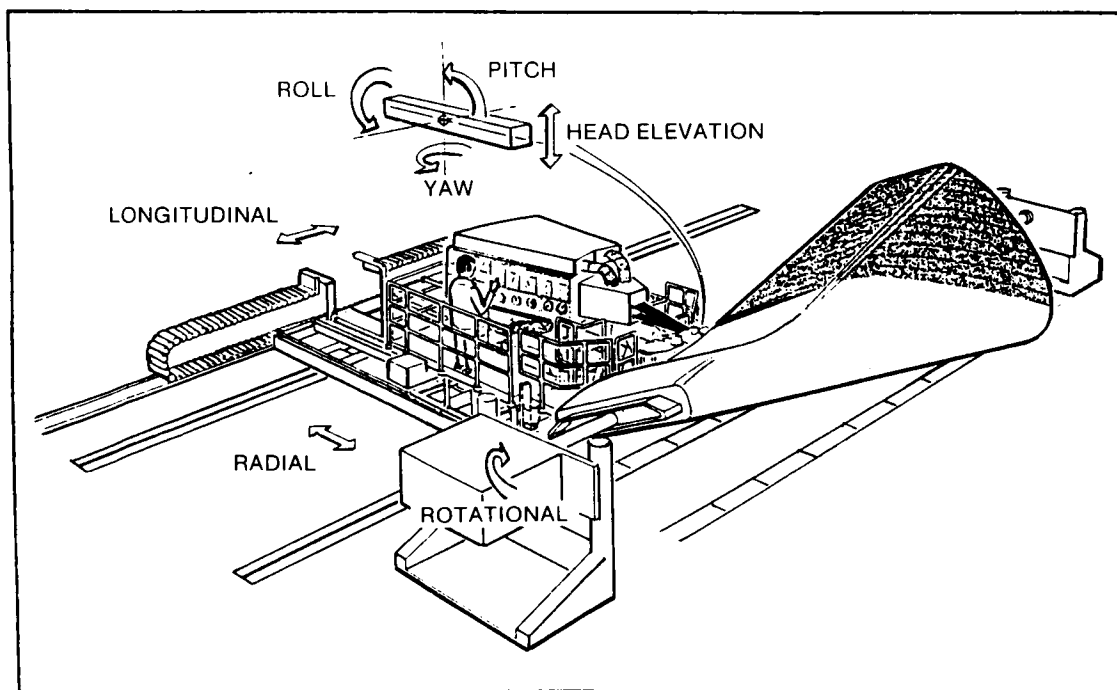


Figure 5.

The panelized design for the V-22 FSD aft fuselage consists of a basic skin of four layers of AS4 fabric for a total thickness of 0.75 mm (0.030 inch). The fiber placed design consists of a skin with five plies of IM6 prepreg tow (equivalent to grade 145 tape) for a total thickness of 0.71 mm (0.028 inch). In subscale testing, fiber placed test panels were the equivalent of the baseline test panels.

The panelized FSD design utilized outside mold line (OML) tooling, which required building the fuselage component from the outside in. Once laid up, they are bagged on the IML surface and cured. Each component is limited in size by the workers' ability to reach the middle of the tool during processing.

In contrast, the fiber placed design utilizes a knockdown, male IML mandrel. The internal stiffeners are assembled into the tooling which locates them exactly. The stiffener doublers are laid up in sections on recesses built into the surface of the full-size composite mandrel so that the resultant inner skin surface is smooth. See figure 6. The mandrel can be rotated so that workers can lay up sections of doubler material from a convenient position. The skin is then fiber placed on the mandrel surface using continuous, full-length, 9 cm (3.50 inch) wide bands of prepreg tows.

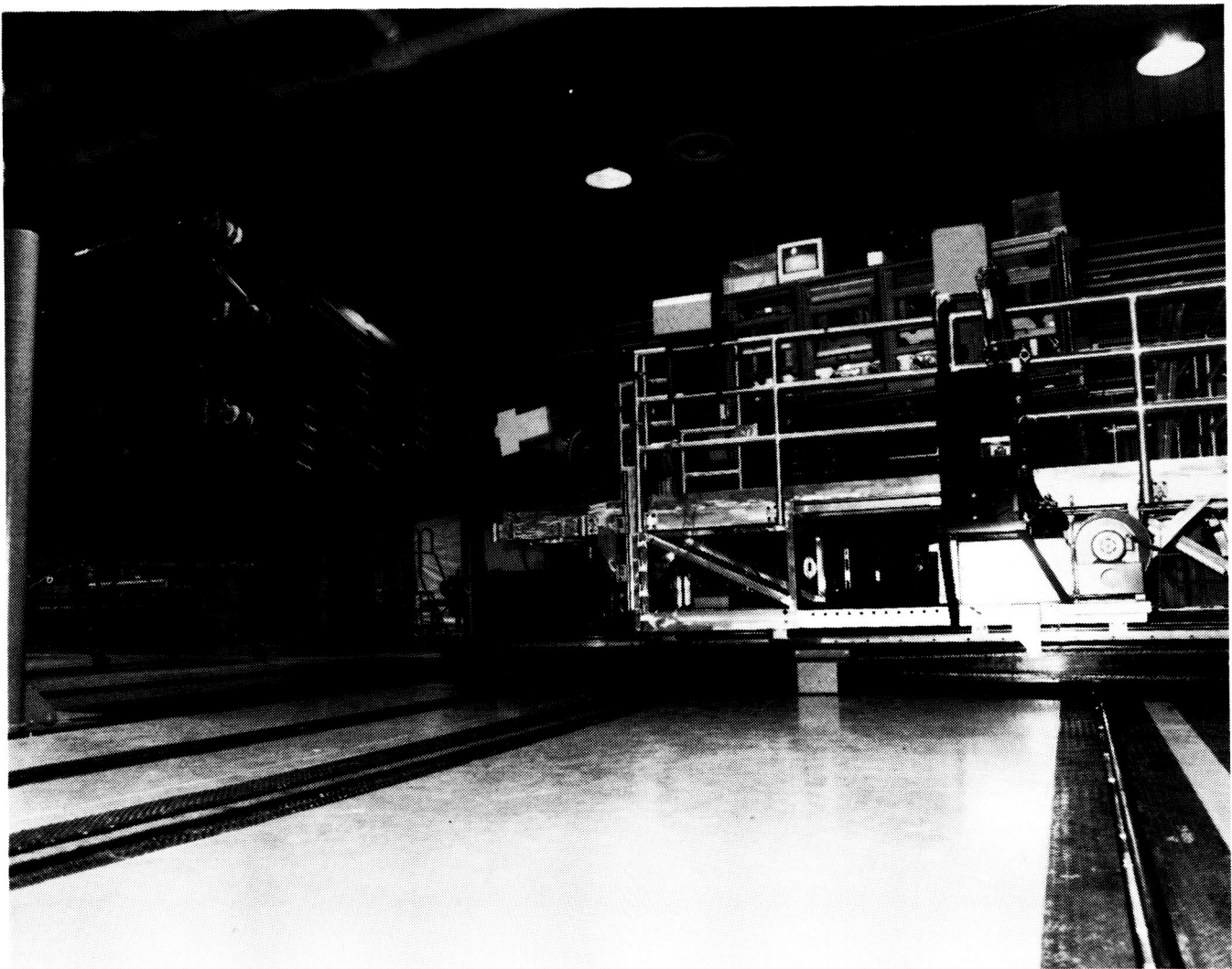


Figure 6.

The hand layup design of the V-22 aft fuselage consisted of 10 skin panels; 2 in the ramp and 8 in the upper fuselage. The fiber tow placed aft fuselage was cured in one piece, with the mandrel components being disassembled from within. For ease in manufacturing, and since the ramp is a separate assembly from the upper fuselage section, the ramp is cut before cure. Both components remain on the mandrel through the cure cycle. Manufacturing the aft fuselage in fewer pieces results in fewer subassemblies and fewer fasteners. This reduces handling, part control, and traceability costs as well as component, subassembly and inspection costs. The completed aft fuselage one-piece shell with the ramp skin and mandrel removed is shown in figure 7.

BOEING HELICOPTERS AFT FUSELAGE ASSEMBLY

The three aft fuselage shells and frame details supplied by Hercules, Teledyne-Ryan and Xerkon were trimmed to net shape, ultrasonically and dimensionally inspected, and shipped to Boeing Helicopters for final assembly. The detail components were reinspected by Boeing and the additional components required, (frame splice plates, angles, and fasteners) were procured. A new assembly fixture was fabricated to accommodate the large one-piece shell and to locate the frames and other details.

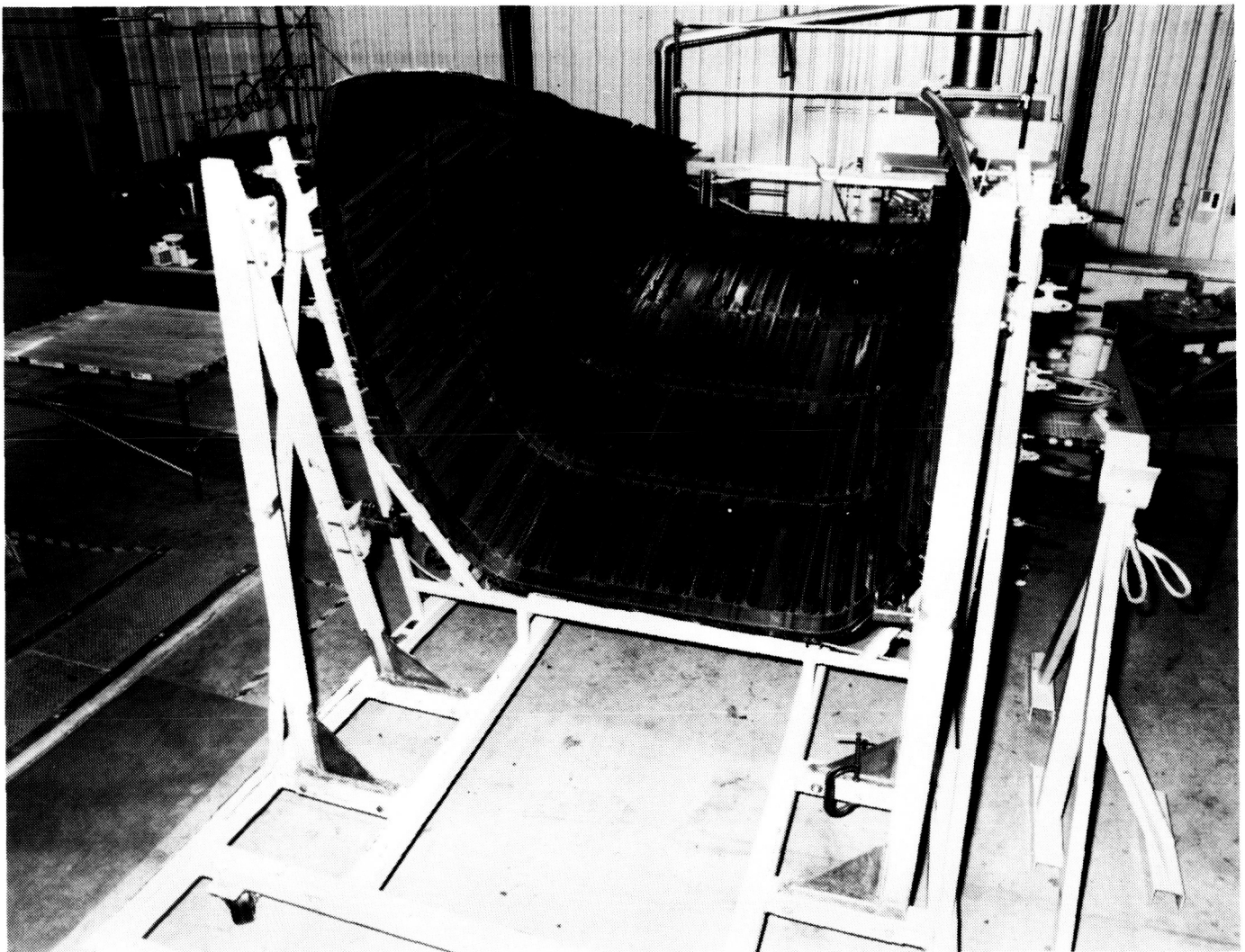


Figure 7.

Frame-fastener hole locations were pilot drilled on the bench, and the frames were located in the assembly fixture by means of tooling holes defined in the CAD data supplied to each frame contractor. The one-piece shell was positioned over the frames and pinned to the assembly fixture by means of tooling tabs located at each end of the shell. Fastener holes were located in the one-piece shell skin by back drilling through the frame pilot holes. All fastener holes were drill reamed to final size and titanium fasteners installed with wet polysulfide sealant. The one-piece shell eliminated eight individual hand layup panels and reduced from thirty-two to eight the number of trim lines required to be hand fitted, pressure sealed, and electrically connected for EMI protection.

Since the frame/skin mating surfaces were all tool controlled, no shims were needed for fit up and thus no need for fasteners of various lengths to accommodate shimming. Substantial assembly cost savings were realized. A completed aft fuselage skin/frame assembly is shown in figure 8.



Figure 8.

COST PROJECTIONS, COMPARISONS AND SAVINGS

At the completion of design modifications in 1987, we projected a cost savings in production basic factory labor for the V-22 Aft Fuselage as a result of automating key operations. In 1988 we performed time studies for fiber tow placement of the stiffened skin to validate the earlier projections. The time study costs have been evaluated and are first broken down as cost by operation, then as production basic factory labor savings. The latter includes a direct comparison with the 1987 projections.

1987 Cost Savings Projection. We projected a cost savings for the V-22 production aft fuselage section of 54% in basic factory labor. This cost savings is due to automation of the frame and stiffener forming and skin fabrication (see figure 9). This projection also included material cost (converted to a labor equivalent) and assembly labor. During the program, we performed studies to validate the projection.

1988 Time study by Operation. Figure 10 illustrates the results of the time study performed on automated stiffened skin fabrication. This study included all fabrication operations for the stiffened skin on the first two deliverable units (SS-001 and SS-002).

In referring to figure 10 note that the mandrel assembly and fiber placement are the largest cost contributors. However, expectations for labor and material savings for this operation were not fully realized on SS-001 and SS-002. Further improvements to the fiber placement

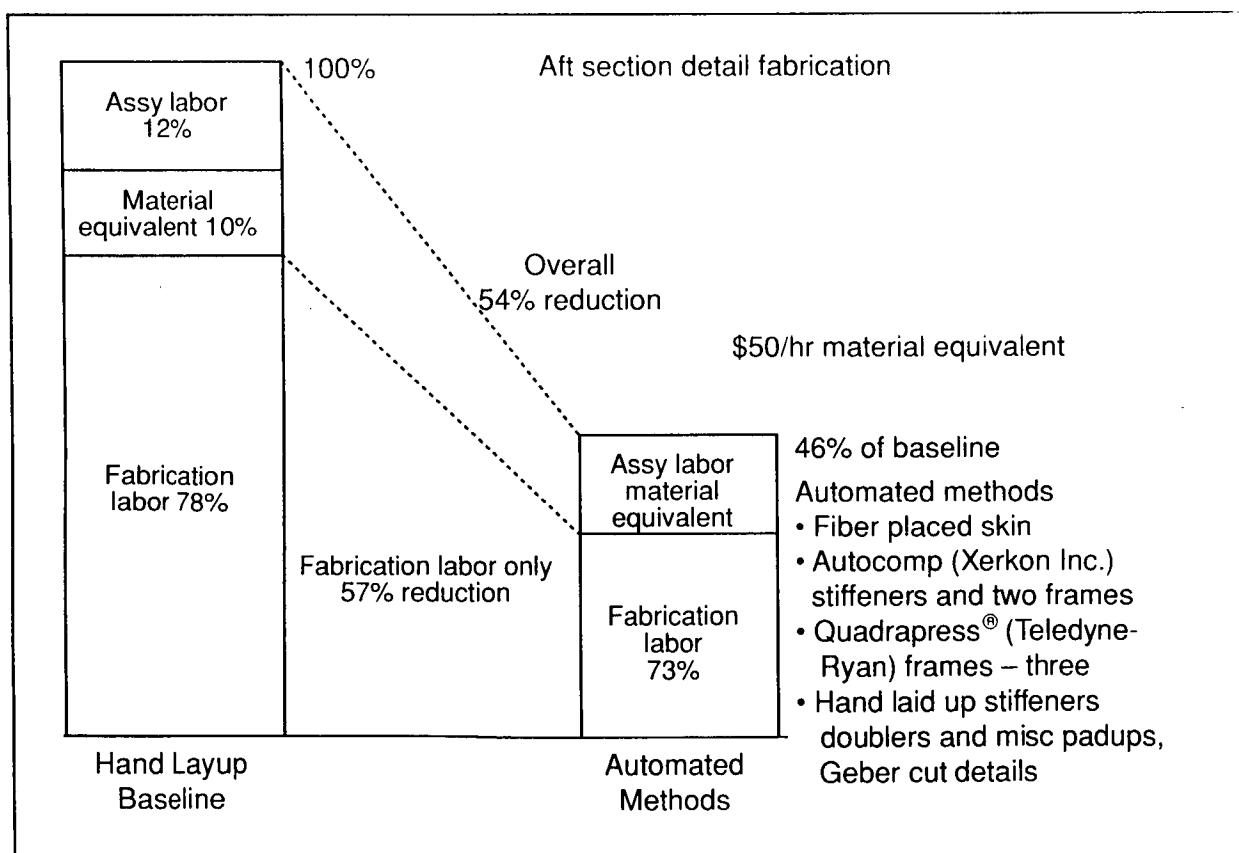


Figure 9. Automated Technology Application to V-22 Production
Hand Lay Up Versus Automated Methods

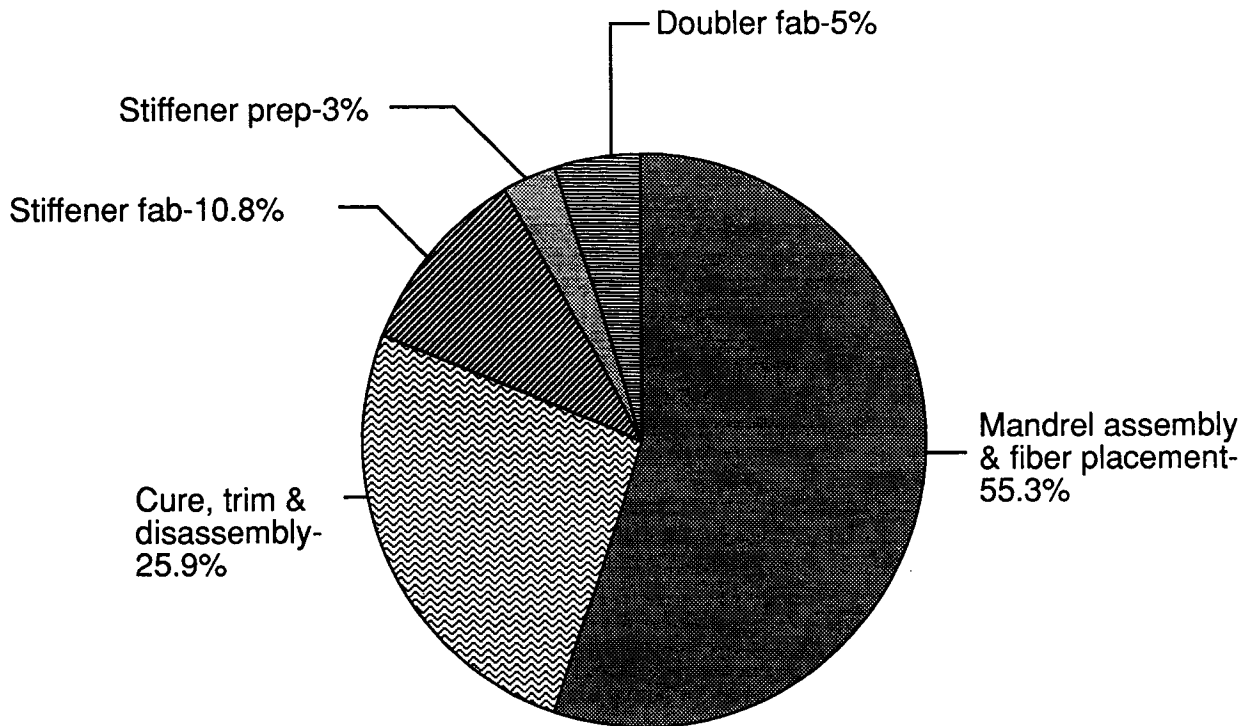


Figure 10. Automated Technology Application to V-22
Time Study Costs by Operation

machine as well as process improvements were integrated into the production rated fiber placement machine (FPM2) and upgraded tow placement heads. These were used to fabricate the final deliverable aft fuselage SS-003. Projected lower prepreg tow costs also contribute to a lower projected production cost.

PROGRAM RESULTS

Significant direct labor cost savings were demonstrated throughout the program. Direct labor savings, when compared to the V-22 FSD hand layup costs, were more than 50% for the detail composite component fabrication and their assembly. The demonstrated direct labor savings for the Xerkon Autocomp® and Teledyne-Ryan Quadrapress® frame processes are shown in figures 11 and 12. Figure 12 shows the Hercules Fiber tow placement process results.

A segmented learning curve based on prior composite component fabrication experience was used to calculate the average cost for the 912 production units: Units 1 through 165 follow an 83% curve, and units 166 through 912 a 90% curve for an average of approximately 84%. In an effort to more equitably compare the benefit of the fiber tow placement process in making large cocured fuselage skins, the actual data obtained in the hand layup fabrication of the first seven shipsets of V-22 components was collected and used to recompute the baseline cost, figure 13. The reduction found was due to improvement in the manufacturing process, reduction in the number of stiffener configurations, and improved adhesives and copper shielding materials. Several of these changes were also incorporated into the fiber-tow automated shell.

The final assembly operations, mechanical fastening of the five frames, frame splices, and the fiber-placed one-piece cocured skin also resulted in substantial savings in direct labor

costs, as shown in figure 14. These were due to reasons previously presented. An 80% curve was used through unit 240 and a 90% through unit 912 to calculate the savings.

Preliminary analysis of the data currently available shows that the 84 kg (185 pound) aft fuselage structure fabricated by the advanced manufacturing techniques demonstrated in this program can be produced in quantity for the equivalent direct labor cost of approximately 400 hours. This represents a 64% savings when compared to the hours required for the conventional fabrication and assembly of the multicomponent baseline structure.

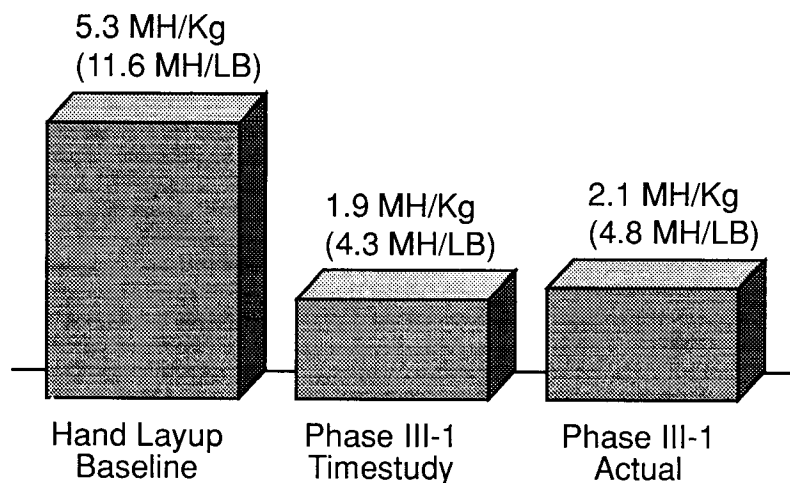


Figure 11. Manufacturing Costs —
Frame Fabrication: Xerkon Autocomp Process
Average for 912 Production Units

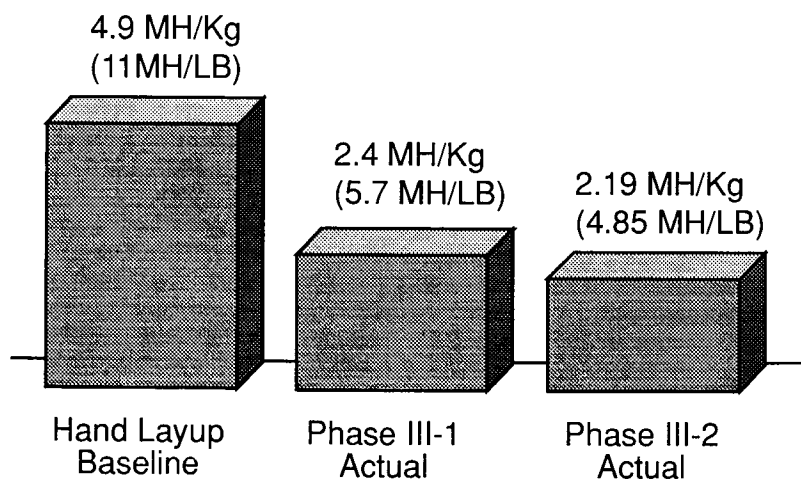


Figure 12. Manufacturing Costs —
Frame Fabrication: Teledyne Quadrapress Process
Average for 912 Production Units

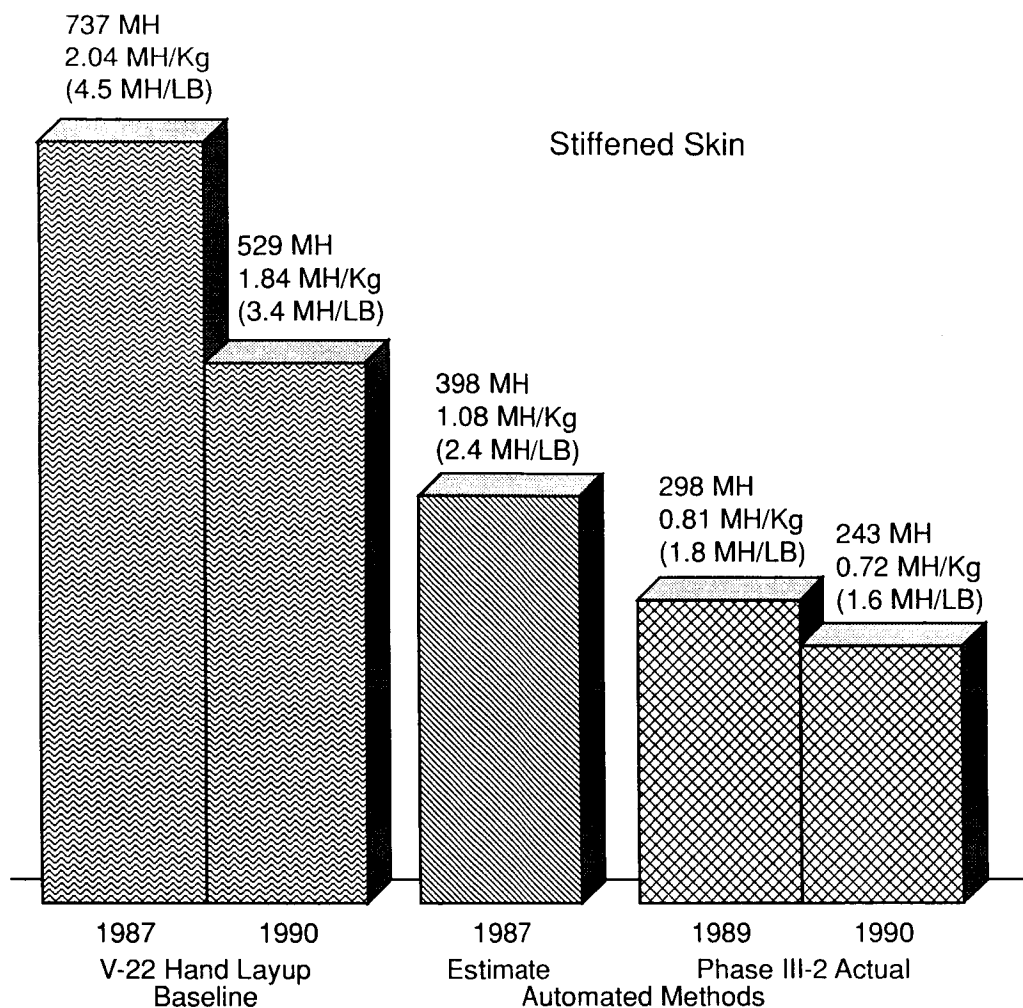


Figure 13. Manufacturing Costs —
Skin Fabrication: Hercules Fiber Tow Placement
Average for 912 Production Units

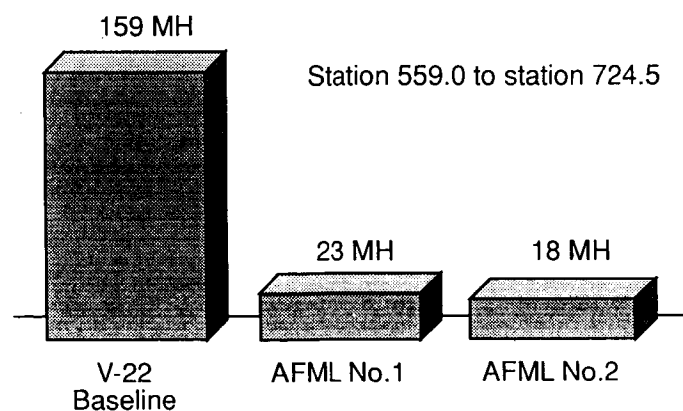


Figure 14. Costs of Aft Fuselage Assembly by Boeing
Average for 912 Production Units

LESSONS LEARNED FOR COMPOSITE STRUCTURES

R. S. Whitehead
Northrop Corporation

SUMMARY

Lessons learned for composite structures are presented in three technology areas: materials, manufacturing and design. In addition, future challenges for composite structures are presented.

Composite materials have long gestation periods from the developmental stage to fully matured production status. Many examples exist of unsuccessful attempts to accelerate this gestation period. Experience has shown that technology transition of a new material system to fully matured production status is time consuming, involves risk, is expensive and should not be undertaken lightly. The future challenges for composite materials require an intensification of the science based approach to material development, extension of the vendor/customer interaction process to include all engineering disciplines of the end user, reduced material costs because they are a significant factor in overall part cost and improved batch-to-batch pre-preg physical property control.

Historical manufacturing lessons learned are presented using current in-service production structure as examples. Most producibility problems for these structures can be traced to their sequential engineering design. This caused an excessive emphasis on design-to-weight and schedule at the expense of design-to-cost. This resulted in expensive performance originated designs, which required costly tooling and led to non-producible parts. Historically these problems have been allowed to persist throughout the production run. The current/future approach for the production of affordable composite structures mandates concurrent engineering design where equal emphasis is placed on product and process design. Design for simplified assembly is also emphasized, since assembly costs account for a major portion of total airframe costs. The future challenge for composite manufacturing is, therefore, to utilize concurrent engineering in conjunction with automated manufacturing techniques to build affordable composite structures.

Composite design experience has shown that significant weight savings have been achieved, outstanding fatigue and corrosion resistance have been demonstrated, and in-service performance has been very successful. Currently no structural design show stoppers exist for composite structures. A major lesson learned is that the full scale static test is the key test for composites, since it is the primary structural "hot spot" indicator. The major durability issue is supportability of thin skinned structure. Impact damage has been identified as the most significant issue for the damage tolerance control of composite structures. However, delaminations induced during assembly operations have demonstrated a significant nuisance value.

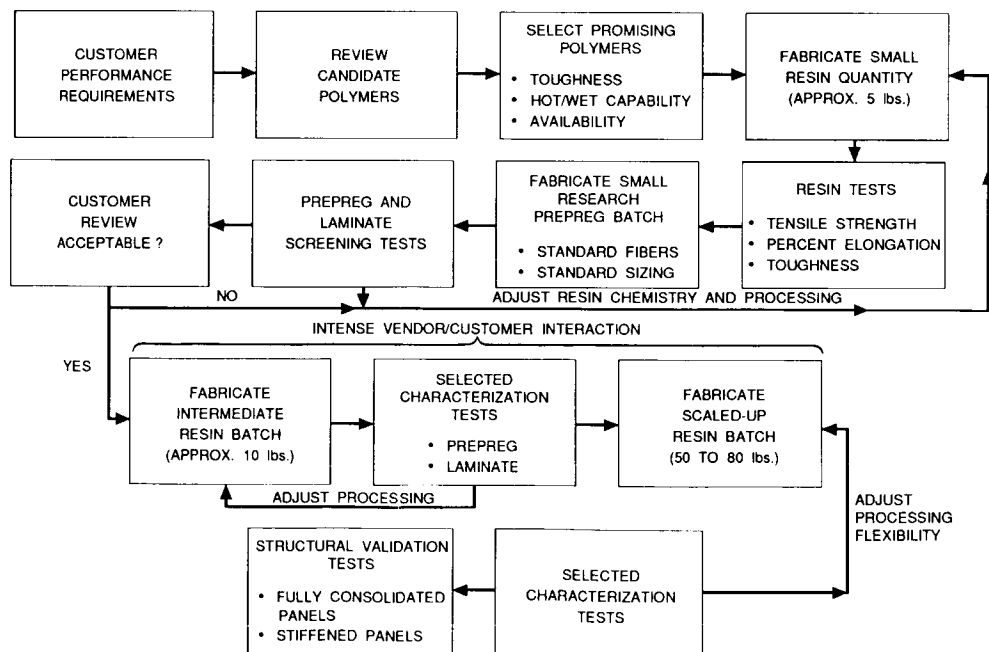
The future challenges for composite structures are threefold. Firstly, composite airframe weight fraction should increase to 60%. At the same time, the cost of composite structures must be reduced by 50% to attain the goal of affordability. To support these challenges it is essential to develop lower cost materials and processes.

Agenda

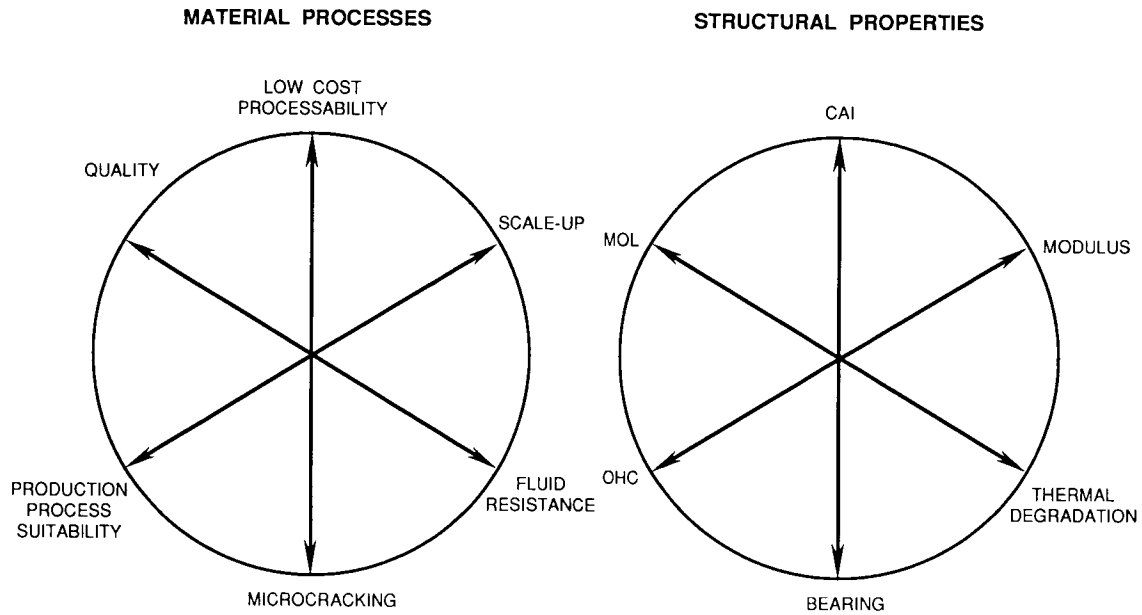
- **MATERIALS**

- Manufacturing
- Design
- Future Challenges

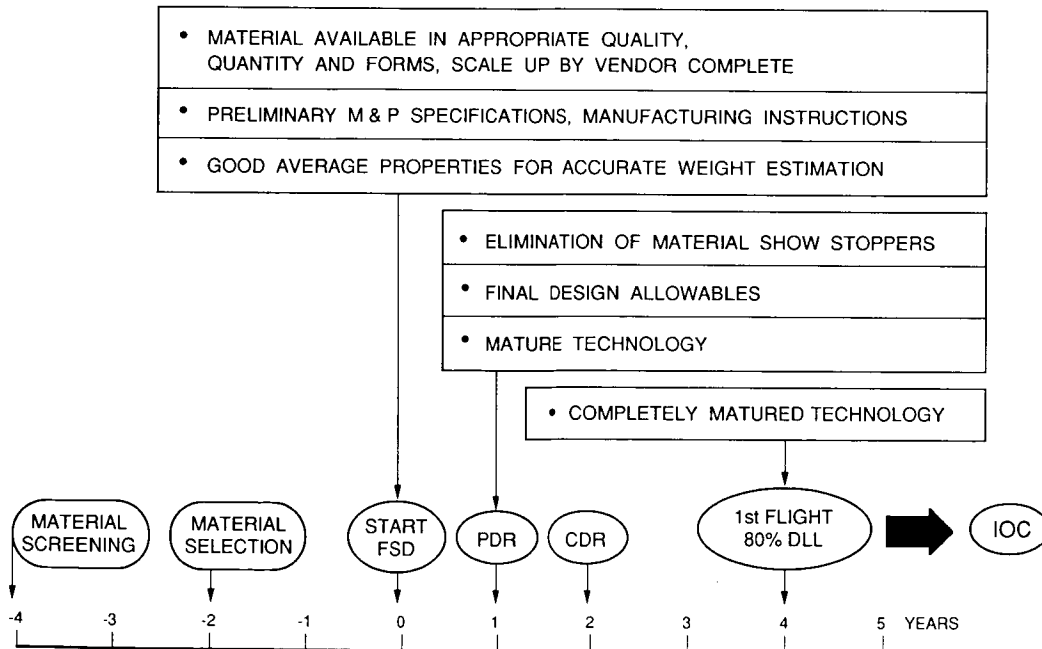
Material Development Process



Material Performance Requirements



Technology Transition Milestones



Technology Transition Problems

Examples

- TOUGH BISMALEIMIDE
- HIGH TEMPERATURE THERMOPLASTIC
- GALVANIC CORROSION INDUCED DEGRADATION OF BISMALEIMIDES AND POLYIMIDES

Lessons Learned

- ALL MATERIALS HAVE LONG GESTATION PERIODS FROM THE DEVELOPMENTAL STAGE TO FULL PRODUCTION STATUS
- ATTEMPTS TO ACCELERATE THE GESTATION PERIOD INVOLVE SIGNIFICANT TECHNOLOGY TRANSITION RISKS
- THERE ARE MANY EXAMPLES OF UNSUCCESSFUL TECHNOLOGY TRANSITION FOR MATERIALS
- TECHNOLOGY TRANSITION OF A NEW MATERIAL TO FULL PRODUCTION STATUS IS TIME CONSUMING, INVOLVES RISK, IS EXPENSIVE, AND SHOULD NOT BE UNDERTAKEN LIGHTLY

Future Challenges

- INTENSIFY SCIENCE BASED APPROACH TO MATERIAL DEVELOPMENT
- EXTEND VENDOR/CONTRACTOR INTERACTION PROCESS TO INCLUDE ALL DISCIPLINES OF END USERS
- REDUCE MATERIAL COSTS BECAUSE THEY ARE A SIGNIFICANT FACTOR IN OVERALL COMPOSITE PART COST
- DRIVE TOWARDS TIGHTER PRE-PREG PHYSICAL PROPERTIES CONTROL ON A BATCH-TO- BATCH BASIS

Agenda

- Materials

- **MANUFACTURING**

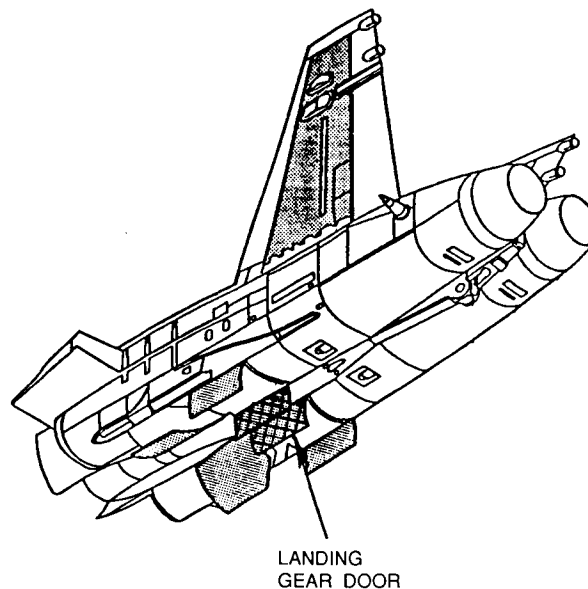
- Design

- Future Challenges

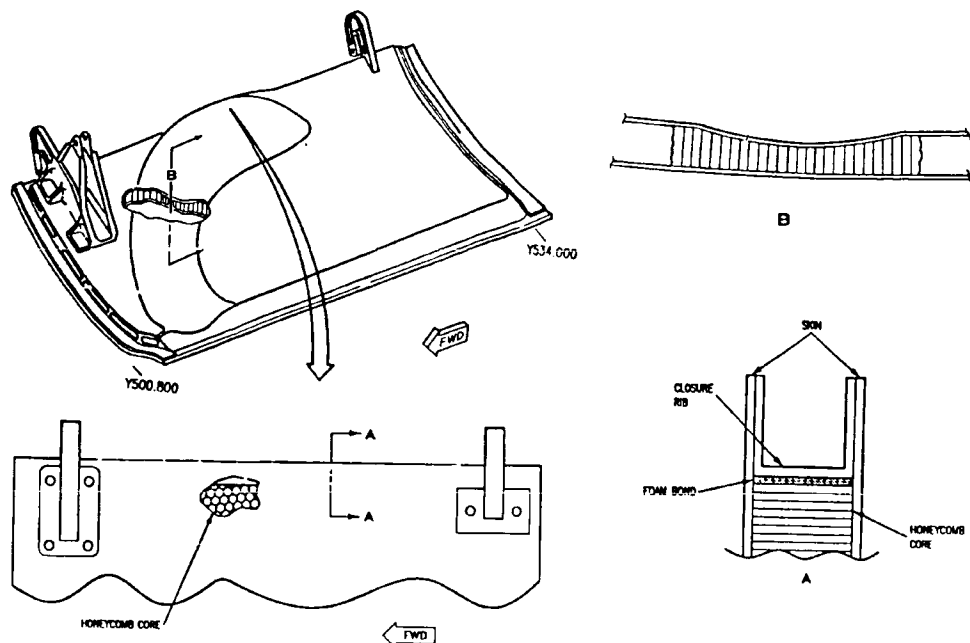
Analysis of Current Approach

- PART PRODUCIBILITY NOT DESIGNED IN
 - Manufacturing Problems With Initial Production
- EXTENSIVE MRB ACTION REQUIRED FOR PART DISPOSITION
 - Substantial Increase in Support Costs
- PART "BUY-OFF" WITH AN EXPENSIVE TEST PROGRAM
 - Inadequate QA and Effects of Defects Database
- RESISTANCE TO REDESIGN FOR PRODUCIBILITY
 - Avoid Design Cost Increase
 - Schedule Driven Production Program
 - Avoid Process Development Costs
- PROBLEM PERSISTS THROUGHOUT PRODUCTION

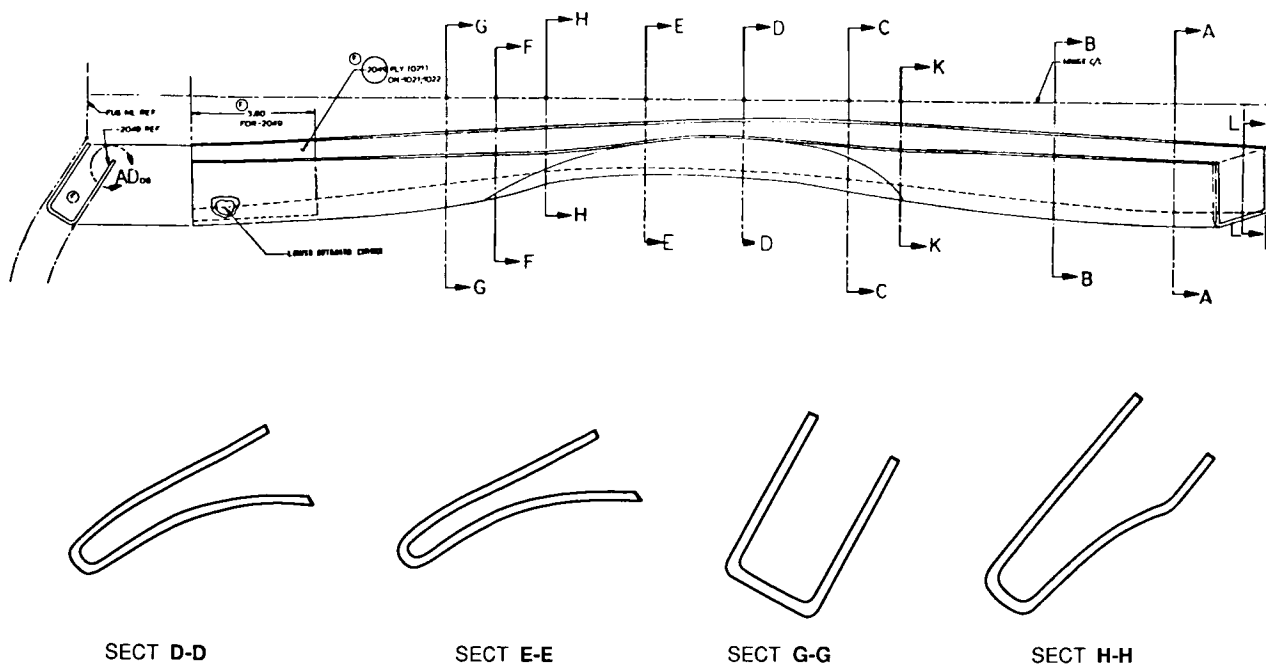
Example F-18 Landing Gear Door



F-18 Landing Gear Door



F-18 Landing Gear Door Stiffener



Door Stiffener Analysis

- NON - PRODUCIBLE SHAPE, I.E., COULD NOT BE PRODUCED REPEATABLY AND COST EFFECTIVELY
- RADIUS DESIGNED FOR FLIGHT LOADS WITHOUT ACCOUNTING FOR TOOL/PART INTERACTION
- PART DIFFICULT TO REMOVE FROM FEMALE TOOL (DICTATED BY ASSEMBLY REQUIREMENTS)
- HIGH REJECT RATE AND MRB ACTIONS DUE TO DELAMINATIONS AND POROSITY IN NARROW REGION

Historical Lessons Learned

- PAY-AS-YOU-GO RATHER THAN SUBSCRIPTION PRICE APPROACH
- DESIGN-TO-WEIGHT AND SCHEDULE WERE PRIMARY DRIVERS
- DESIGN-TO-COST NOT EMPHASIZED DUE TO A LACK OF COST MODELS/METHODOLOGY
- PERFORMANCE ORIENTED DESIGNS REQUIRED EXPENSIVE TOOLING AND SEVERELY AFFECTED PART PRODUCIBILITY
- M&P SPECIFICATIONS DEVELOPED WITHOUT ACCOUNTING FOR 3-D CONFIGURATION
- INSUFFICIENT LEAD TIME FOR TOOL DESIGN AND PROCESS DEVELOPMENT
- QA PLAN NOT INCORPORATED IN PART DESIGN
- NO MECHANISM AND IMPETUS FOR INTERDISCIPLINARY COMMUNICATION AT DESIGN STAGE

Current/Future Approach

- IMPLEMENTATION OF CONCURRENT ENGINEERING
 - Co-Located Multi-Disciplinary Dedicated Teams
 - Personnel Skills Are a Significant Contributor
 - Systematic Checks and Balances
- PROCESS DEVELOPMENT UNDERTAKEN INDEPENDENTLY
 - Separate Design and Manufacturing Development Articles
- DESIGN FOR SIMPLIFIED ASSEMBLY
 - Reduced Part Count
 - Shimless Designs in Certain Areas
- REDUCTION OF POST DRAWING RELEASE CHANGES
- DESIGN-TO-WEIGHT AND DESIGN-TO-COST USUALLY IN CONFLICT
 - Design-To-Weight Dominates
 - D / MI a Key to Balanced Design

Agenda

- Materials
- Manufacturing
- **DESIGN**
- Future Challenges

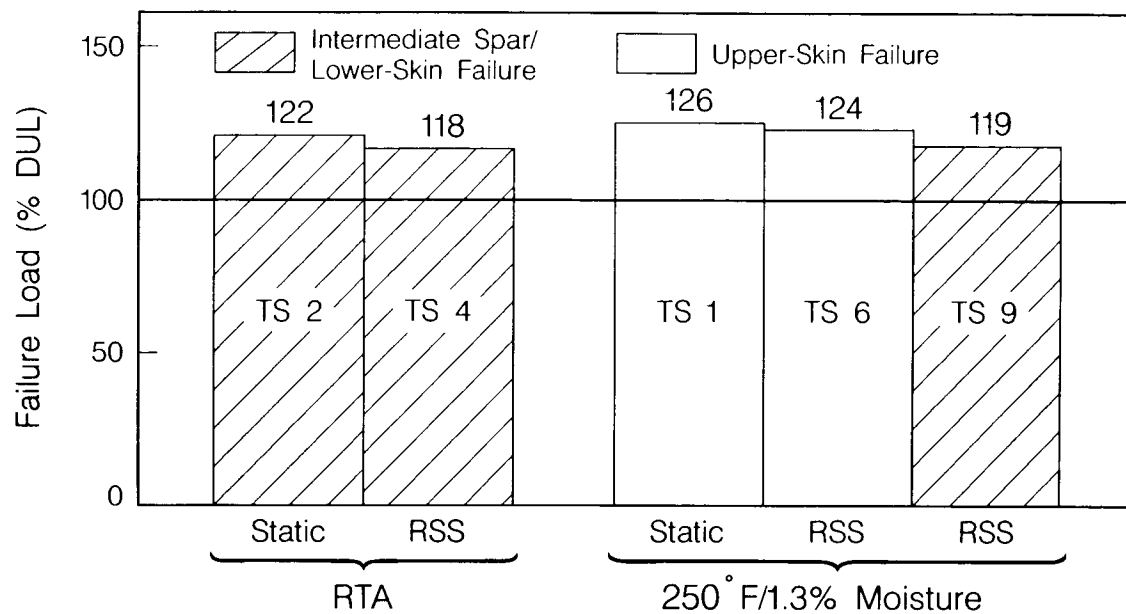
Historical Factors

- SIGNIFICANT WEIGHT SAVINGS
- EXCELLENT FATIGUE AND CORROSION RESISTANCE
- MIXED CERTIFICATION EXPERIENCE
- SUCCESSFUL IN-SERVICE EXPERIENCE
(Except Early Vintage Sandwich Structure With Metallic Core)
- NO STRUCTURAL DESIGN SHOW STOPPERS

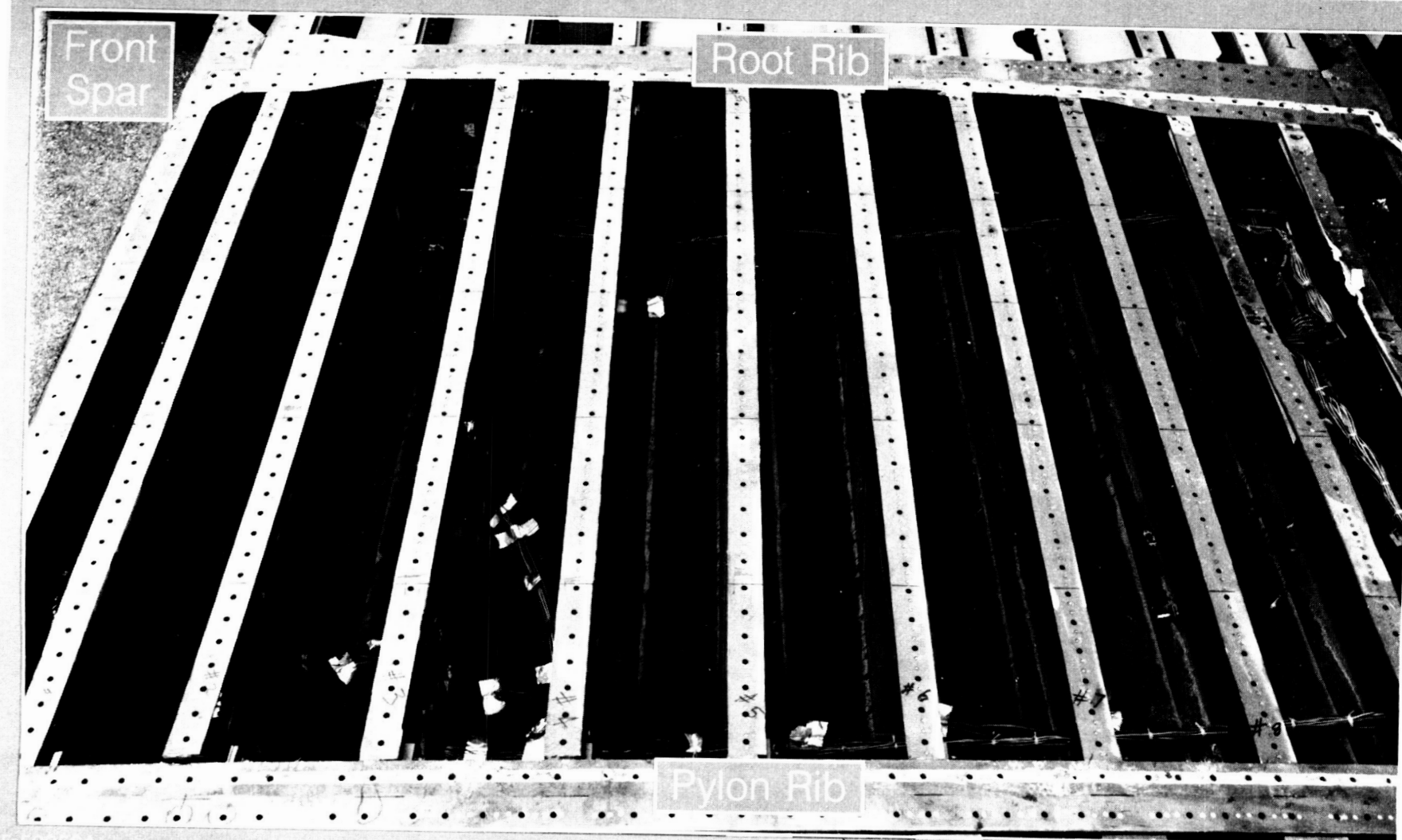
Lessons Learned – Static Strength

- INHERENT PROPERTY DIFFERENCES EXIST BETWEEN COMPOSITES AND METALS
- COMPOSITE STRUCTURES ARE SENSITIVE TO OUT-OF-PLANE LOADS
- MULTIPLICITY OF POTENTIAL FAILURE MODES
- FAILURE MODES OF FULL-SCALE STRUCTURES ARE DIFFICULT TO PREDICT
- STATIC-STRENGTH TEST IDENTIFIES STRUCTURAL "HOT SPOTS"

Wing Component Failure Loads



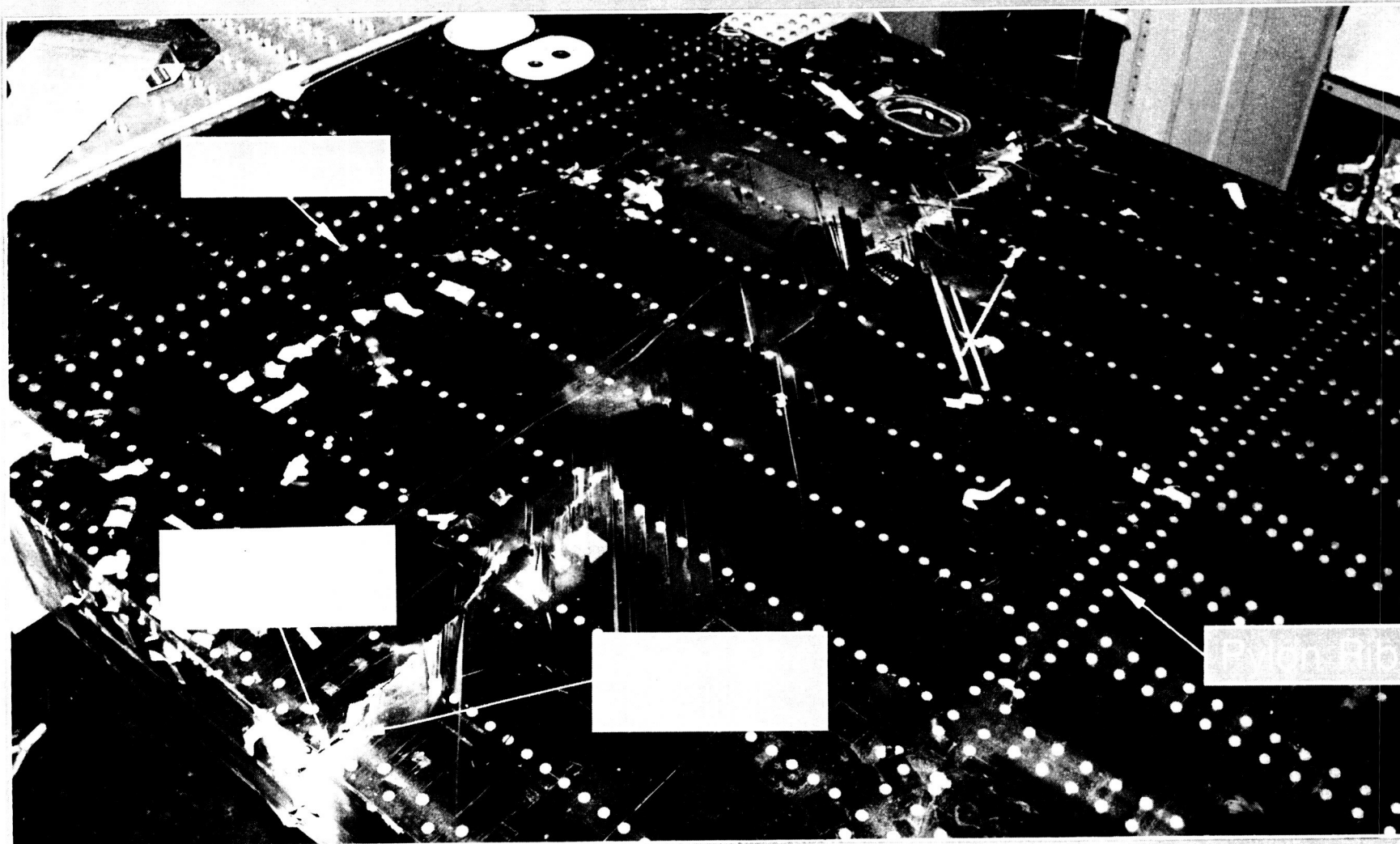
RTA Static Test (TS 2) Failure



550956A
OE INS

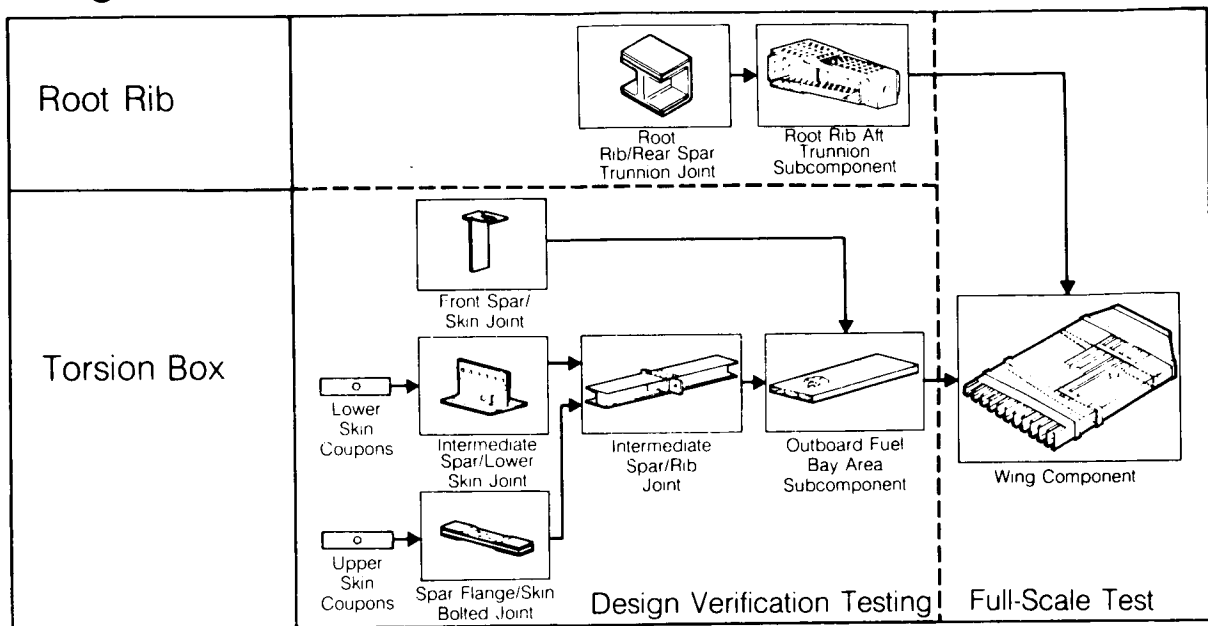
83-0

250°F Wet Static Test (TS 1) Failure



Building-Block Approach

Wing Structure



Lessons Learned – Durability

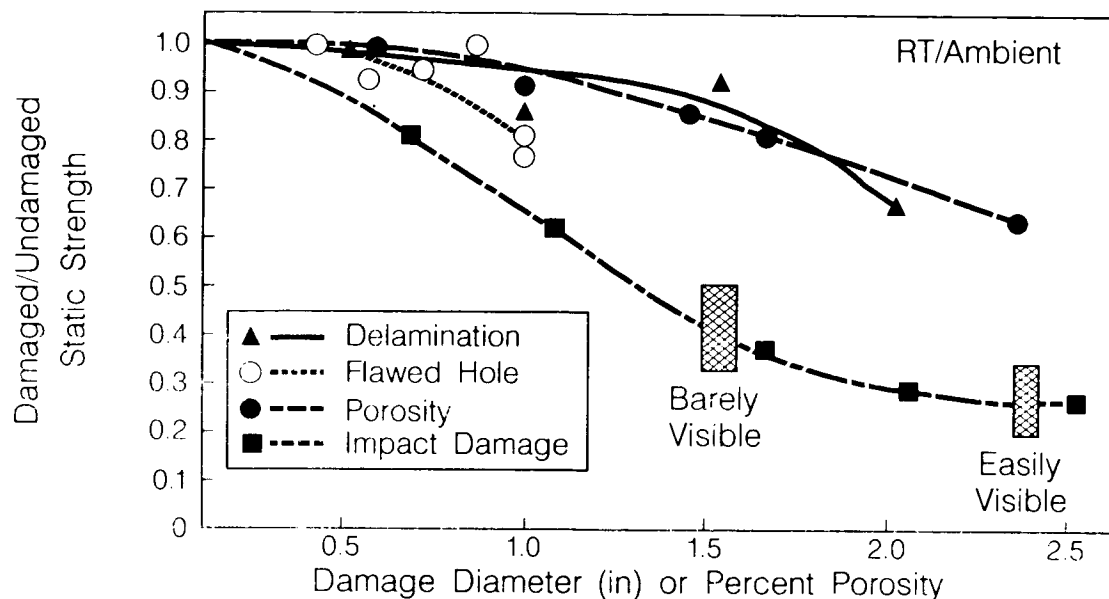
- DURABILITY IS A MEASURE OF ECONOMIC LIFE
- THIN COMPOSITE STRUCTURES ARE SENSITIVE TO LOW-LEVEL (<10 ft-lb) IMPACTS
 - Visible Skin Damage
 - Nonvisible Skin/Core Damage
 - Accelerated Moisture Ingression
 - High Repair Frequency
 - Part Replacement



HIGH MAINTAINABILITY COSTS

Defect/Damage Severity Comparison

Compression



Lessons Learned – Damage Tolerance

- IMPACT DAMAGE IS THE MOST SEVERE DEFECT/DAMAGE TYPE
- IMPACT-DAMAGE AREAS AND STATIC STRENGTH ARE STRONGLY DEPENDENT ON STRUCTURAL CONFIGURATION
- FAILURE MODES OF IMPACT-DAMAGED BUILT-UP STRUCTURE ARE SIGNIFICANTLY INFLUENCED BY STRUCTURAL CONFIGURATION
- SIGNIFICANT IMPACT-DAMAGE TOLERANCE SCALE-UP EFFECTS EXIST FOR BUILT-UP STRUCTURE
- IMPACT-DAMAGED STRUCTURES ARE RELATIVELY INSENSITIVE TO FATIGUE LOADING
- DELAMINATIONS INDUCED DURING ASSEMBLY OPERATIONS HAVE DEMONSTRATED A SIGNIFICANT NUISANCE VALUE

Lessons Learned – Design Criteria

- STATIC STRENGTH, FATIGUE/DURABILITY AND DAMAGE TOLERANCE
- THERE ARE SIGNIFICANT DIFFERENCES BETWEEN USAF, NAVY, ARMY AND FAA REQUIREMENTS
- RATIONALIZATION OF DAMAGE TOLERANCE REQUIREMENTS INTO A SINGLE DOCUMENT IS IN PROGRESS BY J. JAEB (BOEING) THROUGH AIA
- BEWARE OF THESE DIFFERENCES WHEN DESIGNING AN AIRFRAME FOR MORE THAN ONE AGENCY

Agenda

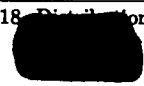
- Materials
- Manufacturing
- Design

- **FUTURE CHALLENGES**

Future Challenges

- REDUCE THE COST OF COMPOSITE AIRFRAME STRUCTURES THROUGH MULTIDISCIPLINARY (MATERIALS, MANUFACTURING, DESIGN) CONCURRENT ENGINEERING
- INCREASE COMPOSITE AIRFRAME WEIGHT FRACTION TO 60%
- DEVELOP LOW COST MATERIALS AND PROCESSES ESSENTIAL IN ORDER TO MEET THESE GOALS

Report Documentation Page

1. Report No. NASA CP-3104, Part 1		2. Government Accession No.		3. Recipient's Catalog No.	
4. Title and Subtitle First NASA Advanced Composites Technology Conference				5. Report Date January 1991	
				6. Performing Organization Code	
7. Author(s) John G. Davis, Jr., and Herman L. Bohon, Compilers				8. Performing Organization Report No. L-16889	
9. Performing Organization Name and Address NASA Langley Research Center Hampton, Virginia 23665-5225				10. Work Unit No. 510-02-11	
				11. Contract or Grant No.	
12. Sponsoring Agency Name and Address National Aeronautics and Space Administration Washington, DC 20546-0001				13. Type of Report and Period Covered Conference Publication	
				14. Sponsoring Agency Code	
15. Supplementary Notes John G. Davis, Jr.: NASA Langley Research Center, Hampton, Virginia. Herman L. Bohon: Lockheed Engineering & Sciences Company, Hampton, Virginia.					
16. Abstract This document is a compilation of papers presented at the first NASA Advanced Composites Technology (ACT) Conference held in Seattle, Washington, from October 29–November 1, 1990. The ACT program is a major new multiyear research initiative to achieve a national goal of technology readiness before the end of the decade. Conference papers recorded results of research in the ACT Program on new materials development and processing, innovative design concepts, analysis development and validation, cost effective manufacturing methodology, and cost tracking and prediction procedures. Papers presented on major applications programs approved by the Department of Defense are also included in this document.					
17. Key Words (Suggested by Authors(s)) Thermoplastics Aircraft Thermosets Composite design Stitching Manufacturing Graphite fibers Analysis Processing				18. Distribution Statement  Review for General Release January 1993 Subject Category 24	
19. Security Classif. (of this report) Unclassified		20. Security Classif. (of this page) Unclassified		21. No. of Pages 426	
22. Price					